



<https://theses.gla.ac.uk/>

Theses Digitisation:

<https://www.gla.ac.uk/myglasgow/research/enlighten/theses/digitisation/>

This is a digitised version of the original print thesis.

Copyright and moral rights for this work are retained by the author

A copy can be downloaded for personal non-commercial research or study,
without prior permission or charge

This work cannot be reproduced or quoted extensively from without first
obtaining permission in writing from the author

The content must not be changed in any way or sold commercially in any
format or medium without the formal permission of the author

When referring to this work, full bibliographic details including the author,
title, awarding institution and date of the thesis must be given

Enlighten: Theses

<https://theses.gla.ac.uk/>
research-enlighten@glasgow.ac.uk

SEISMOLOGICAL STUDIES OF UPPER CRUSTAL STRUCTURE OF
THE SOUTHERN MIDLAND VALLEY OF SCOTLAND

Kenneth Alexander Stuart Davidson

Thesis submitted for the degree of Ph.D at the University of Glasgow

January 1986

ProQuest Number: 10991709

All rights reserved

INFORMATION TO ALL USERS

The quality of this reproduction is dependent upon the quality of the copy submitted.

In the unlikely event that the author did not send a complete manuscript and there are missing pages, these will be noted. Also, if material had to be removed, a note will indicate the deletion.



ProQuest 10991709

Published by ProQuest LLC (2018). Copyright of the Dissertation is held by the Author.

All rights reserved.

This work is protected against unauthorized copying under Title 17, United States Code
Microform Edition © ProQuest LLC.

ProQuest LLC.
789 East Eisenhower Parkway
P.O. Box 1346
Ann Arbor, MI 48106 – 1346

to Heather,

with all my love

Acknowledgments

This project was funded by a NERC research studentship (GT4/81/GS/34) and included two NERC seismic equipment pool loans (102 & 112). This financial and material support is gratefully acknowledged.

I am very grateful to Prof. B.E. Leake for sanctioning this research and for allowing me the use of the facilities of the Department of Geology at Glasgow University to carry out and complete this project.

I am also very grateful to Dr. J. Hall for his advice and supervision at all stages of the project, and for his critical, yet always constructive appraisal of this manuscript.

This project has benefited much from the comments and suggestions of many members of staff and research students at the Department of Geology, and in particular from Drs. D.W. Powell, J.J. Doody and the late A.C. McLean. Their contributions to the contents of this manuscript are acknowledged with thanks.

Many thanks are due to the technical staff at the Department of Geology, in particular Messers R.T. Cumberland and E. Speirs, for their assistance throughout many long, often wet, hours of field work; and to Mr. G. Gordon for maintaining and repairing field equipment. Mrs. S. Hall gave invaluable assistance with much of the draughting work.

My appreciation goes to the staff of the Glasgow University Computing Service, in particular to Messers D. Fildes and J. Beck for their help and patience with my many and varied programming problems, but also to Mrs. E. Hammond and the operators who coped with every type (and size) of job I threw at them.

The facilities of the Global Seismology Unit of the British Geological Survey were generously made available by Dr. C. Browitt. Mr. C. Fyffes and Dr. A. McDonald gave invaluable advice and help with the use of the replay

and digitising equipment.

The field work was carried out only with the kind permission and generous cooperation of all the quarry owners and managers, the blasting contractors; Boskalis Westminster Construction Ltd. and Ritches Ltd., and the landowners, farmers and tenants throughout the survey area. The staff of the NCB Opencast Division are also thanked for their assistance.

Finally, I would like to thank my wife for her encouragement of, and considerable patience with, my work; - despite the number of hours it has consumed. Her help with the field work has also been much appreciated.

List of contents

	Section headings	Page No.
Chapter 1	Regional geology and geophysical background.	
1.1	Introduction	1
1.2	Regional framework	1
1.3	Geological succession within the project area	5
1.3.1	Ordovician rocks of the Midland Valley	5
1.3.2	Silurian rocks of the Midland Valley	8
1.3.3	Old Red Sandstone rocks in the southern Midland Valley	8
1.3.3.1	Lower Old Red Sandstone	8
1.3.3.2	Distinkhorn complex	10
1.3.3.3	Upper Old Red Sandstone	13
1.3.4	Carboniferous rocks in the southern Midland Valley	15
1.4	Geological evidence for the nature of the basement in the Midland Valley	21
1.4.1	Crustal xenoliths	21
1.4.2	Lower Palaeozoic conglomerate provenance	23
1.5	Regional geophysical background in the Midland Valley	25
1.5.1	Regional gravity studies	25
1.5.2	The LOWNET array	26
1.5.3	The LISPB study	29
1.5.4	The Broughton array and subsequent studies	34
1.6	Summary	38

Chapter 2 Equipment, data acquisition and procedure

2.1	Introduction	40
2.2	Field recording equipment	40
2.2.1	The Geostore system	40
2.2.2	The Glasgow FM cassette system	43
2.3	Digitisation procedure	47

Chapter 3 Data acquisition, presentation and processing

3.1	Data collection	50
3.2	Data presentation	54
3.2.1	Data from the Hillhouse - Broughton profile	54
3.2.2	Data from the LES and BTN arrays	63
3.2.3	Spectral analysis	63
3.2.3.1	Introduction	63
3.2.3.2	Spectral analysis of the Hillhouse - Broughton profile sections	81
3.2.4	Description of available filters	83
3.2.5	Filter application to the Hillhouse - Broughton profile	94
3.3	The time-distance data	107

Chapter 4 Interpretation

4.1	Interpretation of the surface structure	120
4.1.1	Introduction	120
4.1.2	Wiechert-Herglotz-Bateman inversion	120
4.1.2.1	Method	120

4.1.2.2	Application of the WHB method to field data	121
4.1.3	Plane layer interpretation	138
4.1.4	Tau-p inversion	153
4.1.5	Summary of the initial surface layer velocity interpretation	160
4.2	Interpretation of the deep structure	166
4.2.1	Time-term study	166
4.2.1.1	Introduction	166
4.2.1.2	Application of the time-term method to this study	169
4.2.2	Ray-trace modelling	176
4.2.2.1	Procedure	176
4.2.2.2	The ray model and surface velocity structure	178
4.2.2.3	Thin layers	199
4.2.2.4	Basement (a_0) refractor	202
4.2.2.5	Deep structure	215
4.2.3.1	Apparent velocity interpretation	216
4.2.3.2	Use of the apparent velocity dataset	221
4.3	S-wave interpretation	224
4.4	Summary of the interpretation of these data	227

Chapter 5 Discussion and conclusions

5.1	Nature of the a_0 refractor	229
5.1.1	Introduction	229
5.1.2	Summary of the seismic evidence	229
5.1.3	Summary of the geological evidence	230
5.1.4	Comparisons and predictions of possible lithologies	231

5.2	Relationship of the a_0 refracting layer with the overlying sedimentary sequence	236
5.2.1	Geometry of the basement structure compared with known and deducible sediment thicknesses	236
5.2.2	Effect of surface faults on the interpretation of basement structure	239
5.3	Seismic character of faults	241
5.4	Geological interpretation of the a_1 refracting layer	242
5.5	Conclusions and recommendations for further work	248
5.5.1	Conclusions	248
5.5.2	Recommendations for further work	249
References		251
Appendices		
Appendix 1	Site locations	265
Appendix 2	Quarry locations and shot origin times	266
Appendix 3A	Travel-times and ranges (P-waves)	267
Appendix 3B	Travel-times and ranges (S-waves)	275
Appendix 4	LES and BTN array velocity and azimuth data	278
4.1	Cornstones shot into LES array	
4.2	Middle Croft shot into LES array	
4.3	Greivehill shot " " "	
4.4	Cairngryffe Q. " " " 26 Aug 1982	
4.5	Cairngryffe Q. " " " 14 Sept 1982	
4.6	Hillhouse Q. " " "	
4.7	Craigie Q. " " "	
4.8	Kirkconnel Opencast " " "	
4.9	Benbain Opencast " " "	
4.10	Waterside Opencast " " "	
4.11	Dumbuck Q. " " "	
4.12	Craigpark Q. " " "	

4.13	Morvern Q.	"	"	"	
4.14	Westgate Q. (P _n)	"	"	"	
4.15	Westgate Q. (?a ₁)	"	"	"	
4.16	Cloburn Q. (P) into BTN array				
4.17	Cloburn Q. (S)	"	"	"	
4.18	Craigpark Q. (P)	"	"	"	23/2/77
4.19	Craigpark Q. (S)	"	"	"	"
4.20	Craigpark Q. (P)	"	"	"	30/3/77
4.21	Craigpark Q. (S)	"	"	"	"
4.22	Hillhouse Q. (P)	"	"	"	
4.23	Hillhouse Q. (S)	"	"	"	
4.24	Duntilland Q. (P)	"	"	"	
4.25	Duntilland Q. (S)	"	"	"	
4.26	Croy Q.	"	"	"	
4.27	Craighouse Q.	"	"	"	
4.28	Coatsgate Q.	"	"	"	
4.29	Levens Seat O/cast	"	"	"	
4.30	Haywood Opencast	"	"	"	
4.31	Kaimes Q.	"	"	"	
4.32	Middleton Q.	"	"	"	
4.33	Tams Loup Q. (P)	"	"	"	
4.34	Tams Loup Q. (S)	"	"	"	
4.35	Cairryhill Q. (P)	"	"	"	
4.36	Cairryhill Q. (S)	"	"	"	
4.37	Cruicks Q.	"	"	"	

Appendix 5	Calculated and field travel-times for the ray model	315
Appendix 6	Program listings: BJARRY DIGFLT DRAW4 RAYVZ TAUP TX3E	318

List of figures

Figure captions	Page No.
Chapter 1 Regional geology and geophysical background	
1.1 Location map for Central Scotland.	2
1.2 Simplified geological map of Central & Southern Scotland showing the major tectonic and stratigraphic units.	4
1.3 Palaeogeographical reconstruction of the Girvan region during Ordovician times.	6
1.4 Palaeogeographical reconstruction of the Girvan region as 1.3 with radiometric age dates from boulders within the conglomeratic units.	7
1.5 Distribution of Silurian rocks in the Midland Valley and Southern Uplands.	9
1.6 Geological map of the Distinkhorn complex.	11
1.7 Distribution of Upper Old Red Sandstone rocks in the Midland Valley.	14
1.8 Thickness variations of Carboniferous rocks across the western Midland Valley.	16
1.9 Summary of the distribution of ages and lateral extent of Carboniferous lavas in the Midland Valley.	17
1.10 Map showing basement controls of volcanism and sedimentation during Carboniferous times.	18
1.11 Changes in conglomerate composition from Ordovician to Silurian times.	24
1.12 LOWNET site locations and details.	27
1.13 LOWNET travel-times and their interpretation.	28
1.14 Location map for the LISPB study.	30
1.15 Crustal structure of northern Britain from the LISPB study.	31
1.16 t_s / t_p ratio data from the LISPB study.	33
1.17 Geological interpretation of the portion of the LISPB study across northern Britain.	35
1.18 Velocity-depth distributions for the Southern Uplands.	37

Chapter 2 Equipment, data acquisition and procedure

- | | | |
|-----|---|----|
| 2.1 | Comparison of the frequency responses of the Geostore & Glasgow FM cassette recorder systems. | 44 |
| 2.2 | Comparison of the frequency responses of various geophones & seismometers used in this study. | 45 |
| 2.3 | Flow diagram summarising the stages involved in producing final digital sections from field recordings. | 48 |

Chapter 3 Data acquisition, presentation and processing

- | | | |
|-------|---|-------|
| 3.1 | Location map for the Hillhouse - Broughton profile. | 52 |
| 3.2 | Sketch geological section under the Hillhouse - Broughton profile. | 53 |
| 3.3-5 | 10 or 8 second, unfiltered record sections ($V_{red} = 6.0 \text{ km s}^{-1}$) for Hillhouse, Dunduff and Cairngryffe-Cloburn quarries. | 55-57 |
| 3.6-8 | 10 or 8 second, unfiltered record sections ($V_{red} = 3.5 \text{ km s}^{-1}$) for Hillhouse, Dunduff and Cairngryffe-Cloburn quarries. | 58-60 |
| 3.9A | Location map of all sources referenced in the array study. | 65 |
| 3.9B | Summary of all P-wave data identified into the LES & BTN arrays. | 66 |
| 3.10 | Summary diagram for the dataset in 3.9B, but showing the spread of ranges for each identified event. | 67 |
| 3.11 | Summary of the S-wave dataset identified into the BTN array. | 68 |
| 3.12 | Unfiltered record section ($V_{red} = 6.0 \text{ km s}^{-1}$) for Cairngryffe Q. into LES array, 26 Aug 1982. | 69 |
| 3.13 | Unfiltered record section ($V_{red} = 6.0 \text{ km s}^{-1}$) for Cairngryffe Q. into LES array, 14 Sept 1982. | 70 |
| 3.14 | Unfiltered record section ($V_{red} = 6.0 \text{ km s}^{-1}$) for Greivehill shot into LES array. | 71 |
| 3.15 | Unfiltered record section ($V_{red} = 6.0 \text{ km s}^{-1}$) for Hillhouse Q. into LES array. | 72 |
| 3.16 | Unfiltered record section ($V_{red} = 6.0 \text{ km s}^{-1}$) for Craigie Q. into LES array. | 73 |
| 3.17 | Unfiltered record section ($V_{red} = 6.0 \text{ km s}^{-1}$) for Cloburn Q. into BTN array. | 74 |
| 3.18 | Unfiltered record section ($V_{red} = 6.0 \text{ km s}^{-1}$) for Hillhouse Q. into BTN array. | 75 |

3.19	Unfiltered record section ($V_{red} = 6.0 \text{ km s}^{-1}$) for Tams Loup Q. into BTN array.	76
3.20	Unfiltered record section ($V_{red} = 6.0 \text{ km s}^{-1}$) for Duntilland Q. into BTN array.	77
3.21	Unfiltered record section ($V_{red} = 6.0 \text{ km s}^{-1}$) for Craigpark Q. into BTN array.	78
3.22	Unfiltered record section ($V_{red} = 6.0 \text{ km s}^{-1}$) for Coatsgate Q. into BTN array.	79
3.23	Unfiltered record section ($V_{red} = 6.0 \text{ km s}^{-1}$) for Craighouse Q. into BTN array.	80
3.24	Plot of dominant frequency against range for the Hillhouse - Broughton profile.	82
3.25, 26	Impulse response and amplitude spectrum for a causal, tapered Robinson BP filter.	86, 87
3.27, 28	Impulse response and amplitude spectrum for a two-sided, tapered Robinson BP filter.	88, 89
3.29, 30	Impulse response and amplitude spectrum for a two-sided, untapered Robinson BP filter.	90, 91
3.31, 32	Impulse response and amplitude spectrum for a two-sided Hanning BP filter.	92, 93
3.33	Hillhouse Q. record section ($V_{red} = 6.0 \text{ km s}^{-1}$) with a Hanning BP filter.	95
3.34	Hillhouse Q. record section ($V_{red} = 6.0 \text{ km s}^{-1}$) with a two-sided, tapered Robinson BP filter.	96
3.35	as for 3.33 but with ($V_{red} = 3.5 \text{ km s}^{-1}$).	97
3.36	as for 3.34 but with ($V_{red} = 3.5 \text{ km s}^{-1}$).	98
3.37	Dunduff Q. record section ($V_{red} = 6.0 \text{ km s}^{-1}$) with a Hanning BP filter.	99
3.38	Dunduff Q. record section ($V_{red} = 6.0 \text{ km s}^{-1}$) with a two-sided, tapered Robinson BP filter.	100
3.39	as for 3.37 but with ($V_{red} = 3.5 \text{ km s}^{-1}$).	101
3.40	as for 3.38 but with ($V_{red} = 3.5 \text{ km s}^{-1}$).	102
3.41	Cairngryife-Cloburn record section ($V_{red} = 6.0 \text{ km s}^{-1}$) with a Hanning BP filter.	103
3.42	Cairngryife-Cloburn record section ($V_{red} = 6.0 \text{ km s}^{-1}$) with a two-sided, tapered Robinson BP filter.	104
3.43	as for 3.41 but with ($V_{red} = 3.5 \text{ km s}^{-1}$).	105

3.44	as for 3.42 but with ($V_{red} = 3.5 \text{ km s}^{-1}$).	106
3.45-	Hillhouse, Dunduff and Cairngryffe-Cloburn quarries,	108-
47	unfiltered record sections with first break picks superimposed.	110
3.48-	First break picks from analogue records for Hillhouse, Dunduff	112-
50	and Cairngryffe-Cloburn quarries.	114
3.51-	Shear wave picks from analogue records for Hillhouse, Dunduff	115-
53	and Cairngryffe-Cloburn quarries.	117
Chapter 4 Interpretation		
4.1	P-wave T-X data for Dunduff Q. E with V-Z curve from WHB inversion.	123
4.2	S-wave T-X data for Dunduff Q. E with V-Z curve from WHB inversion.	124
4.3	Combination plot of 4.1 & 4.2, with V_p/V_s and Poisson's ratio -depth curves.	126
4.4	P-wave T-X data for Cairngryffe Q. W with V-Z curve from WHB inversion.	127
4.5	Combination plot of 4.3 & 4.4, with V_p/V_s and Poisson's ratio -depth curves.	129
4.6	P-wave T-X data for Cloburn Q. E with V-Z curve from WHB inversion.	130
4.7	P-wave T-X data for Cornstones shot into the LES array with V-Z curve from WHB inversion.	132
4.8	P-wave T-X data for Mid Croft shot into the LES array with V-Z curve from WHB inversion.	133
4.9	P-wave T-X data for Dunduff Q. W with V-Z curve from WHB inversion.	135
4.10	P-wave T-X data for the Greivehill shot into the LES array with V-Z curve from WHB inversion.	137
4.11	as for 4.1 but with the WHB interpretation extended down to the first velocity discontinuity.	139
4.12	as for 4.9 but with the WHB interpretation extended down to the first velocity discontinuity.	140
4.13	as for 4.4 but with the WHB interpretation extended down to the first velocity discontinuity.	141
4.14	as for 4.6 but with the WHB interpretation extended down to the first velocity discontinuity.	142

4.15	Plane layer interpretation of the Mid Croft and Cornstones shot data.	144
4.16	Plane layer interpretation of the Hillhouse Q. E and Dunduff Q. F data.	145
4.17	Plane layer interpretation of the Dunduff Q. E S-wave data.	146
4.18	Plane layer interpretation of the Dunduff Q. W and Cairngryffe Q. W data.	147
4.19	Plane layer interpretation of the Cloburn Q. E P & S-wave data.	148
4.20	Comparison of WHB inversion vs plane layer interpretation for the Cornstones and Mid Croft shot datasets.	150
4.21	Comparison of WHB inversion vs plane layer interpretation for the Dunduff Q. E P & S-wave datasets.	151
4.22	Comparison of WHB inversion vs plane layer interpretation for the Cairngryffe Q. W and Cloburn Q. E datasets.	152
4.23	Comparison of WHB inversion vs Tau-p inversion for the Cornstones and Mid Croft shot datasets.	155
4.24	Comparison of WHB inversion vs Tau-p inversion for the Greivehill shot and Dunduff Q. E S-wave datasets.	156
4.25	Comparison of WHB inversion vs Tau-p inversion for the Cairngryffe Q. W and Cloburn Q. E datasets.	157
4.26	Comparison of the plane layer interpretation vs the Tau-p inversion for the Dunduff Q. F dataset.	159
4.27	Comparison of the LISPB & LGWNET upper crustal models with all the WHB model V-Z curves.	161
4.28	Comparison of the LISPB & LGWNET upper crustal models with all the plane layer interpretation V-Z curves.	162
4.29	Comparison of the LISPB & LGWNET upper crustal models with 4.5	165
4.30	Weighting scheme for the time-term analysis.	167
4.31	Tabulation of all time-term results.	170
4.32	Comparison of calculated time-terms from the ray model with those from an iteration using a fixed a_0 refractor velocity of 6.05 km s^{-1} .	174
4.33	Diagram showing the results in 4.32.	175
4.34	The final raymodel for the Hillhouse - Broughton profile.	179
4.35,	P-wave velocity distribution for the final raymodel down to	180,
36	-11 km and -5 km.	181

4.37- 41	Ray diagrams for Hillhouse, Dunduff, Cairngryffe-Cloburn and Craigie quarry datasets.	182- 186
4.42- 46	Diagrams showing field and model T-X points for each of the ray diagrams in 4.37-41.	187- 191
4.47- 50	Record sections showing field seismograms and the model T-X points for the ray diagrams in 4.37-40.	192- 195
4.51	Table of standard errors for the fit of each layer in the raymodel.	196
4.52	Apparent velocity & attenuation as functions of layer thickness for P-wave refractions along thin layers.	200
4.53	Comparison of the LISPB & LOWNET upper crustal models with the P-wave velocity for the a_0 refractor from this study.	203
4.54	Ray model constructed by downwards extrapolation of the surface geology.	206
4.55	Ray diagram for all sources for the raymodel in 4.54.	207
4.56	Diagram showing the fit of the predicted geological model T-X points to the field T-X data.	208
4.57, 58	P-wave velocity models for the raymodel in 4.54 down to -13 km and -5 km.	209, 210
4.59	Simplified geological map of the Lesmahagow Inlier showing the positions of all the stations in the LES array and the line of section in 4.60.	213
4.60	Sketch geological section across the Lesmahagow Inlier with plots of time-terms from sites on or near the section.	214
4.61, 62	Plots of apparent velocity-azimuth and apparent velocity-range for all P-wave data between 15-55 km received into the LES & BTN arrays.	217. 218
4.63	Plots of apparent velocity-azimuth and apparent velocity-range for all S-wave data between 15-55 km received into the LES & BTN arrays.	219
4.64	Map of the distribution of apparent P-wave velocity data used to produce the map in 4.65.	220
4.65	Contoured depth map to the a_0 refractor produced from the Hillhouse - Broughton raymodel, the MAVIS profile preliminary interpretation and all apparent velocity data shown in 4.64.	223
4.66	Plane layer interpretation of the LISPB shot E (south) into alpha and beta segments.	225

Chapter 5 Discussion and conclusions

5.1	Summary of the seismic characteristics of the a_0 refractor.	229
5.2	Comparison of the model a_0 refractor V-Z curve with V-Z curves from cores of Ordovician clastic sediments from the Girvan region.	233
5.3	Comparison of the model a_0 refractor V-Z curve with V-Z curves from cores of acid gneisses.	234
5.4	Comparison of the model a_0 refractor V-Z curve with V-Z curves from cores of quartzite.	235
5.5	Summary of the velocity information on the a_1 refractor.	243
5.6	C.I.P.W. norms from Midland Valley granulite xenoliths compared with norms calculated from seismic data for the lower crustal layer (a_2).	246
5.7	Summary diagram showing the suggested mineralogical composition of the crust under the Midland Valley of Scotland.	247

Synopsis

The aim of this project has been to investigate the crustal structure, in particular the upper crustal structure, of the southern Midland Valley of Scotland using quarry blast and controlled-shot seismic refraction methods. The study was designed as a follow-up of the LISPB and LOWNET crustal refraction studies in Central Scotland, extending their interpretations of upper crustal structure into southern and western parts of the Midland Valley of Scotland.

The acquisition and presentation of new data collected over a period of 2 1/2 years is discussed, along with results from the application of various interpretational methods. This new data is grouped for convenience into the results from the Lesmahagow array (LES), and the Hillhouse - Broughton profile. Some older data, from the Broughton array (BTN; El-Isa 1977), are also presented and interpreted in the light of this new data.

These data were interpreted using a variety of methods depending on the amount of data available and its distribution.

Individual shot/quarry profiles were interpreted for the near surface velocity structure using the Wiechert-Herglotz-Bateman (WHB) inversion and planar-layer modelling methods. Most of the near surface data were independently interpreted by both of these methods, providing some measure of the consistency of the near surface velocity structures, rather than as a direct comparison of each method. The suspected existence of velocity inversions under some of these profiles suggested that an inversion technique such as the tau-p method might provide a means of directly modelling these low velocity zones. Initial tests were encouraging, but further development had to be abandoned.

High apparent velocity arrivals were noticed on a number of profiles and these were initially interpreted using time-term analysis. This provided a

reasonable statistical solution proving the existence of a high velocity refractor ($V_p > 6.0 \text{ km s}^{-1}$) under the study area (southern Midland Valley), but the site time-terms did not obviously correlate with those expected from downwards extrapolation of the surface geology. The reasons for this are twofold. The variable velocity-depth structures modelled for different stratigraphic units within the southern Midland Valley makes the depth conversion of each site time-term an individual process, dependent on knowledge of the geological structure under each site.

The other factor affecting the geological interpretation of the time-term solution was the realisation, from ray trace modelling and the regional apparent velocity modelling, that the structure of this high velocity layer (now designated a_0 to conform to the LISPB standard nomenclature) does not appear to conform to the structure predicted by the downwards extrapolation of the surface geological structure. Even after quantifying the errors involved in the field data and ray trace modelling procedure, the expected vertical relief on the a_0 refractor is much less than predicted.

Ray modelling of the Hillhouse - Broughton profile also highlighted the existence of several high velocity layers within the sedimentary layer. These can be related to hyperbyssal intrusive suites seen at the surface.

From these interpretations, it is concluded that both the LISPB and LOWNET P-wave velocity models for the near surface layer (a_s) have oversimplified the ranges of velocity found to characterise the three main litho-stratigraphic groups within the study area (ie the Upper Old Red Sandstone & Carboniferous, the Lower Old Red Sandstone, and the Silurian). This can be summarised as below:

Stratigraphic Unit	P-Wave velocity range
Carboniferous & Upper O.R.S.	3.2 - 4.0 km s ⁻¹
Lower Old Red Sandstone	4.0 - 5.2 km s ⁻¹
Silurian (& ?Ordovician)	3.5 - 5.5 km s ⁻¹

Evidence is presented from this study, and collated from other applicable sources, such as ultrasonic measurements on rock cores and other field studies over cratonic areas, that the LISPB interpretation of the geological nature of the a_0 refracting layer (as Lower Palaeozoic clastic sediments) is erroneous. On the basis of the near surface velocity interpretations and a series of lithological comparisons, it was concluded that the seismic characteristics of this layer would be best matched by a quartz-feldspar rich, crystalline layer.

The geological impact of the velocity and structural information on the a_0 refracting layer is discussed, highlighting the difference between the apparently low relief, near planar a_0 refractor and the highly variable Palaeozoic sedimentary thickness recorded at the surface. It is suggested that the major faults of the southern Midland Valley (the Kerse Loch, Carmichael and Southern Uplands faults) may not give displacements on the a_0 refractor commensurate with those found at the surface. A major basement strike-slip zone, producing a 'flower' fault pattern whose branching 'petals' are these major faults, might be one explanation for the above evidence.

Some new data are presented from the a_1 (LISPB 6.4 km s⁻¹) refracting layer, and its interpretation fitted into the existing LISPB structural model. The geological nature of this layer is discussed using all available seismic information, and geochemical/petrological data available from local volcanic xenoliths.

The conclusion from this is that the interpretation of the a_0 refracting

layer is consistent with quartz-rich, probably granulitic lithology, and the simplest interpretation for the nature of the a_0/a_1 interface is as a metamorphic facies change, from amphibolite to granulite.

The basic granulitic xenolith suite from within the Midland Valley and previously assumed by some workers to be derived from the a_1 refracting layer, is now, on the basis of simple mineral modelling of the LISPB a_2 refractor data, suggested to have a lower crustal origin.

In summary, a generalised crustal model of the Midland Valley is presented showing the surface sedimentary layer extending to between 2 - 4 km depth and overlying quartz-rich gneissose basement, possibly with localised hornblende granite intrusions. This in turn overlies a quartz-rich, granulitic layer extending from 6 - 8 km to 18 - 20 km depth which may be the granulite facies equivalent of the overlying layer. The lower crust, from 18 - 20 to 34 - 35 km depth, is suggested to be composed predominantly of basic, pyroxene granulites.

Further work is required to extend the structural models of the a_0 and a_1 refractors throughout the Midland Valley and further into the Southern Uplands. Additionally, preliminary interpretation of S-waves from this study suggest that much extra geological information would result from a fuller study of the S-wave velocity distribution, used in conjunction with a P-wave velocity model.

Localised seismic reflection profiling could provide rigorous tests of the structural hypotheses suggested in this study.

Chapter 1 Regional geology and geophysical background

1.1 Introduction

This study investigates the structure of the upper crust within the Midland Valley of Scotland using seismological techniques. The area under investigation here extends from the Ayrshire coast around Troon eastwards across to Broughton in the Southern Uplands (for locations see figure 1.1), and comprises outcrops of predominantly Old Red Sandstone or older sedimentary rocks (see figure 1.2). Particular attention has been paid in this study to the relations between the known surface geology and crystalline basement in view of the significance of the Midland Valley in Caledonian tectonic studies.

1.2 Regional framework

The Midland Valley of Scotland is defined in terms of surface geology as being the area of predominantly weakly deformed Palaeozoic sedimentary and volcanic rocks bounded to the north by the Highland Boundary Fault (HBF), and to the south by the Southern Uplands Fault (SUF) (see figure 1.2). The tectonic significance of the Midland Valley lies in the fact that it separates highly deformed Dalradian rocks in the Highlands from more mildly deformed Ordovician and Silurian rocks in the Southern Uplands. No Caledonian structures can be correlated between these two areas.

Much early speculation centred over whether the Midland Valley basement was of continental or oceanic origin (Kennedy 1958; George 1960; McLean & Qureshi 1966; Dewey 1971; Mitchell & McKerrow 1975), but with the publication of the results of the LOWNET study (Crampin et al 1970) and the LISPB crustal profile (Bamford 1979; Bamford et al 1976; 1977; 1978), the existence of continental crust was confirmed. The geological relationship of sedimentary cover and basement within the Highlands, Midland Valley and Southern Uplands was still not known and one of the aims of this project is to establish this

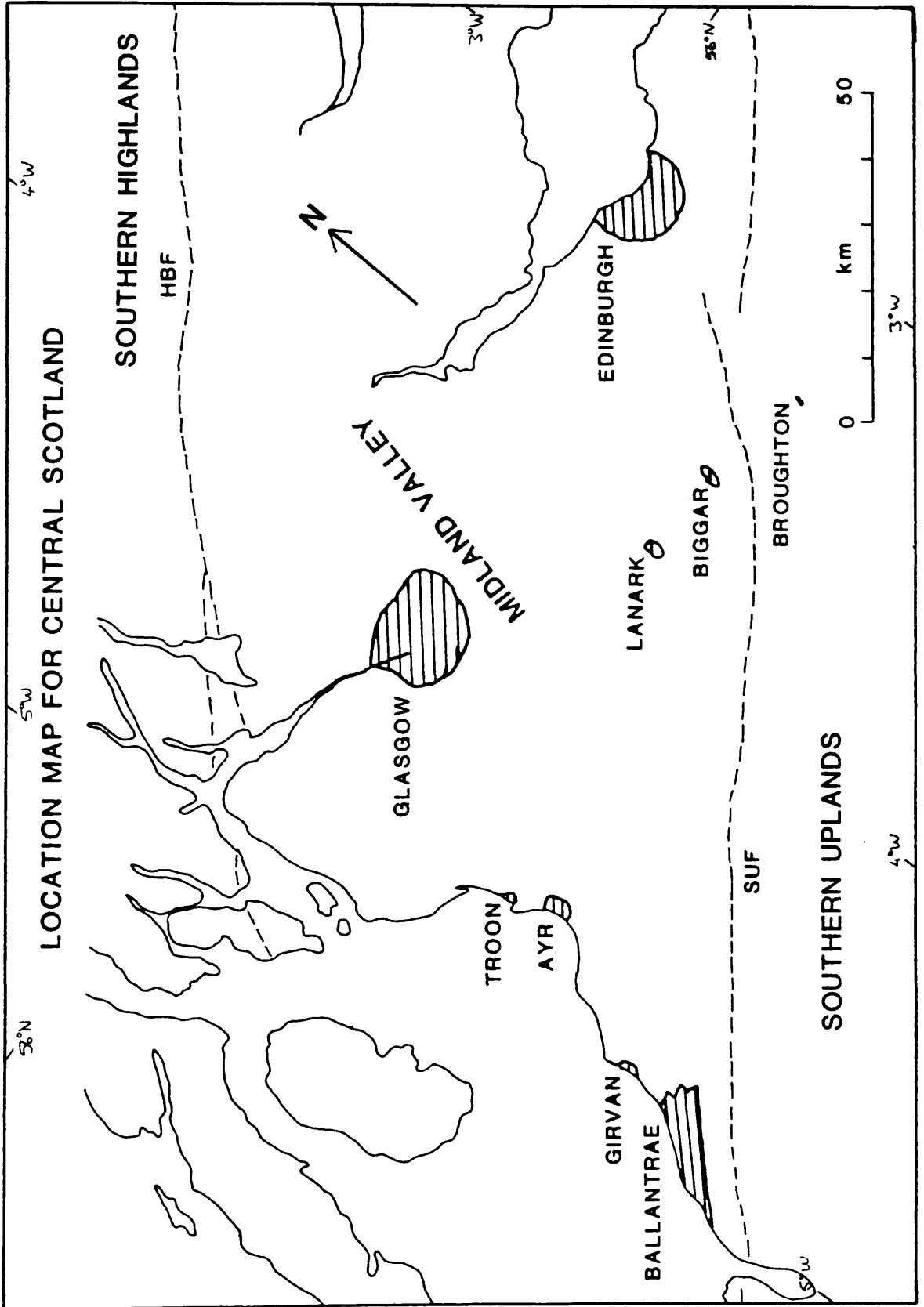


Figure 1.1 Location map for Central Scotland.

HBF - Highland Boundary fault, SUF - Southern Uplands fault.

Figure 1.2 Key.

HBF - Highland Boundary fault
OF - Ochil fault
CPF - Clyde Plateau fault
DWF - Dusk Water fault
IGF - Inchgotrick fault
KLF - Kerse Loch fault
PF - Pentland fault
STF - Straiton fault
CF - Carmichael fault
SUF - Southern Uplands fault
LF - Leadburn fault

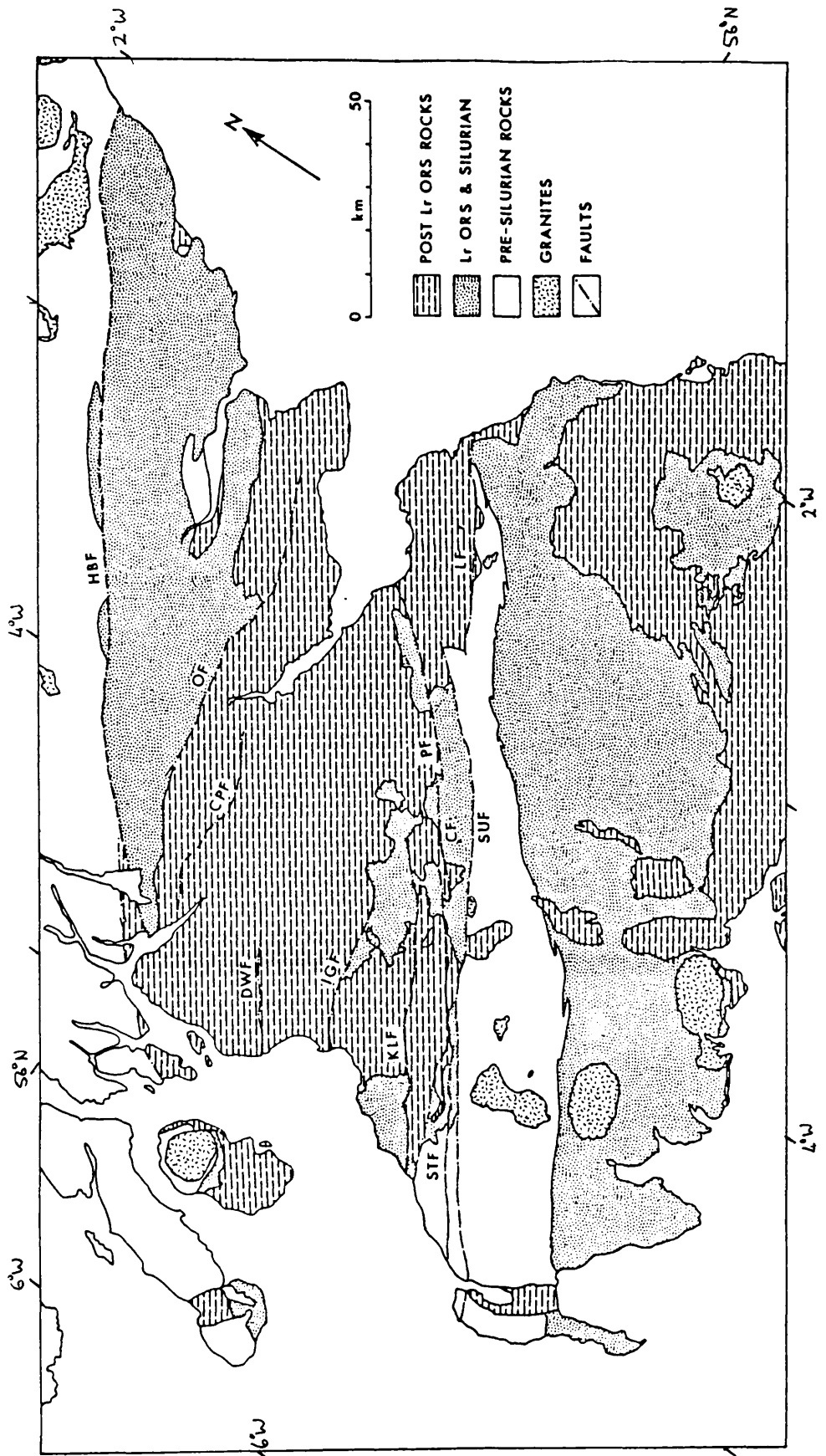


Figure 1.2 Simplified Geological map of Central and Southern Scotland, showing the major tectonic and stratigraphic units.

relationship in the southern part of the Midland Valley of Scotland.

1.3 Geological succession within the project area

A brief summary of the major features of the geological succession in the Midland Valley is given with particular reference to the southern part of the Midland Valley.

1.3.1 Ordovician rocks of the Midland Valley

The oldest rocks seen at the surface within the Midland Valley are found in its SW corner, at Ballantrae (see figure 1.1 for localities). These rocks comprise a suite of intrusive and extrusive, predominantly basic igneous rocks and associated marine sediments, known as the Ballantrae ophiolite (Church & Gayer 1973; Dewey 1974). This allochthonous complex, of Arenig age (Stone & Rushton 1983), is thought to represent the remnants of a Pacific type ocean island (Barrett et al 1982) or part of a marginal basin (which may have included small oceanic islands) (Bluck et al 1980; Bluck & Halliday 1982; Bluck 1983; Thirlwall & Bluck 1984), which was then obducted, probably northwards at 478 ± 4 Ma.

The Ballantrae complex is overlain by a thick sequence of conglomerates, sandstone turbidites and shallow water reefal limestones of Upper Llanvirn to Ashgill age (Ingham 1978; Ince 1984), which were laid down in a series of NE - SW striking basins which had contemporaneous and probably parallel faults at their northwestern margins (Williams 1962) (see figure 1.3), and were probably formed in a strike- or oblique- slip stress regime relating to oblique subduction further S (Ince 1984; Phillips et al 1976). Successively younger basins formed towards the NW so that a progressive fault-controlled overstep was achieved in that direction (Williams 1962). Radiometric dating of clasts within the conglomerate sequences (Longman 1980; Longman et al 1979; Longman et al 1982) (figure 1.4) have shown the close proximity of the

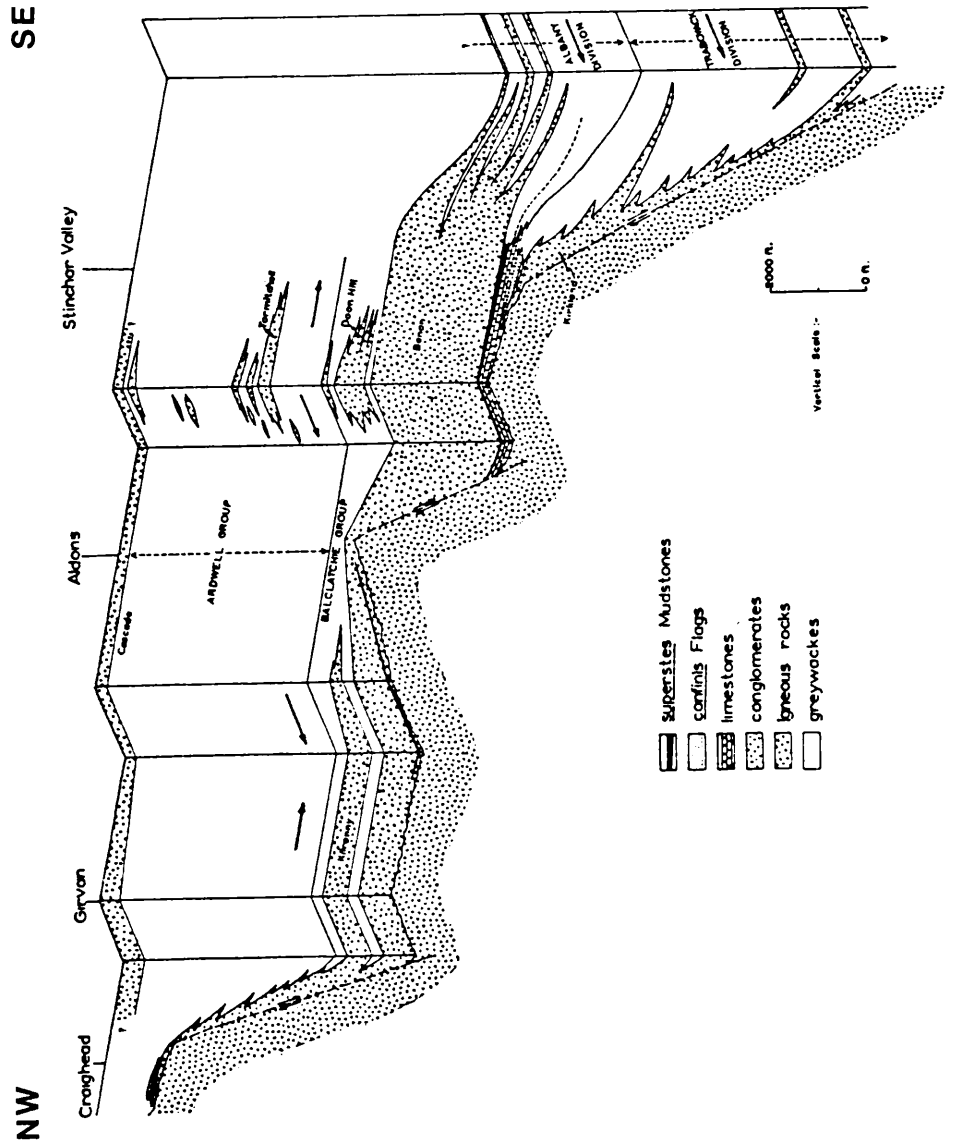


Figure 1.3 Palaeogeographical reconstruction of the Girvan region during Ordovician times (from Williams 1962).

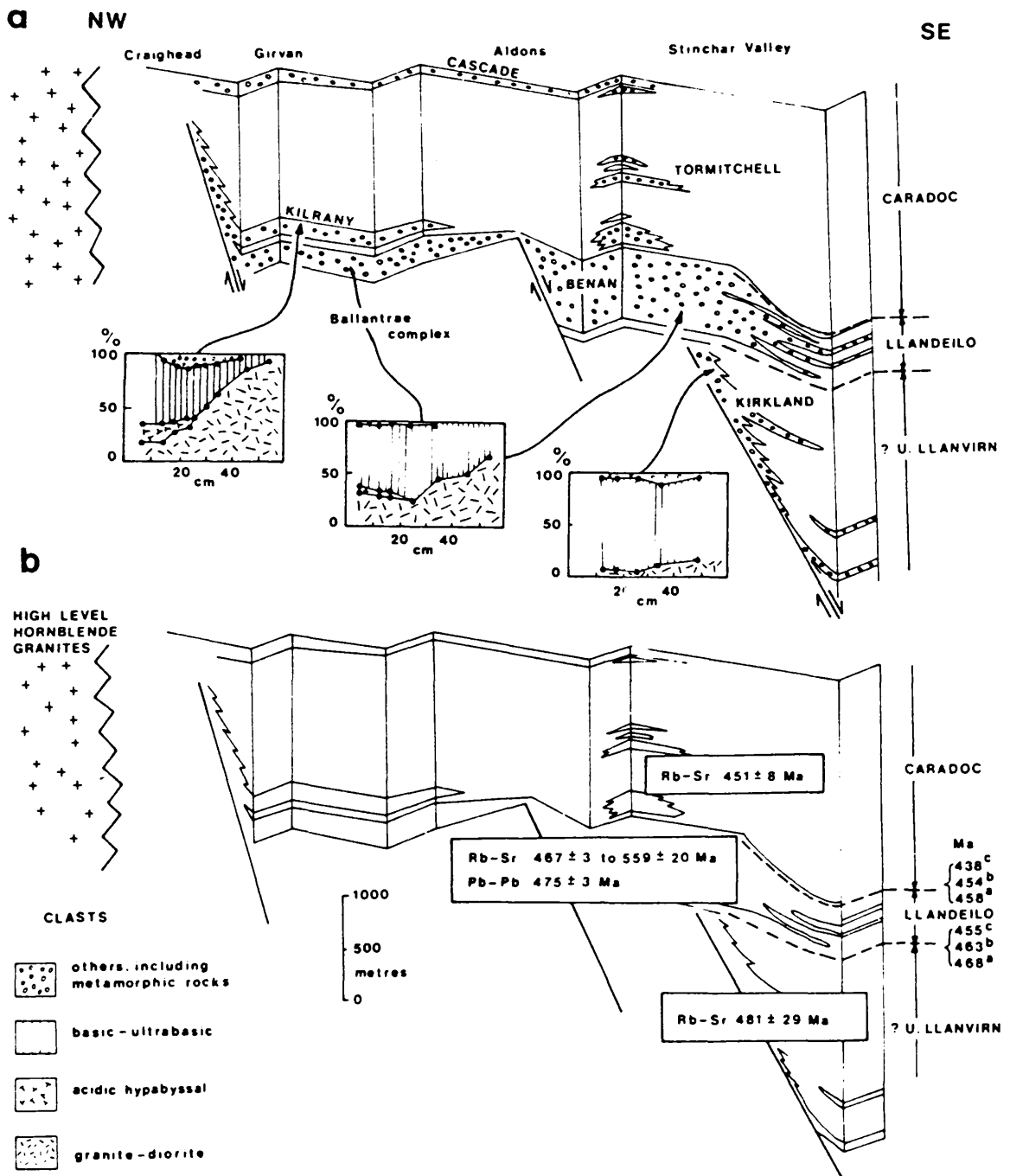


Figure 1.4. Section through the Girvan district (after Williams 1962 & Bluck 1983).

a) Clast composition varying with size.

b) Ages of youngest granite clasts with the addition of a Pb-Pb age and the age of the oldest clast in the Benan Conglomerate; data from Longman (1980) & Longman et al (1979; 1982). Stage-boundary age determinations: a Harland et al (1982), b McKerrow et al (1984), c Odin (1982).

large granite clasts to their original source , and a source-basin relationship has been proposed where continuous uplift of this source accompanied the granite intrusion, while flanking, coeval and genetically related basin underwent complementary subsidence (Bluck 1983).

1.3.2 Silurian rocks of the Midland Valley

A number of inliers of Silurian rocks occur within the Midland Valley ranging in age from Llandovery to Ludlow (see figure 1.5) (Cocks et al 1971). A base for this sequence is seen only at Craighead, near Girvan where a patchy conglomerate oversteps Ashgillian rocks of the Girvan sequence (Ingham 1978). Up to 2 km of sediments have been preserved and palaeofacies analysis indicates a lagoonal, occasionally shallow marine, environment predominating throughout the Llandovery until the appearance of the first of the three major conglomerate wedges, the 'igneous conglomerate', at around the base of the Wenlock. After this, the sediments become progressively terrigenous in nature and indicate a transition to fluvial, lacustrine and inter-tidal environments (McGiven 1967).

1.3.3 Old Red Sandstone in the southern Midland Valley

1.3.3.1 Lower Old Red Sandstone

The Lower Old Red Sandstone rocks of the southern margin of the Midland Valley occur as a series of fault bounded outcrops between the Southern Upland fault and a number of parallel, en echelon faults towards the NW and often associated with older Silurian outcrops. The sequence is characterised by red, drab conglomerates and lithic arenites which often interstratify with lavas of basalt, andesite, trachyte, dacite and rhyolite (Bluck 1978). These are accompanied by many minor intrusions of felsite, dolerite and various porphyries. The thickest development of Lower Old Red Sandstone in the southern part of the Midland Valley is probably to be found in the Pentland Hills (Mykura 1960), where around 2 km of lavas can be demonstrated; although

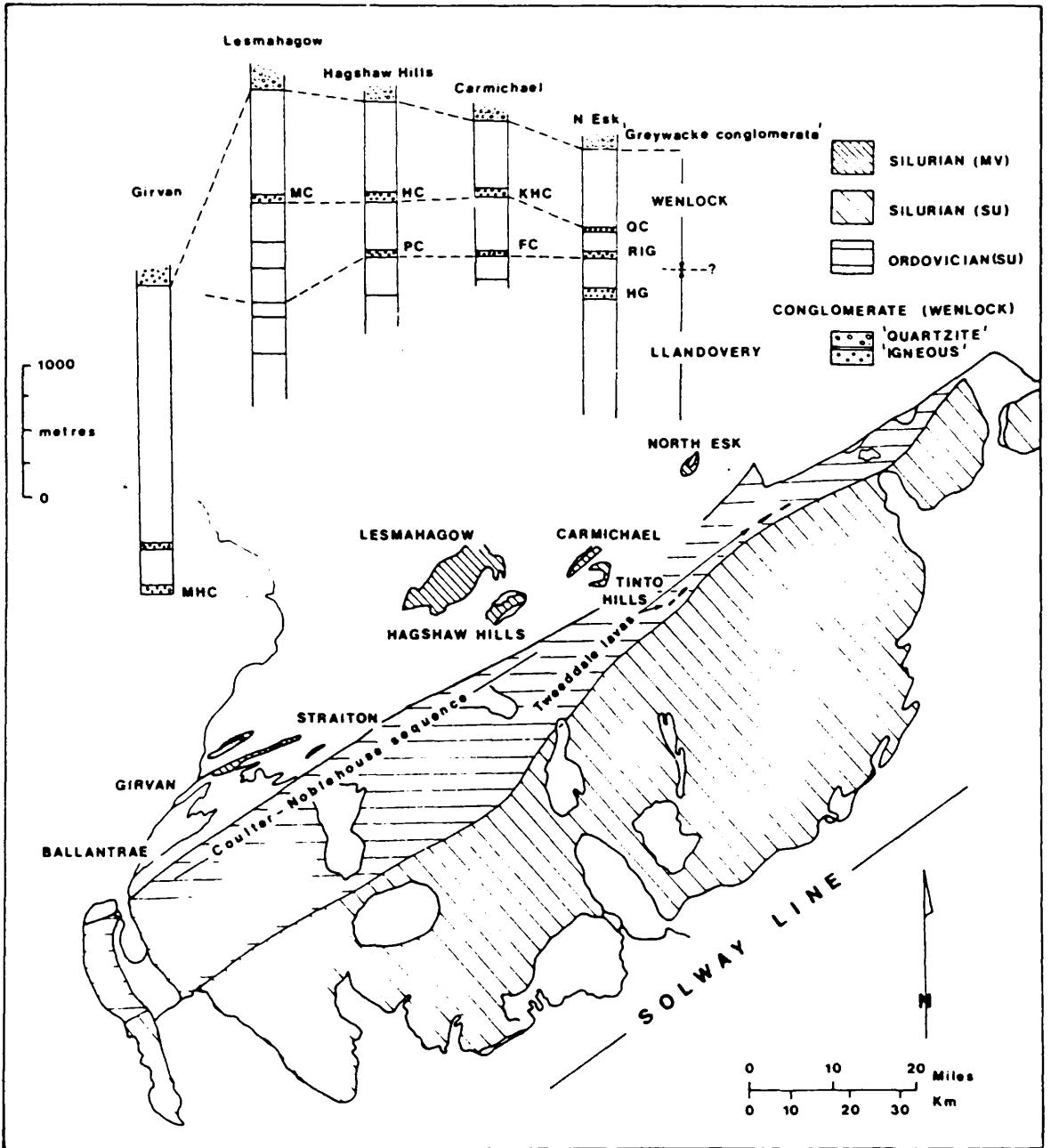


Figure 1.5 Distribution of Silurian rocks in the Midland Valley (MV) and Southern Uplands (SU) (after Bluck 1983).

some of these, at least, have been subsequently shown to be sub-aqueous, soft-sediment intrusions (Kokelaar 1982). These pass southwestwards into a thinner sequence of conglomerates and sandstones. Around Cumnock the thickness is estimated as 1.7 km and in the Maybole inlier as 1.5 km.

Throughout the Midland Valley the Lower Old Red Sandstone lies unconformably on Silurian rocks, except possibly in the Lesmahagow and Hagshaw Hills inliers (see figure 1.5 for locations) where the succession may be conformable (Thirlwall 1981).

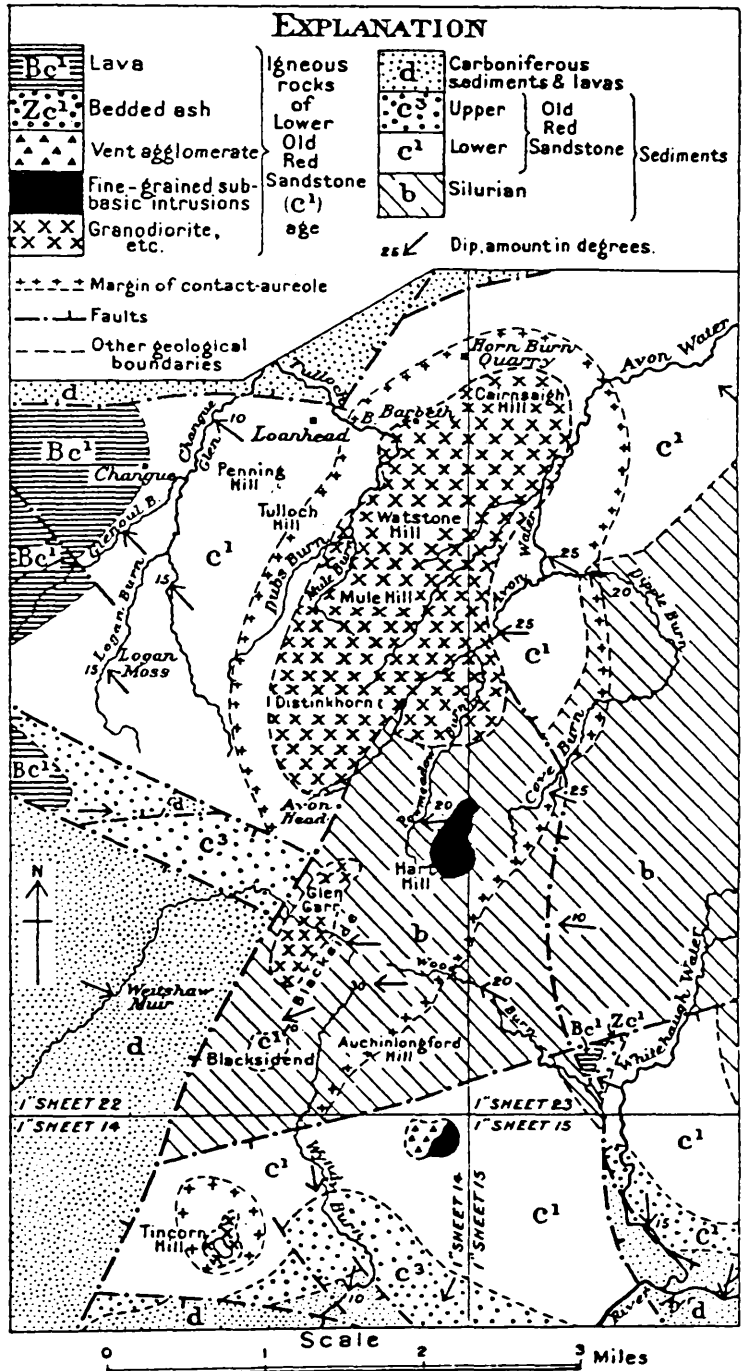
Geochronological studies have placed most or possibly all this vulcanicity in the late Silurian (Thirlwall 1983) and also suggest that some of the minor acidic intrusions around Tinto are late Silurian in age (Herriot 1956; Bluck 1984).

With these new age date constraints, it is clear that the Lower Old Red Sandstone is predominantly, if not totally, a late Silurian continental facies, and thus the unconformity with the Upper Old Red Sandstone may mark a considerable hiatus.

1.3.3.2. Distinkhorn complex

The Distinkhorn igneous complex is an enigmatic plutonic complex cropping out over about 6 km² and intruded into Lower Old Red Sandstone and Silurian sediments at the northwestern corner of the Lesmahagow Inlier (see figures 1.1 & 1.5 for locations). It is the only known Caledonian plutonic intrusion in the Midland Valley yet very little is known about it. The only detailed field and petrological studies are found in the Geological Survey Memoirs (Sheet 22, Richey et al 1930) and MacGregor & MacGregor (1936) (see figure 1.6).

There are very few exposures of the plutonic rocks owing to the extensive post-Glacial cover of peat and boulder clay. Of the variety of igneous rock-types present, none are found in contact with each other and there is only



Map of neighbourhood of Distinkhorn Plutonic Complex, south-east of Darvel; minor intrusions omitted.

Figure 1.6 from Richey et al (1930).

one contact with the country rocks.

Two main groups of plutonic rocks are present. The older and less extensive group are dioritic to quartz-dioritic, thermally altered rocks which, when the original petrology can be recognised, contain plagioclase (often zoned) in the andesine-labradorite range, with biotite, augite (sometimes diopside) and occasionally hypersthene. Quartz and K feldspar are always subordinate in volume, if present at all. Hornblende and biotite are the common products of the thermal metamorphism which replaced the second suite of rocks.

The second, and more extensively outcropping, group consist of a medium grained tonalite containing andesine, orthoclase (often sodic), biotite and primary hornblende with interstitial quartz.

Isotopic age dates have been obtained for the tonalite (Pidgeon & Aftalion 1978) using U-Pb from zircon fragments, and give an age of emplacement of 386 ± 3 Ma. This age is equivalent to dates obtained by the same method for the Criffel-Dalbeattie (391 ± 19 Ma) and Fleet (382 ± 54 Ma) granites from the Southern Uplands (Pidgeon & Aftalion 1978; Aftalion et al 1984), and is distinctly younger than the 405-410 Ma ages quoted by Thirlwall (1983) for the Lower Old Red Sandstone lavas of the northern Midland Valley. The relationship in time between these lavas and the petrologically similar lavas of the Lower Old Red Sandstone in the southern Midland Valley is not clear, but stratigraphic evidence (Bluck 1984) suggests that the base of sedimentary sequence in the southern Midland Valley could be older. Thus the contemporaneous lavas must be at least 405 Ma in age, so that the Distinkhorn Complex cannot relate to that episode of igneous activity.

Regional maps of the gravity and aeromagnetic fields over the complex show only small anomalies compared to the surrounding country rocks, implying either that the density and magnetic susceptibility values are comparable (which, from the above petrological descriptions, appears unlikely), or that

the igneous complex has no great vertical thickness or buried lateral extent.

1.3.3.3 Upper Old Red Sandstone

The Upper Old Red Sandstone is everywhere separated from the Lower Old Red Sandstone by a marked unconformity. It is a more thinly developed sequence than the Lower Old Red Sandstone and it is characterised by generally finer grained sediments. The thickest development of the Upper Old Red Sandstone, at 1 km, is at the NW margin of the Midland Valley (see figure 1.7). The formation thins to a uniform 0.5 km to the south and east. On the basis of palaeocurrent analysis on the constituent groups of the Upper Old Red Sandstone, Bluck (1978) has proposed an E or NE drainage direction throughout the Upper Old Red Sandstone. Changes in distribution, grain-size and provenance of these sediments indicate that in the lower division of the Upper Old Red Sandstone, sedimentation was confined to a series of small, fault controlled basins in the NW corner of the Midland Valley, whose existence may be linked to a local tensional, or transtensional, stress regime, possibly linked to strike slip movement along the HBF itself (Bluck 1978). The middle division of the Upper Old Red Sandstone is characterised by mature, braided stream type sediments, indicating a highland source to the W and SW but outwith the present limits of the Midland Valley of Scotland.

The southern Midland Valley also received some sedimentary input from a mature Southern Upland source area at this time. The upper division of the Upper Old Red Sandstone is characterised by finer grained sediments, suggesting a more locally confined but also possibly a more mature source area. Some locally derived and locally developed conglomerates may indicate a minor reactivation of the HBF at the top of the Upper Old Red Sandstone sequence (Bluck 1978).

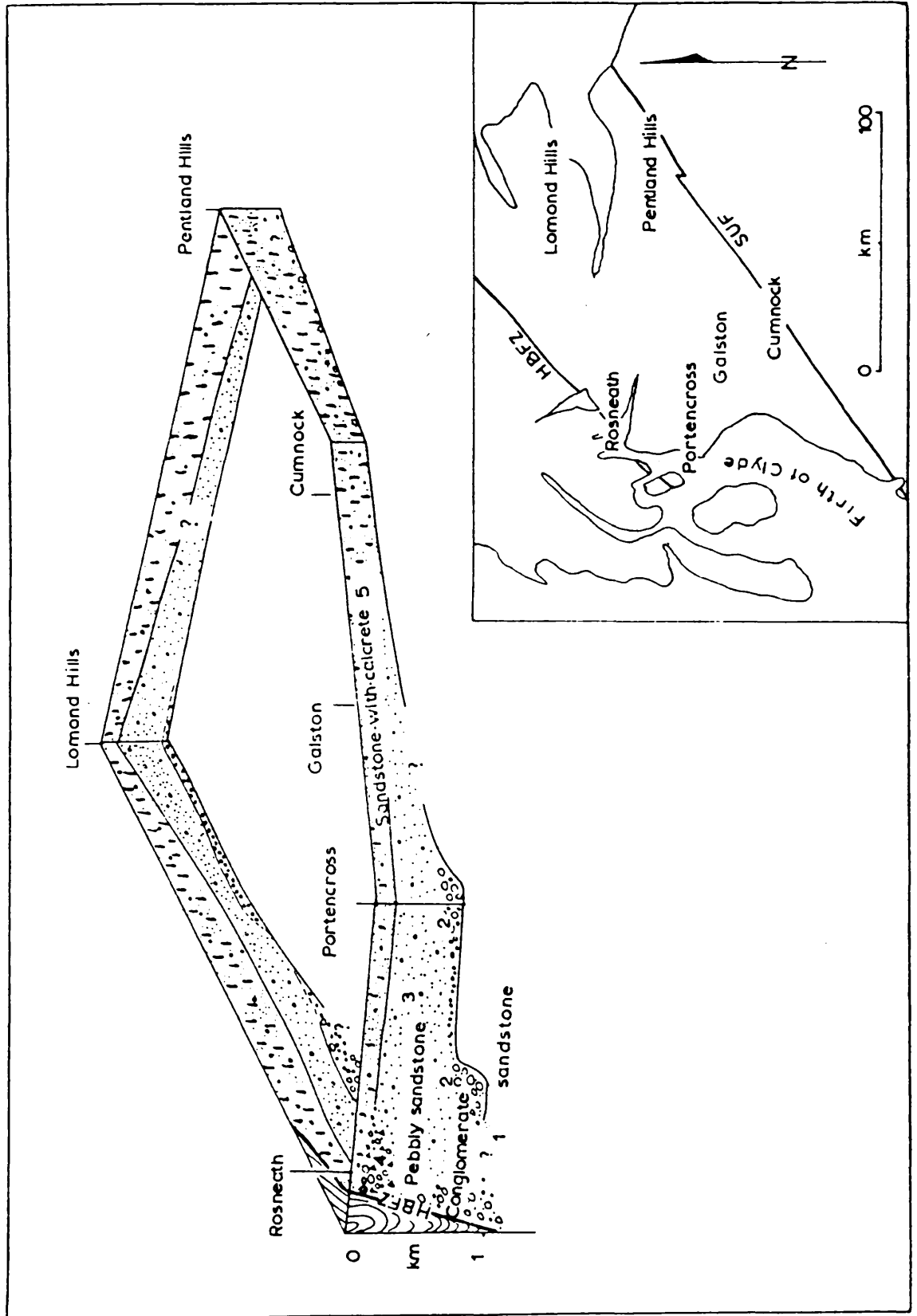


Figure 1.7 Distribution of Upper Old Red Sandstone rocks in the Midland Valley (after Bluck 1973).

1.3.4 Carboniferous rocks in the southern Midland Valley

The base of the Carboniferous in the Midland Valley is ambiguous. It is conventionally placed at the base of the lowest cementstone bed, but it can be argued (Lumsden & Wilson 1979), that the immediately underlying Upper Old Red Sandstone is Tournaisian in age and that the base of the Tournaisian is enclosed within the unfossiliferous Upper Old Red Sandstone fluvial sequence.

Total thicknesses vary considerably across the western half of the Midland Valley as shown by figure 1.8, with the greatest thickness of Carboniferous sediments found in Ayrshire.

The Carboniferous sedimentary sequence formed entirely in either shallow marine or fluvial environments with localised, often persistent, volcanic activity contemporaneous with, and often exerting control over, sedimentation (Francis 1978; 1983). A summary of the age ranges and lateral extents of Carboniferous igneous activity is provided in figure 1.9. However the major control on sedimentation from early Dinantian to mid-Silesian, was differential subsidence along NE-SW trending basement fractures, bounded by the HBF and SUF (see figure 1.10). Within the western Midland Valley, the near surface expressions of these are the Duskwater, Inchgotrick and Kerse Loch faults (Eyles et al 1949; McLean 1966; 1978) and elsewhere by sharp gradients on isopach contours produced for various stratigraphic levels within the Midland Valley (Kennedy 1958; Francis 1983).

The source of basement instability at this time has not been traced to one particular cause. Anderson (1951) showed that a period of compressional stress with the major axis oriented N-S, would result in sinistral transpressive movement along these fractures. The field evidence is equivocal. According to McLean (1966) there is no conclusive evidence of such movements along major faults in S Ayrshire, but Williams (1962) does report evidence of post-Caledonian wrench movement along major NE-SW faults in the Girvan region. An alternative hypothesis relates the apparent relative

Thickness of Carboniferous rocks in the western Midland Valley

Ballycastle	Machrihanish	Arran	South and central Ayrshire	North Ayrshire
<u>Namurian</u> c. 100 m	<u>Lower and Middle Coal Measures</u> c. 150 m	<u>Coal Measures</u> ?200-300 m (an attenuated sequence with no coals)	<u>Barren Red Measures</u> Volcanics (Stephanian) up to c. 205 m Sediments up to 550 m	<u>Barren Red Measures</u> up to 380 m (variable thickness)
<u>Lower Carboniferous</u> c. 540 m (arenaceous with coals and marine bands)	<u>Passage Group</u> c. 137 m (lavas with sedimentary intercalations)	<u>Passage Group</u> c. 59 m (sandstones, marls and volcanics, cut out northwards)	<u>Lower and Middle Coal Measures</u> 427 m at Dalmellington	<u>Lower and Middle Coal Measures</u> 150-220 m
	<u>Upper Limestone Group</u>	<u>Carboniferous Limestone Series</u> c. 138 m	<u>Passage Group</u> up to 128 m (entirely sedimentary sequence)	<u>Passage Group</u> Upper sedimentary Group thin and variable Volcanics up to 150 m Lower Sedimentary Group thin and variable
	<u>Limestone Coal Group</u> 77 m (with good coals)	<u>Calciferous Sandstone Series</u> thickness unknown	<u>Upper Limestone Group</u> c. 215 m	<u>Upper Limestone Group</u> 90 m+
	No <u>Calciferous Sandstone</u> sediments recognised but an unknown thickness of lavas is present		<u>Limestone Coal Group</u> c. 60 m	<u>Limestone Coal Group</u> 150 m+
			<u>Lower Limestone Group</u> up to 30 m	<u>Lower Limestone Group</u> up to 60 m
			<u>Calciferous Sandstone Series</u> 490 m (max.)	<u>Calciferous Sandstone Series</u>
			<u>Upper Group</u> Cementstone Group Shale Subgroup Cornstone Beds Basal Sandstones	<u>Upper Sedimentary Group</u> up to 45 m Clyde Plateau Lavas Cementstone Group

Figure 1.8 after McLean & Deegan (1978).

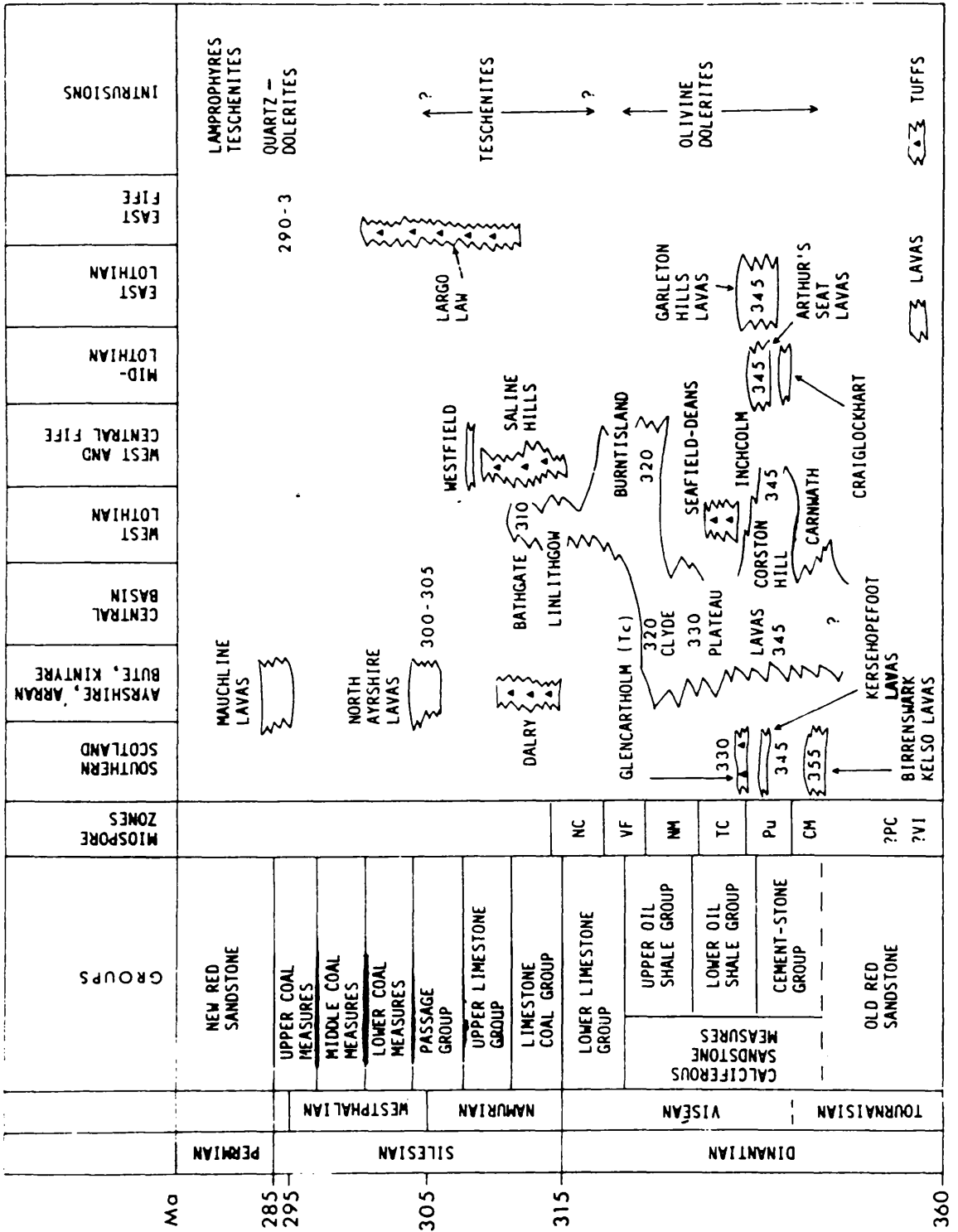
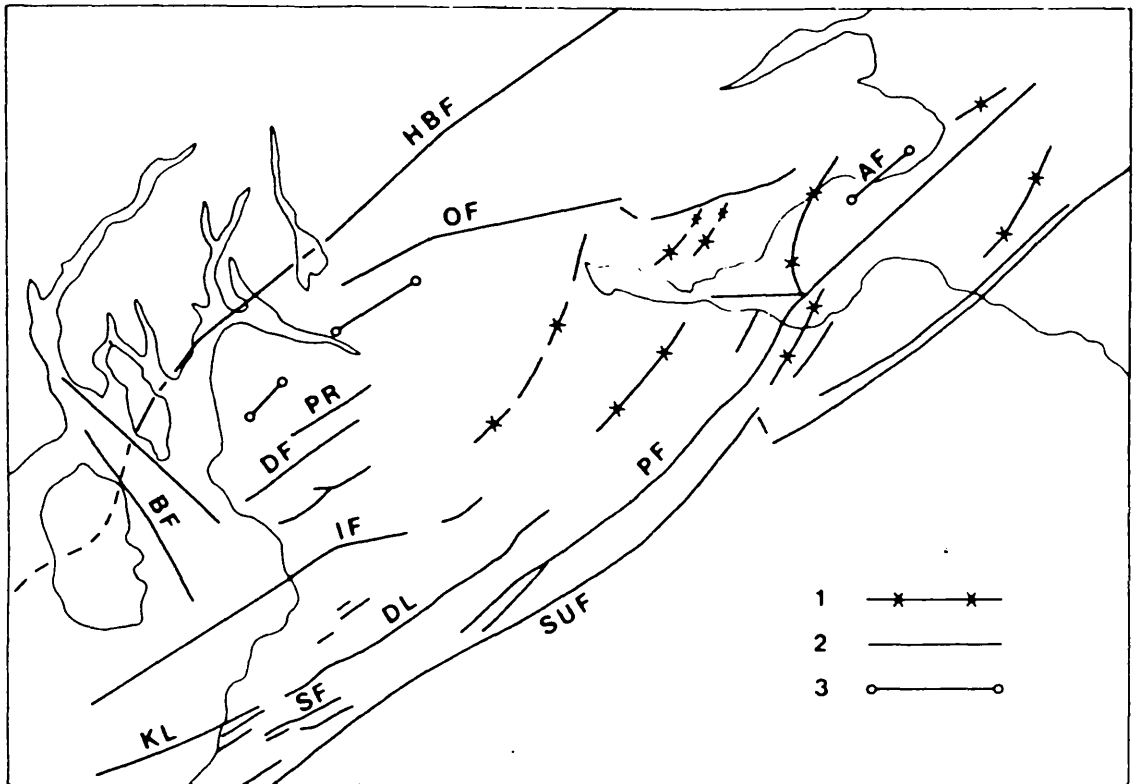


Figure 1.9 Summary of the distribution of ages and lateral extent of Carboniferous lavas in the Midland Valley (from Francis 1983; data from De Souza 1979).



Map showing basement controls of volcanism and sedimentation during the Carboniferous. 1. Axes of syndepositional basins; 2. Syndepositional fractures; 3. Tectovolcanic lineaments. AF Ardross Fault; BF Brodick Bay Fault; DF Dusk Water Fault; DL Dron Line; HBF Highland Boundary Fault; IF Inchgotrick Fault; KL Kerseloch Fault; OF Ochil Fault; PF Pentland Fault; PR Paisley Ruck; SF Straiton Fault; SUF Southern Uplands Fault.

stability of the Highlands and the Southern Uplands compared with the Midland Valley, to the increased buoyancy of the crust under these two regions due to the presence of large volumes of late-Caledonian granite (Bott 1976; Leeder 1976).

During late Westphalian or early Stephanian times the stress regime changed abruptly producing E-W trending fractures which are directly associated with extensive tholeiitic dyke and sill emplacement dated c295 Ma (Fitch et al 1970; Klingspor 1976) covering an approximately 200 km wide belt extending into northern England and which can be correlated both geochemically and geochronologically with a similar suite of intrusions in Norway (MacDonald et al 1981).

During the late Carboniferous, the direction of principal regional stress switched from a N-S tension to a NE-SW tension, giving rise in the western Midland Valley to a series of broad fault-bounded basins in which subsidence kept pace with sedimentation through to New Red Sandstone times. In Ayrshire, the Mauchline Basin is separated from the East Arran Basin to the NW by a block bounded by the Dusk Water and Inchgotrick faults in which there is no evidence of structural continuity. To the SE, the Kerse Loch and Southern Uplands faults, similarly divide the Mauchline Basin from the Sanquhar Basin. Associated with this linear feature is the anticlinal swell running from Renfrew to Lesmahagow which exposes the Clyde Plateau Lavas N of the Inchgotrick fault and the Silurian rocks of the Lesmahagow Inlier to the south. McLean (1978) has proposed that these zones of subsidence may be correlated with other similarly aligned basins to produce a 400 km long linear zone of contemporaneous subsidence, the 'Clyde Belt', which is linked with local volcanic activity. As this NW-SE tension is recognisable elsewhere in northwestern Europe during the early Mesozoic times, McLean proposed that the subsidence could be due to stress transmitted regionally due to

initiation of plate movement from a new spreading axis. Failure would then have occurred along this lineament either due to a focusing of stress relating to the geometry of the spreading axis or due to the presence of a previous line of weakness in the crystalline basement. The latter point suffers from the problem that the 'Clyde Belt' crosses the Caledonian suture and so links two cratons with separate pre-Caledonide crustal identity and development.

However, as mentioned in 1.3.3.2, Bluck (1978) invoked the presence of a series of approximately NW trending faults generated in Upper Old Red Sandstone times as a result of transtensional stress along the HBF, producing (a) pull-apart basin(s) in the region of Renfrew and the Firth of Clyde. The situation of the East Arran Basin in late-Carboniferous might then be related to reactivation of these fractures. This hypothesis may be extended to account for the position of the Mauchline and possibly Sanquhar Basins, depending on the lateral extent of propagation of these fractures during Upper Old Red Sandstone times. (The original assumption was of a local tensional or transtensional stress regime centred around that part of the HBF, and arising from dextral strike-slip movement along it. Sedimentological evidence does not offer any support for continuing these fractures much further south than N Ayrshire). This hypothesis cannot explain the existence of aligned basins developed NW of the HBF, if indeed this alignment is more than coincidental, nor basins found considerably further south of the SUF. The absence of any subsidence between the Dusk Water and Inchgotrick faults may be a problem within the hypothesis, but may also be due to a major difference in upper crustal structure in this region compared with the areas to the N and S.

1.4 Geological evidence for the nature of the basement in the Midland Valley.

The geological evidence for the nature of the basement within the Midland Valley comes from two main sources: crustal xenoliths from volcanic vent agglomerates (Upton et al 1976; Graham & Upton 1978; Upton et al 1983; 1984) and provenance relations obtained from clasts found in Lower Paleozoic conglomerates now cropping out along the marginal regions of the Midland Valley (Longman et al 1979; Bluck 1983).

1.4.1 Crustal xenoliths

Within the Midland Valley, xenoliths are found in vents exclusively Carboniferous in age (figure 1.9), and comprise a suite of rocks yielding information on crustal and upper mantle composition down to around 100 km, as it was during late Paleozoic times. Since then, there have been only vertical movements within this region, and so a study of these xenoliths can provide a useful source of information on lithological types, as distinct from physical properties, present within given depth ranges in the lithosphere. As this project is concerned with upper crustal structure, there is no need for a discussion of the ultrabasic, mantle-derived portion of this xenolith suite, although it provides more than half the number of crystalline samples.

The petrographic similarity of all pyroxene-feldspar basic granulite inclusions across the region from the N of Scotland to central Ireland, along with the absence of any other common xenolith lithology compatible with the observed LISPB $c7 \text{ km s}^{-1}$ lower crustal velocity (Bamford 1979), implies that the lower crust is dominantly gabbroic to dioritic in composition, but possibly containing localised zones with anorthositic fractions (Upton et al 1983; Collette et al 1970).

Within the Midland Valley, quartz-feldspar gneiss xenoliths with very occasional garnet are found in vents in Renfrewshire, Ayrshire and along the

Fife coast, and are inferred to be samples of the sub-Palaeozoic basement (Upton et al 1976). There is no evidence of a lower-grade metamorphic basement layer as might be expected if Dalradian rocks underlie the Lower Palaeozoic sediments (Upton et al 1983; cf Dewey 1971). Samples similar to Southern Uplands sedimentary sequence are also conspicuously absent (Upton et al 1976). On the assumption of a chemically-zoned continental crust becoming more siliceous upwards (Rogers 1977), the acid gneisses generally may be derivatives from more superficial crustal layers than those that supplied the basic granulites (Upton et al 1983). Xenoliths from this residual but intermediate composition do not appear to be present, or have not yet been recognised.

Unfoliated igneous xenoliths are not common, but where found they can be correlated with exposed Caledonian plutons or with granitic bodies proposed from geophysical evidence (eg Tweeddale granite, Lagios & Hipkin 1979). Crustal xenoliths from vents in the Southern Uplands also show a continental affinity instead of oceanic as would be expected if the Southern Uplands accretionary prism was floored by oceanic crust. The results of interpretation of the WINCH profile N of the Solway Basin (Brewer et al 1983; Hall et al 1984), show that the northern edge of the Baltic Continent does not extend for any great distance northwestwards under the Southern Uplands, and so continental crust beneath these vents must be related to the Midland Valley continental crust. This then suggests that an allochthonous contact may exist between the continental basement and the Lower Palaeozoic sedimentary prism.

1.4.2 Lower Palaeozoic conglomerate provenances.

Within the Ordovician (Llanvirn to Ashgill) sedimentary sequence around Girvan, there exist a series of NW derived conglomerates (see 1.3.1). Provenance relations indicate sources which comprised basic and ultrabasic, predominantly intrusive, igneous rocks (see figure 1.11). Later conglomerates record the influx of granitic material which is petrographically and isotopically dissimilar to possible Highland sources (van Breemen & Bluck 1981; cf Yardley et al 1982). The size of these clasts indicate that much of this material was derived from sources no more than 50 km to the NW (ie N Ayrshire) and probably within an active island-arc environment (Longman et al 1979; Bluck 1983).

The oldest two of the three major Silurian conglomerates, the 'igneous' and 'quartzite' conglomerates (McGivern 1967; Bluck 1983)(see 1.3.2), indicate a provenance from the SE (except around Girvan, NW) for the derived acid and basic, intrusive and extrusive igneous rocks; and a prolific source of metaquartzite. Again, on the basis of geochemical and isotopic evidence, this has been proposed as indicating derivation from an island-arc regime, but now situated a short distance to the SE. This movement may be in line with the coincident southeasterly migration of the Iapetus trench margin. This island-arc is not visible in the northern part of the Southern Uplands at present, and Yardley et al (1982) maintain that this, along with the continental source of the southerly derived Southern Highland Group of the Dalradian (Phillips 1976; Harris et al 1978), has been removed by strike-slip movement during the Upper Palaeozoic and cannot now be traced. However Upton et al (1976), Longman et al (1979), Thirlwall (1981; 1983) and Bluck (1983;1984) have, with an increasing volume of evidence, proposed that the Southern Uplands accretionary prism is allochthonous on crystalline basement of Midland Valley continental/island-arc affinity; and that this over-thrusting took place sometime between the deposition of the 'quartzite conglomerate'

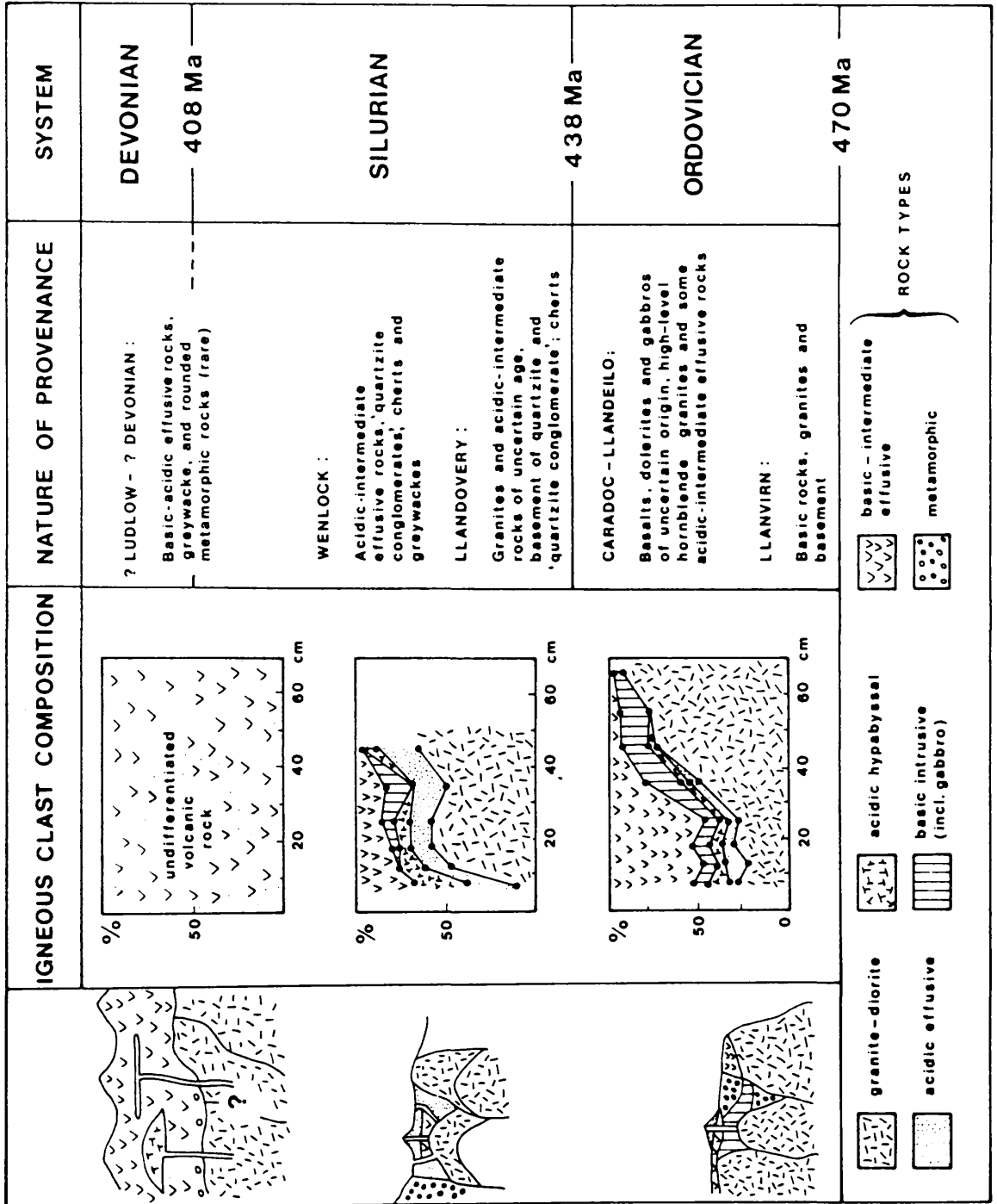


Figure 1.11 Change in conglomerate composition and possible configuration of the Midland Valley source during Ordovician to Silurian time (from Bluck 1983).

and the final Silurian conglomerate - the 'greywacke conglomerate' (see figure 1.5 for stratigraphy), when at last, southeasterly derived sediment, recognisably from the Lower Palaeozoic accretionary prism, is found in Midland Valley sediments.

1.5 Regional geophysical background in the Midland Valley

1.5.1 Regional gravity studies

The earliest regional geophysical study of the crustal structure of the Midland Valley was performed by Mclean & Qureshi (1966) who used the gravity coverage then available to construct a profile across the western part of the Midland Valley and perpendicular to the HBF and the SUF. These data were stripped to the base of the Old Red Sandstone so that the sedimentary cover could be represented by an equivalent thickness of Lower Palaeozoic sediments of density 2720 kg m^{-3} . From this, they produced a two layer crustal model which showed the crust within the Midland Valley to have a thickness of approximately 32 km, and bounded to the N and S by thickened crust; this thickening of 5 km occurring only within the upper crust and required at this shallow level to provide the marginal gradients.

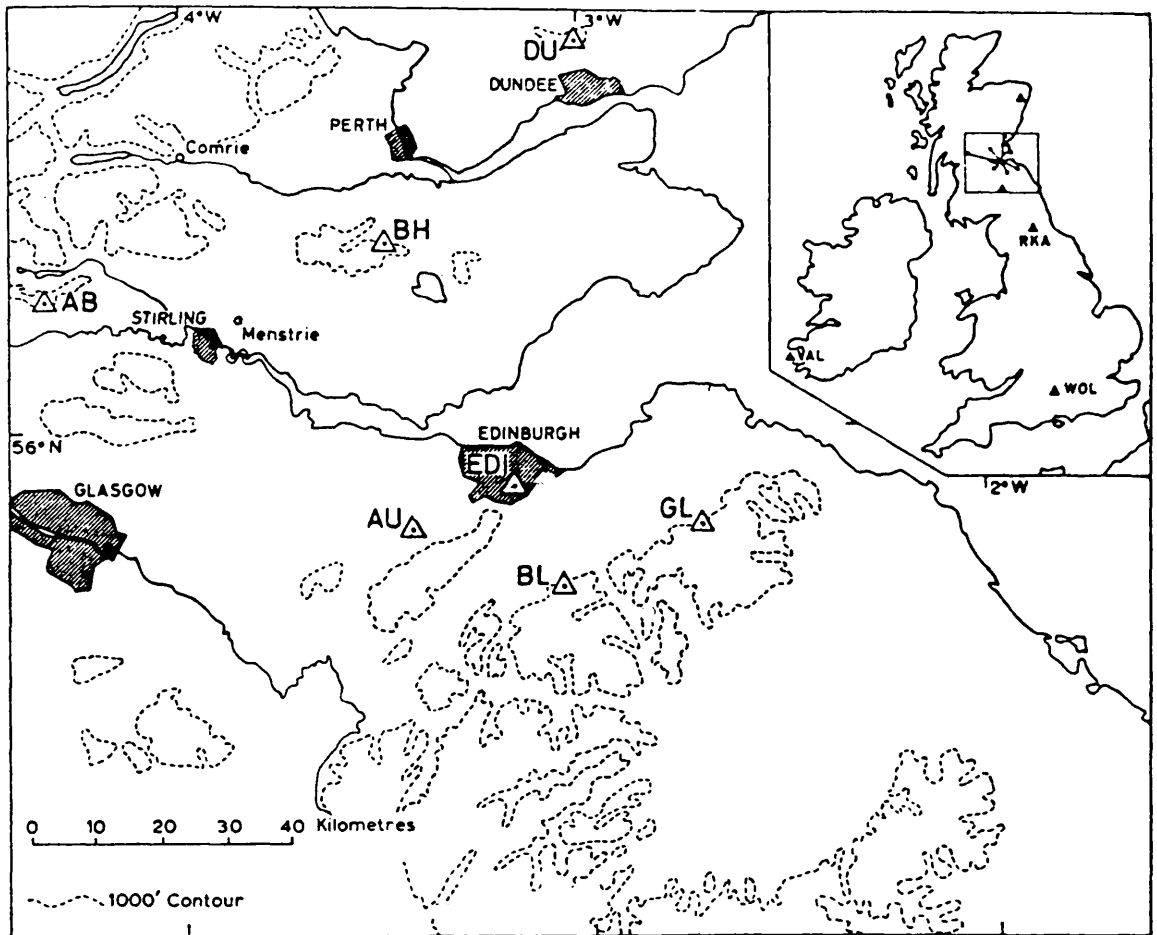
With a complete gravity coverage of northern Britain now available (Hussain & Hipkin 1981), it is apparent that the gravity gradients do not closely relate to the boundary faults defining the Midland Valley. The gravity low with amplitude -100 mgal, elongated to the SE of and parallel to the SUF NE of the Sanquhar basin has been postulated as being the result of a large granite intrusion at shallow depth with a density of 2650 kg m^{-3} , giving a density contrast with the country rock of -70 kg m^{-3} (the Tweeddale granite; Lagios & Hipkin 1979). Also, modelling of the gravity field in the southwestern portion of the Southern Uplands around the post-Caledonian acidic intrusions of Loch Doon, Cairnsmore of Fleet and Criffell (El-Batroukh 1975), has suggested that the Loch Doon and Cairnsmore of Fleet bodies are

connected at a depth of around 7.5 km by a saddle-like structure, and that they rest on a 4.5 km thick slab of material of intermediate composition. This slab thins to around 2 km in thickness between Cairnsmore of Fleet and Criffell, and extends under the Criffell body at a depth of around 10 km. From this study, it has been concluded that all the exposed post-Caledonian granites in the southwestern Southern Uplands are connected at depth, but no evidence has been produced to indicate that this batholith may have a connection at depth to the NE with the concealed Tweeddale body. Seismic refraction investigations are at present underway to attempt to resolve the relationship between the basal, intermediate compositional layer and the Midland Valley basement in southern Ayrshire (D.Majid, private communication). The implications of these studies of the gravity field have been to postulate a very large volume of granitic material existing at present at shallow depths in the NE and SW of the Southern Uplands.

The regional gravity gradient on the northern margin of the Midland Valley is now seen to be centred some 20 km to the N of the HBF. It has been proposed as relating to the -100 kg m^{-3} density contrast between the Dalradian and Moine rocks of the Central Highlands (Hipkin & Hussain 1983).

1.5.2 The LOWNET array

A network of short-period seismometers sited around the eastern part of the Midland Valley and named LOWNET, was established in 1969 by the then Institute of Geological Sciences with the aim of monitoring local seismological activity (see figure 1.12 for locations). With this purpose in mind, a preliminary upper crustal model based on observations of P-wave arrivals generated mainly from commercial quarry blasts within the Midland Valley was published in 1970 (see figure 1.13) (Crampin et al 1970). This model took the form of a three layered upper crust. The top two layers were characterised by P-wave velocities of 3 km s^{-1} and 5.67 km s^{-1} , and assumed



Details of station sites

Code	Site	Co-ordinates	Height above sea level, (m)	Geological location
EDI	Royal Observatory, Edinburgh	55° 55' 24" N 3° 11' 10" W	125	Extrusive pyroxene-andesite of Lower Old Red Sandstone age.
AU	Auchinoon Hill	55° 50' 40" N 3° 27' 17" W	350	Sill of dolerite intruded into Carboniferous sandstones.
BH	Blackhill	56° 14' 57" N 3° 30' 43" W	375	Volcanic tuff, of Lower Old Red Sandstone age.
GL	Gala Law	55° 51' 40" N 2° 44' 33" W	245	Hard compacted Old Red Sandstone.
AB	Aberfoyle	56° 11' 17" N 4° 20' 24" W	250	Lower Old Red Sandstone conglomerate.
BL	Broad Law	55° 46' 24" N 3° 02' 37" W	365	Granodiorite intruded into Ordovician shales.
DU	Craigowl Hill, Dundee	56° 32' 51" N 3° 00' 51" W	275	Lower Old Red Sandstone conglomerate.

Figure 1.12 LOWNET locations and site details (after Crampin et al 1970).

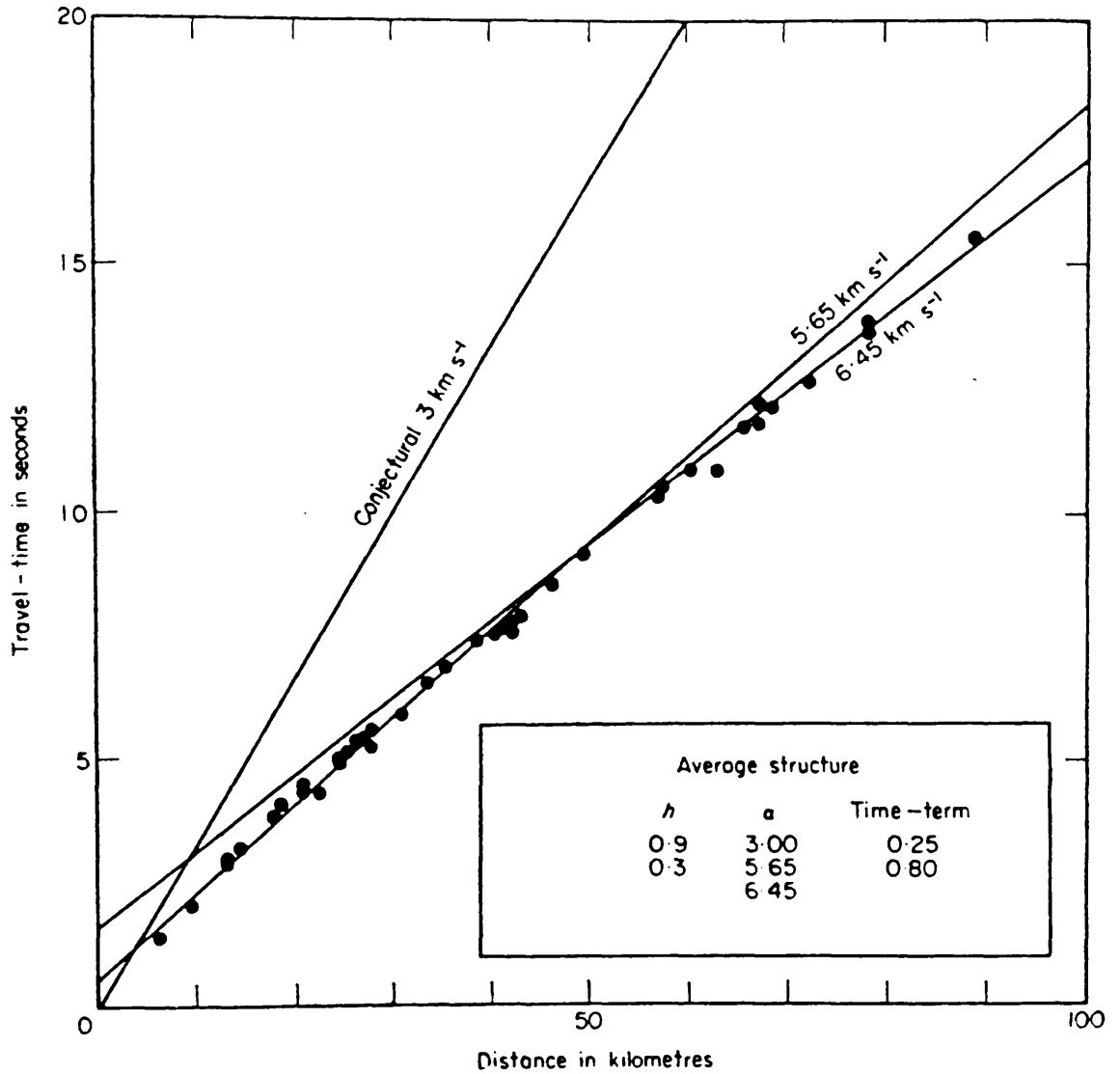


Figure 1.13 LOWNET travel-times and their interpretation (from Crampin et al 1970).

to represent the Palaeozoic sedimentary sequence. At between 7 km and 8 km depth, a refractor characterised by a P-wave velocity of 6.4 km s^{-1} was assumed to represent the top of the crystalline basement. The nature of this interpretation, together with the wide distribution of quarries and receiver stations result in a broad interpretation of the regional crustal structure which bears very little relationship to surface geology and structure.

1.5.3 The LISPB study

In 1974, the Lithospheric Seismic Profile across Britain (LISPB) was recorded (Bamford 1979; Bamford et al 1978; 1977; 1976). It crossed the Midland Valley on a N-S line centred on Edinburgh (see figure 1.14 for locations). Again, the interpretation defined a three layered upper crust with boundaries at between 2-3 km and between 7-8 km depth (figure 1.15). The P-wave velocities quoted for Layer 1, $4.0\text{-}5.0 \text{ km s}^{-1}$ (figure 1.15a), were interpreted as the direct arrival (a_3) through Carboniferous and Old Red Sandstone sediments. This was followed by the a_0 refracted phase giving a velocity from plus-minus analysis of $5.93 \pm 0.03 \text{ km s}^{-1}$ between shotpoints 1 and E, and $5.84 \pm 0.02 \text{ km s}^{-1}$ between shotpoints E and 2. With ray-trace modelling, this phase was best fitted using a velocity of 5.8 km s^{-1} increasing to 6.0 km s^{-1} at 7 km depth. This layer, Layer 2, was attributed to Lower Palaeozoic sediments. The refractor generated from the top of Layer 3 and interpreted as the top of crystalline basement (a_1) was, in the absence of suitable reversed coverage for a plus-minus analysis, poorly constrained from plane-layer modelling to have a P-wave velocity of $6.50 \pm 0.17 \text{ km s}^{-1}$. Subsequent ray-tracing showed that a value of 6.40 km s^{-1} increasing to 6.45 km s^{-1} at the base, gave a tolerable fit to the travel-time data, while still remaining within the error estimates of the mean apparent velocity determination.

The interpretation of the a_1 refractor phase as being generated from the

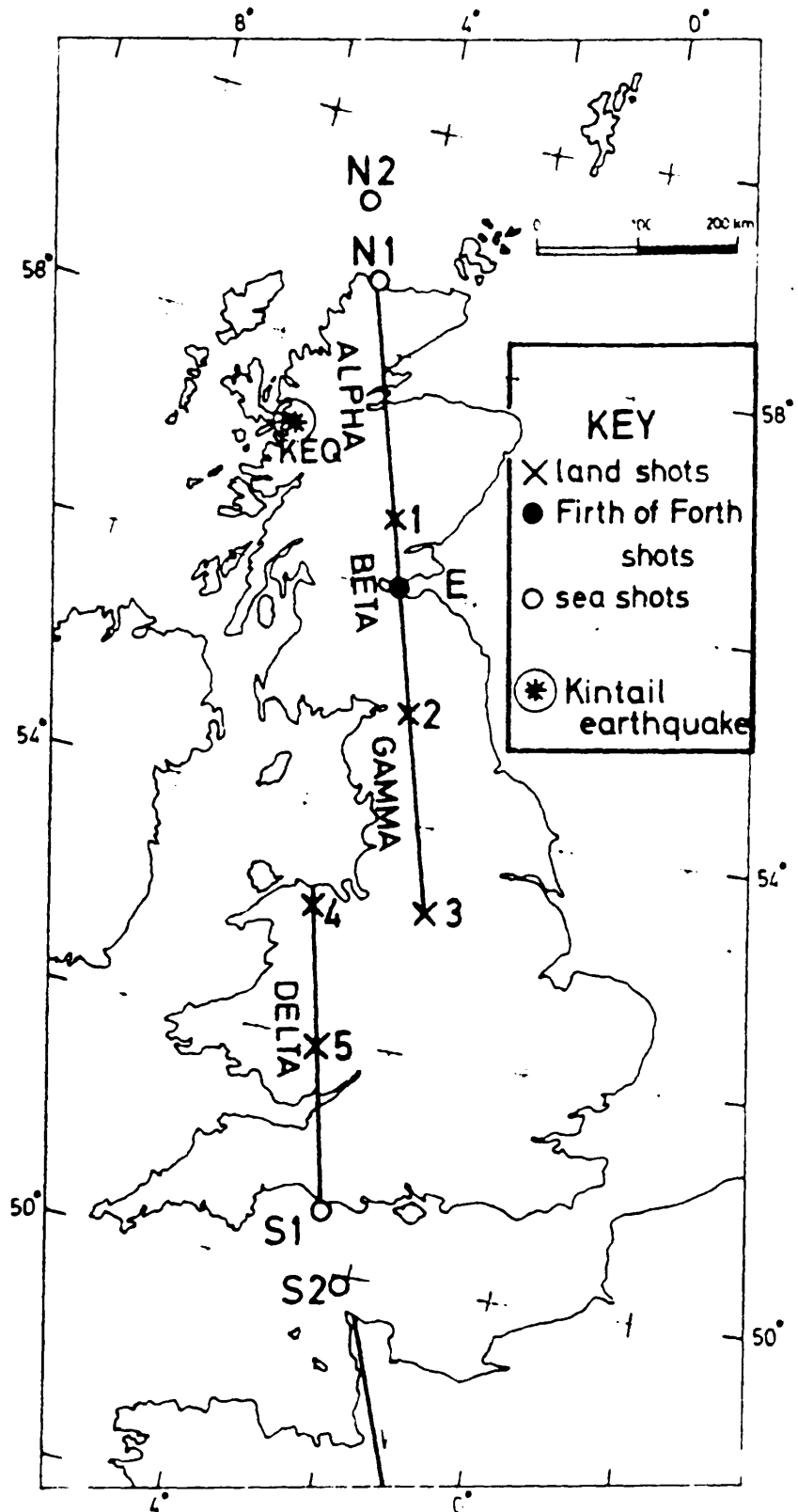


Figure 1.14 Location map for the LISPB study
(from Bamford et al 1976).

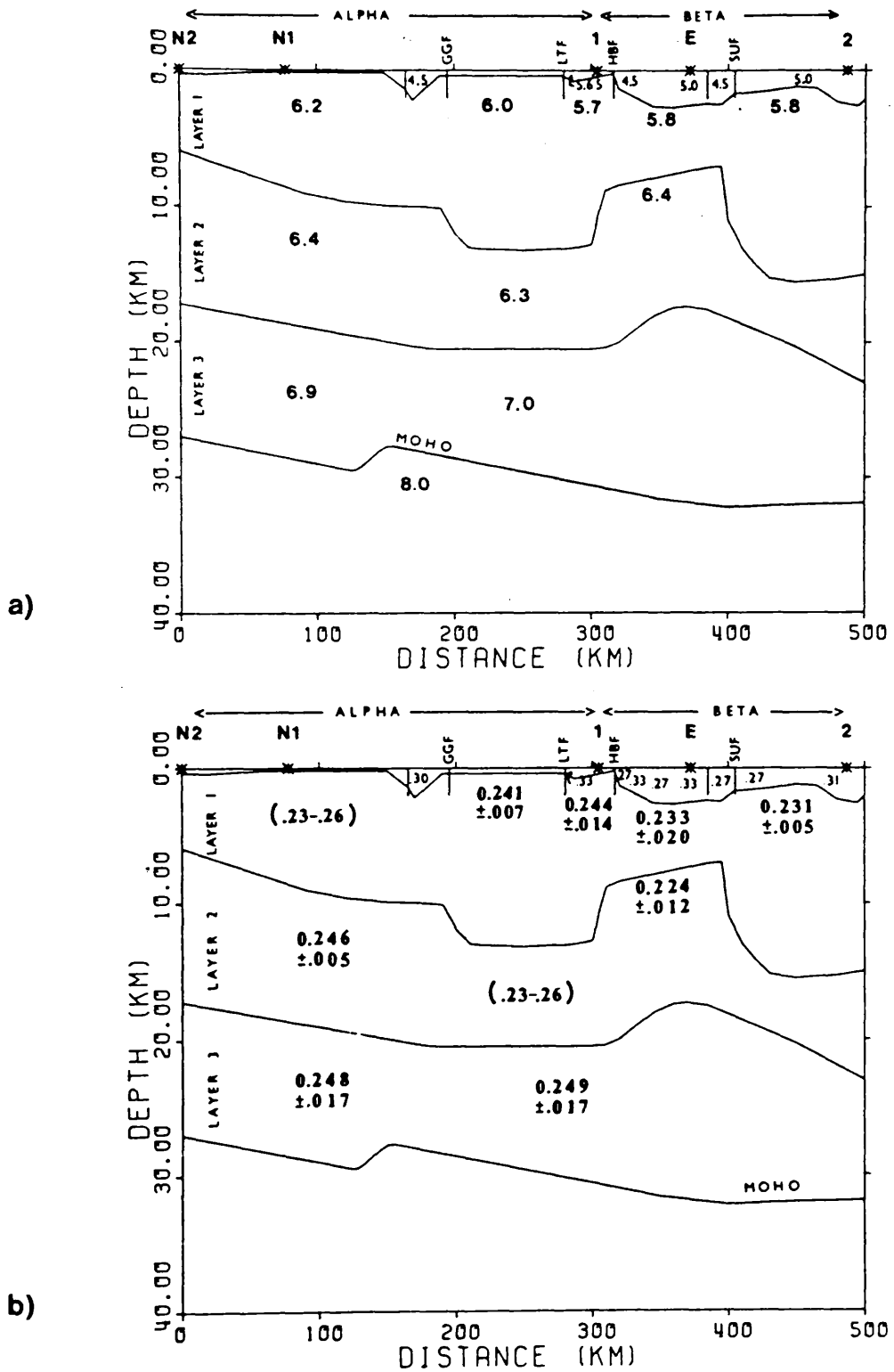


Figure 1.15 Crustal structure of northern Britain from the LISPB study (after Assumpcao & Bamford 1978).

a) P-wave structure.

b) Poisson's ratio structure using the t_s/t_p method.

top of the crystalline basement was confirmed by ultrasonic P and S-wave measurements on cores of Lewisian rock samples (Hall & Al-Haddad 1979; Hall & Simmons 1979; Al-Haddad 1977), who concluded that anhydrous pyroxene granulites, similar to those found in the Central Belt of the Lewisian foreland, would give the best lithological match to these data.

The LISPB profile was conceived as a lithospheric experiment with shotpoints spaced at less than 1 per 100 km and with an average receiver spacing of 3 km. This geometry precludes the accurate determination of detailed crustal structure within the top 2-3 km of crust (Bamford 1979).

Shear wave studies of the Midland Valley portion of the LISPB dataset (Assumpcao and Bamford 1978; Assumpcao 1978), allowed the modelling of Poisson's ratio distribution using the t_S/t_P method (figure 1.15b). The use of both P and S-wave data allows greater confidence to be placed in any resulting lithological interpretation as P and S-wave velocities are not linearly related in their response to variations in constituent mineral proportions. This technique has been used successfully in detecting subtle variations in lithology and porosity by a number of authors (eg Tatham 1982; Hall & Ali 1985). Unfortunately, due to the limitations of the dataset mentioned above, the upper layer (Layer 1) was modelled across the eastern Midland Valley with a bimodal distribution of blocks which has only a very loose association with the surface distribution of Upper Palaeozoic sediments and volcanic rocks. Similar modelling of Layers 2 and 3 show values of Poisson's ratio which are significantly lower than the crustal average of 0.25 and lower than the values obtained for the surrounding crust to the N and S of the Midland Valley. Figures 1.16 a, b, c, d show the t_S/t_P data on which the upper crustal model for the Midland Valley is based.

The t_S/t_P method has both an advantage and a disadvantage over the normal V_P/V_S method of calculating Poisson's ratio. The former is that t_S and t_P can

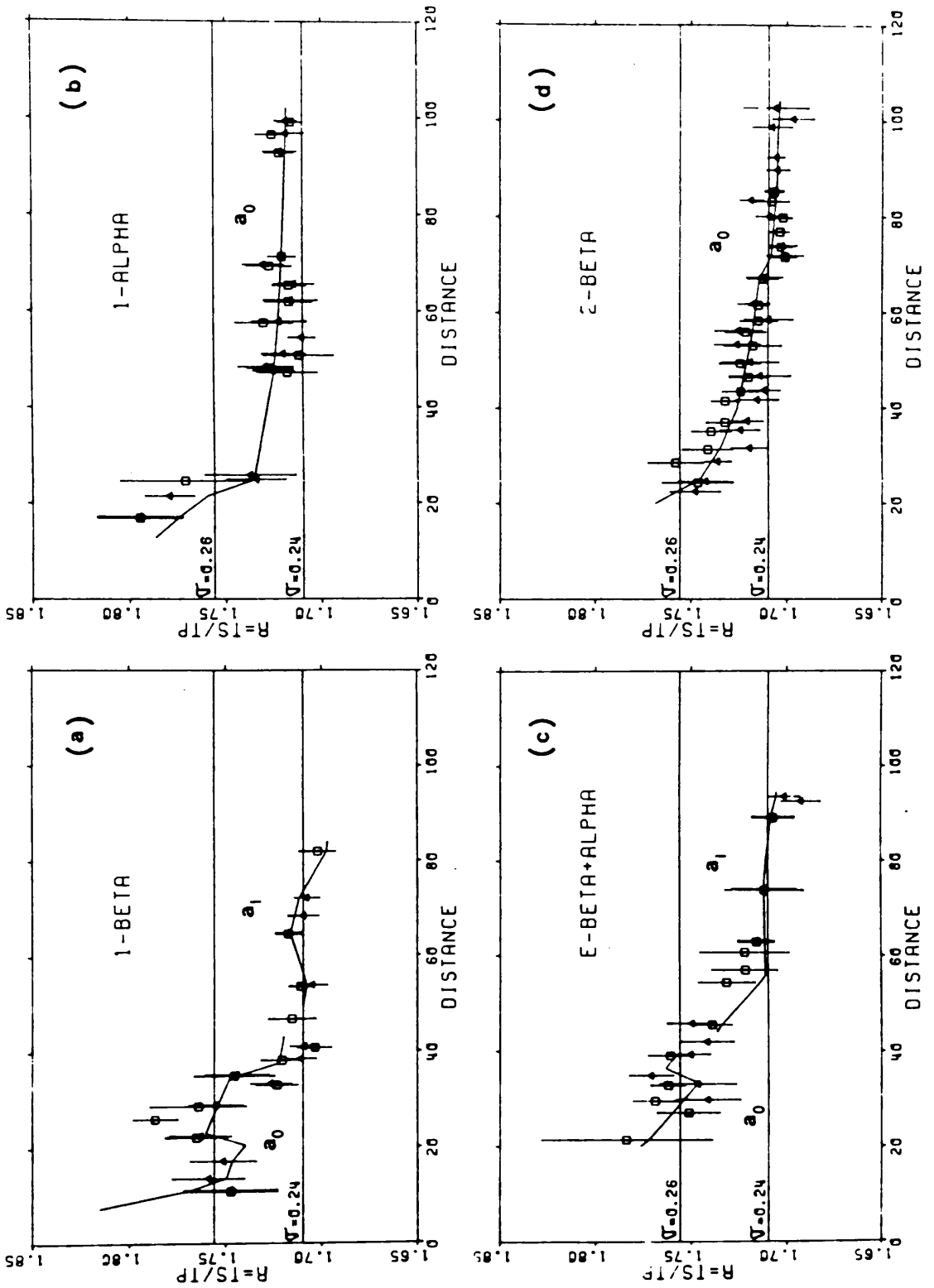


Figure 1.16 t_s/t_p ratio data from LISPB. Diagrams a), c) & d) give a reversed coverage across the Midland Valley and Southern Uplands (from Assumpcao & Bamford 1978).

be measured directly from the data, removing the need to calculate V_P and V_S , and so minimising the cumulative effect of errors in the calculation. The disadvantage is in the assumption of common raypaths and raypath lengths for both P and S waves. This could be a serious deficiency in a medium of laterally varying physical properties.

The published geological model of the LISPB data interpretation (figure 1.17) (eg Bamford 1979), was acknowledged by the authors as being the simplest and therefore most likely solution given the background geological knowledge at that time. Since then, this model has been used, by geophysicists at least, as a basis for further research with the inevitable result that some of the original assumptions have been proven either invalid or only partially correct.

1.5.4 The Broughton array and subsequent studies

One of the first tests of localised aspects of the LISPB model was in the attempt to reconcile the 12 km thick Lower Palaeozoic sedimentary layer of LISPB in the Southern Uplands with the previously published proposal (Powell 1970; 1971) that magnetic crystalline basement should underlie the Southern Uplands at shallow depth.

To this end, a temporary 9-seismometer Geostore array was operated in the Broughton area some 10 km SE of the SUF, with the intention of recording quarry blast data from either side of the fault (El Isa 1978). Due to the limited distribution of active quarries recorded during that time, the results in themselves were not completely conclusive, but they did suggest the occurrence of a high velocity layer ($V_P > 5.8 \text{ km s}^{-1}$) at no more than a few kilometers depth beneath the array and dipping to the NW. This work and measurements from a similar study over the Eskdalemuir array (EKA), have been combined with a later study into the physical properties of Lower Palaeozoic sediments using ultrasonic measurements on small rock cores to pressures of 5

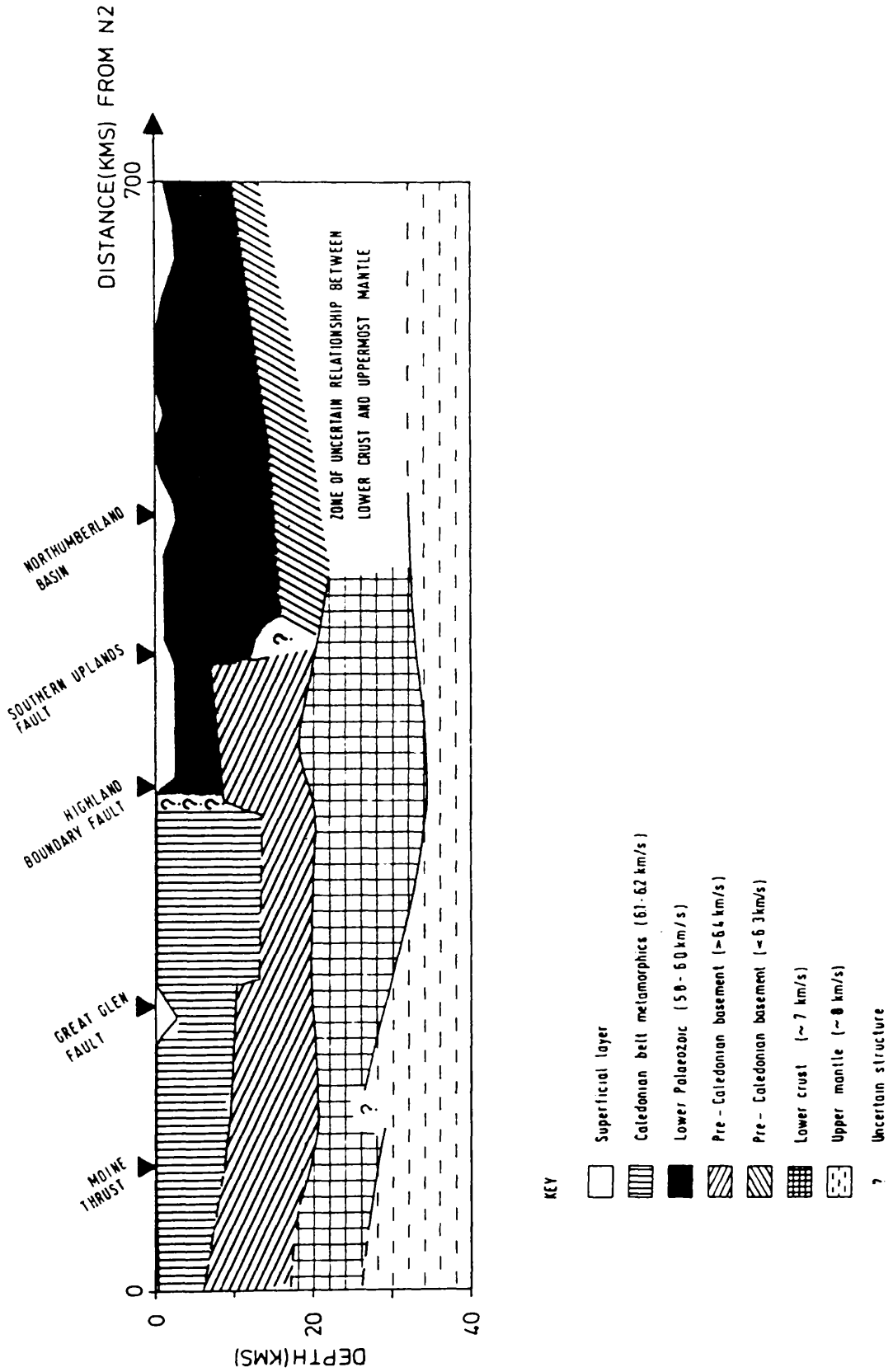
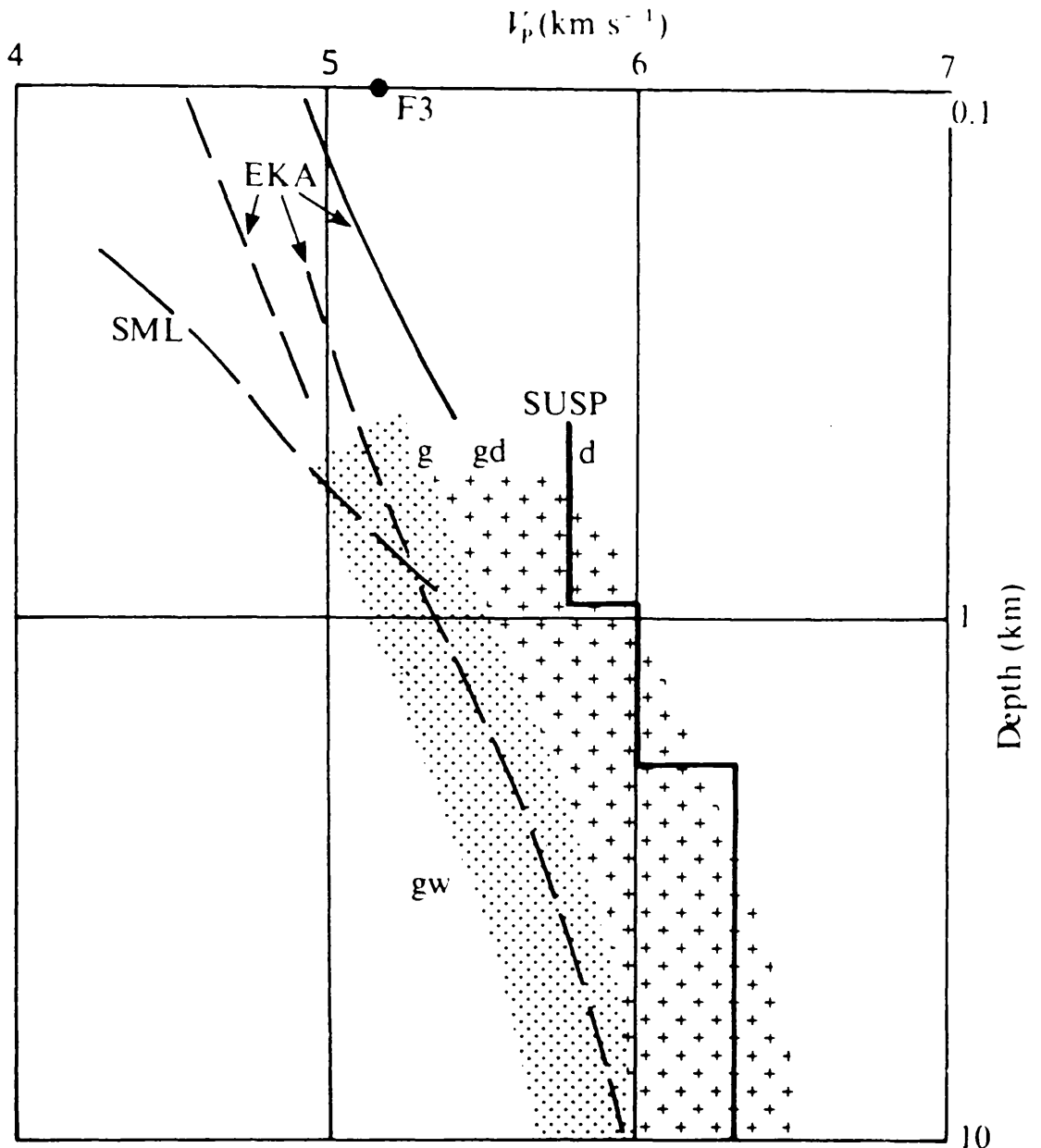


Figure 1.17 Geological interpretation of the portion of the LISPB study across northern Britain (from Bamford 1979).

kbars (Adesanya 1982). These results have been summarised by Hall et al (1984) (figure 1.18). It was found that the velocity-depth ranges of the Lower Palaeozoic sediments, regardless of the ratio of greywacke to shale used, were much lower than the P-wave velocities quoted from LISPB for either the Southern Uplands or the Midland Valley Layer 2 at equivalent depths. Similarly the values of Poisson's ratio obtained from these cores show values distinctly higher than predicted by LISPB for the Lower Palaeozoic layer, and more in line with the expected values for clastic sedimentary rocks. Velocity-depth information from the Southern Uplands Profile (SUSP) (see figure 1.18, and Warner et al 1982) also tend to confirm these results, although the aim of this profile was more to confirm the presence of high-velocity, 'granite-like' material under the large Tweeddale gravity low (Lagios and Hipkin 1979).

As a result of a magnetometer study along the line of the LISPB profile across the Midland Valley, Powell (1978) proposed the sub-division of the LISPB Layer 3 into two groups, one more highly magnetised than the other. He proposed that the more highly magnetised layer could represent hornblende granulite retrogressed from pyroxene granulite.

Subsequent work on the Lewisian Units Seismic Traverse (LUST, Hall 1978) (Ali 1983; Hall & Ali 1985) has shown the potential of using S-waves to produce a Poisson's Ratio model obtained from the combination of P-wave and S-wave velocity models, to resolve zones of regression and changes in lithology across the Northern and Central Belts of the Lewisian. The application of such a technique to an extensive, good quality dataset from this refracting layer could provide a means to test this hypothesis. Unfortunately this dataset does not yet exist.



Velocity–depth distributions for the Southern Uplands (note: depth scale is logarithmic). Solid lines show along-strike velocities and dotted lines across-strike velocities. EKA curves combine observations at short range (2 shallow-depth curves) and longer range dominantly across strike. SML is from an array study at St Mary's Loch in slow belt S2. F3 is from a shallow refraction survey in the northern fast belt. Dotted area (gw) shows range of velocities measured in Lower Palaeozoic greywackes. Plusses indicate range of velocities in plutonic rocks from measurement on Spango granodiorite (gd) with estimates for diorite (d) and granite (g). SUSP, Southern Uplands Seismic Profile.

1.6 Summary

Both laboratory and field experiment studies in the Southern Uplands have suggested that the velocity discontinuity at shallow depth is not the change between weathered rock and its physically sound equivalent, (that can be shown to occur at a higher crustal level) but due to a change in rock type, like that found with a change from sedimentary to crystalline rock (Adesanya 1982; Hall et al 1983; Bott et al 1985). Oliver and Leggett (1980) and Oliver et al (1984) have proposed, on the basis of conodont colour, graptolite reflectance and illite crystallinity, that this discontinuity could be due to a change in metamorphic facies such as that from prehnite-pumpellyite to greenschist facies; but the weight of data at present supports the hypothesis that this discontinuity marks the top of a moderately high grade metamorphic, probably continental, layer.

This reinterpretation has considerable significance to the upper crustal structure of the Midland Valley, as the predicted structural continuity of this inferred crystalline basement into the Midland Valley forces a reappraisal of certain aspects of the tectonic reconstructions of the Caledonides N of the Iapetus Suture. In particular, by postulating basement at 3 km depth instead of 7 km (cf 1.5.3) in the southern and western parts of the Midland Valley, this reinterpretation does not allow for the expected thick Lower Palaeozoic sedimentary succession in this region, as predicted by the models of Dewey (1971), Mitchell and McKerrow (1975), Lambert and McKerrow (1976), Leggett et al (1979; 1983), and Yardley et al (1982), who envisage the Midland Valley as a fore-arc basin receiving sediment from the rapidly uplifting and eroding Dalradian highlands to the N.

This project has been to investigate the nature of the LISPB layers 2 and 3 in the southern part of the Midland Valley, relating them to both the LISPB profile and the Broughton array study. It compliments a parallel project which is investigating the sub-Carboniferous structure beneath the Central

Coalfield, with particular reference to the nature of the Bathgate Bouguer gravity and aeromagnetic anomalies (Hall & Dagley 1970; Hossain 1978; Alomari 1980; Sola & Powell 1983; Davidson et al 1983; 1984; and Sola 1985).

Chapter 2 Equipment, data acquisition and procedure

2.1 Introduction

The data presented here were collected over the full three year duration of this project. Two equipment systems were used: NERC Seismic Equipment Pool Geostore recorders with Willmore Mk 3 seismometers, and Glasgow FM cassette recorders (designed and built within the Department of Geology) with either Mark Products or Mandrel 4.5 Hz geophones.

The Geostore data was collected during two loan periods: three weeks from the end of August to mid September 1982, and eight weeks from mid May to early July 1983. The Glasgow recorders have been used intermittently from November 1981 through to August 1984, primarily to fill in data around the areas covered by the Geostore loans.

2.2 Field recording equipment

The following section gives a brief review of the technical specification and field implementation of both types of equipment.

2.2.1 The Geostore System

The technical specification of the Geostore recording system is generally well known so only brief details will be given here.

The Geostore recording system is based on a low-speed, reel-to-reel tape recorder using 1/2", 2400ft magnetic tapes on 8" reels. It can record up to 14 channels (7 using bi-directional mode) of which 10 (4) are conventionally available for seismic data. Only one of the five Geostores employed was used in this bi-directional mode, as the others were used (or were intended to be used) for recording more than seven channels. The remaining channels record the Vela-encoded internal clock, an external time-code (in this case the MSF code from Rugby), and a wow-and-flutter monitor for each tape head. As the primary intention for these Geostore loans was to record quarry blasts in the

15-50 km range, a tape speed of 15/160 in s⁻¹ was used throughout, giving a high frequency cutoff of 32 Hz.

Vertically-sensitive Willmore Mk 3 seismometers were used for all stations. These were calibrated and set to a natural frequency of 1 Hz prior to each loan by staff at the NERC Seismological Equipment Pool centre in Edinburgh. The output from a seismometer was amplified and frequency modulated around 676 Hz by a Racal D6230 amp-mod.

For the 1982 loan, two Geostore recorders and 15 Willmore Mk 3 seismometers were employed: all sited on cement bases, with all but two in direct contact with rockhead. One seismometer was sited on stiff boulder clay some 5 m above rockhead, the other on a large boulder which could be no more than a few metres above rockhead. All sites were protected from the elements by turf and/or stone cairns surrounding and enclosing them, and were seismically quiet. The only exceptions to this were those sites which had to be placed close to the only main road in the area, and which suffered severe but transient noise on an infrequent and random basis due to the passing road traffic. Problems were encountered consistently throughout the loan period with faulty radio telemetry links. This entailed daily repairs to some part of the array, and precluded my recording of shot instants of quarry sources of interest to the project. Thus this loan accumulated a large amount of good quality, apparent velocity data, but with very few timed events.

For the second loan, in 1983, three Geostore recorders and 15 seismometers were installed in a similar manner to the 1982 loan. At the suggestion of staff at the Global Seismology Unit in Edinburgh, the alignment bias between the two recording heads on each Geostore was checked for any misalignment prior to field deployment. For this, all 14 input channels were connected in parallel and a series of pulses from a signal generator recorded onto tape. In one of the Geostores, the misalignment was found to be equivalent to a time difference of greater than 100 ms; the others gave slightly lower

values. Subsequent checks on the uncalibrated data from the 1982 loan has not revealed any obvious large systematic differences.

The only difference in field techniques for the 1983 loan was the use of small triangular Tufnol bases in place of cement for the Willmore seismometers, and which were leveled by adjusting screws at each corner of the base. The base was sited on rock and bonded using an industrial wax which was melted over the base and surrounding rock to form a solid join. This was found to be a much quicker and less weather dependent method of site preparation than cement, and has been used subsequently for all rock-site recordings. Again problems were experienced with the radio telemetry links, but in addition there were many problems with faulty seismometers, and seismometer - amp-mod cables. The seismometer faults were only traced when NERC Seismic Pool staff came out, near the end of the loan period, with more sophisticated and effective test equipment than was available to me initially. Thus up until the last 10 days of recording, I did not get better than 50% return on timed events (and never the same set of channels); frequently less. The 1983 Geostore Loan proved to be a very poor investment of my time and effort, and required further fieldwork during the following year in an attempt to fill in some of the gaps in my dataset.

The Geostore playback system has been designed to provide analogue playback or digitisation, or both simultaneously. The Store 14 replay deck is connected to a bank of Kemo analogue filters (one for each seismic channel) via a patch-panel. The filtered output is then sent back to the patch-panel, where it is then directed to either the jet-pen recorder or the digitiser. The normal fast paper output speed used for analogue playbacks was 50 mm s^{-1} .

2.2.2 The Glasgow FM cassette system

The Glasgow FM Mk 1 cassette recorders were designed and built in 1981 as a cheaper, portable and more readily available alternative to the Geostore recording system. It was designed specifically for use in short to medium range seismic refraction recording, and its immediate application was to be in resolving basement/cover relations in the Midland Valley and Southern Uplands particularly in the light of the LISPB interpretation.

Initially six recorder sets were constructed, allowing the deployment of up to either 18 vertically oriented geophones or 6 three-component geophone sites. The system is based on a standard commercial audio cassette deck mechanism, but with a 4-track recording tape head replacing the normal 2-track (stereo) record/playback head. This allows 60 minutes of recording time using a C120 cassette. Comparison of the frequency responses of this system (both the Mk 1 and the later Mk 2 versions) and the Geostore system are shown in figure 2.1. The system was primarily designed for use with Mark Products L15B 4.5Hz or Mandrel EV22B 7.5Hz geophones, but also available were Teledyne-Geotech S500 1Hz piezoelectric seismometers. The frequency responses of all geophone and seismometer types used throughout this study and earlier referenced work (eg El-Isa 1978) are shown in figure 2.2.

The output from a geophone is amplified and frequency-modulated on to a 3 KHz carrier before being recorded onto one of the three available channels in the recorder. In addition to the three seismic channels, a time signal is recorded onto channel 4 thus providing a time calibration for the tape. The source used has been the MSF signal from Rugby. During recording this is also modulated onto the 3 KHz carrier and thereafter can be handled similarly. This value of 3 KHz for the carrier frequency was found to be best suited to the frequency-response characteristics of the cassette deck and is also well placed within the optimum frequency bandwidth of the human ear, thus allowing easy audio monitoring of the tapes signal both in the field and in the

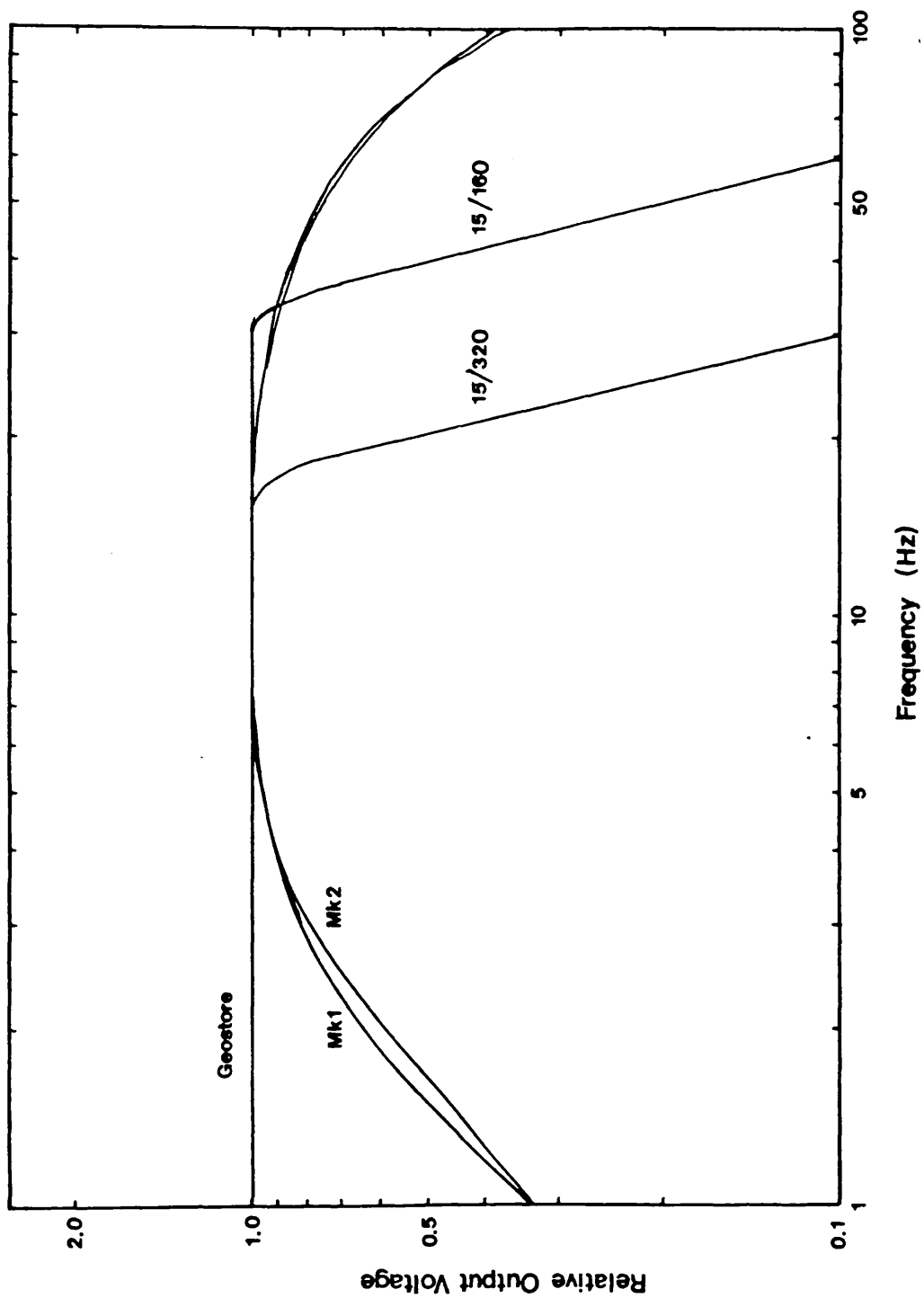


Figure 2.1 Comparison of the frequency responses of the Geostore system using the 15/160 & 15/320 in/s recording speeds, and the Mk 1 & Mk 2 Glasgow FM cassette recorders.

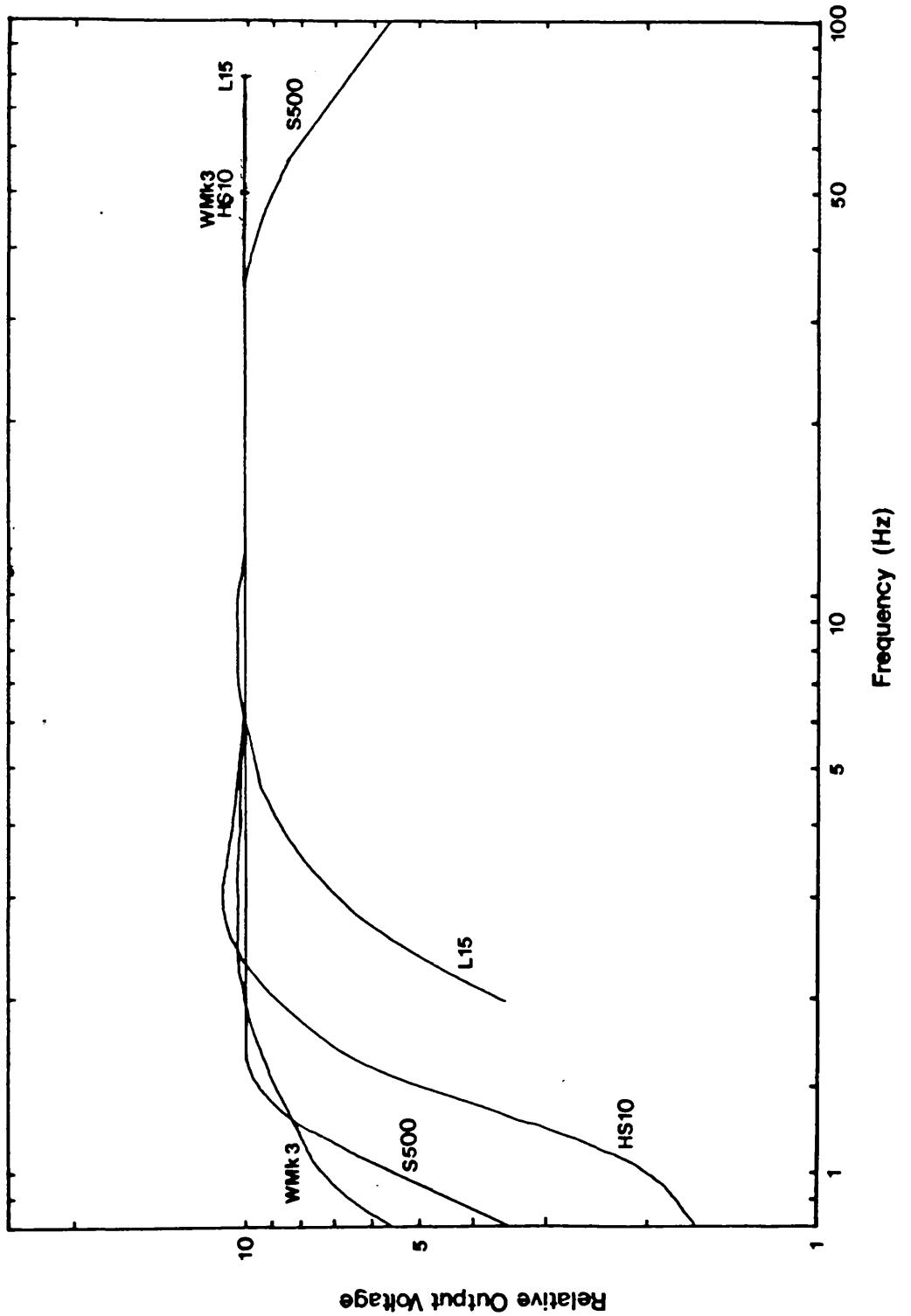


Figure 2.2 Comparison of the frequency responses of the four types of seismometer and geophone used in this study.

laboratory.

The original equipment was manually operated only, but by 1983 a remote start facility had been developed which allowed independent operation of recorders. Field experience had shown this feature to be of extreme importance as technical assistance was only available under exceptional circumstances. However, the remote start facility only became more than 90% reliable by mid-1984 with the arrival of the Mark 2 recorders.

The analogue playback facility for these cassettes recorders comprises a similar cassette deck mechanism to the field recorders, but with the tape head wired for playback only. The signal on each seismic channel is passed through a separate demodulator and then through a Kemo analogue bandpass filter. Each channel is then amplified before being output on a Bryans 40000 W oscillograph. The time channel is demodulated in a similar manner before being output direct to the oscillograph via an amplifier. If required, the MSF signal can be cleaned by being passed through a Schmitt trigger filter immediately after demodulation. As the Bryans oscillograph can handle up to six channels, the normal practice has been to have the time signal fed to channels 1 and 5, thus straddling the three seismic channels. The dynamic range of the complete system is 38 db (at maximum gain; 46 db for Mark 2 recorders) and rising to 60 db on the lower gain settings.

Allowing for teething problems during the initial stages of use, these sets have performed consistently well, often with the only limiting factor being the unpredictably variable quality of the MSF radio reception. However, even given reasonable radio reception conditions, the quality of the MSF signal is superior to the Cambridge Instruments Ltd. receivers used with the Geostore recorders. One area in particular in which these sets have exceeded the original specification has been in their ability to record useful information at ranges of up to 100 km, even with the L15B geophones.

2.3 Digitisation procedure

Most of the data presented here was digitised at the Global Seismology Unit of the British Geological Survey at Murchison House, Edinburgh. The digitisation procedure is summarised by figure 2.3. It involves using a DEC PDP 11/50, connected via a patch-panel to the Kemo analogue filters and finally to the playback tape deck. Both the Geostore tapes and the Glasgow FM cassettes were digitised using this system, although the cassettes required the transportation to Edinburgh of the dedicated playback and demodulation sections of the Analogue Playback System installed at Glasgow. The Geostore tapes were played back using the standard Store 14 tape deck. The Kemo analogue bandpass filters are used as predigitising, anti-aliasing filters on each input channel, and for all files were set at 0.001 - 45 Hz.

The Global Seismology Unit have developed a package of programs available to external users which relate to the creation and handling of digital data files. For Geostore tapes, the digitising could be carried out automatically by programs DIGTRN or DIG2 (both of which read and decode the internal clock), or manually by MTDIG. The cassettes, having no internal clock system could only be digitised using program MTDIG. Thereafter, all data files were handled the same way.

All files were digitised at 100 Hz. The cassettes and some tapes had the digitiser gain set at 2.5 V cm^{-1} , while the remaining tapes were digitised at 10 V cm^{-1} .

The conversion from binary to character format is achieved by programs DIGCFM or D2, both of which also demultiplex the data. At any time in this process, the contents of a digital data tape could be checked numerically by program MTANAL or sent to the jet-pen recorder by program MTREAD.

From there, the demultiplexed character files were delivered to the Data Transfer Service of the Computing Centre at Glasgow University. There they were transferred from IBM to ICL character format and copied onto ICL 2900

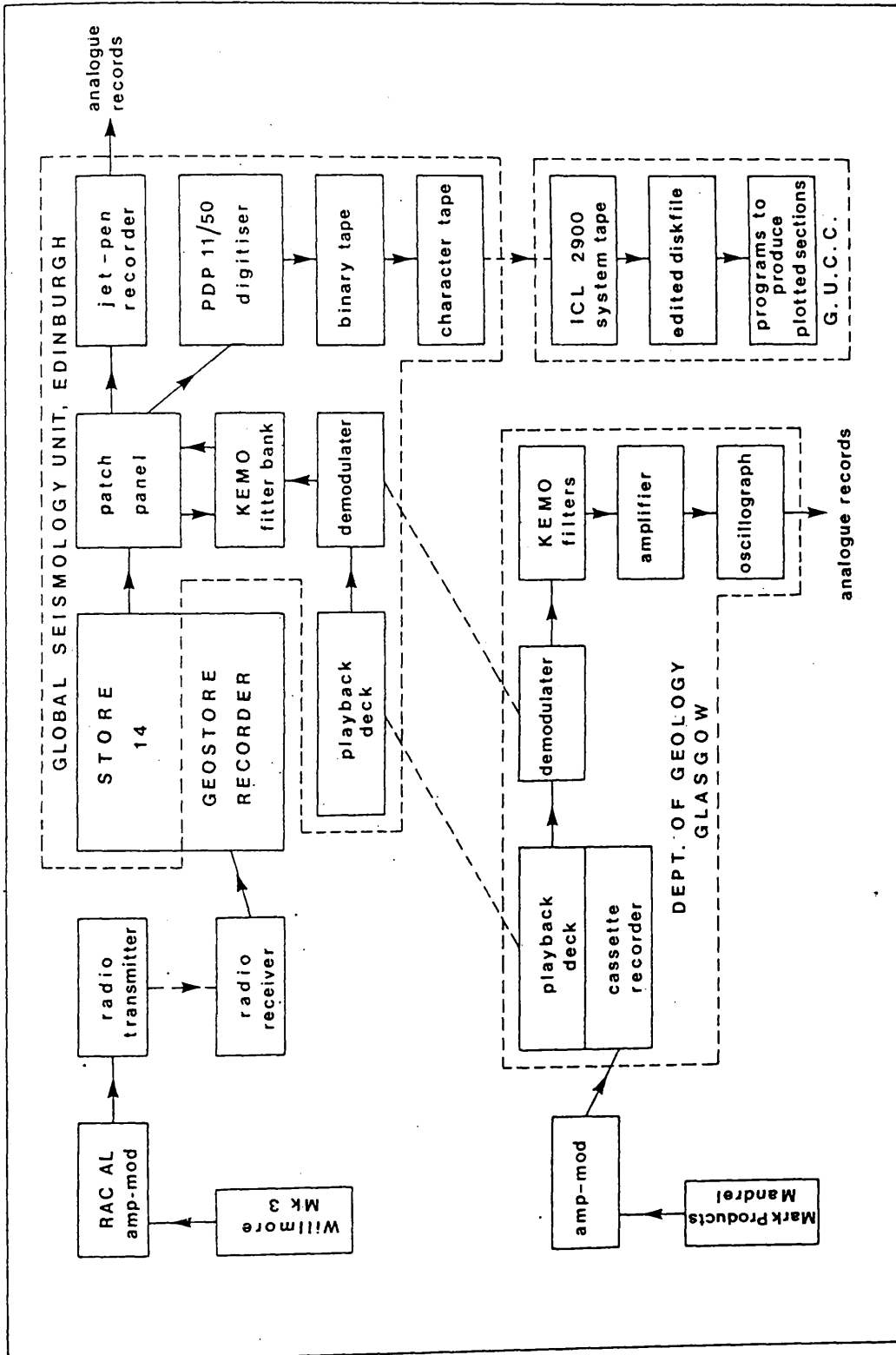


Figure 2.3 Flow diagram summarising the stages involved in producing final digital travel-time sections from either Geostore or Glasgow FM cassette field recordings.

system tapes using a Computer Industries Ltd. System 90 minicomputer. This last stage in the process tended to be the longest as the time required to transfer a standard 2400 ft magnetic tape with approximately 30 Mb of data was in the order of 14 hours. If this crashed for any reason during a job, which was a frequent occurrence, the whole job had to be rescheduled and rerun. As long jobs such as this took a low priority, this further increased the time required before the digital data could be accessed from the mainframe system.

Once the contents of a data tape were successfully transferred onto an ICL 2900 system tape, the data files could be copied across to disc and prepared for use with various handling and processing programs developed within the Department.

Since the Glasgow FM cassette system uses a 1:1 ratio of record and playback tape speeds, the digital files obtained from these could be short, typically 10 - 20 seconds in length, and therefore not in need of any further editing. However the Geostore tapes have a record/playback speed of 1:10 or 1:20, and particularly when coupled with the automatic digitising programs, these resulted in very long files, normally 4 minutes (2 Mb) but occasionally 6 or 8 minutes in length. These files had to be plotted out in full before editing which again added time to the whole process. Program DIGPLT (listing Appendix 6) was written to handle the data, regardless of the input format and digitising voltages used. The next stage is to relate the first sample on the file to the time of the first arrival as picked from the analogue paper playbacks. Seismometer polarity was standardised at this stage.

By this stage, the files were ready for plotting as a digital time-distance seismogram. The program used here is DRAW4 (listing Appendix 6), a considerably modified version of DRAW (Ali 1983) and which was used for all stages of digital data handling as described in Chapter 3.

Chapter 3 Data acquisition, presentation and processing

3.1 Data collection

Data acquisition started in October 1981 using six cassette-based seismographs built in the Department with recordings from the recently reopened Dunduff quarry near Lesmahagow, in southern Lanarkshire. These recordings provided an introduction to the area and the equipment, and gave a preliminary velocity-depth function for the top kilometre of Lower Old Red Sandstone sediments. From the local geology, it was expected that these rocks could be less than 2 km thick and overlie a Lower Palaeozoic sedimentary sequence similar to that seen in the Lesmahagow Inlier. According to the LISPB interpretation (Bamford 1979), Lower Palaeozoic sediments should produce refracted arrivals with a velocity of around 5.8 km s^{-1} , so the presence of a refractor with V_p approximately equal to 5.8 km s^{-1} at around 2 km depth or less, would confirm the applicability of the LISPB model to this region. Three blasts, at around 1200–1500 kg total and 120–150 kg per delay, were recorded before complaints from the village caused the curtailment of blasting. As a result, this potentially valuable source could not be used for longer range recordings until 16 months later, when the charge size had gradually, and unofficially, increased to around its earlier values.

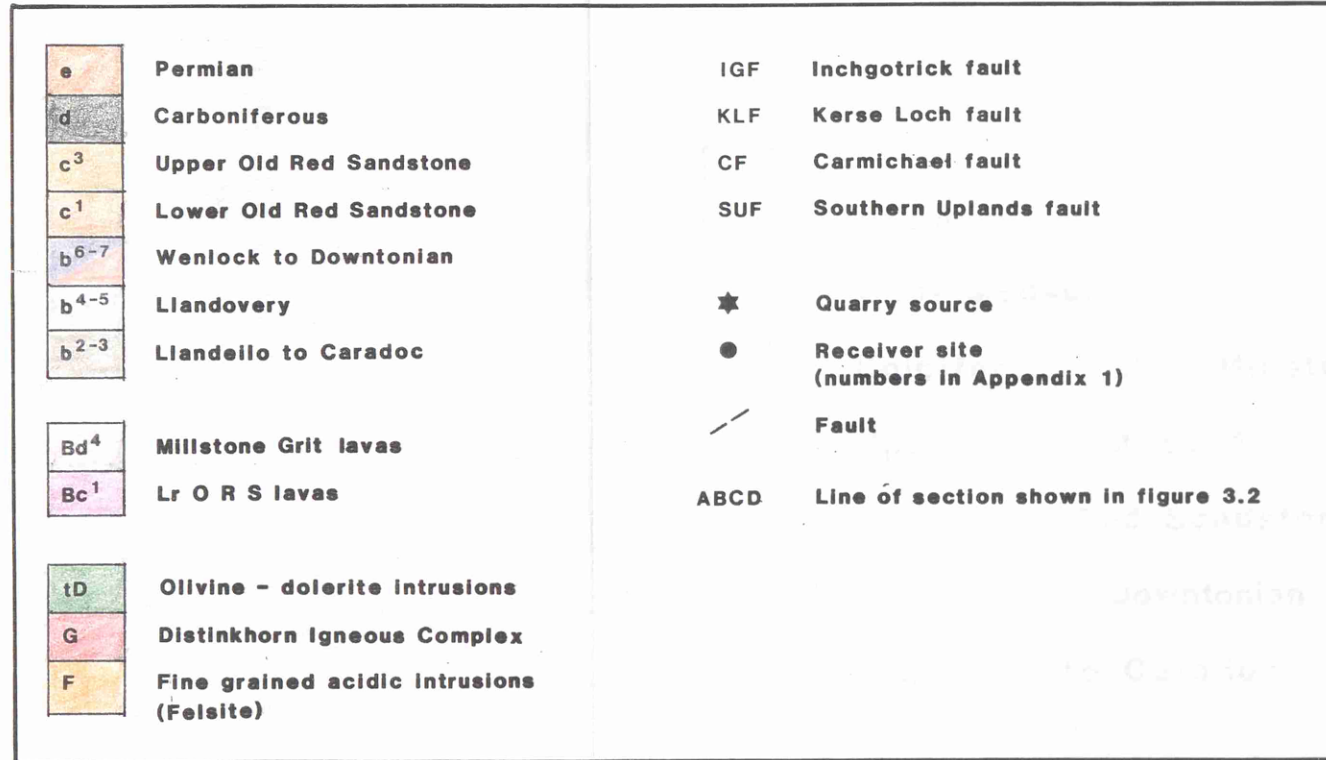
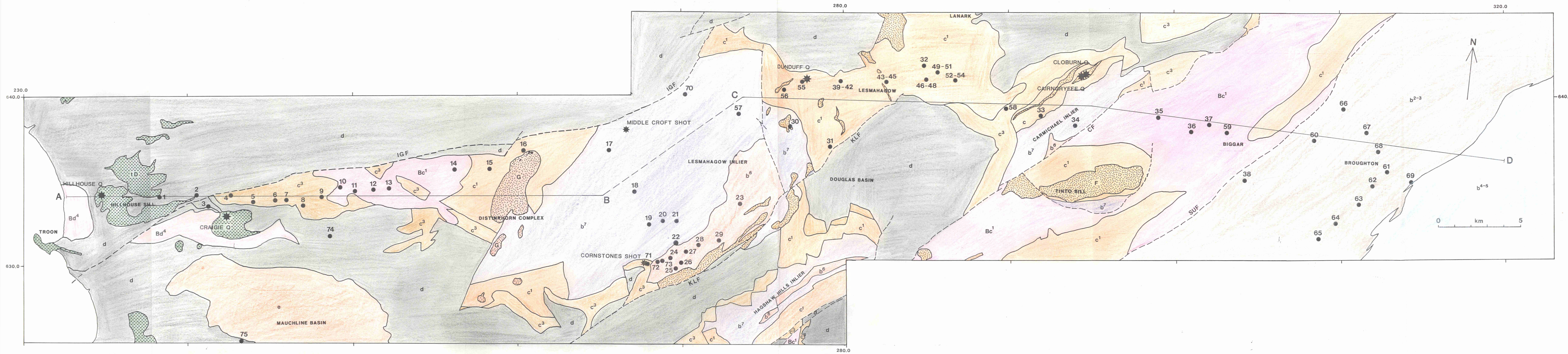
For three weeks during late August and September 1982, a fifteen station Geostore array was operated over part of the Silurian Lesmahagow Inlier (see figure 3.1). The Lesmahagow Array (LES), formed an asymmetrical cross with one arm of approximately 10 km along strike, and the other 10 km arm perpendicular to strike. Two arm-end shots (Cornstones and Middle Croft) were recorded to give information on the surface velocity-depth structure, and two quarry blasts (Hillhouse and Cairngryffe (twice)) and a larger shot at Greivehill near Cunnock, were timed into the array to investigate the deeper structure (see figure 3.1 for locations). Apparent velocities of over 6 km s^{-1}

¹ (see Appendix 4.4,5,6) were obtained across the array from both Hillhouse and Cairngryffe quarries at ranges of greater than 17 km, and so it was decided that the data from these two quarries should be expanded into a 60 km E - W profile, which would allow the data recorded over the inlier to be extended laterally into the surrounding regions.

Hillhouse quarry was particularly useful throughout the period of data acquisition as, at that time, it was regularly blasting charges of 7 -10 tonnes total, with 250-350 kg per delay, thus increasing the range of weather conditions in which recording was still feasible. Throughout the winter of 1982-83, the Glasgow FM seismographs were used to build up the profile, particularly at the western end.

For ten weeks from May to July 1983, 15 Willmore Mk3 seismometers and three Geostores were employed mainly in the central and eastern ends of the profile, to allow its expansion eastwards towards the SUF. Shots were timed from Hillhouse, Dunduff and Cloburn Quarries (the latter being adjacent to Cairngryffe Quarry) This also allowed the linking up of the previously occupied Broughton Array (BTN) (El-Isa 1977) and coincided with my rediscovery of these data tapes in Murchison House, Edinburgh after seven years of misplacement.

The data set compiled from these various sources thus consists of an 80 km long E - W profile which is sub-parallel to the predominant Caledonian trend of surface structures in the southern Midland Valley, and two mid-profile 10 km aperture cross-arrays which were intended to extend the profile model laterally. The locations of all quarries and recording sites are shown in figure 3.1. A geological sketch section (figure 3.2) shows all the expected major lithological and stratigraphic units from the Ayrshire coast eastwards across the Midland Valley to the Southern Uplands fault (SUF), and across the northern belt of the Southern Uplands. All the source locations and shot origin times are listed as part of Appendix 1. The receiver locations and



Location map for the Hillhouse - Broughton profile and adjacent regions.

d5	Coal Measures
d1-4	Calcareous Sst to Millstone Grit
c3	Upper Old Red Sandstone
c1	Lower Old Red Sandstone
b6-7	Wenlock to Downtonian
b2-4	Llandeilo to Caradoc & Llandovery

V	assumed Permian volcanic vent
Bd4	Millstone Grit lavas
Bd1	Lr Carboniferous lavas
Bc1	Lr ORS lavas
tD	Olivine-dolerite intrusions
G	Distinkhorn Igneous Complex
F	Fine grained acidic intrusions (Felsite)

IGF	Inchgotrick Fault
KLF	Kerse Loch Fault
CF	Carmichael Fault
SUF	Southern Uplands Fault

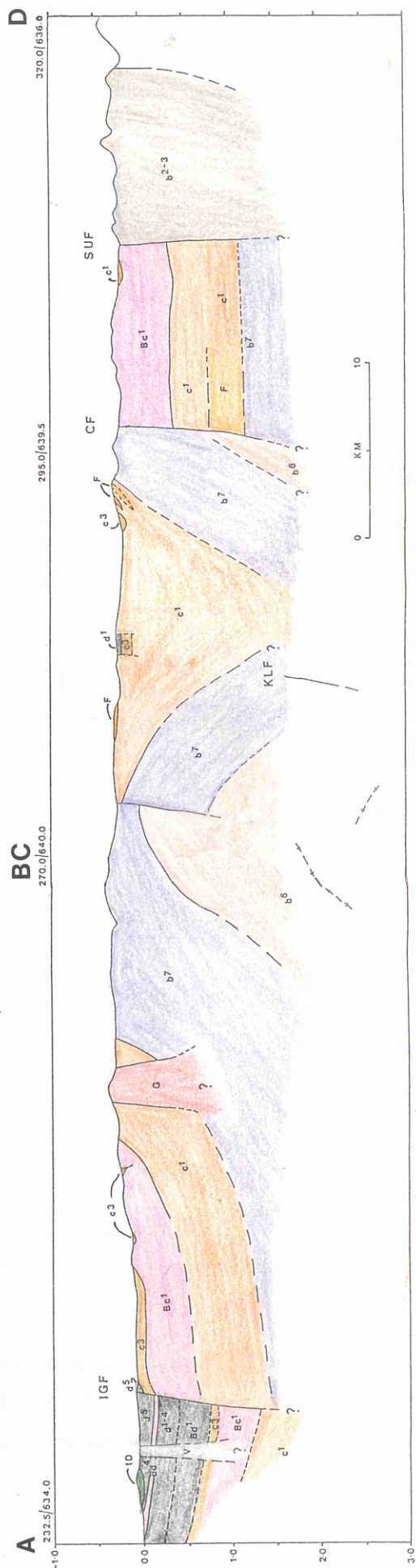


Figure 3.2 Sketch geological section under profile ABCD from figure 3.1 and based on the BGS one-inch geological maps of this area. Colour code is as for figure 3.1.

arrival times are listed in Appendix 2.

3.2 Data presentation

3.2.1 Data from the Hillhouse - Broughton profile

Record sections were prepared for the Hillhouse - Broughton profile and some of the data obtained from the LES and BTN arrays using digital data. Full 8 or 10-second record sections for each of the three quarries comprising the Hillhouse - Broughton profile are shown in figures 3.3, 3.4 and 3.5. All these record sections are unfiltered and have been normalised with respect to the largest amplitude on each trace. The signal-noise ratio for first arrivals is excellent on all three lines, even out to 80 km (eg figure 3.3). However, secondary arrivals are very much poorer: - there are no distinct secondary P-wave arrivals on any of the record sections and S-waves are only patchily recognised (figures 3.6,7,8) By far the best set of S-waves are seen on the Dunduff line (figure 3.7), particularly to the E of the quarry. Here also, longer wavelength surface waves are well recorded.

The traces on the 10-second record section from Hillhouse quarry (figure 3.3) generally give a true representation of the vertical component of the ground motion at each recording site. Three traces, however, do not represent accurately the local ground motion due to instrumental problems. The trace at 5 km from the source gives a response which is typical of signal overload on the Glasgow built FM amp-mods. The overload period is of the order of 4 seconds and covers the section of the trace immediately after the first break, through to a point at which the surface wave energy has dissipated sufficiently for the internal circuitry to recover.

The traces at 8 km and 25 km from the source were recorded correctly but have been affected by D.C. shift in the digitising process resulting in only the portion of the trace within the digitiser gain range being sampled, and the remainder being lost. The first break on these traces will not represent

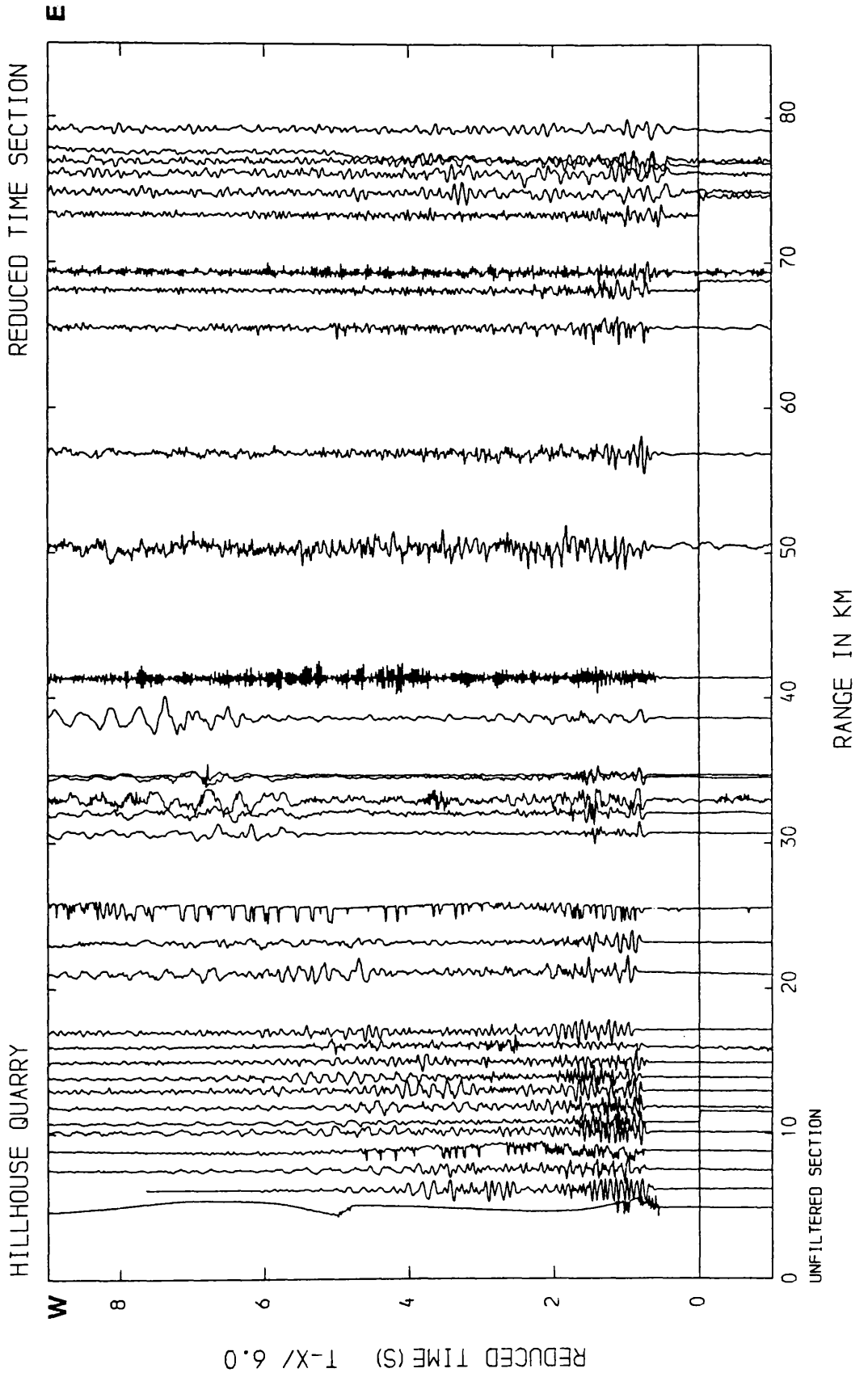


Figure 3.3

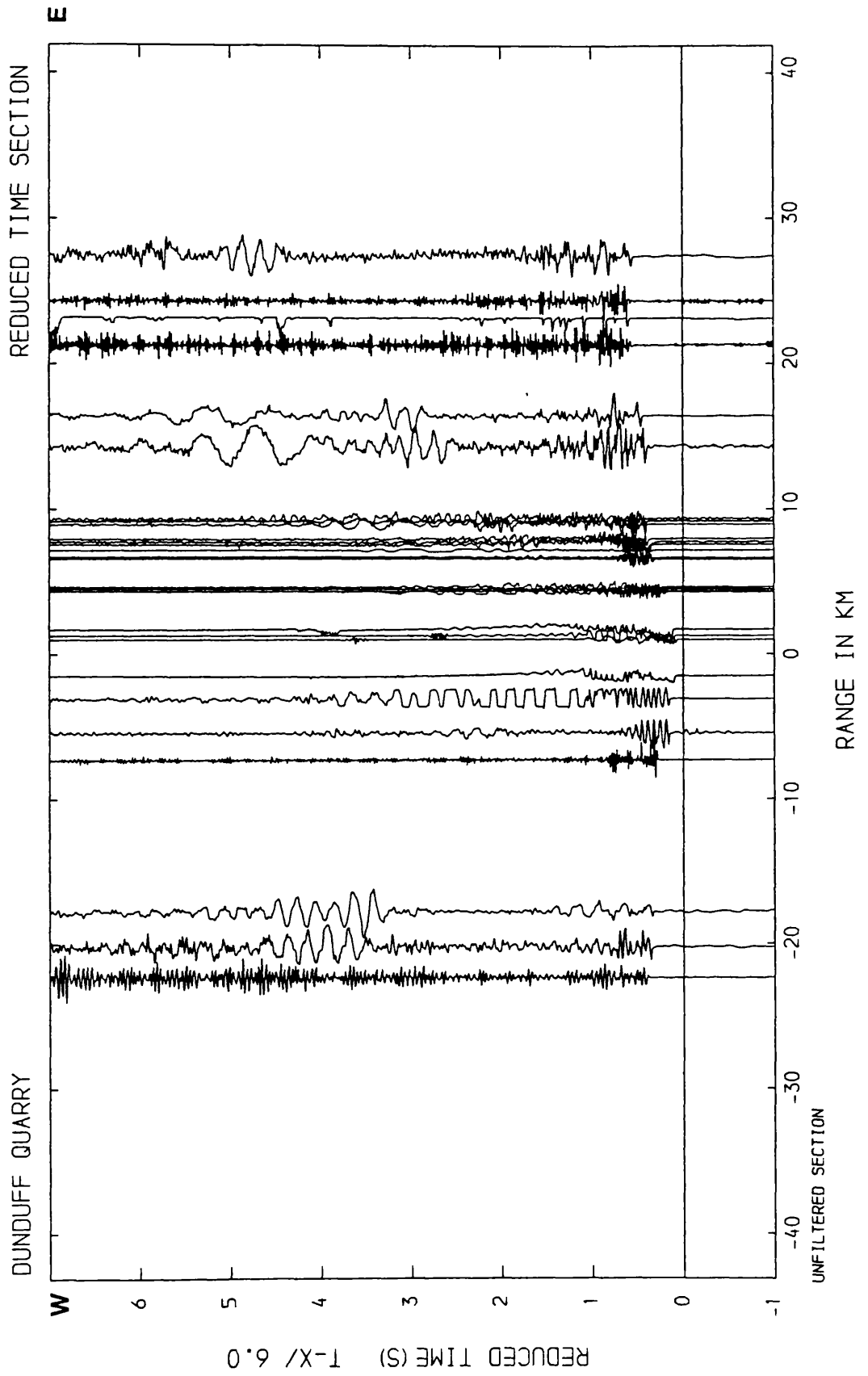


Figure 3.4

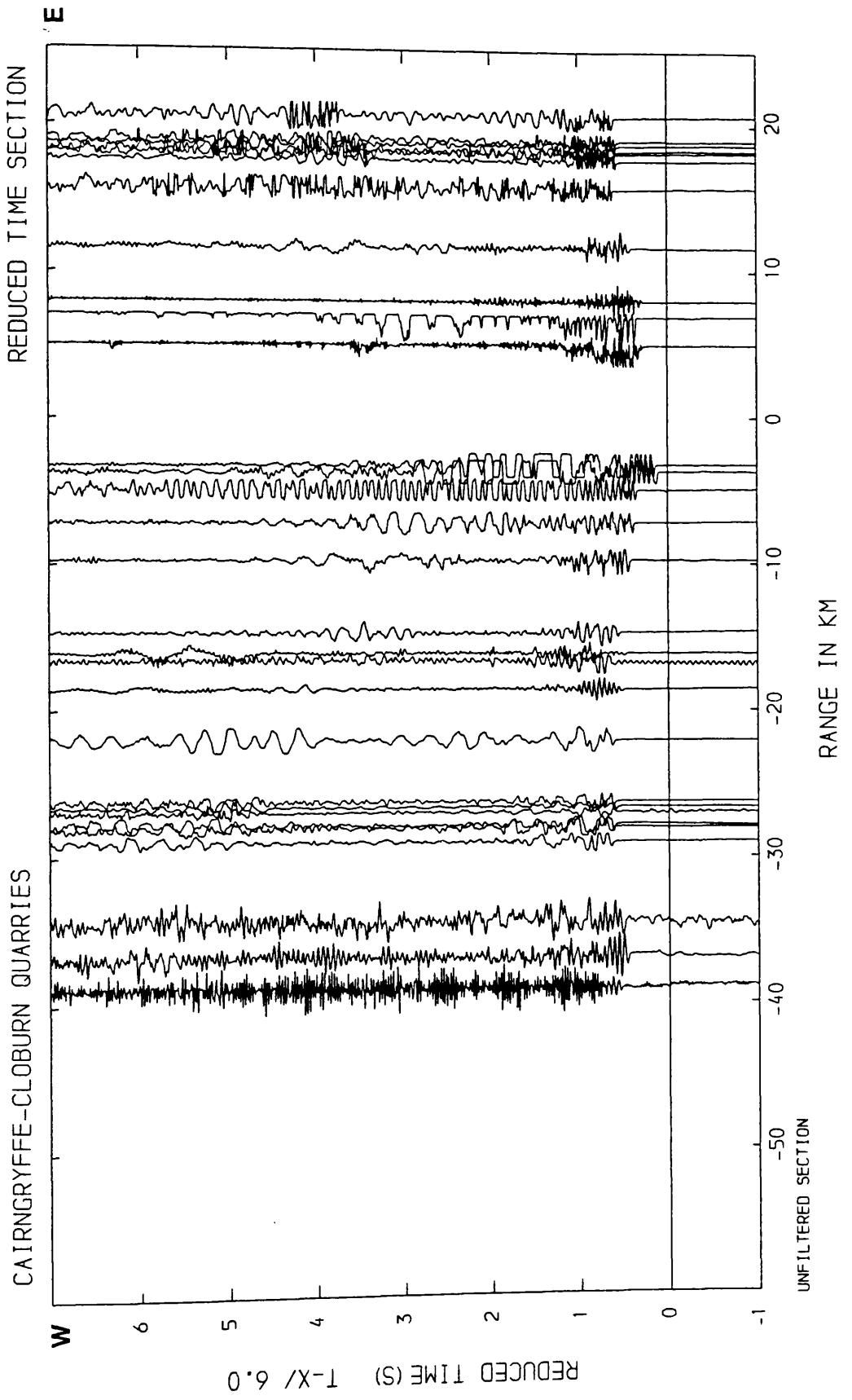


Figure 3.5

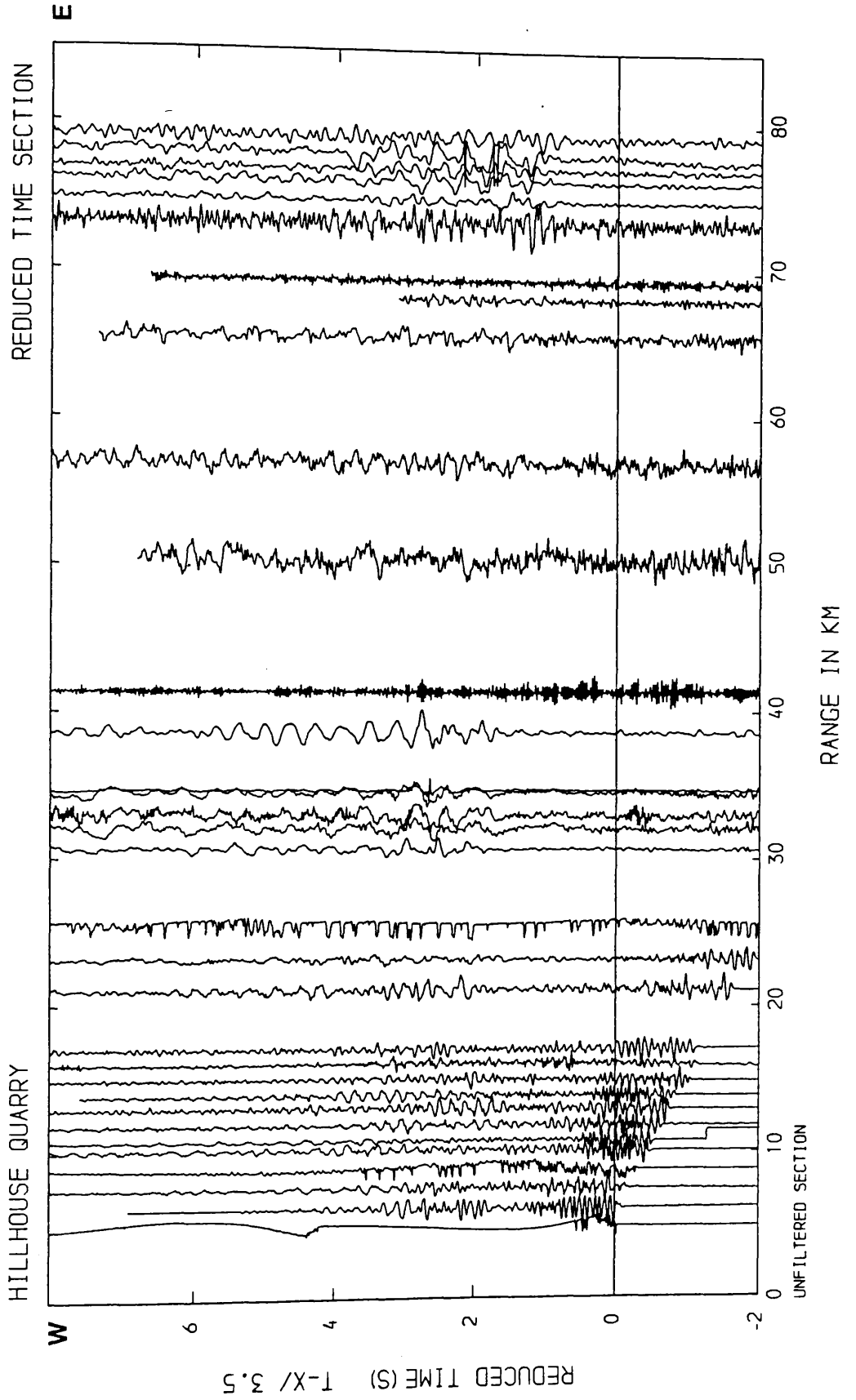


Figure 3.6

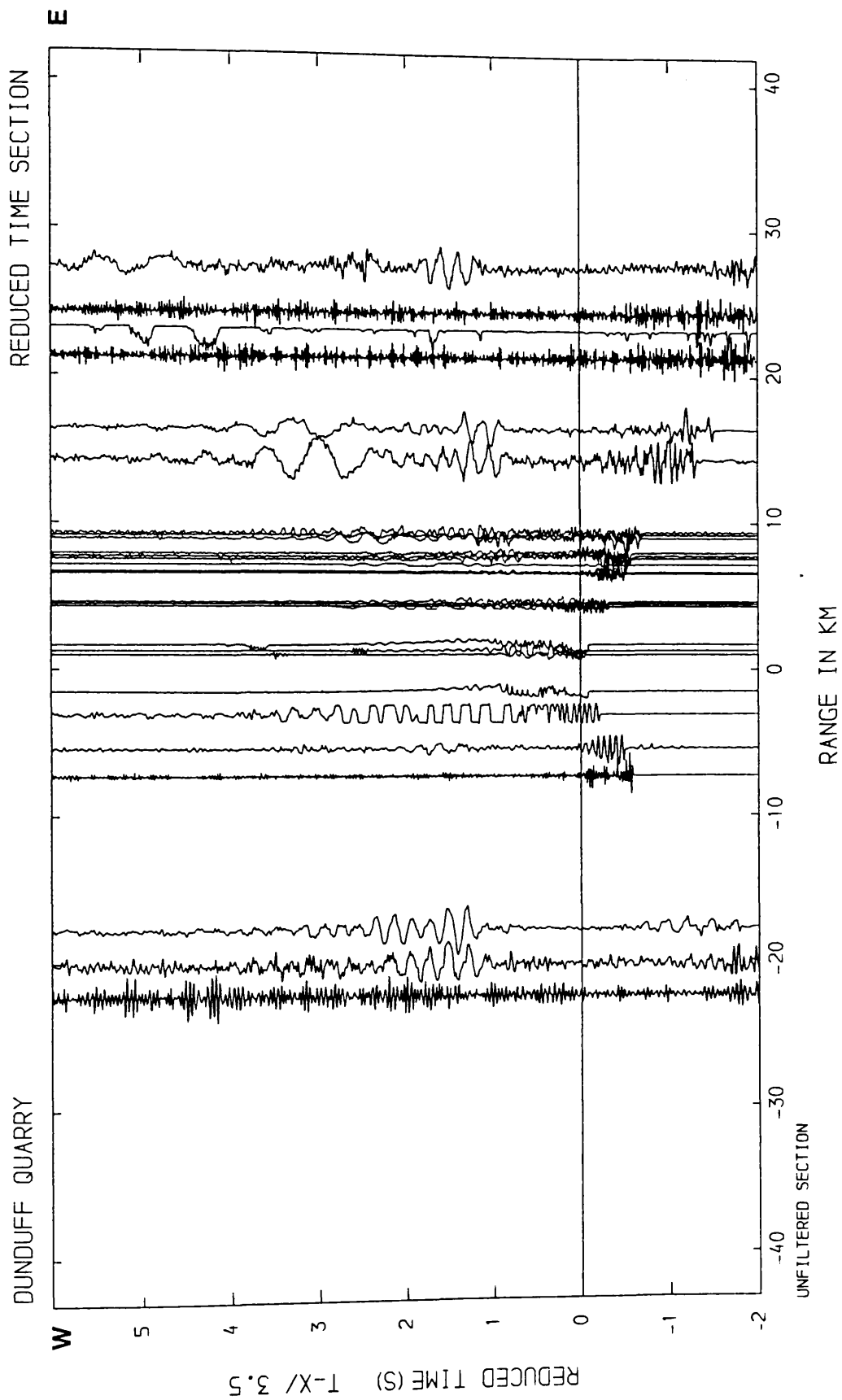


Figure 3.7

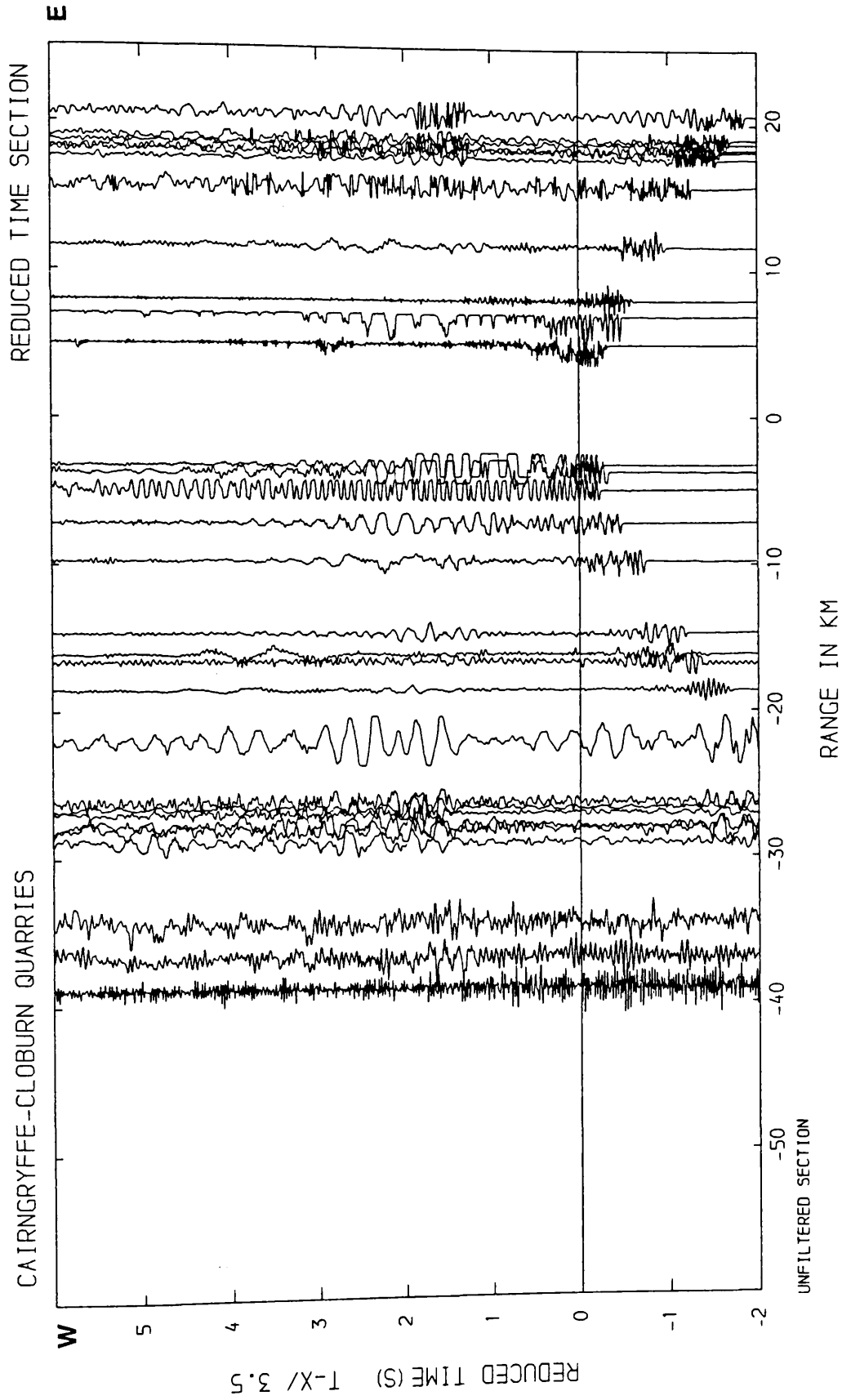


Figure 3.8

the first arrival, but instead will come from a segment on the first cycle.

Two other traces, at 41 km and 69 km give responses which may be corruptions of the local ground motion. Both traces contain predominantly high frequencies which could be caused by either poor seismometer-ground coupling, internal seismometer problems or incorrect damping due to an incompatibility between the Willmore seismometer and its supposedly tuned amp-mod. Alternatively, a geological explanation for this screening could be found in the filtering effect of a near surface, high velocity layer such as a sill. Unless such a body crops out near the site or can be inferred from the local geological structure, the only method of deducing a geological explanation for the high frequency response is to have different equipment record the same effect at the same site.

During the course of the recording season, an internal fault was diagnosed in the seismometer at 41 km. Its replacement recorded the traces at -4 km and -19 km from Dunduff and Cloburn quarries respectively, neither of which show the same predominance of high frequencies, and so confirming that the seismometer itself was the source of the anomalous high frequencies.

The site at 69 km was not used for any other recordings so no direct comparisons can be made. However, notes on the field sheets for that recording suggest that the problem may have originated with poor ground coupling of the geophone base.

The record section compiled from Dunduff quarry (figure 3.4) shows all of the features described above. Most of the traces are accurate representations of the vertical ground motion, although close to the source in particular, the three Willmore seismometers (at -4 km, +4 km, and +7 km) all show P-wave and surface wave overloading. The trace at +23 km shows a D.C. digitising problem similar to that described for two of the traces from the Hillhouse record section. Three traces, at -22 km, +21 km and +24 km all show anomalous

high frequency content. Of these three sites, only the one at -22 km was successfully re-recorded with different equipment, giving an acceptable trace at 23 km from Hillhouse quarry.

The two other sites (at +21 km and +24 km) did not record Hillhouse quarry and so it is not possible to relate their high frequency response directly to any source. However, given the problems experienced with Willmore Mk3 seismometers described above and in section 2.2.1, it is reasonable to assume that the problems were with the equipment rather than invoking a geological solution for which there is no real evidence.

The Cairngryffe-Cloburn quarries record section (figure 3.5), is unique amongst the three record sections comprising the Hillhouse - Broughton profile, in that all the data presented was recorded from only three separate quarry blasts. As a result, the only duplication of recordings is across the LES array.

Close to the source, there are the usual over-modulation effects (eg from -5 km to -3 km), with an interesting comparison of the effects of over-modulation between the Geostore system (-3 km and -4 km) and the Glasgow FM cassette system (-5 km). The three traces between +5 km and +8 km, and the trace at -38 km were recorded on the same day as the traces at +21 km, -23 km and +24 km from Dunduff quarry and so show similar trace characteristics. While more than adequate for interpretation, the general quality of individual traces on these record sections is not as good as that of the original analogue records. This is due to the low sampling rate of 100 Hz used throughout and originally dictated by limitations on the maximum amount of computer storage space available to this user. Cleaner records would have been produced using sampling rates of 200 or 250 Hz.

3.2.2 Data from the LES and BTN arrays

Arrivals recorded at the LES and BTN arrays form the remainder of the data presented in this study. Source locations are shown in figure 3.9A. These arrivals are shown in Appendix 4 as a series of plots of timed and detected events at either array, and fitted by least squares with best fit straight lines to give the indicated apparent velocities. Origins and origin times, where recorded, are presented as part of Appendix 1, and travel times, where timed, as part of Appendix 2. The standard errors quoted in the plots in Appendix 4 are a measure of the quality of a best-fit source azimuth, and do not give bounds to the apparent velocity values which were dependent also on the data quality itself. These data are summarised in figures 3.9B,10,11, along with the standard errors on each apparent velocity. Most of this data is of good quality and limited in usefulness only by the paucity of timed origins. Examples of some of the data are shown in figures 3.12 - 3.23 as normalised but unfiltered records. The use of this dataset will be discussed in section 4.2.3.

3.2.3 Spectral analysis

3.2.3.1 Introduction

Analysis of peak frequencies for primary arrivals on each of the three record sections comprising the Hillhouse - Broughton profile was carried out for two main reasons. Firstly, the spectral content of shallow refracted first arrivals was useful during the raytrace modelling in providing minimum bounds for the thicknesses of several thin layers recognised across the profile (see section 4.2.2.3), and showing how the apparent true refractor velocity might relate to the actual refractor velocity. Secondly, information on the dominant frequencies of P and S-waves allowed the 'cleaning up' of record sections by filtering, in particular, enhancing any S-wave energy present in these sections by hopefully removing all frequencies outwith the

$\frac{1}{2} \frac{d}{dt} \left(\frac{1}{2} \frac{d^2 x}{dt^2} \right) = \frac{1}{4} \frac{d^3 x}{dt^3}$

$\frac{1}{2} \frac{d}{dt} \left(\frac{1}{2} \frac{d^2 x}{dt^2} \right) = \frac{1}{4} \frac{d^3 x}{dt^3}$

$\frac{1}{2} \frac{d}{dt} \left(\frac{1}{2} \frac{d^2 x}{dt^2} \right) = \frac{1}{4} \frac{d^3 x}{dt^3}$

$\frac{1}{2} \frac{d}{dt} \left(\frac{1}{2} \frac{d^2 x}{dt^2} \right) = \frac{1}{4} \frac{d^3 x}{dt^3}$

$\frac{1}{2} \frac{d}{dt} \left(\frac{1}{2} \frac{d^2 x}{dt^2} \right) = \frac{1}{4} \frac{d^3 x}{dt^3}$

$\frac{1}{2} \frac{d}{dt} \left(\frac{1}{2} \frac{d^2 x}{dt^2} \right) = \frac{1}{4} \frac{d^3 x}{dt^3}$

$\frac{1}{2} \frac{d}{dt} \left(\frac{1}{2} \frac{d^2 x}{dt^2} \right) = \frac{1}{4} \frac{d^3 x}{dt^3}$

$\frac{1}{2} \frac{d}{dt} \left(\frac{1}{2} \frac{d^2 x}{dt^2} \right) = \frac{1}{4} \frac{d^3 x}{dt^3}$

$\frac{1}{2} \frac{d}{dt} \left(\frac{1}{2} \frac{d^2 x}{dt^2} \right) = \frac{1}{4} \frac{d^3 x}{dt^3}$

$\frac{1}{2} \frac{d}{dt} \left(\frac{1}{2} \frac{d^2 x}{dt^2} \right) = \frac{1}{4} \frac{d^3 x}{dt^3}$

$\frac{1}{2} \frac{d}{dt} \left(\frac{1}{2} \frac{d^2 x}{dt^2} \right) = \frac{1}{4} \frac{d^3 x}{dt^3}$

$\frac{1}{2} \frac{d}{dt} \left(\frac{1}{2} \frac{d^2 x}{dt^2} \right) = \frac{1}{4} \frac{d^3 x}{dt^3}$

N Event location

- 1 Hillhouse quarry
- 2 Craigie quarry
- 3 Cairngryffe - Cloburn quarries
- 4 Mid Croft shot
- 5 Cornstones shot
- 6 Greivehill shot
- 7 Waterside Opencast
- 8 Kirkconnel Opencast
- 9 Benbain Opencast
- 10 Cairnyhill quarry
- 11 Tams Loup quarry
- 12 Duntilland quarry
- 13 Haywood Opencast
- 14 Leven's Seat Opencast
- 15 Craigpark quarry
- 16 Kaines quarry
- 17 Cruicks quarry
- 18 Dumbuck quarry
- 19 Croy quarry
- 20 Middleton quarry
- 21 Craighouse quarry
- 22 Coatsgate quarry
- 23 Morvern quarry
- 24 Westgate quarry

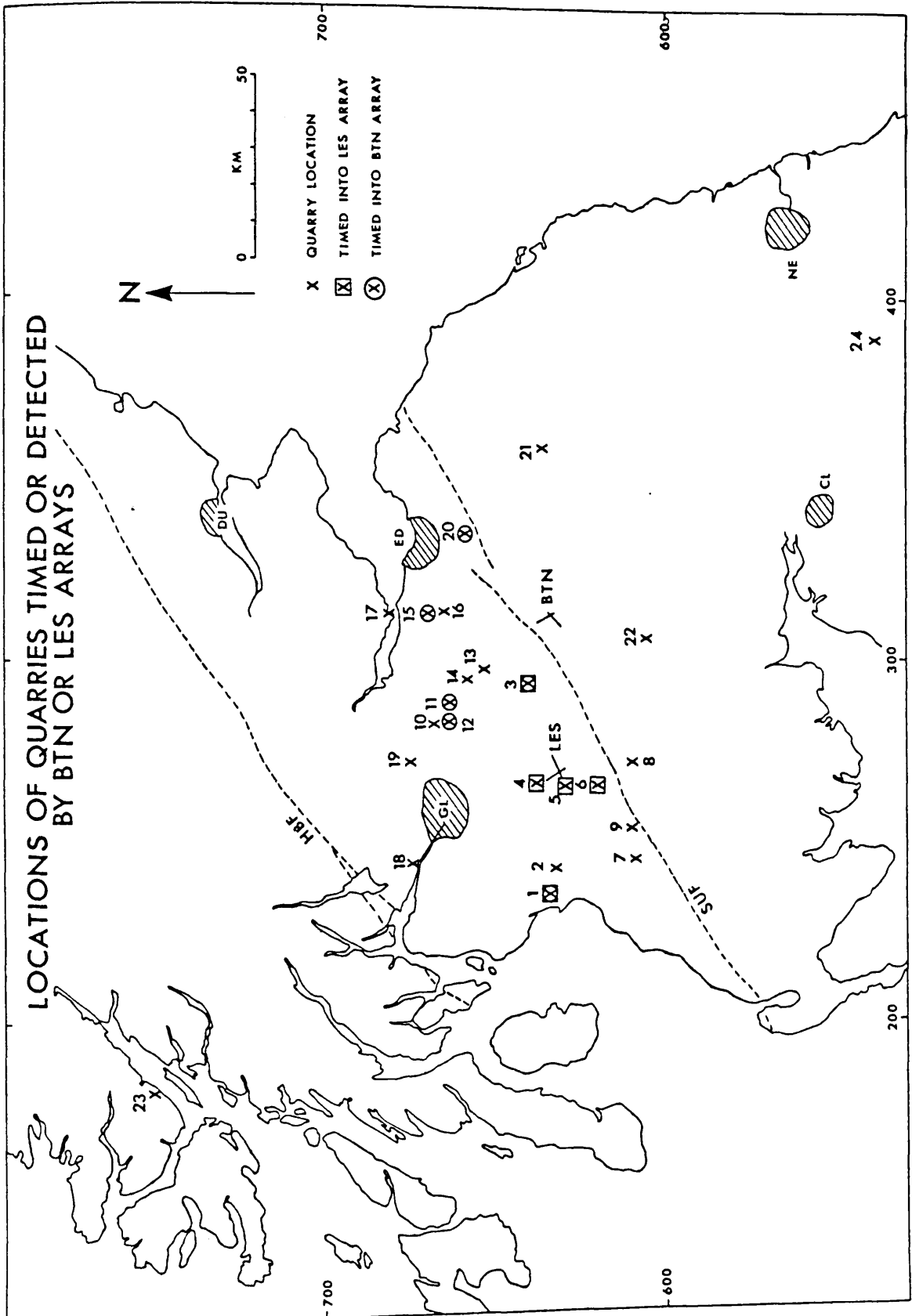


Figure 3.9A Location map of all sources referenced in this study.
 Key is on the facing page.

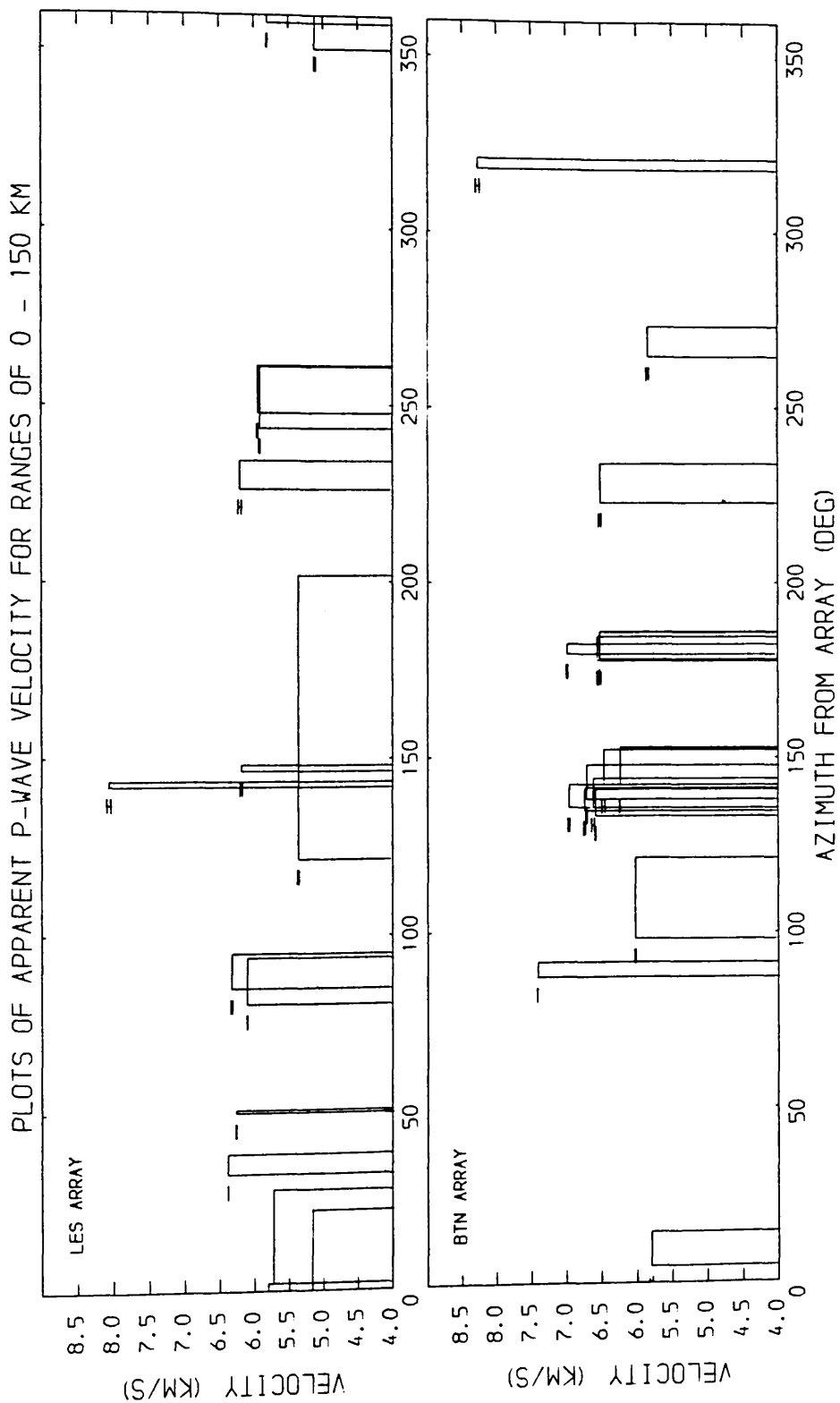


Figure 3.9B Summary of all P-wave data identified into the LES & BTN arrays.

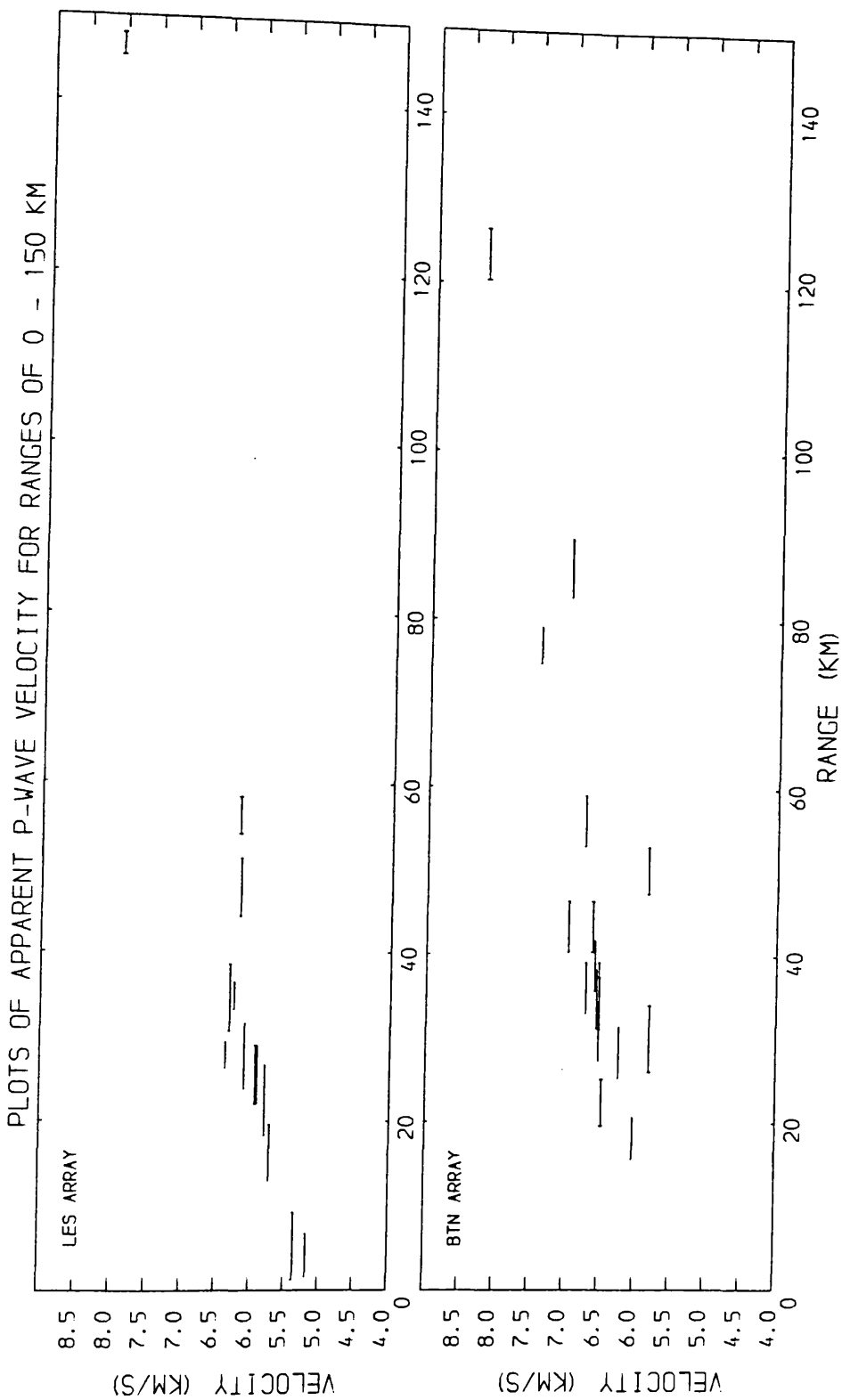


Figure 3.10 Summary diagram for the same dataset as shown in Figure 3.9B, but showing the spread of ranges for each identified event.

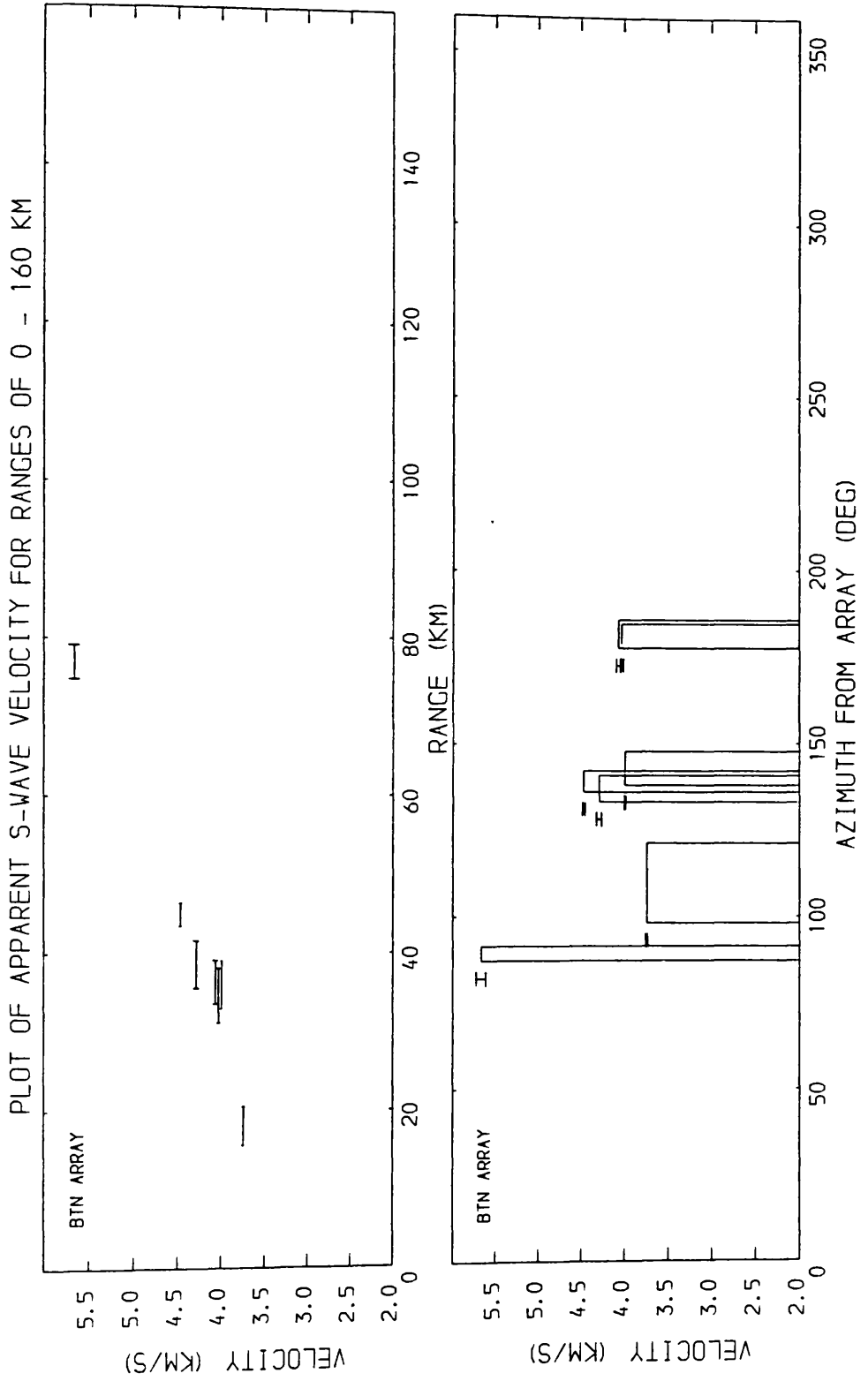


Figure 3.11 Summary of the S-wave dataset identified into the BTN array.

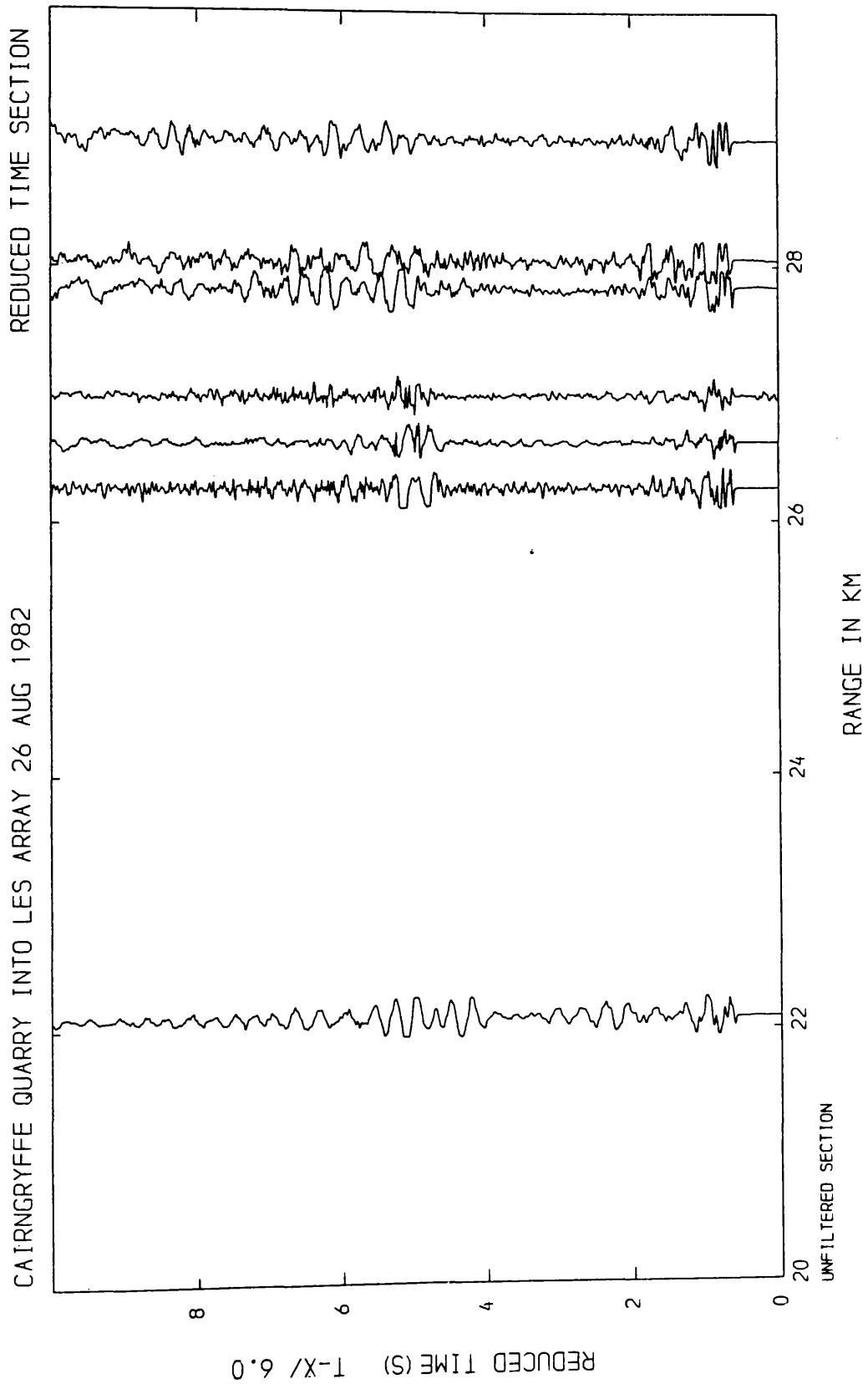


Figure 3.12

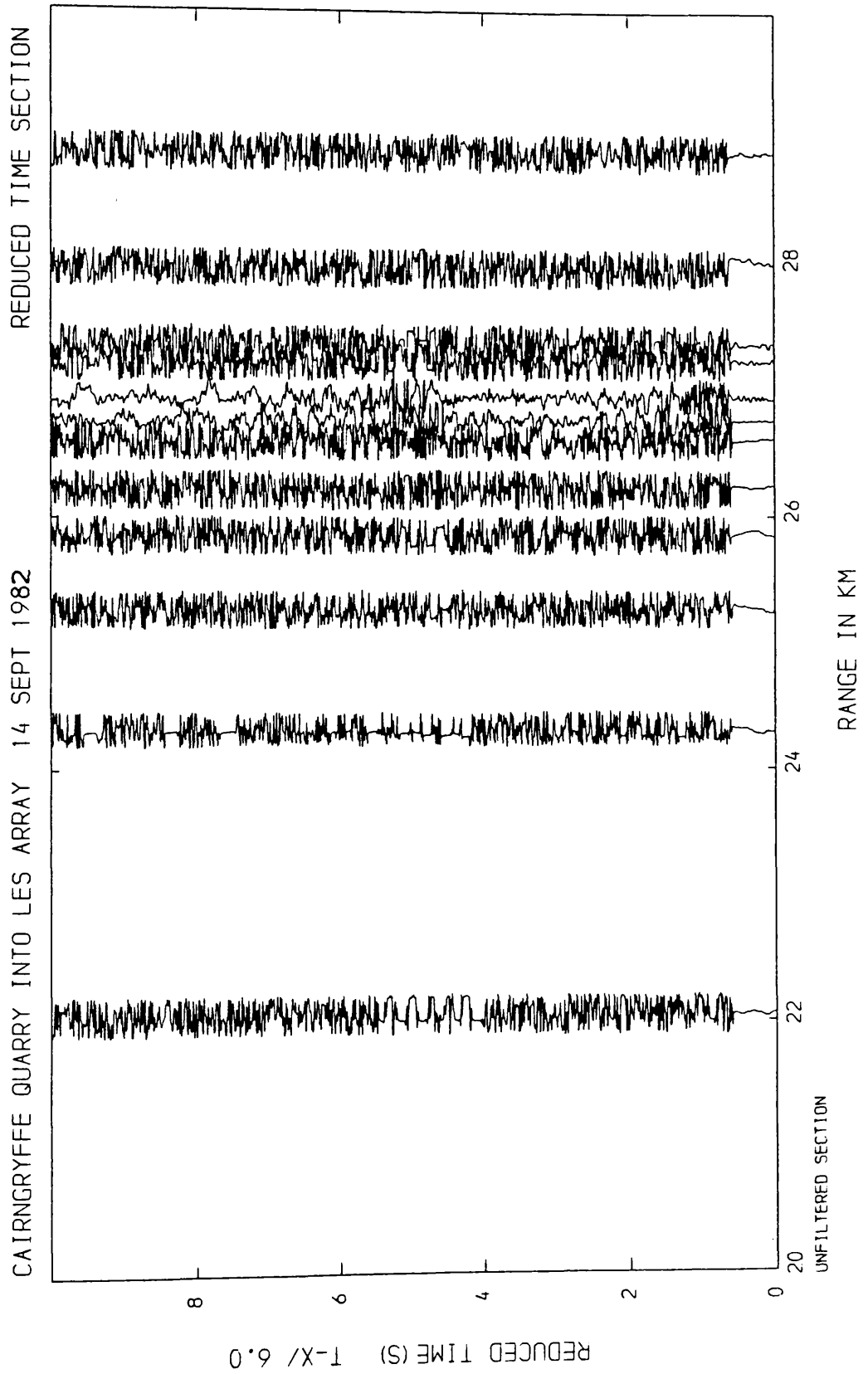


Figure 3.13

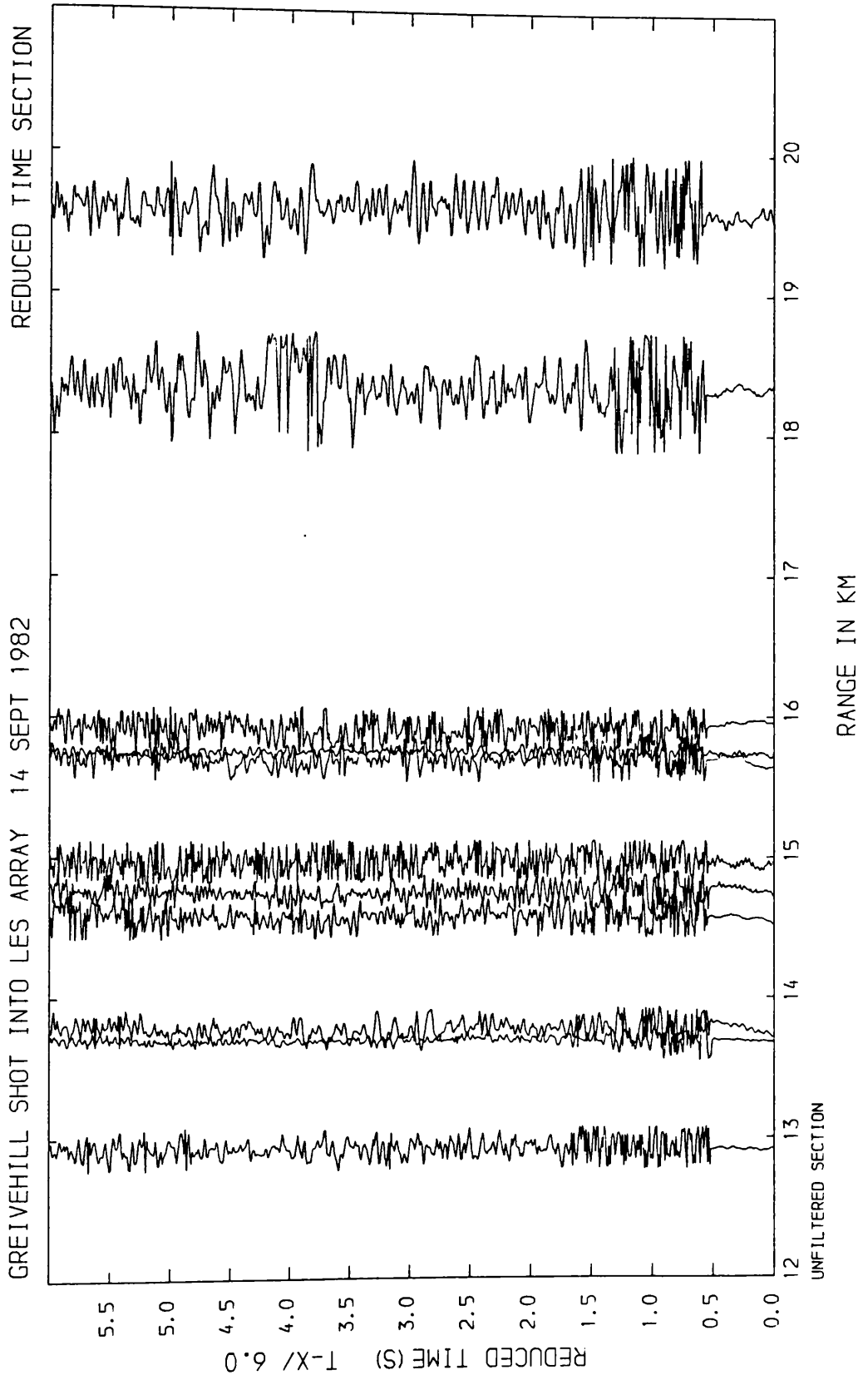


Figure 3.14

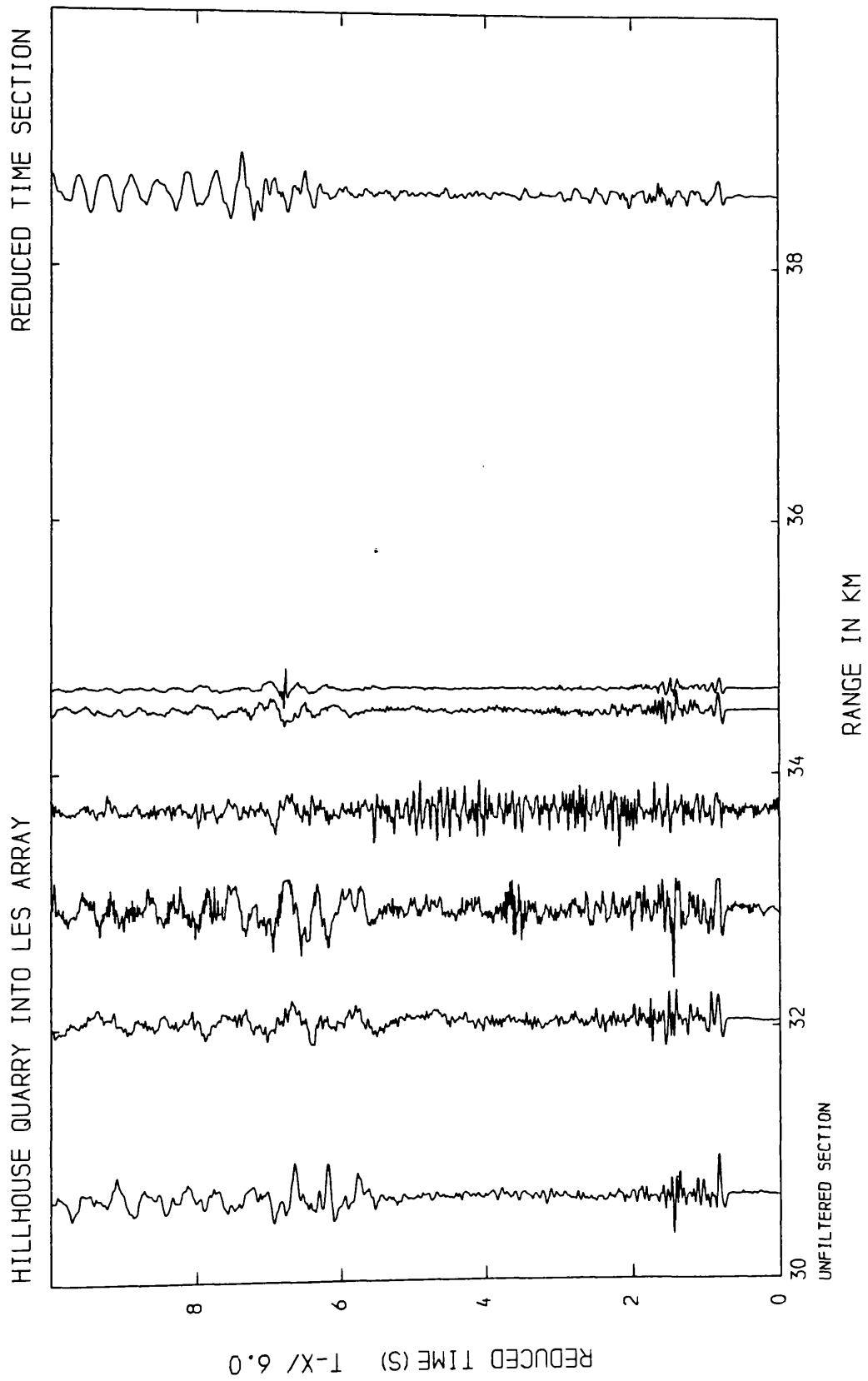


Figure 3.15

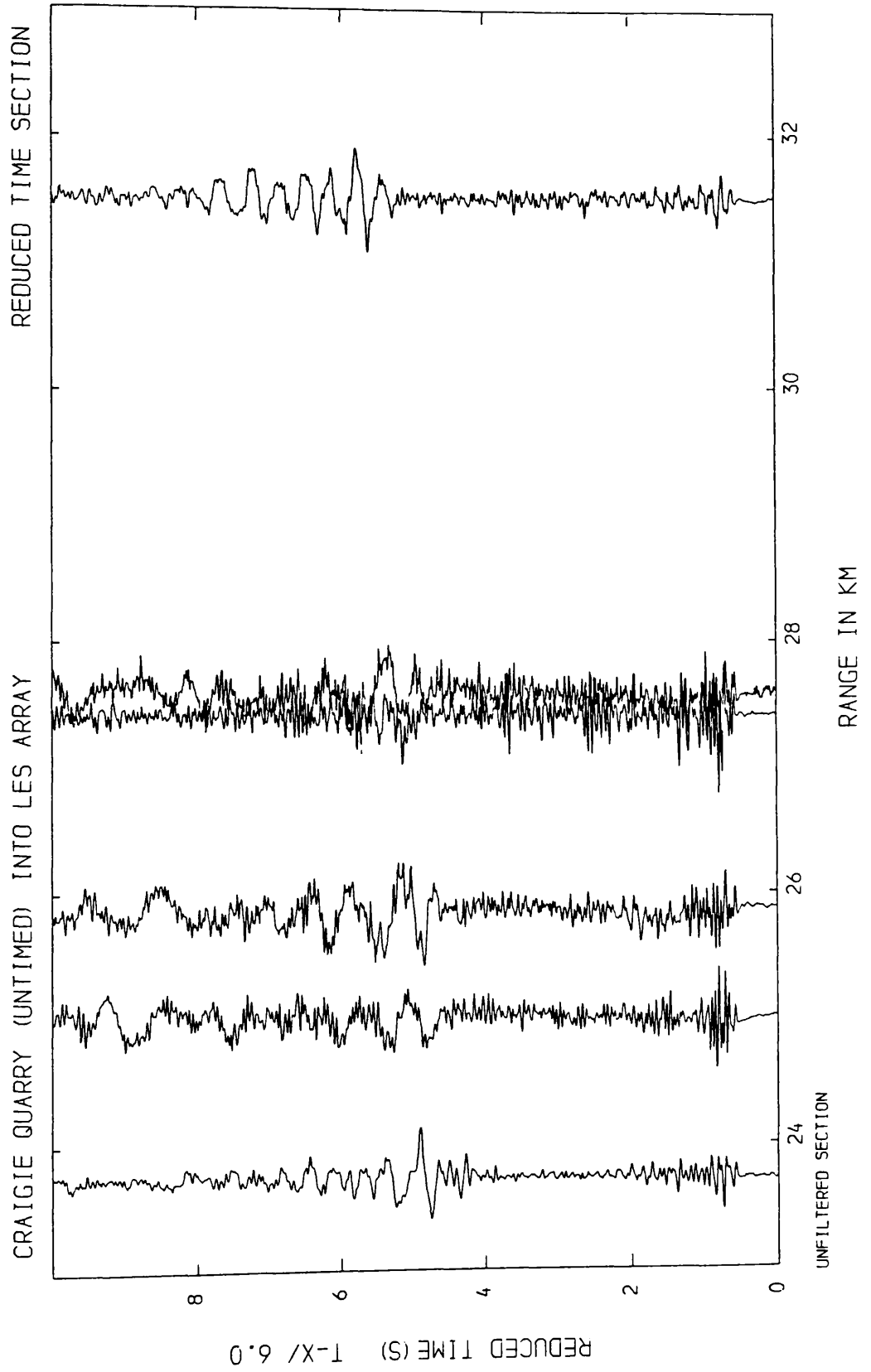


Figure 3.16

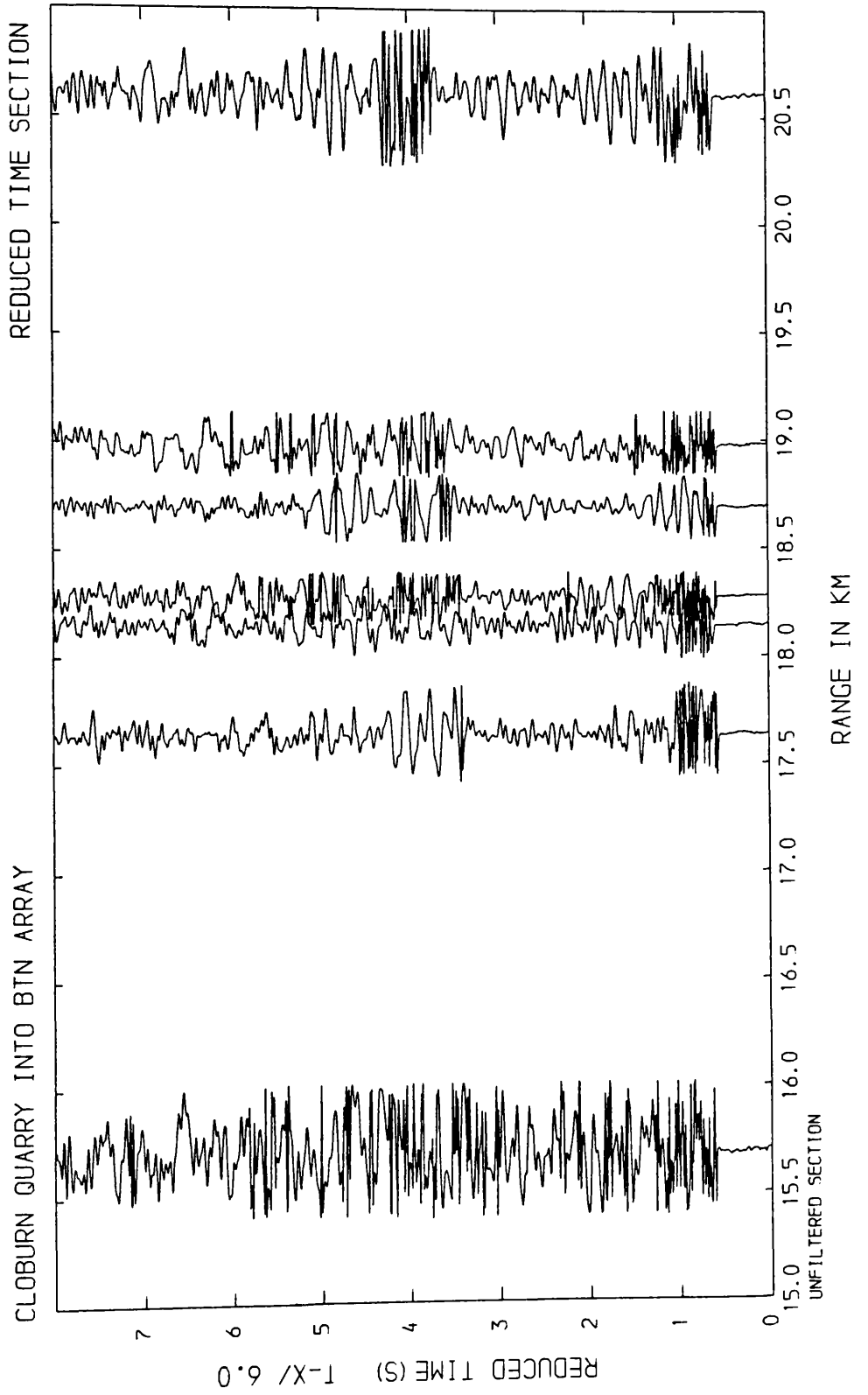


Figure 3.17

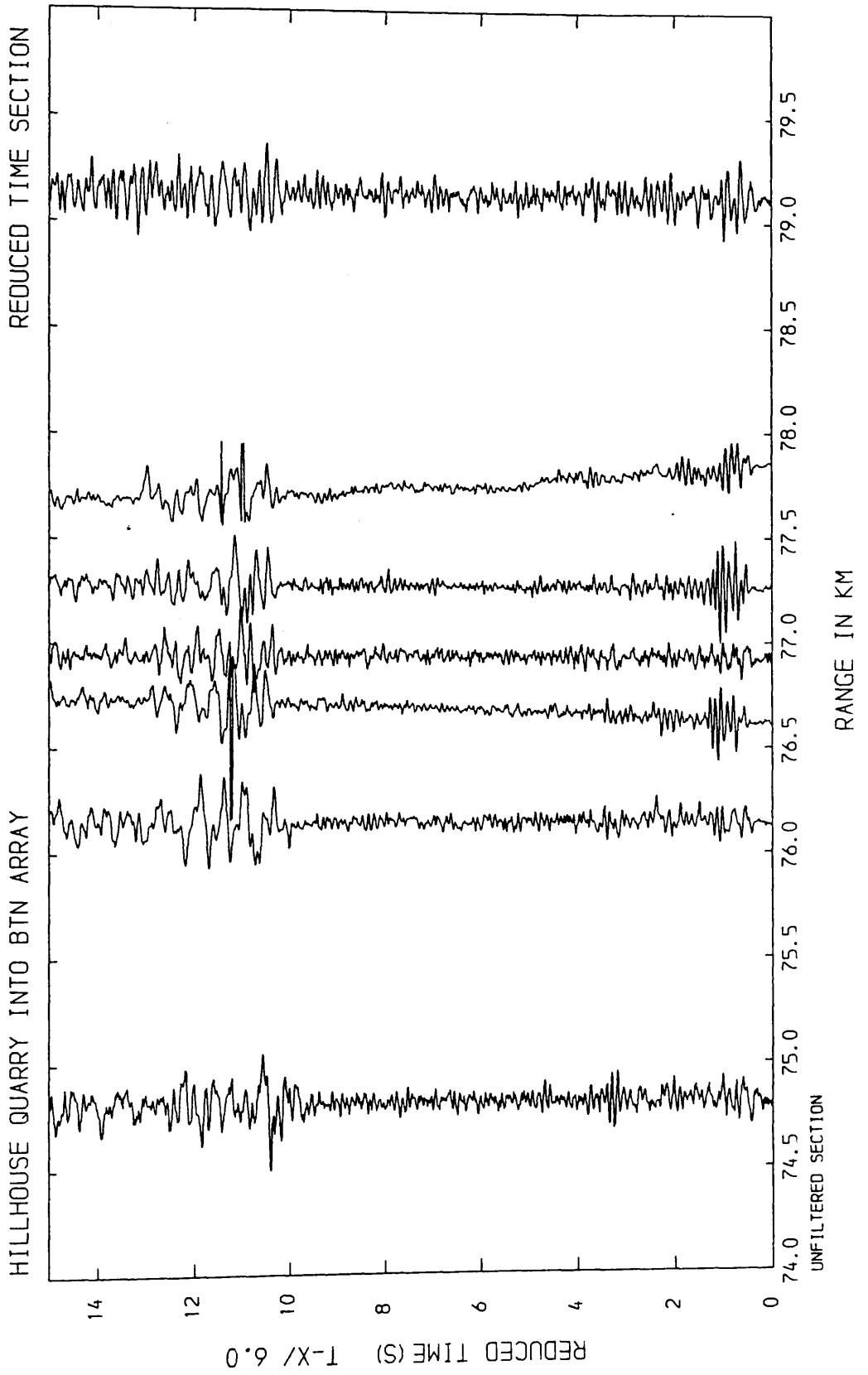


Figure 3.18

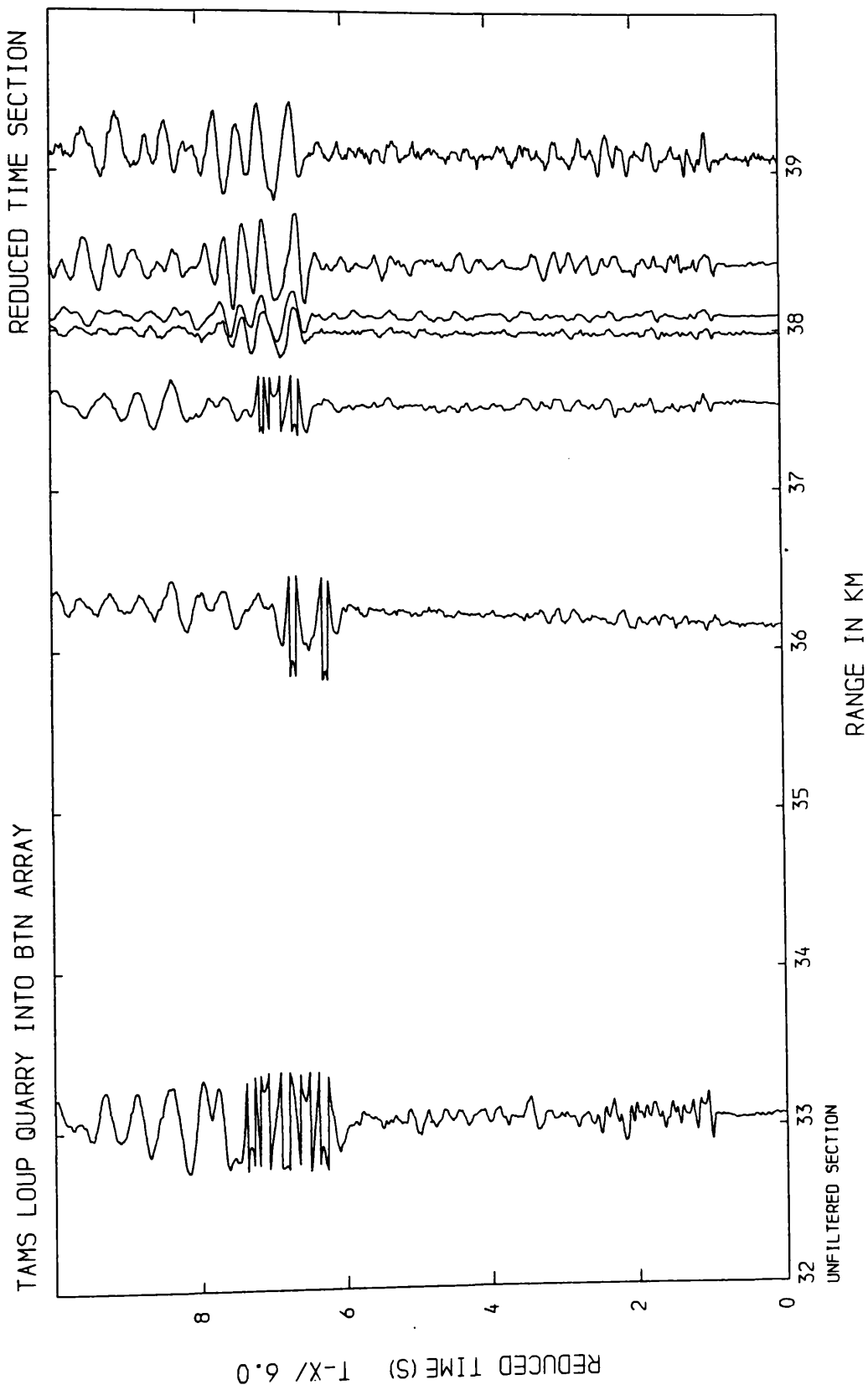


Figure 3.19

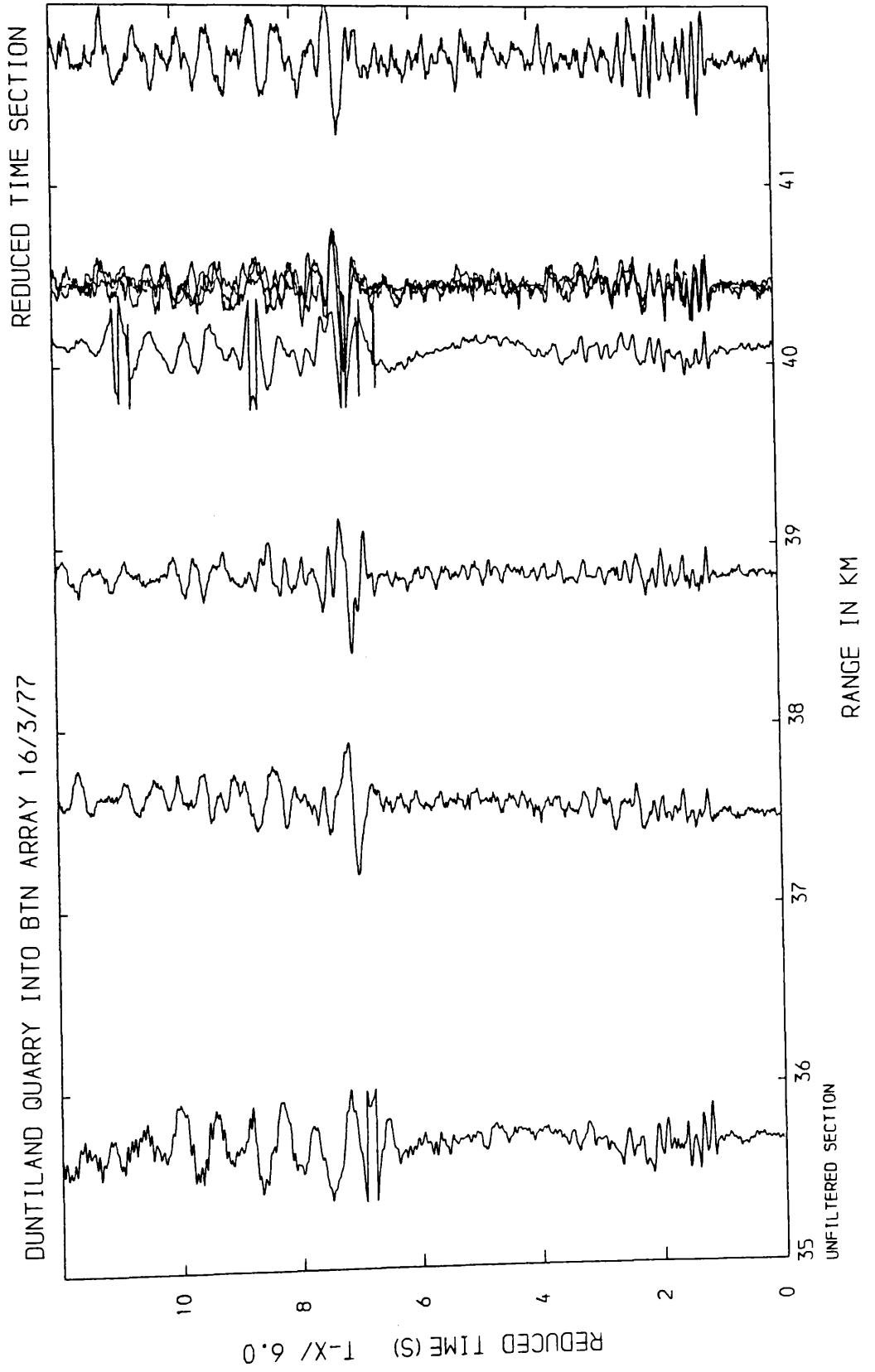


Figure 3.20

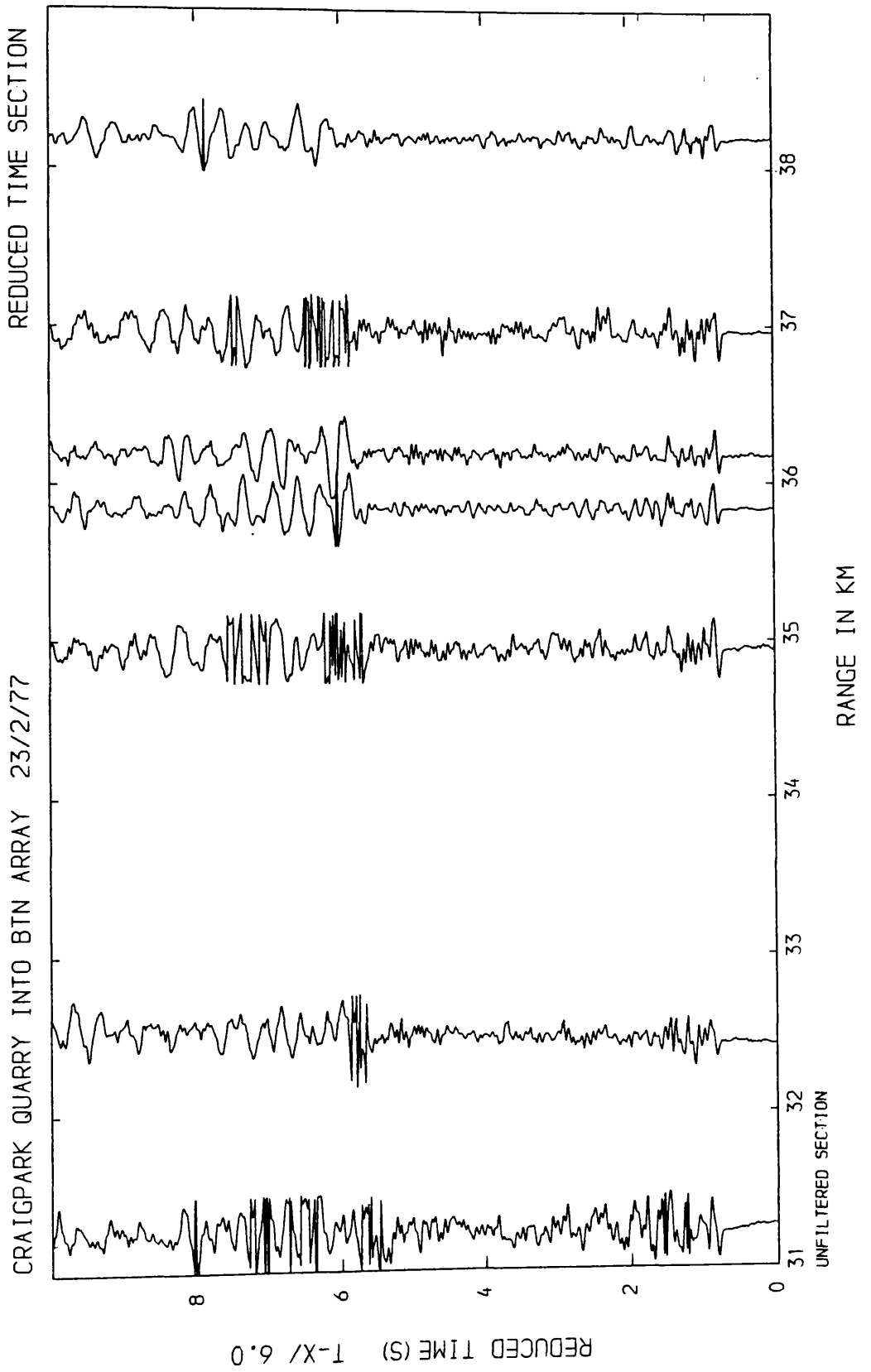


Figure 3.21

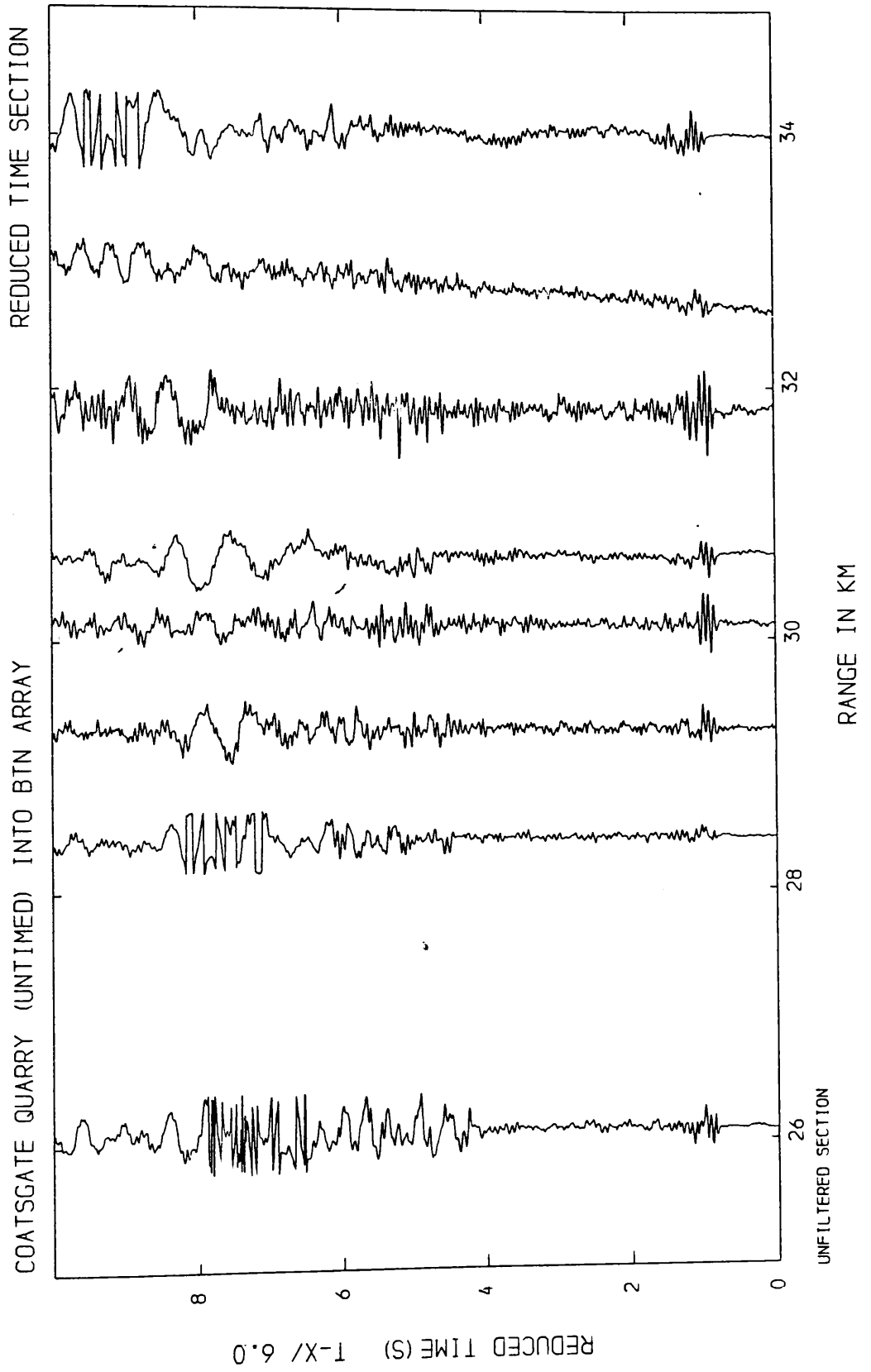


Figure 3.22

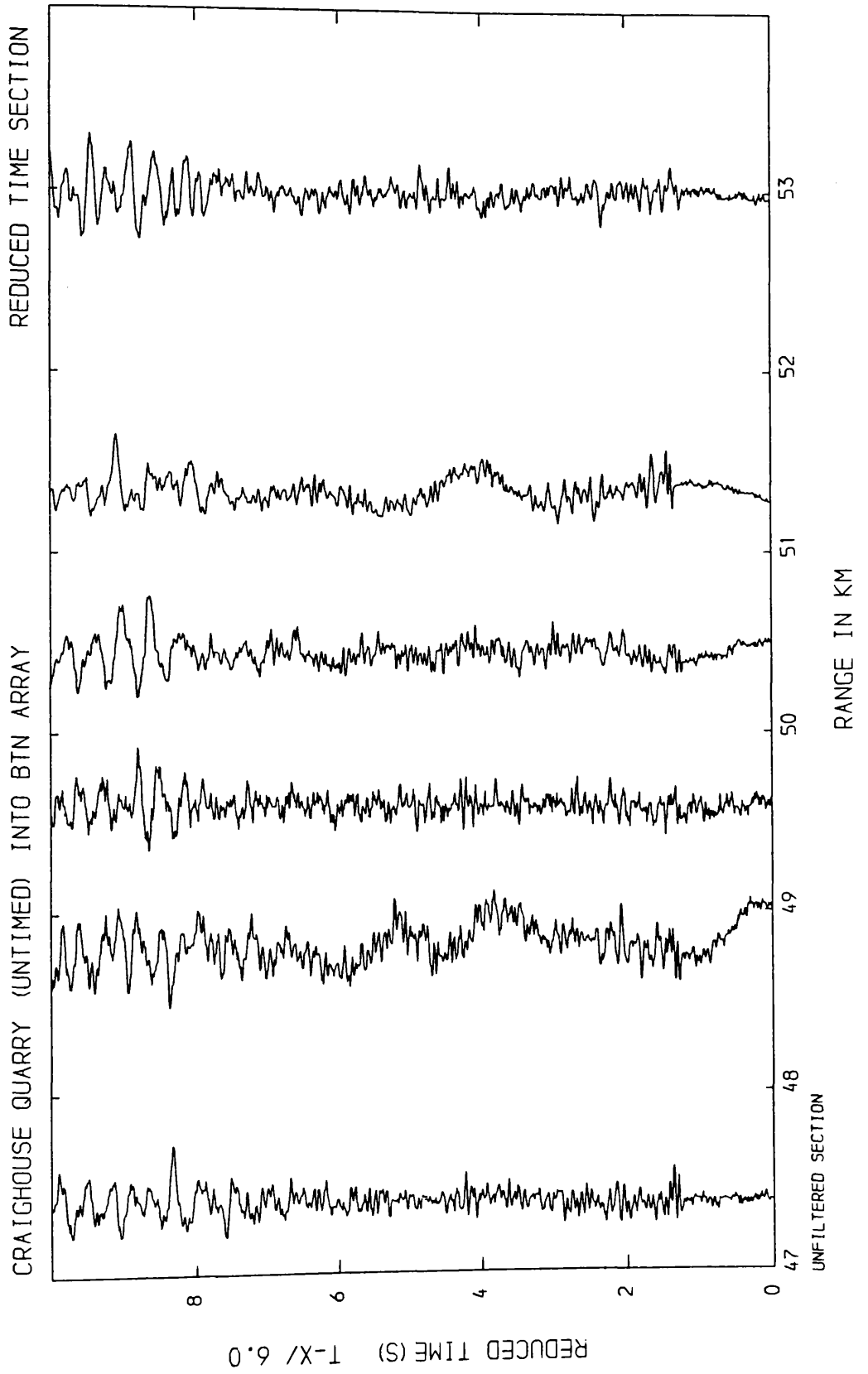


Figure 3.23

dominant S-wave frequency spectrum.

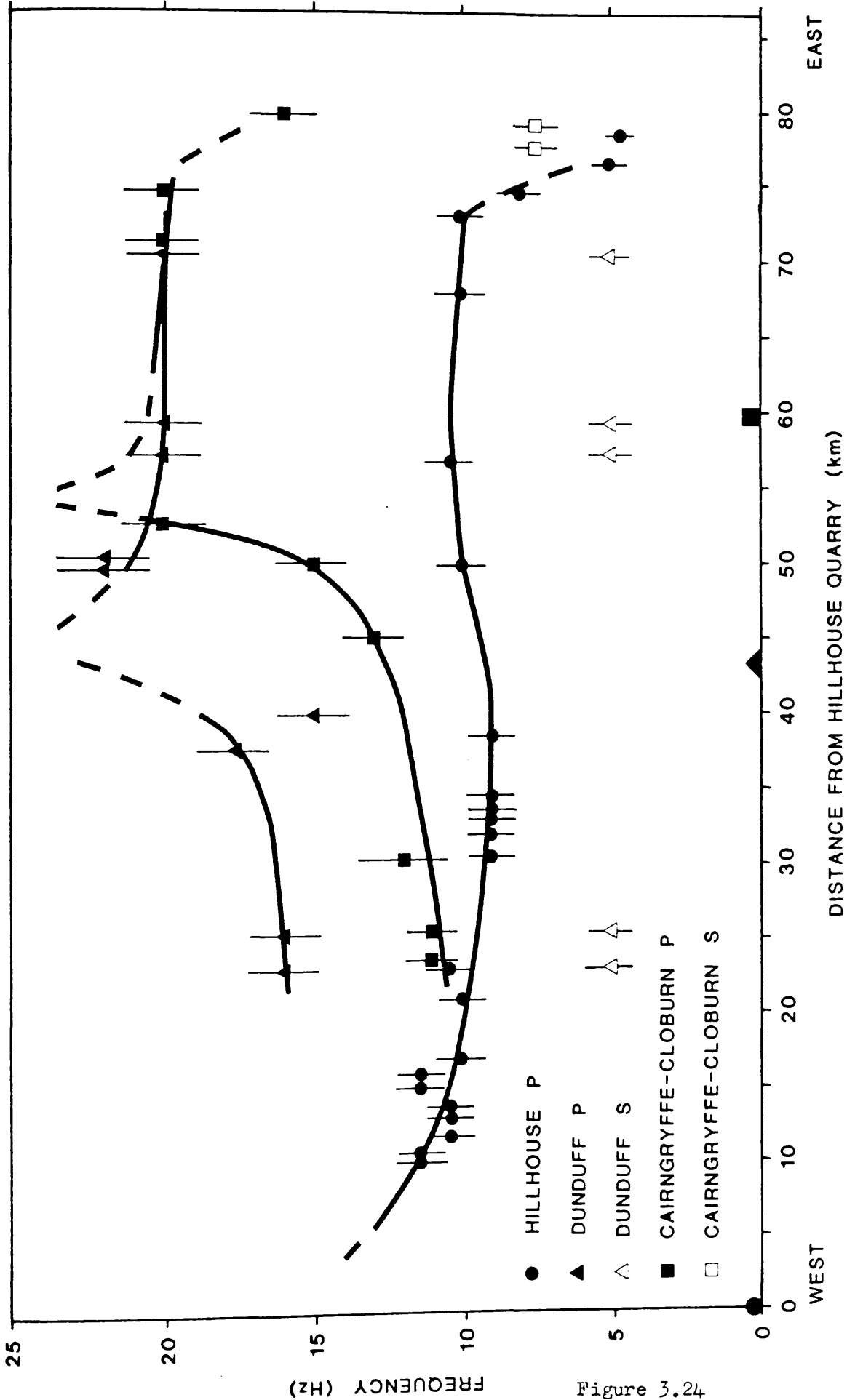
The analysis of dominant frequencies for clear P-wave first arrivals and S-waves was carried out by the physical measurement of prominent adjacent peaks (or troughs) close to the onset, as the eye automatically discriminates between these dominant, source-produced frequencies and other spurious, often digitiser-produced, frequencies. On each section, traces which were known, or suspected to be, distorted by instrumentation or digitising problems were excluded from analysis.

3.2.3.2 Spectral analysis of the Hillhouse - Broughton profile record sections

Plots of the dominant P-wave frequencies for all three record sections are shown in figure 3.24. The most obvious feature (apart from rapid high-frequency attenuation away from each source), is the clear difference in frequencies obtained from each quarry. Despite the discontinuous and protracted nature of the data acquisition, this effect has been consistent over many blasts, and therefore must be related to either local subsurface geological effects or to consistent, although individual, blasting practices by the blasting engineer at each quarry. On closer inspection of these peak frequencies, there is another frequency variable, apparently quarry independent. From Dunduff and Cairngryffe-Cloburn quarries all frequencies between about 50 km and 80 km from the western end of the profile are higher than those measured at equivalent ranges to W. The frequencies measured from Hillhouse quarry between these ranges are also slightly higher than expected, compared with the frequency trend for the rest of this line, although here the difference is small.

On the basis of later ray modelling of these data see (4.2.2.2), the origin of this frequency variation must be in the surface, sedimentary layer to the E of Cloburn quarry. From the surface geology, the most obvious major

PLOT OF DOMINANT FREQUENCY AGAINST RANGE



lithological change in this area is the occurrence of predominantly andesitic lavas in place of sandstone in the Lower Old Red Sandstone. Not far to the NE of the profile, in the Pentland Hills, these lavas have their maximum recorded thickness of 2 km (Mykura 1960) and so it is reasonable to assume a thickness under this part of the profile of at least 1.5 km. The presence of such a thickness of layered crystalline rocks could provide a suitable explanation for this low-frequency screening due to high frequency resonance being produced by wave propagation through the relatively thin lava flows.

A small number of good quality S-waves were analysed and plots of the peak frequencies are also shown in figure 3.24. The dominant frequency throughout is 5 Hz.

3.2.4 Description of the available filters

At a late stage in this project, all data were available in digital form and filtering was considered as a possible means of enhancing the amount of clear S-wave energy in the three record sections of the Hillhouse - Broughton profile. In particular, S-wave energy is only weakly recognisable in the Hillhouse quarry record section (figures 3.3,6) and not at all in the first 25 - 30 km. This is to be expected considering the complex nature of the P-wave first arrival phases and the existence of a 0.5 sec source wavelet. However, if distinct differences exist in the frequency content of the P and S-waves, then filtering should provide a method of selective discrimination.

Several bandpass filtering options are available in a program package (DRAW4, listing Appendix 6) compiled by M. Ali (see Ali 1983; also Warren 1981; and Robinson 1966; 1983) and modified by the writer. These comprise one-sided Robinson filters, two-sided Robinson filters, a two-sided Hanning filter and *highcut/lowcut* filters based on either half of a one-sided Robinson filter.

As a summary, a frequency filter is a device which discriminates against

predefined unwanted frequencies. A digital filter is a time series of predefined length, which when convolved with the seismic trace, or time series, will sequentially concentrate at each point on the trace, an amplitude which is dependent on the frequencies determined around that point. For the purposes of the discussion below, $t=0$ refers to the point on the trace which, at any time in the convolution process, is defined as being the origin. Negative t -values signify the future segment of the trace, and positive t -values the past segment.

One-sided (causal) filters have all filter coefficients for values of $t < 0$ set to zero, so the filter has only a memory component and can only operate on the present and past components of a time series. The resulting output will have no time shift.

Two-sided filters have anticipation and memory components, centred symmetrically about $t=0$. This allows the operation of the filter on the part of the trace in front of $t=0$ (ie in the future), giving greater control over the desired frequency response. This results in a time-shift in the output time series which if linear can be balanced by a complementary shift of origin in the time series.

The one-sided Robinson bandpass filter (Robinson 1966) is a minimum-phase filter whose frequency response is designed to approximate to a box-car filter. It has been modified (Warren 1981) by the addition of a cosine taper to give smoother high and low frequency cutoff slopes and so reduce the oscillatory effect from the Fourier transform produced by sharp points on the frequency response.

The response of this filter (with a passband of 1-15Hz and length of 99 samples (ie 0.99 s)) to an impulse function defined as :

$$X = (1, 0, 0, 0, 0, \dots)$$

is shown in figure 3.25. The input spike function has been transformed into a

minimum phase wavelet with some oscillatory energy still present after 200-300 ms. Taking the Fourier transform of this filter allows the calculation of its amplitude spectrum (figure 3.26). This shows an asymmetric frequency response across the predefined passband range, and poor suppression of frequencies above 15 Hz.

The two-sided Robinson bandpass filter, again modified by a cosine taper (Warren 1981), has an anticipation as well as a memory component and so can operate on the future component of the input time series as well as the present and past. A time delay is introduced which is linear with respect to frequency and so can be removed.

The response of this filter, with identical parameters to the previous example, to the same impulse function is shown in figure 3.27. The resulting zero-phase wavelet is symmetrical about the point;

$$T = \text{filter length} / 2 = \text{time shift}$$

and with each half a mirror image of the one-sided filter described above.

The amplitude response is noticeably smoother than figure 3.28 and is symmetrical about a central frequency. Attenuation is zero within the passband, and very high outwith it, giving superior performance to the one-sided filter.

The cosine taper has been incorporated into these filters to remove oscillations in the impulse away from the central spike. For comparison, the impulse response of the original two-sided Robinson bandpass filter is shown in figure 3.29. Oscillations are present for over 500 ms on either side of the central spike. Comparing amplitude spectra (figures 3.28,30) shows the cosine smoothing of the corners of the passband spectrum which results in a damping of most of the minor oscillations.

However, removing the corners from the amplitude spectrum does result in a broader central pulse (compare figures 3.27,29).

An extension of this smoothing of box-car bandpass filters is given by the

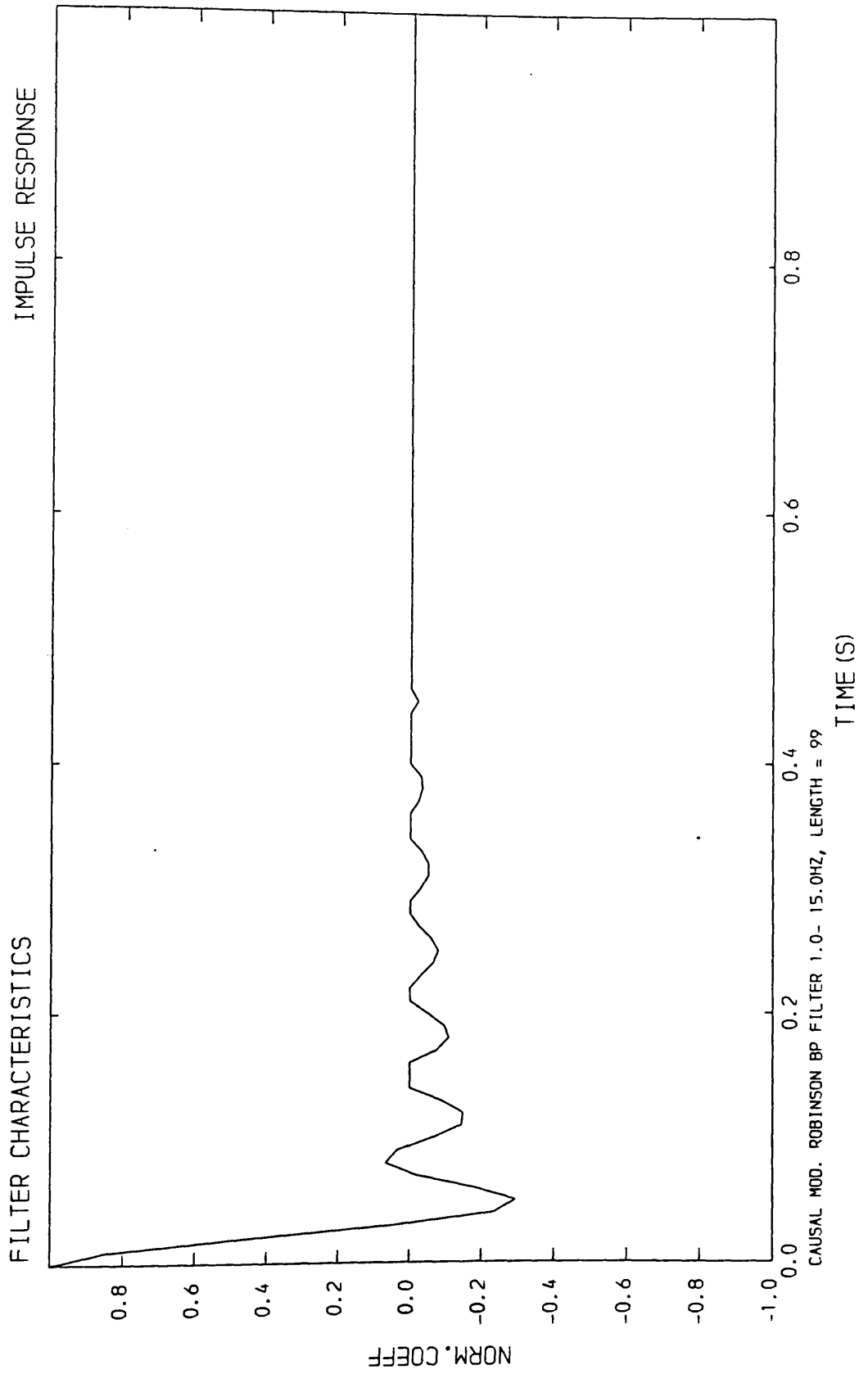


Figure 3.25 Impulse response for a causal, tapered Robinson bandpass filter.

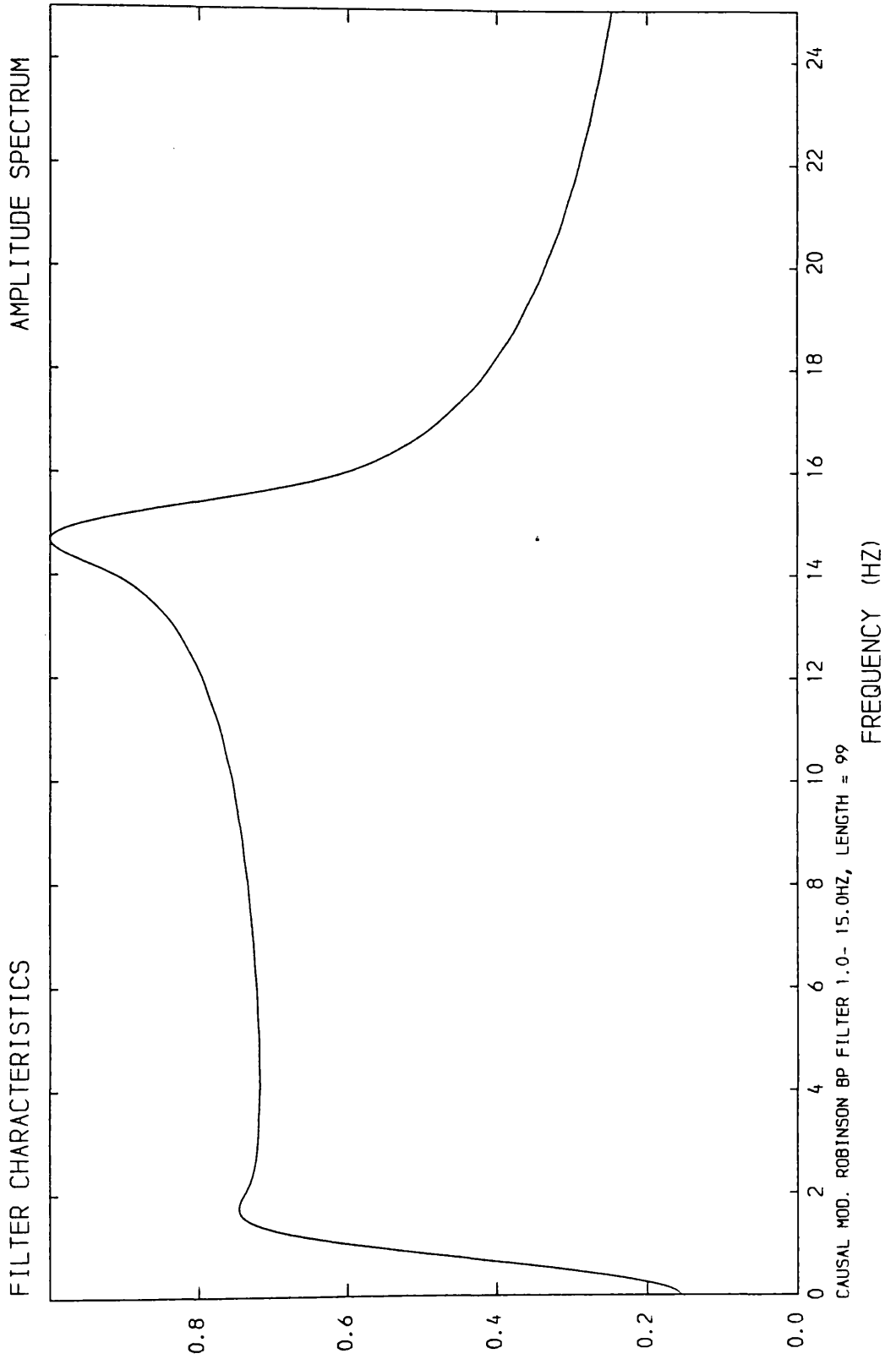


Figure 3.26 Amplitude spectrum of the filter shown in Figure 3.25.

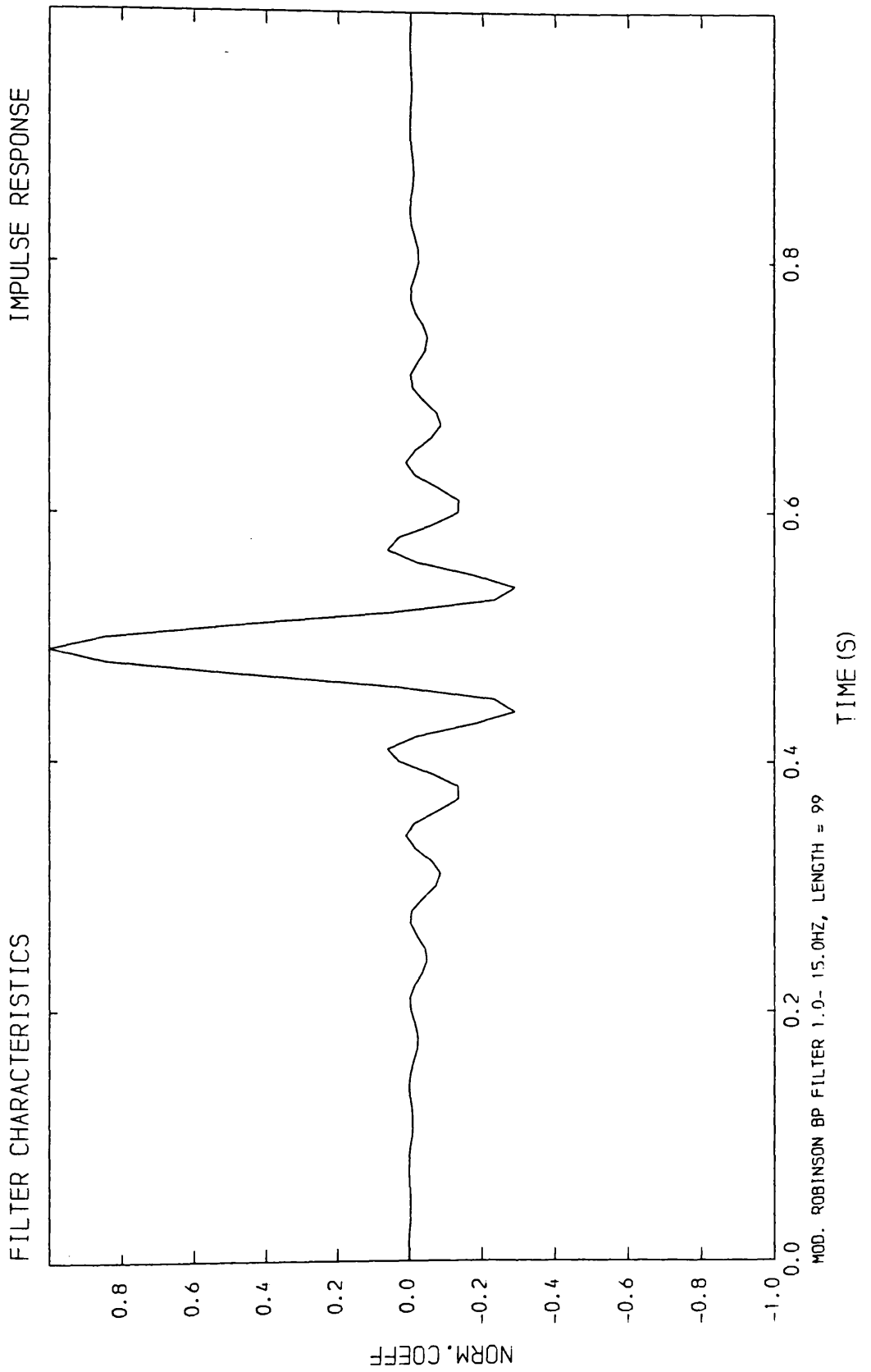


Figure 3.27 Impulse response for a two-sided, tapered Robinson bandpass filter.

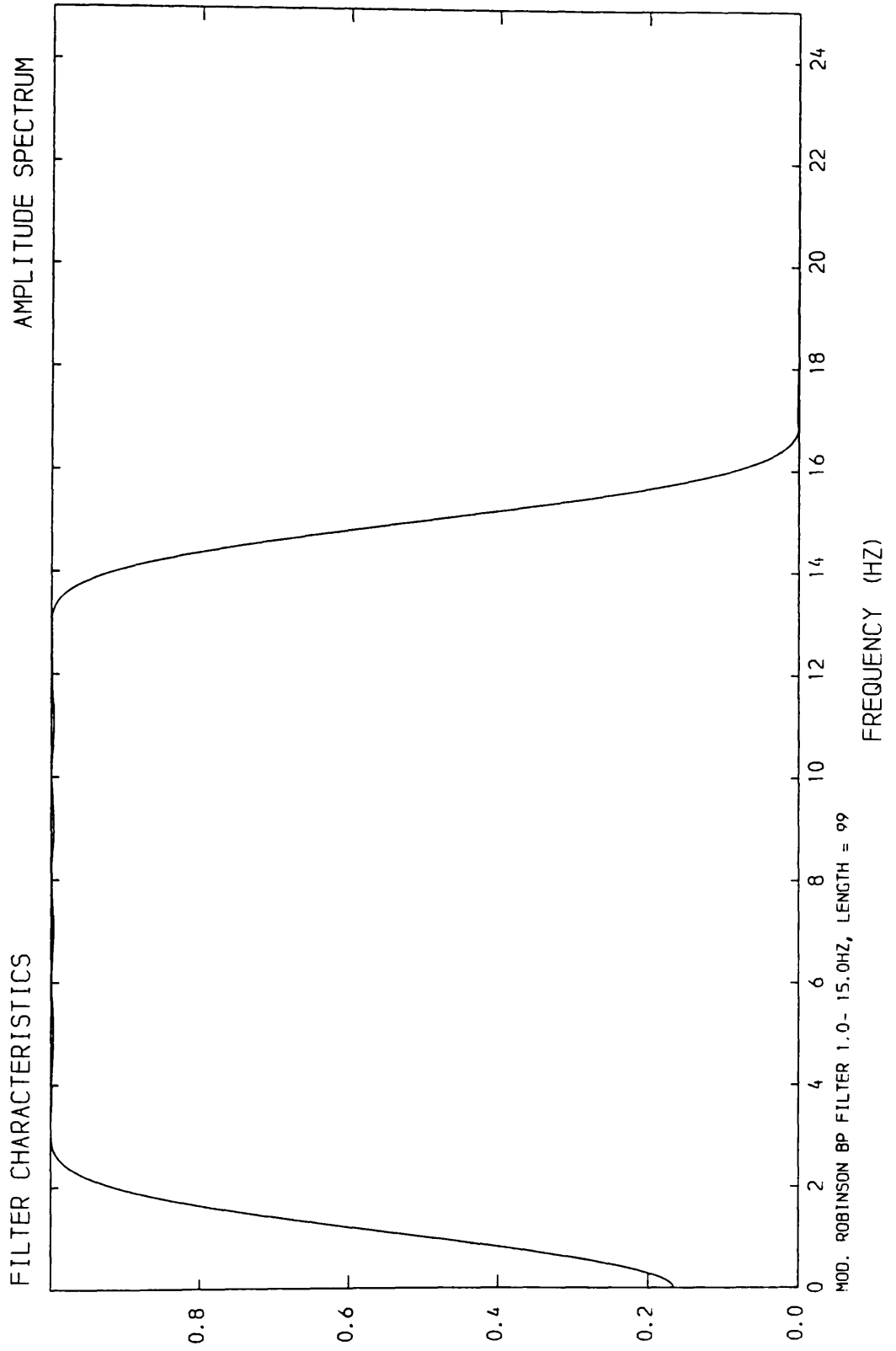


Figure 3.28 Amplitude spectrum for the filter shown in Figure 3.27.

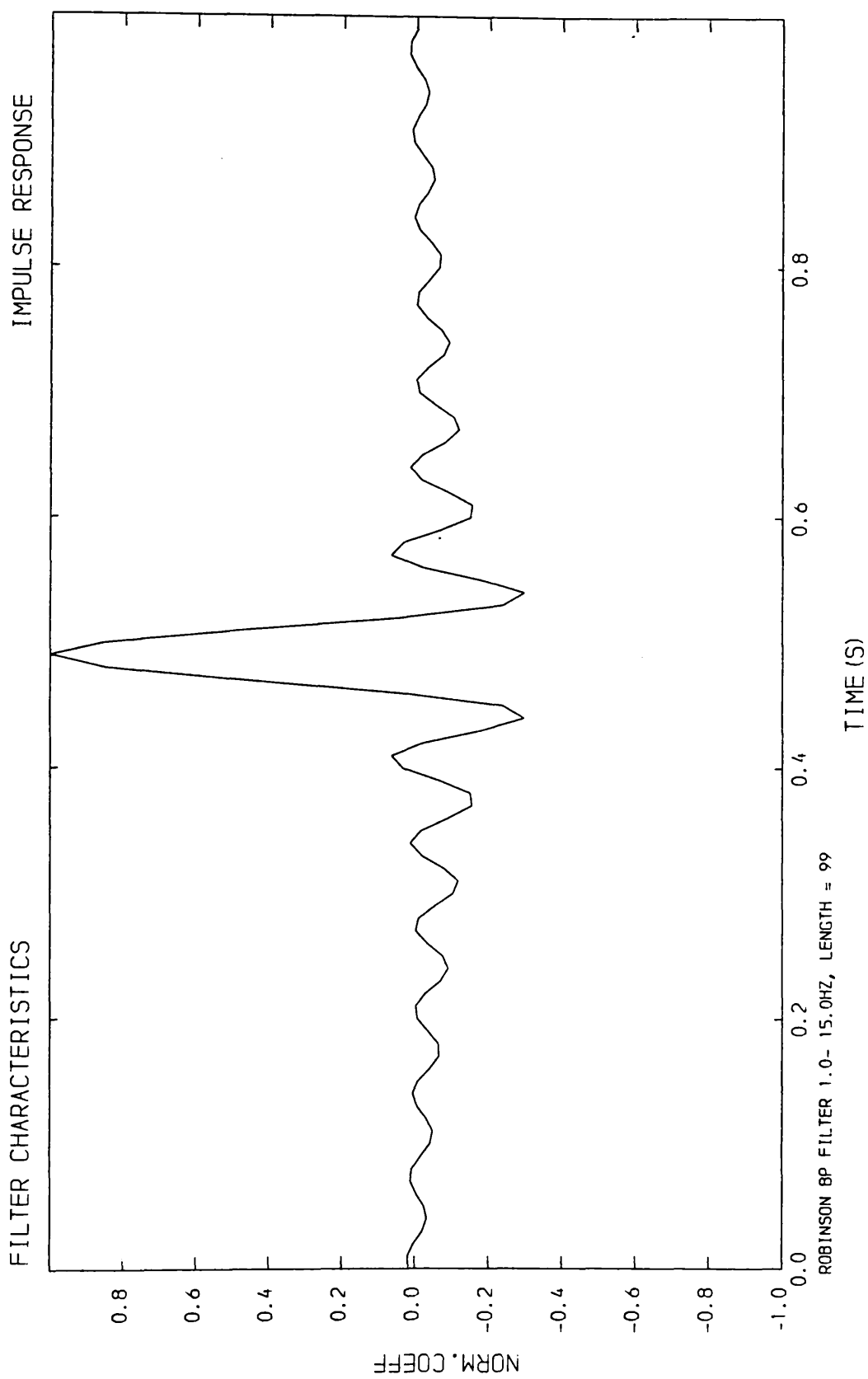


Figure 3.29 Impulse response for a two-sided, untapered Robinson bandpass filter.

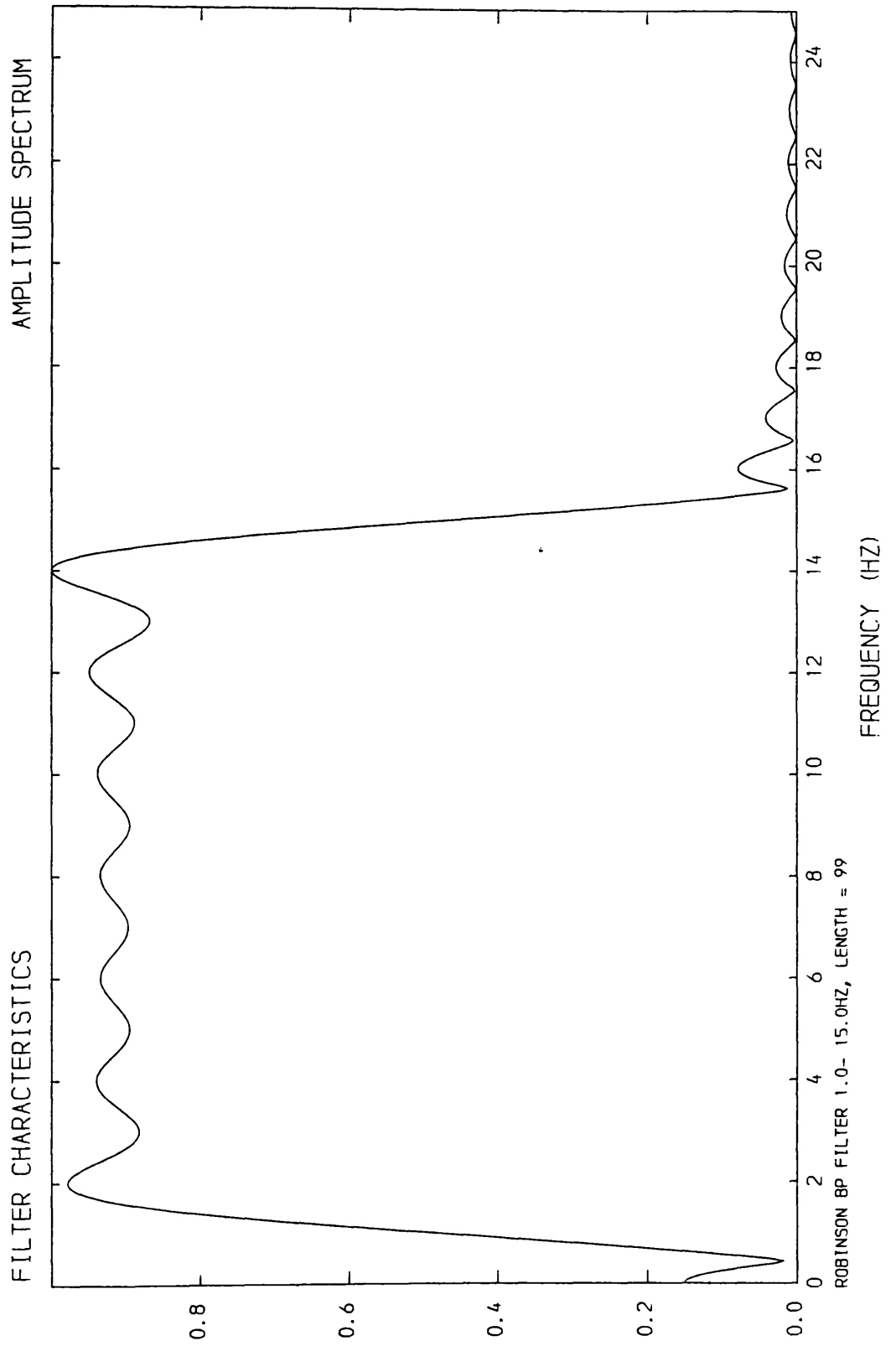


Figure 3.30 Amplitude spectrum for the filter shown in Figure 3.29.

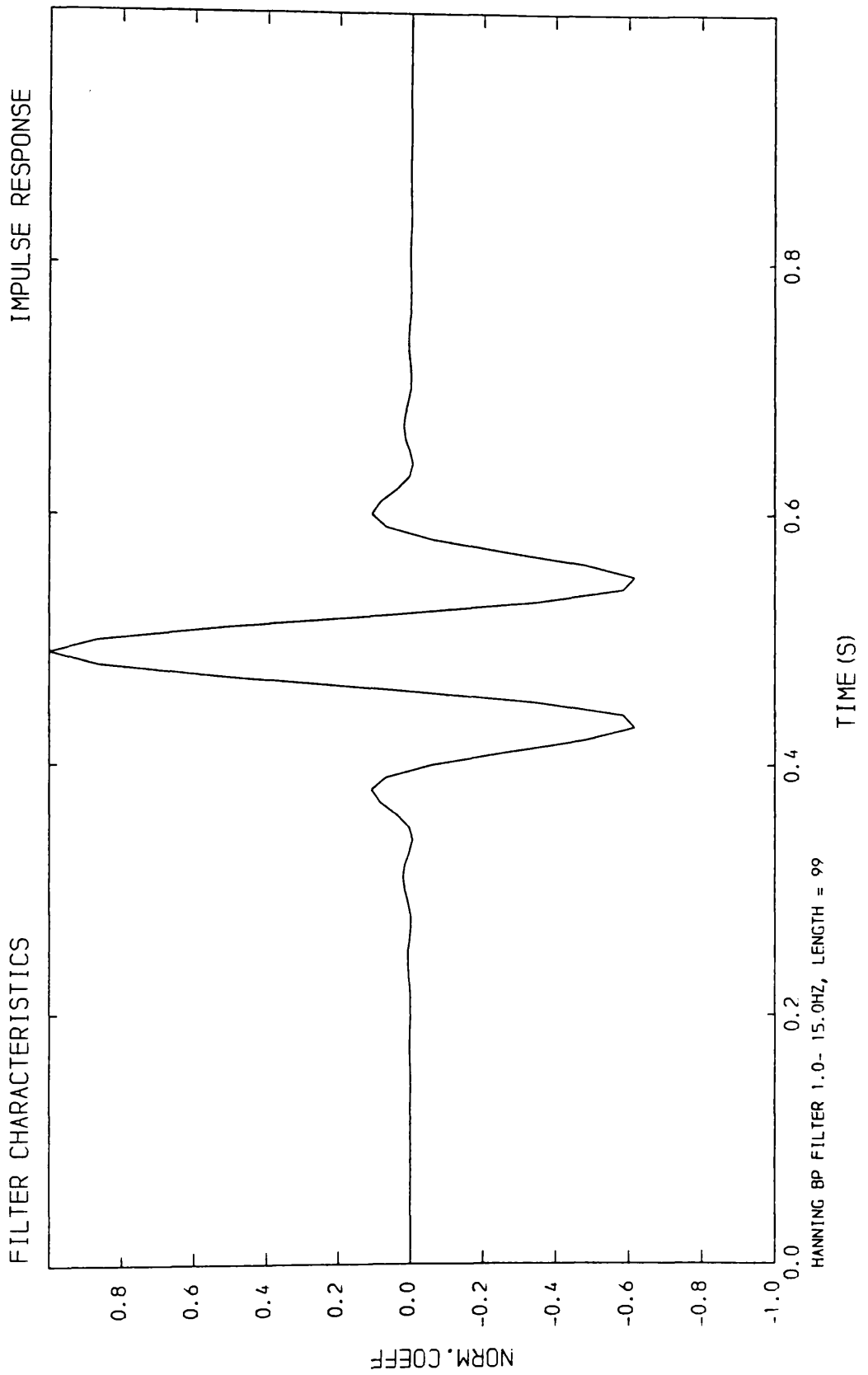


Figure 3.31 Impulse response for a two-sided Hanning bandpass filter.

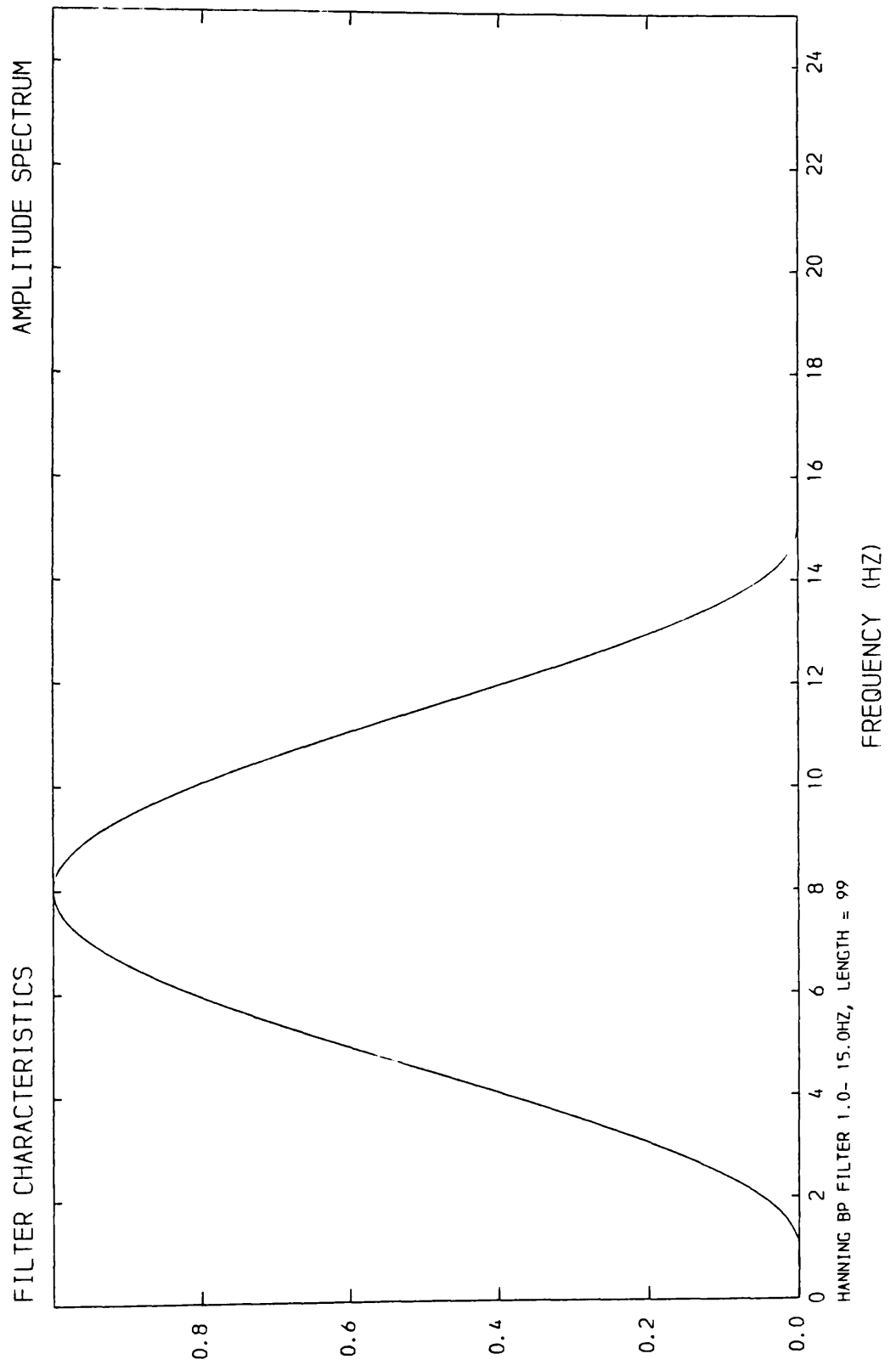


Figure 3.32 Amplitude spectrum for the filter shown in Figure 3.31.

Hanning or bell filter. Here a cosine² taper is applied symmetrically to either side of a central, allpass frequency. The resulting filter (figure 3.31) has an amplitude spectrum with no sharp edges (figure 3.32) giving an impulse response with only two side-lobes. As expected, the central pulse is much broader than either of the Robinson bandpass central pulses, due to the more extreme smoothing in this filter.

3.2.5 Filter application to the Hillhouse - Broughton profile

Filtered record sections from each quarry on the Hillhouse - Broughton profile were prepared on the basis of the above discussion (3.2.4), and the information gained from peak frequency spectral analysis of the P and S-wave arrivals in figure 3.24. As the merits of the two-sided Robinson and Hanning bandpass filters were taken to be about equal, both filters were used with identical parameters so that a qualitative, visual judgement could be made.

Figures 3.33,34 (reduction velocity of 6.0 km s^{-1}) and 3.35,36 (reduction velocity of 3.5 km s^{-1}) show the results of application of 1-10 Hz filters to the Hillhouse record section. Compared with figures 3.2,5, there is a increase in recognisable S-wave energy between 1.5 and 2.0 seconds in the range 0-40 km. Comparison between both filtered sections does not reveal any striking superiority, although it is noticeable that the Robinson filter has retained slightly more background noise whereas the Hanning filter shows a fairly rigorous discrimination of all frequencies away from the central frequencies of 5-6 Hz.

Figures 3.37,38 ($V_{\text{red}} = 6.0 \text{ km s}^{-1}$) and 3.39,40 ($V_{\text{red}} = 3.5 \text{ km s}^{-1}$) show the results of application of both filters to the record section from Dunduff Quarry. A wider bandwidth was used due to the greater high frequency content of this section. As the unfiltered record section shows the best quality S-waves of any of the unfiltered sections (see figures 3.3,6), little improvement has been achieved except for a slight increase in the S-wave

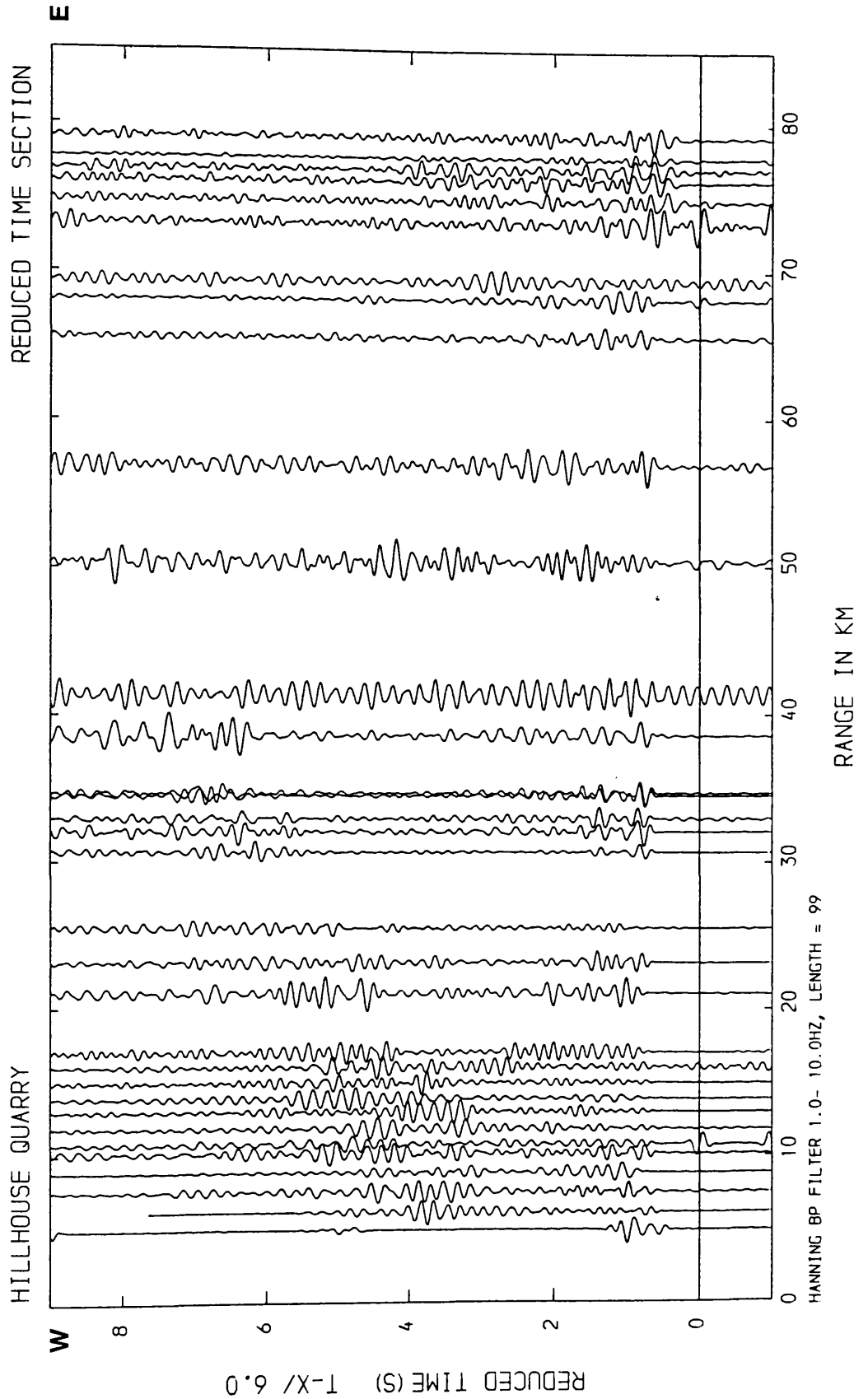


Figure 3.33 Filtered record section: Hanning BP filter.

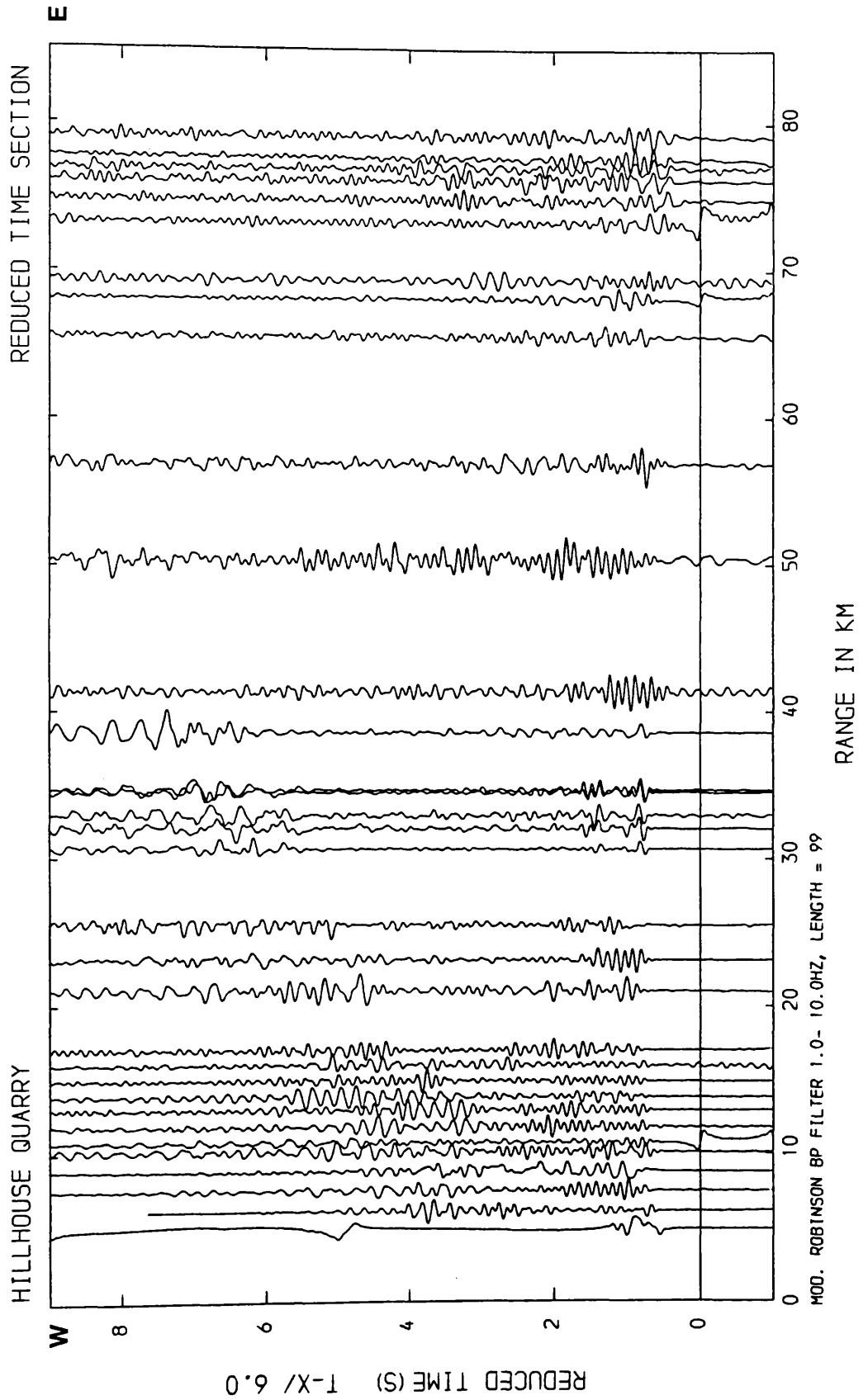


Figure 3.34 Filtered record section; two-sided, tapered Robinson BP filter.

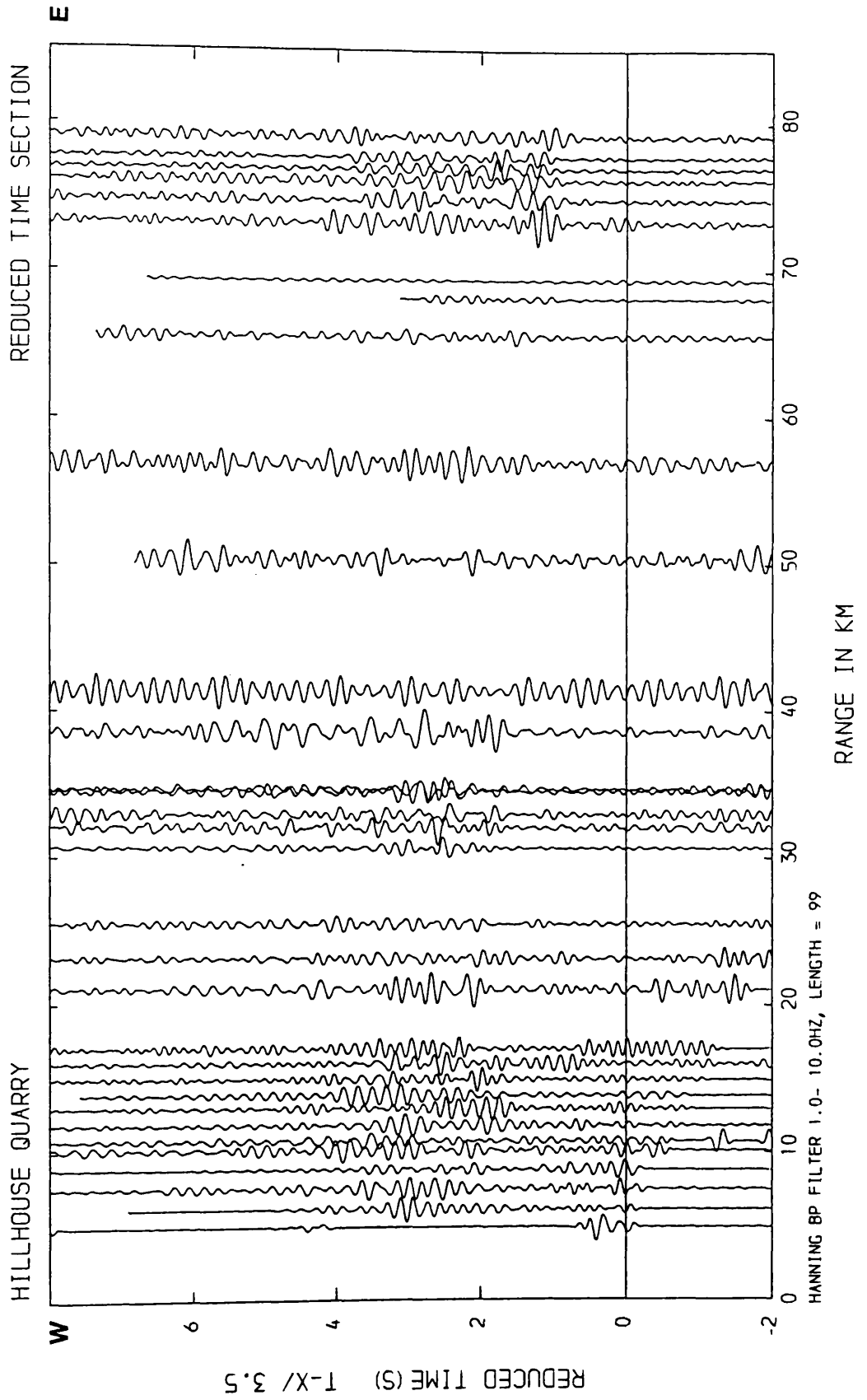


Figure 3.35 Filtered record section: Hanning BP filter.

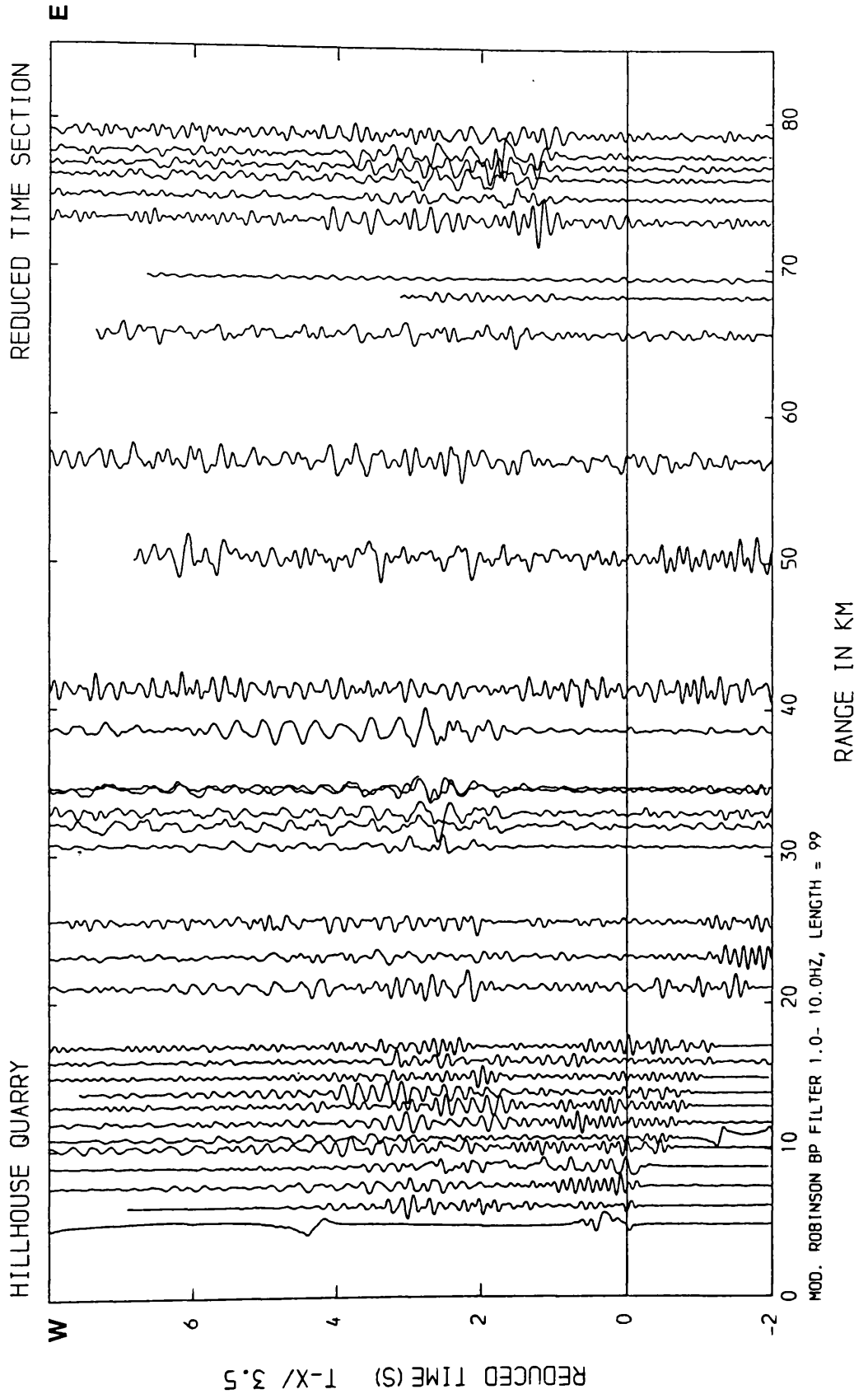


Figure 3.36 Filtered record section: two-sided, tapered Robinson BP filter.

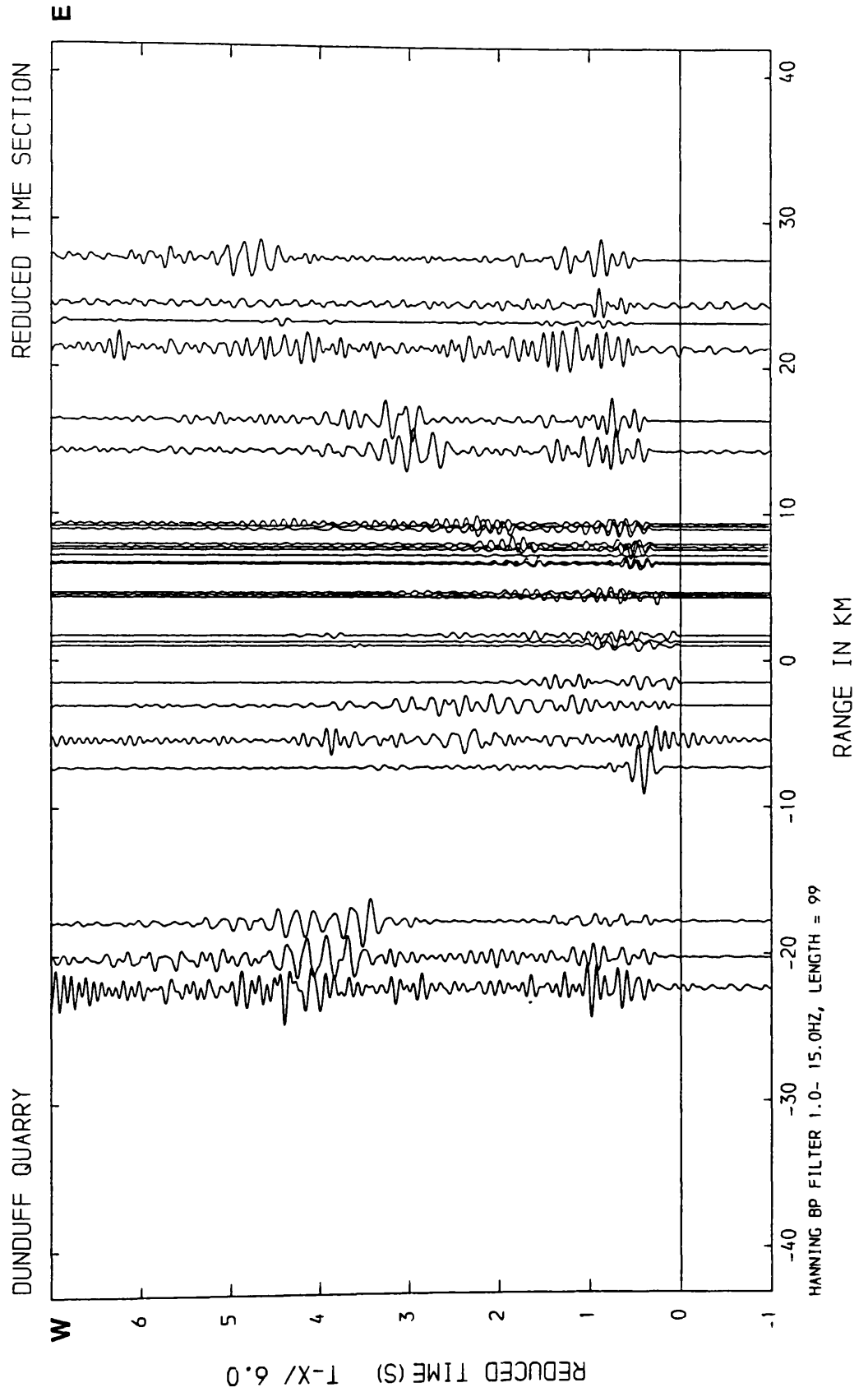


Figure 3.37 Filtered record section: Hanning BP filter.

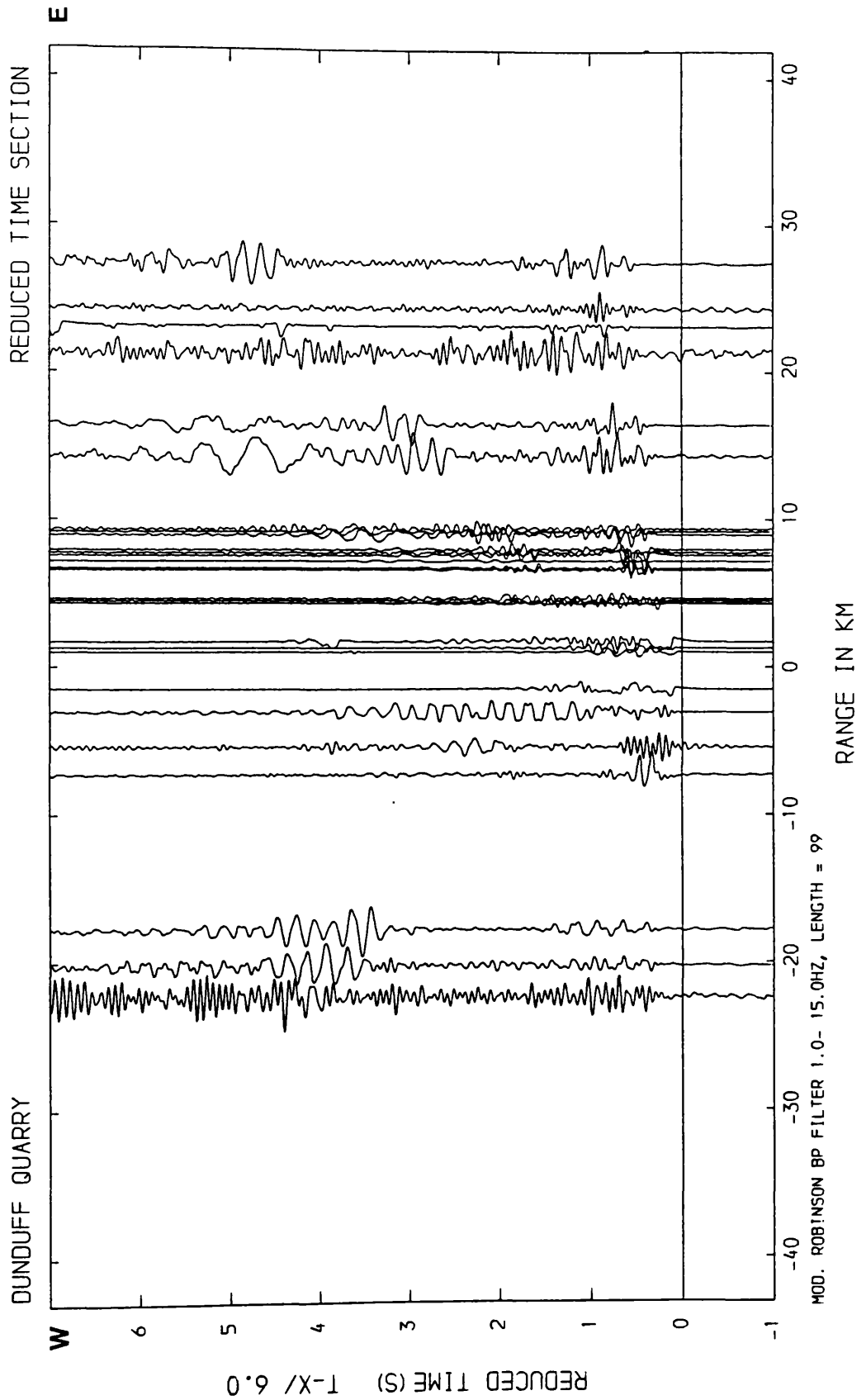


Figure 3.38 Filtered record section: two-sided, tapered Robinson BP filter.

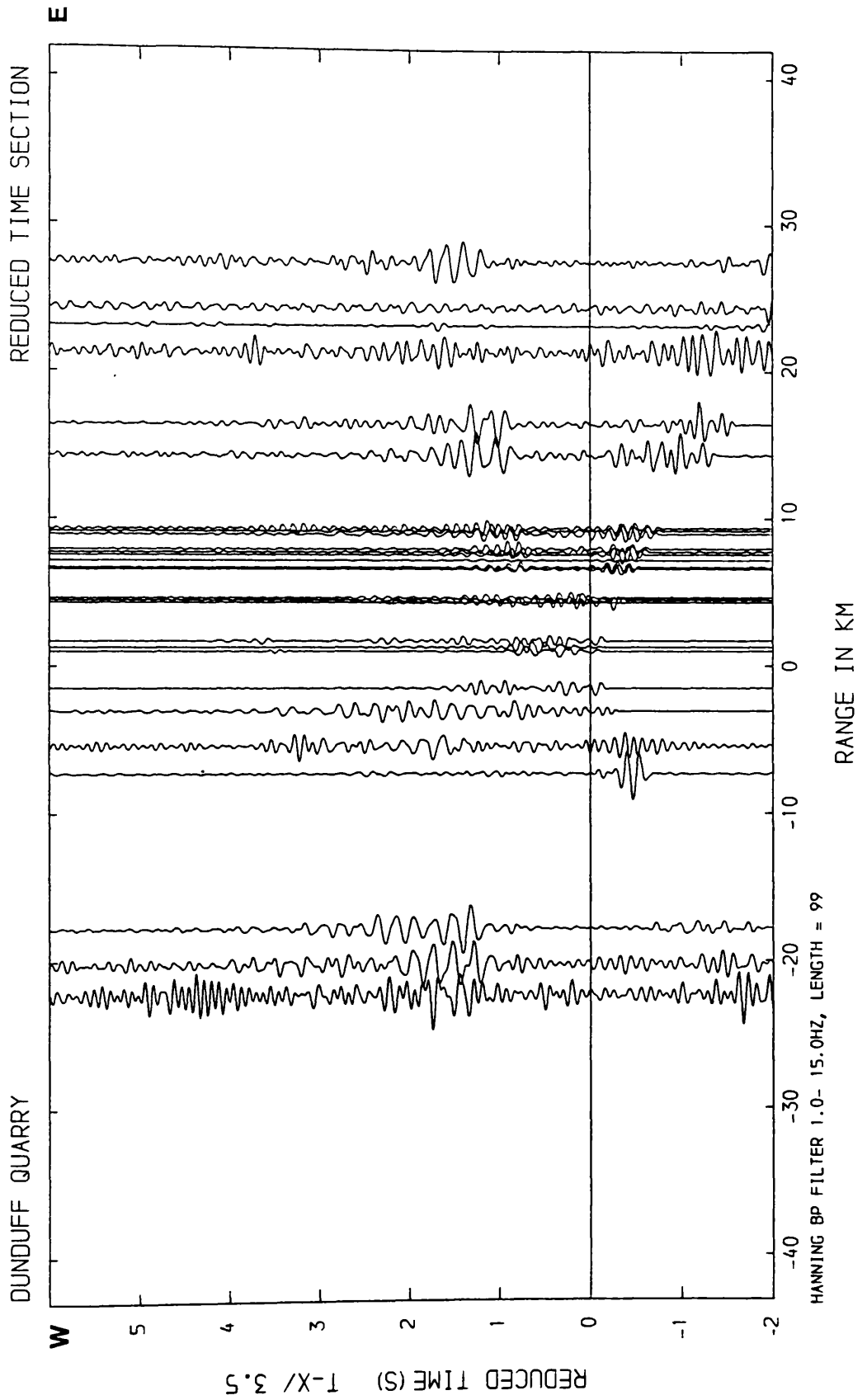


Figure 3.39 Filtered record section: Hanning BP filter.

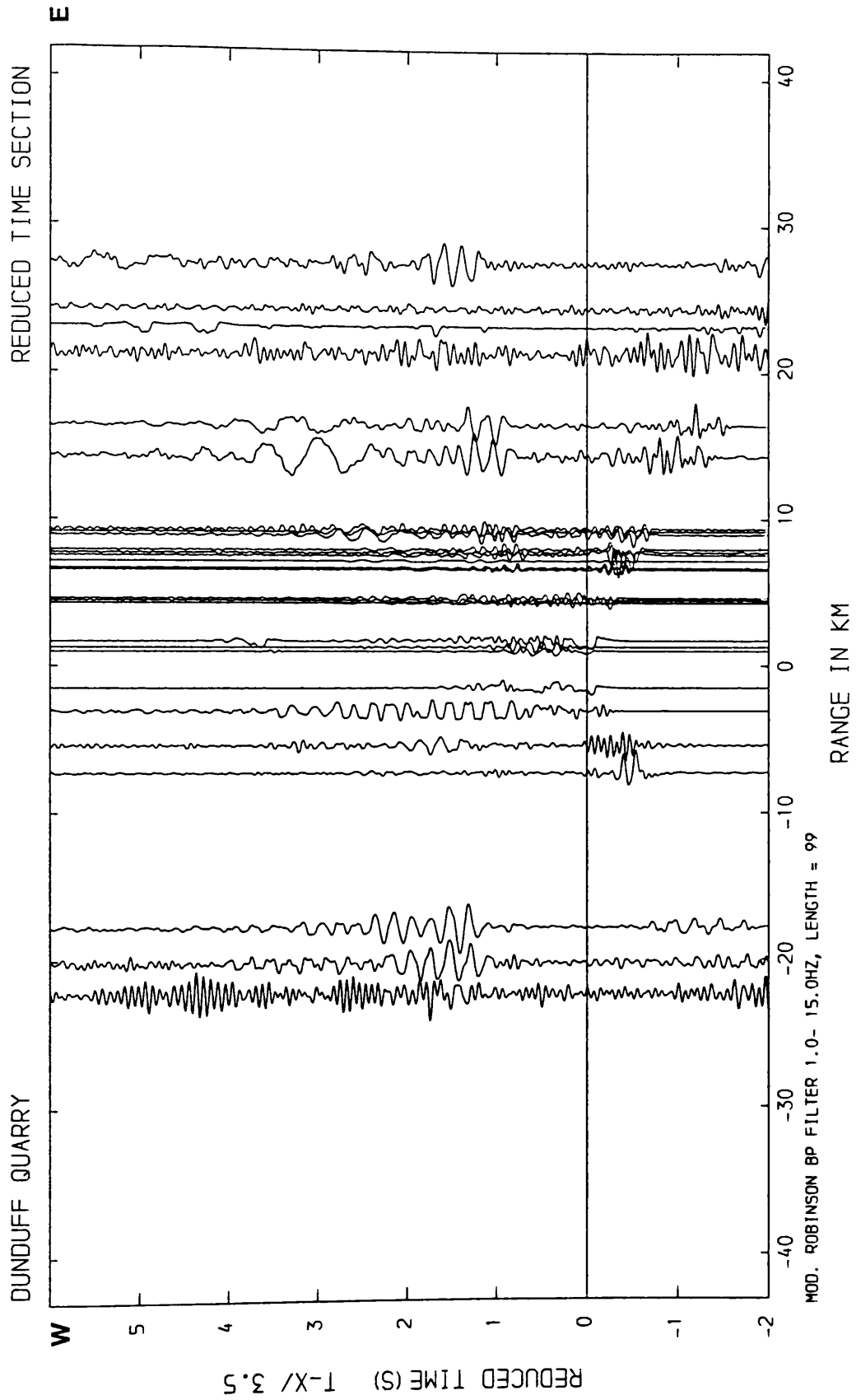


Figure 3.40 Filtered record section: two-sided, tapered Robinson BP filter.

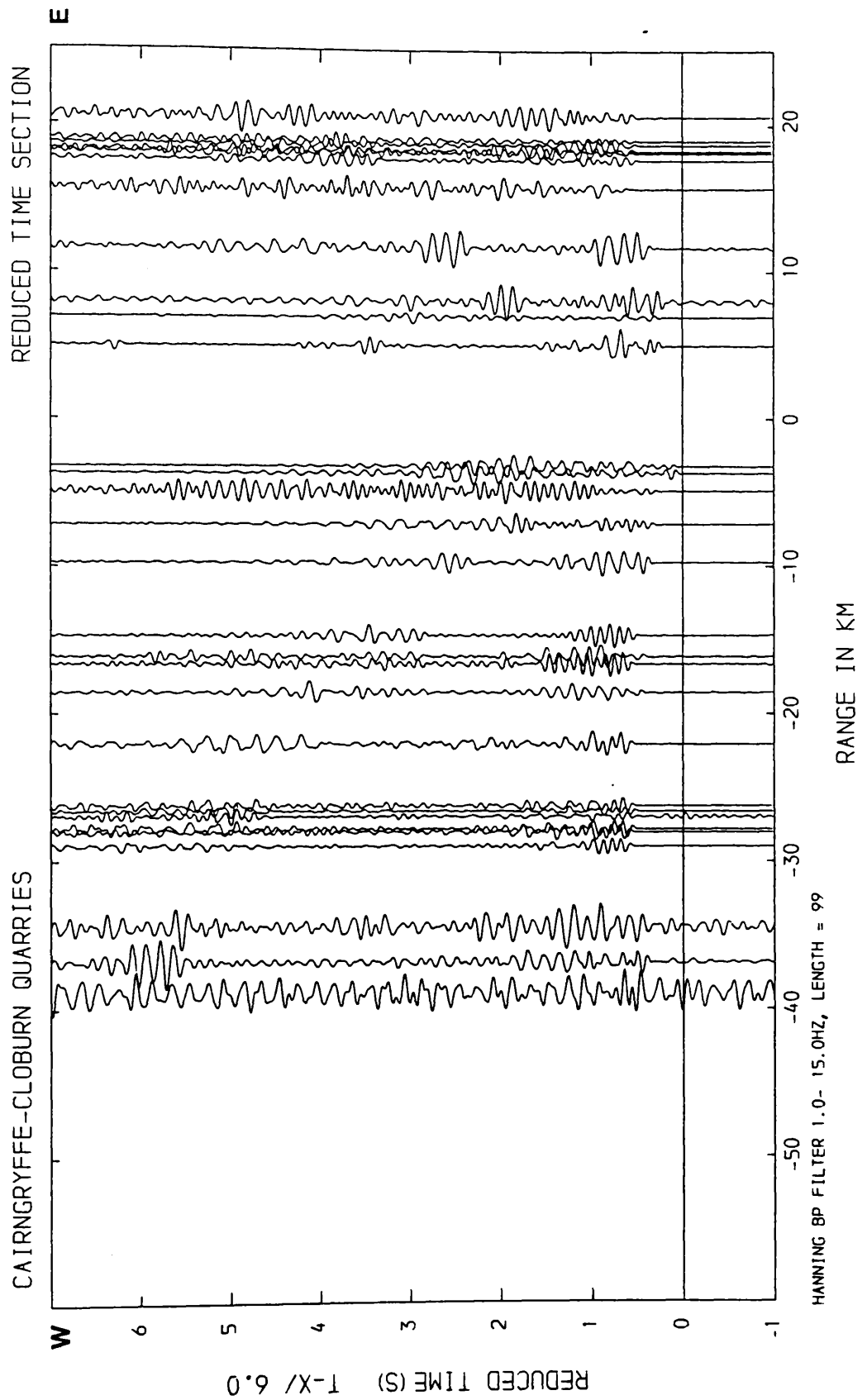


Figure 3.41 Filtered record section: Hanning BP filter.

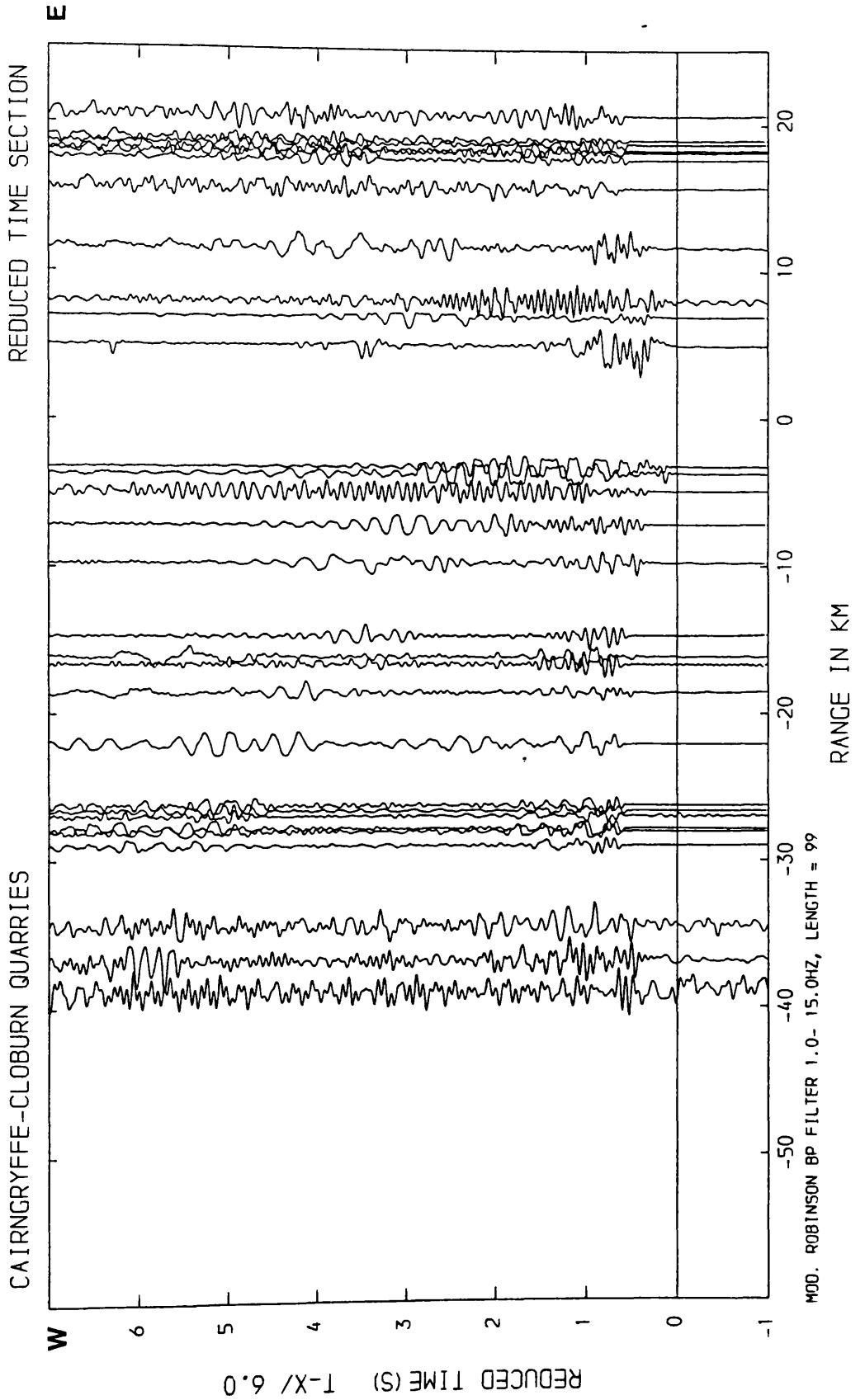


Figure 3.42 Filtered record section: two-sided, tapered Robinson BP filter.

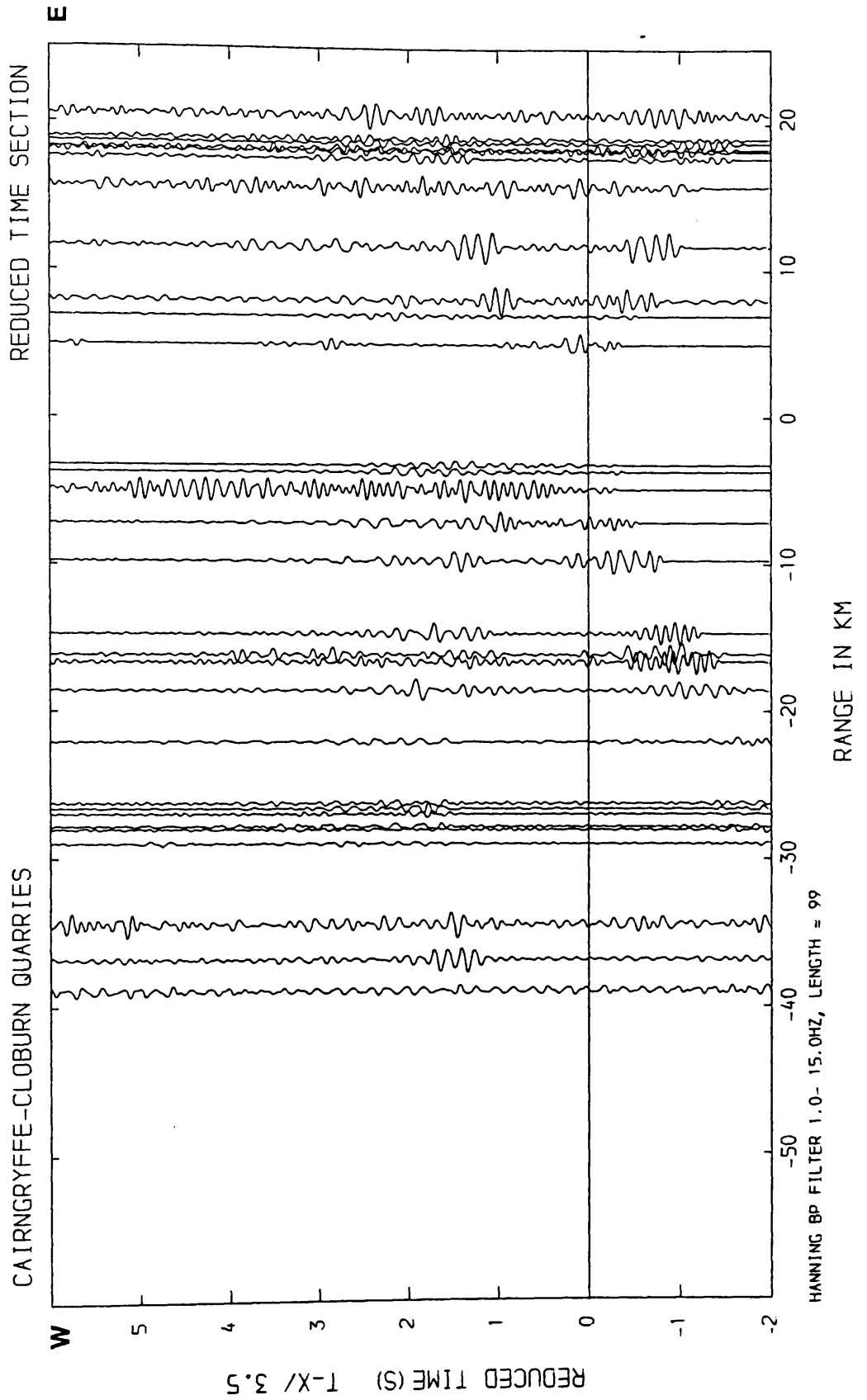


Figure 4.43 Filtered record section: Hanning BP filter.

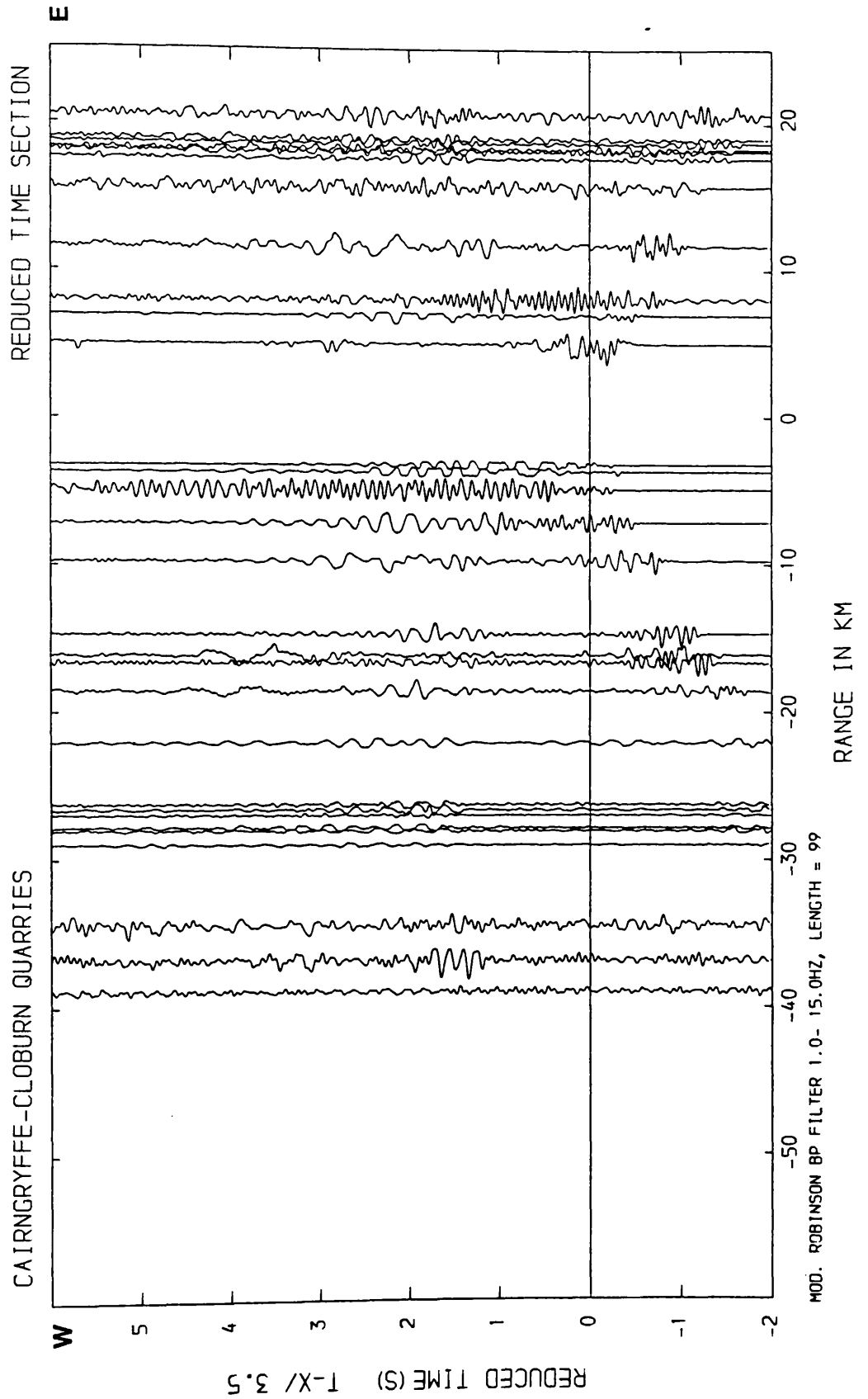


Figure 4.44 Filtered record section: two-sided, tapered Robinson BP filter.

signal noise ratio. Again, the Hanning filter proves to be marginally more effective.

Figures 3.41,42 ($V_{\text{red}} = 6.0 \text{ km s}^{-1}$) and 3.43,44 ($V_{\text{red}} = 3.5 \text{ km s}^{-1}$) show the results of the application of both filters to the Cairngryffe - Cloburn record section. Most of the traces in the unfiltered section (figures 3.4,7) do not show any clear S-wave energy and contain large amounts of higher frequency noise. The filtered sections, and in particular using the Hanning filter, show a considerable reduction in this noise giving the best improvement in the S-wave signal/noise ratio of all the sections.

3.3 The time-distance data

Each time-distance pick was acquired originally as a pair of Ordnance Survey grid coordinates with elevation, and an arrival time for the first break on the oscillograph record. Measures of the observational uncertainty are included in all quantities. A program was written (TX3E; listing Appendix 6) to take source and receiver parameters for each recording, and calculate the range, travel and reduced times with standard errors for each receiver.

Groups of data from the same source recorded on separate days could be plotted on the same diagram as well as other data groups from different sources but on the same profile. The 3-second unfiltered record sections have the analogue P-wave pickings (figures 3.45-47) superimposed for direct comparisons. For various reasons, a few analogue records were not digitised and so their position is marked on the 3-second record sections by crosses only. Also across the LES and BTN arrays, the high density of traces has meant that some have been omitted for clarity. However all traces for these events are shown in figures 3.12,13,15,17,18. The internal consistency of data recorded on different days in the same line was monitored by rerecording several sites. If the data are consistent, then the variation between records obtained at the same site on different days should be within the

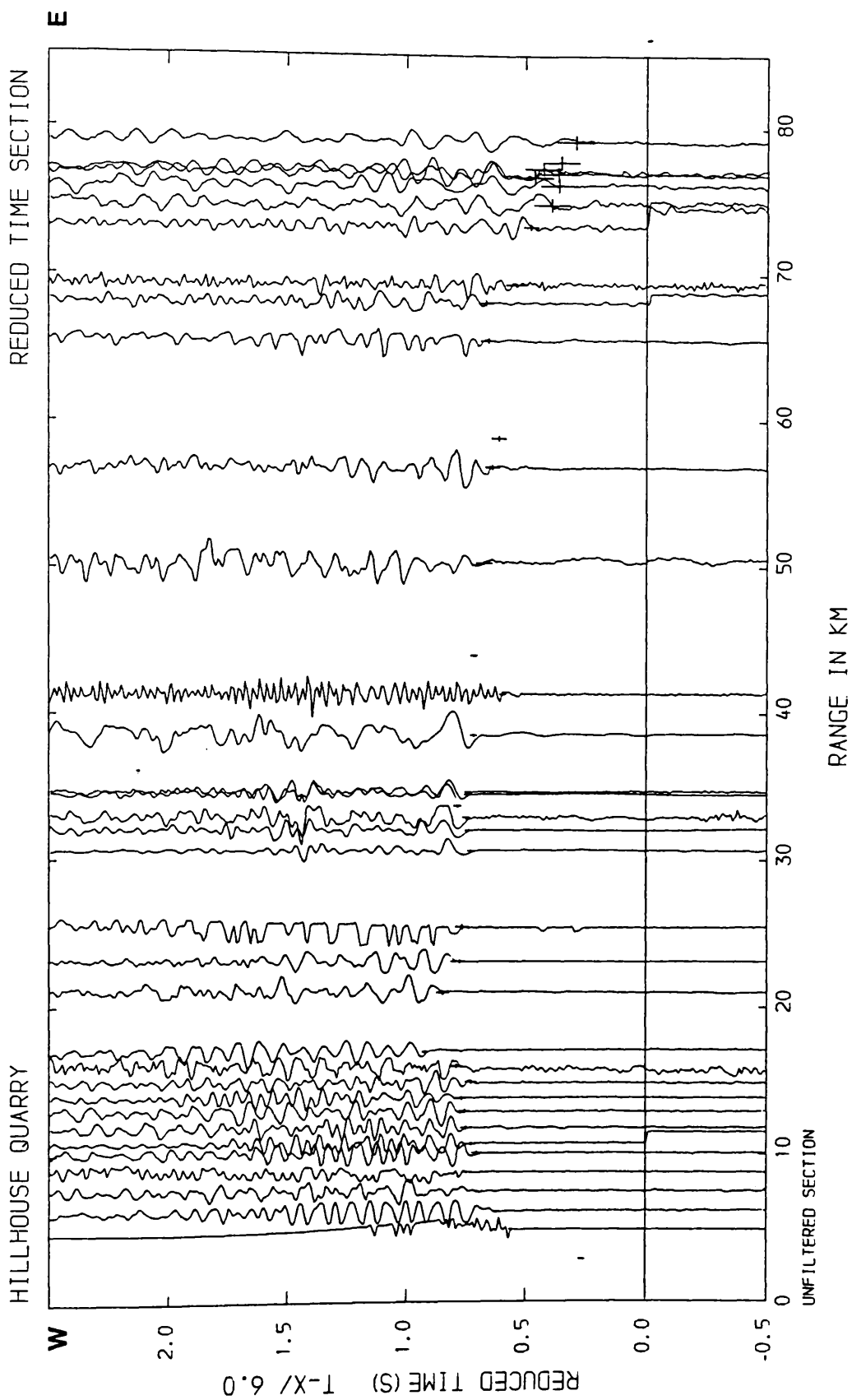


Figure 3.45 Unfiltered record section with first break picks.

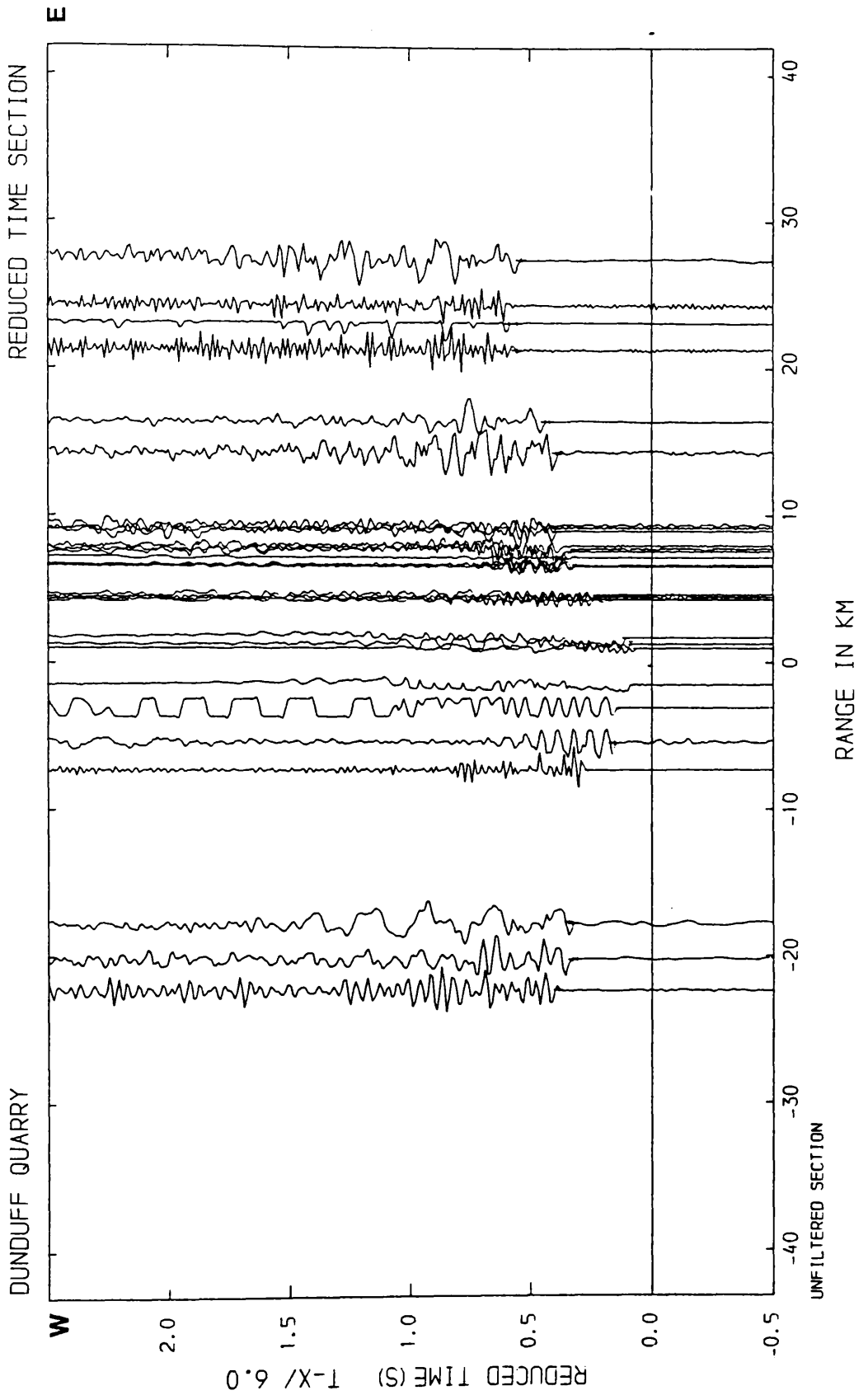


Figure 3.46 Unfiltered record section with first break picks.

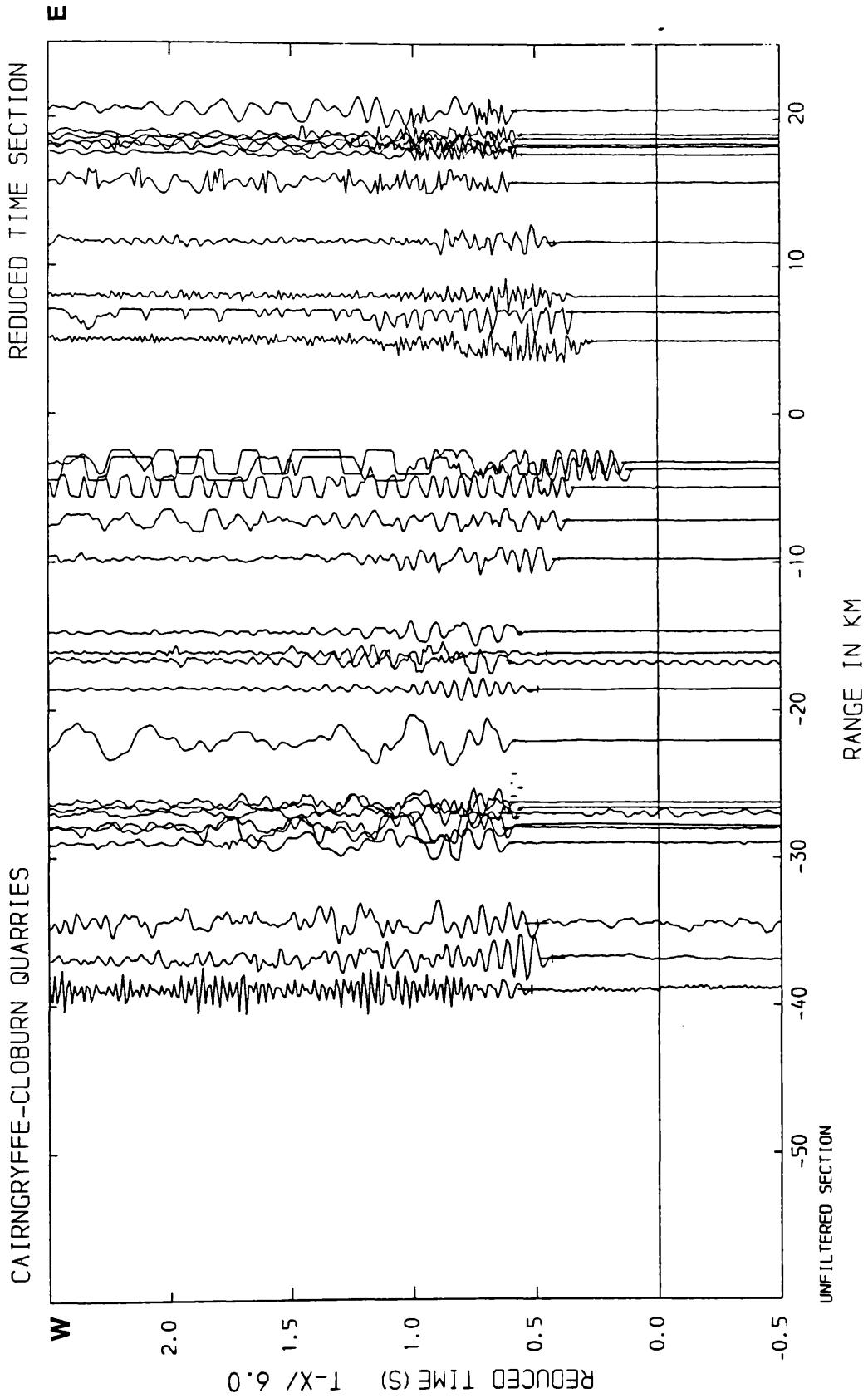


Figure 3.47 Unfiltered record section with first break picks.

observational errors. Time - distance sections from the three quarry lines (figures 3.48-50) show all the data recorded and the magnitude of the tie-in errors produced by this method of recorded. Qualitatively, the tie-in errors do not appear unreasonably large. Statistically, the mean observational error for all records is 0.008 ± 0.004 (s^2 , $n=133$), whereas the mean of the tie-in variance is 0.017 ± 0.019 (s^2 , $n=18$) - a random set of variances. When one large tie-in discrepancy is removed (85 ms at site 8A from Cairngryffe quarry 1982), the mean becomes 0.013 ± 0.009 (s^2 , $n=17$). This mean value is still weighted by a few large variance values but is now in line with the observations on figures 3.45-47. The mean tie-in error (for $n=17$) is marginally outwith the field of observational errors but there is some overlap of error ranges, allowing the general conclusion that the data is internally consistent.

The number of recording sites providing data for these profiles is Hillhouse 39, Dunduff 31, and Cloburn-Cairngryffe 30. This gives average station spacings with regards to the range of coverage for each quarry line of 2.0 km, 1.6 km, and 2.0 km, respectively. These compare well with previous work of this type carried out in the Midland Valley and elsewhere (eg LISPB 3 km, Bamford et al 1976; SUSP 2 km, Warner et al 1982; SWESE 2-3 km, Brooks et al 1984; S Wales-Bristol Channel 2-5 km, Mechie & Brooks 1984).

Occasionally, apparent shear wave arrivals were of sufficient strength and coherency on the analogue records to be picked with reasonable confidence. Where sufficient picks are present in any direction to make a profile from the same source, these have been incorporated into the dataset and interpreted accordingly. Figures 3.51-53 show picks of all clearly identifiable S-wave arrivals with observational errors.

A list of all travel times is given in Appendix 3. These standard data groups have been used with all the interpretive processes to compare model

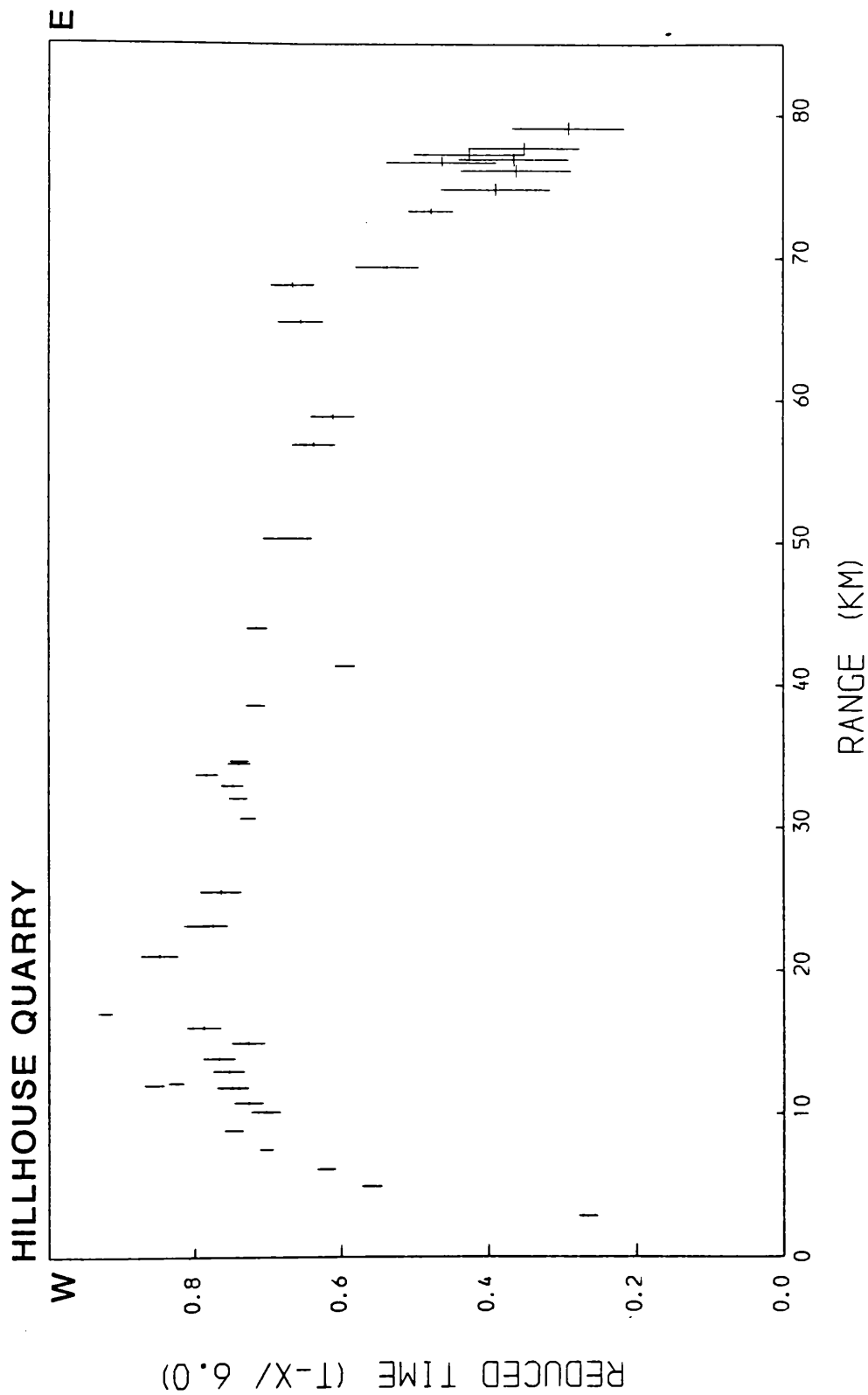


Figure 3.48 First break picks from analogue record sections.

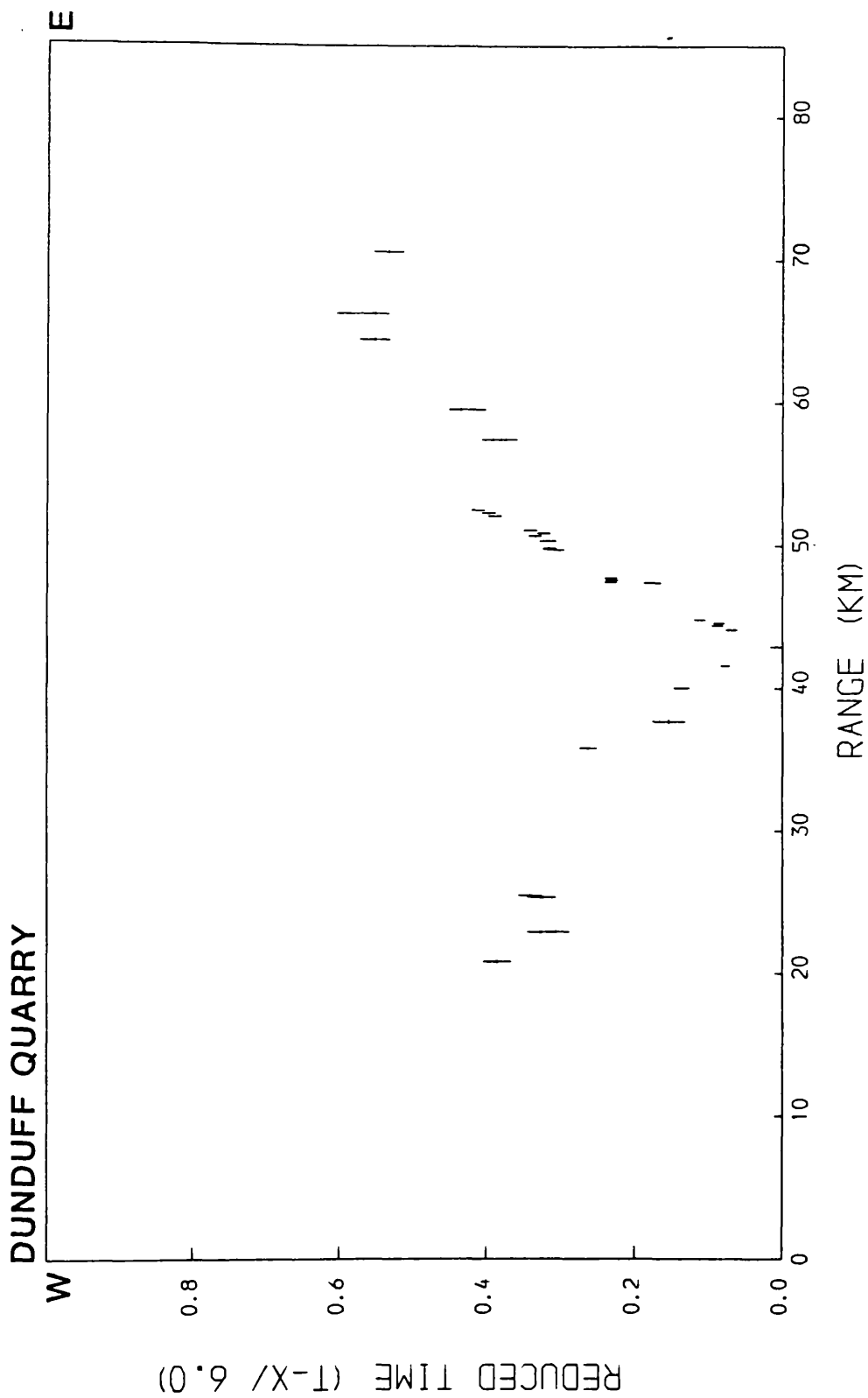


Figure 3.49 First break picks from analogue record sections.

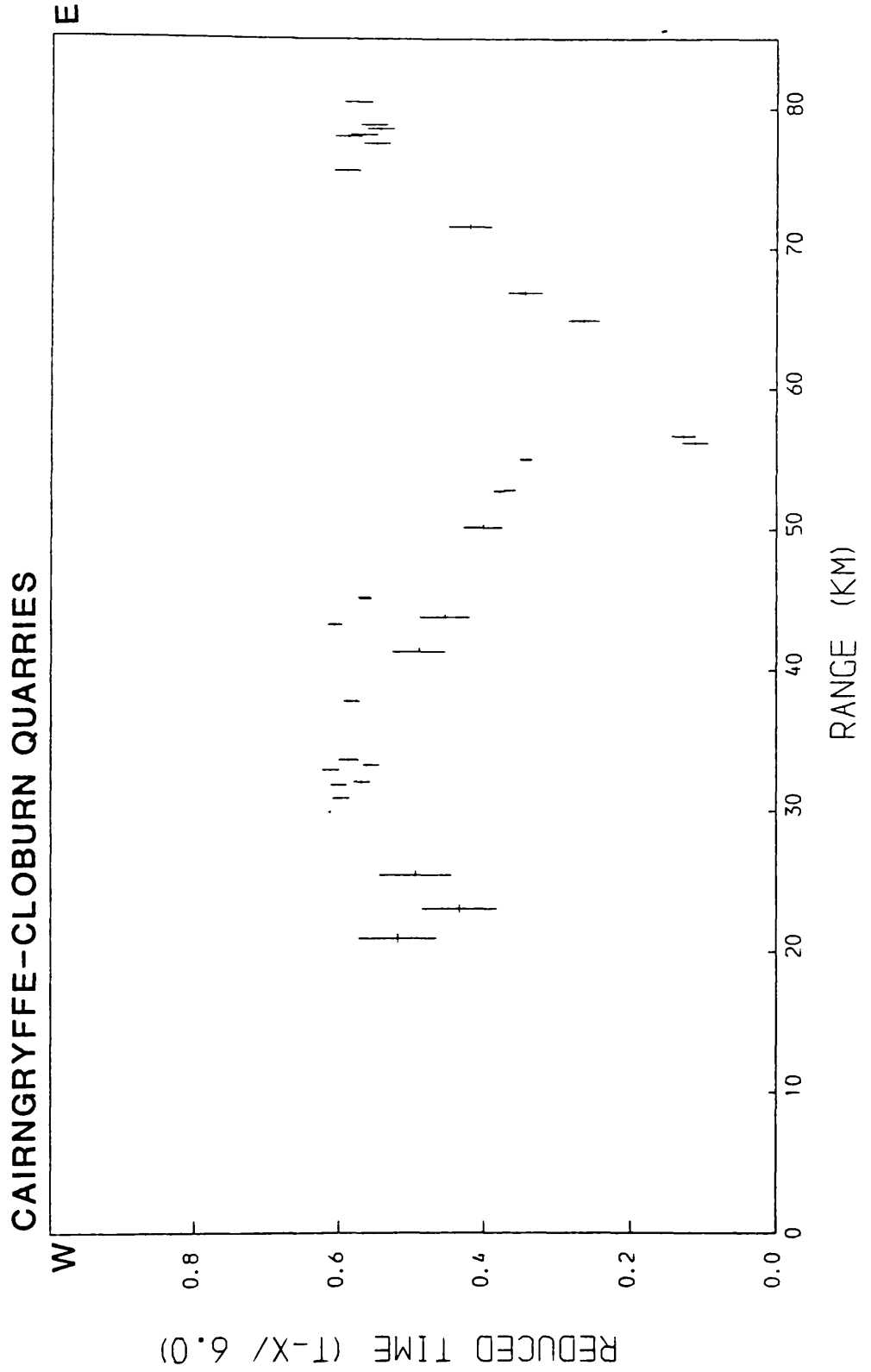


Figure 3.50 First break picks from analogue record sections.

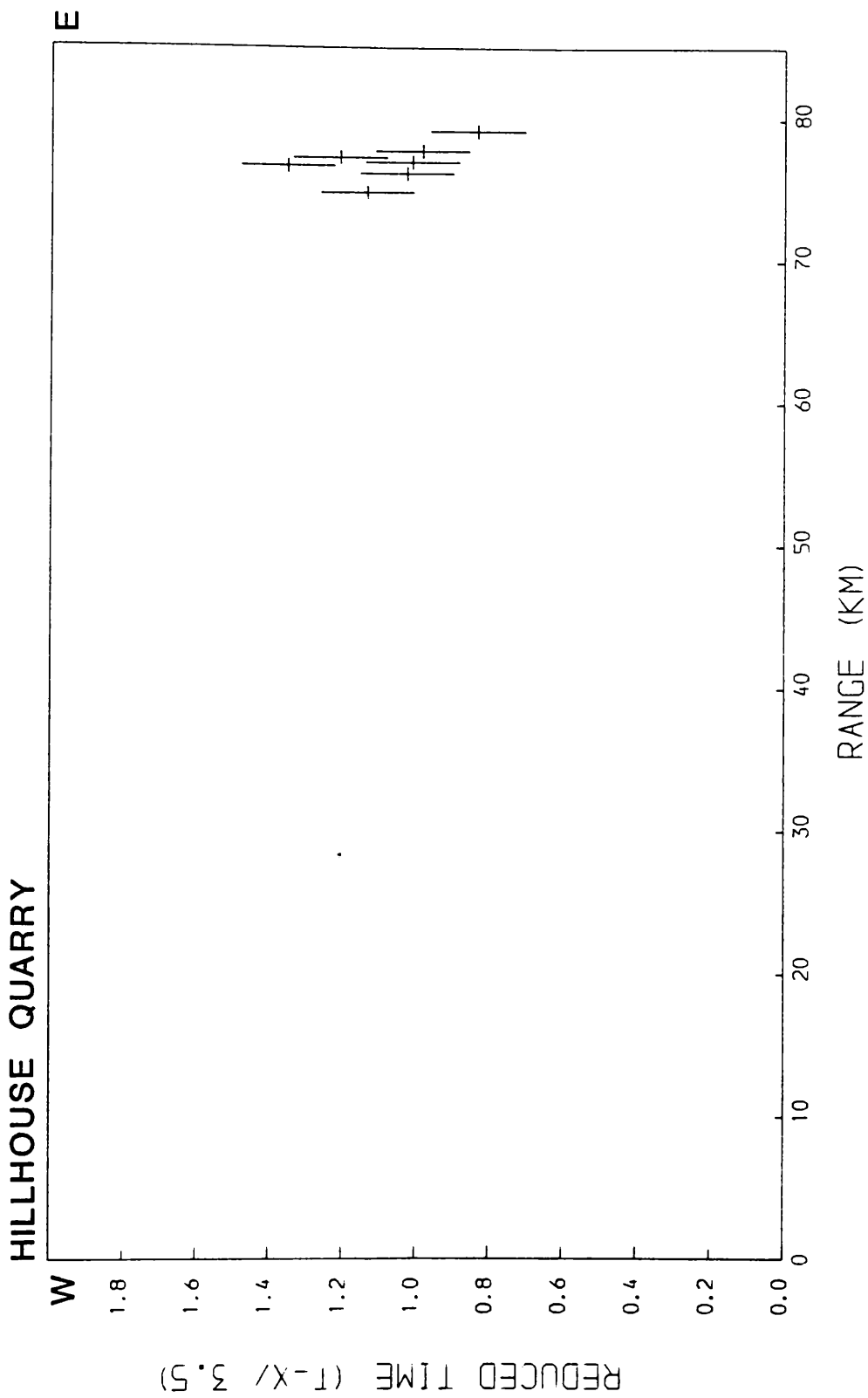


Figure 3.51 Shear wave picks from analogue records.

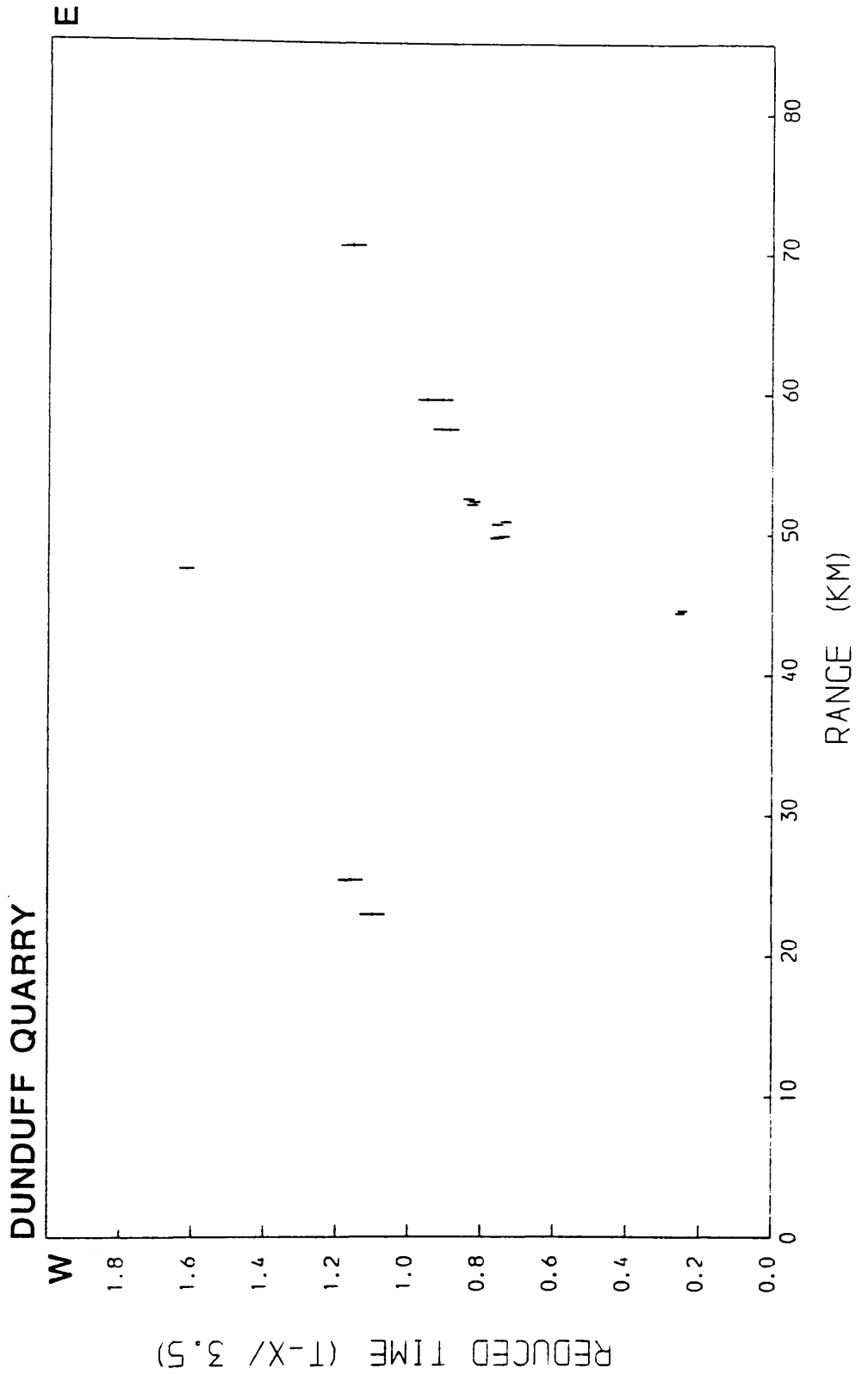


Figure 3.52 Shear wave picks from analogue records.

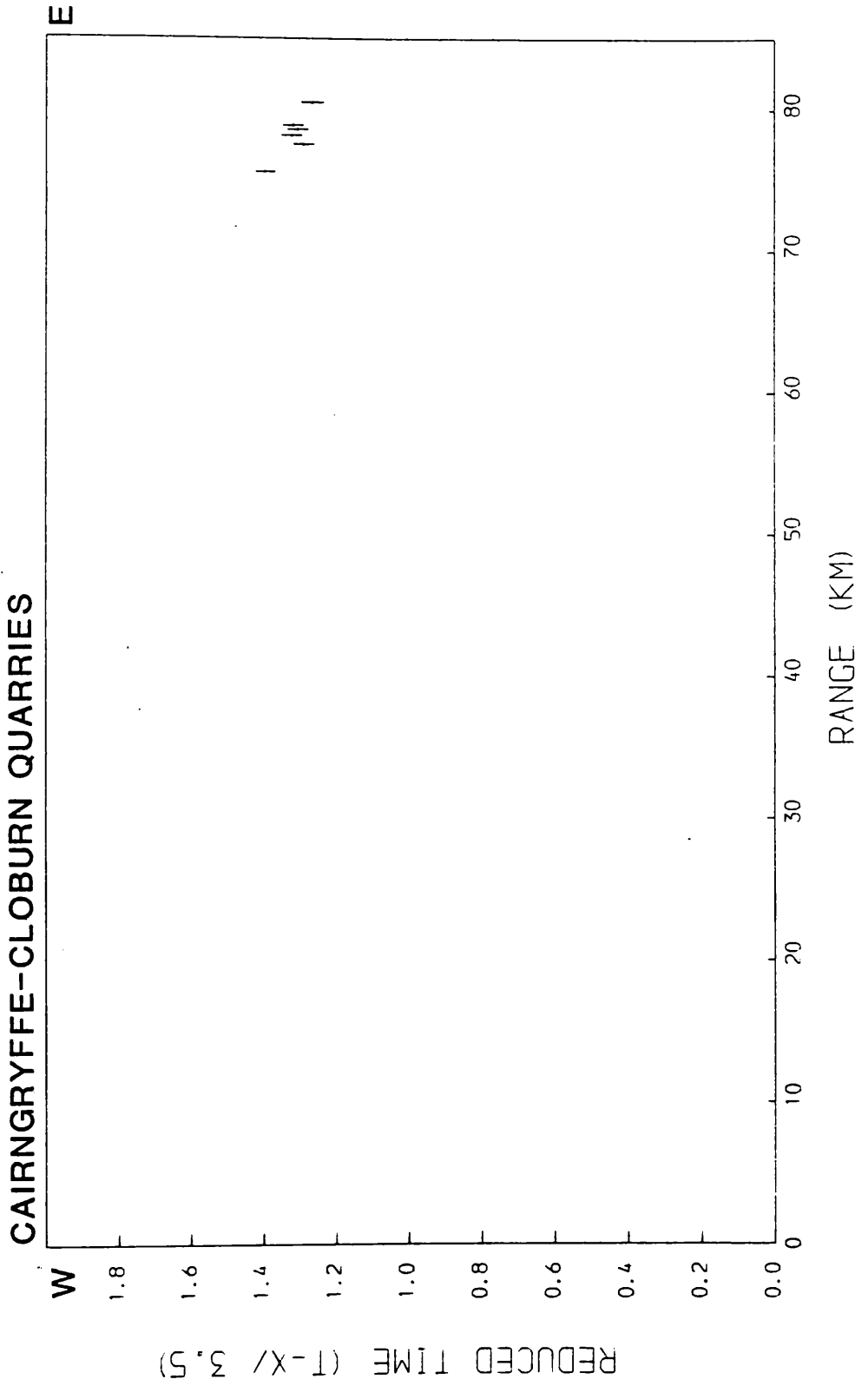


Figure 3.53 Shear wave picks from analogue records.

time distance data with the original field data.

As mentioned in section 3.2.1, secondary arrivals in particular P-wave arrivals are very poorly recognised (if at all) on the three profile record sections. The main reason for this non-detection of secondary arrivals lies in the nature of the source used in this study. Quarry blasts have some advantages over customised shots. They are cheap (free), repeatable (although recording over several months (or years) can lead to location problems unless the quarry resurvey the active faces regularly), and their use of large amounts of ammonium nitrate slurry provides a high proportion of low frequency energy in the source, so giving the potential for recording out to quite long ranges even though the amount of available recording equipment at any one time was limited. There are some logistic disadvantages, but from the point of view of the record sections and their interpretation, the most serious disadvantages are in the control of amplitudes between different blasts and in the variability and extreme length of the generated source wavelet.

Commercial quarry blasts consist of a large number of holes aligned parallel to, and set back by around 5 m from, the working face. To achieve the most effective yield of rock, the holes are fired in sequence starting at one end of the face, with each hole detonation being delayed, usually by 20 ms, relative to the preceding hole. The number of holes used and the weight of charge in each hole varies according to the needs of that particular blast so that at least one station must be held in common for all repeated blasts to allow amplitude and wavelet shape correlation across the profile. Logistic restrictions precluded the use of this technique here.

The use of delays produces a ripple blast creating a complex source wavetrain which is normally around 500 ms in length, but can be longer. The only useable part of the wavetrain is the energy from the first delay or hole. The remaining energy is dissipated as a poorly controlled series of

constructive and destructive interference.

Other workers, notably at the Global Seismology Unit of the B.G.S., have expended much time and effort, using well controlled quarry blast data, into a method of reliably predicting an accurate far-field signature for the source wavelet, in the hope that the deconvolution of this operator with record traces would result in the efficient collapsing of the total source energy back into a single, simple pulse at the onset. To date, this work has not been entirely successful mainly due to the problems of predicting a far-field signature (A. McDonald, private communication), although future work may provide a means to overcome this problem.

Until then, quarry blasts will remain a useful source of P-wave first breaks often with good shear and surface wave energy, but limited in resolution compared with customised shots.

Chapter 4 Interpretation

4.1 Interpretation of the surface structure

4.1.1 Introduction

As this dataset was built up over a period of almost three years, so similarly the interpretation expanded as a wider and fuller coverage of this area became available. The early data were predominantly single-ended, and so the conventional reversed-coverage methods of interpretation were not suitable. Discussion of the interpretation procedures used on this dataset will concentrate initially on the direct arrivals through the topmost rock layer, since a knowledge of near surface velocity structure is critical to the later interpretation of deeper structure.

Two differing interpretational approaches are described involving forward and inverse modelling techniques. The WHB method provides a means of direct inversion from (T,X) to (V,Z) , but is limited in its operation to areas where the vertical velocity gradient is always positive. The plane-layer method provides an iterative means of forward modelling which can incorporate variations in the vertical velocity gradient. Both methods were applied here to provide a measure of the consistency of the interpretations for each set of field data rather than to provide any comparisons between interpretational methods.

4.1.2 Wiechert-Herglotz-Bateman inversion

4.1.2.1 Method

It was noticed that most of the travel time data corresponding to direct arrivals (a_s) and recorded across the Lower Old Red Sandstone and Silurian sediments over, and to the E, of the Lesmahagow Inlier showed a continuous velocity increase with range, independent of azimuth, over the first 10 or 15 km (see figure 3.1 for site and quarry locations). Thus these data were suitable for direct inversion with a velocity-depth model using a solution to

the Wiechert-Herglotz-Bateman (WHB) integral (Grant & West 1965; p139). This represents the velocity V , at a depth Z , defined as the turning point of a ray received at a distance X from the source as:

$$Z(v) = \int_{x=0}^{x=X} \cosh^{-1}(V * dt/dx) dx$$

where $V = (dx/dt)_{x=X}$

A program has been written (program WHB (listing Appendix 6): a modified version of an original program written by J. Hall, Glasgow University) which accepts a series of travel times corresponding to equal increments of range away from the source, and obtained from a pre-smoothed curve of field data. The program checks that the model-travel-time data have continuously decreasing time increments. If not, the relevant values are incrementally reduced until this condition is met. At the end of the calculation sequence, the model and field travel time data are plotted on the same graph for comparison.

4.1.2.2 Application of the WHB method to field data

The following figures show the application of this technique to direct arrival data (a_g). All field time-distance data are presented with the computed observational errors, and all model time-distance data as a series of straight line segments.

The sampling interval of these time-distance curves for inversion by the WHB method reflects the density of data in each profile. For all the data sets modelled using the WHB method, the sampling density was determined by the number of field points to be modelled and range of data coverage across each profile. Obviously, detail is lost using a coarse sampling interval but where data was limited or data coverage sparse, it was felt that loss of

detailed resolution was preferable to over-modelling.

The data recorded to the E of Dunduff quarry (see locations in figure 3.1) were the first set of data recorded in this project and have the advantage of reasonably predictable lithological as well as stratigraphical homogeneity across the region of interest (cf geological section figure 3.2). It was expected that Silurian sediments similar to those cropping out in the Lesmahagow Inlier would be present beneath the line at depths of around 1 km. Only the first 10 km of these data will be considered here for, as with the line to the W of the quarry, there is a discontinuity in the time distance data suggesting a complexity either laterally or with increasing depth under this part of the line.

A smooth curve was fitted through the data as shown in figure 4.1a giving the V-Z curve in figure 4.1b. This shows a high surface velocity of around 4 km s⁻¹ with an initial velocity gradient in the top 0.5 km of about 1 s⁻¹ reducing with depth to 0.6 s⁻¹ below 1 km depth, while 5 km s⁻¹ is reached at only 0.6 km depth.

As described in 3.2.1 and shown in figure 3.3/6 a number of good quality S wave arrivals were picked from the data recorded east of Dunduff. It was considered worthwhile to model these because of the considerable potential in lithological discrimination with the use of V_p/V_s (or Poisson's ratio) compared with V_p alone. V_p/V_s varies among minerals from 1.48 for quartz to around 1.85 for hydrated minerals (Alexandrov & Ryzhova 1961a,b; Alexandrov & Ryzhova 1962; Christensen & Fountain 1975), and so greater lithological discrimination is possible on the basis of this extra parameter. Picking of S-waves at sites close to a quarry source involves the difficulty of distinguishing the S-wave arrival from the generally high energy surface waves following close behind in time. Assuming that the highest mode surface waves will have a velocity of 0.9 times that of the S-waves, then the late arrivals at around 7 km in figure 4.2a could be explained as mis-identified

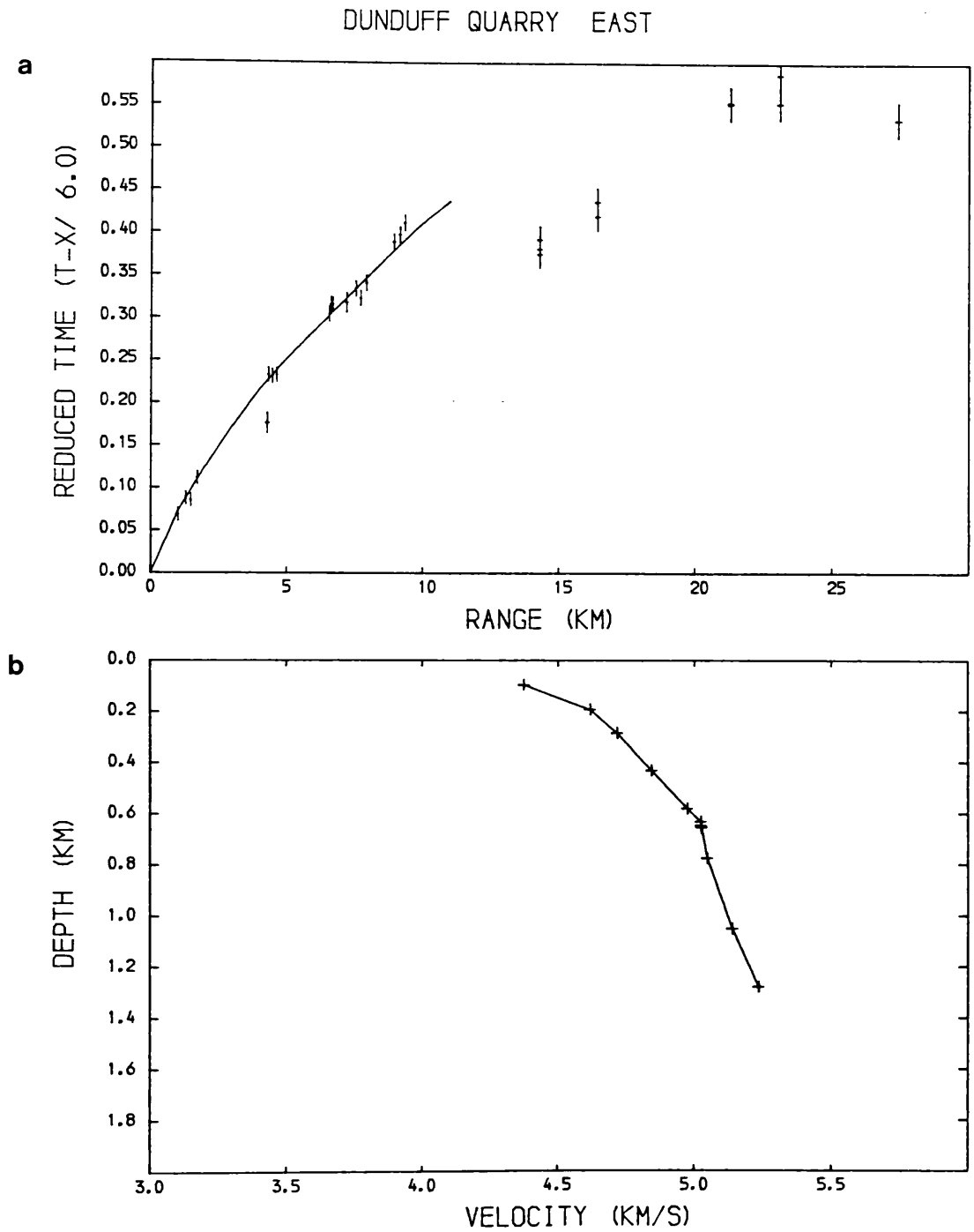


Figure 4.1 Time-distance data (with st. errors) and modelled WHB interpretation, along with the modelled WHB velocity-depth curve.

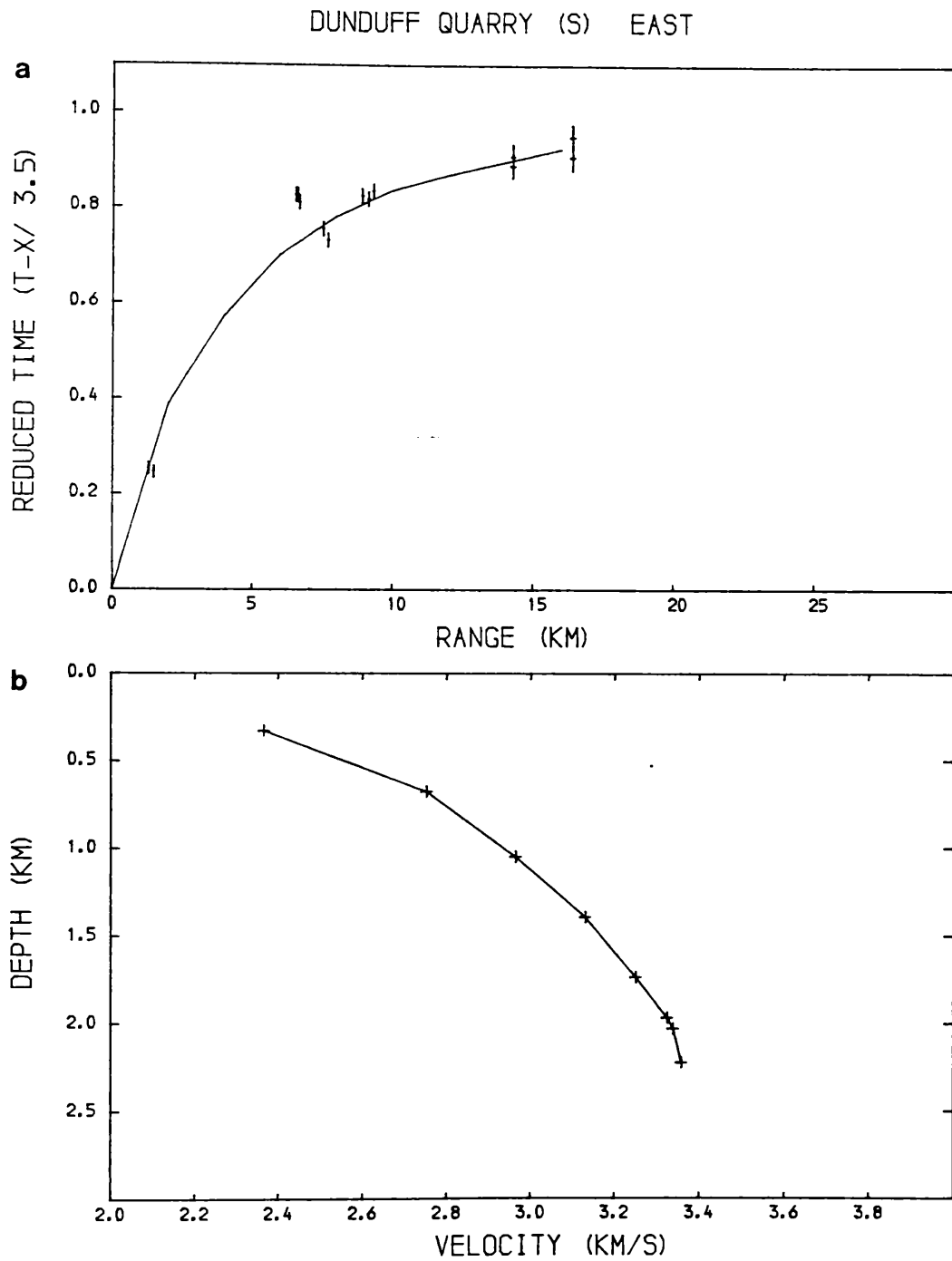


Figure 4.2 Time-distance data (with st. errors) and modelled WHB interpretation, along with the modelled WHB velocity-depth curve.

surface waves. Elsewhere on this part of the line, the separation is large enough to be noticeable.

A smooth curve through the data in figure 4.2a gives the V-Z curve in figure 4.2b. This again shows a high initial velocity gradient of around 1 s^{-1} , reducing with depth, and reaches 3 km s^{-1} at a depth of just over 1 km.

A more useful diagram is figure 4.3, where both P and S-wave V-Z curves have been combined onto one diagram and plotted along with the V_P/V_S and Poisson's ratios. Both the V_P/V_S and Poisson's ratio curves show a sharp decrease over the initial 0.4 km depth and then flatten out with increasing depth. The initial gradient relates to the S-wave velocity gradient being higher than the P-wave gradient near the surface and is due to the closure of flat cracks and larger scale fractures within the sandstone, and the corresponding reduction in porosity.

Cairngryffe and Cloburn quarries (locations figure 3.1) are adjacent quarries working the same felsite intrusion, intruded into the base of the local Lower Old Red Sandstone, on either side of a hill. The working faces are separated by no more than 0.5 km and in the direction of the Hillhouse - Broughton profile, the effective separation is less than 100 m. For all purposes, the two quarries have been assumed to be at the same point on the profile.

The data recorded to the W of Cairngryffe quarry (figures 4.4a, b) comprise four temporary stations, closest to the quarry and defining the direct arrival, and the LES array where the recorded apparent velocity is 5.95 km.s^{-1} (Appendix 4.4,5). The first point, at 5 km range, is seen to be around 50 ms slower than expected from the predicted model. This station was sited on boulder clay overlying Upper Old Red Sandstone sediments and around 20 m from the site of a shallow B.G.S. borehole giving the depth to rockhead as 12 m (see figure 3.1). The Upper Old Red Sandstone sequence here is thin but has

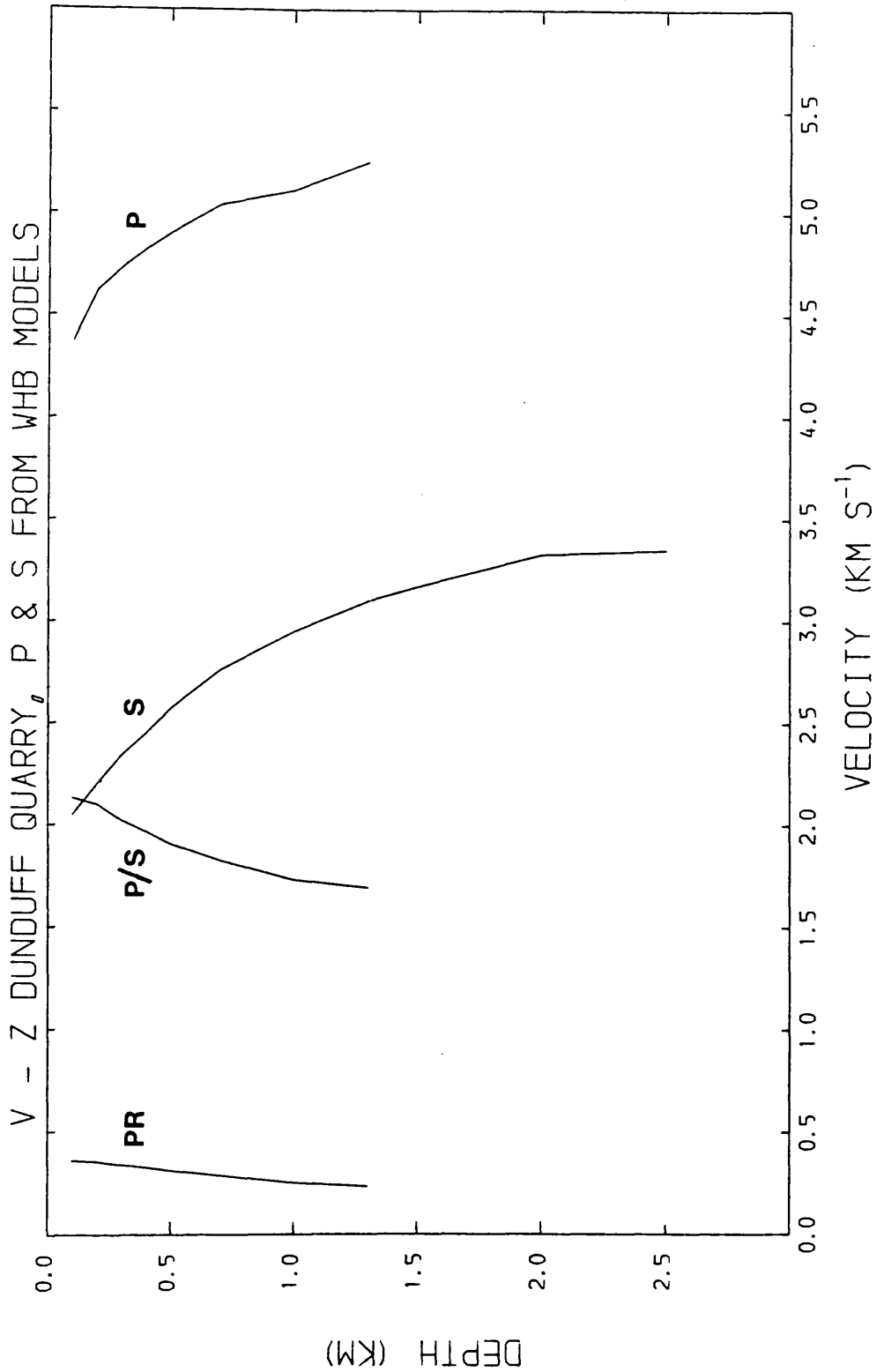


Figure 4.3 Combination of the WHB interpretations of Figures 4.1/2 giving V_P/V_S and Poisson's ratio variations with depth for the area to the east of Dunduff quarry.

CAIRNGRYFFE QUARRY EAST 26 AUG 1982

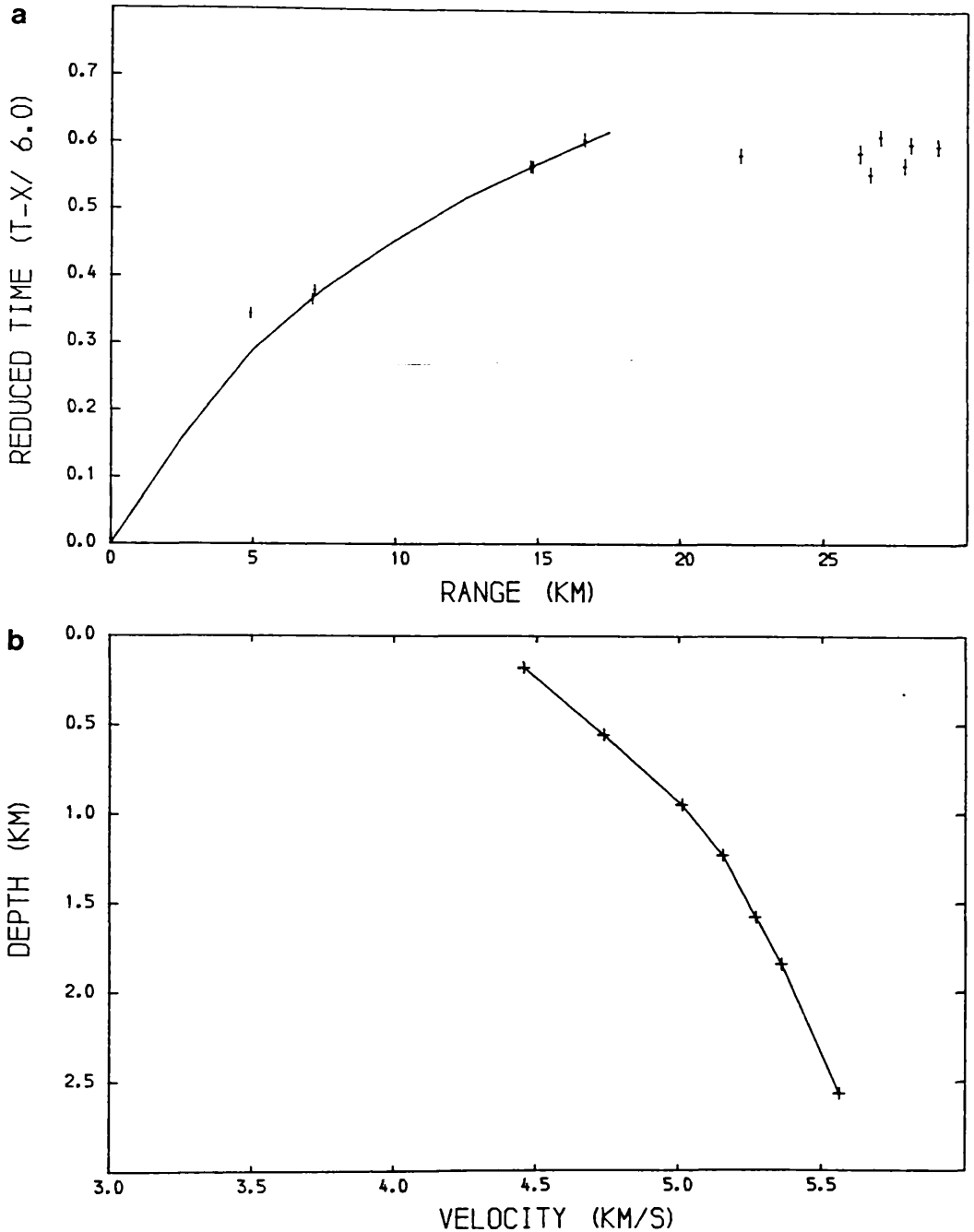


Figure 4.4 Time-distance data (with st. errors) and modelled WHB interpretation, along with the modelled WHB velocity-depth curve.

an outcrop length in line with the expected ray-path from the quarry of 1.5 km. Assuming a ray-path length of about 1 km, velocities for the Lower and Upper Old Red Sandstone of 4.5 and 3.8 km s⁻¹, and for boulder clay of 2.0 km s⁻¹, gives a delay relative to a Lower Old Red Sandstone ray-path of 47 ms which is of the right order of value to explain this delayed travel-time point. The remaining points were fitted to a smooth curve based originally on the curve from the Dunduff E line, and the resulting V-Z curve is shown in figure 4.4b. The surface velocity is similar to that seen around Dunduff quarry, but down to 1 km depth the velocities are slightly lower, indicating a small lateral change in V_p across the Lower Old Red Sandstone sediments between Dunduff and Cairngryffe quarries.

As the estimated maximum depth of penetration of S-waves from Dunduff quarry (figure 4.2b) is similar to that of the P-waves from Cairngryffe quarry, effective reversal of these data can be assumed. An attempt can then be made to estimate the range of V_p/V_s and Poisson's ratio values expected with depth under this region assuming that the S-wave velocities are laterally constant between the two quarries. Figure 4.5 shows the P-wave V-Z curves from Dunduff and Cairngryffe quarries, and the S-wave V-Z curve from Dunduff. Obtained from these curves are estimates of V_p/V_s and Poisson's ratio values for this region down to 2.5 km depth. As expected for a region of predominantly, if not entirely, quartz-rich clastic sediments, the V_p/V_s and Poisson's ratios are very low, once the near surface flat cracks and fractures close with increasing pressure.

To the E of Cloburn quarry, the data were collected on two separate occasions; the three close points as part of the Hillhouse - Broughton profile and the remaining data as arrivals into the BTN array (see Appendix 4.17). The station at around 12 km range was sited some 3-4 km S of the line of profile, just across the SUF, and it appears on the time-distance diagram (figure 4.6a) as about 90 ms fast of the interpretation of the remaining

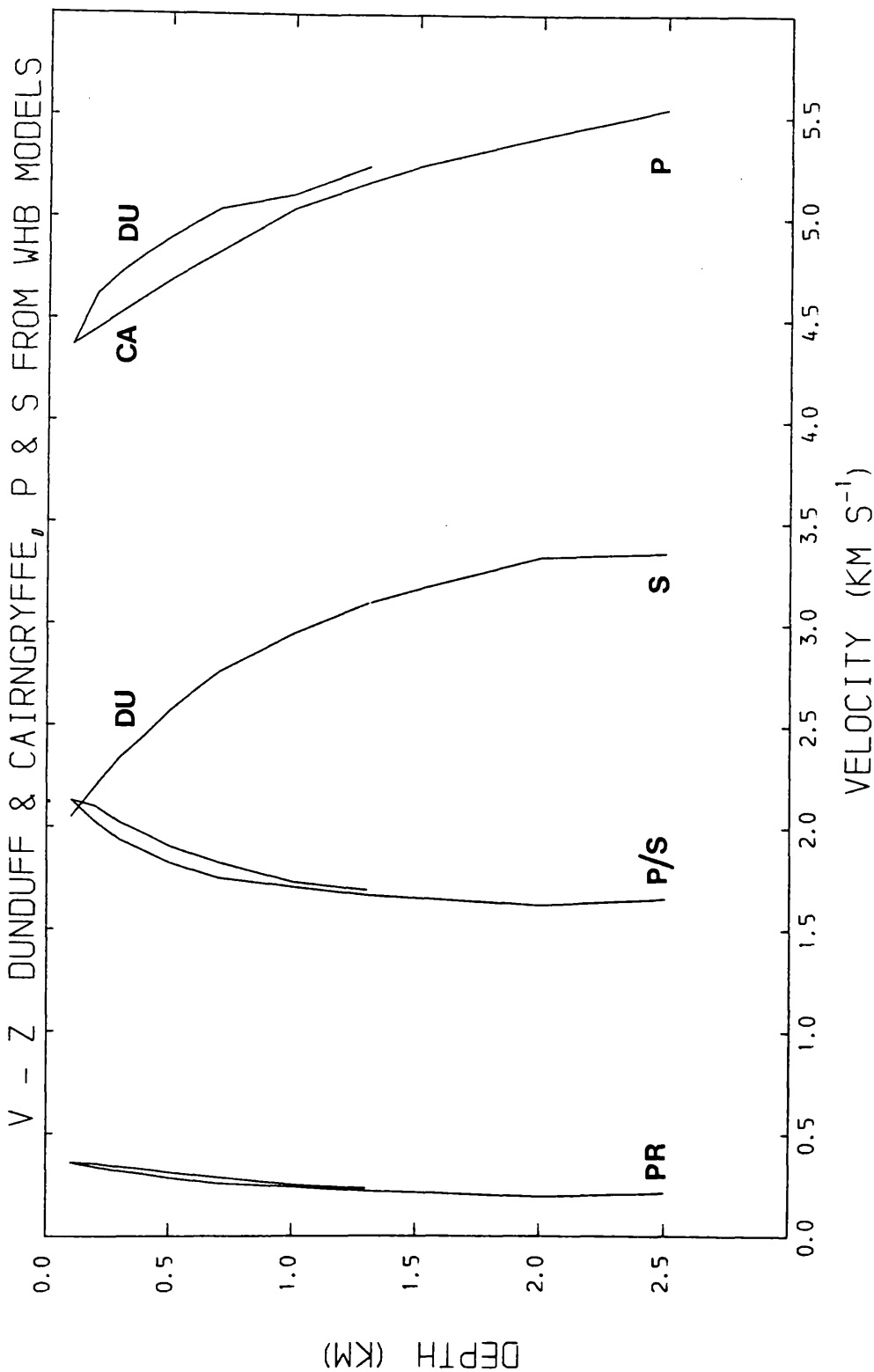


Figure 4.5 Combination of the WHB interpretations of Figures 4.1-4.4 giving V_P/V_S and Poisson's ratio variations with depth for the area between Dunduff and Cairngryffe quarries. Assumes the S-wave V-Z structure is laterally constant.

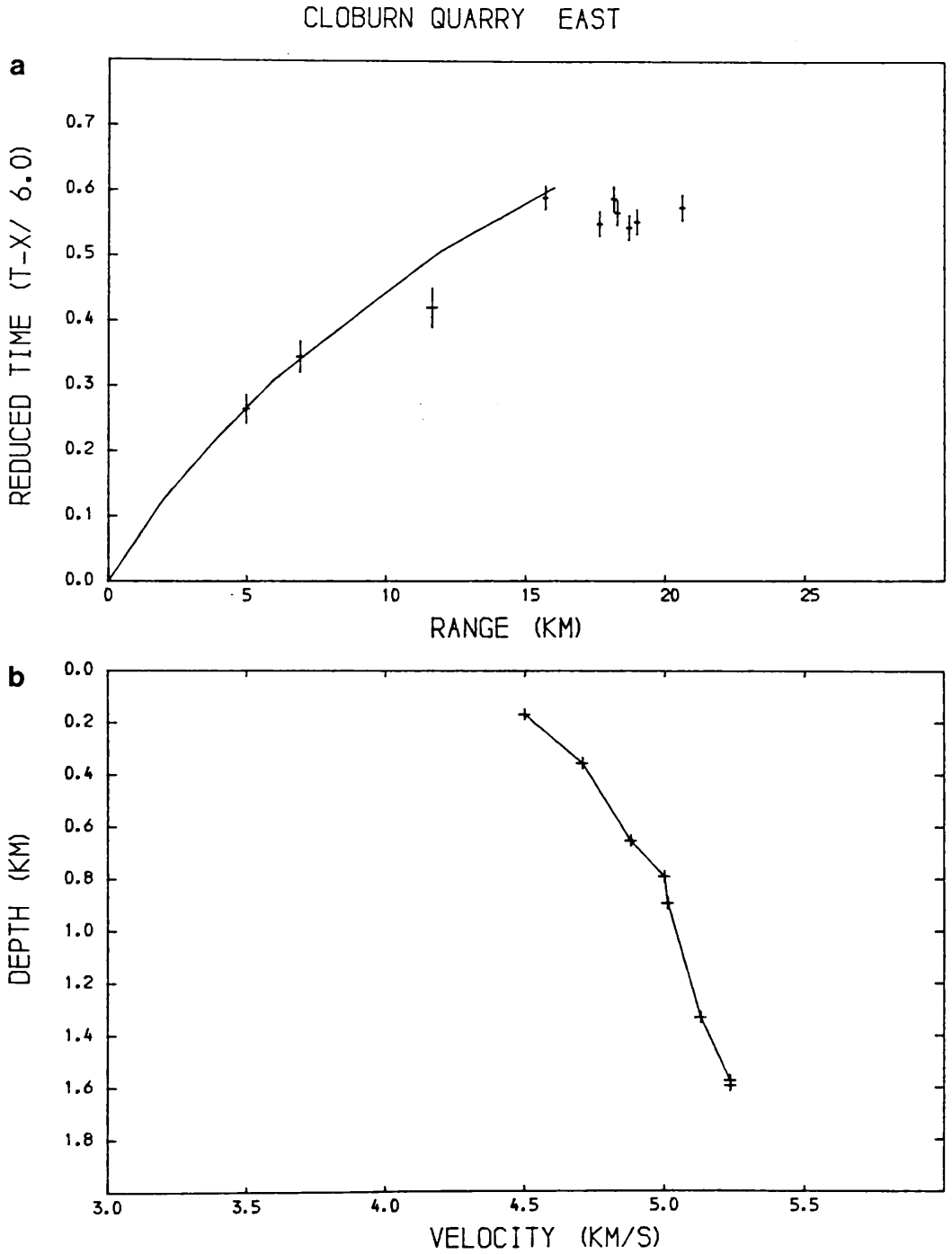


Figure 4.6 Time-distance data (with st. errors) and modelled WHB interpretation, along with the modelled WHB velocity-depth curve.

points on the direct segment of the curve. This early arrival can be explained by using some knowledge of the local geology. A direct line from Cloburn quarry to this site (6E) passes close to the eastern margin of the Tinto felsite intrusion (see figures 3.1,2) which is a large concordant, laccolithic body up to 2 km in thickness and dipping to the NW at around 40° . If this body extends laterally underground for a few kilometres towards the E or NE, then it will cross the quarry-receiver ray-path at a depth of around 1 km. Assuming a velocity at this depth of 5.7 km s^{-1} compared with 5.0 km s^{-1} for the surrounding rocks, and a path length of 4 km through the intrusion, which is not unreasonable, the resulting decrease in travel-time would be 98 ms. Given that the above assumptions do not involve much extrapolation from either the known local geology or previous geophysical work (presented in this study or previously published), simple calculations can be used to explain locally anomalous data as found in figures 4.4a and 4.6a.

The curve fitted to the remaining data in figure 4.6a produced the V-Z curve in figure 4.6b. This was based on the curve fitted to the data from the W of Cairngryffe, and little modification was required.

Figures 4.7,8 show the data from the two off-end shots into the LES array. The Cornstones Shot (location figure 3.1) was situated in a small disused limestone quarry around 100 m off the southwestern margin of the Lesmahagow Inlier and recorded approximately along strike. The Middle Croft Shot (location figure 3.1) was situated off end of the northern limits of the array and within the upper most part of the Silurian succession, and recorded across strike. The cluster of data on figure 4.8a between 8-9 km range is due to arrivals from stations on the along-strike arm and is a measure of the amount of lateral variation in velocity within the top 1 km under the array.

The inversion to velocity-depth of the Cornstones and Middle Croft datasets produces curves which can be split into two segments at a depth of 0.5 km

CORNSTONES SHOT

10 SEPT 1982

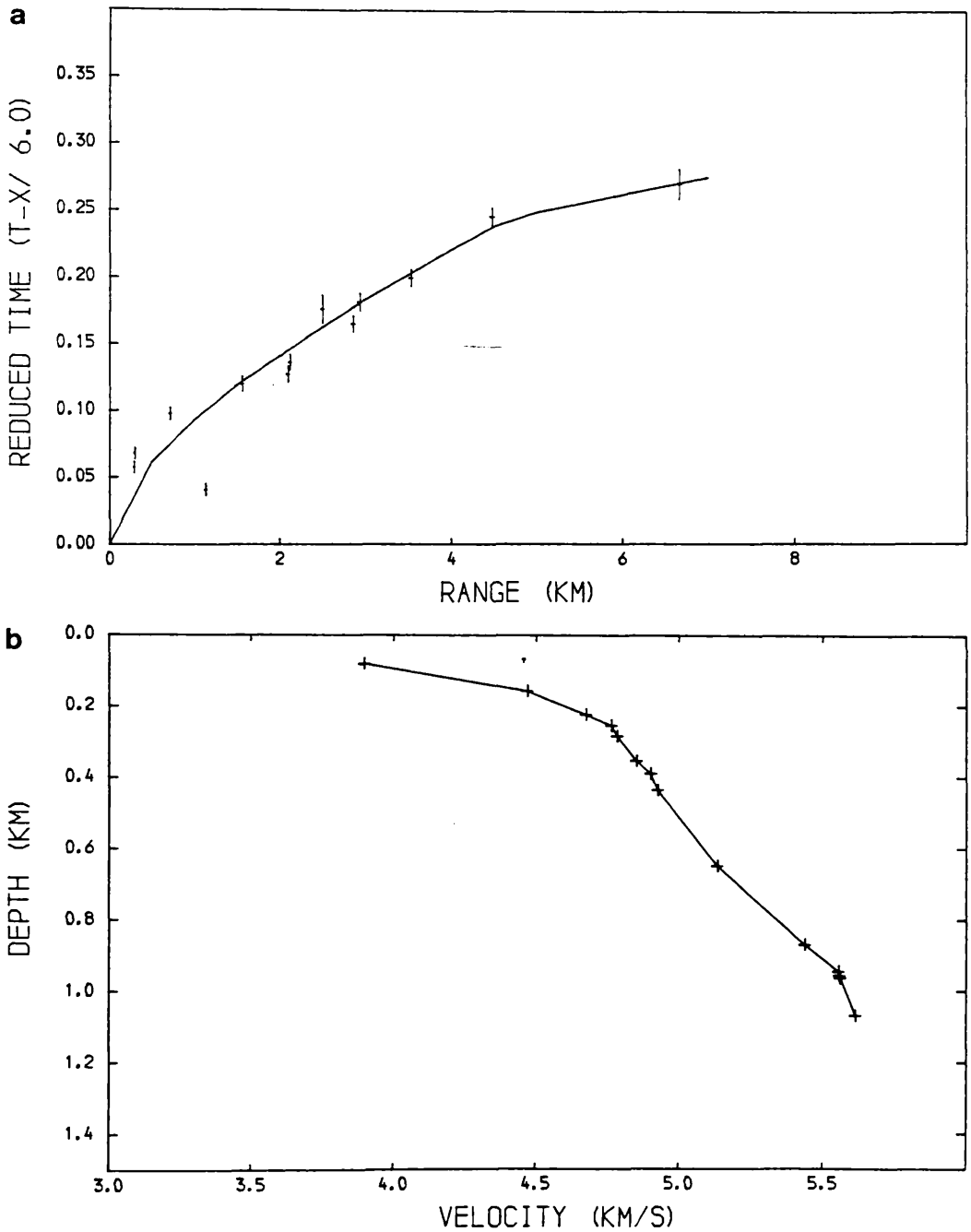


Figure 4.7 Time-distance data (with st. errors) and modelled WHB interpretation, along with the modelled WHB velocity-depth curve.

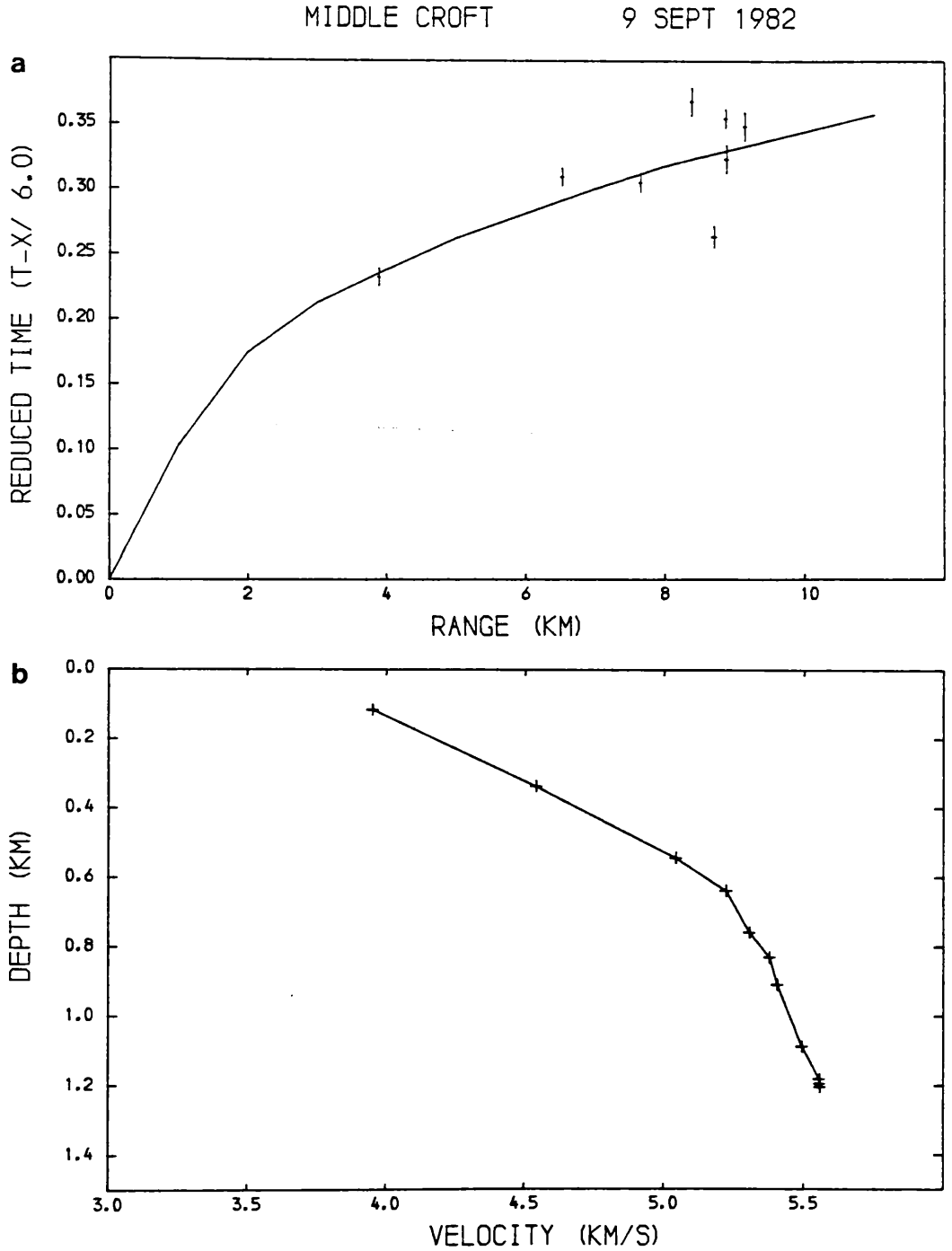


Figure 4.8 Time-distance data (with st. errors) and modelled WHB interpretation, along with the modelled WHB velocity-depth curve.

(figures 4.7b & 8b). Although constrained by only one point close to the shot, the Middle Croft V-Z curve indicates lower initial velocities than from Cornstones over the same range, a fact which is confirmed by the comparison of the travel times between the two datasets. Over comparable ranges, the Middle Croft data is consistently around 50 ms slower.

Beneath 0.5 km, both V-Z curves are very similar, indicating maximum penetration of just over 1 km and predicting P-wave velocities of up to 5.5 km s⁻¹. With both curves, the indicated velocity gradients are high, with initial gradients of over 2 s⁻¹ reducing to around 1 s⁻¹ below 0.5 km.

Figures 4.9a,b show the data and its interpretation for recordings made to the W of Dunduff quarry. W of the quarry Lower Old Red Sandstone sediments outcrop for 3 km until a fault brings up the Silurian rocks of the inlier (cf figures 3.1,2). Only four of the first five points on the line recorded W of Dunduff quarry have been included in this interpretation. The cluster of points between 18 and 23 km were considered outwith the range of direct arrivals, and also being recorded over or to the W of the Distinkhorn intrusive complex, were expected to show complexities relating to this igneous body. The unmodelled point at 6 km range was sited on a small felsite intrusion and the position of its travel time on figure 4.9a implies that this body must be more extensive depth. From the site locations shown in figure 3.1, not all sites, especially in the central parts of the Hillhouse - Broughton profile, are located exactly on a straight line. This was due to the need to locate suitable outcrops of rock as sites in areas with thin but uniform drift cover. This particular site (1D), is slightly to the S of the profile and so any inferred localised mass of felsitic rock need not affect the arrivals to other sites further N.

The remaining sites allow the fitting of a smooth curve (figure 4.9b) which reveals high surface velocities and much lower velocity gradients than modelled from the Cornstones or Middle Croft shot data. This, along with the

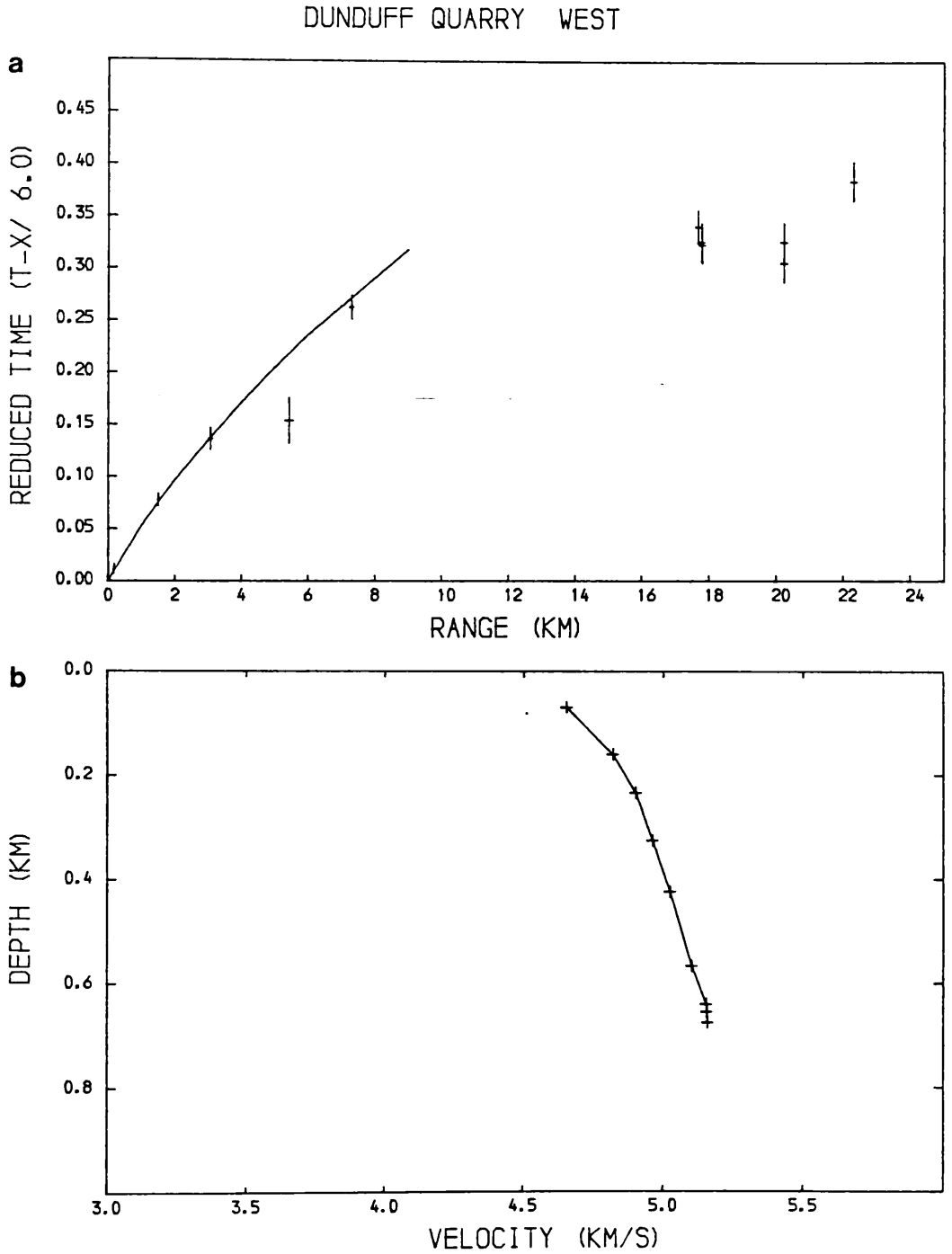


Figure 4.9 Time-distance data (with st. errors) and modelled WHB interpretation, along with the modelled WHB velocity-depth curve.

discussion of the data from E of Dunduff quarry, led to the view that this area is one of considerable lateral as well as vertical velocity variations, and as such the WHB method is not suitable for its interpretation.

Figures 4.10a,b show the time-distance data and their interpretation from the Greivehill Shot. This was a 52.5 kg Plaster Gelatine shot fired in a N.C.B. borehole in Lower Carboniferous sediments near New Cummnock, central Ayrshire, and recorded by the Lesmahagow array. No intermediate recording sites were used, so the interpretation of this data is limited. The intervening region between the shot and the array is composed initially of a 3 km wide outcrop of Carboniferous sediments followed by a 4 km wide outcrop of Lower Old Red Sandstone sediments, the SW extension of the Hagshaw Hills Inlier and the 4 km wide Douglas Coalfield which is terminated at its northern margin by the Kerse Loch fault. To the north of the Kerse Loch fault lies the Lesmahagow Inlier. The close proximity of the Douglas basin to the array may affect the closest stations by imposing an extra delay due to transmission of those rays through the base of the Carboniferous succession but the remaining arrivals do not appear to be affected.

The interpreted curve stops at 17 km range as evidence from Hillhouse and Cairngryffe quarries suggests that the cross-over point to a refracted arrival should occur at around this range. The apparent velocity across the last three points between 16 and 20 km is around 5.8 km s^{-1} , which although less than the values from Hillhouse and Craigie quarries (Appendices 4.6/7) is similar to that received from Cairngryffe quarry and also the Kirkconnel opencast site (Appendix 4.8), which has a similar azimuth although greater range. Thus the final two points in this dataset were tentatively associated with refracted arrivals and therefore not considered further in this section.

The remaining data have an aperture of less than 4 km and so it is difficult to produce a unique interpretation. Therefore an initial model based on the

GREIVEHILL SHOT 14 SEPT 1982

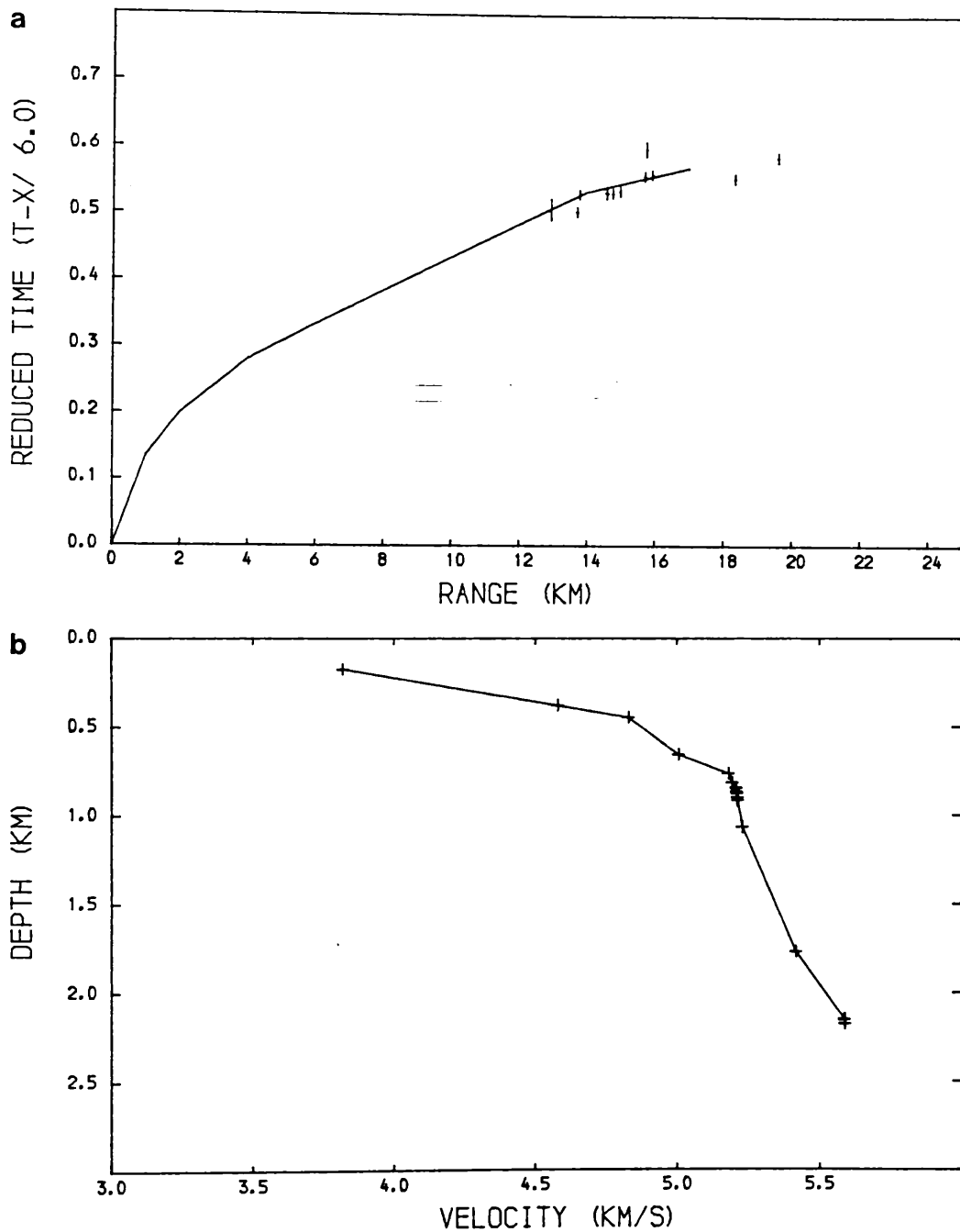


Figure 4.10 Time-distance data (with st. errors) and modelled WHB interpretation, along with the modelled WHB velocity-depth curve.

main features of the Cornstones and Middle Croft V-Z interpretations was used and extended by extrapolation to fit this remaining data. It was felt that this was a geologically reasonable approach as no confidence can be placed upon the independent interpretation of the dataset.

The close-shot data from Hillhouse quarry were not included in the WHB analysis due to the early refracted arrivals and the subsequent difficulty in defining a good series of direct arrivals.

The short range time-distance data have been used in two ways with the WHB inversion: by ignoring the time-distance points on the refractors, estimates of the velocity-depth structure for the sedimentary layer up to the maximum depth of penetration were obtained (eg figures 4.1 to 4.10); whereas by including the first few points on the refractor and assuming a realistic refractor velocity (based on estimates from reversed or near reversed segments if available, otherwise using the apparent velocity), an estimate of depth to the refractor could be obtained (see figures 4.11 to 4.14). This did result in some distortion of the V-Z curve for the region immediately above the refractor due to the smoothing effect of the WHB function on a now discontinuous V-Z curve, but this did prove a useful method of obtaining a quick, direct estimate of the depth to a refractor for incorporation into the ray-model.

4.1.3 Plane layer interpretation

The results of the WHB inversion were compared with results obtained using a plane layer interpretation where the continuous velocity increase with depth has been simulated by using many thin layers, each with an increasing velocity. Program LAUFZEIT (Kaminski & Muller, Karlsruhe University) is designed to calculate the various phases produced by an input velocity-depth curve, using plane-layered geometry. Modelling of the headwaves produced from refracting horizons is possible, as is the delimiting of delays produced by

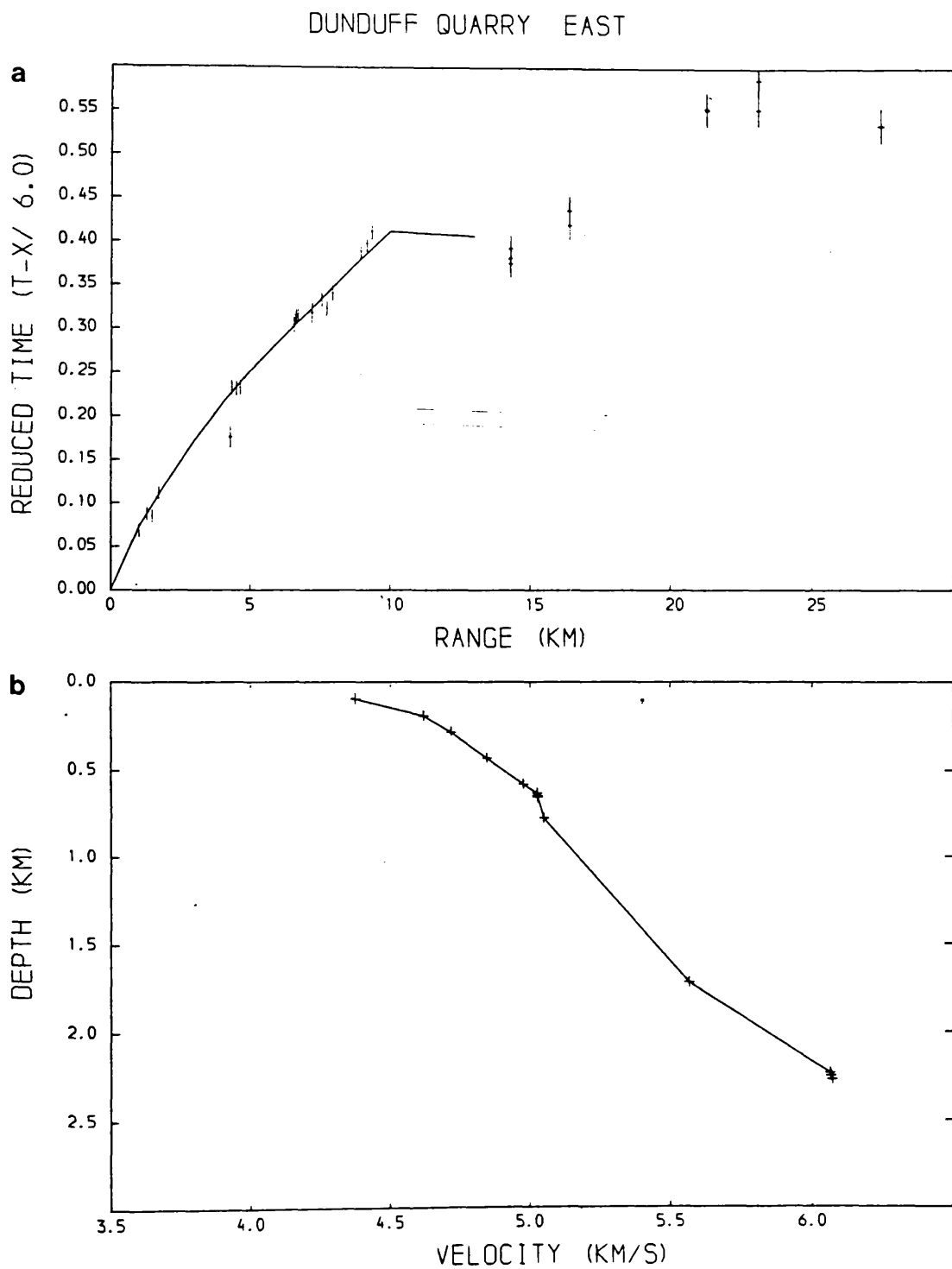


Figure 4.11 Time-distance data (with st. errors) and modelled WHB interpretation, along with the modelled WHB velocity-depth curve to determine depth to the discontinuity.

DUNDIFF QUARRY WEST

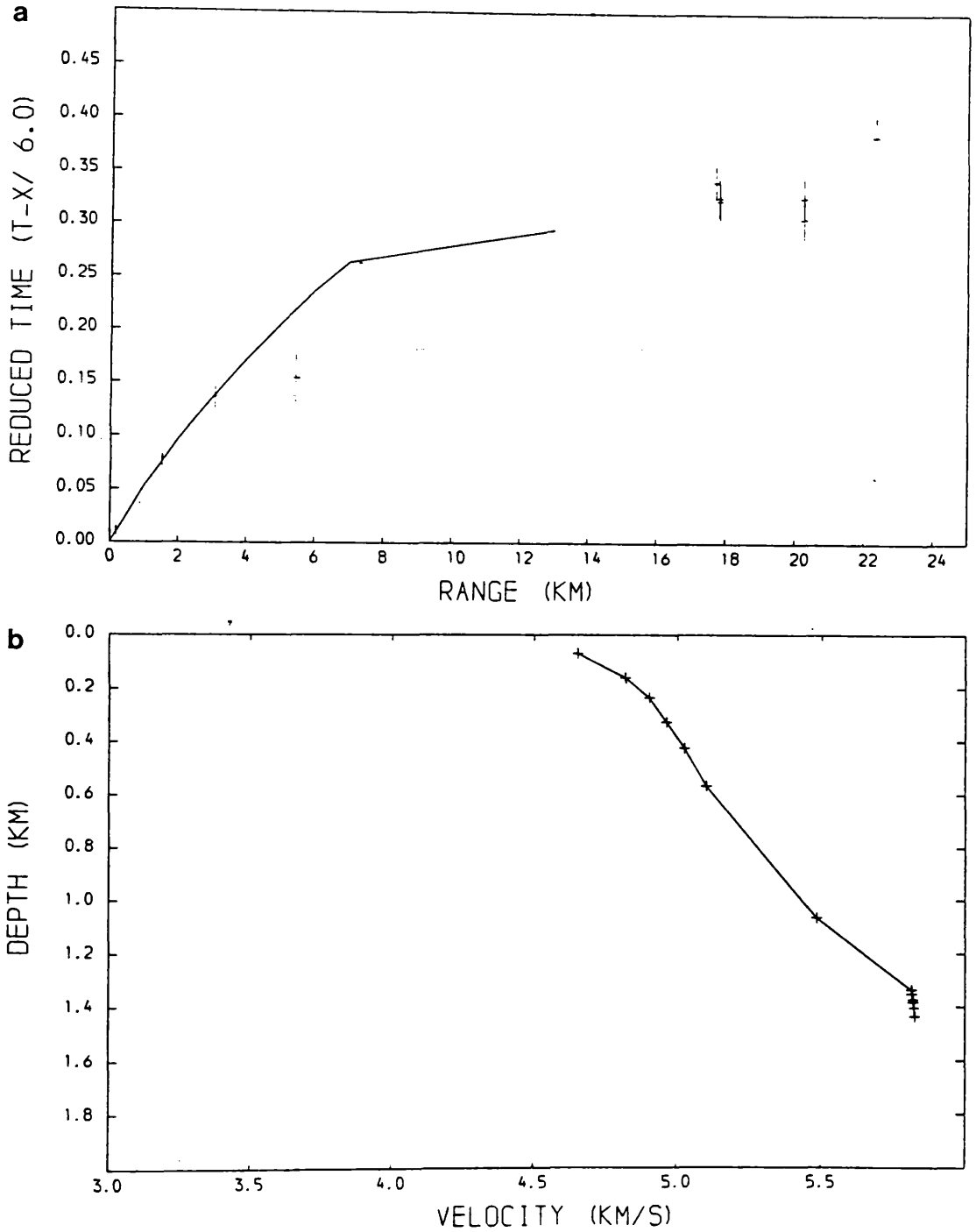


Figure 4.12 Time-distance data (with st. errors) and modelled WHB interpretation, along with the modelled WHB velocity-depth curve to determine depth to the discontinuity.

CAIRNGRYFFE QUARRY WEST 26 AUG 1982

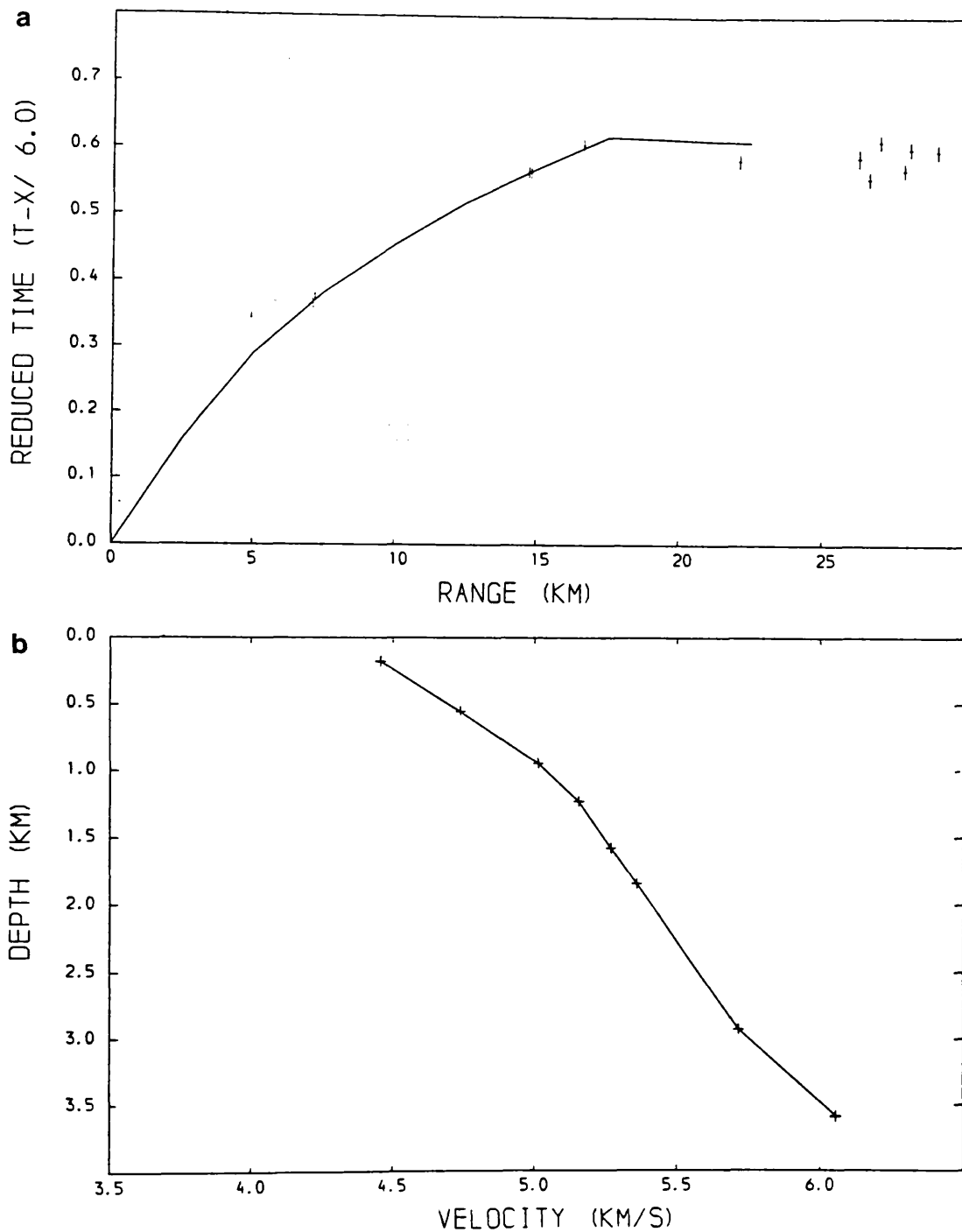


Figure 4.13 Time-distance data (with st. errors) and modelled WHB interpretation, along with the modelled WHB velocity-depth curve to determine depth to the discontinuity.

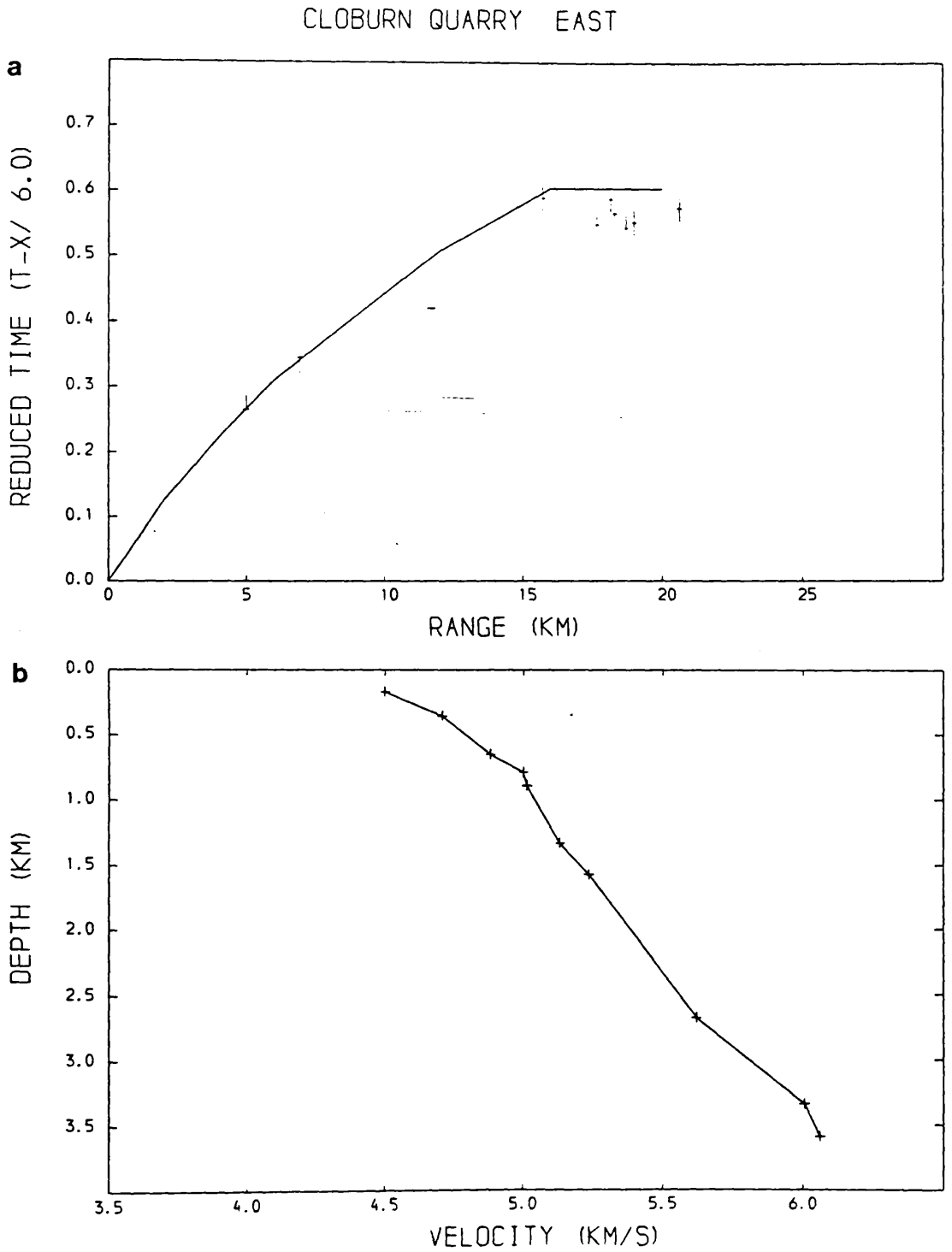


Figure 4.14 Time-distance data (with st. errors) and modelled WHB interpretation, along with the modelled WHB velocity-depth curve to determine depth to the discontinuity.

reversed velocity gradients and low-velocity-zones. This process is iterated until a satisfactory fit to the field data is achieved. As with the WHB method, this program assumes lateral velocity homogeneity within each dataset and so the results must be interpreted with caution. This technique was applied independently to all the field data presented in the WHB inversion section and the resultant synthetic time-distance graphs are shown for comparison in figures 4.15 to 4.19. The post-critical reflection branch was always calculated and plotted by the program although not used in any of these interpretations. The errors in the field observations are not plotted. The range of depths produced from the WHB inversion give a measure of the depth of penetration of direct arrivals within each dataset as any refracted arrivals were excluded from the inversion and should also provide minimum possible velocity values at any given depth. However both direct and refracted arrivals can be modelled using the plane layer method with the result that the region between the deepest penetrating direct ray and the refractor has to be interpreted indirectly as a time delay between the known surface velocity structure and the refractor. This zone was always assumed to have a velocity-depth structure which is a downwards continuation of that directly interpreted from the direct arrival data. Where a refractor was encountered within any dataset, the first priority was made to match the crossover point with a refractor velocity obtained either from refractor reversal or, if this was not available, from a reasonable geological estimate.

From the interpretations shown in figures 4.16a,b and 4.18a, it became apparent that high velocity, probably discrete layers existed within the surface sedimentary layer. The thicknesses of these layers could not be controlled directly for the reasons described above, but a measure of their limited lateral extent could be appreciated from the length of each refractor segment compared with the length of the plane-layer synthetic segment. Where

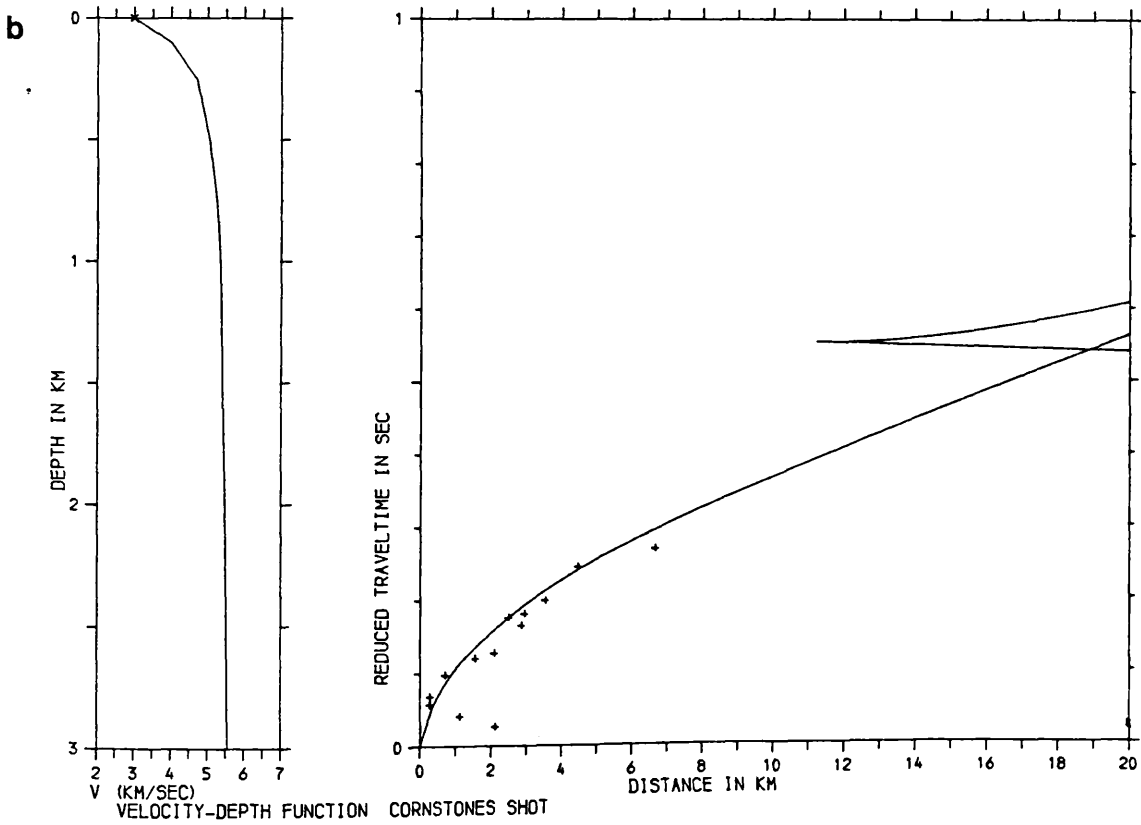
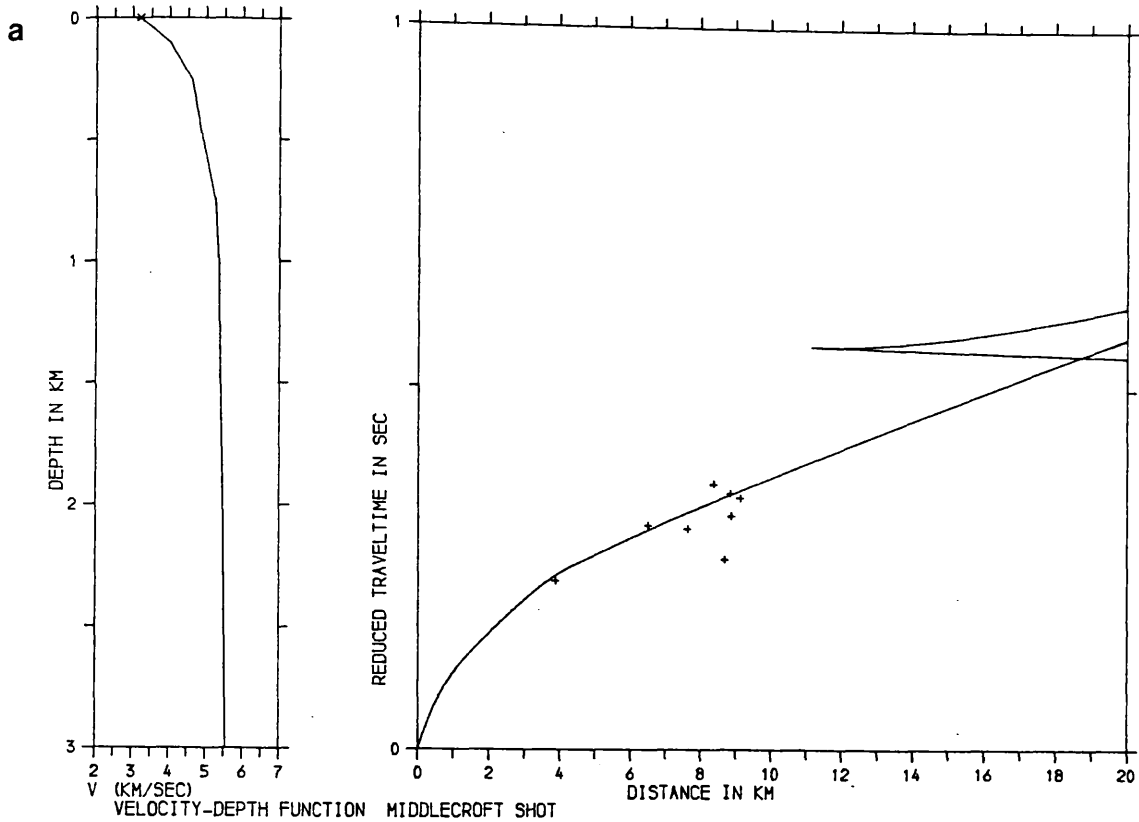


Figure 4.15 Time-distance data and its interpretation using the plane-layer method.

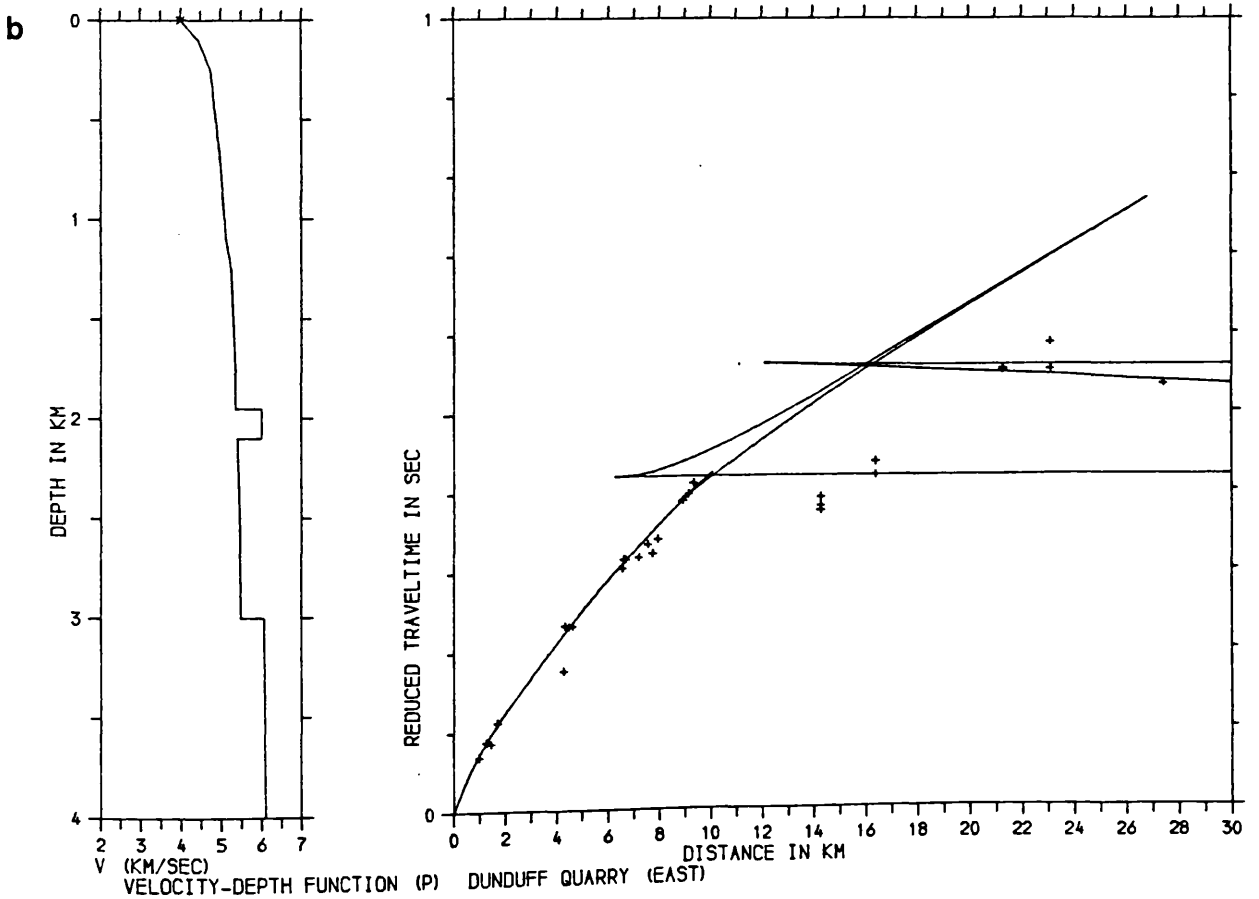
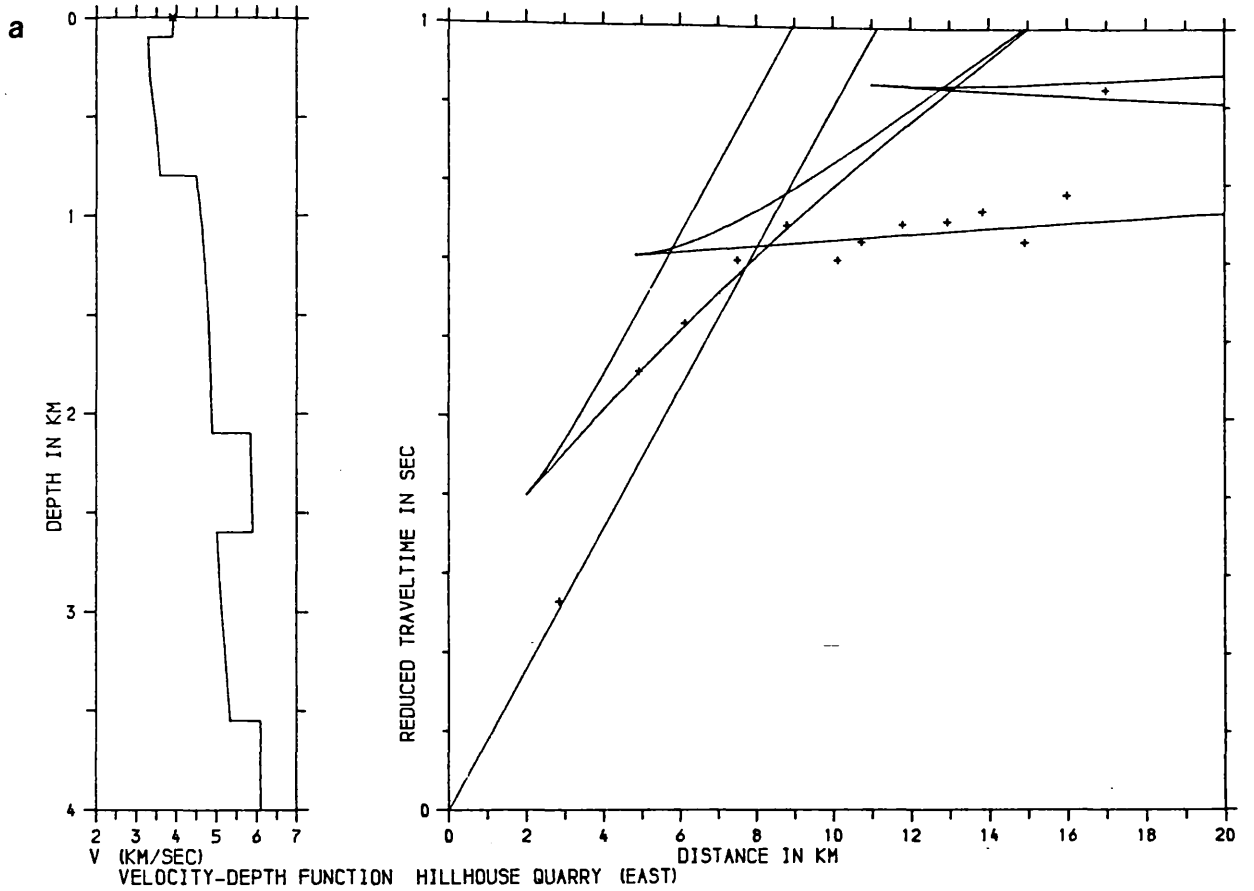


Figure 4.16 Time-distance data and its interpretation using the plane-layer method

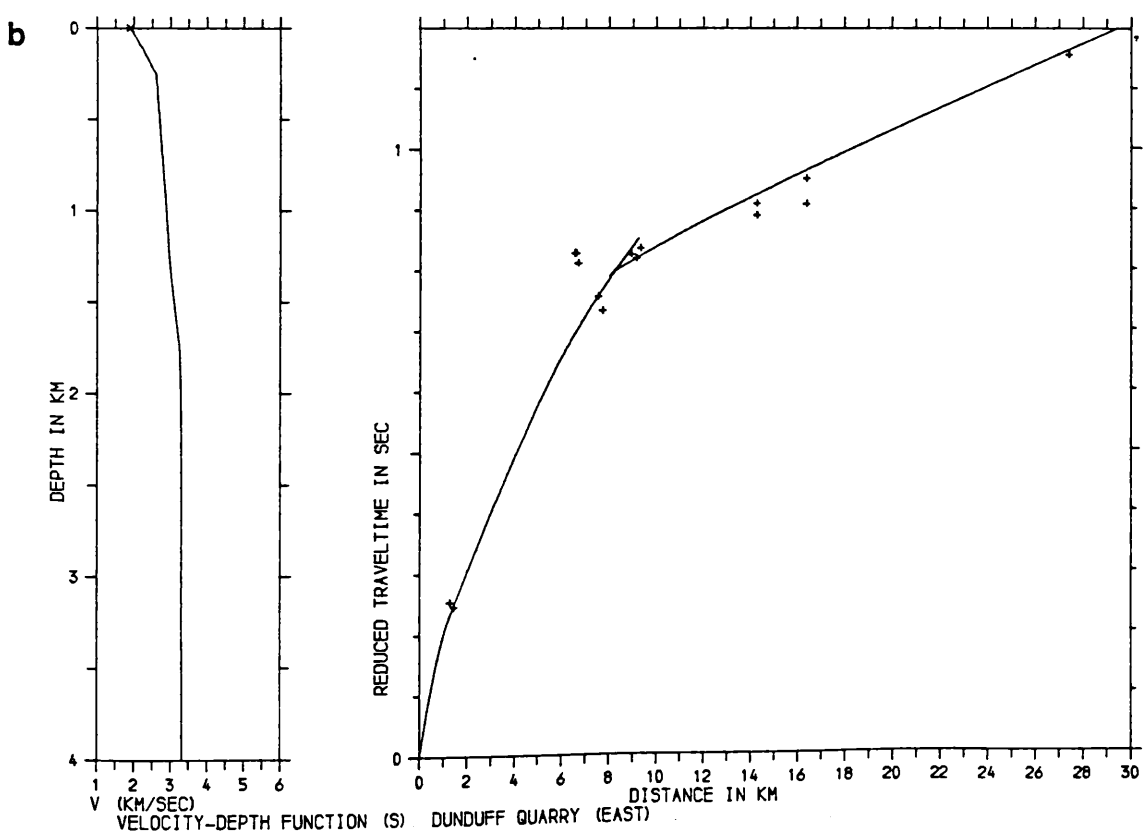
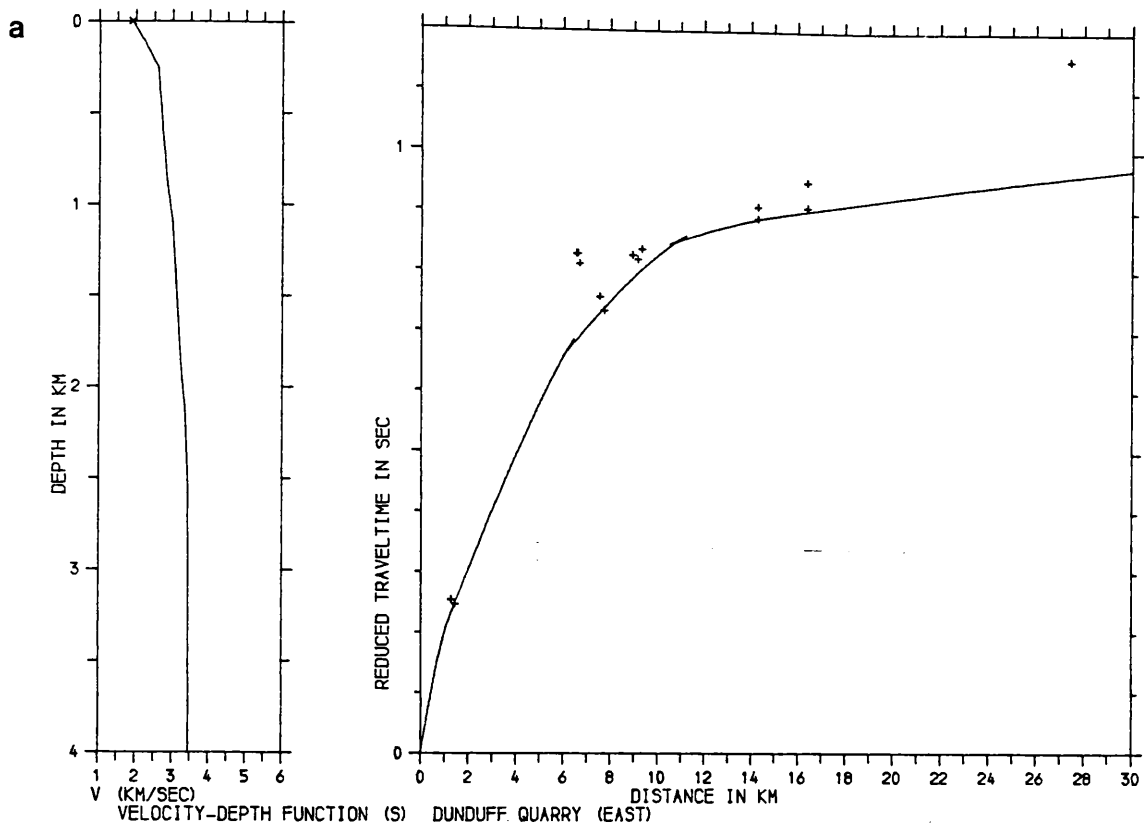


Figure 4.17 Time-distance data and its interpretation using the plane-layer method.

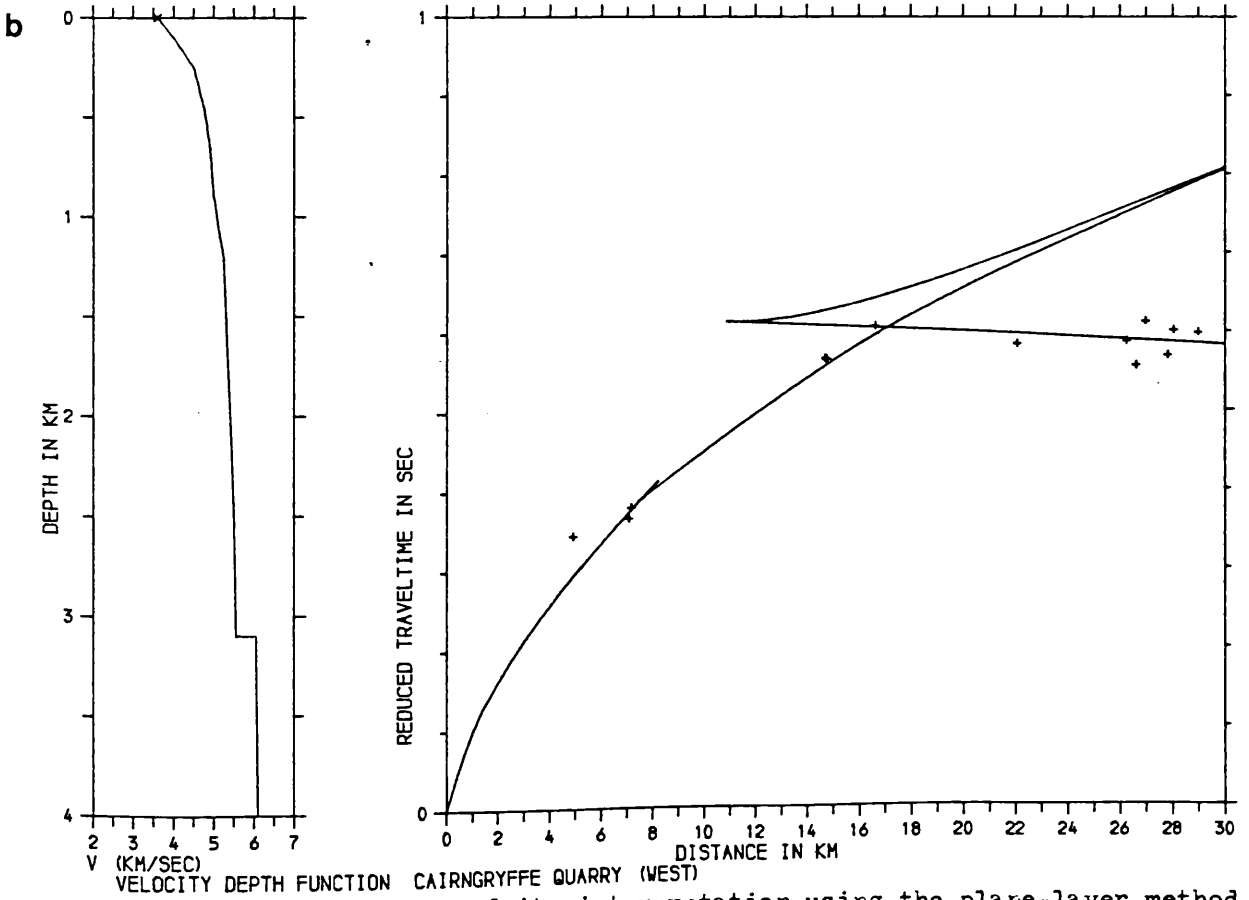
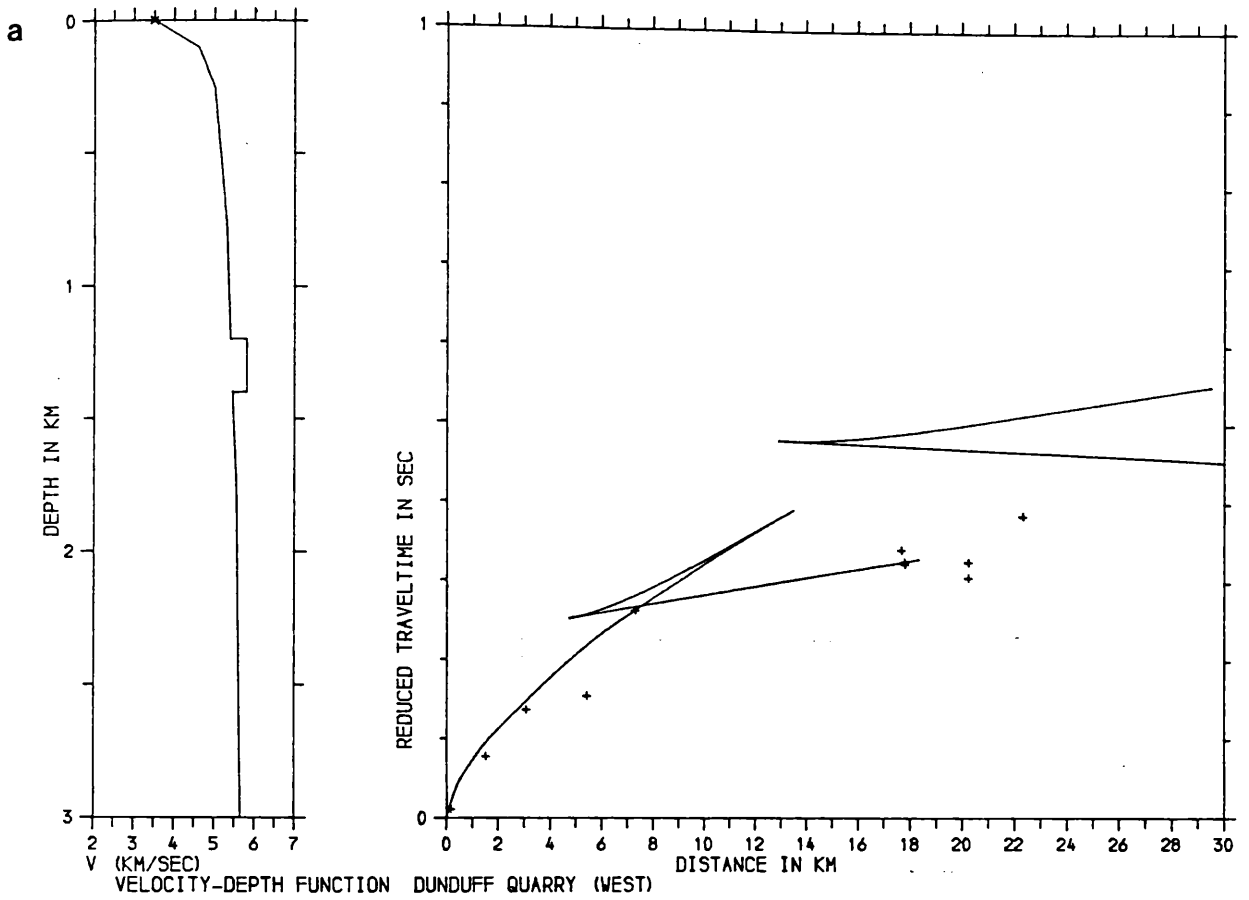


Figure 4.18 Time-distance data and its interpretation using the plane-layer method.

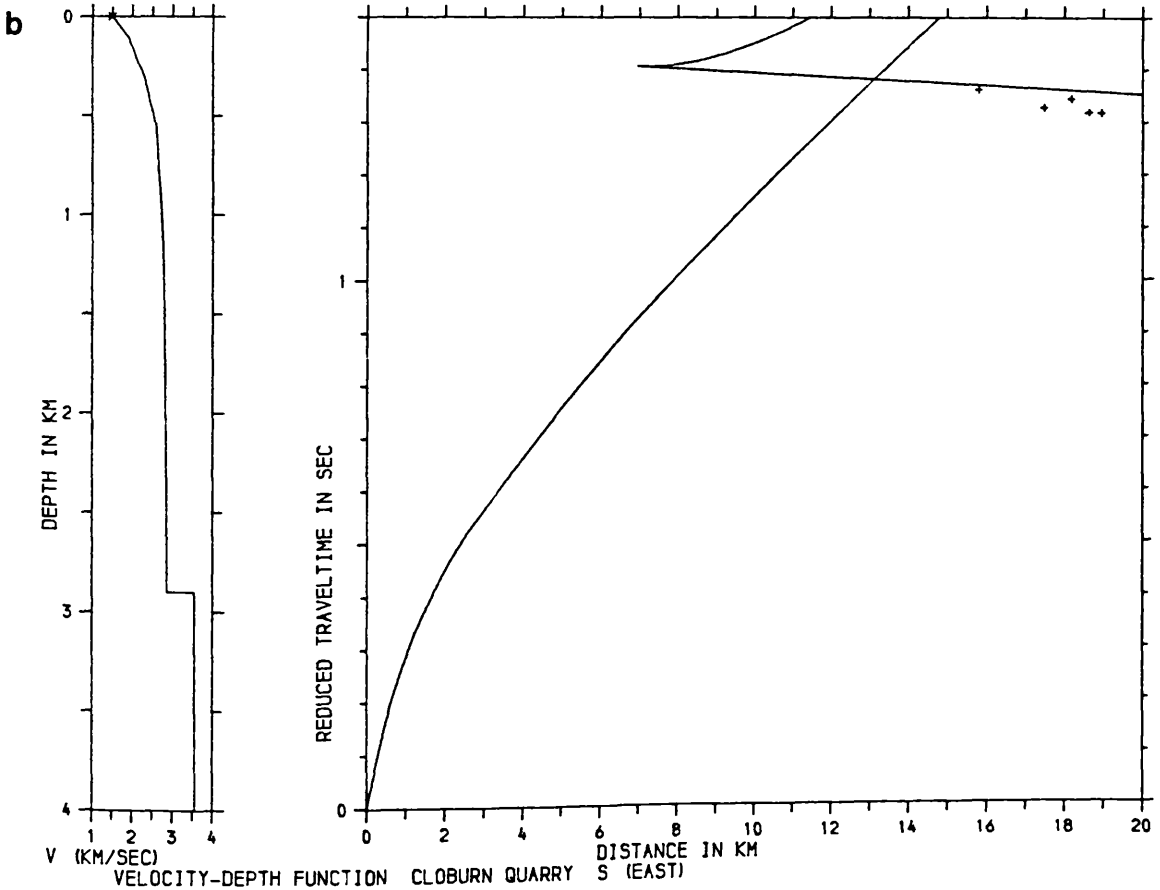
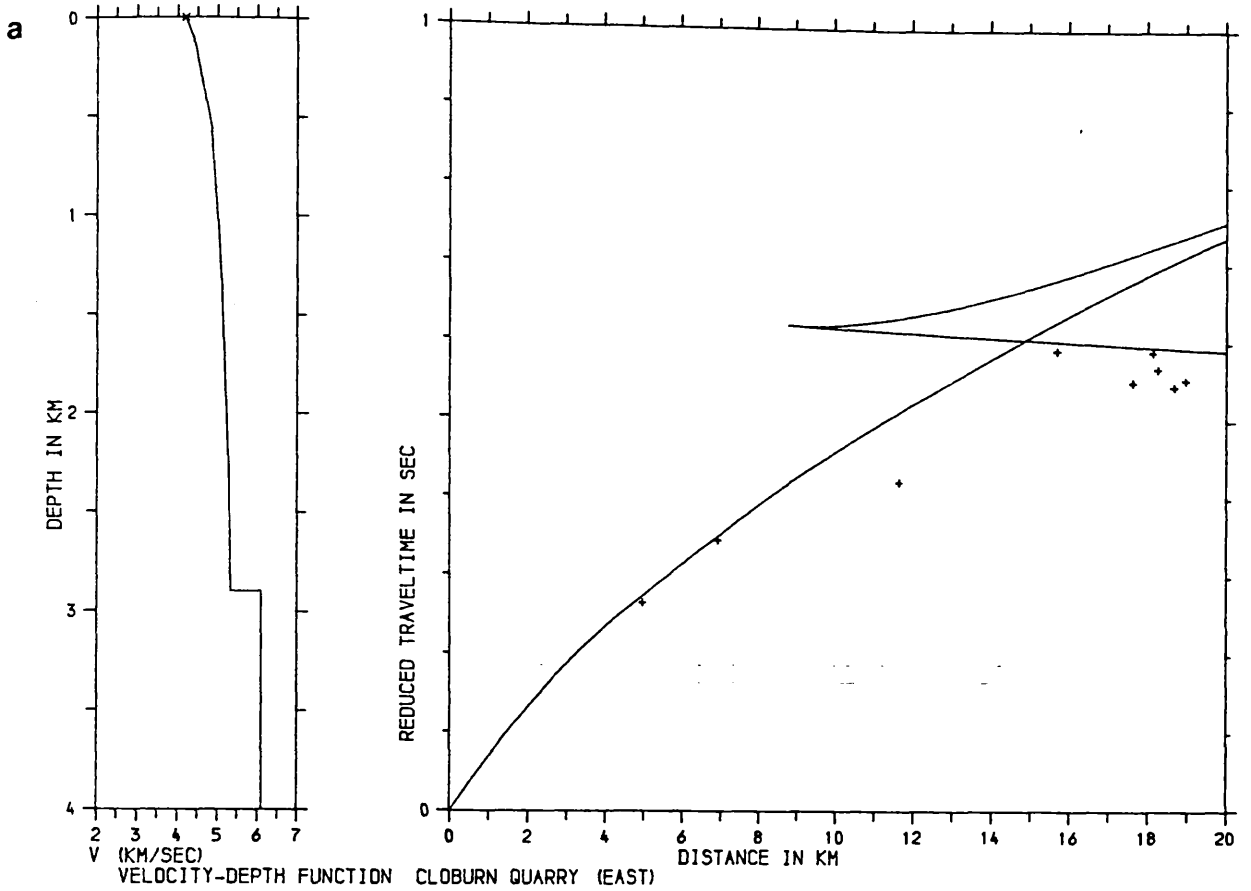


Figure 4.19 Time-distance data and its interpretation using the plane-layer method.

the apparent refractor velocity was higher than the expected range of values encompassing all realistic geological possibilities, such as the short segment with an apparent velocity of 6.3 km s^{-1} between +9 km and +14 km from Dunduff quarry (figure 4.16b), then it was inferred that these arrivals were up-dip from the body and some minimum value could be placed on this dip, in this case $3-4^{\circ}$. No lower limit could be placed on the velocity, as realistic geological interpretations in this area can account for most velocities up to about 6 km s^{-1} . Values greater than this would imply rock types whose density is sufficiently large to create regions of anomalously high density, which would then be obvious on the regional Bouguer anomaly map (Hussain & Hipkin 1983).

With the exception of the data to the W of Dunduff quarry (4.18a) and the minimum and maximum S-wave velocity interpretations from Dunduff E (figure 4.17a,b), all lines with data recorded beyond 16-17 km range require the presence of a high velocity (V_p around $6.0-6.1 \text{ km s}^{-1}$) refractor at depths of about 3 km. This consistency of apparent velocity and indicated depth implies that this refractor must be continuous and may underlie the whole profile. This will be considered further in the following sections.

Comparisons of the V-Z curves produced by both methods are shown in figures 4.20 to 4.22. The curves produced by both methods are similar in shape and were fitted using the same philosophy as outlined earlier. It was found that the WHB integral produces velocities which are generally higher by $0.1 - 0.2 \text{ km s}^{-1}$ for any given depth than the plane-layer method. This was initially unexpected as, due to the assumption of curved raypaths (the COSSH integral), the WHB method should provide velocity values which are always slower with depth than those obtained from plane-layer modelling. The difference arises from the fact that both methods were independently applied to each dataset and the resulting interpretations differ by virtue of fitting different lines

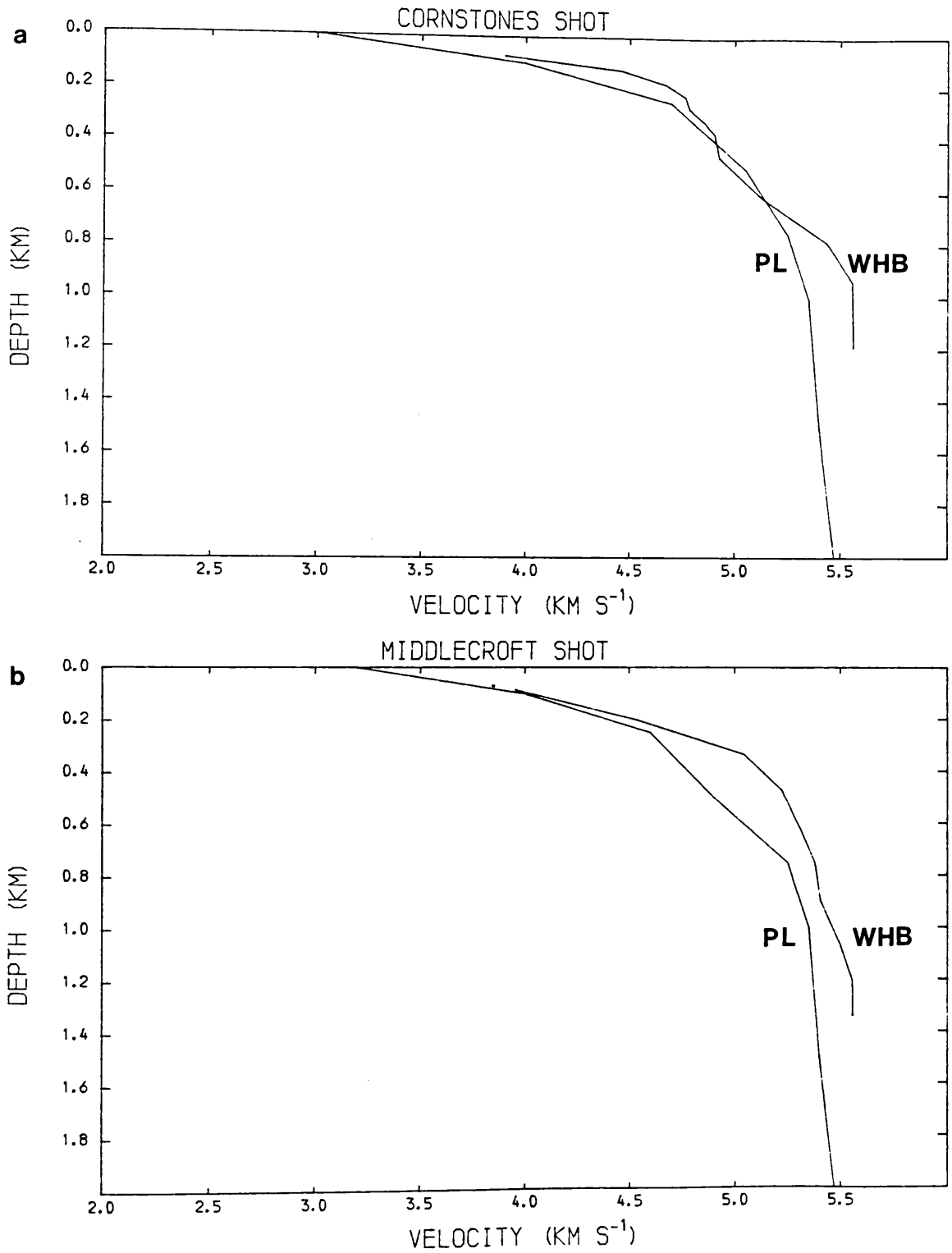


Figure 4.20 Comparison of WHB and plane-layer velocity-depth curves.

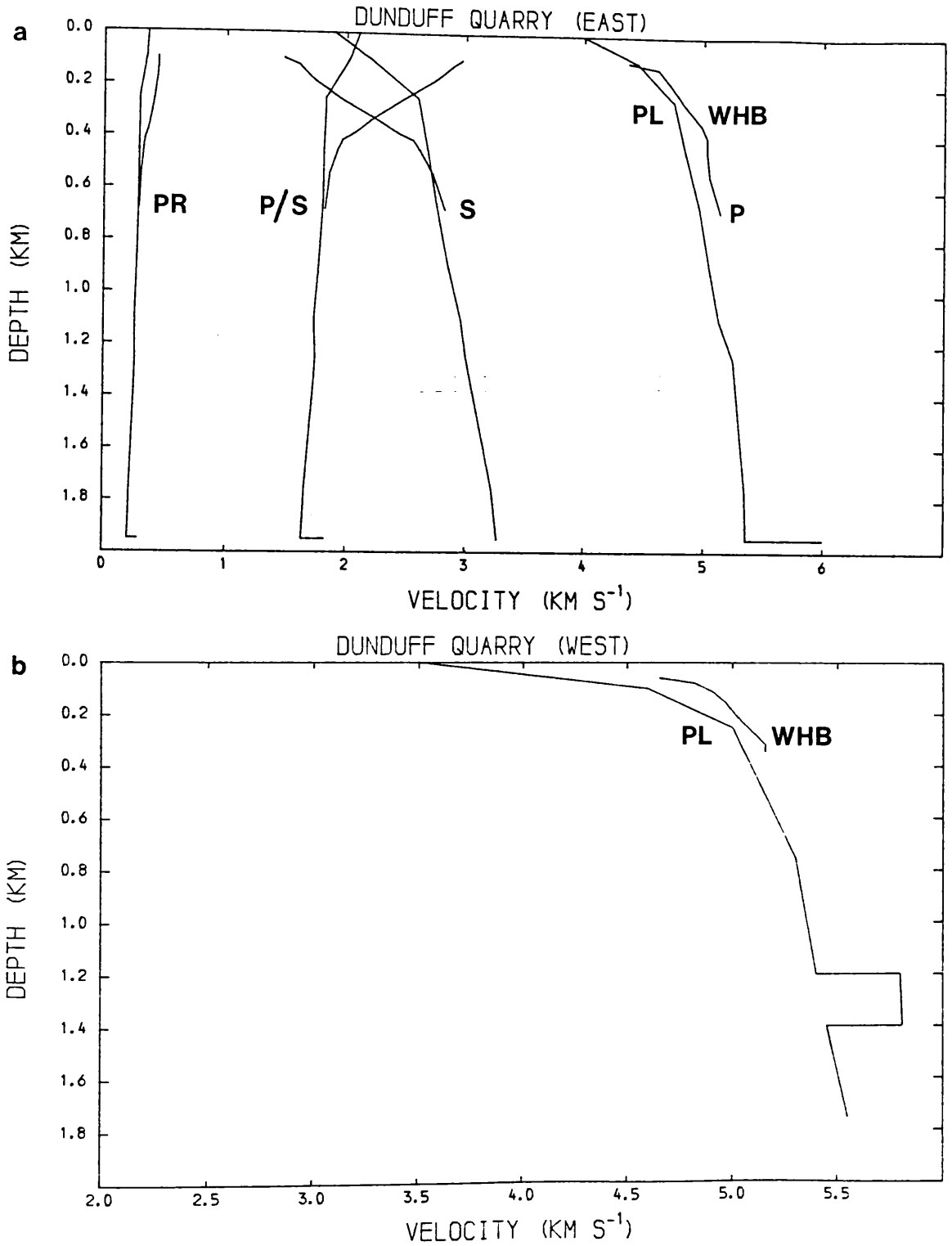


Figure 4.21 Comparison of WHB and plane-layer velocity-depth curves.

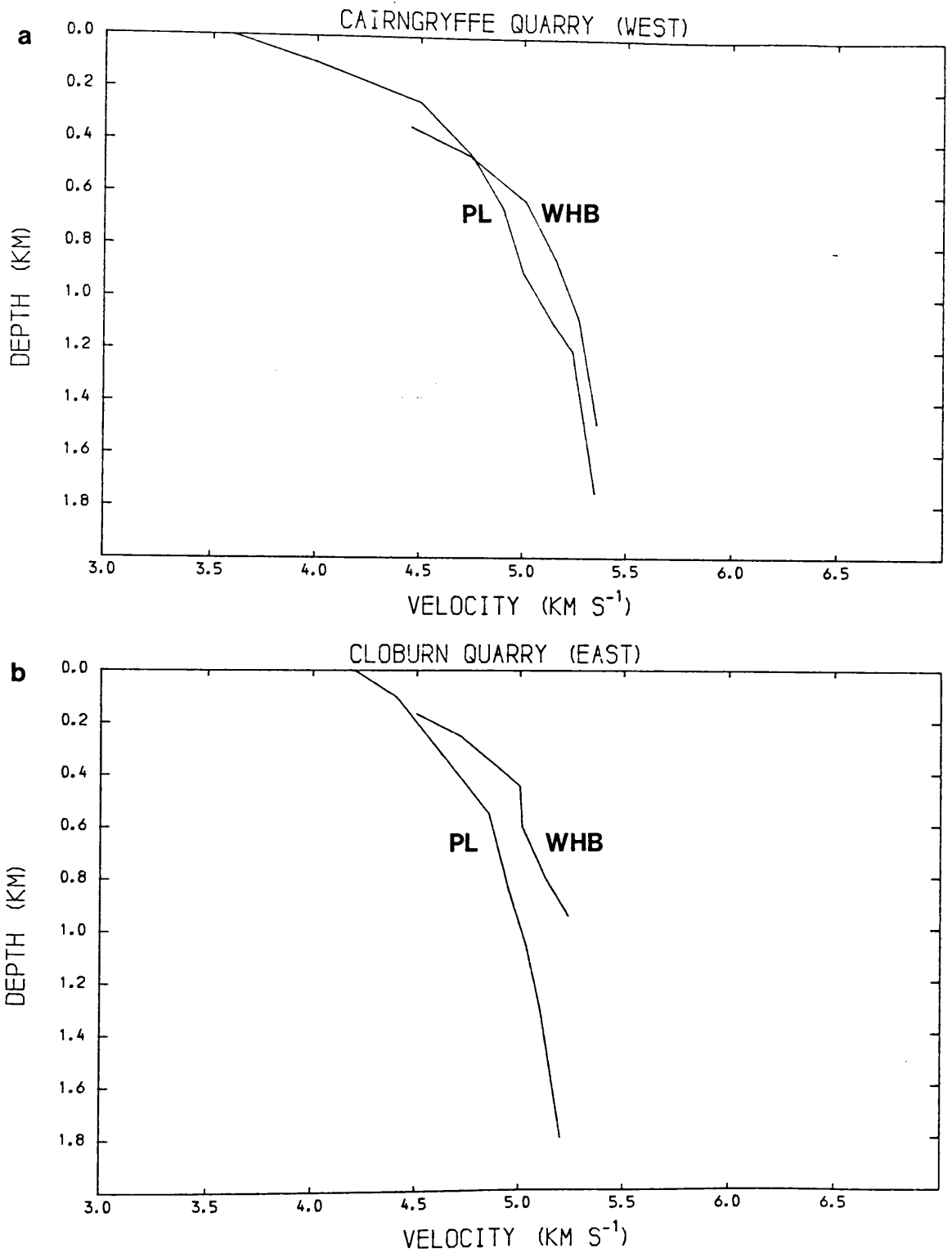


Figure 4.22 Comparison of WHB and plane-layer velocity-depth curves.

to the same sets of data. These comparisons must therefore be treated as a measure of the breadth of possible solutions obtainable by the fitting of curves to these field data in addition to any discrepancies produced by these two different interpretation approaches.

4.1.4 Tau - P inversion

Since the WHB inversion method cannot be used for direct inversion of data containing suspected velocity reversals, it was felt that an attempt should be made to use another, preferably more robust, inversion technique to investigate further the implications of low-velocity-zones under parts of the Hillhouse - Broughton profile. Tau-P inversion (Bessonova et al 1974; Kennett 1976; Garmann et al 1979; Diebold & Stoffa 1981, amongst others) is a method of directly converting time-distance points (or complete seismograms (Clayton & McMechan 1981; McMechan 1983a;b) from the (T,X) plane, to the (Tau,P) plane and then inverting to produce a velocity-depth curve. It can be used for both refraction and Common Mid Point (CMP) reflection data.

For a fixed source refraction profile, the wave slowness U , in any part of the medium under the profile can be expressed as:

$$U = 1/V = (P^2 + Q^2)^{1/2}$$

where P = horizontal slowness

Q = vertical slowness

V = velocity of the medium

Thus at any point (X_i, T_i) on the time-distance graph, the tangent at that point is P_i and the time intercept is Tau_i . If the surface velocity is known, then assuming a horizontally travelling ray, $U_1 = P_1$, ($Q_1 = 0$). Otherwise if the offset from the source to the first receiver (X_1) is small then:

$$U_1 = 1/V_{app 1}$$

If a laterally homogeneous medium with horizontal layers is assumed then:

$$U_i = P_i \quad \text{ie } Q = 0$$

Thus it is now possible to use the relationship

$$Z_1 = \frac{\text{Tau } (P_2)/2}{(U_1^2 - P_2^2)^{1/2}}$$

to derive Z_1 , and then

$$Z_i = \frac{\text{Tau}(P_{i+1})/2 + \sum_{j=1}^{j=i-1} Z_j (U_j - P_{i+1})^{1/2}}{(U_i^2 - P_{i+1}^2)^{1/2}}$$

to derive values for $Z_{i=1, n-1}$ (after Diebold & Stoffa 1981, equation 15). The above relation for Z_1 is analogous to the plane-layer solution for two horizontal layers using the head-wave intercept time. Similarly, the relation for Z_i is analogous to the plane-layer solution for the i^{th} layer. More recent work (Milkereit et al 1985) has demonstrated the potential extension of this method to a laterally inhomogeneous medium.

The original method of applying the Tau-P inversion was tested firstly on some of the data used in the WHB integral interpretation, since velocities and depths for these data were already known. The results of these comparisons are shown in figures 4.23 and 4.25. In general the agreement is good, but with a tendency of the Tau-P method to produce slightly higher velocities for any given depth (as expected for a method similar to the plane-layer method). However some of the local discrepancies, where present, may be due to the rather coarse sampling intervals used in some of the WHB

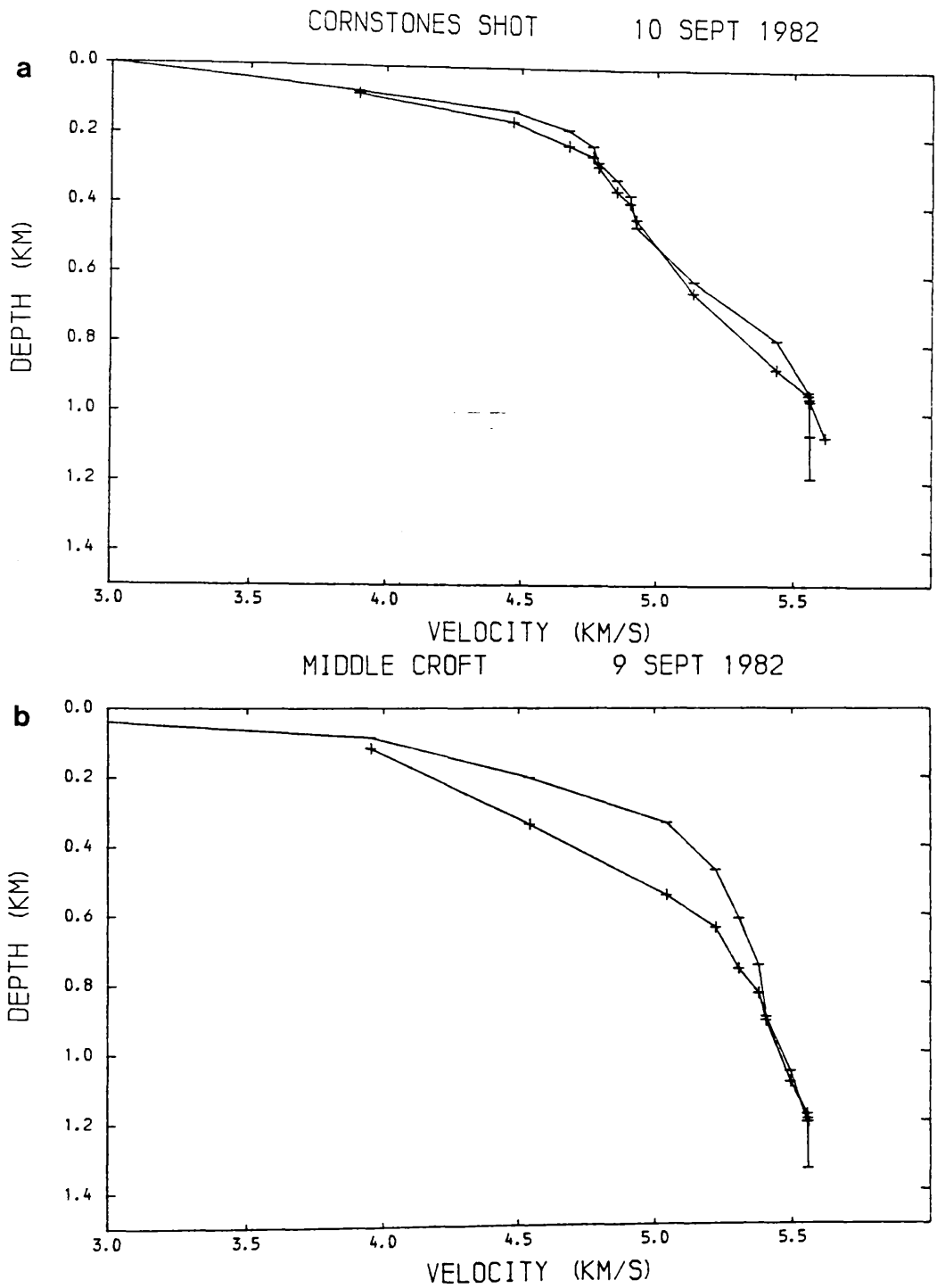


Figure 4.23 Comparison of WHB and Tau-P velocity-depth curves.
(+ WHB, - Tau-P)

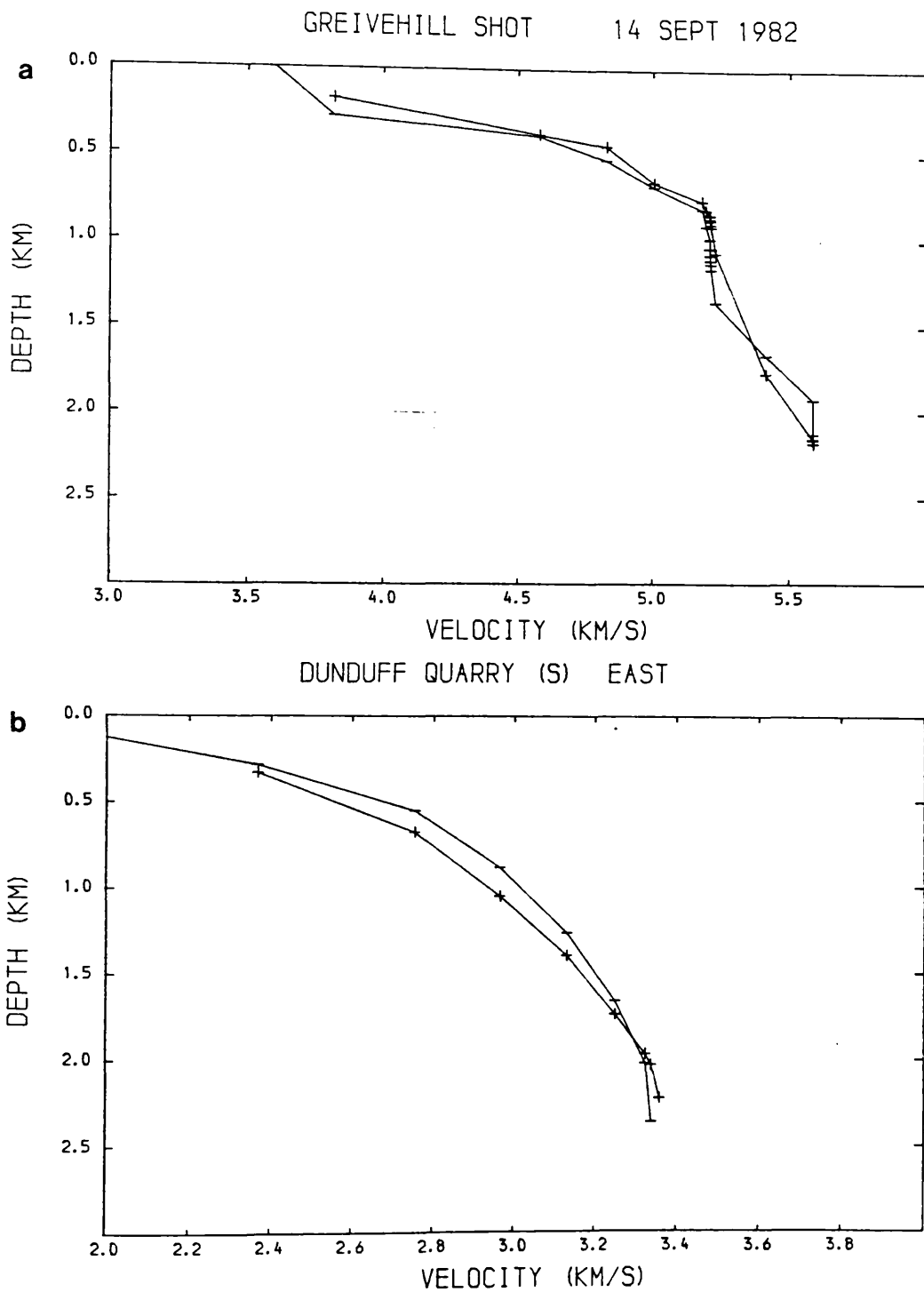


Figure 4.24 Comparison of WHB and Tau-P velocity-depth curves.
 (+ WHB, - Tau-P)

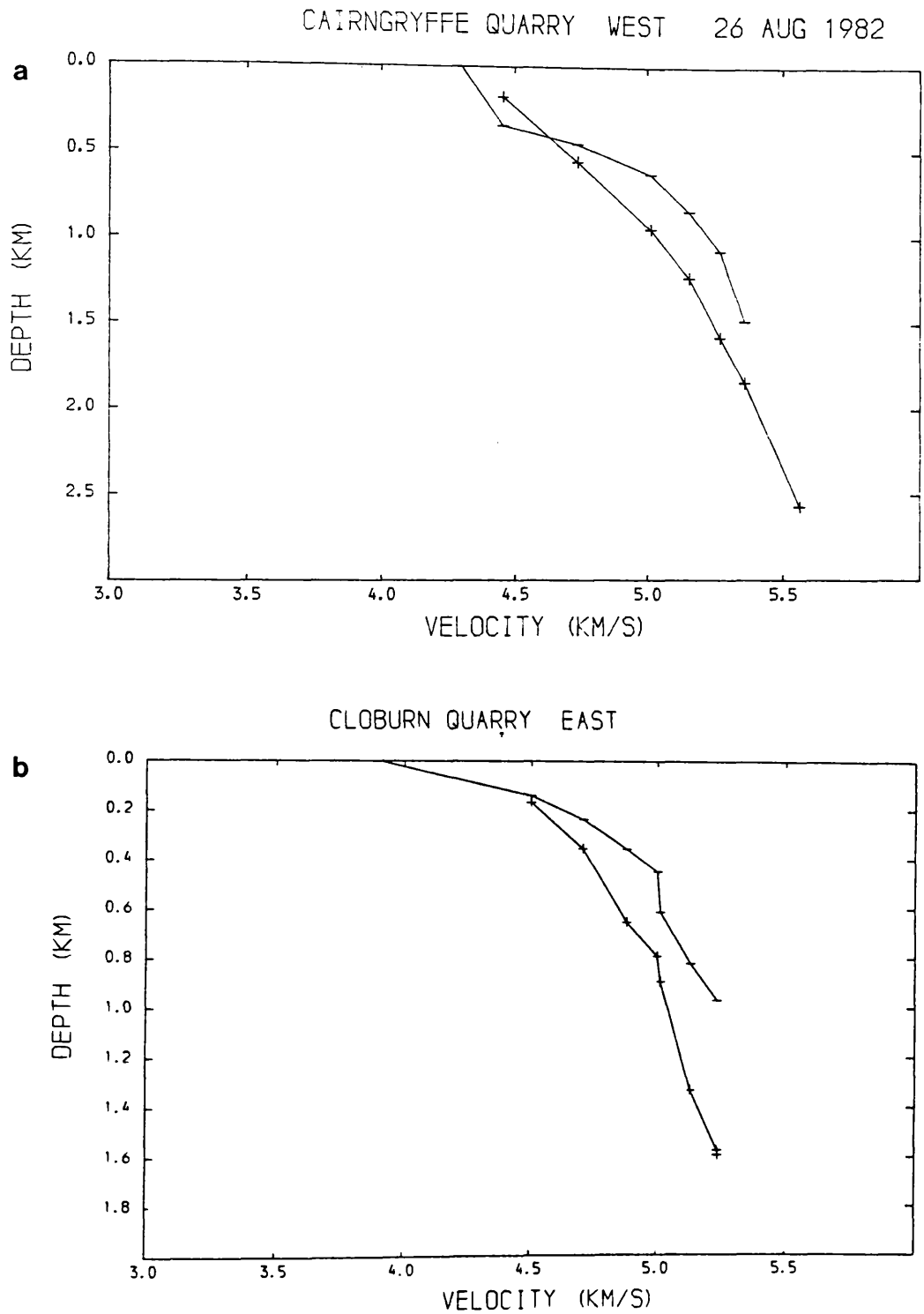


Figure 4.25 Comparison of WHB and Tau-P velocity-depth curves.
(+ WHB, - Tau-P)

datasets.

This technique was written into a simple program (TAUP; listing Appendix 6) and then applied to time-distance data generated from the velocity-depth curve supplied to the plane layer interpretation program LAUFZEIT for the Dunduff dataset recorded to the east of Dunduff Quarry. As with the previous two interpretation methods, this technique suffers from the serious limitation in an area of considerable geological complexity such as the Midland Valley, in that it assumes lateral velocity homogeneity. As a result of this, it was decided to test this method on the data obtained E of Dunduff, where it was felt that lateral velocity homogeneity was most probable. Here it was suspected that a velocity reversal might be present at around 2.0 - 2.5 km depth, and so if the method is sound, then the program TAUP should reduce the synthetic-time-distance dataset back to something resembling the original LAUFZEIT input V-Z curve (see figure 4.26). The LAUFZEIT output produces synthetic time-distance curves which are calculated from equal increments of the emergent ray angle resulting in a large number of (T,X) points at irregular but generally very small intervals (particularly for the direct arrival and also at short ranges). In this way, any effects produced by the coarse sampling on the WHB tests should be nullified, but the irregular spacings possibly coupled with insufficient precision in the calculations then resulted in a wide scattering of data at short ranges. Under testing with the direct and refracted arrivals only, the main features of the direct arrival are reproduced as are the velocities of the two refractors. The depth to the tops of the refractors are reasonably well fixed but thickness estimates are somewhat exaggerated. Further development and refinement of this technique would involve slant-stacking of the digital traces used in this example using the method outlined by McMechan (1983a; b), but lack of time has precluded its implementation here.

The strength of this method over the plane layer method is that it provides

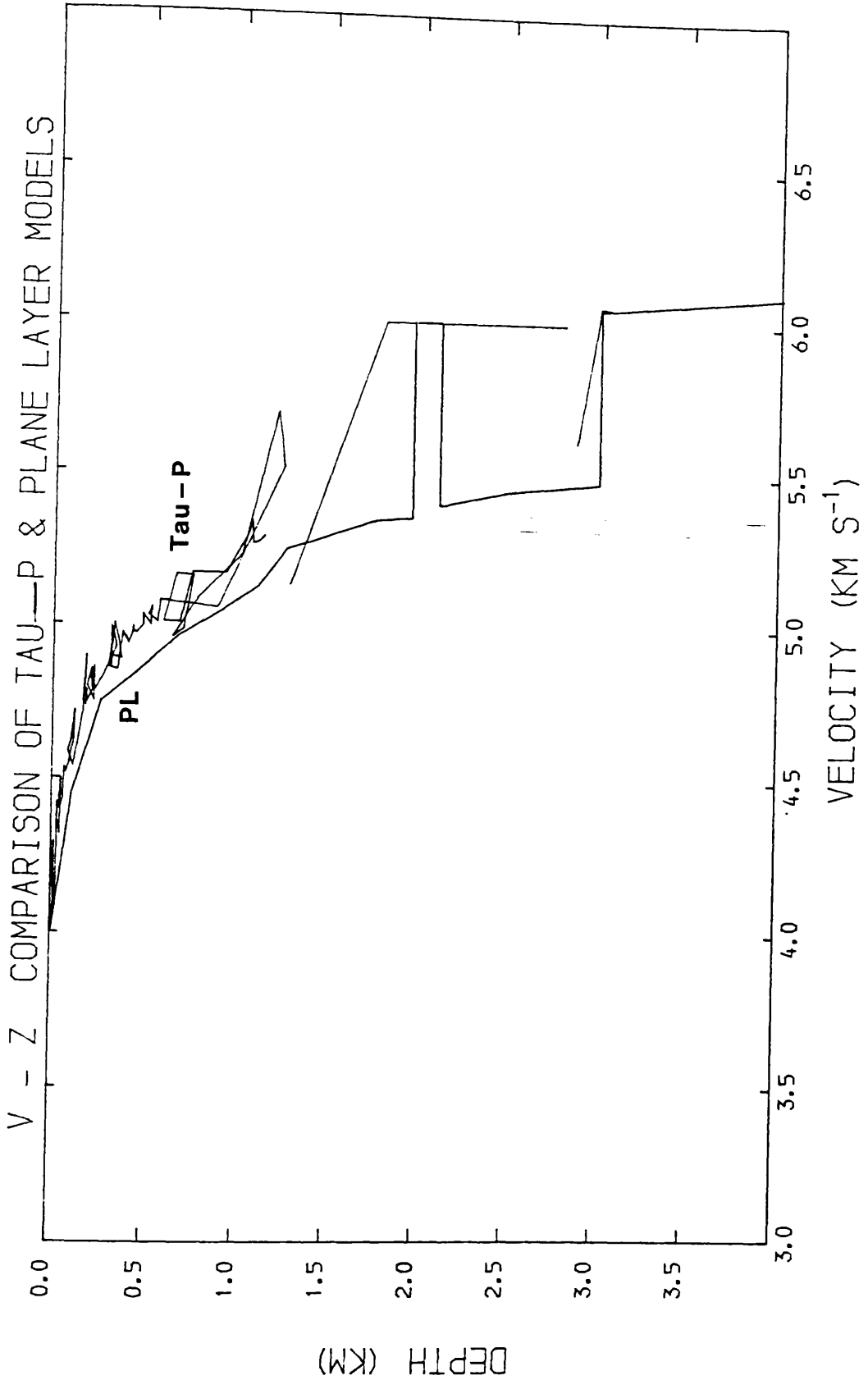


Figure 4.26 Comparison of plane-layer and Tau-P velocity-depth curves for the Dunduff quarry East dataset.

direct inversion of field data, while (unlike the WHB inversion) retaining the potential to model low-velocity-zones. It does however rely heavily on all segments of the T-X curve to provide accurate determinations of the depths and thicknesses of refracting layers (eg see Garmany et al 1979) Milkereit et al 1985), and so its application here to first-arrival data at unequally spaced intervals does not show this technique to fullest advantage.

4.1.5 Summary of the initial surface layer velocity interpretation

The initial velocity-depth interpretation produced using the WHB integral and plane layer methods are summarised in figures 4.27 and 4.28. In both figures, the internal consistency is good with the exception of the curve corresponding to the plane layer interpretation of the P-waves from the initial 16 km of the Hillhouse East line (this *dataset* was not suitable for direct inversion using the WHB integral). This line differs from the other two in starting from within a basic sill in Carboniferous sediments and the correspondingly lower near surface velocities confirm this. Below 0.8 km depth, a layer with a similar vertical velocity gradient but lower velocities to the other curves was inferred to represent the local Old Red Sandstone on the basis of modelling of the local gravity field (McLean 1966). This disparity was better quantified with later ray modelling.

The remaining V-Z curves show P-wave velocity distributions which below about 0.5 km depth are consistently within a band of velocities with a width of around 0.5 km s^{-1} . Above this surface velocities appear to be directly related to near-surface lithology with lower velocities across the shale-siltstone-sandstone sequence of the Lesmahagow Inlier, and higher velocities across the arenaceous sandstones of the Lower Old Red Sandstone further E.

These curves are plotted along with the published V-Z curves for the Midland Valley from the LISPB profile (Assumpcao & Bamford 1978) and the LOWNET study (Crampin et al 1970). Referring firstly to the P-wave curves,

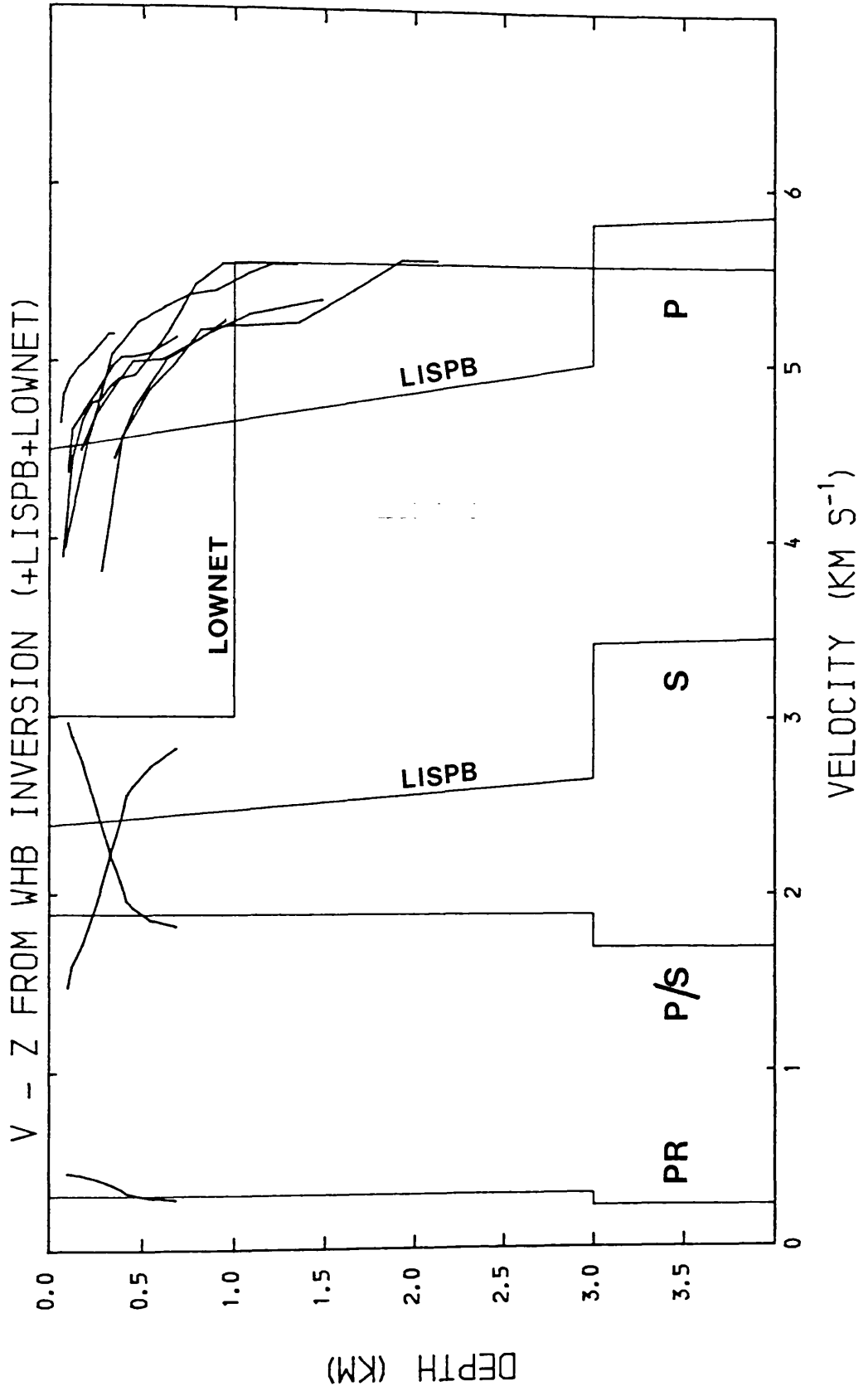


Figure 4.27 Velocity-depth curves for all the WHB interpretations plotted alongside those for the LISPB & LOWNET models.

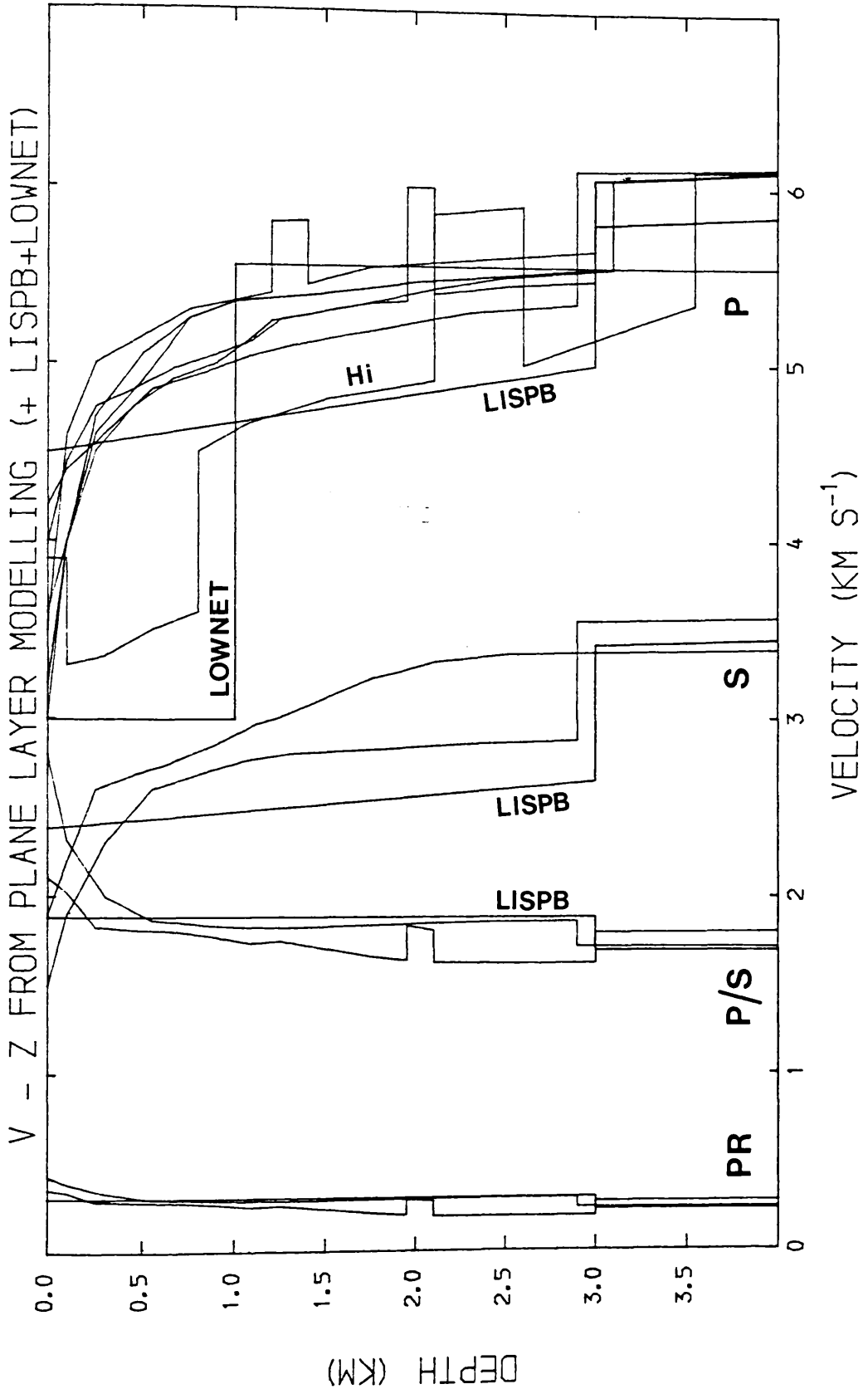


Figure 4.28 Velocity-depth curves for all the plane-layer interpretations plotted alongside those for the LISPB & LOWNET models.
(Hi = Hillhouse Q. East)

the LISPB estimate for surface sedimentary velocities is seen to be a poor estimate of these velocities across most of the area of Lower Old Red Sandstone and Silurian outcrop in the southern Midland Valley, being consistently slow with depth from depths of less than 0.5 km down to 3 km. The only exception to this is the line recorded from Hillhouse quarry where the layer extending from 0.8 - 3.5 km and attributed to the local Lower Old Red Sandstone, forms a good fit to the LISPB V-Z curve. On this line the overlying Carboniferous sediments give much lower velocities as expected from previous work (Hall 1974;1971). Thus the LISPB surface layer velocity can be shown to be an average of lower velocity Carboniferous sediments and higher velocity Lower Old Red Sandstone and Silurian sediments.

From figures 4.27 and 4.28 the 5.56 km s^{-1} from the LOWNET study can be seen to provide a reasonable upper limit to the range of P-wave velocities found below 1 km depth. Above this, the LOWNET model velocity of 3 km s^{-1} is much lower than anything found in this study. In fact this layer occurs in the published LOWNET dataset (Crampin et al 1970) only as a delay on the 5.56 km s^{-1} refractor and was justified by the fact that all the LOWNET receiver sites are sited on Lower Old Red Sandstone or older rocks, whereas the majority of sources were from within areas of Carboniferous outcrop. The 3 km s^{-1} value represents a best estimate at that time for the Carboniferous sedimentary sequence and the 1 km depth value is the resulting average thickness of Carboniferous sediments as limited by the extent of their data.

The only direct measurements of surface S-wave structure come from data recorded to the E of Dunduff quarry. Combining these data with an assumed average P-wave model for this region gives Poisson's ratio values (figure 4.5) which are always less than 0.25 below 1 km depth, and are less than or equal to 0.21 below 1.5 km depth. As discussed in section 4.1.2, these results are compatible with the existence of a sequence of dominantly quartz-

rich, clastic sediments and confirm that the lithology observed at the surface in this region can be considered to extend unchanged to at least 2.5 km depth.

Figure 4.29 shows the above results plotted for comparison with the LISPB and LOWNET V-Z curves. The higher S-wave velocities recorded between Dunduff and Cairngryffe quarries result in values of V_p/V_s and Poisson's ratio which are considerably lower than those recorded to the N and S of Edinburgh by the LISPB profile (Assumpcao & Bamford 1978).

The results described above along with the results of the interpretation of the LES close shots fulfill one of the initial aims of this project as outlined in section 3.1.

There is no evidence from the LES close shots of P-wave velocities approaching 5.8 km s^{-1} over the Lower Palaeozoic outcrop, neither is there any evidence of such high velocities within 2 km depth under the region between Dunduff and Cairngryffe quarries. Geological evidence suggests that Lower Palaeozoic sediments should be continuous from the Lesmahagow Inlier to the Carmichael Inlier, and so should be present under the region between these two quarries at depths of less than 2 km. A high velocity refractor ($V_p > 6.0 \text{ km s}^{-1}$) is present under this area at a depth of around 3 km, but it is continuous under the Lesmahagow Inlier and so cannot represent any of the lithologies seen at the surface. From these results, it must be concluded that the LISPB interpretation of the a_0 refractor ($V_p = 5.8 \text{ km s}^{-1}$) is erroneous. Alternative interpretations will be discussed in the following sections.

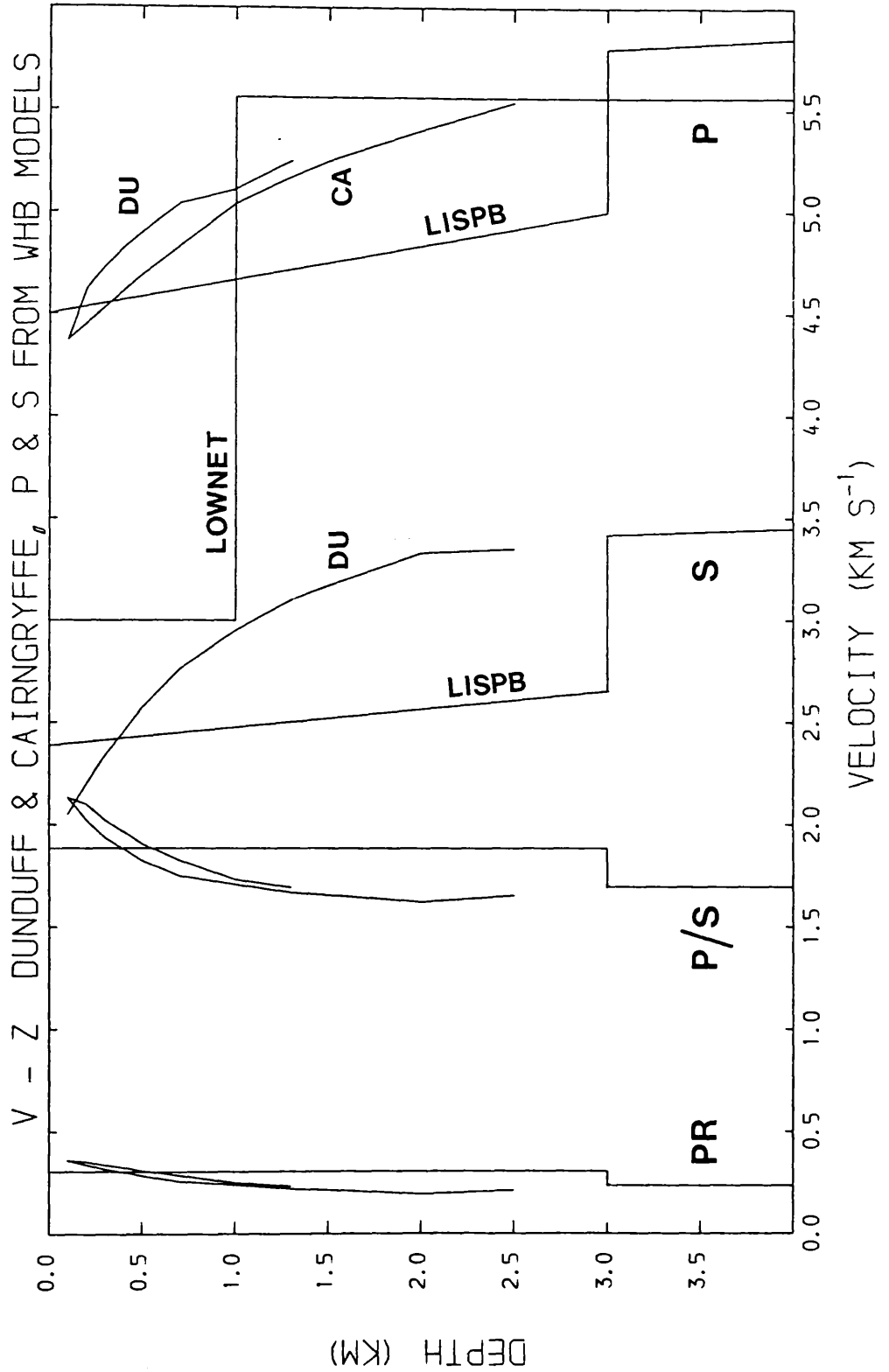


Figure 4.29 Velocity-depth curves from the WHB interpretations of Dunduff P & S-wave data, and Cairngryffe P + Dunduff S-wave data, plotted alongside those for the LISPB & LOWNET models.

4.2 Interpretation of deep structure

4.2.1 Time-term study

4.2.1.1 Introduction

The time-term method (Willmore & Bancroft 1960) is a method of obtaining delay times for recording sites over a given refractor and obtaining a least-squares value for the velocity of this refractor. It is best suited to 2D recording arrays rather than profiles, and particularly where data from many sources are present.

The relation of a recorded travel time to its range and time-terms can be represented by:

$$T_i = a_s + a_r + X_i/V_{ref}$$

where T_i = the i^{th} travel time

X_i = the i^{th} range

$a_{s/r}$ = the source and receiver time-terms
respectively

The time-term for any station is related to the thickness Z , and the velocity-depth structure $v(z)$, of the overlying layer by:

$$a_i = \sum_{z=0}^{z=Z} v^2 - v^2(z)/V * v(z) dz$$

A series of simultaneous equations can be constructed from the travel time data and solved to give values with standard errors for all the source and receiver sites, and the refractor velocity. This type of solution is most meaningful if the residual formed from the degree of each time-term equation is of similar magnitude to the observed travel-time standard errors. It is assumed that all the travel-time data has similar observational error values, and an equal weighting is assigned to each on this basis. In addition it is

assumed that the refractor velocity is constant across the region of study. In order to attempt to correct for variations in observational error within a given dataset, a system of equation weighting was introduced using an empirical relation which assigns an integer to each travel-time equation on a scale of 1 - 10 based on the magnitude of the travel-time error for that equation. The relation used here was :

$$W_i = \text{integer component of } (1/DT) * 20$$

where W_i = weighting factor

DT = standard error on travel time

This gives the following table

W	DT (sec)
10	< 0.005
8	0.006
7	0.007
6	0.008-0.009
5	0.010-0.011
4	0.012-0.014
3	0.015-0.020
2	0.021-0.033
1	> 0.034

figure 4.30

The value of W is used to produce W identical equations which can then be used in the normal way.

The error in the travel-times can be compared with the solution residuals by using the F ratio method (Whitcombe & Maguire 1979; Whitcombe & Rogers 1981). This method computes a value for the variance of the travel time data by the following means;

$$s_0^2 = \sum_{i=1}^{i=I} \sum_{k=1}^{k=K_i} (\text{Tobs}_{ik} - \bar{\text{Tobs}}_i)^2 / S$$

where Tobs_{ik} = the k^{th} observation of the i^{th} time

$\bar{\text{Tobs}}_i$ = the mean observed value of Tobs_i

k = number of pickings of the i^{th} time

i = number of travel times in the dataset

and where $S = \sum_{i=1}^{i=I} (K_i - 1)$

The time-term solution variance is given by;

$$s_s^2 = \sum_{i=1}^{i=I} r_i^2 / I - N - 1$$

where r_i = i^{th} equation residual

i = the number of the observation

The F ratio for any solution is then

$$F = s_s^2 / s_0^2$$

In practice, the quantity s_0^2 is impossible to calculate precisely as it is derived from the variance of travel-time picks around a mean value, and it is not normally possible to be totally objective and repick a travel time several times in isolation. However, if an arrival is picked and a realistic measure of the uncertainty is included then intuitively, this range should cover all possible values of picking. Thus

$$s_0^2 = \sum_{i=1}^{i=I} t_i / I - 1$$

where t_i = error in the i^{th} arrival time picking

This is easily calculable and should be of the same magnitude, although generally slightly smaller than, the predicted theoretical value. As a result the F ratio calculated by this means will be somewhat lower than its theoretical value.

4.2.1.2 Application of the time-term method to this study

Three overlapping datasets were prepared so as to provide comparisons between each of the geographical regions for which travel time data was available. Set A comprised the data from the Hillhouse - Broughton profile only; set B incorporated A with data from Middleton and Craigpark (twice) quarries; and set C included B plus the Central Coalfield quarries. This subdivision of the data was designed to allow a comparison of set A with other interpretive methods used on the profile data, as well as checking for any along strike continuity of the model towards Edinburgh (set B), and finally into the Central Coalfield (set C). In particular, set A could be compared with the ray model, allowing calibration of the time-terms and their depths. All sources were used where timed data within the ranges of 18 - 50 km were available.

In order to test the effect of weighting the travel time equations, solutions for all three sets were obtained using both unweighted and weighted equations and these results are shown in figure 4.31. Two types of standard error are included for each time-term: E1 represents the standard error due to the fit of the site time-term to the solution, whereas E2 represents the

DATASET A				DATASET B				DATASET C				SITE NAME						
UNWEIGHTED		WEIGHTED																
TT	E1	E2	TT	E1	E2	TT	E1	E2	TT	E1	E2	TT	E1	E2				
0.702	0.026	0.007	0.700	0.006	0.002	0.664	0.038	0.008	0.669	0.009	0.003	0.502	0.039	0.013	0.613	0.011	0.003	HILLHOUSE Q
0.240	0.019	0.001	0.241	0.004	0.001	0.253	0.028	0.015	0.253	0.006	0.005	0.181	0.035	0.033	0.235	0.008	0.006	DUNDUFF Q
0.481	0.022	0.003	0.477	0.005	0.001	0.443	0.032	0.003	0.447	0.007	0.001	0.290	0.029	0.008	0.397	0.008	0.002	CLOUBURN Q
0.298	0.029	0.032	0.297	0.007	0.014	0.293	0.045	0.033	0.295	0.012	0.014	0.325	0.059	0.025	0.299	0.014	0.001	GREIVEHILL SHOT
0.303	0.030	0.023	0.300	0.006	0.007	0.297	0.045	0.025	0.298	0.010	0.007	0.128	0.060	0.028	0.302	0.013	0.007	1A
0.276	0.032	0.003	0.275	0.007	0.001	0.268	0.050	0.007	0.274	0.011	0.002	0.297	0.066	0.014	0.277	0.015	0.002	2A
0.307	0.029	0.007	0.307	0.006	0.002	0.302	0.045	0.006	0.305	0.010	0.002	0.335	0.060	0.010	0.309	0.015	0.002	3A
0.273	0.029	0.008	0.273	0.006	0.002	0.267	0.045	0.009	0.271	0.010	0.002	0.299	0.060	0.015	0.275	0.013	0.003	4A
0.261	0.029	0.007	0.260	0.006	0.002	0.258	0.044	0.002	0.259	0.010	0.001	0.295	0.059	0.011	0.265	0.130	0.001	5A
0.259	0.030	0.011	0.257	0.006	0.003	0.252	0.046	0.008	0.255	0.010	0.002	0.282	0.059	0.013	0.259	0.013	0.002	6A
0.280	0.038	-----	0.279	0.008	0.000	0.277	0.058	-----	0.279	0.014	0.000	0.314	0.077	-----	0.284	0.018	0.000	1B
0.267	0.038	-----	0.266	0.008	0.000	0.284	0.058	-----	0.286	0.014	0.000	0.321	0.077	-----	0.291	0.018	0.000	3B
0.284	0.037	-----	0.284	0.008	0.000	0.265	0.058	-----	0.267	0.013	0.000	0.304	0.077	-----	0.272	0.018	0.000	4B
0.253	0.037	-----	0.253	0.008	0.000	0.284	0.057	-----	0.285	0.013	0.000	0.327	0.076	-----	0.293	0.018	0.000	5B
0.271	0.037	-----	0.271	0.008	0.000	0.254	0.057	-----	0.255	0.013	0.000	0.299	0.076	-----	0.263	0.017	0.000	6B
0.271	0.037	-----	0.271	0.008	0.000	0.273	0.056	-----	0.274	0.013	0.000	0.323	0.075	-----	0.284	0.017	0.000	7B
0.338	0.035	-----	0.336	0.007	0.000	0.350	0.055	-----	0.349	0.012	0.000	0.440	0.071	-----	0.376	0.016	0.000	CAIRNHILL FM
0.299	0.029	0.003	0.295	0.006	0.001	0.279	0.043	0.015	0.283	0.010	0.005	0.292	0.058	0.043	0.281	0.012	0.009	1C
0.230	0.028	0.016	0.228	0.006	0.005	0.211	0.043	0.026	0.217	0.010	0.008	0.226	0.057	0.050	0.215	0.013	0.012	2C
0.216	0.028	0.014	0.210	0.006	0.004	0.198	0.042	0.020	0.194	0.010	0.005	0.216	0.056	0.037	0.190	0.013	0.007	3C
0.157	0.032	0.020	0.157	0.007	0.004	0.150	0.049	0.003	0.153	0.011	0.001	0.140	0.066	0.041	0.154	0.014	0.003	1D
0.315	0.046	-----	0.309	0.009	0.000	0.287	0.070	-----	0.292	0.015	0.000	0.262	0.093	-----	0.275	0.020	0.000	2D
0.317	0.050	-----	0.309	0.019	-----	0.279	0.076	-----	0.285	0.031	-----	0.227	0.101	-----	0.258	0.041	-----	3D
0.489	0.040	-----	0.483	0.013	0.000	0.441	0.059	-----	0.447	0.022	0.000	0.388	0.069	0.026	0.362	0.021	0.017	4E
0.481	0.042	-----	0.476	0.009	0.000	0.355	0.047	0.073	0.370	0.012	0.023	0.404	0.071	0.014	0.390	0.025	0.008	6E
0.202	0.035	-----	0.203	0.009	0.000	0.218	0.039	0.018	0.229	0.011	0.008	0.321	0.047	0.014	0.262	0.014	0.007	S1
0.192	0.035	-----	0.193	0.009	0.000	0.214	0.040	0.011	0.217	0.011	0.006	0.319	0.046	0.012	0.258	0.013	0.006	S2
0.212	0.035	-----	0.213	0.009	0.000	0.214	0.040	0.009	0.219	0.001	0.004	0.318	0.047	0.009	0.259	0.014	0.009	S3
0.190	0.035	-----	0.191	0.009	0.000	0.220	0.042	0.009	0.222	0.012	0.006	0.324	0.050	0.017	0.264	0.014	0.009	S4
0.217	0.035	-----	0.219	0.009	0.000	0.277	0.050	0.035	0.235	0.015	0.016	0.313	0.058	0.028	0.262	0.017	0.014	S5
0.232	0.035	-----	0.233	0.009	0.000	0.250	0.044	0.018	0.248	0.013	0.008	0.390	0.045	0.025	0.313	0.014	0.012	N1
0.232	0.035	-----	0.233	0.009	0.000	0.232	0.048	0.166	0.236	0.015	0.052	0.304	0.054	0.744	0.238	0.017	0.037	N2
0.215	0.016	-----	0.216	0.009	0.000	0.268	0.041	0.020	0.270	0.012	0.010	0.340	0.047	0.025	0.312	0.014	0.012	N3
			0.216	0.009	0.000	0.268	0.040	0.009	0.270	0.011	0.005	0.343	0.047	0.025	0.312	0.014	0.012	N4
			0.690	0.050	0.020	0.642	0.052	0.014	0.641	0.013	0.009	0.456	0.046	0.025	0.608	0.016	0.014	MIDDLETON Q
			0.650	0.054	0.020	0.650	0.054	0.020	0.655	0.014	0.011	0.372	0.044	0.021	0.530	0.015	0.018	CRAIGPARK Q (1)
												0.398	0.050	0.014	0.560	0.017	0.008	CRAIGPARK Q (2)
												0.505	0.063	0.026	0.596	0.019	0.008	HEADLESSCROSS OC
												0.721	0.051	0.026	0.901	0.017	0.022	DUNTILLAND Q
												0.574	0.053	0.013	0.742	0.017	0.007	TAMS LOUP Q

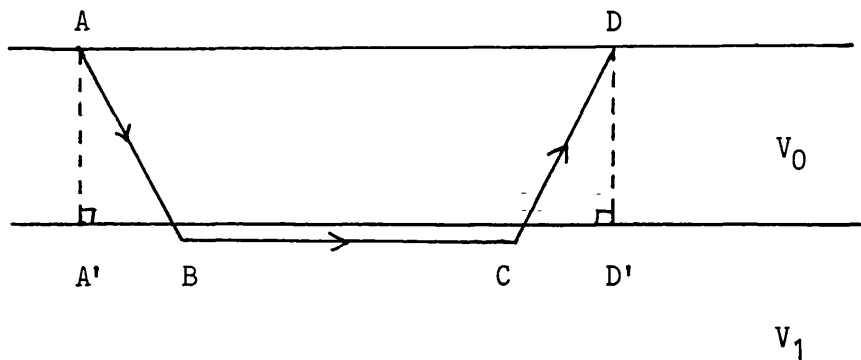
Figure 4.31 Time-terms and residuals calculated for datasets A, B & C. For each time-term, the E1 error represents the time residual with respect to the overall solution, and the E2 error the residual attributable to local variations under each site. Where only one travel-time exists for any site, the E2 error is not calculated.

variation in time-terms of individual rays incident at that site. The weighting factors resulted in a 5-fold increase in the number of equations used, a halving of the standard error in the solution and a 4-fold decrease in the standard error on the refractor velocity determination. Thus the weighting process results in a more precise solution for each of the three datasets. Set against this, a 5-fold increase in program memory storage was required and the job timing increased similarly. The enlarging of the memory storage requirement created operational problems as regards the execution of jobs during the normal working day, and so all jobs had to be specially labelled and run individually during quiet times in the computer schedule (usually very early in the morning).

The largest variations between unweighted and weighted solutions is seen in set C, which also has the poorest solution fits, and refractor determinations which are inconsistent with the other sets. As a result, it was concluded that the sets A and B are representative of sites above a uniform continuous refracting horizon, whereas the time-terms obtained from the Central Coalfield must have additional variables to affect the solution, either in refractor type or in structure. This observation is further strengthened by noting that the anomalous sources all have unusually high apparent velocities for ranges of less than 50 km. It is conceivable that these velocities could be coming from an updip section of the 6.4 km s^{-1} refractor, itself at an unusually high crustal level, but to confirm this more evidence would be required, perhaps along the lines of direct determination of the depth to this layer under the quarries by reversed refraction coverage. Set C was therefore excluded from further analysis. Set A was not considered any further as it could be assumed to be a subset of set B.

The value for the refractor velocity from set B at $6.20 \pm 0.06 \text{ km s}^{-1}$ (figure 4.31) is slightly but significantly larger than the velocities derived from the plane layer and WHB interpretations. In view of this and

also of the ray modelling of the Hillhouse - Broughton profile which placed the refractor velocity at around $6.05\text{--}6.10 \text{ km s}^{-1}$, it was suspected that the solutions were being affected by complexities in the overlying sedimentary layer. In order to test this, the calculations were repeated assuming that the refractor velocity was known (and so could be fixed), and constant across the region of set B. These values were compared with time-term values calculated directly from the ray model. Calculated time-terms were produced by the following method:



The total travel time can be represented by either

$$t_{AD} = t_{AB} + t_{BC} + t_{CD}$$

or

$$t_{AD} = a_s + a_r + A'D' / V_{ref}$$

this can be rewritten as

$$t_{AD} = a_s + a_r + (A'B/V_{ref} + BC/V_{ref} + CD'/V_{ref})$$

since

$$t_{BC} = BC / V_{ref}$$

then

$$\begin{aligned} a_s + a_r &= t_{AD} - t_{BC} - A'B/V_{ref} - CD'/V_{ref} \\ &= t_{AB} + t_{CD} - A'B/V_{ref} - CD'/V_{ref} \end{aligned}$$

$$a_s + a_r = (t_{AB} - A'B/V_{ref}) + (t_{CD} - CD'/V_{ref})$$

and assuming the source and receiver structures are independent, and can be isolated, gives

$$a_s = t_{AB} - A'B / V_{ref}$$

and

$$a_r = t_{CD} - CD' / V_{ref}$$

This information was available in numerical form from the output of the ray plotting program RAYPLT (see 4.2.2.1) and the results of this test are shown in figures 4.32 and 4.33 in comparison with the calculated values of the time-terms for sites on the Hillhouse - Broughton profile. Where standard errors are quoted for the calculated time-terms, these were produced from the range of values resulting from more than one ray being incident at that site and so can be used to give a measure of the variation in surface layer velocity structure around that site.

The general trends of these two independent sets of data are comparable. There are two areas of significant difference; under Hillhouse quarry and under, and to the E of, Cloburn quarry. The unweighted time-term under Hillhouse quarry is almost 20% greater, implying a greater true depth to the refractor compared with the ray model or lower velocities in the overlying surface layer. From the interpretations of surface structure across the profile already presented in section 4.1.2 and 4.1.3, and summarised in figures 4.27-29, there is good evidence to support the argument for lower surface velocities in this area. The three large time-term values between 60 - 70 km are similarly unexpectedly slow. The same explanations as above can

TIME-TERMS PRODUCED WITH DATASET B FOR REFRACTOR VELOCITY FIXED AT
6.05 KM/S, AGAINST CALCULATED TIME-TERMS FROM THE RAY MODEL

UNWEIGHTED			WEIGHTED			RAY MODEL			SITE NAME
TT	E1	E2	TT	E2	E2	CL	TT	ST E	
0.604	0.033	0.011	0.601	0.008	0.004	0.525	0.003	HILLHOUSE Q	
0.230	0.029	0.011	0.227	0.007	0.004	0.279	-----	DUNDUFF Q	
0.400	0.029	0.004	0.402	0.007	0.002	0.300	0.014	CLOBURN Q	
0.227	0.041	0.032	0.226	0.012	0.013	0.306	0.018	1A	
0.228	0.041	0.025	0.227	0.009	0.013	0.282	0.027	2A	
0.199	0.046	0.009	0.202	0.011	0.002	0.291	0.022	3A	
0.235	0.041	0.007	0.236	0.009	0.002	0.302	0.030	4A	
0.200	0.041	0.012	0.201	0.009	0.003	0.300	0.030	5A	
0.195	0.041	0.008	0.194	0.009	0.002	0.359	0.052	6A	
0.182	0.041	0.016	0.184	0.009	0.005	0.261	0.038	8A	
0.212	0.057	-----	0.209	0.014	0.000	-----	-----	1B	
0.218	0.057	-----	0.216	0.014	0.000	-----	-----	3B	
0.201	0.057	-----	0.199	0.014	0.000	-----	-----	4B	
0.224	0.057	-----	0.221	0.014	0.000	-----	-----	5B	
0.196	0.057	-----	0.193	0.014	0.000	-----	-----	6B	
0.219	0.057	-----	0.217	0.014	0.000	-----	-----	7B	
0.342	0.059	-----	0.345	0.014	0.000	0.448	-----	CAIRNHILL	
0.212	0.038	0.033	0.222	0.010	0.012	0.334	0.064	1C	
0.146	0.038	0.043	0.152	0.010	0.015	0.284	0.046	2C	
0.136	0.038	0.033	0.128	0.009	0.011	0.266	0.001	3C	
0.082	0.046	0.034	0.079	0.010	0.008	0.304	0.012	1D	
0.171	0.059	-----	0.174	0.013	0.000	0.289	-----	2D	
0.138	0.059	-----	0.141	0.013	0.000	0.330	-----	3D	
0.372	0.057	-----	0.374	0.034	0.000	0.314	-----	4E	
0.292	0.044	0.050	0.299	0.012	0.016	0.316	-----	6E	
0.186	0.041	0.018	0.193	0.013	0.008	0.274	-----	S1	
0.177	0.041	0.010	0.177	0.013	0.005	0.274	-----	S2	
0.176	0.041	0.010	0.177	0.013	0.005	0.274	-----	S3	
0.180	0.043	0.002	0.179	0.013	0.002	0.273	-----	S4	
0.174	0.050	0.036	0.176	0.017	0.016	-----	-----	S5	
0.232	0.047	0.020	0.228	0.015	0.009	0.278	-----	N1	
0.205	0.050	0.115	0.205	0.017	0.051	-----	-----	N2	
0.239	0.043	0.019	0.236	0.013	0.010	0.274	-----	N3	
0.209	0.041	0.008	0.208	0.012	0.004	0.278	-----	N4	
0.598	0.039	0.020	0.597	0.012	0.011	-----	-----	MIDDLETON Q	
0.538	0.037	0.011	0.536	0.011	0.007	-----	-----	CRAIGPARK Q (1)	
0.542	0.039	0.020	0.542	0.012	0.011	-----	-----	CRAIGPARK Q (2)	
0.049			0.033					SR ERR SOLN	
14.782			6.684					F RATIO	
6.050			6.050			6.050		REFR VEL	

Figure 4.32 Comparison of the time-term solution obtained by fixing V_{ref} at 6.05 km s^{-1} , and time-terms calculated from the ray model (where V_{ref} at 3 km depth is modelled at 6.05 km s^{-1}). These results are shown graphically in figure 3.33

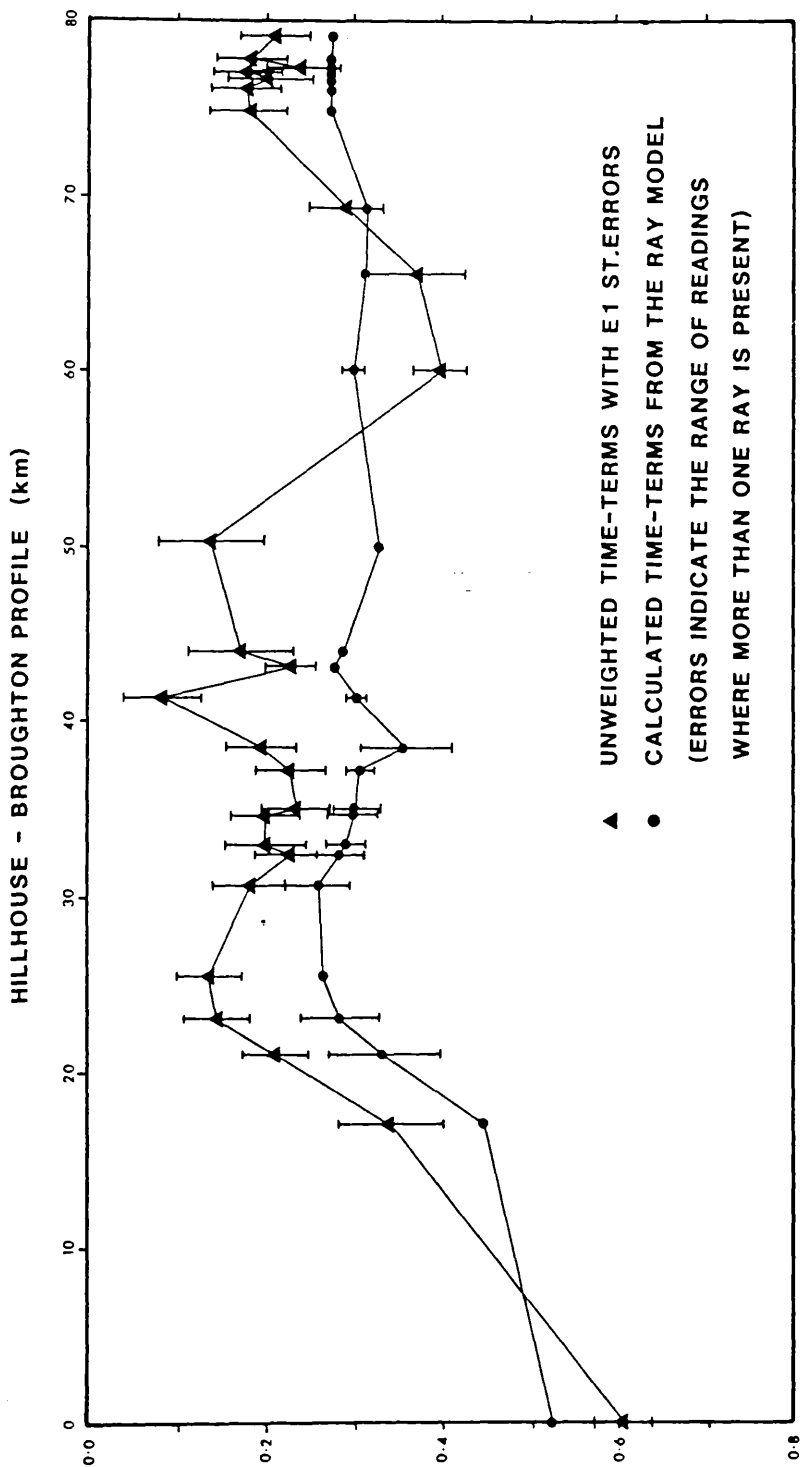


Figure 4.33 Comparison of time-terms across the Hillhouse-Broughton profile.

be offered, but there is less geological evidence to support the argument for significantly lower surface velocities in the area E of Cloburn quarry (although see 3.2.3.2 & 4.3) compared with the known Carboniferous sequence under Hillhouse quarry. The alternative is that the basement refractor is deeper in this region; a view predicted by the downwards extrapolation of the local surface geology. This apparent contradiction between these two interpretations will be discussed in section 4.2.2.4. While the validity of the ray model as an exact solution may be dubious, it is significant that the calculated values often show large variations at any given site thus indicating the presence of lateral inhomogeneity in the overlying sediments. This is in accordance with what can be deduced from the surface geology and also with the results of all the direct wave interpretations (see 4.1.2/3). However, the E2 standard errors, which are a measure of the variation of individual site time delays around its time-term value, rarely give such large values indicating that the simultaneous equations are oversimplifying the solution in the attempt to minimise all residuals. Thus in a region such as this where there is considerable lateral velocity inhomogeneity in the sedimentary layers, the time-term method will tend to produce solutions which are geologically erroneous and also give a false impression of accuracy. In this last respect, the weighting factor increases the illusion of accuracy of the solution and so may be quite misleading. However, in an area more suited to time-term analysis, the ability to grade and weight data could be a useful addition.

4.2.2 Ray-trace modelling

4.2.2.1 Procedure

As mentioned in 4.1.2.3, considerable lateral velocity and structural inhomogeneity has been found to exist across the Hillhouse-Broughton profile. The ray-trace method with its ability to model lateral changes in velocity as

well as structure, has proven to be the most useful interpretative method, and as a result has been used from an early stage in the data collection and interpretative process. The ray-trace program used during the first two years of this project was a slightly modified version of the Cerveny & Psencik 1971 program, as used by D. Bamford and co-workers on the LISPB project. While it was possible to model velocity variations within a layer reasonably satisfactorily, the use of interfaces was very limited, and so this constrained quite severely the number of possible structural interpretations which could be realistically achieved at that stage.

However, the arrival in the autumn of 1983 of the Karlsruhe University version of the SEIS81 package (Cerveny & Psencik 1981) gave a considerable increase in the interpretative potential of ray-tracing to this project.

The SEIS81 package consists of two main sections: the SEIS81 ray-tracing program with an attendant plotting program, and the programs SYNTPL and SEISPL which would calculate and plot the synthetic seismograms resulting from the ray model. Because of the methods used to obtain this dataset and the complexity of a typical quarry-blast source wavelet secondary arrivals are difficult to recognise and correlate between traces, and so the synthetic seismogram programs were not used as part of the interpretive procedure.

The SEIS81 program is a two-point ray-tracing program using the 'shooting' method of initiating a ray. This is an iterative process whereby, for each receiver station in turn, a trial ray is generated using specified initial ray parameters and is traced through the model back to the surface. The difference between the position of the ray termination at the surface and the intended receiver point is calculated and a new initial ray parameter chosen. This ray is then traced through the model and the difference between the termination point and the intended receiver measured. This process continues until the traced ray terminates at the chosen receiver point (or within the

supplied tolerances). Each ray is dealt with similarly.

The other major improvement of the SEIS81 program over the earlier program is in its ability to accept a wide variety of shapes and configurations of crustal interfaces, thus allowing much greater realism to be built into a crustal model. Modifications to the program have been to produce an output of the final velocity-range-depth matrix to a secondary program (RAYVZ, listing Appendix 6) which can then plot this matrix as either an isometric block diagram or as a sequence of isovelocity lines, and the addition of a subroutine to calculate linear interpolation of the velocity matrix (P. Tsumakous, private communication) which can be used in place of the standard bicubic spline interpolation for any layer within the model. This has proved useful where large lateral velocity changes (either real or fictitious) are required within one layer, so provoking instability from the bi-cubic interpolation routine.

4.2.2.2 The ray model and surface velocity structure

An initial velocity model was produced for the Hillhouse - Broughton profile from the methods described in sections 4.1.2 and 4.1.3, and used as a basis for ray modelling using the ray-tracing packages described above. The resulting ray model (figure 4.34, velocity model figures 3.35,36) confirms the existence of a surface layer with considerable lateral as well as vertical variations in velocity structure, overlying a layer where little, if any, lateral inhomogeneity appears to be present. Ray-tracing was continued until the computed travel times were within 30 ms of the field data travel times. The ray diagrams are shown in figures 4.37 to 4.41 and the fit of the model to travel time picks and field seismograms is shown in figures 4.42 to 4.50. The origin and nature of the extended sill-like body at 2 km depth beneath the western end of the modified model (figure 4.38) are discussed further in 4.2.2.3). All computed and field travel time data are listed in

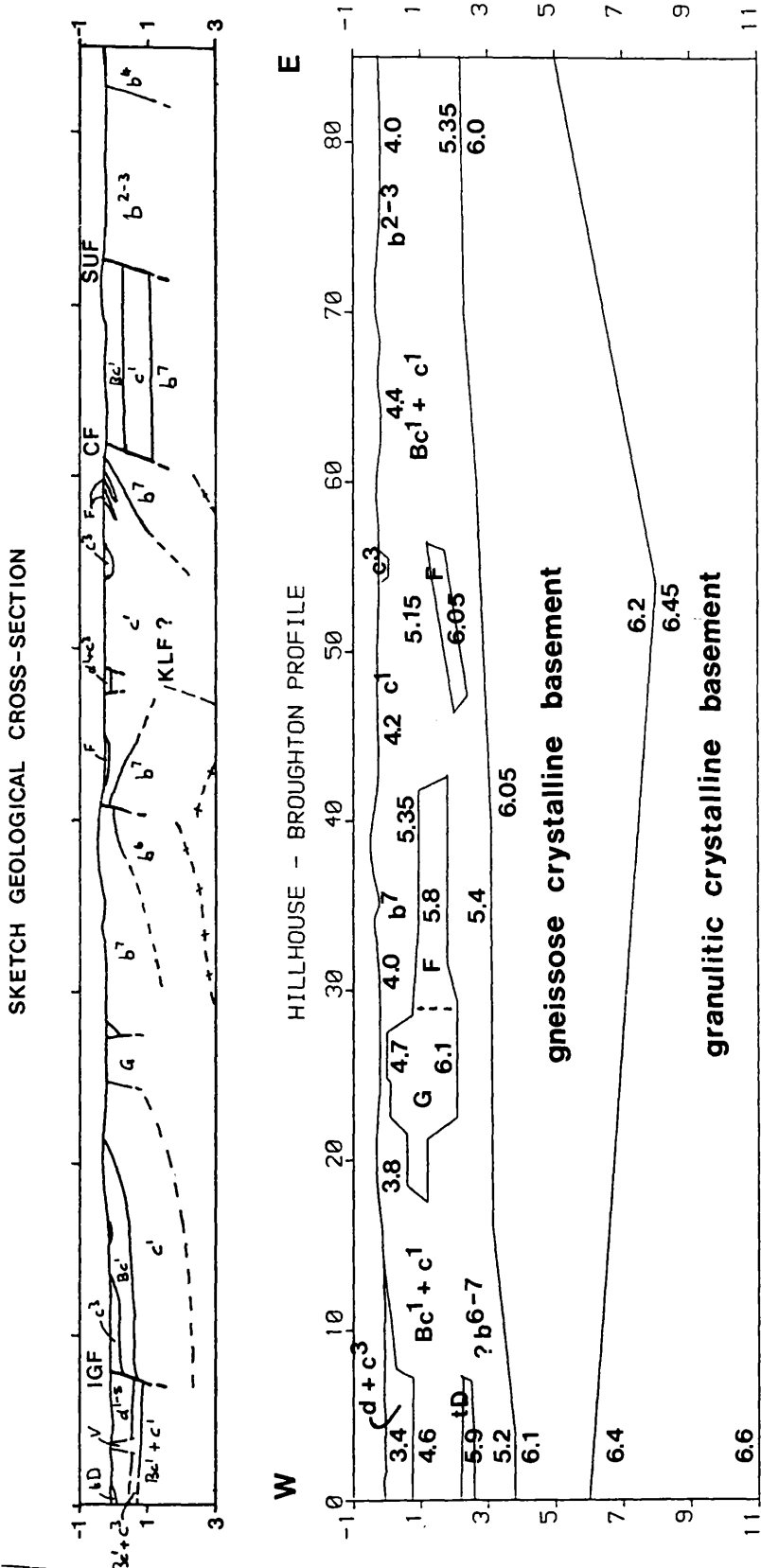


Figure 4.34 Interpretation of the Upper Crustal Structure under the Hillhouse-Broughton profile using ray-tracing techniques. (Velocities in km.s⁻¹) (key to geological symbols in figure 3.1).

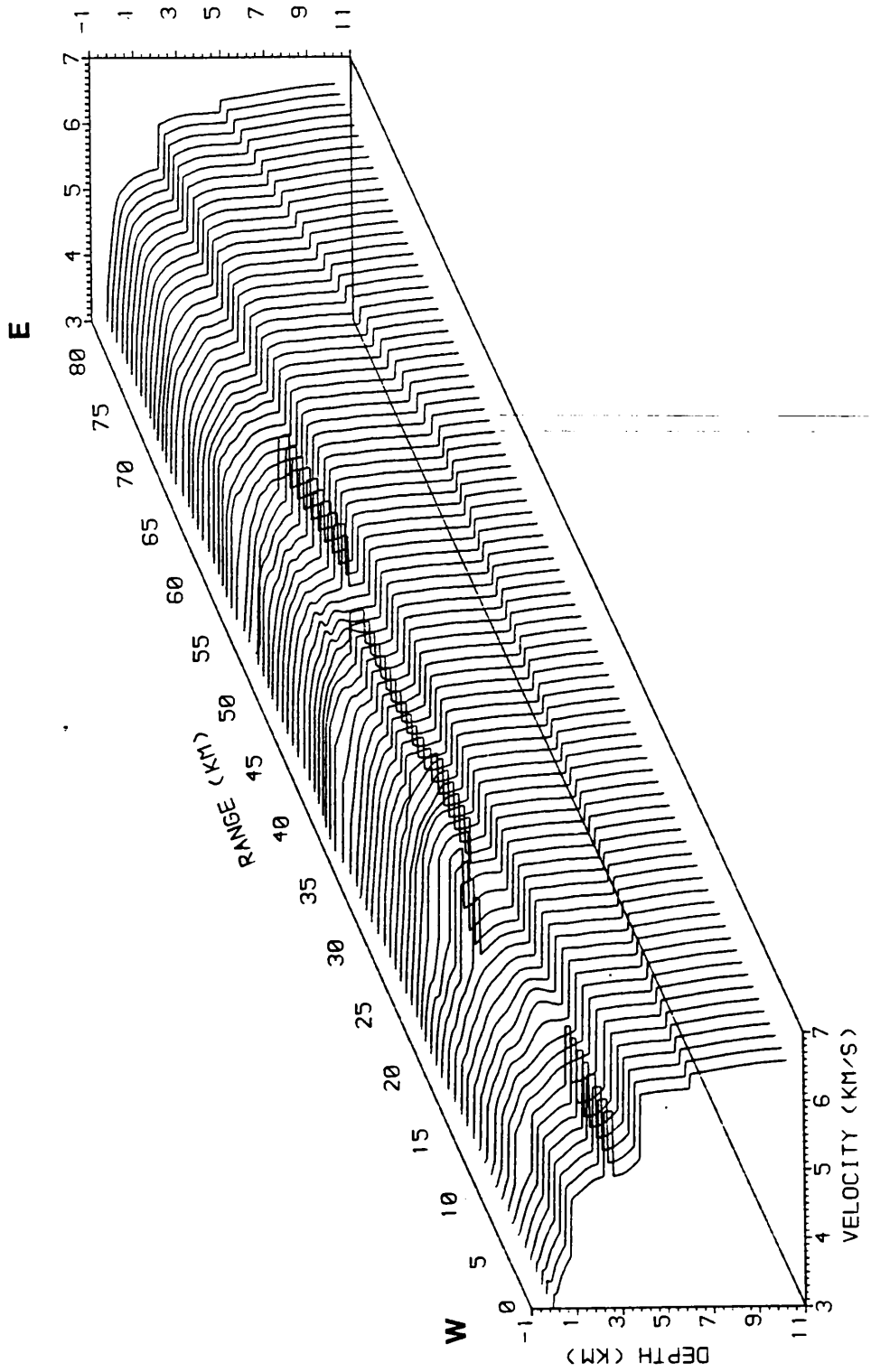


Figure 4.35 P-wave velocity structure under the Hillhouse-Broughton profile as derived from the ray model in Figure 4.34.

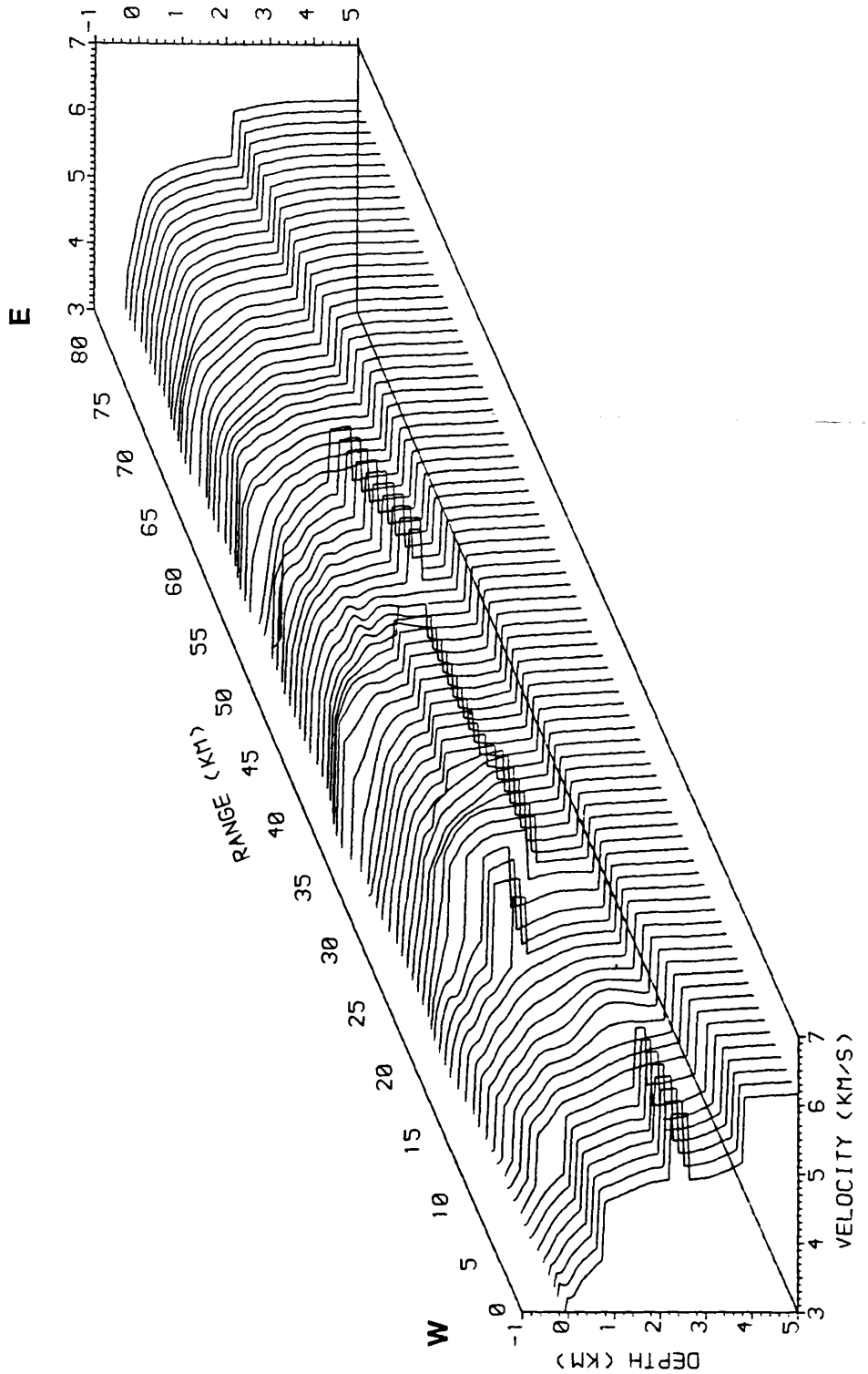


Figure 4.36 Enlargement of Figure 4.35 showing the P-wave velocity structure of the upper 5 km of crust.

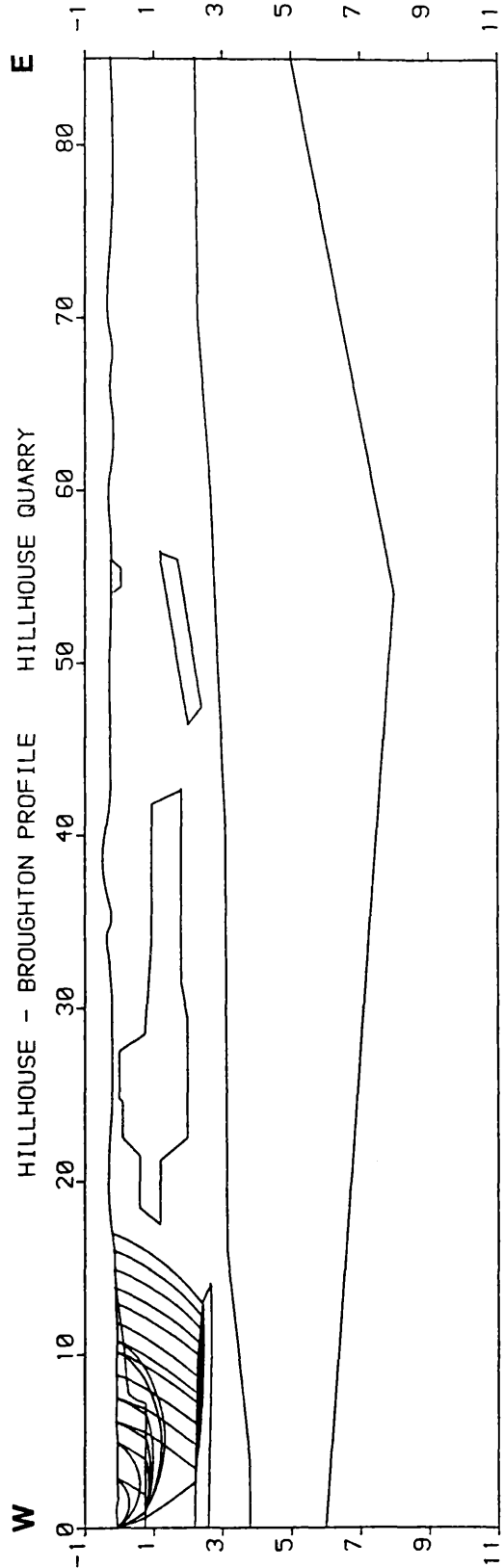


Figure 4.37 Ray diagram for Hillhouse quarry with phases a_s & a_{sr} .

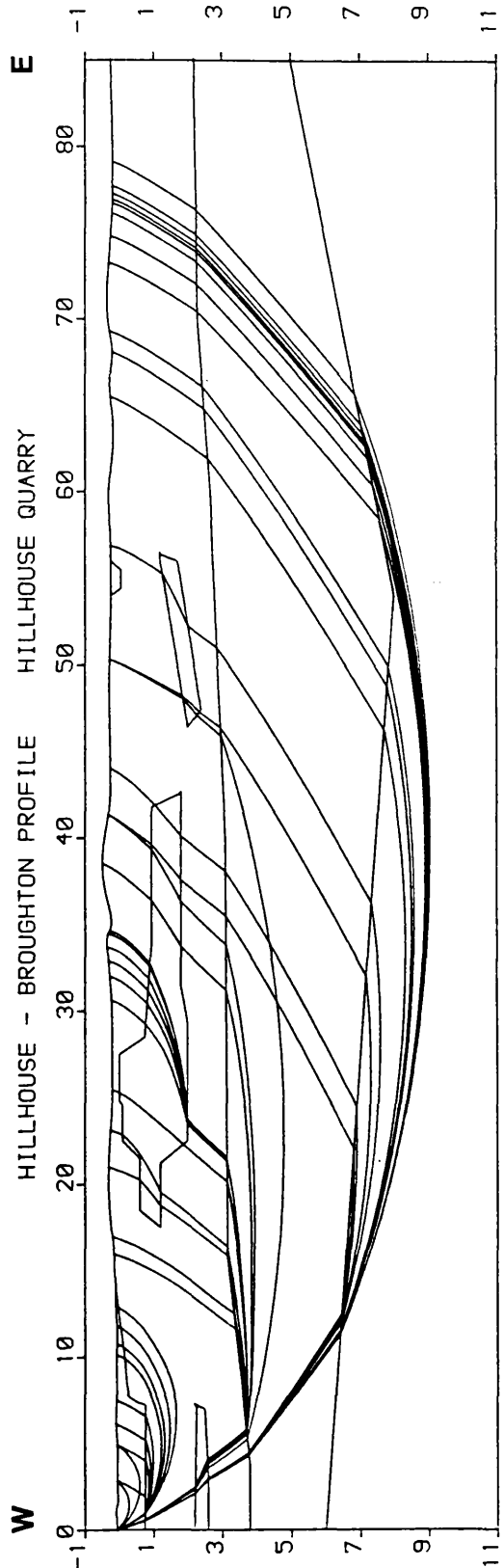


Figure 4.38 Ray diagram for Hillhouse quarry with phases a_s , a_0 & a_1 .

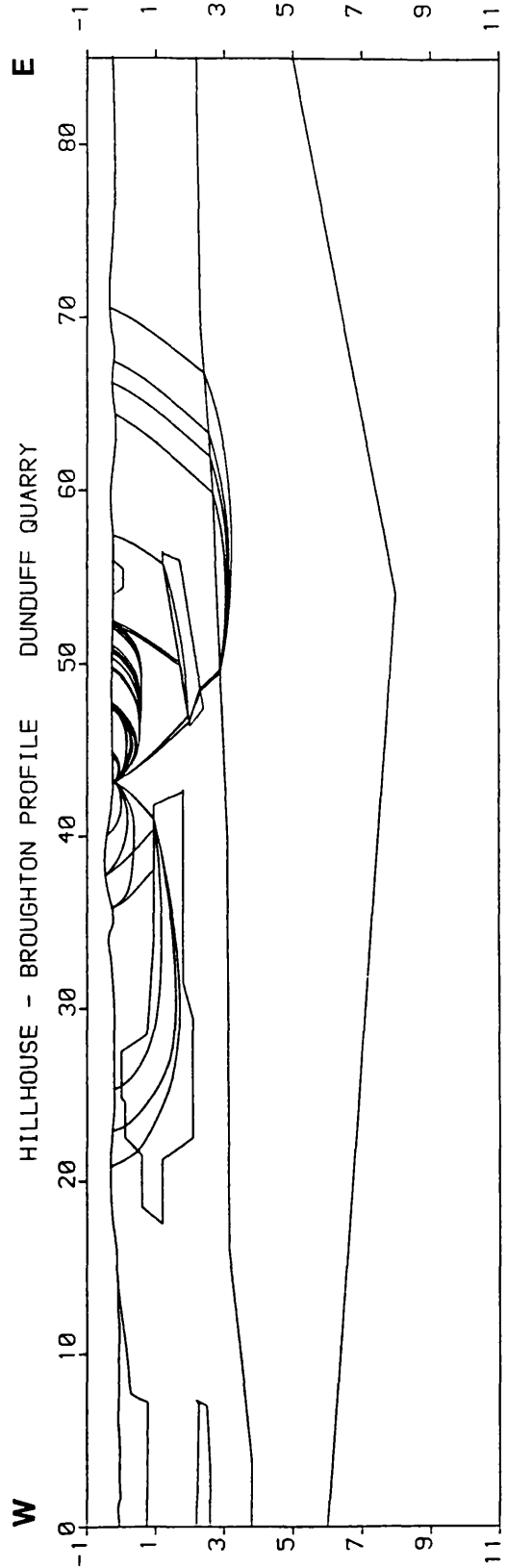


Figure 4.39 Ray diagram for Dunduff quarry with phases a_s , a_{sr} & a_0 .

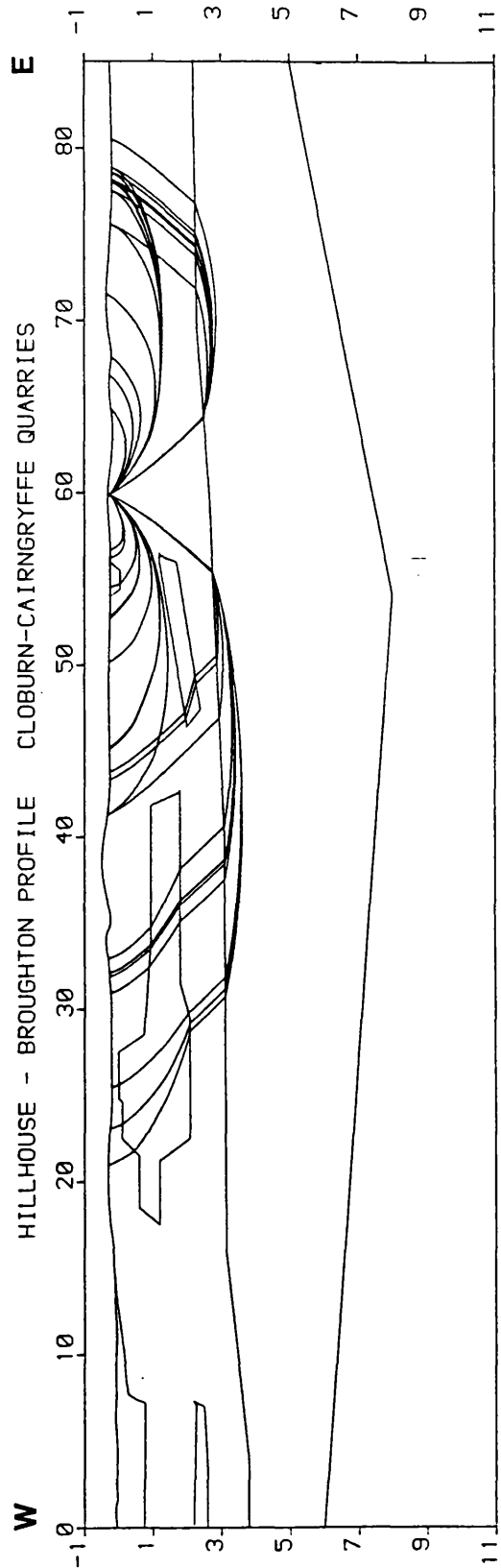


Figure 4.40 Ray diagram for Cairngryffe-Cloburn quarries with phases a_s & a_0 .

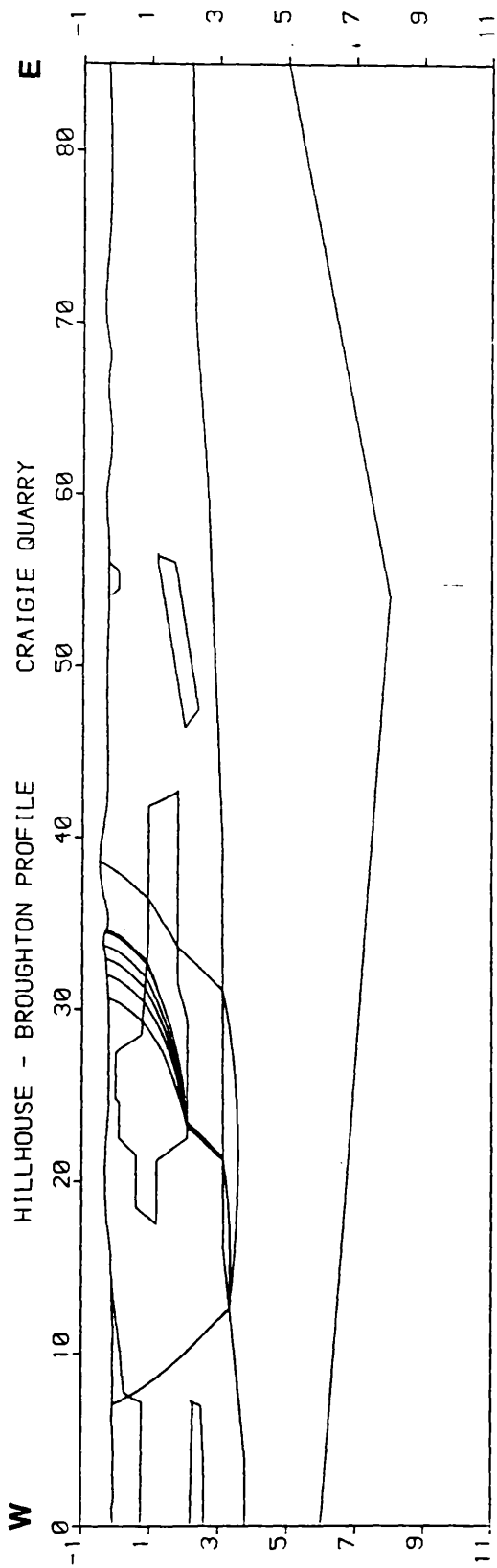


Figure 4.41 Ray diagram for Craigie quarry with apparent a_0 phase.

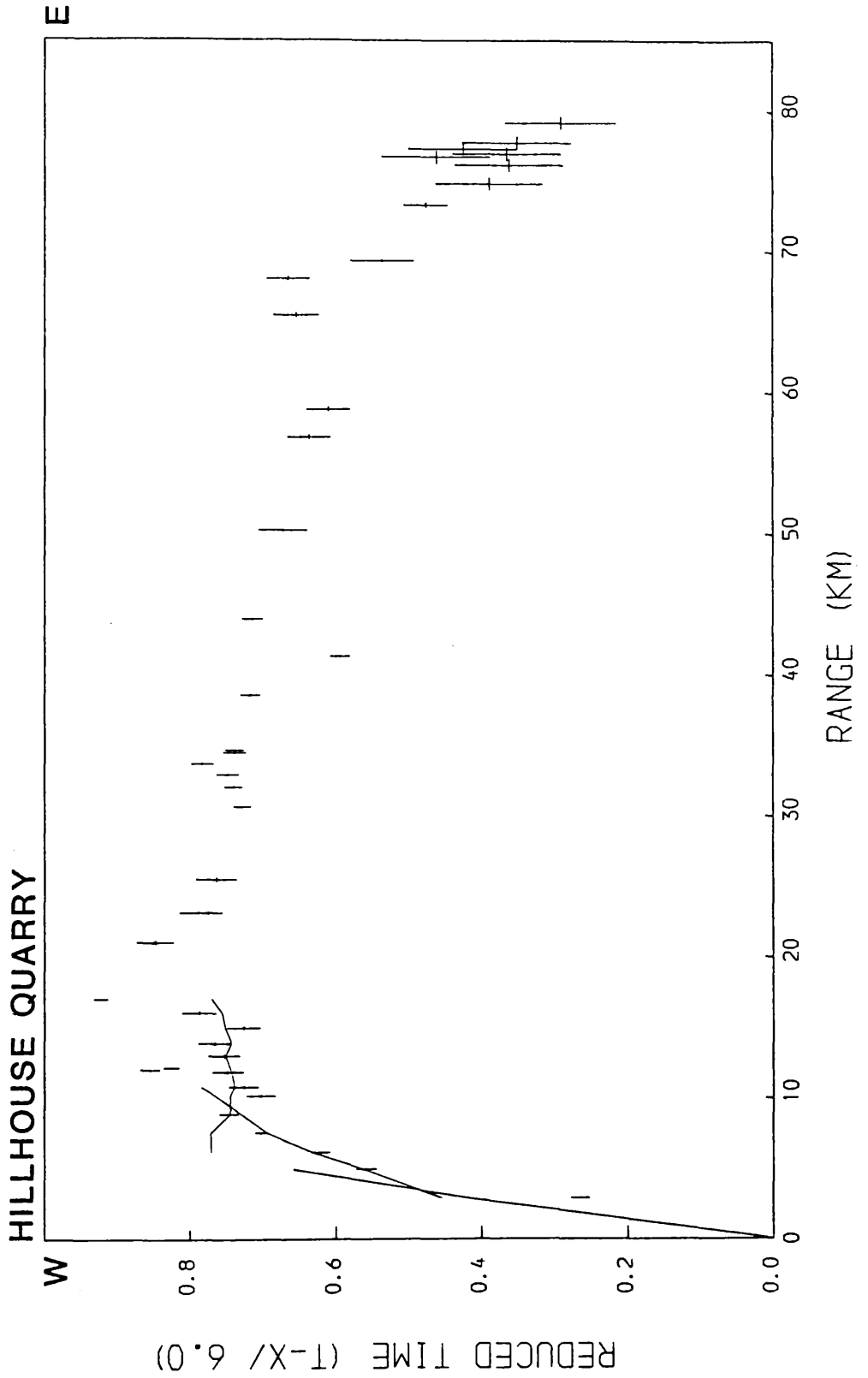


Figure 4.42 Computed and field travel-times for Hillhouse quarry, phases a_s & a_{sr} .

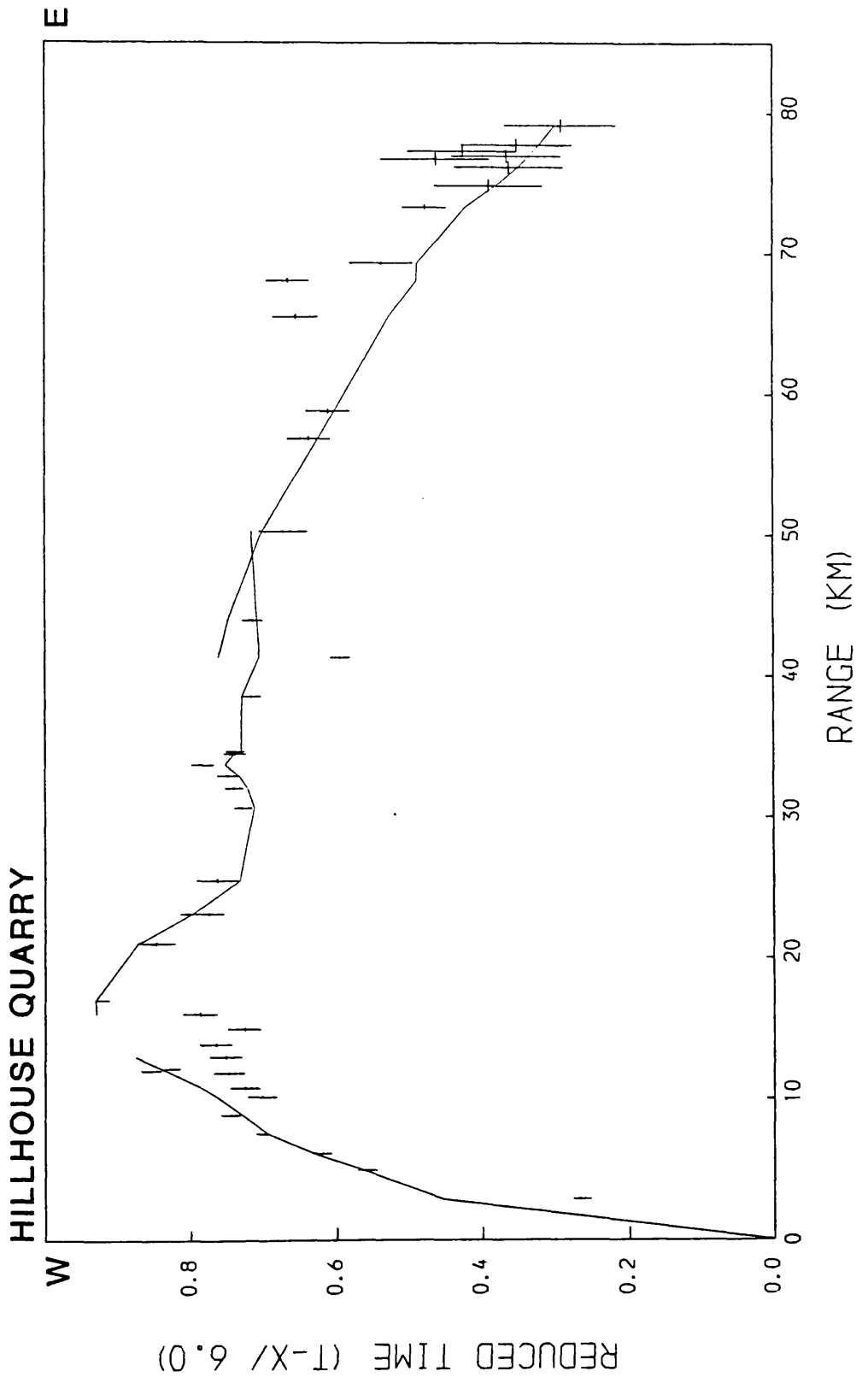


Figure 4.43 Computed and field travel-times for Hillhouse quarry, phases a_s , a_0 & a_1 .

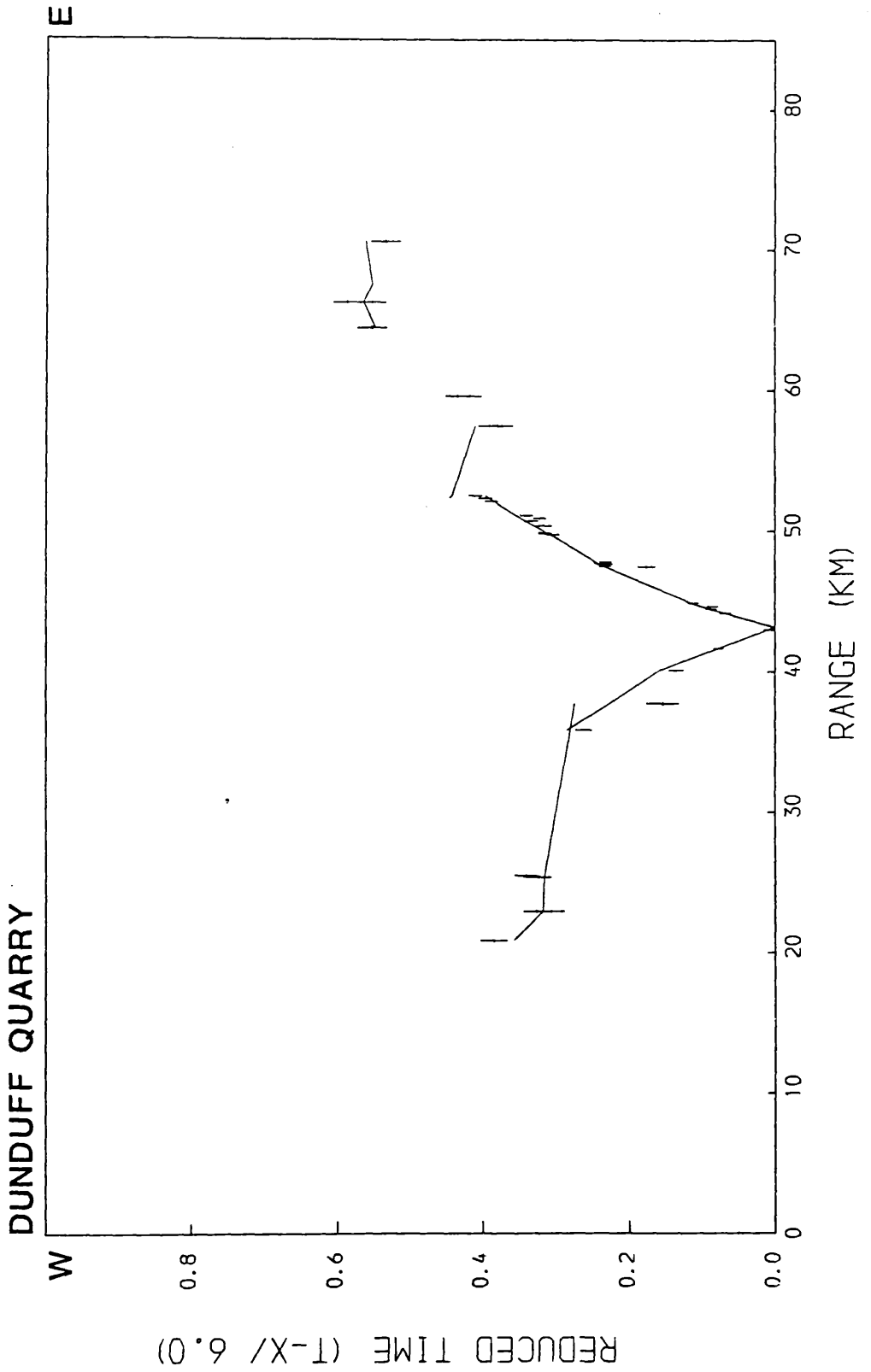


Figure 4.44 Computed and field travel-times for Dunduff quarry.

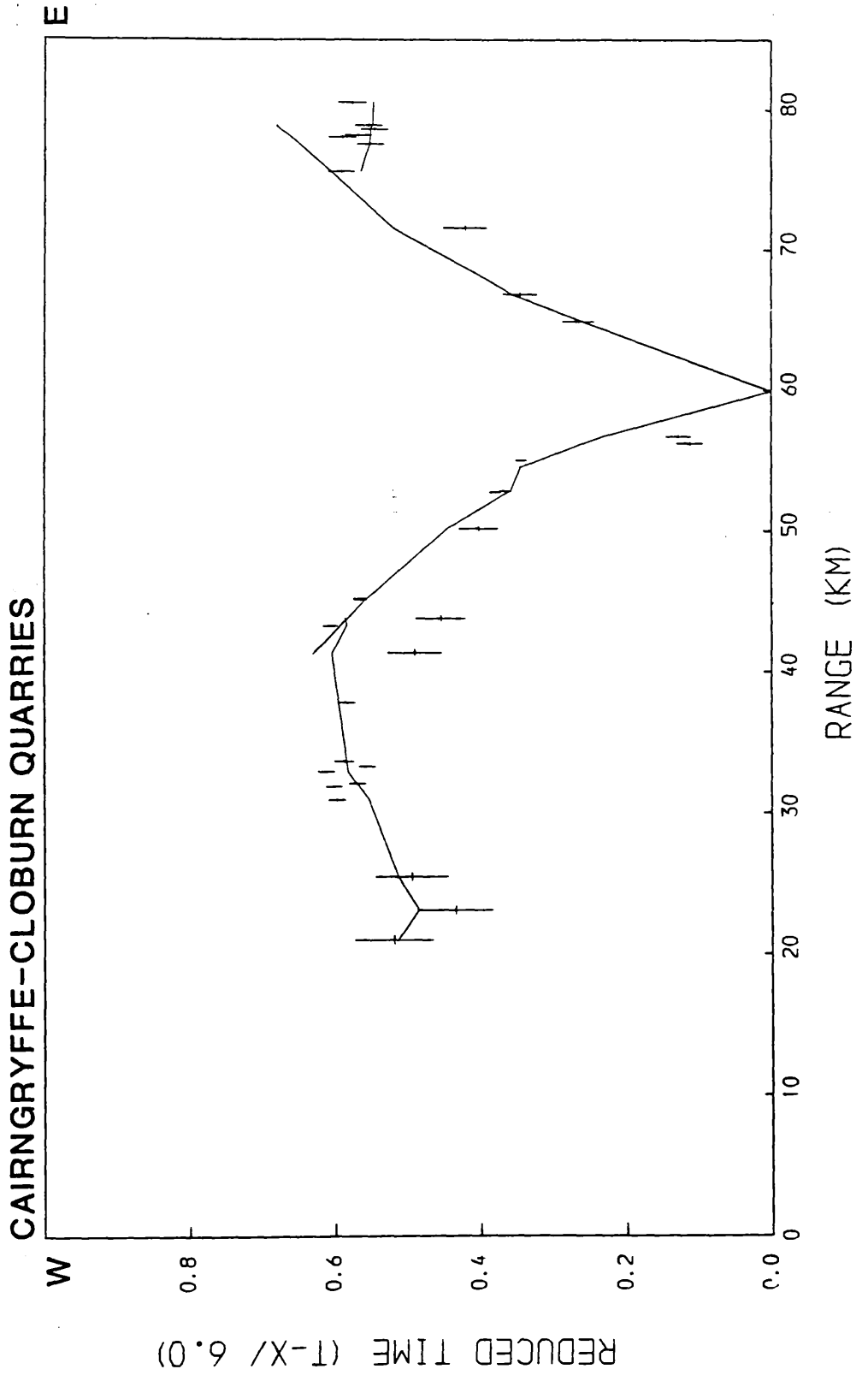


Figure 4.45 Computed and field travel-times for Cairngryffe-Cloburn quarries.

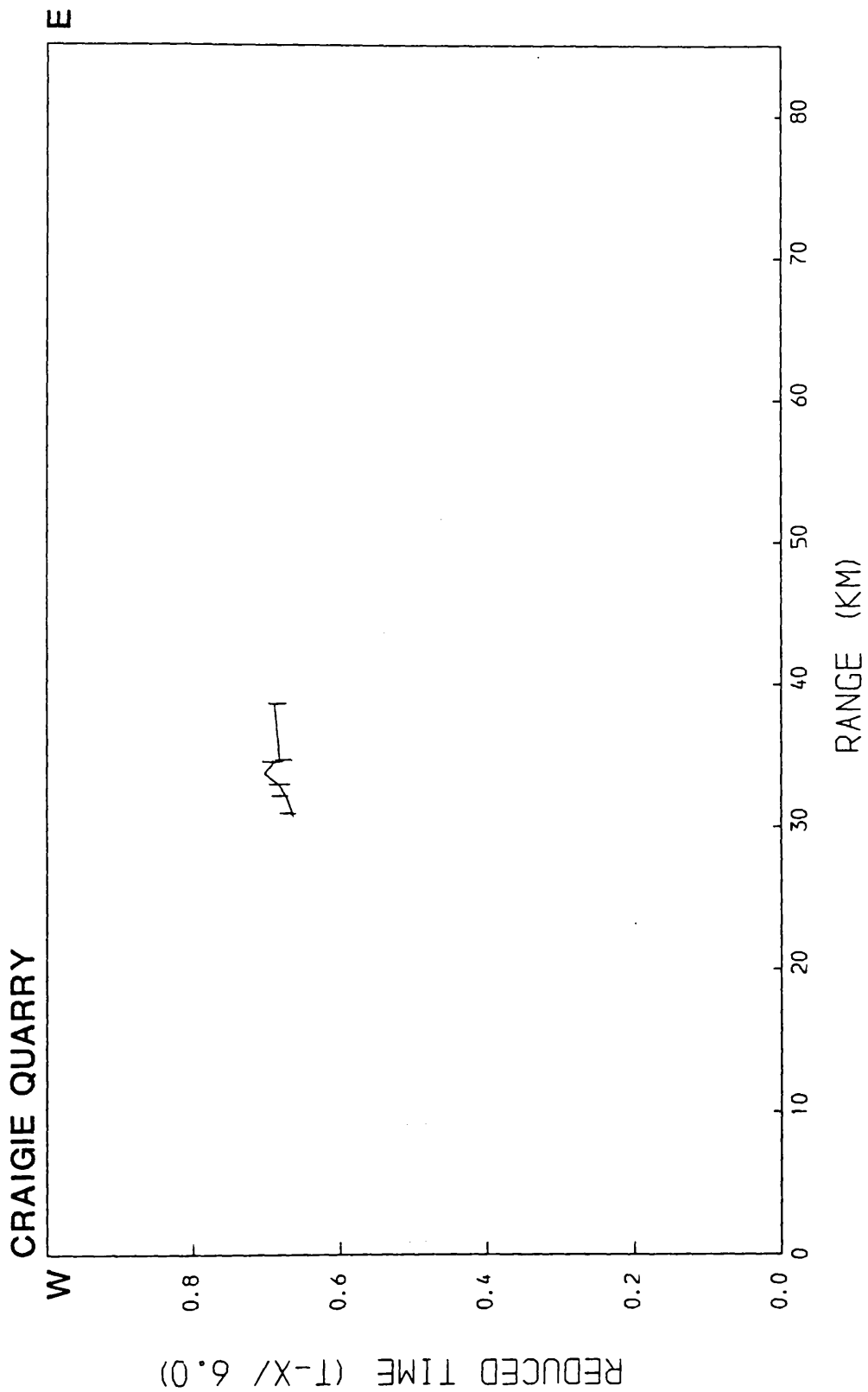


Figure 4.46 Computed apparent velocity against field apparent velocity for Craigie quarry.

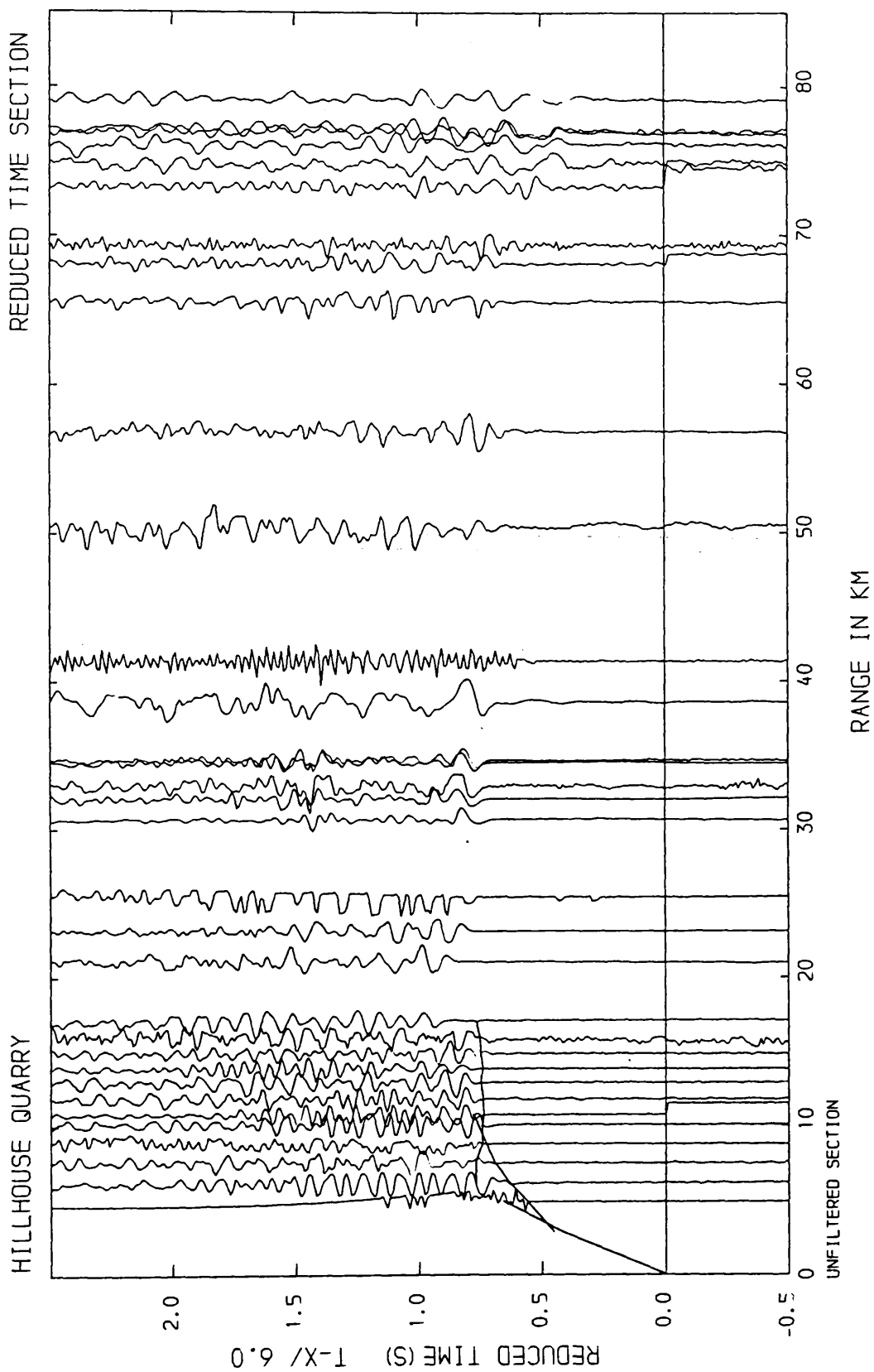


Figure 4.47 Computed travel-times of Figure 4.42 with unfiltered seismograms for Hillhouse quarry.

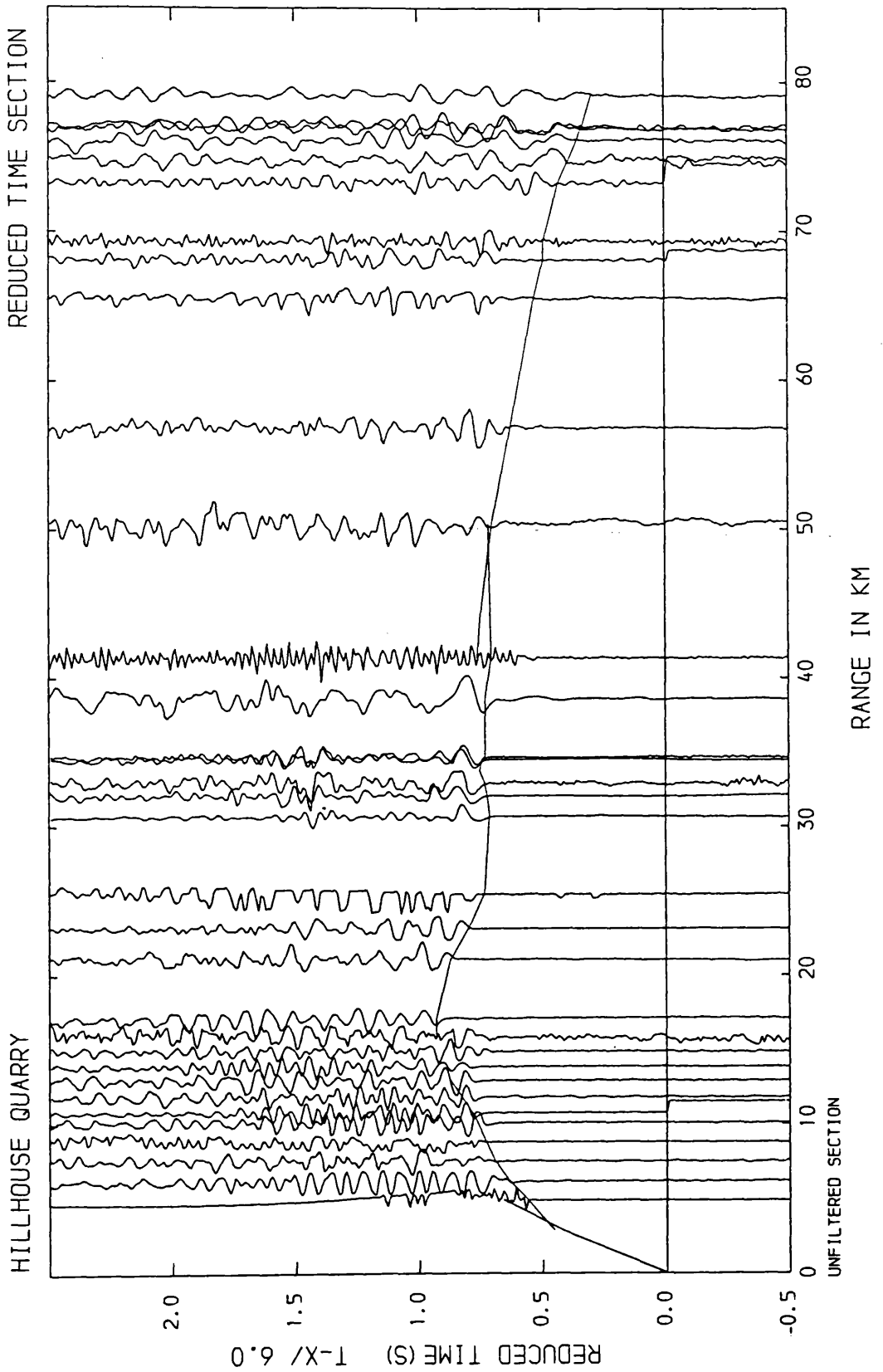


Figure 4.48 Computed travel-times of Figure 4.43 with unfiltered seismograms for Hillhouse quarry.

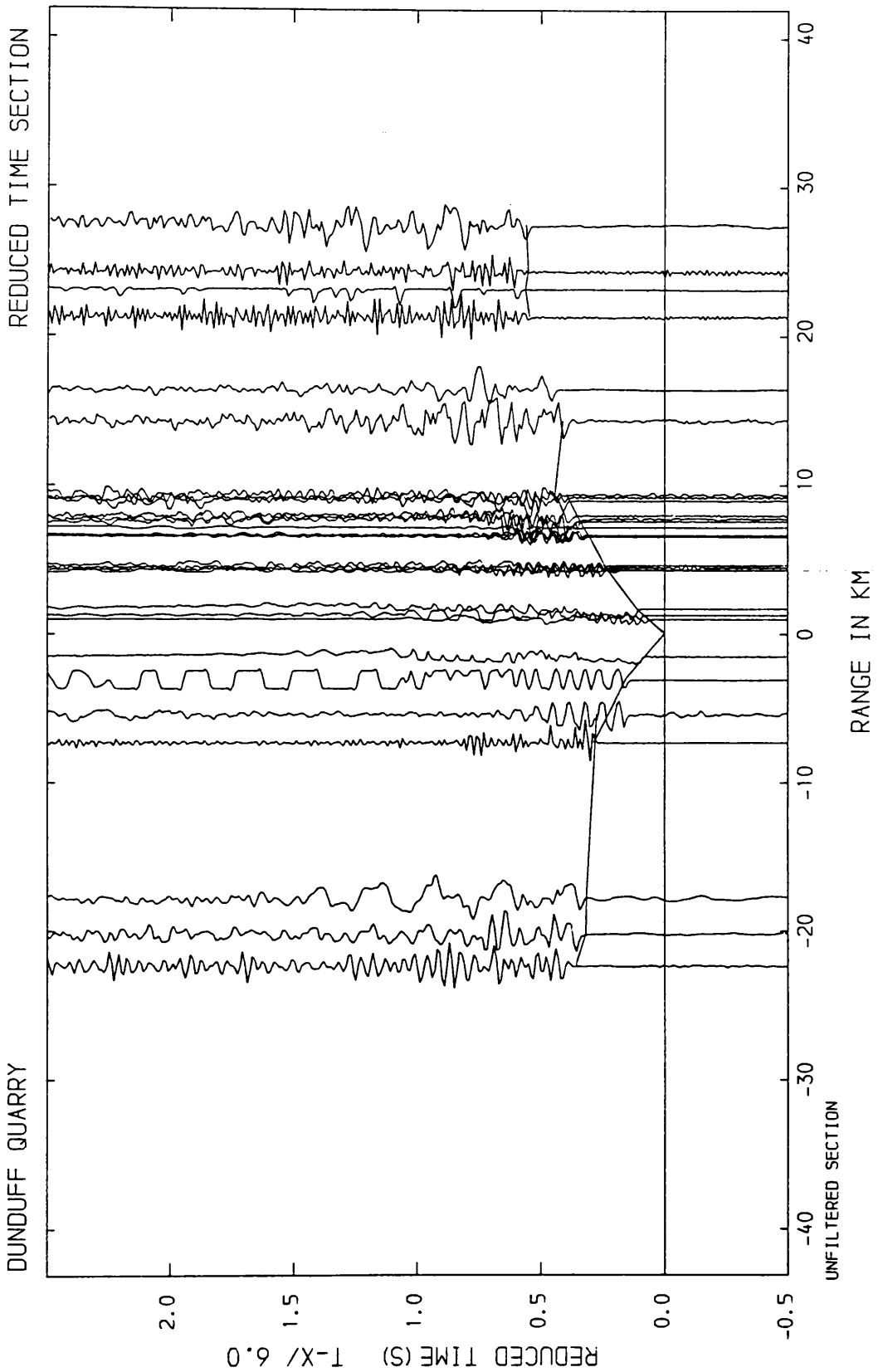


Figure 4.49 Computed travel-times of Figure 4.44 with unfiltered seismograms for Dunduff quarry.

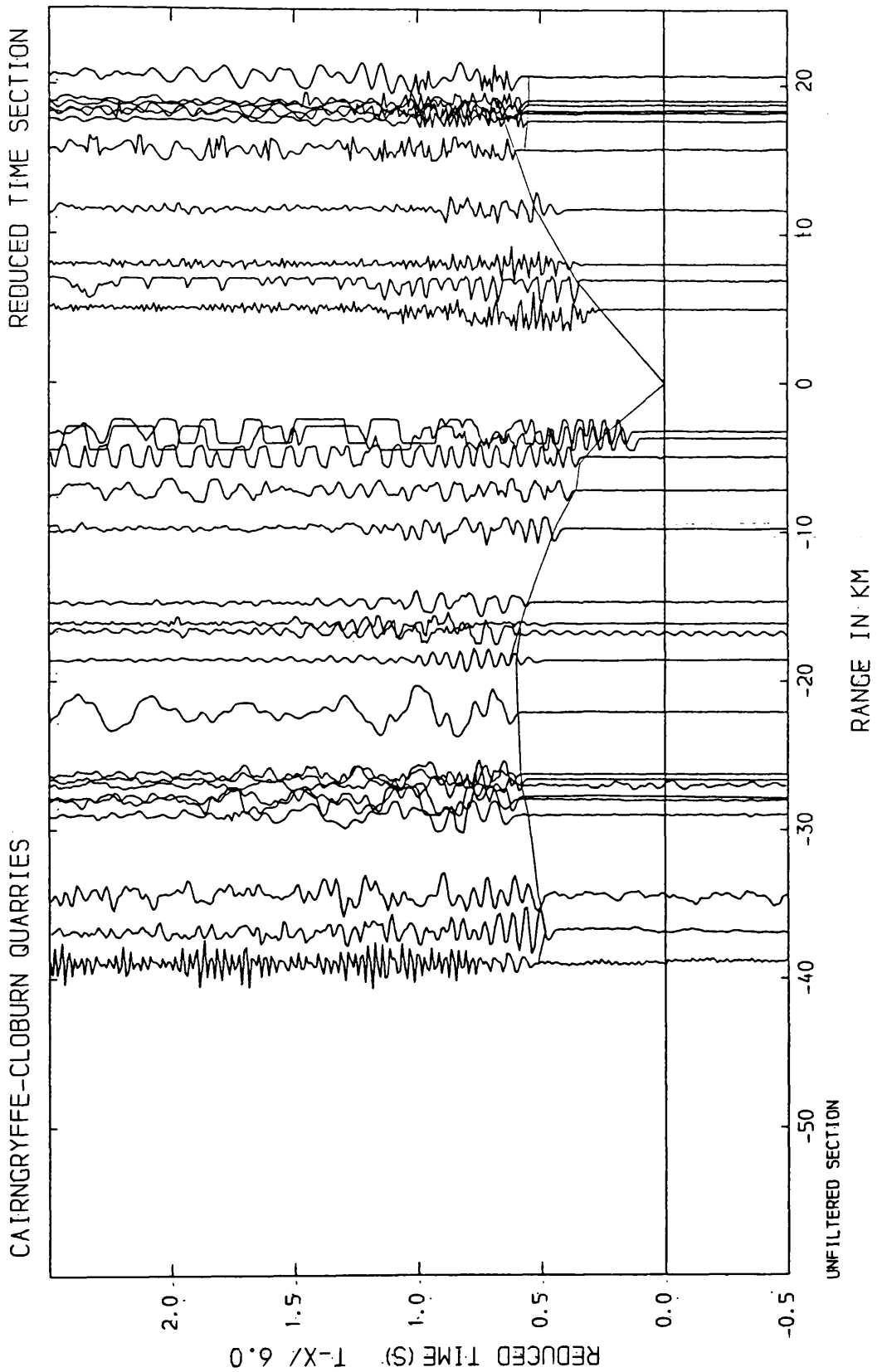


Figure 4.50 Computed travel-times of Figure 4.45 with unfiltered seismograms for Cairngryffe-Cloburn quarries.

Phase	St.deviation of picking errors from field data (s)		Residual times for the ray model (s)	
	mean	st.dev.of mean	mean	st.dev.of mean
a _s	0.009	0.009 (n=33)	-0.025	0.044 (n=33)
	0.007	0.002 (n=32) ₁	-0.009	0.020 (n=28) ₂
			-0.007	0.016 (n=27) ₃
a _{sr}	0.010	0.002 (n=13)	-0.002	0.021 (n=13)
a ₀	0.008	0.003 (n=30)	0.0002	0.038 (n=30)
			0.011	0.020 (n=28) ₄
a ₁	0.014	0.010 (n=14)	0.056	0.081 (n=14)

n = number of points
1 - one large value omitted
2 - five residuals, all over -0.080, omitted
3 - six residuals, all over -0.070, omitted
4 - two residuals, all over -0.110, omitted

figure 4.51

The magnitude of the mean residual for any phase gives the average difference in time between the model and the field travel times for that phase, whereas its polarity describes whether the modelled phase is consistently fast or slow. The size of the st.deviation of the mean residual indicates the scatter of residuals about the mean value. This can be usually ascribed to the model being an oversimplification of the real geological structure.

Negative values of mean residual for any phase show that the modelled values are generally slow compared with the field travel time data.

A target threshold residual of 30 ms was used as a compromise figure between the generally lower mean values for the st. deviations on picked first arrivals, the limited total amount of data coverage over the survey area, and its uneven distribution.

With the exception of the a₁ phase, all the st. deviations from the mean of residuals are within this limit. After removing a few points, particularly on the a_s phase, where provable or inferable anomalous geology exists locally beneath the recording sites (see section 4.1.2.2), the mean residuals become still lower.

The ideal model fit would have all the mean residuals equal to zero and all the st. deviations around the mean residuals equal to, or less than, the sums of the mean and st. deviations of the mean errors on the picked field data for each phase. While this is not true for the ray model presented here, a clear overlap exists between modelled and field travel times showing that this model is a statistically meaningful solution to the Hillhouse - Broughton profile dataset.

Appendix 5. The standard deviations of the model for various arrival phases are shown on the page opposite (figure 4.51).

The apparent velocity data from Craigie quarry is included as it provides an extra check on the structure under the Lesmahagow Inlier.

As discussed in 4.1.5, the Carboniferous and Upper Old Red Sandstone sequences as sampled in the western section of the profile have distinctly lower velocities compared with the Lower Old Red Sandstone and Silurian sequences further east. This agrees well with the results of similar work over the Carboniferous of the Central Coalfield (Sola 1985; Sola & Powell 1983) and of North Ayrshire (McLean & Deegan 1978; Hall 1971; 1974).

The velocities obtained over the Lower Old Red Sandstone sequence to the west of the Distinkhorn complex, and which includes andesitic lavas which are often weathered, are consistently lower by 0.5 km s^{-1} than equivalent rocks further E. This may relate to the absence of any felsitic intrusive suite in this region. Also, velocities over the Lower Old Red Sandstone sequence exposed to the E of Cloburn are slightly lower ($0.1 - 0.2 \text{ km s}^{-1}$) in the top 1 km than those found across the Lesmahagow Inlier. A thick sequence of dominantly andesitic lavas is predicted in the area E of Cloburn quarry (Mykura 1960), and where seen at the surface, they appear unweathered. In addition these lavas have been used extensively locally as a building

material, again implying unweathered rock. From this it is concluded that typical Lower Old Red Sandstone sediment velocities are probably best represented west of Distinkhorn, giving velocities which are lower than the contemporaneous lavas east of Cloburn quarry. The high near surface velocities around Lesmahagow must then be due to a large volume of minor, acidic intrusions occurring throughout this area. It is then proposed that the two large refracting bodies between 27 and 60 km from Hillhouse quarry are due to larger intrusions of the same suite.

Differences in surface velocity between the Silurian and Lower Old Red Sandstone sediments around Lesmahagow are probably due to the differences in lithology as well as compaction history. The Silurian sequence is predominantly a mixture of sandstones, siltstones and shales, whereas the Lower Old Red Sandstone is almost entirely comprised of arenaceous sandstones. Much of the scatter of arrival times in the close shots around the LES array can be attributed to this (as well as the probable presence of local felsite bodies in the south of the inlier). The differences in velocity gradient can then be explained by the different crack spectra characters of these two stratigraphic groups. A lithological sequence with a high aggregate proportion of sheet silicate minerals, as found in siltstones and shales, will contain a greater proportion of flat and ellipsoidal cracks. These will close more rapidly with increasing confining pressure than the round pores which are prevalent in sandstones. The Lower Old Red Sandstone sequence contains a very high proportion of sandstones, so it is logical to expect a higher proportion of round pores to be present and therefore the velocity gradient should be lower. This would appear to be supported by the field V - Z evidence.

As described above, felsitic intrusions are prolific in the region to the east of the Distinkhorn complex and appear to be around 20 Ma older than it

(390 ± 6 Ma, U - Pb from zircons; Pidgeon & Aftalion 1978), and so need not be related to the same magma generating episode. The existence of generally higher sedimentary rock velocities in this area, as well as several discrete zones of high velocity within the sedimentary layer, point to a regionally extensive and locally voluminous acidic intrusive suite emplaced at the end of the Silurian.

Although not a distinct target for investigation in this project, the Distinkhorn granodiorite is inferred to conceal a much higher velocity root. This when combined with the coincidence of a Bouguer gravity high of 4 mgals and an aeromagnetic high of 200 nT, tends to suggest the presence of an igneous body of intermediate to basic composition which appears to be slightly more extensive at depth than the outcropping granodiorite. The base of the intrusion cannot be well defined from this survey, but the apparent base on the ray model is most likely to represent sideswipe from the northern flank of a body deepening to the south.

At the western end of the profile, the Carboniferous sequence is exactly as predicted from local gravity surveys by McLean (1966). His problem with matching the magnitude of the long wavelength Bouguer anomaly over the region to the north of the Inchgotrick fault and its gradient at the fault edge to the known or immediately predictable sub-surface geology, may be explained by the presence of the high velocity refractor at around 2 km depth representing an intrusive (presumably basic) intrusive body. However, no detailed gravity modelling has been attempted to confirm this theory. The absence of data received from this refractor in other directions precludes modelling of any elaborate structure on this body.

4.2.2.3 Thin layers

In this ray model, the thickness of the three sill-like bodies have been assumed to be purely functions of the refracting velocity and a delay requirement dictated by the rest of the data. However, theoretical constraints on the transmission of refracted waves through thin layers must be taken into consideration in any model where thin layers are suspected to be present.

Synthetic materials studies (Poley & Nooteboom 1966) have shown that the transmission of refracted arrivals through a thin, high-velocity medium is possible without a significant reduction in the apparent arrival velocity, or increase in attenuation, until the layer thickness/wavelength (d/l) ratio is less than 0.5 (figure 4.52). Thereafter, with decreasing d/l , transmission effects involving energy interactions with the surrounding low-velocity medium result in non-linear behaviour of the apparent arrival velocity and attenuation values. This, the limit of 'normal' transmission of refracted energy in a thin layer, occurs at the threshold of vertical resolution for seismic reflection recording.

In the ray model shown, all three bodies are approximately 1 wavelength in thickness (ie $d/l = 1$) at which point the apparent refractor velocity should be 99% of the true refractor velocity (figure 4.52). With each body the lowest possible refractor velocity and simplest structure compatible with all the data was assumed. Surface geological structure was also used as a constraint on the possible options. As a result, the Dunduff 'sill' is modelled with a similar dip (5°) to that seen at the surface, although this is probably less than the dip found at depth closer to Cloburn quarry, where the surface strata are dipping more steeply.

The Hillhouse 'sill' was originally considered as a sub-horizontal body terminating at the northern margin of the Inchgotrick fault (IGF). However, from the raymodelling exercise, the continuation of the refractor further E

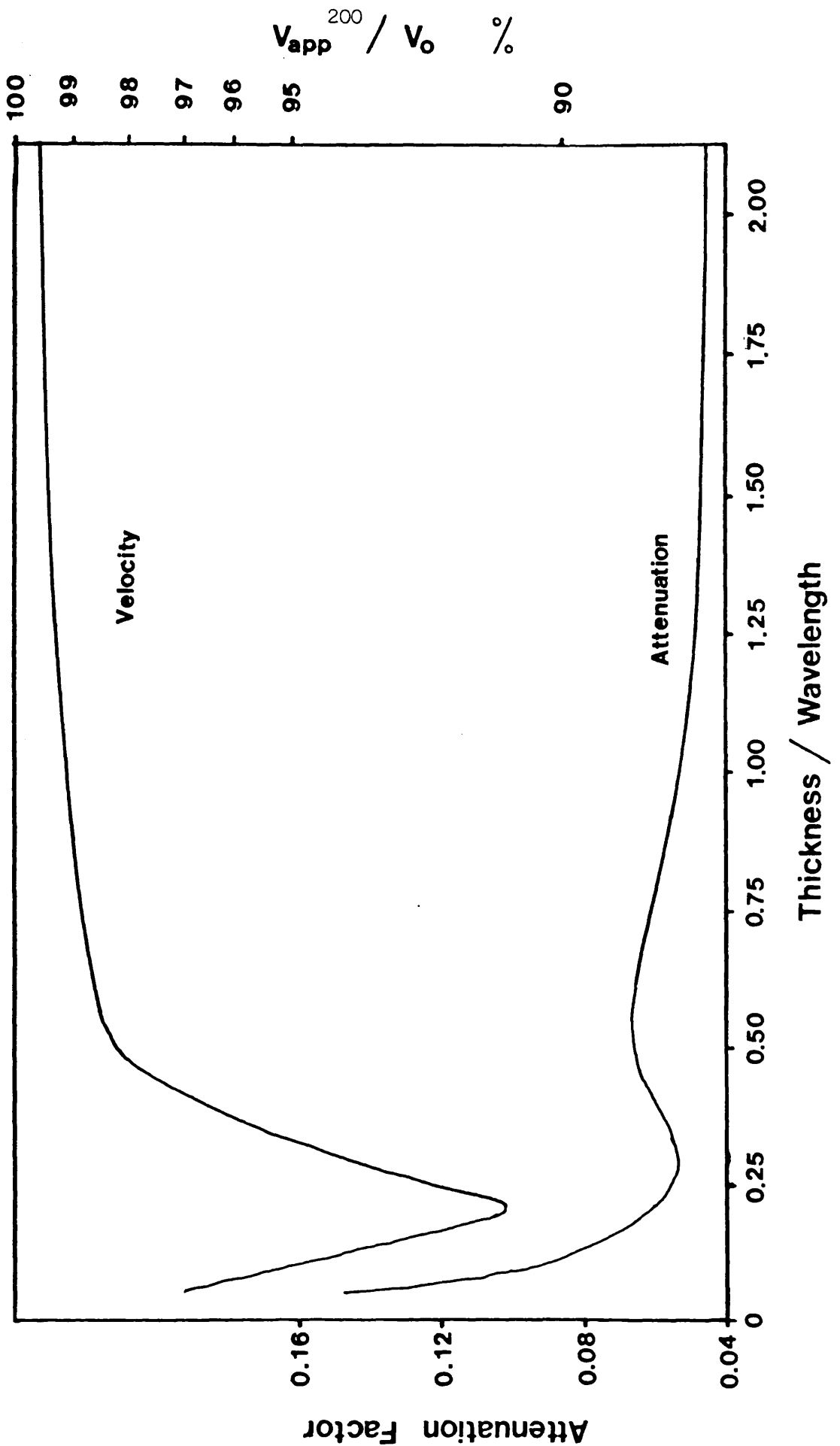


Figure 4.52 Apparent velocity & attenuation as functions of the layer thickness/wavelength ratio (after Poley & Nooteboom 1966).

than predicted leads to one of two conclusions: either that this body continues across the fault - which considering that this fault controlled sedimentation throughout much of the Carboniferous, and that all the exposed basic sills in this region were intruded during Carboniferous times, would appear unlikely; or that the shallow angle with which the profile crosses the fault has resulted in sideswipe from the north and westwards continuation of the sill. Simple calculations from the B.G.S. 1 inch Geological map of Ayrshire predict pseudo-depths produced by sideswipe that fit this model remarkably well. From this it is concluded that the second alternative is the more likely.

This hypothesis was tested by placing two recording sites off-line to the S of the profile, in the the Mauchline Basin, so that the ray-paths should be as far as possible separate from the body to the N of the fault. Figures 4.42,43 show both points at ranges of around 14 km from Hillhouse quarry and delayed relative to equivalent points on the profile by about 100 ms. Their travel-times indicate ray-paths through a sedimentary sequence similar to that under the profile, but without a high velocity layer, and provide some confirmation that the Hillhouse 'sill' is confined to the northern side of the IGF.

The Lesmahagow Inlier 'sill' occurs in an area which from the surface geology and the velocity evidence presented in 4.2.2.1, must contain a large volume of mainly thin, laterally discontinuous felsitic sills. There are two possible alternatives for explaining the nature of this refracting body: either that it represents a single large intrusion, or that it represents a discrete zone with a very high percentage of thin sills, giving a zone giving a zone which seismically appears as a single body.

The second alternative bears the greater similarity with the surface geology, but geologically, they are both tolerable. In the ray model, the

western margin of the body is shown as being coincident with the eastern margin of the Distinkhorn complex. This is a modelling artifact and need not necessarily imply geological contact or petrological equivalence.

4.2.2.4 Basement (a_0) refractor

The position of this refractor in the model is broadly similar to that of the a_0 refractor defined by LISPB to the N and S of Edinburgh. Bamford and co-workers based their velocity determination on plus-minus analysis of segments of coverage between shots 1 & E and E & 2 (see figure 1.14 for LISPB shot locations), giving velocities of $5.93 \pm 0.03 \text{ km s}^{-1}$ and $5.84 \pm 0.02 \text{ km s}^{-1}$ respectively. The evidence presented in the preceding sections of this chapter suggest that the a_0 refractor in the southern Midland Valley has a velocity of $6.05 \pm 0.05 \text{ km s}^{-1}$, where the standard error is a semi-qualitative estimate of the amount of tolerable variance in velocity before the model would cease to fit with the field data. The velocity gradient used in the ray modelling process was initially derived from the typical gradients measured from ultrasonic tests using gneissose cores. This was used as a basis for the iterative ray modelling, and required minimal modification to give the final ray model.

This P-wave velocity is slightly higher than that determined between shots 1 & E (see figure 4.53), but more significantly, it is higher than the value obtained between shots E & 2, which given the doubts expressed on this interpretation (Hall et al 1983) must now be regarded as an oversimplification of the true structure in the area to the S of Edinburgh.

From figure 4.34 it is clear that the structure of the a_0 basement refractor presented here is a much smoother structure than might have been expected from the downwards extrapolation of the surface geology (cf geological section, figure 3.2). There are a number of possible explanations for this. Firstly the nature of the propagation, and the modelling of the

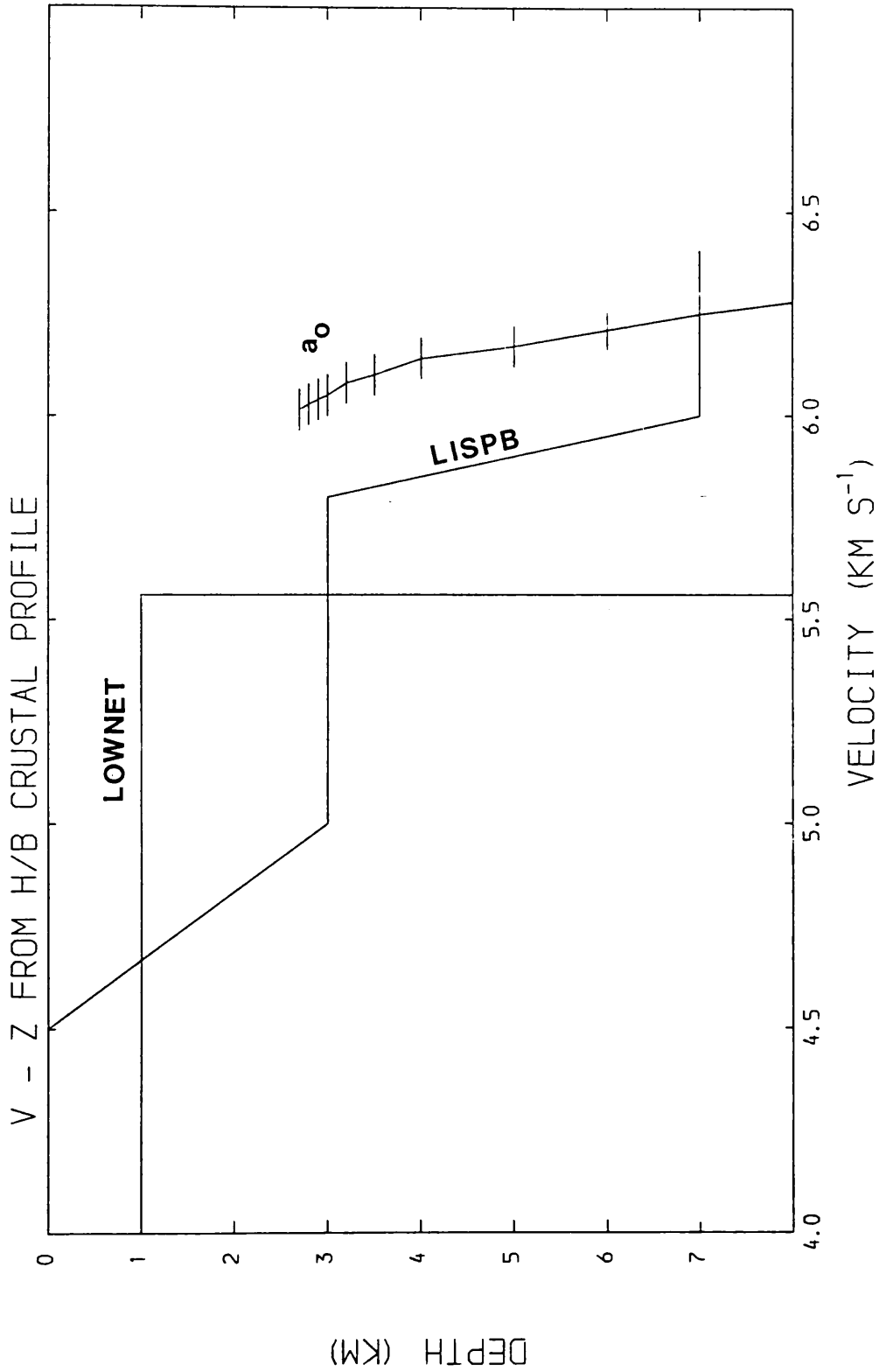


Figure 4.53 Modelled velocity-depth curve for the southern Midland Valley basement (a_0) compared with those for the LISPB & LOWNET models.

propagation of seismic headwaves will tend to average any complex structure present in an area, so any model produced by ray-tracing in particular will be invariably a smoothed representation of the actual structure. The use of amplitudes and secondary arrivals often can provide an improvement in the accuracy of the model. However as described in section 3.3, these were not applicable to this dataset due to the complexity of the source pulse produced by the quarry blasts.

The second possible explanation for the smooth nature of the basement refractor is that the surface geology bears little relation to the deeper structure. This then produces problems in the geological interpretation which will be dicussed later.

A qualitative estimate of the allowable vertical range of depths to the refractor along the profile has been made by considering the ranges of travel time values possible within each travel-time standard error.

The area to the E of Cloburn quarry towards the BTN array is covered by both downgoing and upcoming rays from Cloburn quarry, and upcoming rays only from Dunduff quarry. The change in depth to produce a 10 ms change in the refractor arrival times is ~ 110 m. 10 ms is also the average standard error in the field data arrival-times in this area although a further 5 ms should be added to cover timing inconsistencies resulting from repeated measurements. Thus around ± 170 m is the maximum allowable relative vertical movement across the SUF before a significant change is produced in the arrival times in this area.

The region between 30 - 50 km from Hillhouse quarry, and underlying the Lesmahagow Inlier and part of the Lower Old Red Sandstone outcrop further E has a reversed coverage of ray-paths from Hillhouse and Cairngryffe-Cloburn quarries, although complicated by the presence of the discrete, high-velocity bodies in the surface, sedimentary layer. The standard errors in the refractor arrivals in this region are consistently less than 10 ms (Appendix

3), so that allowing for the generally higher sedimentary velocities and an additional 5 ms potential error due to repeated measurements from these quarries, the allowable range of relative vertical movement on the refractor is again around ± 170 m.

The area of the refractor between 50 - 60 km, under the Carmichael Inlier and to the N and W of the Carmichael fault (CF), is constrained only by westward, downgoing rays from Cairngryffe quarry. A rise of 1 km in the refractor to the N and W of the CF would produce an acceleration in the refractor travel-times received in the E over the Lesmahagow Inlier of ~ 90 ms. As discussed above, the model under the Lesmahagow Inlier can be regarded as a reasonable fit to the field data, and so an additional ~ 90 ms acceleration would provide a significant discrepancy between the field data and this model. However, until the segment of the profile between the Carmichael Inlier and the BTN array is reversed, there cannot be any quantitative statement on the amount of vertical throw across the CF.

Comparison of the ray model with one produced from the downwards extrapolation of the surface geology (assuming no significant extra thickness of Silurian strata) shows a number of similarities as well as differences (figure 4.54). The average depth to basement is similar, at around 3 km, but a number of features predicted from the geological model do not show on the ray model. For example, there is no evidence for a structural high in the basement under the Lesmahagow Inlier, nor under the northwestern side of the CF. Also the SUF does not appear to produce any seismic discontinuity in the basement. This predicted geological model was raytraced from the same sources into the same receivers as the model in figure 4.34, so as to compare these calculated travel-times with the field data. The ray diagram is shown in figure 4.55 and the travel-time comparison in figure 4.56. The velocity model is illustrated in figures 4.57,58. The more complex refractor structure

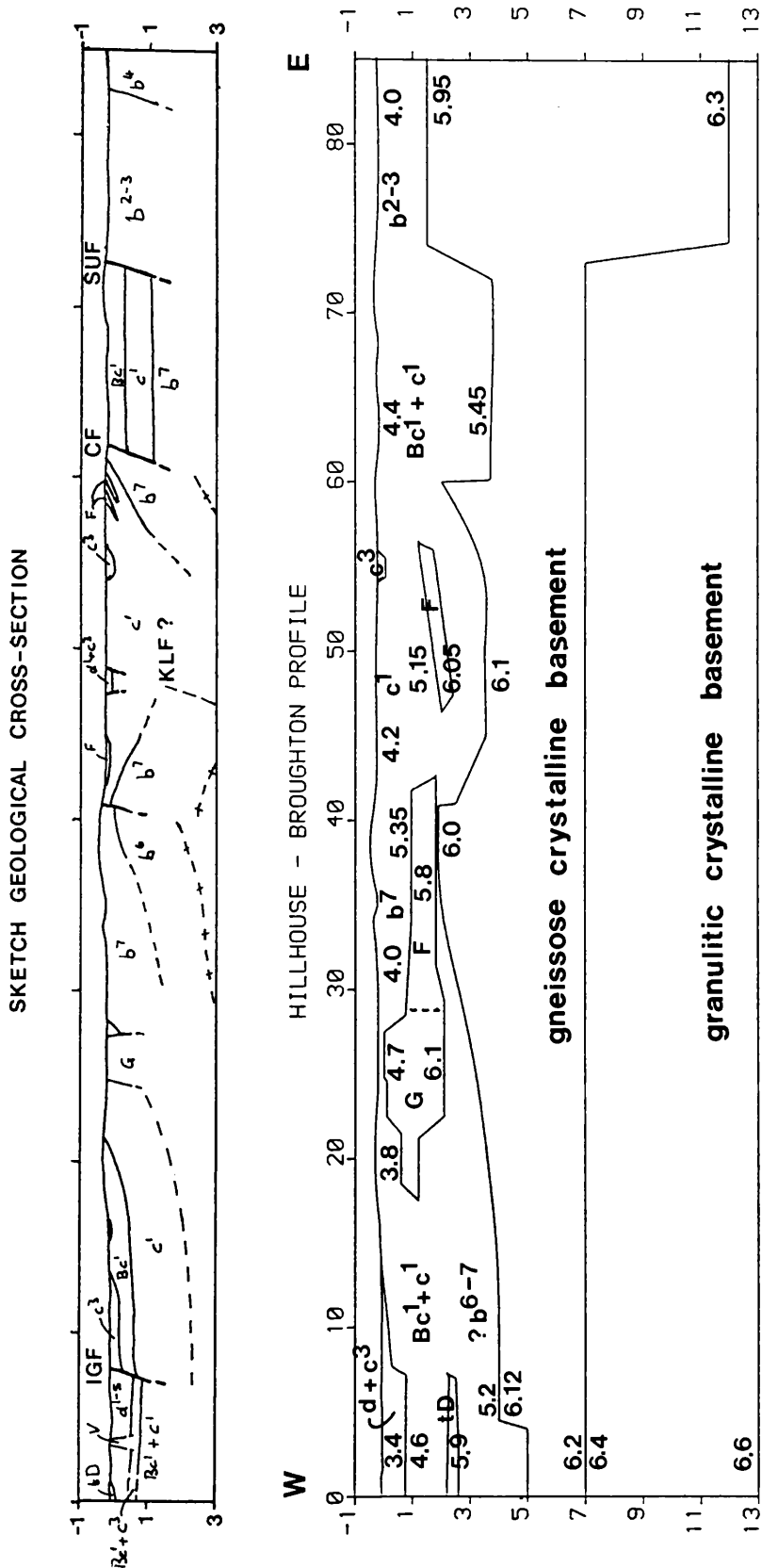


Figure 4.54 Ray model of the Upper Crustal structure under the Hillhouse Broughton profile as predicted from downwards extrapolation of the surface geological structure. (Velocities in km.s⁻¹, key to geological symbols is in figure 3.1).

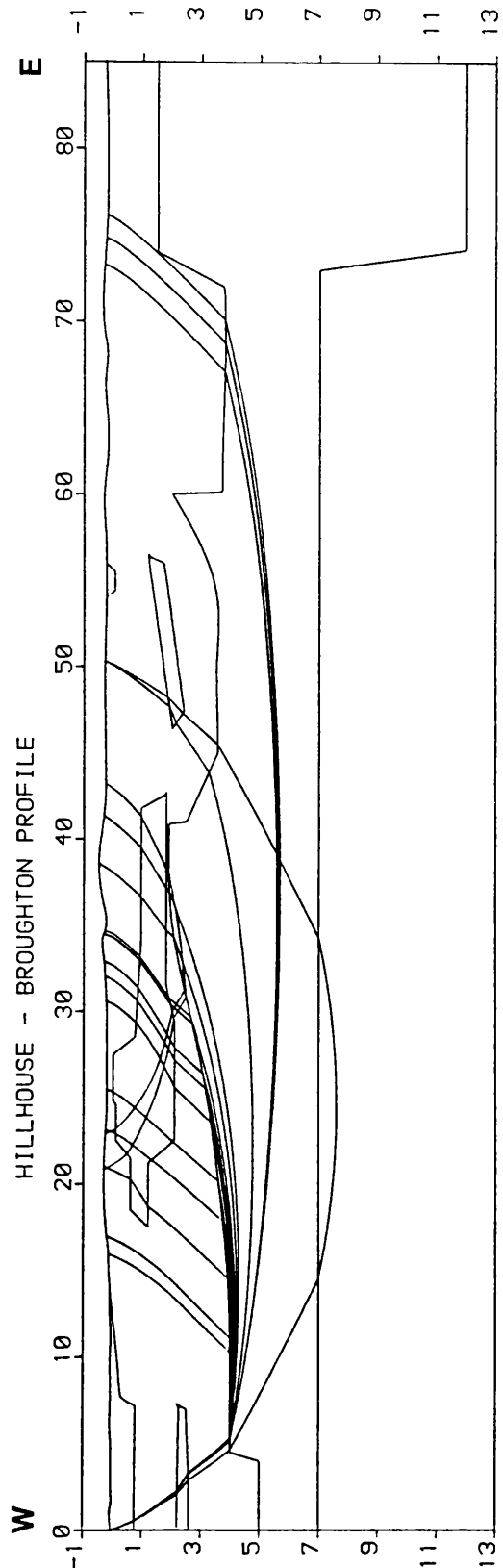


Figure 4.55 Ray diagram of Figure 4.5 showing all modelable raypaths through the a_0 basement.

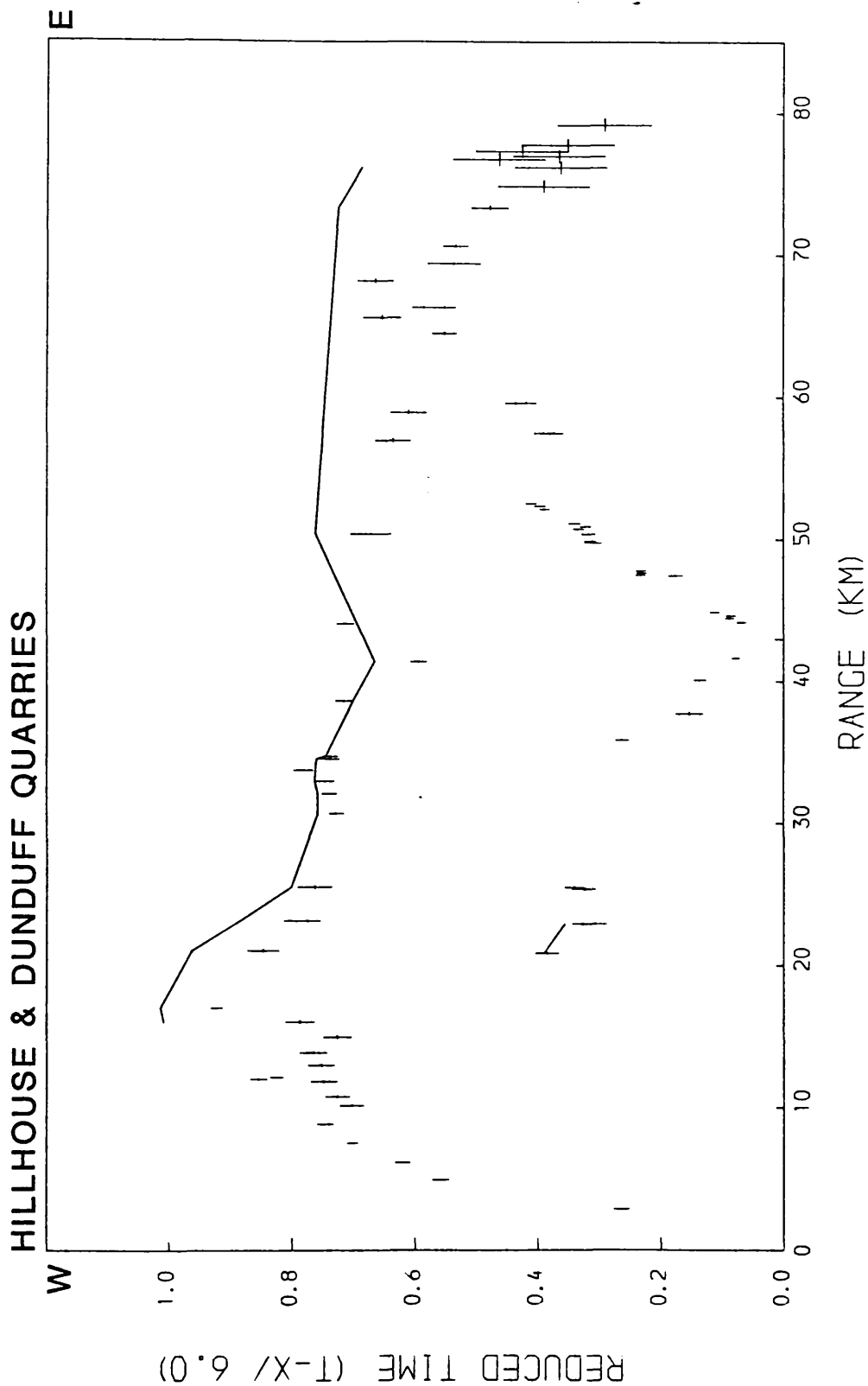


Figure 4.56 Computed and field travel-times for the predicted basement structure model.

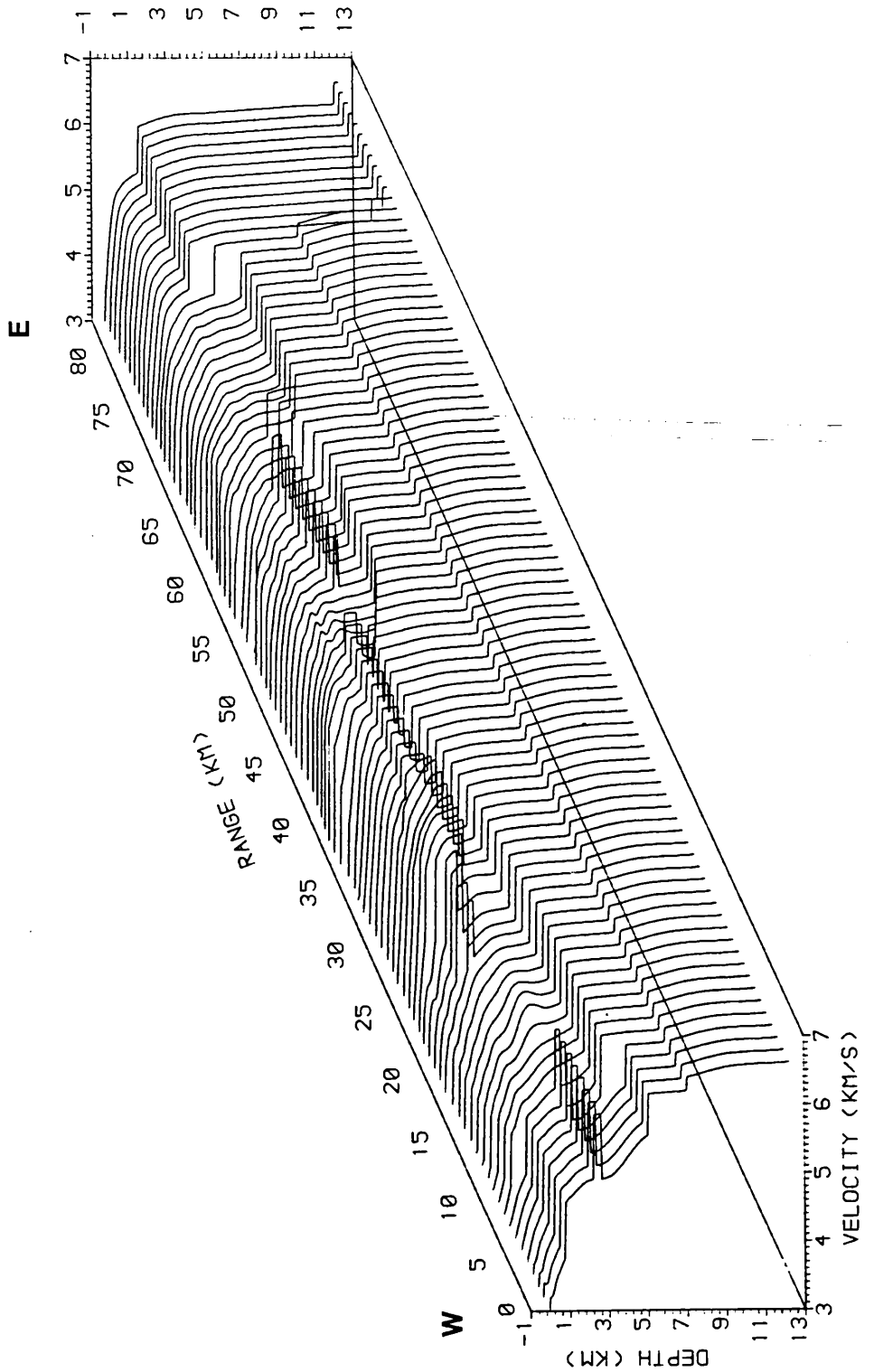


Figure 4.57 P-wave velocity structure under the Hillhouse-Broughton profile as derived from the ray model in Figure 4.54.

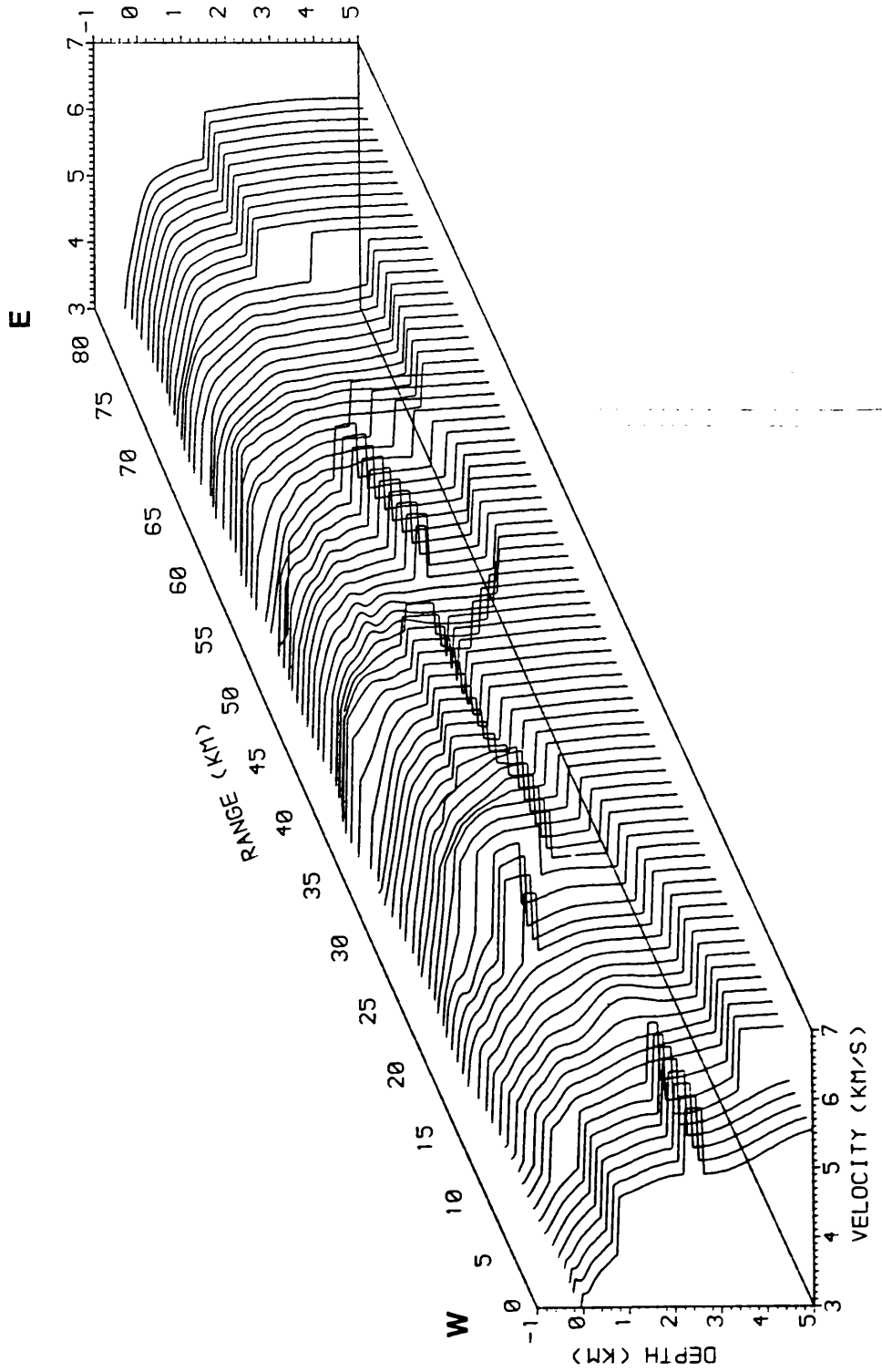


Figure 4.58 Enlargement of Figure 4.57 showing the P-wave velocity structure of the upper 5 km of crust.

creates geometrical problems which have prevented the successful transmission of most of the refracted rays, but these successful refracted arrivals do not fit the field data as well as those from the original ray model.

Comparing the shape of the predicted geological basement interface in figure 4.53 with the results of the time-term analysis along the profile (figure 4.33), does not show the expected correlation between the group of large time-term values at between 60 - 70 km range on figure 4.33 and the deeper basement area between the Carmichael and Southern Uplands faults (figure 4.54). For this correlation to be tenable, the time-terms between 45 and 60 km should have similarly large values, since the predicted basement in that region is broadly horizontal at a depth of around 4 km. From figure 4.33, it is obvious that this is not the case as these time-terms increase from 0.1 - 0.4 sec between 50 and 60 km.

As both the ray model (figure 4.34) and the predicted geological model (figure 4.54) imply a near planar refracting surface in this region, the jump in time-terms does not fit either model. The reduction in surface velocity E across the Carmichael fault (see 4.2.2.2) would produce an additional delay of no more than 90 ms, a factor of three times less than the observed difference. Two of these points, at 65 and 69 km, are sites connected into the system of simultaneous equations only by connection to Dunduff quarry and one connection to Craigpark quarry, near Edinburgh. Both of the arrivals from Dunduff quarry can be shown from the ray diagram (figure 4.39) to have travelled through the Dunduff 'sill', resulting in an increased path length through the surface layer. As a result, these points are slower than expected on the time-distance sections (eg figure 4.44). Although this delay is concentrated under the shot, the other arrival at Dunduff quarry site (from Cairngryffe quarry) does not pass through the high velocity layer. As a result, the quarry delay will be reduced, forcing the excess residual delay into the two receiver sites. Being from a peripheral source, the arrivals

from Craigpark quarry would not significantly influence this distribution of delays.

Thus, it appears that these anomalously large delays can be explained as an artifact of the operation of the simultaneous equations. This does not immediately explain the equally large delay value under Cairngryffe-Cloburn quarries.

Bearing in mind the qualifications mentioned earlier, it appears that the basement refractor structure is not rigorously controlled by surface geological structures but is to some extent independent. One consequence of this is that the thicknesses of the Lower Palaeozoic sediments, as seen across the profile, cannot be constant: a greater thickness of these sediments must be present under the Lesmahagow and Carmichael Inliers than elsewhere in the profile. This hypothesis can be tested by the comparison of time-terms measured across the LES array, with a geological section across the inlier showing the predicted variation in depth of the known base of the sedimentary sequence in this area. Figure 4.60 is a combination plot of the estimated geological section across the Lesmahagow Inlier in a NW - SE orientation (profile location on figure 4.59). Alongside, but plotted with a time-axis in place of depth-axis, are time-terms from the two major datasets described in section 4.2.1.2. The Hillhouse - Broughton profile crosses the section near the northwestern margin of the inlier, and the modelled depth to the a_0 refractor, 3.1 km, provides a common base for both geological and time-term sections. The time-terms have not been depth-converted but are only used to highlight the absolute differences in values between the two datasets. However, as no significant lateral changes in the surface layer V-Z profile are expected (eg the absence laterally of the 0.7 km thick Lesmahagow 'sill' would add only 15 ms on to any time-term value), the time-terms give an accurate representation of the variation in depth to the refractor across

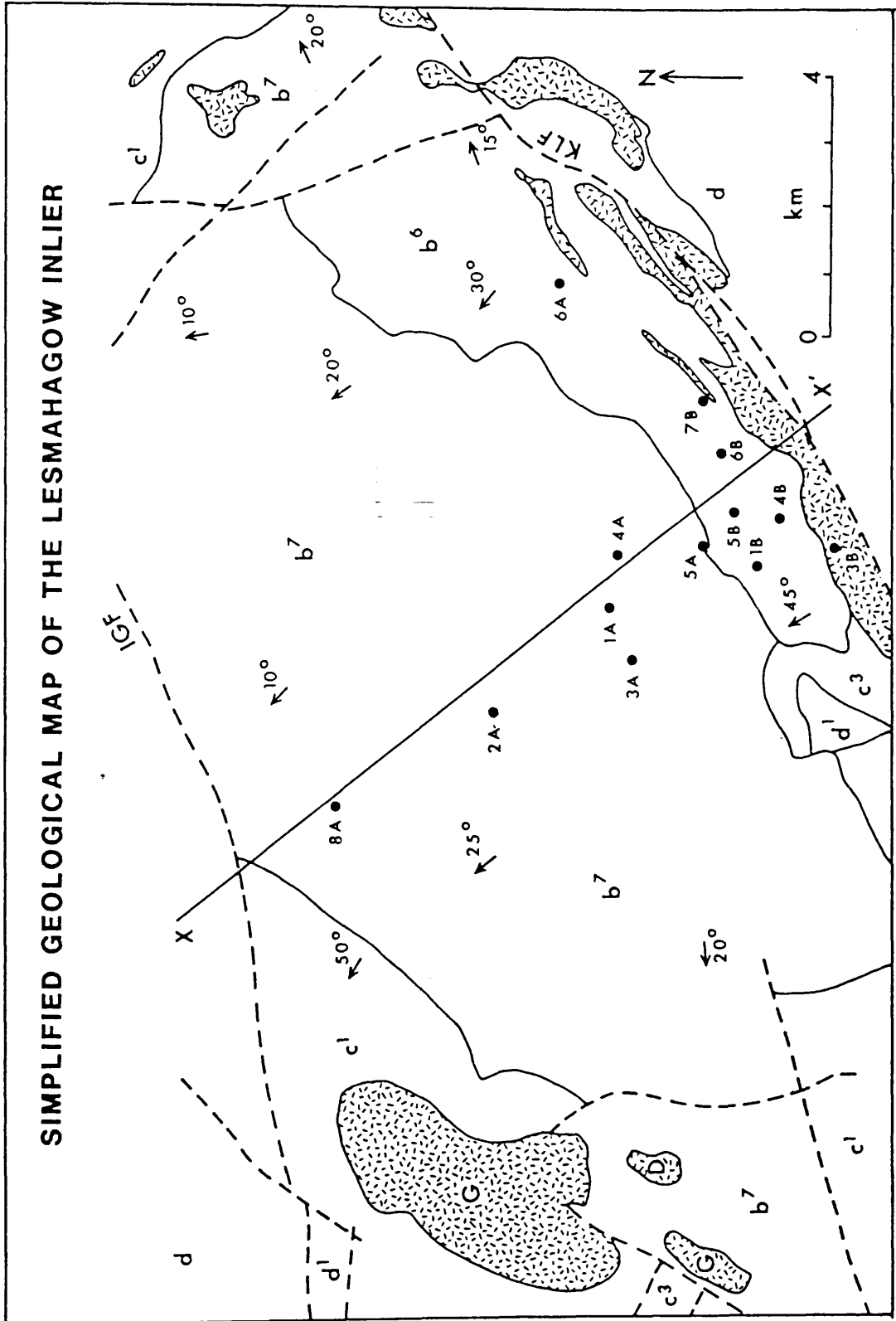


Figure 4.59 (key in figure 3.1).

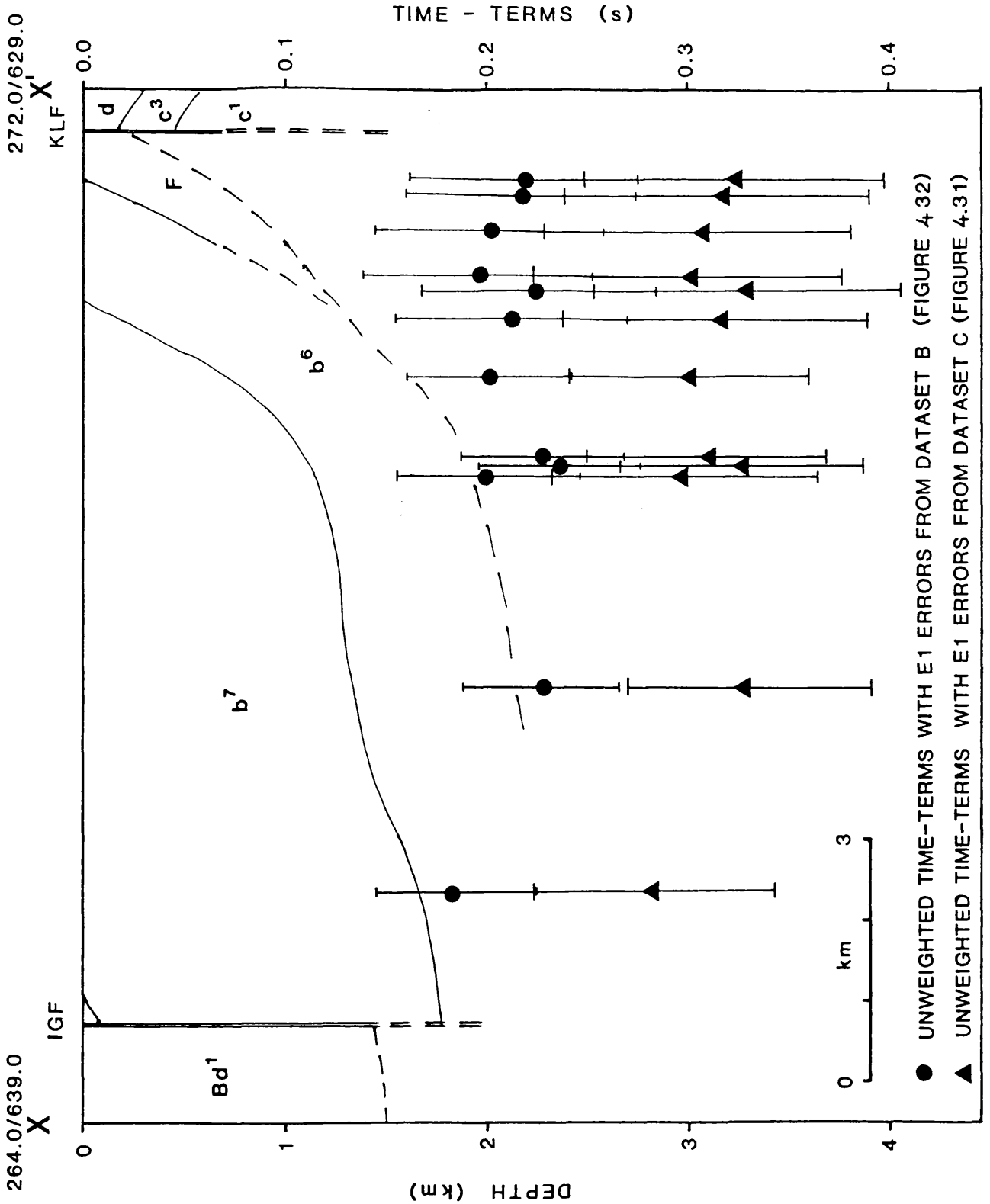


Figure 4.60 Sketch geological section with time-terms from two sample datasets for sites on or close to the line of section. Locations are shown on figure 4.59.

the regional strike, and which can in turn be compared to true depths by the intersection with the Hillhouse - Broughton profile.

It is obvious from figure 4.60 the the time-terms do not rise towards the Kerse Loch fault, implying that the a_0 refractor maintains a constant average depth irrespective of the surface geological structure. Further geological implications of this interpretation will be explored in later sections.

4.2.2.5 Deep structure

The only data from the Hillhouse - Broughton profile which can be attributed to energy propagating along a deeper refracting interface than the a_0 basement are found on the line recorded eastwards from Hillhouse quarry. Arrivals recorded from Hillhouse quarry into the BTN array (El-Isa 1977) show an apparent velocity of $7.64 \pm 0.27 \text{ km s}^{-1}$ at ranges of between 74 and 80 km. During this project, it was hoped that additional data could be recorded to fill in the gap up to 74 km and so relate this high apparent velocity to the known upper crustal structure of this area. Out of the ten recording sites placed between 50 and 70 km, only five gave any information and four were successfully digitised.

The LISPB and LOWNET studies both show a clearly defined a_1 refractor in the Midland Valley with a velocity of around 6.4 km s^{-1} and with a crossover point at around 50 km. An inflexion in the Hillhouse East travel time curve can be seen at 50 km with an apparently short segment of velocity 6.4 km s^{-1} continuing to between 60 and 65 km. Then follow several 'slow' points, some of which are part of the BTN dataset, and which appear to define the start of an approximately 7.0 km s^{-1} segment. This sort of complexity is not seen on the LISPB or LOWNET datasets.

The evidence of these previous studies suggests that the a_1 refractor occurs relatively uniformly at a depth of around 7 km throughout the Midland Valley. Because of the limited and single-ended nature of the available data,

it was felt that this pre-existing model should be used as a basis for a relative study of structure. The resultant ray model (figure 4.34) shows a ramp of 2° in the refractor extending from the western end of the profile (at 6 km depth) to a point at about 54 km (8 km depth), after which the refractor rises steeply (at around 6°) to reach a depth of 5 km under the BTN array. This model does not completely fit all the available data, in particular the slow points around 68 km, but it does represent the simplest likely explanation to this seismic data.

4.2.3.1 Apparent velocity interpretation

As mentioned in 2.2.1, the problems encountered with the Geostore equipment reliability and maintenance resulted in a reasonable number of good quality but untimed events being recorded by the LES array. In addition, the data obtained from the BTN array also contained many similar events, and it was felt that these should be used as far as possible to extend regionally the model obtained from ray-tracing and the time-term analysis. Untimed events were located, where necessary, by program BJARRY (a modified and extended version of a program originally written by B. Jacob, listing Appendix 6). The dataset used for this study comprises all timed and detected events in Appendix 4 with ranges of between 15 and 55 km from either array. Plots of P-wave apparent velocity-azimuth and apparent velocity-range are shown in figures 4.61,62 (S-waves; figure 4.63), and a map of the areal distribution of sources and apparent velocities is shown in figure 4.64.

For the purpose of this study, it was assumed that the velocity-depth structure to the refractor and the depth to the refractor were all known for some reference point in each array (the crossover point), that the refractor velocity was known and constant over the whole region of interest - assumptions considered reasonable in the light of the conclusions of sections

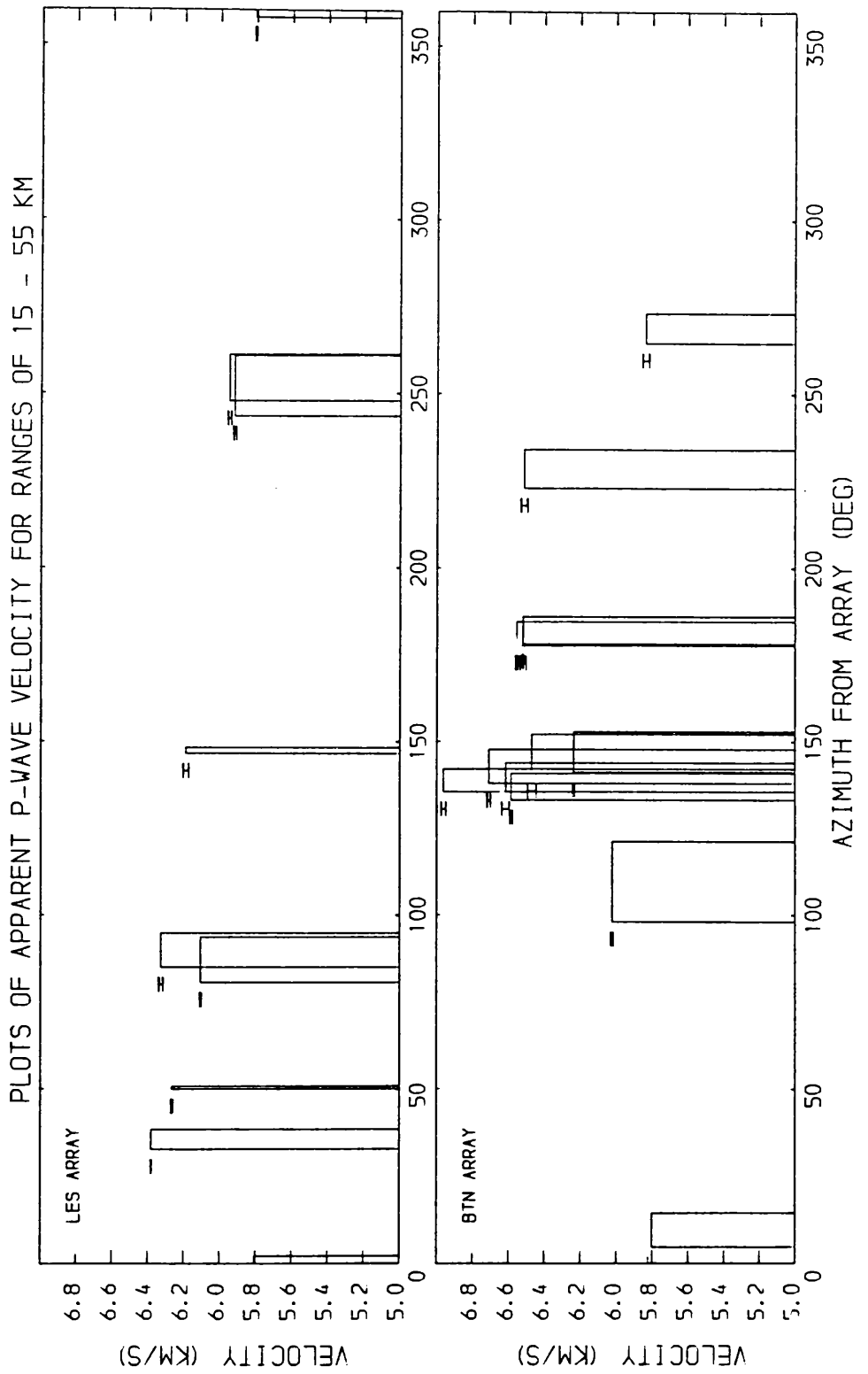


Figure 5.61 Apparent velocity against azimuth from array.

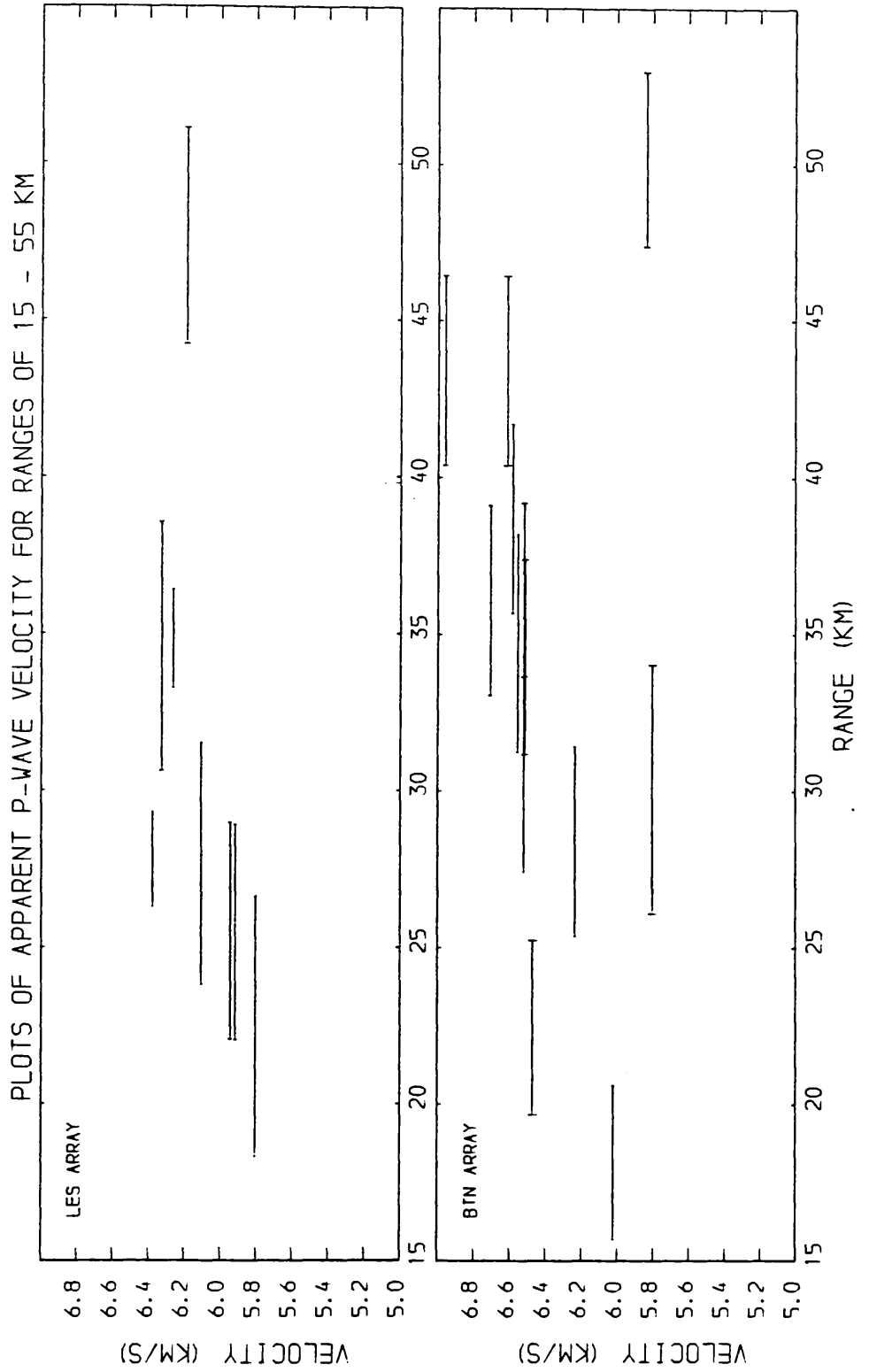


Figure 4.62 Apparent velocity against range.

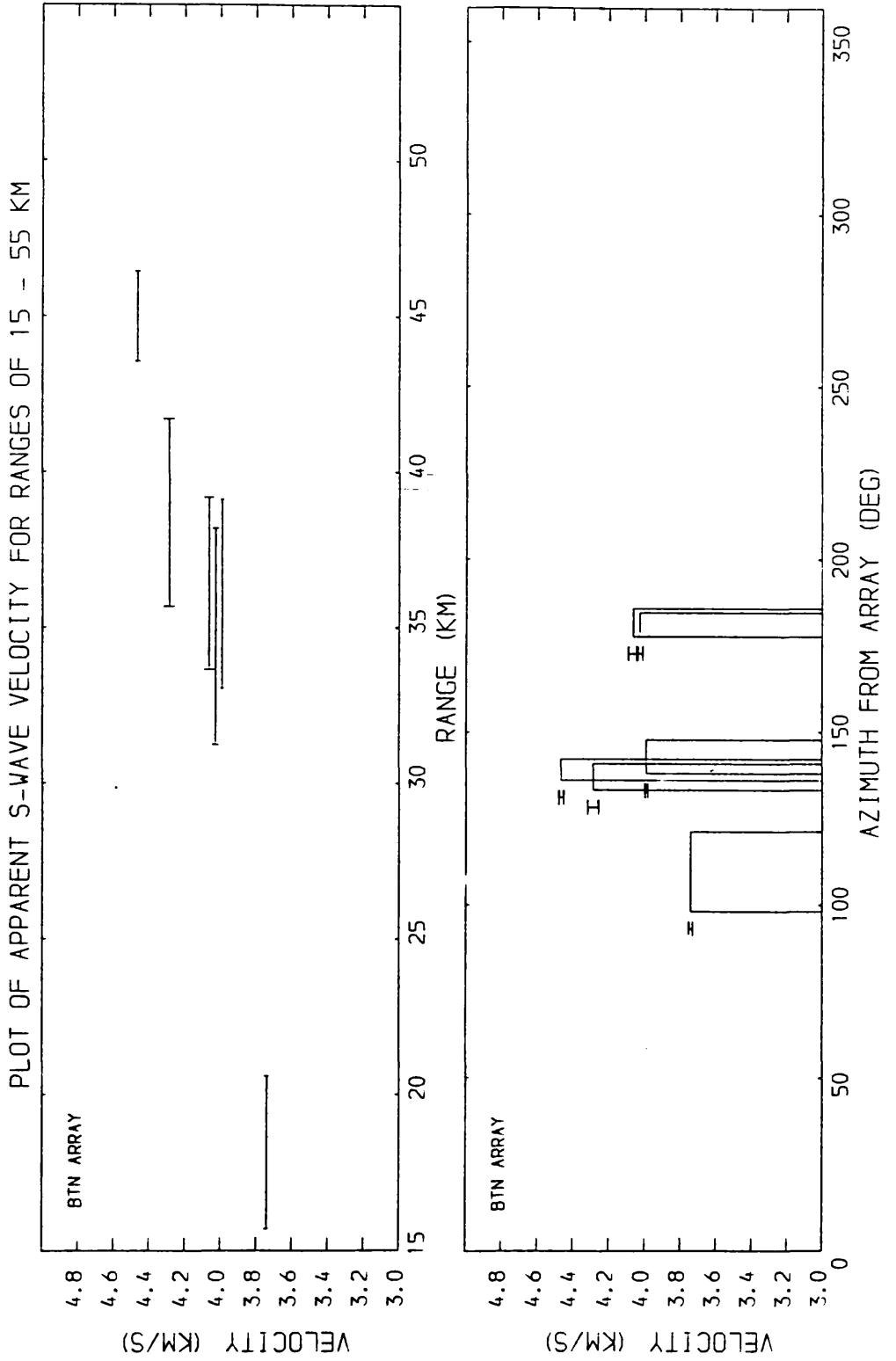


Figure 4.63 Apparent S-wave data into the BTN array.

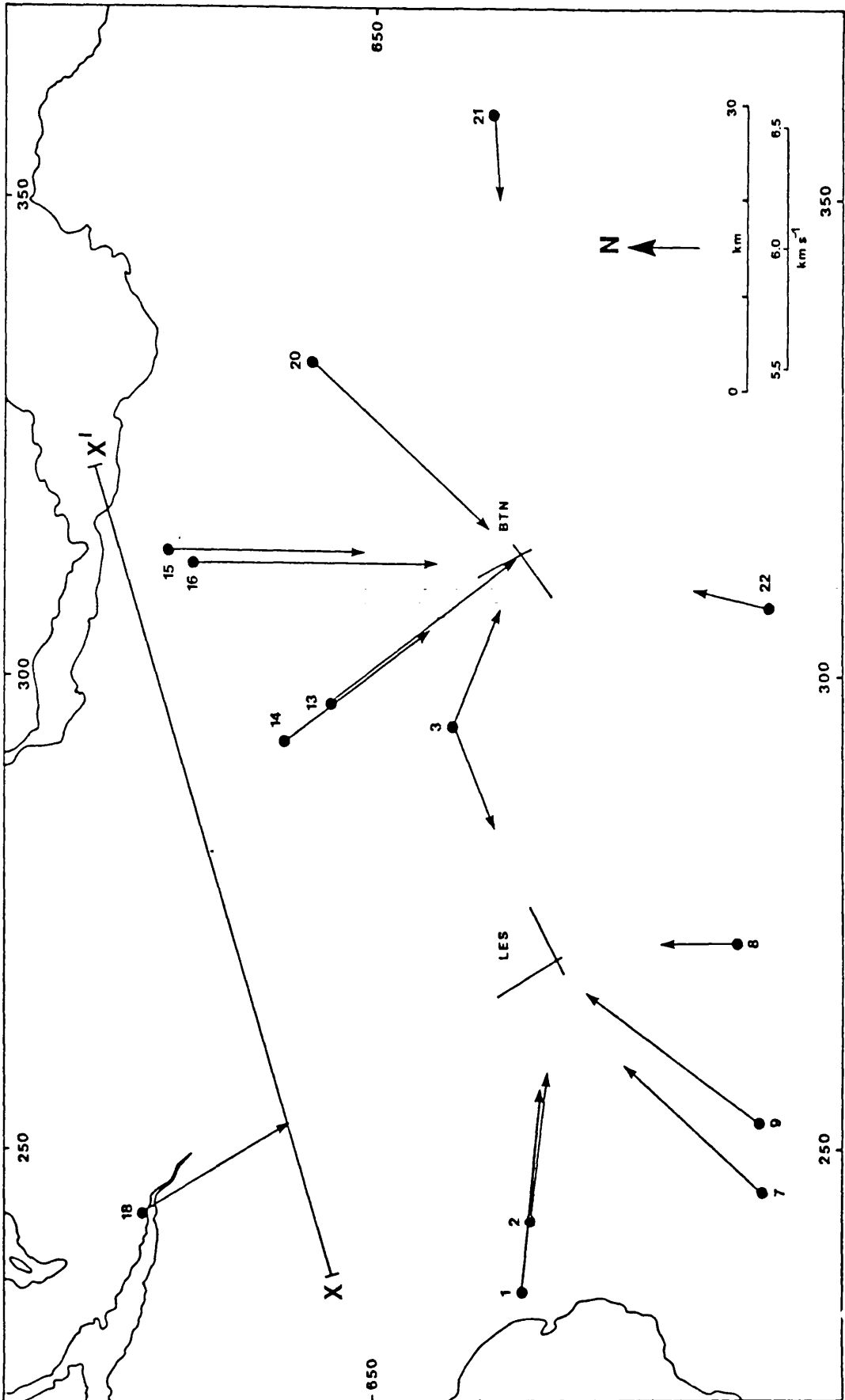


Figure 4.64 Summary of the apparent velocity data used to build up Figure 4.6. The length of each arrow is proportional to its P-wave apparent velocity. The MAVIS (south) profile is denoted by the line X-X'.

4.2.1.2 and 4.2.2.5. Thus the apparent velocity at any azimuth must be directly related to the average angle of dip on the refractor from that range as :

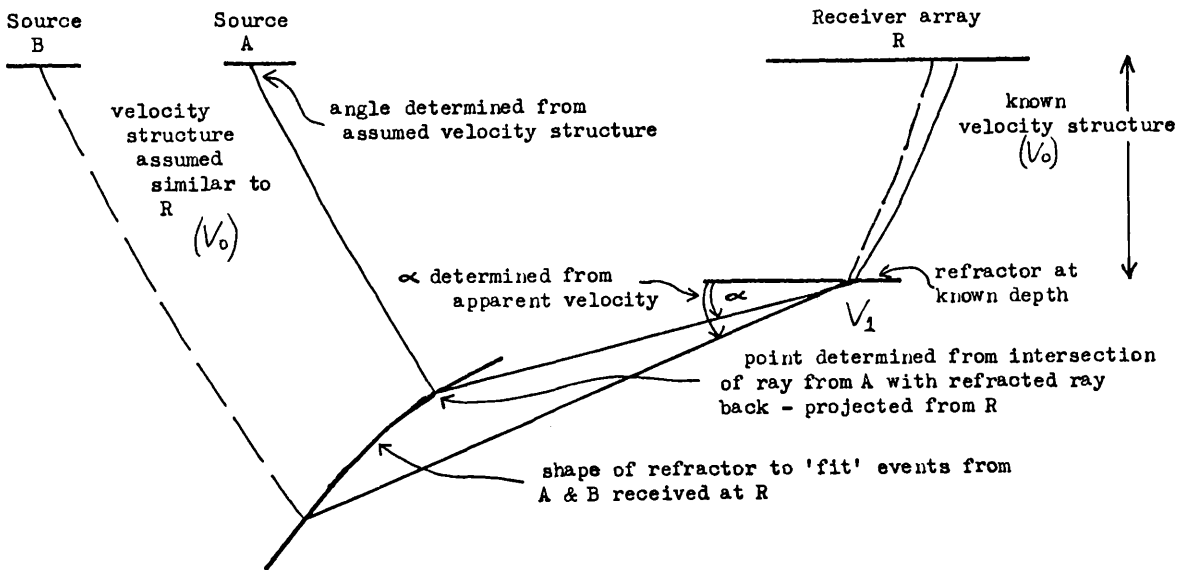
$$\alpha = \sin^{-1} (V_0/V_{app}) - \sin^{-1} (V_0/V_1)$$

where V_0 = the surface layer velocity at the array

V_1 = the true refractor velocity

V_{app} = the apparent refractor velocity received at the array

Where more than one event has been received at similar azimuths but different ranges to the same array, it has been assumed that each apparent velocity represents a series of raypaths which represent the shortest distances through the refracting layer and do not necessarily follow the refractor interface. This construction is summarised below.



4.2.3.2 Use of the apparent velocity dataset

The above technique was applied to the sets of apparent velocity data obtained from the LES and BTN arrays and combined with pre-existing data comprising the ray model described in 4.2.2.2, the preliminary ray models from data obtained around the Bathgate area (Davidson et al 1984; Sola &

Powell 1983), and selected preliminary depth values from the MAVIS South line (J. Hall, private communication), to build up a semi-quantitative view of the basement refractor topography of a part of the southern and central Midland Valley. While recognising that the use of the apparent velocity data in this way represents an extrapolation away from known and fixed depth points which probably will be only valid for as long as it takes to collect and interpret new, timed data in the surrounding regions, any new interpretation must still satisfy all existing data and so will be constrained to some extent by it. Thus the map presented in figure 4.65 is in essence correct, although suspect in detail, and will serve as a basis for further interpretations.

The most striking observation is that a large proportion of the area covered by these data is consistently at relatively shallow depth: the 3.5 km depth contour covers a large area of the Central and Southern Midland Valley and includes the southern part of the Central Coalfield. The region of predominantly Lower Palaeozoic rocks in the southern Midland Valley is, as expected from the interpretation of the Hillhouse - Broughton profile, a zone with consistently shallow basement and which appears to continue shallowing across into the Southern Uplands. On the basis of two quarry sources from within the Southern Uplands, these contours can be continued parallel to the Caledonide regional strike until they would surface before or close to their sources. Since there is no evidence for any high velocity layer cropping out in the Southern Uplands, it must be concluded that the a_0 refractor terminates or drops to a much greater depth at a distance of somewhere between 10 and 20 km SE from the SUF. This could be confirmed by timing either of these quarries into a reoccupied site in the BTN array. This conclusion is in general agreement with the 'block model' for the Southern Uplands basement of Hall et al (1983).

Slightly separate from the main shallow area, is another shallow region

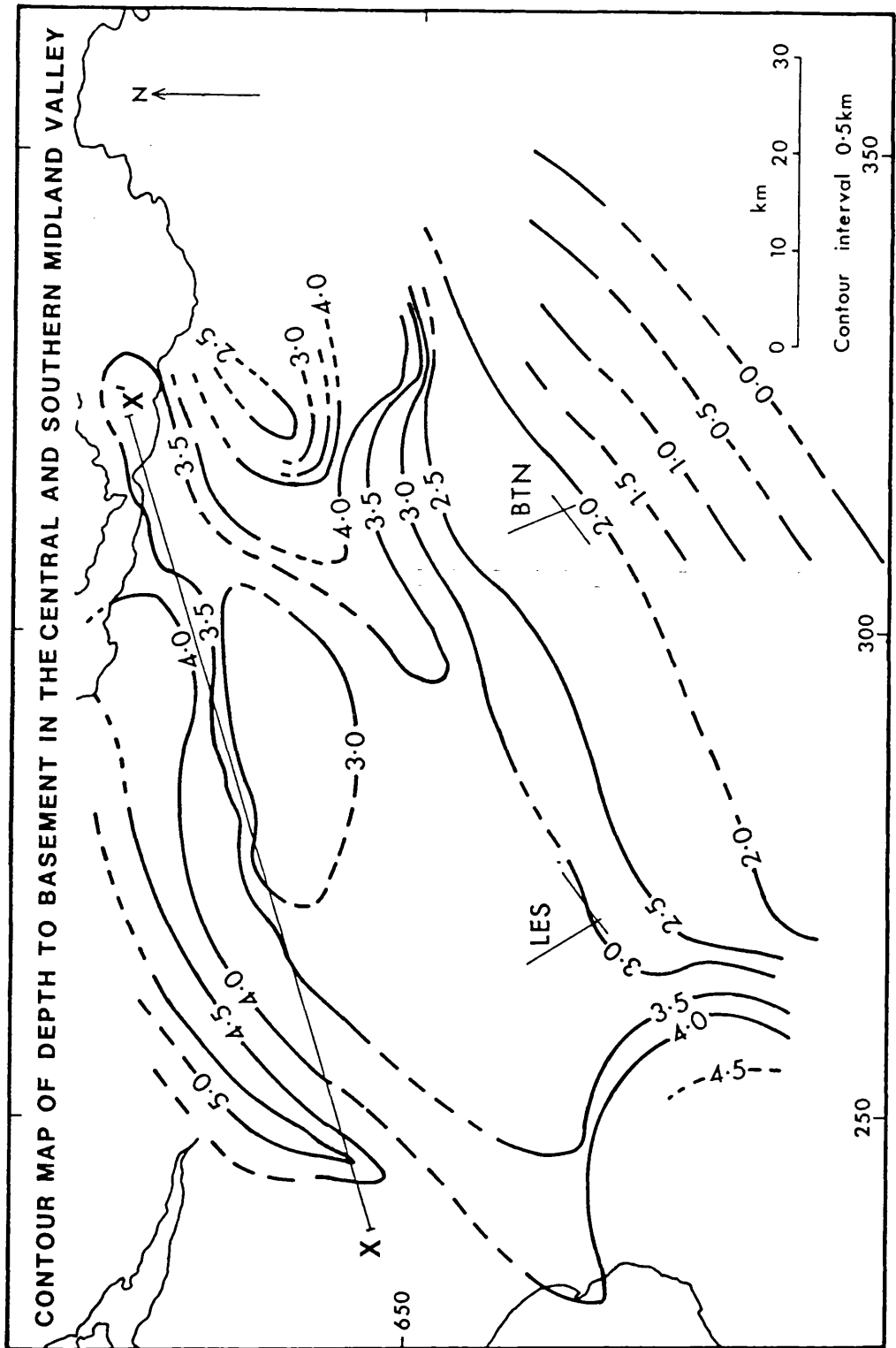


Figure 4.65 Depth values are relative to fixed depths under each array. The MAVIS (south) profile is denoted by the line X-X'

under the northeastern part of the Pentland hills. This can be confirmed by a plane layer inspection model of the first 20 km of data from the LISPB shot E (south) into alpha & beta (figure 4.66, locations in figure 1.14). To the S and E of the Pentland hills and separated from them by the Pentland fault, lies deeper basement under the E Lothian Coalfield. The resolution of this technique is insufficient to predict whether this movement took place along the Pentland or Leadburn faults.

In the southwestern corner of the map, the northeastern margin of the Mauchline basin is quite clearly defined by this data and is known from geological evidence to have formed during late Carboniferous times.

The overall conclusion from this study of the apparent velocity data is of a broadly planar refractor surface which has been warped by subsidence late in the history of evolution of the Midland Valley. This deformation must have occurred in relation to the late Carboniferous faulting which was widespread within the basins forming at that time. However this interpretation does not appear to hold for the region around the southern margin of the Central Coalfield which does appear to have been stationary at that time. New information across the Central Coalfield is required to delimit the structure more accurately.

Early interpretation of data recorded across the Maybole Inlier in the SW corner of the Midland Valley (D. Majid, private communication) confirms that basement is at a similar, shallow depth in that region and that the Mauchline basin is in fact a late, synclinal structure.

4.3 S - wave interpretation

Along the Hillhouse - Broughton profile, the S-wave dataset is limited (for reasons given in 3.2.4) to good quality analogue pickings of two groups of arrivals: those recorded E of Dunduff quarry and those recorded E of Cloburn quarry. These have been interpreted using the plane layer and WHB methods

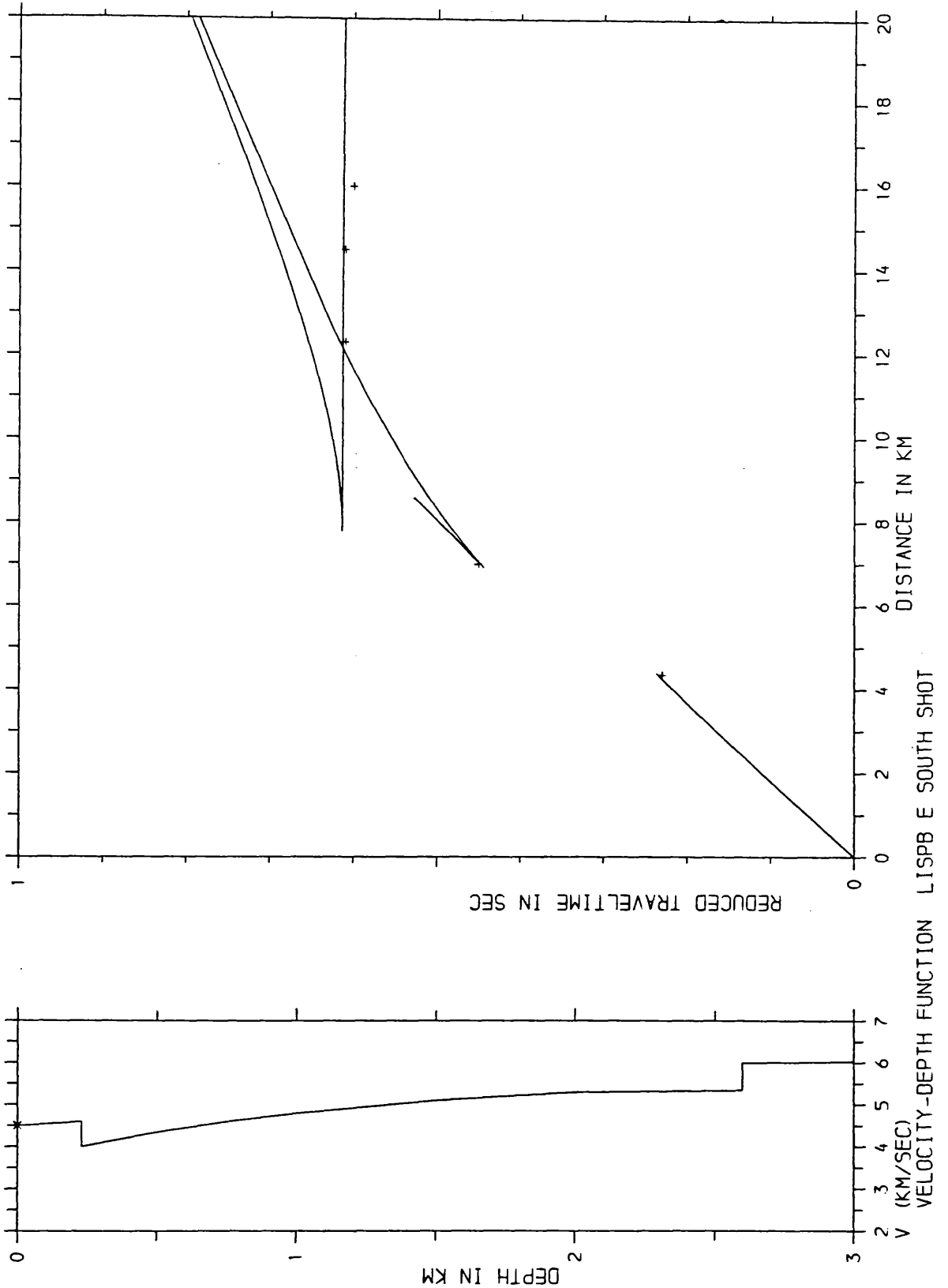


Figure 4.66 Plane-layer interpretation of the LISPB shot E into BETA (south). Surface geology from BGS 1:50000 maps, surface P-wave velocities from Davidson et al (1984).

(see figures 4.2a, 4.5, 4.17a,b). Because of the limited S-wave coverage across the profile no S-wave ray model was produced. Instead, comparisons were made with the S-wave interpretation of the Midland Valley section of the LISPB profile (Assumpcao & Bamford 1978; Assumpcao 1978) where, for the surface layer, a bimodal Poisson's ratio distribution of 0.33 ± 0.03 and 0.27 ± 0.03 was produced, loosely associated with the distribution of sediments and lavas in the eastern Midland Valley, and overlying the a_0 refractor with a Poisson's ratio of 0.233 ± 0.020 (0.231 ± 0.005 in the Southern Uplands).

From figures 4.27,28, it was noticed that the data recorded E of Dunduff quarry show Poisson's ratios which, apart from the first few hundred metres (where open cracks and therefore the effect of porosity will reduce S-wave velocities), are significantly lower with depth than either of the above estimates for the surface layer Poisson's ratio. This dataset is not well enough constrained beyond 10 km range to distinguish between direct and refracted S-wave arrivals, so no distinction was included in the model. However, the computed WHB results for this region (figure 4.3,5) confirm the presence of low Poisson's ratio values over the region between Dunduff and Cairngryffe quarries.

For the data recorded E of Cloburn quarry across the thick sequence of Lower Old Red Sandstone lavas (Mykura 1960) to the W of the SUF, no direct arrival was recorded and so the surface layer S-wave structure was modelled as a delay on a best fit refractor velocity at a depth fixed from the P-wave model, but using realistic velocity gradients similar to those modelled E of Dunduff quarry. Thus this direct S-wave velocity - depth curve represents realistic maximum velocities down to the refractor. Interestingly, after the initial 0.5 km of low V_S and high Poisson's ratio, the modelled Poisson's ratios are very similar with depth to the 0.27 figure suggested by Assumpcao (1978) for Midland Valley lavas, pointing to a significant change in lithological composition from predominantly sandstone to predominantly lavas

on either side of the Carmichael fault. These results also confirm the observations on the change in peak frequency of P-waves either side of this fault (section 3.2.3.2 and figure 3.24).

The only clearly defined group of a_0 refractor S-waves are found from Cloburn quarry, giving an apparent velocity of $3.74 \pm 0.05 \text{ km s}^{-1}$. After correction for the modelled refractor dip, this gives an estimate of 3.55 km s^{-1} for V_S . If the error on V_S is assumed to be the same as that of the apparent velocity fit, then a value of 0.237 ± 0.018 is obtained for the Poisson's ratio. As only one dataset has been used, this value must be treated with some caution. However, the value for the Poisson's ratio is compatible with the figure of 0.233 ± 0.020 quoted above for the a_0 refractor in the Midland Valley, and almost equivalent to the figure of 0.231 ± 0.005 obtained for the Southern Uplands.

4.4 Summary of the interpretation of this data

Various interpretation methods have been used to interpret the data presented, culminating in the ray models which show the existence of considerable lateral as well as vertical P-wave velocity inhomogeneity. The gross lateral velocity differences in the surface layer can be related to major changes in lithology as observed or predicted from the surface geology. In addition, there is evidence of several large high velocity bodies enclosed within the surface layer, which are interpreted as igneous intrusions of a similar type but a larger scale to those seen locally at the surface.

The a_0 refractor recognised by LISPB further E in the Midland Valley is also recognised in this area, but with a slightly, but possibly geologically significant, higher velocity. Possible geological interpretations will be discussed in the next chapter. Preliminary work indicates that this refractor is present at shallow depths over a wide area in the southern and central Midland Valley.

New information on the a_1 refractor is limited and ambiguous. It does not, however, appear to indicate a simple planar refractor structure.

Vertical velocity gradients can be demonstrated throughout the region covered by the Hillhouse - Broughton profile. As expected from previous work (Ali 1983; Adesanya 1981), these are greatest in the top 3 to 4 km (0 - 1 kb), and can be shown to depend on whether round pores or flat, grain-boundary cracks are dominant.

Chapter 5 Discussion and conclusions

5.1 Nature of the a_0 refractor

5.1.1 Introduction

The interpretation of the a_0 refracting horizon presented in section 4.2.2.4 and 4.2.3.1 concentrated almost exclusively on its velocity-depth structure and its position in the upper crust of the Midland Valley. This was done to highlight the similarities and differences in the interpretation presented in this study with previous interpretations, notably of LISPB.

No direct statement has yet been made as to the composition of this refracting layer or to its geological relationship with the overlying sedimentary layer.

5.1.2 Summary of seismic evidence

A summary of the seismic characteristics of the a_0 refractor determined in this study are given in figure 5.1 below,

V_P	$6.05 \pm 0.05 \text{ km s}^{-1}$ at 3 km
V_S	$3.55 \pm 0.05 \text{ km s}^{-1}$ " "
dV_P / dZ	$0.10 - 0.02 \text{ s}^{-1}$ (3 - 7 km)
Poisson's ratio	0.24 ± 0.02 at 3 km

figure 5.1

The velocity gradient is that used in the modelling process as discussed in section 4.2.2.4, and is based on estimates of the expected behaviour of flat-cracked rocks at equivalent confining pressures.

The inference from laboratory measurements of figure 5.1 on the geological nature of this refractor is that this combination of moderately high V_p and

low Poisson' ratio values would be best matched to a quartz rich, well compacted (either crystalline or highly cemented) lithology (Evans 1980; Hall & Al-Haddad 1979; Hall & Simmons 1979; Christensen & Fountain 1975; Christensen 1965; 1966; Alexandrov & Ryzhova 1962; and 1961a,b; Birch 1960; 1961 amongst others). Examples of seismic studies across continental (particularly cratonic) crust and confirming this interpretation are numerous in the literature (eg Hall & Ali 1985; Mechie & Brooks 1984; Mechie et al 1983; Drummond 1983;1981; Finlayson 1981; and Assumpcao & Bamford 1978).

5.1.3 Summary of geological evidence

This section reviews geological evidence which may provide some control on the interpretation of the nature of the a_0 refractor layer. Xenoliths from Midland Valley volcanic vents reveal a suite of almost exclusively metamorphic rocks whose petrogenesis indicate origins ranging from the mantle up to the upper crust (Upton et al 1983; Upton et al 1984). The lowest grade metamorphic xenoliths are quartz-feldspar gneisses (occasionally quartz-feldspar-garnet gneisses) containing minor amounts of sillimenite and biotite but no hornblende. As discussed in section 1.4.1, no xenoliths of Dalradian rocks or rocks of similar metamorphic facies have been found from these vents.

Assuming the rising magma in these vents systematically sampled all lithologies during its journey to the surface, then the upper most basement rocks must be represented by these acid gneiss xenoliths.

Longman (1980) noted the presence of a suite of exotic lithologies in clasts from Ordovician conglomerates of the Girvan region, which geochemically have island-arc affinity, and whose emplacement ages are coeval with the disposition of the conglomerates. Longman et al (1979) and Bluck (1983; 1984) have proposed for the Midland Valley the existence of an Ordovician arc sited on continental crust.

From both these lines of geological evidence the basement in the Midland Valley would be predicted to be composed of host lithology acid-gneisses penetrated by island-arc granites. McGiven (1967) and Bluck (1983; 1984) have also shown the need for a source, in Silurian times of a substantial volume of metaquartzite.

5.1.4 Comparisons and predictions of possible lithologies.

In order to gain some quantitative feel for the types of lithology which would give an acceptable fit with the velocity information on the a_0 refractor in the Midland Valley and summarised in figure 5.1, a series of comparisons are shown for the a_0 refractor against three sets of ultrasonic measurements on rock cores. In each figure, the original velocity-pressure measurements have been converted to velocity-depth assuming lithostatic loading, as the modelled low velocity gradient would imply predominately closed cracks and therefore negligible pore-pressures. An overlying layer of average density 2700 kg m^{-3} can be assumed to be representative of the average density of Lower Palaeozoic sediments (McLean 1961; Powell 1970; 1971; Bott & Masson-Smith 1960; Adesanya 1982). Overestimation of the surface layer density by 50 kg m^{-3} will result in an error in depth of around 50 m at 3 km depth. Similarly, an underestimation of the overburden density at 7.5 km results in a discrepancy of around 140 m. As a result, all depth conversions of core data are considered accurate to within 2%.

P and S-wave velocities were compensated for the effects of the regional temperature gradient using the temperature coefficients quoted by Hall & Simmons (1979). For confining pressures of less than 2 kbars, this gives values of $-0.0006 \text{ km.}(s \text{ } ^\circ\text{C})^{-1}$ for P-waves and $-0.0003 \text{ km.}(s \text{ } ^\circ\text{C})^{-1}$ for S-waves (where applicable), and was combined with the estimate from Ingham & Hutton (1982) for the regional temperature gradient in the top 10 km of the Midland Valley, of 22°C km^{-1} . An overestimation of the temperature gradient by 5°C

would only produce an error in V_p of $< 0.2\%$ (assuming V_p in the range of $6.0 - 6.5 \text{ km s}^{-1}$).

Figure 5.2 shows the a_0 refractor V-Z curve plotted alongside the compiled data from a study of P and S-wave velocities in cores of Ordovician clastic sediments from the Girvan area (Adesanya 1982). The wide range of core velocities represents the variability in composition of these sandstones, but is distinct from the V-Z curve derived for the a_0 refractor. This confirms the inferences of sections 4.1.4 and 4.4 which invalidate the interpretation by LISPB of the geological nature of this refractor.

Figure 5.3 shows the refractor V-Z curve plotted against three examples of acid gneiss cores from Christensen (1965), chosen to be within the density range of $2650 - 2850 \text{ kg m}^{-3}$. These velocity values are the calculated means of three component measurements, and the error bars are a measure of the anisotropy range. There is a much closer agreement between the field V-Z curve and these samples, with the best correlation occurring with sample Gneiss 3 (Christensen 1965).

Figure 5.4 shows the refractor V-Z curve plotted against two samples of metaquartzite also from Christensen (1965). The curve indicating higher velocities corresponds to the 'feldspathic-mica quartzite' and contains 30% plagioclase and biotite, whereas the other sample contains 96% quartz.

From this, it can be deduced that if a quartzite layer exists as part of the basement sequence, it must occur at around 3 km depth, as below this depth the modelled velocities are greater than the single crystal velocities for quartz (eg $V_p = 6.2 \text{ km s}^{-1}$ at 5 km; V_p for quartz is 6.05 km s^{-1} (Christensen & Fountain 1975)). The Poisson's ratios for these quartzite samples are also much lower than the value of 0.24 ± 0.02 implied for the uppermost basement by this study and also by LISPB (Assumpcao & Bamford 1978; Assumpcao 1978). It is therefore unlikely that this lithology comprises a significant proportion of even the uppermost basement.

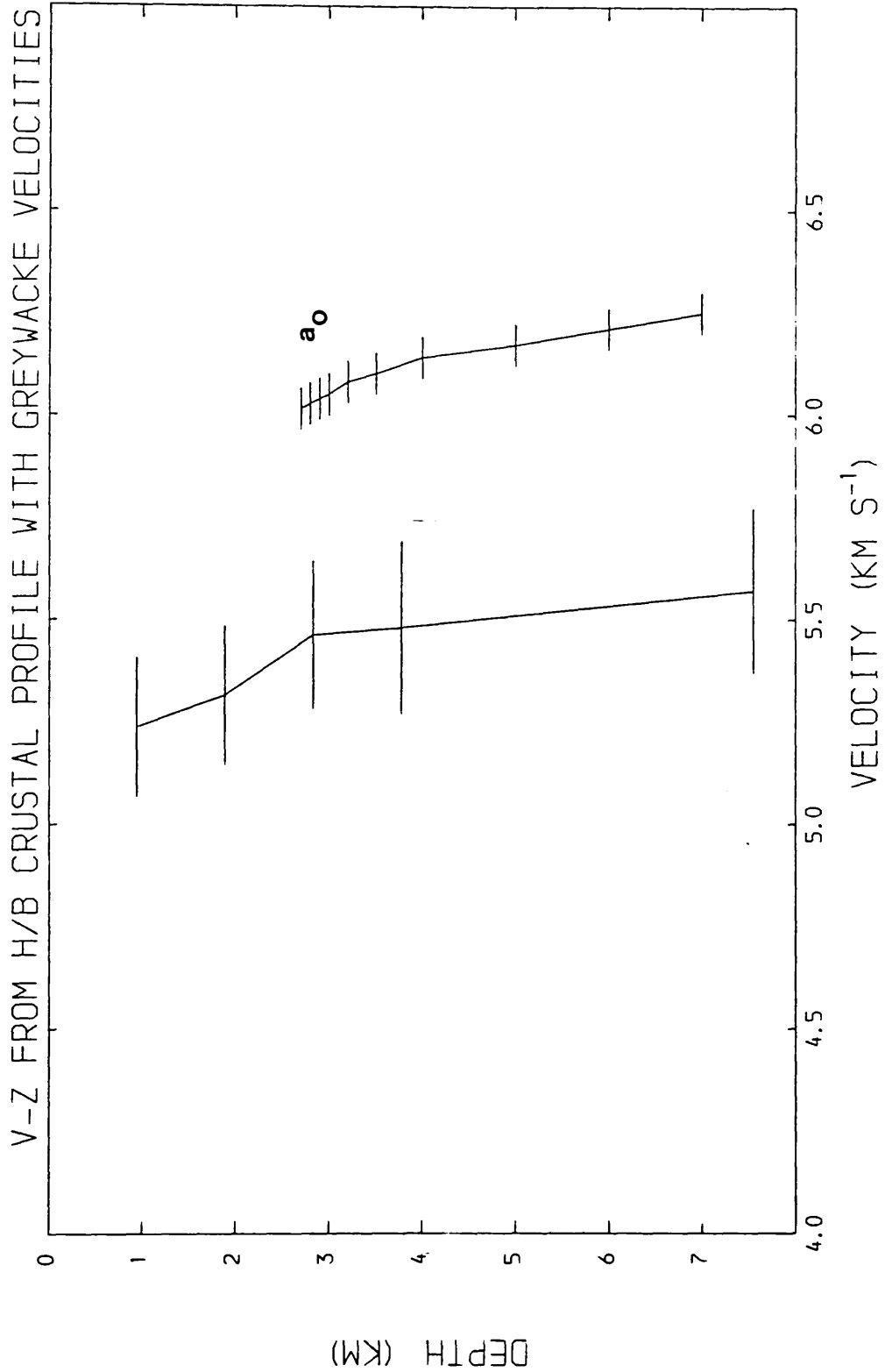


Figure 5.2 Velocity-depth curve for the a_0 refractor in the southern Midland Valley compared with the mean velocity-depth curve from a suite of greywacke cores from the Girvan region (Adesanya 1982).

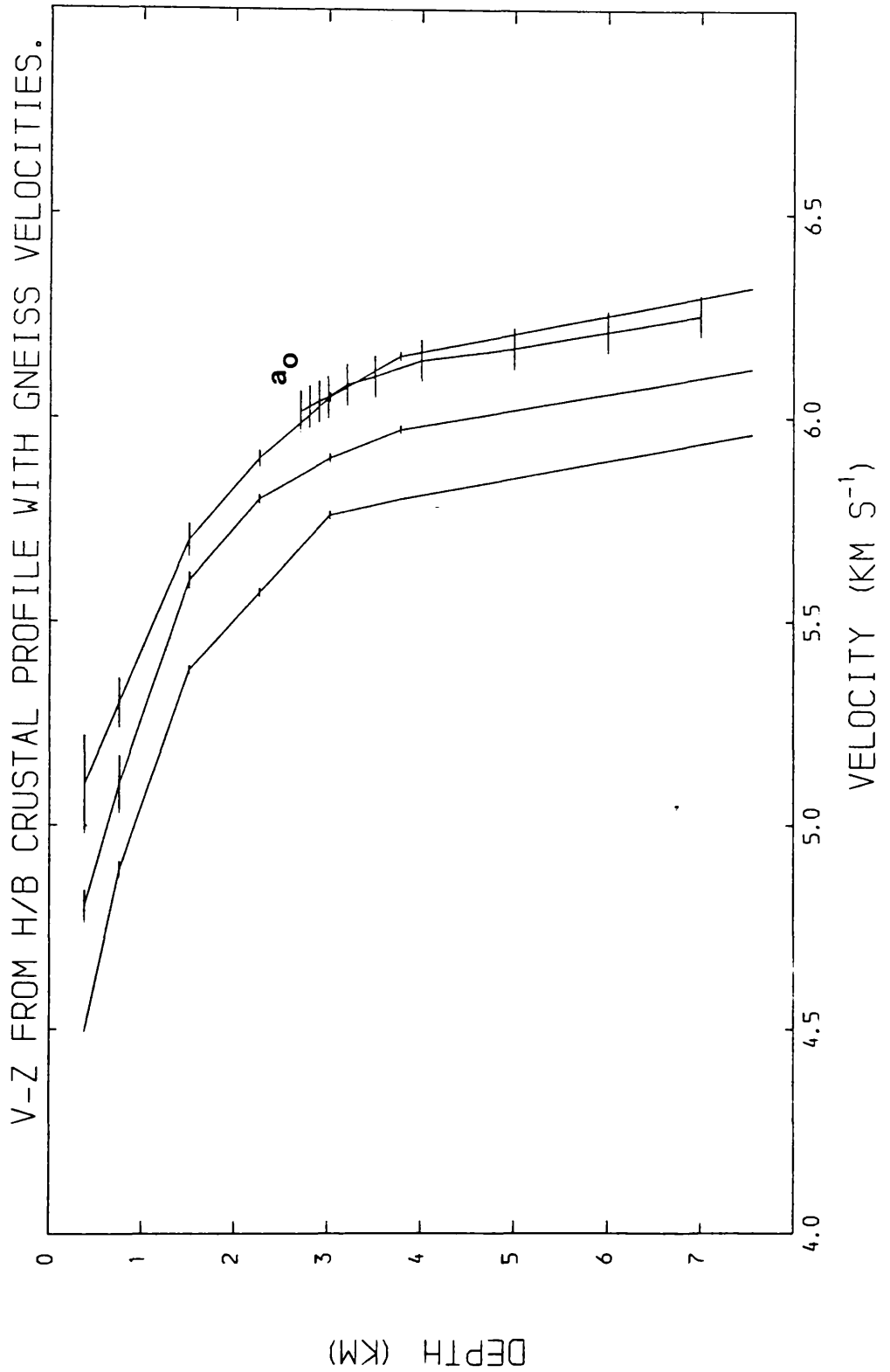


Figure 5.3 Velocity-depth curve for the a_0 refractor in the southern Midland Valley compared with velocity-depth curves for 3 sets of acid gneiss cores (Christensen 1965).

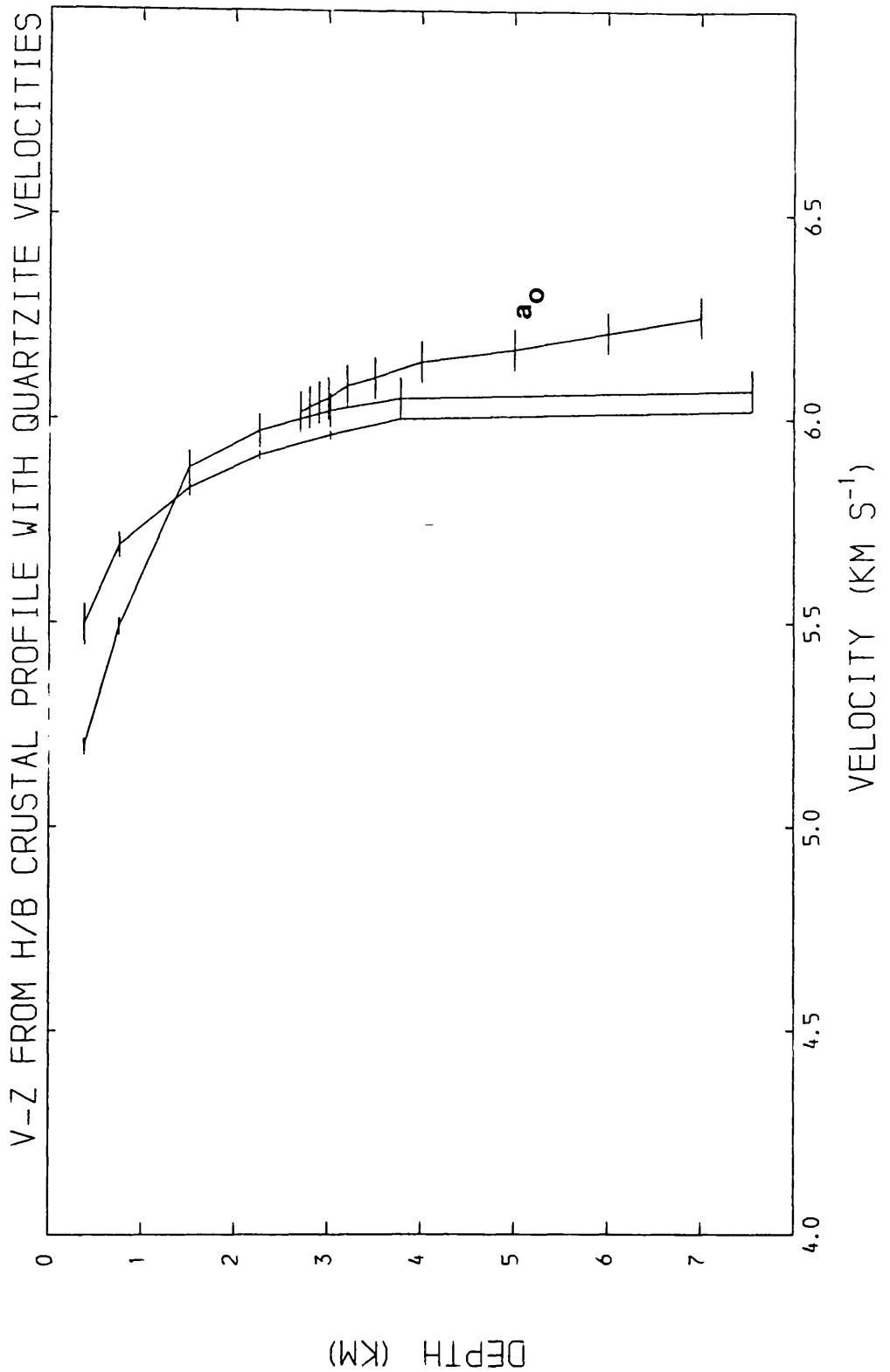


Figure 5.4 Velocity-depth curve for the a_0 refractor in the southern Midland Valley compared with velocity-depth curves for 2 sets of metaquartzite cores (Christensen 1965).

To summarise this section, three groups of quartz-rich lithologies, as represented by the above core samples, have been compared with the V-Z curve of the a_0 refracting layer in the southern Midland Valley. These comparisons serve to contrast differing types of quartz-rich rocks, more than to search for one matching lithology. The contrast between quartz-rich, well cemented sandstones (figure 5.2), a series of quartz-feldspar (+biotite +hornblende) crystalline rocks (figure 5.3), and quartz-rich metasediments (figure 5.4), indicates a clear preference for crystalline rocks (figures 5.3,4). Potentially any coarse-grained plutonic or metamorphic rock type predominantly composed of quartz and feldspar with minor proportions of higher velocity accessory minerals such as biotite and hornblende (or garnet) would fit with the V_p and Poisson's ratio limits supplied in section 5.1.1. Biotite and garnet are common accessory minerals in most samples found in the Midland Valley xenolith suite.

The gneissose xenoliths do not contain hornblende, whereas clasts in the Ordovician conglomerates indicate an abundance of high-level, hornblende granites (Longman 1979; Bluck 1983; 1984). Since these intrusions would have formed localised sources within the Ordovician basement, it is less likely that the Carboniferous vents would have sampled them, and so the absence of hornblende in the xenolith suite should not preclude the presence of that mineral locally within the roots of these intrabasement granites.

5.2 Relationship of the a_0 refracting layer with the overlying sedimentary sequence

5.2.1 Geometry of the basement structure compared with known or deducible sediment thicknesses

The modelled structure of the a_0 refractor was compared with the structure expected on it taking into consideration surface late-Caledonian structural movement and Upper Palaeozoic fault movements (section 4.2.2.4 and figures

4.34 & 4.54). It has been noted that the modelled surface is much smoother than expected and that even allowing for generalisations within the raytracing technique and the limitations of the present dataset, these differences remain. On a regional scale, the depth contoured surface of the a_0 refractor in the southern and central Midland Valley implies considerably reduced thicknesses of sediments throughout this region than would be predicted from extrapolation of the surface geology.

For example, in the area between the Lesmahagow and Carmichael Inliers, a reasonable estimate of the total thickness of Lower Old Red Sandstone and Silurian sediments based on the surface stratigraphy would be at least 4 km. Similarly, under the Central Coalfield, a value of 2 km for the Carboniferous sediments and lavas (confirmed seismically by Sola 1985; and Sola & Powell (1983)), would imply a total sedimentary thickness in this region of at least 6 km (the uncertainty being due in part to the thickness of the Upper Old Red Sandstone sediments, if present).

However, based on the results of the time-term study across the LES array (figure 4.60) which show time-terms under the across-strike arm of the array maintaining consistent values despite the rise in geological structure towards the SE, a further 2.5 - 3.0 km of sediment must exist under this southeastern part of the inlier. If this extra material is added to the stratigraphic column, then the total thickness of pre-Ludlow sediments in the inlier must be around 5 km. Since the basement must be at a constant depth across the inlier (figure 4.60), around 2 km of sediment must be 'lost' within the 10 km width of the inlier under this arm of the array. At the same time, the basement under and between Dunduff and Cairngryffe quarries is modelled at 3 km depth while between 1.0 - 1.5 km of Lower Old Red Sandstone sediments are estimated to be present from stratigraphic evidence. A reduction of 3.0 - 3.5 km in the thickness of the pre-Ludlow sediments must

have occurred eastwards across this 15 - 20 km distance.

An even more considerable reduction in sedimentary thickness is inferred in the southern part of the Central Coalfield and flanking the Bathgate Bouguer gravity and aeromagnetic high. Here basement has been modelled at 3.5 km depth (Sola 1985; Davidson et al 1984) and removing a 2 km thickness of Carboniferous sediments and lavas leaves only around 1.5 km of older sediments: 4 km less than would be expected from the total thicknesses inferred above on stratigraphic and seismological grounds.

Areas which do show a distinct deepening of the basement are the E Lothian Coalfield and the Mauchlin Basin. The total subsidence in the latter area has been computed by gravity modelling (McLean 1966) as 1.5 km, which is of similar order to the observed deepening from figure 4.65. Subsidence in the Mauchlin Basin was initiated during the late-Carboniferous and continued into the Permian (McLean 1978), making it one of the youngest surface tectonic features in the Midland Valley.

The apparent flatness of this basement refractor over such a wide area suggests two alternative explanations. It could represent an original topographic surface which has subsequently suffered only minor vertical warping since the Ordovician. Alternatively, it could represent a major planar tectonic movement zone. There is a problem with this second hypothesis. Any major thrust zone must have a surface trace corresponding to the outcrop of the lowest member of the thrust stack. As this refractor continues across the Central Coalfield, this boundary should be seen cropping out in the Lower Old Red Sandstone outcrop further N towards the HBF. There is no field evidence to support such a feature.

Given the limited extent of the present dataset, the topographic origin for the refractor appears the more likely explanation. The variations in thickness described above for pre-Ludlow sediments could then be related to differential erosion of these sediments by later fluvial action. This would

produce a buried landscape with regions such as the Lesmahagow Inlier remaining as high ground. This differential erosion must have taken place before the end of the Llandovery, as after that time, the stratigraphic record does not show any significant evidence for large scale, localised erosion. Unfortunately the only way of proving or disproving this hypothesis is by drilling close to the outcrop of the oldest (Llandovery) sediments, for example in the Lesmahagow Inlier. If the drilled sequence were to be a downwards continuation of the exposed sequence, with no tectonic breaks, then an erosive cycle would have to be invoked for all other regions to explain reduced thicknesses of pre-Ludlow sediments.

5.2.2 Effect of surface faults on the interpretation of basement structure.

Another enigmatic feature of this basement refractor is its continuation undeviated, or apparently so (see section 4.2.2.4), under several major faults such as the Kerse Loch (KLF), Carmichael (CF) and Southern Uplands faults (SUF), all of which can be shown to have exerted considerable vertical control on sedimentation throughout long periods from the Silurian to the Carboniferous. In particular, the SUF has been long considered to mark the southern margin of the Midland Valley 'graben' and the Laurentian continent in the UK, and has been considered by some workers as the site of early Caledonian subduction of the Iapetus Ocean (eg Leggett et al 1983; Yardley et al 1982).

Further indication of this control has been obtained for Central and Southern Ayrshire by interpretation of the Bouguer gravity field (McClean 1966). In this region, all of these faults show Bouguer anomalies which can be related to density contrasts within the top 1 - 2 km of the crust on either side of these faults, and which can be used to measure relative vertical movement through time. There is no evidence from this region of a longer wavelength component to these anomalies which might indicate

corresponding vertical movements in the basement. This may indicate that no vertical movement has been propagated down to the basement, but may equally be the result of a negligible density contrast between the lowest sediments and the basement rocks.

Direct information on the density of the basement is not available, but a likely range of values can be estimated from the value of V_p quoted in figure 5.1. Using regression analysis on a suite of core samples from the Lewisian (Hall & Al-Haddad 1979; Al-Haddad 1977), a relation between P-wave velocity at 1 kbar and the grain-density can be obtained giving;

$$\text{density} = (0.15 \pm 0.34) + (0.42 \pm 0.05) V_p \quad (r = 0.85, n = 23)$$

This gives a value for the density of the a_0 refractor of $2690 \pm 40 \text{ kg m}^{-3}$. Comparing this value with the accepted value of density for the Lower Palaeozoic sediments in southern Scotland of 2720 kg m^{-3} (McLean 1961; 1966; $2728 \pm 45 \text{ kg m}^{-3}$, Hipkin & Hussain 1983) gives an expected density contrast of approximately $-30 \pm 85 \text{ kg m}^{-3}$, which is negligible. On the basis of these figures, no recognisable anomaly (ie $> 4 \text{ mgal}$) would be produced even by the largest predicted vertical fault movements (up to 2 km) in the basement.

In summary, the seismic interpretation presented here gives no support to the existence of large vertical displacements in the basement in response to a similar scale of movement recognised across the surface faults. There is insufficient density contrast between the Lower Palaeozoic sediments and the basement, based on the above predicted values, to offer any resolution on the above problem based on the regional gravity field.

If this hypothesis regarding the lack of vertical movements in the basement under these faults is valid, then the surface movement along these faults must be taken up in some other way: the only direction which would have minimal effect on the vertical basement structure would be to have curvature on these

faults and have them soling out at, or close to the basement. Gibbs (1984) has provided an analysis which suggests that for much of its Palaeozoic history, the Midland Valley has been an extensional or transtensional regime, and that by the application of balanced cross-section construction techniques to the BGS 1 inch geological maps, has shown that the major faults of the southern Midland Valley could be curved with depth. No relationship was implied for these faults with the basement. Decoupling due to major rheology contrast is common across the basement/cover interface in strike-slip terraines worldwide, and it may provide a suitable decollement zone for these faults in the Midland Valley.

Alternatively, decollement could take place along any convenient incompetent bed unit overlying basement (such as any 'Lower Silurian / Ordovician' shales).

5.3 Seismic characteristics of faults.

The discussion of the previous section (5.2.2) concluded that there is no evidence to confirm large vertical pre-Carboniferous movements in the basement under any of the dominant faults in the southern Midland Valley (eg Inchgotrick, Kerse Loch, Carmichael and Southern Uplands faults).

The question of whether these major surface faults are high angle, strike slip fractures or whether they flatten out at or near the basement/cover interface (with or without a strike slip component of movement) may be answered by looking, in detail, at the attenuation characteristics of the basement under the surface trace of these faults.

The recognition of faults on the seismic refraction record is normally dependent on waves propagating across a velocity discontinuity, and producing a corresponding discontinuity in the arrivals in the record section, which may be either delayed or accelerated relative to earlier arrivals. Diffracted energy will also be produced at any edges in the discontinuity and so any

vertical component of the fault movement may be recognisable if the data quality is sufficiently good.

However, a fault with a purely strike slip component of movement will produce a lateral velocity discontinuity only if the fault movement juxtaposes terranes of differing seismic character; otherwise it will remain seismically transparent.

In certain circumstances, a fault of any type may be seismically recognised. As part of a report on the results of a seismic refraction study in NW Manitoba, Canada, Green (1980) has noted the detrimental effect on S-wave amplitudes by recording across fault zones. The presence along the S-wave ray-path of a highly attenuating zone, such as the region of highly shattered rock normally surrounding major fault planes within competent lithology, will result in severe or complete loss of S-wave arrivals.

If any of the major faults in the southern Midland Valley were to have produced a significant shear zone at depth, then a *carefully* placed, closely spaced profile of receivers should record a similar variation in S-wave amplitude. This could provide a means of detecting major fracture zones at depth and showing whether the major surface faults have near vertical fault planes through the upper crust, or whether they sole out into a decollement zone at or near the basement/cover interface, or indeed whether all these faults might be related to a single strike slip fracture zone within the basement.

5.4 Geological interpretation of the nature of the a_1 refracting layer

As mentioned briefly in section 4.3.3.5, the a_1 refracting layer was first recognised within the Midland Valley by the LOWNET study, and its presence subsequently confirmed by the LISPB study. The seismic properties of this layer are summarised by figure 5.5.

The a_1 refracting layer was originally interpreted as metamorphic basement

(Crampin et al 1970). This interpretation was confirmed and further quantified by the work of Hall & Al-Haddad (1979), Hall & Simmons (1979) and Evans (1980), who concluded that pyroxene granulites petrologically analogous to those found in the Lewisian of NW Scotland provided a good match to the available data. Powell (1978) extended this interpretation by showing that modelling of the smoothed aeromagnetic field over the line of the LISPB profile in the Midland Valley required some of the pyroxene granulite to be replaced by hornblende granulite, indicating metamorphic retrogression.

Summary of velocity information on the a_1 refractor

	V_P km s ⁻¹	V_S km s ⁻¹	V_P/V_S	PR
LOWNET	6.4	-	-	-
LISPB *	6.50 ± 0.17			
**	6.40 at 7 km	3.81	1.678 ***	0.224 ***
**	6.45 at 18 km	3.84	± 0.024	± 0.012
This study	as LISPB			

* plane layer interpretation, averaged unreversed data

** from ray-trace modelling

*** t_S / t_P method (see 1.5.3)

figure 5.5

Assumpcao (1978) carried forward his analytical interpretation of Poisson's ratio distribution under the northern part of LISPB, by comparing his results for the a_1 refractor under the Northern Highlands and the Midland Valley (see figure 1.15) with a suite of aggregate mineral velocity measurements at atmospheric pressure, compiled by Christensen & Fountain (1975). In their study, Christensen & Fountain plotted groups of P & S-wave velocities and

Poisson's ratios for minerals in likely lower crustal combinations onto triangular diagrams.

The use of aggregate mineral velocities to model mineral combinations in the crust is valid only at confining pressures of greater than 1 - 2 kbars (ie when all high aspect ratio cracks should be closed). In the context of Assumpcao's and the present studies, it should provide valid estimates of the likely mineral groups present, and also give a guide as to their volumetric proportions.

Assumpcao's study concluded that the P-wave and Poisson's ratio distribution for the Midland Valley could be matched by a grouping of;

38 % Quartz

56 % Plagioclase (An₂₉)

6 % Bronzite (En₈₅)

This mineralogical breakdown represents a 10 % quartz-enrichment over values obtained for the a₁ refractor under the Northern Highlands, and is due to the unusually low Poisson's ratio values for the a₁ refractor found under the Midland Valley.

This does not concur well with the xenolith evidence reported by Upton et al (1984; 1983), which indicate that quartz is absent in granulites from vents around the Midland Valley.

This contradiction between the directly modelled Poisson's ratio interpretation of the a₁ layer under the Midland Valley and the evidence from xenoliths by magmatic sampling may be resolved if the low Poisson's ratio a₁ layer has not been sampled by any of the magmatic vents or fissures. Intuitively this appears unlikely. Alternatively, quartz disaggregation within the rising magma might provide a means of preferentially removing quartz from the nodules.

The Poisson's ratio structure of the a₂ refractor, taken to correspond to

the top of the lower crust, was also modelled by Assumpcao (1978; Assumpcao & Bamford 1978) giving;

$$V_p = 7.0 \text{ km s}^{-1} \text{ (ray-trace modelling)}$$

$$\text{Poisson's ratio} = 0.249 \pm 0.017$$

for under the Midland Valley.

Using Christensen & Fountain's diagrams in a similar manner to Assumpcao (1978), gives two possible estimated mineralogical compositions for the lower crust under the Midland Valley;

20 %	--	Perthite (Or ₇₉ ; Ab ₁₉ ; An ₂)	
30 %	or 55 %	Plagioclase (An ₂₉)	
50 %	45 %	Bronzite (En ₈₅)	(all \pm 5 %)
(norite)	(gabbro)		

Given the assumptions on the use of this method mentioned earlier, and also the obvious oversimplification of using only two or three minerals, the similarity between these and the average normative compositions for pyroxene granulite xenoliths (see figure 5.6) are encouraging.

From figure 5.6, it appears that both the seismic and geochemical/petrological evidence suggest that the lower crust under the Midland Valley is probably composed primarily of pyroxene granulites, with an overall basic mineralogy.

Thus a model of the crust compatible with the data used in this study would be as shown in figure 5.7. This model matches the seismic data but contains an assemblage (the quartz granulite) not sampled in the xenolith suites, possibly because of quartz disaggregation.

C I P W norms

	A	B	C	D	E	F	1	2
q	-	-	-	-	-	-	-	-
or	0.5	4.4	3.2	5.3	3.8	6.7	16	-
ab	13.1	17.5	15.3	16.5	11.4	26.2	25	30
an	31.9	32.1	21.0	30.6	29.6	28.8	9	16
ne	0.5	-	6.1	5.6	7.2	6.2		
di	24.6	26.2	25.1	18.7	22.5	12.6		
hy	-	6.9	-	-	-	-	50*	45*
ol	19.5	7.3	10.9	14.8	15.9	11.7		
mt	4.1	2.5	4.2	4.5	5.7	3.1	* Eng5	
il	3.0	0.8	1.2	1.9	2.1	2.1		
ap	0.02	0.02	0.3	0.2	0.2	0.4		

A two-pyroxene, Al-spinel granulite (HN43), Hawkes Nib

B two-pyroxene granulite (BdH8), Baidland Hill

C two-pyroxene granulite (Ag6), Ashtree Glen

D clinopyroxene-magnetite granulite (Fd106), Fidra

E retrograded garnet, c/pyroxene, magnetite granulite (Fd157), Fidra

F average of 21 basic granulites from Fidra

1 gabbroic granulite composition from text **

2 noritic granulite composition from text **

(all xenolith data taken from Hunter et al 1984)

** feldspar norms calculated from specified mineral compositions

figure 5.6

Model of the crust under the Midland Valley of Scotland

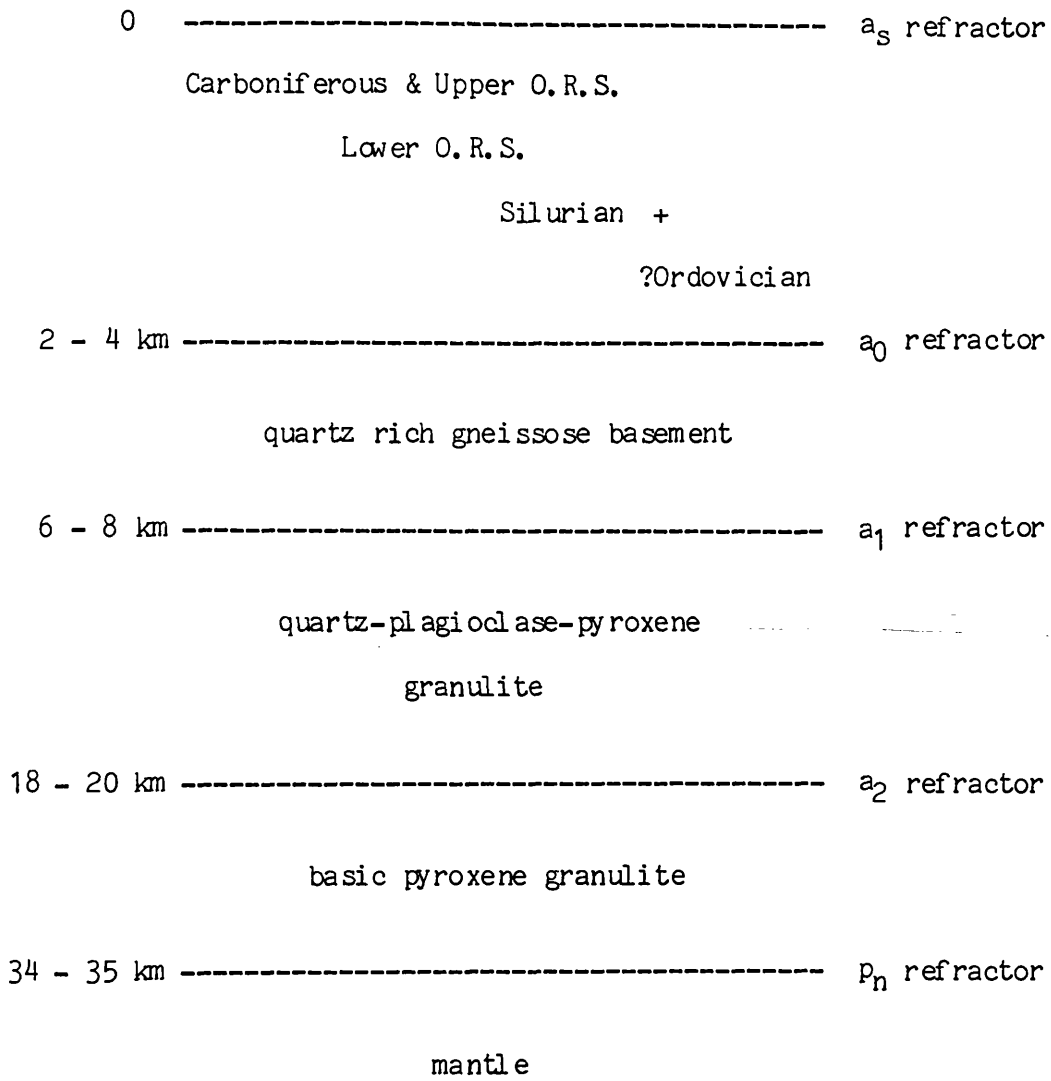


figure 5.7

5.5 Conclusion and recommendations for further work

5.5.1 Conclusions

1. This study (along with Sola 1985) has provided much more information on the range and distribution of P-wave velocities in the Palaeozoic sedimentary sequence of the southern and central Midland Valley of Scotland.

Stratigraphic Unit	P-wave velocity range
Carboniferous & Upper O.R.S.	3.2 - 4.0 km s ⁻¹
Lower Old Red Sandstone	4.0 - 5.2 km s ⁻¹
Silurian (& ?Ordovician)	3.5 - 5.5 km s ⁻¹

These results must therefore supercede previous published velocity values for the surface sediments in the Midland Valley (ie the LOWNET and LISPB velocity models).

2. While the broad geometrical interpretation of the LISPB a_0 refractor is not questioned, its geological interpretation as marking the top of a Lower Palaeozoic sedimentary sequence has been discredited. Comparisons of this study's interpretation of the a_0 refractor both with similar studies worldwide over cratonic areas, and with ultrasonic, high pressure measurements of P & S-wave velocities on cores of various lithologies suggest that the a_0 refractor is probably due to the presence, on a regional scale, of quartz-feldspar rich, crystalline rock (either igneous or metamorphic (or a mixture of both)). This interpretation is consistent with other, independent lines of evidence from within the Midland Valley such as xenoliths (eg Upton et al 1984; Upton et al 1983) and conglomerate provenance studies (eg Bluck 1983; Longman et al 1979).

3. Within the limits of resolution of the ray modelling (± 170 m), there is no evidence to suggest that the a_0 refractor is affected by pre-late

Carboniferous faulting. On the contrary, there is good evidence that in some areas (eg the Lesmahagow inlier and around the Southern Uplands fault near Biggar), there has been no significant vertical movement of the basement in response to variable and often large vertical movements in overlying active faults.

This implies either that these surface faults must sole out into a shallow (< 4 km) decollement zone, and/or route into a major basement strike slip lineament. The SUF cannot now be regarded as the southern margin of the Midland Valley basement, only as the southernmost major fault with a significant dip slip component. Equally it cannot be regarded as the outcrop of the sole thrust of the Southern Uplands accretionary prism allochthon as field evidence suggests a near vertical, near surface fracture whereas a major shallow thrust would have a more sinusoidal surface trace. Also Bluck (1983; 1984) has presented evidence to suggest earlier thrust emplacement during Ludlow or Pridoli times (late Silurian times).

4. Using both geophysical data and geological interpretation from the LISPB study across the Midland Valley has provided an interpretation for the a_1 refracting layer which is consistent with both that data and the evidence available from xenoliths. The a_0 / a_1 interface is considered to be the result of the change in metamorphic facies from amphibolite to granulite in quartz-feldspar rich rocks.

5.5.2 Recommendations for further work

1. Late stage filtering of data from the Hillhouse - Broughton profile showed considerable enhancement in the overall quality of S-waves. It should now be possible to ray-trace this data to obtain a velocity model which would give detailed V_p/V_s and Poisson's ratio distributions across the profile. It might then be possible to attempt modelling of aggregate mineral distributions (eg after Hall & Ali 1985; and Christensen & Fountain 1975). If

successful, this would provide a qualitative geological interpretation of the nature of the a_0 refractor.

2. The recording of more reversed refraction lines (> 50 km) across the central Midland Valley and Northern Belt of the Southern Uplands would allow the extension and qualification of the a_0 regional map presented here.

3. Long refraction lines such as those described in 2. above would also provide information to model the structure of the a_1 (6.4 km s^{-1}) refractor, and if good quality S-waves could be recorded, then some attempt could be made at refining the LISPB Poisson's ratio structure and possibly giving a greater insight into the nature of the a_0 / a_1 interface.

4. The use of modern seismic reflection equipment and interpretive techniques could provide a means of investigating, in greater detail, selected areas within the Midland Valley where modelling of refraction data has highlighted probable structural complexity. The sill-like bodies of the P-wave ray model (figure 4.34) could be investigated in greater detail by this means. If the apparent lack of a density contrast between the lowest Lower Palaeozoic sediments and the top of the a_0 basement is confirmed (eg by mineral modelling), then there is unlikely to be much of an impedance contrast and so mapping of basement structure by this means could be difficult.

5. As described in 5.3, the use of closely spaced receivers in short profiles (spacing around 100 m, profile length around 2.5 km) and a suitable strong source of S-waves, could provide a means of detecting major basement fracture zones. This could have considerable impact on the post-Caledonian tectonic history of the Midland Valley as well as its nature and origins.

References

- Aftalion, M., van Breeman, O. & Bowes, D.R. 1984. Age constraints on basement of the Midland Valley of Scotland. *Trans. R. Soc. Edinburgh Earth Sci.*, **75**, 53-64.
- Alexandrov, R.S. & Ryzhova, T.V. 1962. Elastic properties of rock forming minerals. 3. Feldspars. *Bull. Acad. Sci. USSR Geophys. Ser.*, **2**, 1129.
- Alexandrov, R.S. & Ryzhova, T.V. 1961a. The elastic properties of rock forming minerals. 1. Pyroxenes and amphiboles. *Bull. Acad. Sci. USSR Geophys. Ser.*, **9**, 871.
- Alexandrov, R.S. & Ryzhova, T.V. 1961b. Elastic properties of rock forming minerals. 2. Layered silicates. *Bull. Acad. Sci. USSR Geophys. Ser.*, **9**, 1165.
- Assumpcao, M.S. 1978. Studies of Crustal Shear Waves and Poisson's Ratio. Unpublished Ph.D thesis, Edinburgh University.
- Assumpcao, M.S. & Bamford, D. 1978. LISPB-V. Studies of crustal shear waves. *Geophys. J. R. astr. Soc.*, **54**, 61-73.
- Adesanya, O. 1982. Seismic velocities of the Upper Crust of the Southern Uplands. Unpublished Ph.D thesis, Glasgow University.
- Al-Haddad, F.M. 1977. Seismic Studies of Precambrian Lewisian Metamorphic Complex, NW Britain. Unpublished Ph.D thesis, Glasgow University.
- Ali, M. 1983. Study of shear wave velocities in the Lewisian metamorphic complex of NW Scotland. Unpublished Ph.D thesis, Glasgow University.
- Alomari, M.I. 1980. Geological interpretations of the gravity field of the western Midland Valley of Scotland. Unpublished Ph.D thesis, Glasgow University.
- Anderson, E.M. 1951. The dynamics of faulting. (2nd Ed), Edinburgh.
- Anderson, F.W. 1963. The Geological Survey bore at Rashiehill, Stirlingshire (1951). *Bull. Geol. Surv. UK*, **20**, 43-106.

- Bamford, D. 1979. Seismic constraints on the deep geology of the Caledonides of northern Britain. The Caledonides of the British Isles - Reviewed, edited by A.L.Harris et al., Spec. Publ. Geol. Soc. London, 93-96.
- Bamford, D., Nunn, K., Prodehl, C. & Jacob, B. 1978. LISPB - IV. Crustal structure of northern Britain. Geophys. J. R. astr. Soc., 54, 43-60.
- Bamford, D., Nunn, K., Prodehl, C. & Jacob, B. 1977. LISPB -III. Upper crustal structure of northern Britain. J. Geol. Soc. London, 33, 481-488.
- Bamford, D., Faber, S., Jacob, B., Kaminski, W., Nunn, K., Prodehl, C., Fuchs, K., King, R., & Willmore, P. 1976. A Lithospheric Seismic Profile in Britain - I Preliminary Results. Geophys. J. R. astr. Soc., 44, 145-160.
- Barrett, T.J., Jenkyns, H.C., Leggett, J.K., & Robertson, A.H.F. 1982. Comment and reply on 'Age and origin of the Ballantrae ophiolite and its significance to the Caledonian orogeny and the Ordovician time scale.' Geology, 9, 331-333.
- Bessonova, E.N., Fishman, V.M., Ryaboyi, V.Z., & Sitnikova, G.A. 1974. The tau method for the inversion of travel times, 1, Deep seismic sounding data. Geophys. J. R. astr. Soc., 36, 377-398.
- Birch, F. 1961. The Velocity of Compressional Waves in Rocks to 10 Kbars, Part 2. J. Geophys. Res., 66, 2199-2224.
- Birch, F. 1960. The Velocity of Compressional Waves in Rocks to 10 Kbars, Part 1. J. Geophys. Res., 65, 1083-1102.
- Bluck, B.J. 1984. Pre-Carboniferous history of the Midland Valley of Scotland. Trans. R. Soc. Edinburgh Earth Sci., 75, 275-295.
- Bluck, B.J. 1983. Role of the Midland Valley of Scotland in the Caledonide orogeny. Trans. R. Soc. Edinburgh Earth Sci., 74, 119-136.

- Bluck, B.J. 1980. Evolution of a strike-slip fault-controlled basin, Upper Old Red Sandstone, Scotland. In Ballance, P.F. & Reading, H.G. (eds), Sedimentation in oblique-slip mobile zones, Spec. Publ. int. Ass. Sediment., 4, 63-78.
- Bluck, B.J. 1978. Sedimentation in a late orogenic basin: the Old Red Sandstone of the Midland Valley of Scotland. In Bowes, D.R. & Leake, B.E. (eds) Crustal Evolution in northwestern Britain and adjacent regions. Geol. J. Spec. Issue, 10, 249-278.
- Bluck, B.J., & Halliday, A.N. 1982. Comment and reply on 'Age and origin of Ballantrae ophiolite and its significance to the Caledonian orogeny and Ordovician time scale. Geology, 9, 331-333.
- Bluck, B.J., Halliday, A.N., Aftalion, M. & MacIntyre, R.M. 1980. Age and origin of Ballantrae ophiolite and its significance to the Caledonian orogeny and the Ordovician time scale. Geology, 8, 492-495.
- Bott, M.H.P. 1976. Formation of sedimentary basins of graben type by extension of continental crust. Tectonophysics, 36, 77-86.
- Bott, M.P.H. & Masson-Smith, D. 1960. A gravity survey of the Criffell Granodiorite and the New Red Sandstone deposits near Dumfries. Proc. Yorkshire Geol. Soc., 32, pt 3, no 13.
- Bott, M.P.H., Long, R.E., Green, A.S.P., Lewis, A.H.J., Sinha, M.C. & Stevenson, D.L. 1985. Crustal structure south of the Iapetus suture beneath northern England. Nature, 314, 724-727.
- Brewer, J.A., Matthews, D.H., Warner, M.R., Hall, J., Smythe, D.K. & Whittington, R.J. 1983. BIRPS deep seismic reflection studies of British Caledonides - the WINCH profile. Nature, 305, 206-210.
- Brooks, M., Doody, J.J. & Al-Rawi, F.R.J. 1984. Major crustal reflectors beneath SW England. J. Geol. Soc. London, 141, 97-104.
- Cervený, V. & Psencik, I. 1981. Seismic Ray Package. Charles University, Prague.

- Christensen, N.I. 1966. Shear Wave Velocities in Metamorphic Rocks at Pressures to 10 Kbars. *J. Geophys. Res.*, **71**, 3549-3556.
- Christensen, N.I. 1965. Compressional Wave Velocities in Metamorphic Rocks at Pressures to 10 Kbars. *J. Geophys. Res.*, **70**, 6147-6164.
- Christensen, N.I. & Fountain, D.M. 1975. Constitution of the Lower Continental Crust Based on Experimental Studies of Seismic Velocities in Granulite. *Geol. Soc. Am. Bull.*, **86**, 227-236.
- Church, W.R. & Gayer, R.A. 1973. The Ballantrae ophiolite. *Geol. Mag.*, **110**, 497-510.
- Clayton, R.W. & McMechan, G.A. 1981. Inversion of refraction data by wavefield continuation. *Geophysics*, **46**, 860-868.
- Cocks, L.R.M., Holland, C.H., Rickards, B. & Strachan, I. 1971. A correlation of Silurian rocks in the British Isles. *J. Geol. Soc. London*, **127**, 103-136.
- Collette, B.J., Lagaay, R.A., Ritsema, A.R. & Schouten, J.A. 1970. Seismic investigations in the North Sea, 3 to 7. *Geophys. J. R. astr. Soc.*, **19**, 183-200.
- Crampin, S., Jacob, A.W.B., Miller, A. & Neilson, A. 1970. The LOWNET radio-linked seismometer network in Scotland. *Geophys. J. R. astr. Soc.*, **21**, 207-216.
- Davidson, K.A.S., Hall, J., & Powell, D.W. 1983. Upper Crustal Structure in the South of the Midland Valley of Scotland, *abst. Geophys. J. R. astr. Soc.*, **73**, 284.
- Davidson, K.A.S., Sola, M., Powell, D.W. & Hall, J. 1984. Geophysical model for the Midland Valley of Scotland. *Trans. R. Soc. Edinburgh Earth Sci.*, **75**, 175-181.
- De Souza, H.A.F. 1979. The geochronology of Scottish Carboniferous volcanism. Unpublished Ph.D thesis, London University.

- Dewey, J.F. 1974. Continental margins and ophiolite obduction: Appalachian Caledonian Systems. In Burk, C.A. & Drake, C.L. (eds). *Geology of Continental Margins*, 933-950, Springer-Verlag, New York.
- Dewey, J.F. 1971. A model for the Lower Palaeozoic evolution of the southern margin of the early Caledonides of Scotland and Ireland. *Scott. J. Geol.*, 7, 219-240.
- Diebold, J. & Stoffa, P. 1981. The traveltime equation, tau-p mapping, and inversion of common midpoint data. *Geophysics*, 46, 238-254.
- Drummond, B.J. 1983. Detailed Seismic Velocity/Depth Models of the Upper Lithosphere of the Pilbara Craton, Northwest Australia. *BMR Journal of Australian Geology and Geophysics*, 8, 35-51.
- Drummond, B.J. 1981. Crustal structure of the Precambrian terrains of northwest Australia from seismic-refraction data. *BMR Journal of Australian Geology and Geophysics*, 6, 123-135.
- El-Batroukh, S.L. 1975. Geophysical investigations on Loch Doon Granite South-West Scotland. Unpublished Ph.D thesis, Glasgow University.
- El-Isa, Z.H.M. 1977. Seismic studies of local events received at three arrays in Southern Central Scotland. Unpublished Ph.D thesis, Glasgow University.
- Evans, C.J. 1980. The seismic velocities of the Ox Mountain granulites of Ireland and the implications for the interpretation of the crustal structure of northern Britain. *Geophys. J. R. astr. Soc.*, 63, 417-426.
- Eyles, V.A., Simpson, J.B. & MacGregor, A.G. 1949. *The Geology of Central Ayrshire*. Mem. Geol. Surv. UK., (Sheet 14).
- Finlayson, D.M. 1981. Reconnaissance of upper crustal seismic velocities in the Tennant Creek Block, Northern Territory. *BMR Journal of Australian Geology and Geophysics*, 6, 245-252.

- Fitch, F.T., Miller, J.A. & Williams, S.C. 1970. Isotopic ages of British Carboniferous rocks. C. R. 6e. Congr. Strat. Geol. Carbonif., 2, 771-789.
- Francis, E.H. 1983. Chapter 9 Carboniferous. In Geology of Scotland (2nd Ed), edited by G.Y.Craig, Scottish Academic Press, Edinburgh.
- Francis, E.H. 1978. Igneous activity in a fractured craton: Carboniferous volcanism in northern Britain. In Bowes, D.R. & Leake, B.E. (eds). Crustal Evolution in northwestern Britain and adjacent regions. Geol. J. Spec. Issue, 10, 279-296.
- Garmany, J., Orcutt, J.A. & Parker, R.L. 1979. Travel Time Inversion: A Geometrical Approach. J. Geophys. Res., 84, 3615-3622.
- George, T.N. 1960. The stratigraphic evolution of the Midland Valley. Trans. Geol. Soc. Glasgow, 24, 32-107.
- Gibbs, A.D. 1984. Structural Interpretation with emphasis on extensional tectonics. JAPEC Course Notes, No 28, pt 2.
- Graham, A.M. & Upton, B.G.J. 1978. Gneisses in diatremes, Scottish Midland Valley; petrology and tectonic implications. J. Geol. Soc. London, 135, 219-228.
- Grant, F.S. & West, G.F. 1965. Interpretational theory in Applied Geophysics, McGraw-Hill, New York.
- Green, A.G. 1980. Delineation of geologic contrasts by seismic refraction with application to the fault zone between the Thompson nickel belt and the Churchill Tectonic Province. Can. J. Earth Sci., 17, 1141-1151.
- Hall, D.H. & Dagley, P. 1970. Regional magnetic anomalies: An analysis of the Smoothed Aeromagnetic Map of Great Britain and Northern Ireland. Rep. Inst. Geol. Sci., No.70/10.
- Hall, J. 1978. 'LUST' - a seismic refraction survey of the Lewisian basement complex in NW Scotland. J. Geol. Soc. London, 135, 555-563.

- Hall, J. 1974. A seismic reflection survey of the Clyde Plateau Lavas in North Ayrshire and Renfrewshire. *Scott. J. Geol.*, 9, 253-279.
- Hall, J. 1971. A preliminary seismic survey adjacent to the Rashiehill borehole near Slammanan, Stirlingshire. *Scott. J. Geol.*, 7, 170-174.
- Hall, J. & Ali, M. 1985. Shear waves in a seismic survey of Lewisian basement: an extra control on lithological variation and porosity. *J. Geol. Soc. London*, 142, 677-688.
- Hall, J. & Al-Haddad, F.M. 1979. Variation of effective seismic velocities of minerals with pressure and its use in velocity prediction. *Geophys. J. R. astr. Soc.*, 57, 107-118.
- Hall, J. & Simmons, G. 1979. Seismic velocities of Lewisian metamorphic rocks at pressures to 8 kilobars: relationship to crustal layering in North Britain. *Geophys. J. R. astr. Soc.*, 58, 337-347.
- Hall, J., Brewer, J.A., Matthews, D.H. & Warner, M.R. 1984. Crustal structure across the Caledonides from the 'WINCH' seismic reflection profile: influences on the evolution of the Midland Valley of Scotland. *Trans. R. Soc. Edinburgh Earth Sci.*, 75, 97-109.
- Hall, J., Powell, D.W., Warner, M.R., El-Isa, Z.M.H., Adesanya, O. & Bluck, B.J. 1983. Seismological evidence of shallow crystalline basement in the Southern Uplands of Scotland. *Nature*, London, 305, 418-420.
- Harris, A.L., Baldwin, C.T., Bradbury, H.J., Johnston, H.B. & Smith, R.A. 1978. Ensialic basin sedimentation: the Dalradian Supergroup. In Bowes, D.R. & Leake, B.E. (eds), *Crustal evolution in northwestern Britain and adjacent regions*, *Geol. J. Spec. Issue*, 10, 115-138.
- Herriot, A. 1956. Notes on the occurrence of garnet in felsite of Tinto, Lanarkshire. *Trans. Geol. Soc. Glasgow*, 22, 94-99.
- Hipkin, R.G. & Hussain, A. 1983. Regional gravity anomalies, 1. Northern Britain. *Rep. Inst. Geol. Sci.*, No. 82/10.

- Hossain, M.M.A. 1976. Analysis of the major gravity and magnetic anomalies centred about Bathgate, Central Scotland. Unpublished M.Sc thesis, Glasgow University.
- Hunter, R.H., Upton, B.G.J. & Aspen, P. 1984. Meta-igneous granulite and ultramafic xenoliths from basalts of the Midland Valley of Scotland: petrology and mineralogy of the lower crust and upper mantle. *Trans. R. Soc. Edinburgh Earth Sci.*, **75**, 75-84.
- Hussain, A. & Hipkin, R.G. 1981. Regional Gravity Map of the British Isles, Northern Sheet. (University of Edinburgh).
- Ince, D. 1984. Sedimentation and tectonism in the Middle Ordovician of the Girvan district, SW Scotland. *Trans. R. Soc. Edinburgh Earth Sci.*, **75**, 225-237.
- Ingham, J.K. 1978. Geology of a continental margin 2: middle and late Ordovician transgression, Girvan. In Bowes, D.R. & Leake, B.E. (eds), *Crustal evolution in northwestern Britain and adjacent regions*, *Geol. J. Spec. Issue*, **10**, 163-176.
- Ingham, M.R. & Hutton, V.R.S. 1982. The interpretation and tectonic implications of the geoelectric structure of Southern Scotland. *Geophys. J. R. astr. Soc.*, **69**, 595-606.
- Kennedy, W.Q. 1958. The tectonic evolution of the Midland Valley of Scotland. *Trans. Geol. Soc. Glasgow*, **23**, 106-133.
- Kennett, B.L.N. 1976. A comparison of travel time inversions. *Geophys. J. R. astr. Soc.*, **44**, 517-536.
- Klingspor, I. 1976. Radiometric age-determination of basalts, dolerites and related syenites in Skane, Southern Sweden. *Geol. Foren. Stockh. Fordh.*, **98**, 195-215.
- Kokelaar, B.P. 1982. Fluidization of wet sediments during emplacement and cooling of various igneous bodies. *J. Geol. Soc. London*, **139**, 21-33.

- Lagios, E. & Hipkin, R.G. 1979. The Tweedale Granite - a newly discovered batholith in the Southern Uplands. *Nature*, **280**, 672-675.
- Lambert, R.St.J. & McKerrow, W.S. 1976. The Grampian Orogeny. *Scott. J. Geol.*, **12**, 271-292.
- Leeder, M.R. 1982. Upper Palaeozoic basins of the British Isles - Caledonides inheritance versus Hercynian plate margin processes. *J. Geol. Soc. London*, **139**, 479-491.
- Leggett, J.K., McKerrow, W.S. & Soper, N.S. 1983. A model for the crustal evolution of southern Scotland. *Tectonics*, **2**, 187-210.
- Leggett, J.K., McKerrow, W.S., & Eales, M.H. 1979. The Southern Uplands of Scotland: a Lower Palaeozoic accretionary prism. *J. Geol. Soc. London*, **136**, 755-770.
- Longman, C.D. 1980. Age and affinity of granitic detritus in Lower Palaeozoic conglomerates, SW Scotland: implications for Caledonian evolution. Unpublished Ph.D thesis, Glasgow University.
- Longman, C.D., Bluck, B.J. & van Breeman, O. 1979. Ordovician conglomerates and the evolution of the Midland Valley. *Nature*, London, **280**, 578-581.
- Longman, C.D., Bluck, B.J., van Breeman, O., & Aftalion, M. 1982. Ordovician conglomerates: constraints on the timescale. In Odin, G.S. (ed) *Numerical dating in stratigraphy*, 807-809, Wiley, New York.
- Lumsden, G.I. & Wilson, R.B. 1979. Stratigraphical classification of the Carboniferous succession of Central Scotland. *C. R. 8me. Congr. Int. Strat. Geol. Carb. (Moscow)*, **2**, 27-36.
- McDonald, R., Gottfried, D., Farrington, M.J., Brown, F.W. & Skinner, N.G. 1981. Geochemistry of a continental tholeiite suite: late Palaeozoic quartz dolerite dykes of Scotland. *Trans. R. Soc. Edinburgh Earth Sci.*, **72**, 57-74.
- MacGregor, M. & MacGregor, A.G. 1961. *The Midland Valley of Scotland* (2ndEd). *Br. Reg. Geol.*, HMSO.

- McGivan, A. 1967. Sedimentation and provenance of post-Valentian conglomerates up to and including the basal conglomerate of the lower Old Red Sandstone in the Southern part of the Midland Valley of Scotland. Unpublished Ph.D thesis, Glasgow University.
- McLean, A.C. 1978. Evolution of fault-controlled ensialic basins in northwestern Britain. In Bowes, D.R. & Leake, B.E. (eds), Crustal evolution in northwestern Britain and adjacent regions, Geol. J. Spec. Issue, 10, 325-346.
- McLean, A.C. 1966. A gravity survey in Ayrshire and its geological interpretation. Trans. R. Soc. Edinburgh Earth Sci., 66, 239-265.
- McLean, A.C. 1961. Density measurements of rocks in south-west Scotland. Proc. R. Soc. Edinburgh, 68, 103-110.
- McLean, A.C. & Deegan, C.E. 1978. The solid geology of the Clyde Sheet (55°N/6°W). (eds).Rep. Inst. Geol. Sci., No. 78/9.
- McLean, A.C. & Qureshi, L.R. 1966. Regional Gravity Anomalies in the Western Midland Valley of Scotland. Trans. R. Soc. Edinburgh Earth Sci., 66, 267-283.
- McMechan, G.A. 1983a. p-x imaging by localised slant-stacks of T-x data. Geophys. J. R. astr. Soc., 72, 213-221.
- McMechan, G.A. 1983b. Wavefield inversion of seismic refraction data via the p-x plane. Geophys. J. R. astr. Soc., 72, 809-810.
- Mechie, J. & Brooks, M. 1984. A seismic study of deep geological structure in the Bristol Channel area, SW Britain. Geophys. J. R. astr. Soc. 78, 661-690.
- Mechie, J., Prodehl, C. & Fuchs, K. 1983. The Long-Range Seismic Refraction Experiment in the Rhenish Massif. In-Plateau Uplift, eds Fuchs et al, Springer-Verlag, Berlin Heidelberg.

- Milkereit, B., Mooney, W.D. & Kohler, W.M. 1985. Inversion of seismic refraction data in planar dipping structure. *Geophys. J. R. astr. Soc.*, **82**, 81-104.
- Mitchell, A.M.G. & McKerrow, W.S. 1975. Analogous evolution of the Burma orogen and the Scottish Caledonides. *Bull. Geol. Soc. Am.*, **86**, 305-315.
- Mykura, W. 1960. The Lower Old Red Sandstone Igneous rocks of the Pentland Hills. *Bull. Geol. Surv. GB.*, **16**, 131-155.
- Oliver, G.J.H. & Leggett, J.K. 1980. Metamorphism in an accretionary prism: prehnite-pumpellyite facies metamorphism of the Southern Uplands of Scotland. *Trans. R. Soc. Edinburgh Earth Sci.*, **71**, 235-246.
- Oliver, G.J.H., Smellie, J.L., Thomas, L.T., Casey, D.M., Kemp, A.E.S., Evans, L.J., Baldwin, J.R. & Hepworth, B.C. 1984. Early Palaeozoic metamorphic history of the Midland Valley, Southern Uplands-Longford Down massif and the Lake District, British Isles. *Trans. R. Soc. Edinburgh Earth Sci.*, **75**, 245-258.
- Phillips, W.E.A., Stillman, C.J. & Murphy, T. 1976. A Caledonian plate tectonic model. *J. Geol. Soc. London*, **132**, 579-609.
- Pidgeon, R.T. & Aftalion, M. 1978. Cogenetic and inherited zircon U-Pb systems in granites: Palaeozoic granites of Scotland and England. In Bowes, D.R. & Leake, B.E. (eds), *Crustal evolution in northwestern Britain and adjacent regions*, *Geol. J. Spec. Issue*, **10**, 183-220.
- Poley, J.Ph. & Nooteboom, J.J. 1966. Seismic refraction and screening by thin high-velocity layers. *Geophys. Prosp.*, **14**, 184-203.
- Powell, D.W. 1978. Gravity and magnetic anomalies attributable to basement sources under northern Britain. In Bowes, D.R. & Leake, B.E. (eds) *Crustal evolution in northwestern Britain and adjacent regions*, *Geol. J. Spec. Issue*, **10**, 107-114.

- Powell, D.W. 1971. A model for the Lower Palaeozoic evolution of the Southern margin of the early Caledonides of Scotland and Ireland. *Scott. J. Geol.*, **7**, 367-372.
- Powell, D.W. 1970. Magnetised rocks within the Lewisian of Western Scotland and under the Southern Uplands. *Scott. J. Geol.*, **6**, 353-369.
- Richey, I.E., Anderson, E.M. & MacGregor, A.G. 1930. *The Geology of North Ayrshire*. (Sheet 22). HMSO.
- Robinson, E.A. 1983. Multichannel time series analysis with digital computer programs. (2nd Ed) Goose Pond Press, Houston, Texas.
- Robinson, E.A. 1966. Collection of Fortran II Programs for Filtering and Spectral Analysis of Single Channel Time Series. *Geophys. Prosp.*, **14**, sup no 1., 1-52.
- Rogers, N.W. 1977. Granulite xenoliths from Lesotho kimberlites and the lower continental crust. *Nature*, London, **270**, 681-684
- Sola, M. 1985. The Seismic Structure under the Central Midland Valley from refraction measurements. Unpublished Ph.D thesis, University of Glasgow.
- Sola, M. & Powell, D.W. 1983. Upper Crustal Structure in the Centre of the Midland Valley of Scotland, abstr. *Geophys. J. R. astr. Soc.*, **73**, 284.
- Stone, P. & Rushton, A.W.A. 1983. Graptolite faunas from the Ballantrae ophiolite complex and their structural implications. *Scott. J. Geol.*, **19**, 297-310.
- Tatham, R.H. 1982. V_p/V_s and lithology. *Geophysics*, **47**, 336-344.
- Thirlwall, M.F. 1983. Discussion on implications for Caledonian plate tectonic models of chemical data from volcanic rocks of the British Old Red Sandstone. *J. Geol. Soc. London*, **140**, 315-318.
- Thirlwall, M.F. 1981. Implications for Caledonian plate tectonic models of chemical data from volcanic rocks of the British Old Red Sandstone. *J. Geol. Soc. London*, **138**, 123-138.

- Thirlwall, M.F. & Bluck, B.J. 1984. Sm-Nd isotope and chemical evidence that the Ballantrae "ophiolite", SW Scotland is polygenetic. In Gass, T.G., Lippard, S.J. & Shelton, A.W. (eds), Ophiolites and ocean lithosphere, Spec. Publ. Geol. Soc. London, 13, 215-230.
- Upton, B.J.G., Aspen, P. & Hunter, R.H. 1984. Xenoliths and their implications for the deep geology of the Midland Valley of Scotland and adjacent regions. Trans. R. Soc. Edinburgh Earth Sci., 75, 65-70.
- Upton, B.J.G., Aspen, D. & Chapman, N.A. 1983. The upper mantle and deep crust beneath the British Isles: evidence from inclusions in volcanic rocks. J. Geol. Soc. London, 140, 105-121.
- Upton, B.J.G., Aspen, P., Graham, A. & Chapman, N.A. 1976. Pre-Palaeozoic basement of the Scottish Midland Valley. Nature, 260, 517-518.
- van Breeman, O. & Bluck, B.J. 1981. Episodic granite plutonism in the Scottish Caledonides. Nature, 291, 113-117.
- Warner, M.R., Hipkin, R.G. & Browitt, C.W.A. 1982. Southern Uplands Seismic Refraction Profile. Unpublished NERC Progress Report, Project GST/02/13.
- Warren, R.D. 1981. Signal processing techniques applied to seismic refraction data. Unpublished M.Sc. thesis, Durham University.
- Whitcombe, D.N. & Maguire, P.K.H. 1979. The response of the time-term method to simulated crustal studies. Bull. seis. Soc. Am., 69, 1455-1473.
- Whitcombe, D.N. & Rogers D.E. 1981. The effects of refractor topography and overburden anisotropy on the time-term solution of refractor anisotropy. Geophys. J.R. astr. Soc., 67, 449-464.
- Williams, A. 1962. The Barr and Lower Ardmillan Series (Caradoc) of the Girvan district, south-west Ayrshire. Mem. Geol. Soc. London, 3.
- Willmore, P.L. & Bancroft, A.M. 1960. The time-term approach to refraction seismology. Geophys. J. R. astr. Soc., 3, 419-432.

Yardley, B.W.D., Vine, F.J. & Baldwin, C.J. 1982. The plate tectonic setting of NW Britain in late Cambrian and early Ordovician times. *J. Geol. Soc. London.*, **139**, 455-463.

Appendix 2 Quarry locations and shot origin times.

Quarry No.	Eastng Km	Northing Km	Elevation Km	Origin time (hrs.min.sec)	Shot name
5	267.890	630.010	0.010	13.37.01.028	CORNSTONES SHOT 10 SEPT 1982
4	266.190	637.810	0.005	13.31.17.303	MID CROFT SHOT 9 SEPT 1982
6	265.031	617.043	0.001	14.54.35.185	GREIVHILL SHOT 14 SEPT 1982
1	235.175	634.030	0.010	12.00.26.029	HILLHOUSE Q 2 AUGUST 1984
1	235.175	634.010	0.010	11.59.20.490	HILLHOUSE Q 17 DEC 1982
1	235.175	634.008	0.010	16.06.13.327	HILLHOUSE Q 1 SEPT 1982
1	235.180	634.020	0.010	16.03.42.939	HILLHOUSE Q 16 JUNE 1983
1	235.175	634.010	0.020	12.01.00.188	HILLHOUSE Q 2 JUNE 1983
1	235.000	634.000	0.050	12.08.12.190	HILLHOUSE Q 25/3/77
-	277.750	641.000	0.030	15.40.41.836	DUNDUFF Q 8 JULY 1893
-	277.750	641.000	0.030	13.29.51.447	DUNDUFF Q 8 JUNE 1983 (C)
-	277.640	640.970	0.020	13.37.06.508	DUNDUFF Q 27 JAN 1983
-	277.640	640.970	0.020	13.05.25.348	DUNDUFF Q 11 FEB 1983
-	278.060	641.130	0.010	13.44.14.270	DUNDUFF Q 15 OCT 1981
-	278.060	641.130	0.010	12.40.18.886	DUNDUFF Q 21 OCT 1981
3	294.370	641.080	0.010	12.31.47.123	CAIRNGRYFFE 26 AUG 1982
3	294.270	641.275	0.005	12.47.51.432	CAIRNGRYFFE 14 SEPT 1982 (CORR.)
3	294.650	641.250	0.050	11.35.11.664	CLCBURN 8 JULY 1983
3	294.710	641.350	0.020	12.28.49.010	CLCBURN Q 16/3/77
12	284.240	663.560	0.020	14.52.59.860	DUNTILLAND Q 16/3/77
11	288.230	663.780	0.020	12.57.51.410	TANS LOUP Q 15/2/77
15	312.720	670.280	0.010	16.45.32.570	CRAIGPARK Q 23/2/77
15	312.670	670.280	0.010	15.39.56.700	CRAIGPARK Q 30/3/77
20	335.500	657.400	0.000	00.00.08.810	MIDDLETON Q 14/2/77 (CALC. EVENT)
2	242.200	632.800	0.000	00.00.00.000	CRAIGIE Q 26 AUG 1982 (DFTECTED EVENT)
7	244.000	608.000	0.000	00.00.00.000	WATERSIDE O/CAST 15 SEPT 1982 (DETECTED EVENT)
8	273.000	611.000	0.000	00.00.00.000	KIRKCONNEL O/CAST 14 SEPT 1982 (DETECTED EVENT)
9	254.000	608.000	0.000	00.00.00.000	BENBAIN O/CAST 14 SEPT 1982 (DETECTED EVENT)
10	282.000	668.000	0.000	00.00.00.000	CAIRNHILL Q 14/3/77 (DFTECTED EVENT)
13	298.000	654.500	0.000	00.00.00.000	HATMOOD O/CAST 8/3/77 (DETECTED EVENT)
14	294.500	659.000	0.000	00.00.00.000	LYVENS SEAT O/CAST 16/2/77 (DETECTED EVENT)
15	312.800	670.500	0.000	00.00.00.000	CRAIGPARK Q 1 SEPT 1982 (DETECTED EVENT)
16	313.120	666.400	0.000	00.00.00.000	KAIMES Q 7/3/77 (DFTECTED EVENT)
17	313.500	721.800	0.000	00.00.00.000	CRUICKS Q 21/2/77 (DETECTED EVENT)
18	242.000	674.000	0.000	00.00.00.000	DUNBUCK Q 26 AUG 1982 (DETECTED EVENT)
19	272.500	676.400	0.000	00.00.00.000	CROY Q 16/2/77 (DETECTED EVENT)
21	361.500	636.200	0.000	00.00.00.000	CRAIGHOUSE Q 16/2/77 (DETECTED EVENT)
22	306.600	605.300	0.000	00.00.00.000	COATSGATE Q 16/2/77 (DETECTED EVENT)
23	183.000	749.000	0.000	00.00.00.000	MORVERN Q 14 SEPT 1982 (DETECTED EVENT)
24	390.000	541.000	0.000	00.00.00.000	WESTGATE Q 14 SEPT 1982 (DETECTED EVENT)
24	390.000	541.000	0.000	00.00.00.000	WESTGATE Q 15/2/77 (DETECTED EVENT)

Appendix 3A Travel time data (P-waves)

CORNSTONES SHOT 10 SEPT 1982

RANGE	PT DIST	ST ERR	TR TIME	ST ERR	RED TIME	ST ERR	AZIMUTH	SITE NAME
0.284	0.284	0.006	0.105	0.004	0.058	0.004	162.525	FORKINGS SITE
0.292	0.292	0.006	0.117	0.004	0.068	0.004	160.942	"
0.708	0.708	0.012	0.216	0.004	0.098	0.004	114.209	ROADSIDE SITE
1.128	1.128	0.012	0.229	0.004	0.041	0.004	96.621	STREAM SITE
1.558	1.558	0.014	0.380	0.005	0.120	0.006	87.055	1B
2.097	2.097	0.016	0.477	0.005	0.128	0.006	60.866	5A
2.121	2.121	0.016	0.545	0.005	0.191	0.006	116.625	3B
2.500	2.500	0.018	0.593	0.010	0.176	0.011	22.461	1A
2.860	2.860	0.024	0.642	0.005	0.165	0.007	37.471	4A
2.936	2.936	0.024	0.671	0.005	0.182	0.007	81.773	5B
3.530	3.530	0.021	0.788	0.005	0.200	0.006	80.378	6B
4.106	4.106	0.023	0.894	0.005	0.210	0.007	350.607	2A
4.472	4.472	0.024	0.991	0.005	0.246	0.007	77.471	7B
6.659	6.659	0.029	1.380	0.010	0.270	0.011	61.568	6A

MID CROFT SHOT 9 SEPT 1982

RANGE	PT DIST	ST ERR	TR TIME	ST ERR	RED TME	ST ERR	AZIMUTH	SITE NAME
1.266	1.266	0.008	0.357	0.006	0.146	0.006	201.801	8A
3.689	3.689	0.014	0.881	0.006	0.233	0.006	164.642	2A
6.513	6.513	0.029	1.396	0.006	0.310	0.008	148.116	4A
7.644	7.644	0.020	1.580	0.006	0.306	0.007	152.496	5A
8.379	8.379	0.020	1.765	0.004	0.369	0.005	157.138	1B
8.865	8.865	0.021	1.833	0.006	0.356	0.007	121.502	6A
8.699	8.699	0.033	1.716	0.006	0.266	0.008	148.037	5B
8.878	8.878	0.021	1.804	0.010	0.324	0.011	144.305	6B
9.135	9.135	0.021	1.872	0.010	0.350	0.011	138.395	7B

GREIVEHILL SHOT 14 SEPT 1982

RANGE	PT DIST	ST ERR	TR TIME	ST ERR	RED TME	ST ERR	AZIMUTH	SITE NAME
18.340	18.340	0.022	3.611	0.006	0.554	0.007	28.369	6A
15.698	15.698	0.020	3.174	0.006	0.558	0.007	27.399	7B
14.966	14.966	0.020	3.029	0.006	0.535	0.007	25.060	6B
14.575	14.575	0.038	2.961	0.006	0.532	0.009	23.295	5B
15.916	15.916	0.020	3.213	0.006	0.560	0.007	16.795	4A
14.752	14.752	0.020	2.990	0.006	0.531	0.007	18.533	5A
13.696	13.696	0.019	2.786	0.006	0.503	0.007	21.791	4B
13.773	13.773	0.019	2.825	0.006	0.529	0.007	18.691	1B
15.746	15.746	0.020	3.223	0.010	0.599	0.011	14.018	1A
12.923	12.923	0.018	2.660	0.015	0.506	0.016	21.584	3B
19.604	19.604	0.023	3.854	0.006	0.587	0.007	2.014	8A

HILLHOUSE Q 20 JUNE 1984 (C)

RANGE	PT	DIST	ST	ERR	TR	TIME	ST	ERR	RED	TME	ST	ERR	AZIMUTH	SITE NAME
2.864	2.864	0.035	0.742	0.011	0.265	0.012	90.700	CROOKS FM						
4.925	4.925	0.046	1.379	0.011	0.558	0.013	89.825	FORTACRES FM						

HILLHOUSE Q 2 AUGUST 1984

RANGE	PT	DIST	ST	ERR	TR	TIME	ST	ERR	RED	TME	ST	ERR	AZIMUTH	SITE NAME
11.823	11.823	0.071	2.710	0.004	0.740	0.013	93.613	AIRD FM						
11.978	11.978	0.070	2.851	0.006	0.855	0.013	104.573	TANNOCHILL FM						
12.126	12.126	0.056	2.846	0.004	0.825	0.010	138.055	BURN FM						
68.090	68.090	0.170	12.014	0.004	0.666	0.029	86.956	LANGLEES Q						
73.277	73.277	0.176	12.691	0.004	0.478	0.030	87.462	KIRKLAHILL FM						

HILLHOUSE Q 17 DEC 1982

RANGE	PT	DIST	ST	ERR	TR	TIME	ST	ERR	RED	TME	ST	ERR	AZIMUTH	SITE NAME
4.925	4.925	0.025	1.379	0.006	0.558	0.007	89.593	FORTACRES FM						
6.131	6.131	0.028	1.642	0.011	0.620	0.012	96.650	STAFFLER RES						
7.508	7.508	0.031	1.953	0.007	0.702	0.009	92.672	DONKEY SITE						
8.824	8.824	0.033	2.217	0.011	0.746	0.012	92.735	HILLHOUSE FM						

HILLHOUSE Q 22 MARCH 1983

RANGE	PT	DIST	ST	ERR	TR	TIME	ST	ERR	RED	TME	ST	ERR	AZIMUTH	SITE NAME
10.125	10.125	0.097	2.390	0.011	0.702	0.020	92.038	GATEHEAD FM						
10.746	10.746	0.100	2.517	0.011	0.726	0.020	91.941	DALLARS FM						
11.811	11.811	0.105	2.717	0.011	0.749	0.021	93.412	AIRD FM						
12.962	12.962	0.109	2.913	0.011	0.753	0.021	90.424	OVERLANDS FM						
13.848	13.848	0.113	3.074	0.011	0.766	0.022	88.485	DRUMDROCH FM						

HILLHOUSE Q 10 MARCH 1983

RANGE	PT DIST	ST ERR	TR TIME	ST ERR	RED TME	ST ERR	AZIMUTH	SITE NAME
12.962	12.962	0.109	2.913	0.010	0.753	0.021	90.424	OVERLANDS FM
14.932	14.932	0.118	3.215	0.011	0.726	0.023	89.447	MILRIG FM
16.001	16.001	0.122	3.454	0.011	0.787	0.023	89.141	SORNHILL FM
21.004	21.004	0.139	4.348	0.010	0.847	0.025	86.342	HARDHILL SITE
25.477	25.477	0.154	5.010	0.010	0.764	0.028	84.063	ALLANTON Q SITE

HILLHOUSE Q 1 SEPT 1982

RANGE	PT DIST	ST ERR	TR TIME	ST ERR	RED TME	ST ERR	AZIMUTH	SITE NAME
17.001	17.001	0.046	3.756	0.006	0.923	0.010	88.628	CAIRNHILL FM
21.004	21.004	0.051	4.348	0.006	0.847	0.010	86.337	HARDHILL A SITE
21.026	21.026	0.051	4.353	0.006	0.849	0.010	86.286	HARDHILL B SITE
30.658	30.658	0.062	5.838	0.006	0.728	0.012	85.084	HALLS BURN (8A)
32.046	32.046	0.063	6.081	0.006	0.740	0.012	89.907	2A
32.934	32.934	0.064	6.237	0.010	0.748	0.015	93.408	3A
33.714	33.714	0.065	6.402	0.010	0.783	0.015	92.870	1A
34.499	34.499	0.083	6.489	0.006	0.739	0.015	92.871	4A
34.674	34.674	0.066	6.518	0.006	0.739	0.012	94.927	5A
38.581	38.581	0.069	7.147	0.006	0.717	0.013	91.230	6A

HILLHOUSE Q 16 JUNE 1983

RANGE	PT DIST	ST ERR	TR TIME	ST ERR	RED TME	ST ERR	AZIMUTH	SITE NAME
21.014	21.014	0.051	4.355	0.007	0.853	0.011	86.286	1C
23.123	23.123	0.054	4.656	0.007	0.802	0.012	86.099	2C
41.358	41.358	0.072	7.488	0.005	0.595	0.013	84.079	1D
44.018	44.018	0.074	8.051	0.005	0.715	0.013	86.194	2D
50.329	50.329	0.079	9.061	0.030	0.673	0.033	81.157	3D
56.885	56.885	0.084	10.129	0.007	0.648	0.016	85.160	1E
69.338	69.338	0.093	12.094	0.040	0.538	0.043	89.165	6E

HILLHOUSE Q 2 JUNE 1983

RANGE	PT DIST	ST ERR	TR TIME	ST ERR	RED TME	ST ERR	AZIMUTH	SITE NAME
23.129	23.129	0.099	4.630	0.011	0.775	0.020	86.075	2C
56.891	56.891	0.155	10.119	0.012	0.637	0.029	85.150	1E
58.858	58.858	0.158	10.421	0.012	0.611	0.029	86.000	2E
65.522	65.522	0.167	11.575	0.012	0.655	0.030	86.782	4E

HILLHOUSE Q 25/3/77

RANGE	PT DIST	ST ERR	TR TIME	ST ERR	RED TME	ST ERR	AZIMUTH	SITE NAME
74.812	74.812	0.435	12.859	0.014	0.390	0.074	91.379	S4 BTN
76.143	76.143	0.438	13.053	0.014	0.362	0.074	90.489	S3 BTN
76.704	76.704	0.440	13.247	0.014	0.463	0.075	87.175	N2 BTN
76.940	76.940	0.441	13.189	0.014	0.366	0.075	89.926	S2 BTN
77.275	77.275	0.442	13.305	0.014	0.426	0.075	88.050	N3 BTN
77.722	77.722	0.443	13.305	0.014	0.351	0.075	89.012	S1 BTN
79.132	79.132	0.447	13.480	0.014	0.291	0.076	89.660	N4 BTN

DUNDUFF 8 JULY 1983

RANGE	PT DIST	ST ERR	TR TIME	ST ERR	RED TME	ST ERR	AZIMUTH	SITE NAME
-22.321	20.824	0.101	4.105	0.008	0.385	0.018	255.420	HARDHILL (1C)
-20.237	22.908	0.097	3.699	0.008	0.326	0.018	254.503	2C
-17.801	25.344	0.090	3.290	0.008	0.323	0.017	255.666	ALLANTON (3C)
-3.070	40.075	0.050	0.648	0.006	0.136	0.010	207.834	1D
4.277	47.422	0.061	0.889	0.006	0.176	0.012	161.586	2D
7.200	50.345	0.056	1.518	0.006	0.318	0.011	83.965	3D
14.279	57.424	0.079	2.755	0.008	0.375	0.015	98.782	1E
16.395	59.540	0.085	3.152	0.008	0.420	0.016	100.132	2E
21.270	64.415	0.096	4.097	0.010	0.552	0.019	96.354	3E
23.082	66.227	0.100	4.434	0.008	0.587	0.018	98.250	4E
27.418	70.563	0.111	5.104	0.008	0.534	0.020	102.576	6E

DUNDUFF Q 2 JUNE 1983 (C)

RANGE	PT DIST	ST ERR	TR TIME	ST ERR	RED TME	ST ERR	AZIMUTH	SITE NAME
14.279	57.424	0.079	2.761	0.008	0.381	0.015	98.782	1E
16.395	59.540	0.085	3.169	0.008	0.437	0.016	100.132	2E
21.270	64.415	0.096	4.099	0.010	0.554	0.019	96.354	3E
23.082	66.227	0.100	4.400	0.008	0.553	0.018	98.250	4E

DUNDUFF Q 8 JUNE 1983 (C)

RANGE	PT DIST	ST ERR	TR TIME	ST ERR	RED TME	ST ERR	AZIMUTH	SITE NAME
-20.237	22.908	0.097	3.679	0.008	0.306	0.018	254.503	2C
-17.783	25.362	0.090	3.290	0.010	0.326	0.018	255.897	3C
-7.310	35.835	0.056	1.481	0.006	0.263	0.011	262.532	6C

14.279	57.424	0.079	2.772	0.008	0.392	0.015	98.782	1E
16.395	59.540	0.085	3.169	0.008	0.437	0.016	100.132	2E

DUNDIFF JANUARY/FEBRUARY 1983

RANGE	PT DIST	ST ERR	TR TIME	ST ERR	RED TME	ST ERR	AZIMUTH	SITE NAME
-0.173	42.972	0.009	0.040	0.004	0.011	0.004	236.768	DUND Q CORNER
-1.508	41.637	0.025	0.329	0.004	0.078	0.006	244.880	STARBIRNS FM
-5.437	37.708	0.126	1.060	0.006	0.154	0.022	245.321	ARA BURN
-17.671	25.474	0.087	3.286	0.006	0.341	0.016	255.850	ALLANTON Q

DUNDIFF OCTOBER/NOVEMBER 1981

RANGE	PT DIST	ST ERR	TR TIME	ST ERR	RED TME	ST ERR	AZIMUTH	SITE NAME
-0.200	42.954	0.005	0.038	0.007	0.005	0.007	270.000	MUIRHOUSE FM (E)
0.994	44.148	0.011	0.234	0.007	0.068	0.007	99.273	MUIRSLAND FM 1
1.275	44.429	0.013	0.300	0.007	0.087	0.007	94.950	MUIRSLAND FM 1A
1.462	44.616	0.014	0.329	0.007	0.085	0.007	97.076	MUIRSLAND FM 2
1.700	44.854	0.015	0.395	0.007	0.112	0.007	96.080	MUIRSLAND FM 3
4.314	47.468	0.023	0.952	0.007	0.233	0.008	92.524	BOGSIDE FM 1
4.473	47.627	0.024	0.977	0.007	0.231	0.008	92.050	BOGSIDE FM 2
4.623	47.777	0.024	1.003	0.007	0.233	0.008	91.983	BOGSIDE FM 3
6.561	49.715	0.029	1.398	0.007	0.305	0.009	89.389	DARNFILLAN FM 1
6.620	49.774	0.029	1.419	0.007	0.316	0.009	89.913	DARNFILLAN FM 2
6.692	49.846	0.029	1.431	0.007	0.316	0.009	91.199	DARNFILLAN FM 3
7.540	50.694	0.031	1.591	0.007	0.334	0.009	90.076	GREENHILL FM 1
7.721	50.875	0.031	1.610	0.007	0.323	0.009	90.816	GREENHILL FM 2
7.932	51.086	0.031	1.663	0.007	0.341	0.009	91.373	GREENHILL FM 3
8.932	52.086	0.033	1.878	0.007	0.389	0.009	91.026	LANGSIDE FM 1
9.152	52.306	0.034	1.923	0.007	0.398	0.009	91.252	LANGSIDE FM 2
9.332	52.486	0.034	1.967	0.007	0.412	0.009	91.044	LANGSIDE FM 3

CAIRNGRYFFE 26 AUG 1982

RANGE	PT DIST	ST ERR	TR TIME	ST ERR	RED TME	ST ERR	AZIMUTH	SITE NAME
-4.901	54.999	0.031	1.161	0.005	0.344	0.007	246.417	SANDILANDS FM
-7.087	52.813	0.030	1.547	0.005	0.366	0.007	269.070	LANGSIDE FM A
-7.167	52.733	0.030	1.574	0.005	0.380	0.007	269.120	LANGSIDE FM B
-14.710	45.190	0.043	3.018	0.004	0.566	0.008	270.078	MUIRSLAND FM A
-14.790	45.110	0.043	3.030	0.004	0.565	0.008	270.155	MUIRSLAND FM B
-16.639	43.261	0.046	3.380	0.005	0.607	0.009	268.175	DUNDIFF Q SITE
-22.087	37.813	0.053	4.265	0.005	0.584	0.010	249.042	6A
-26.258	33.642	0.072	4.964	0.005	0.588	0.013	250.420	4A
-26.620	33.280	0.058	4.993	0.005	0.556	0.011	247.819	5A
-26.986	32.914	0.058	5.110	0.005	0.612	0.011	251.058	1A
-27.826	32.074	0.059	5.207	0.005	0.569	0.011	251.064	3A
-28.043	31.857	0.059	5.275	0.005	0.601	0.011	255.503	2A

-28.993 30.907 0.060 5.430 0.005 0.598 0.011 261.181 8A

CAIRNGRYFFE 14 SEPT 1982 (CORR.)

RANGE	PT DIST	ST ERR	TR TIME	ST ERR	RED TME	ST ERR	AZIMUTH	SITE NAME
-22.064	37.836	0.033	4.257	0.007	0.580	0.009	248.476	6A
-24.303	35.597	0.035	4.636	0.007	0.585	0.009	244.938	7B
-25.266	34.634	0.036	4.772	0.007	0.561	0.009	245.007	6B
-25.859	34.041	0.057	4.898	0.007	0.588	0.012	245.204	5B
-26.231	33.669	0.036	4.966	0.007	0.594	0.009	249.945	4A
-26.602	33.298	0.036	4.990	0.007	0.556	0.009	247.349	5A
-26.759	33.141	0.037	5.024	0.007	0.564	0.009	244.512	4B
-27.228	32.672	0.037	5.112	0.007	0.574	0.009	245.746	1B
-26.956	32.944	0.037	5.131	0.011	0.638	0.013	250.597	1A
-27.363	32.537	0.037	5.141	0.007	0.581	0.009	243.486	3B
-27.996	31.904	0.037	5.292	0.007	0.626	0.009	255.065	2A
-28.925	30.975	0.038	5.345	0.007	0.524	0.009	260.769	8A

CLOBURN 8 JULY 1983

RANGE	PT DIST	ST ERR	TR TIME	ST ERR	RED TME	ST ERR	AZIMUTH	SITE NAME
-38.947	20.953	0.314	7.010	0.012	0.519	0.054	261.333	1C
-36.838	23.062	0.305	6.574	0.008	0.434	0.051	261.166	2C
-34.453	25.447	0.295	6.237	0.006	0.495	0.050	262.356	3C
-18.571	41.329	0.217	3.586	0.006	0.491	0.037	260.816	1D
-16.135	43.765	0.202	3.144	0.006	0.455	0.034	254.514	2D
-9.753	50.147	0.157	2.028	0.006	0.402	0.027	272.980	3D
-3.699	56.201	0.097	0.728	0.008	0.111	0.018	228.925	1E
-3.225	56.675	0.090	0.665	0.008	0.127	0.017	193.648	2E
4.975	64.875	0.112	1.094	0.010	0.265	0.021	121.562	3E
6.929	66.829	0.132	1.500	0.008	0.345	0.023	120.937	4E
11.658	71.558	0.172	2.364	0.008	0.421	0.030	122.245	6E

CLOBURN Q 16/3/77

RANGE	PT DIST	ST ERR	TR TIME	ST ERR	RED TME	ST ERR	AZIMUTH	SITE NAME
15.698	75.598	0.082	3.207	0.011	0.591	0.018	98.130	N1 BTN
17.639	77.539	0.087	3.490	0.011	0.550	0.018	121.248	S4 BTN
18.145	78.045	0.088	3.613	0.011	0.589	0.018	105.078	N3 BTN
18.274	78.174	0.088	3.613	0.011	0.567	0.018	115.962	S3 BTN
18.693	78.593	0.089	3.660	0.011	0.544	0.019	112.820	S2 BTN
18.977	78.877	0.090	3.716	0.011	0.553	0.019	108.464	S1 BTN
20.603	80.503	0.094	4.009	0.011	0.575	0.019	109.508	N4 BTN

DUNTILLAND Q 16/3/77

RANGE	PT DIST	ST ERR	TR TIME	ST ERR	RED TME	ST ERR	AZIMUTH	SITE NAME
40.437	40.437	0.193	7.756	0.014	1.016	0.035	136.764	S2 BTN
40.451	40.451	0.193	7.756	0.014	1.014	0.035	138.317	S3 BTN
40.451	40.451	0.193	7.780	0.014	1.038	0.035	140.829	S4 BTN
35.684	35.684	0.182	7.057	0.014	1.110	0.033	133.206	N1 BTN
38.842	38.842	0.190	7.559	0.014	1.085	0.035	133.894	N2 BTN
41.709	41.709	0.196	7.977	0.014	1.026	0.036	134.223	N4 BTN

TAMS LOUP Q 15/2/77

RANGE	PT DIST	ST ERR	TR TIME	ST ERR	RED TME	ST ERR	AZIMUTH	SITE NAME
37.525	37.525	0.186	7.119	0.014	0.865	0.034	139.279	S1 BTN
37.988	37.988	0.187	7.198	0.014	0.867	0.034	141.380	S2 BTN
38.090	38.090	0.188	7.217	0.014	0.869	0.034	143.025	S3 BTN
38.414	38.414	0.189	7.207	0.014	0.805	0.034	147.729	S4 BTN
33.053	33.053	0.175	6.472	0.014	0.963	0.032	138.225	N1 BTN
36.237	36.237	0.183	6.806	0.014	0.766	0.034	138.524	N2 BTN
39.114	39.114	0.190	7.394	0.014	0.875	0.035	138.534	N4 BTN

CRAIGPARK Q 30/3/77

RANGE	PT DIST	ST ERR	TR TIME	ST ERR	RED TME	ST ERR	AZIMUTH	SITE NAME
34.940	34.940	0.122	6.454	0.041	0.631	0.046	179.934	S1 BTN
36.188	36.188	0.124	6.704	0.014	0.673	0.025	181.156	S2 BTN
36.962	36.962	0.125	6.819	0.014	0.659	0.025	182.372	S3 BTN
38.189	38.189	0.127	7.031	0.014	0.666	0.026	184.325	S4 BTN
39.178	39.178	0.129	7.223	0.014	0.693	0.026	185.757	S5 BTN
33.654	33.654	0.120	6.377	0.014	0.768	0.024	180.749	N2 BTN
35.840	35.840	0.123	6.685	0.014	0.712	0.025	177.665	N4 BTN

CRAIGPARK Q 23/2/77

RANGE	PT DIST	ST ERR	TR TIME	ST ERR	RED TME	ST ERR	AZIMUTH	SITE NAME
34.940	34.940	0.122	6.548	0.014	0.725	0.025	180.016	S1 BTN
36.189	36.189	0.124	6.724	0.014	0.693	0.025	181.235	S2 BTN
36.964	36.964	0.125	6.842	0.014	0.681	0.025	182.450	S3 BTN
38.193	38.193	0.127	7.038	0.014	0.673	0.026	184.400	S4 BTN
31.248	31.248	0.115	5.959	0.014	0.751	0.024	184.534	N1 BTN
33.654	33.654	0.120	6.195	0.014	0.586	0.024	180.834	N2 BTN
35.838	35.838	0.123	6.685	0.014	0.712	0.025	177.745	N4 BTN

Appendix 3B Travel time data (S-waves)

HILLHOUSE Q 25/3/77

RANGE	PT DIST	ST ERR	TR TIME	ST ERR	RED TME	ST ERR	AZIMUTH	SITE NAME
74.812	74.812	0.435	22.509	0.014	10.040	0.074	91.379	S4 BTN
76.143	76.143	0.438	22.781	0.014	10.090	0.074	90.489	S3 BTN
76.704	76.704	0.440	23.266	0.014	10.482	0.075	87.175	N2 BTN
76.940	76.940	0.441	22.994	0.014	10.171	0.075	89.926	S2 BTN
77.275	77.275	0.442	23.286	0.014	10.407	0.075	88.050	N3 BTN
77.722	77.722	0.443	23.189	0.014	10.235	0.075	89.012	S1 BTN
79.132	79.132	0.447	23.441	0.014	10.252	0.076	89.660	N4 BTN

DUNDUFF OCTOBER/NOVEMBER 1981

RANGE	PT DIST	ST ERR	TR TIME	ST ERR	RED TME	ST ERR	AZIMUTH	SITE NAME
1.275	44.420	0.013	0.618	0.011	0.405	0.011	94.950	MUIRSLAND FM 1A
1.462	44.607	0.014	0.664	0.011	0.420	0.011	97.076	MUIRSLAND FM 2
6.561	49.706	0.029	2.636	0.011	1.543	0.012	89.389	DARNFILLAN FM 1
6.620	49.765	0.029	2.645	0.011	1.542	0.012	89.913	DARNFILLAN FM 2
6.692	49.837	0.029	2.649	0.011	1.534	0.012	91.199	DARNFILLAN FM 3
7.540	50.685	0.031	2.911	0.011	1.654	0.012	90.076	GREENHILL FM 1
7.721	50.866	0.031	2.939	0.011	1.652	0.012	90.816	GREENHILL FM 2
8.932	52.077	0.033	3.378	0.011	1.889	0.012	91.026	LANGSIDE FM 1
9.152	52.297	0.034	3.434	0.011	1.909	0.013	91.252	LANGSIDE FM 2
9.332	52.477	0.034	3.502	0.011	1.947	0.013	91.044	LANGSIDE FM 3

DUNDUFF Q 8 JUNE 1983

RANGE	PT DIST	ST ERR	TR TIME	ST ERR	RED TME	ST ERR	AZIMUTH	SITE NAME
14.279	57.424	0.079	4.969	0.008	2.569	0.015	98.782	1E
16.395	59.540	0.085	5.634	0.008	2.902	0.016	100.132	2E

DUNDIFF 8 JULY 1983

RANGE	PT DIST	ST ERR	TR TIME	ST ERR	RED TME	ST ERR	AZIMUTH	SITE NAME
-20.237	22.908	0.097	6.880	0.020	3.507	0.026	254.503	2C
-17.783	25.362	0.090	6.239	0.020	3.275	0.025	255.897	3C
4.277	47.422	0.061	2.835	0.010	2.122	0.015	161.586	2D
14.279	57.424	0.079	4.989	0.010	2.609	0.017	98.782	1E
16.395	59.540	0.085	5.592	0.010	2.860	0.018	100.132	2E
27.418	70.563	0.111	8.990	0.010	4.420	0.021	102.576	6E

CLOBURN Q 16/3/77

RANGE	PT DIST	ST ERR	TR TIME	ST ERR	RED TME	ST ERR	AZIMUTH	SITE NAME
15.698	75.598	0.082	5.878	0.011	3.262	0.018	98.130	N1 BTN
17.639	77.539	0.087	6.326	0.011	3.386	0.018	121.248	S4 BTN
18.274	78.174	0.088	6.541	0.011	3.495	0.018	115.962	S3 BTN
18.693	78.593	0.089	6.644	0.011	3.528	0.019	112.820	S2 BTN
18.977	78.877	0.090	6.738	0.011	3.575	0.019	108.464	S1 BTN
20.603	80.503	0.094	7.149	0.011	3.715	0.019	109.508	N4 BTN

DUNTILLAND Q 16/3/77

RANGE	PT DIST	ST ERR	TR TIME	ST ERR	RED TME	ST ERR	AZIMUTH	SITE NAME
40.437	40.437	0.193	13.660	0.014	6.920	0.035	136.764	S2 BTN
40.451	40.451	0.193	13.680	0.014	6.938	0.035	138.317	S3 BTN
40.451	40.451	0.193	13.710	0.014	6.968	0.035	140.829	S4 BTN
35.684	35.684	0.182	12.446	0.014	6.499	0.033	133.206	N1 BTN
38.842	38.842	0.190	13.330	0.014	6.856	0.035	133.894	N2 BTN
41.709	41.709	0.196	13.860	0.014	6.908	0.036	134.223	N4 BTN

TAMS LOUP Q 15/2/77

RANGE	PT DIST	ST ERR	TR TIME	ST ERR	RED TME	ST ERR	AZIMUTH	SITE NAME
37.525	37.525	0.186	12.668	0.014	6.414	0.034	139.279	S1 BTN
37.988	37.988	0.187	12.747	0.014	6.416	0.034	141.380	S2 BTN
38.090	38.090	0.188	12.786	0.014	6.438	0.034	143.025	S3 BTN
38.414	38.414	0.189	12.865	0.014	6.463	0.034	147.729	S4 BTN
33.053	33.053	0.175	11.512	0.014	6.003	0.032	138.225	N1 BTN
36.237	36.237	0.183	12.061	0.014	6.021	0.034	138.524	N2 BTN
39.114	39.114	0.190	13.041	0.014	6.522	0.035	138.534	N4 BTN

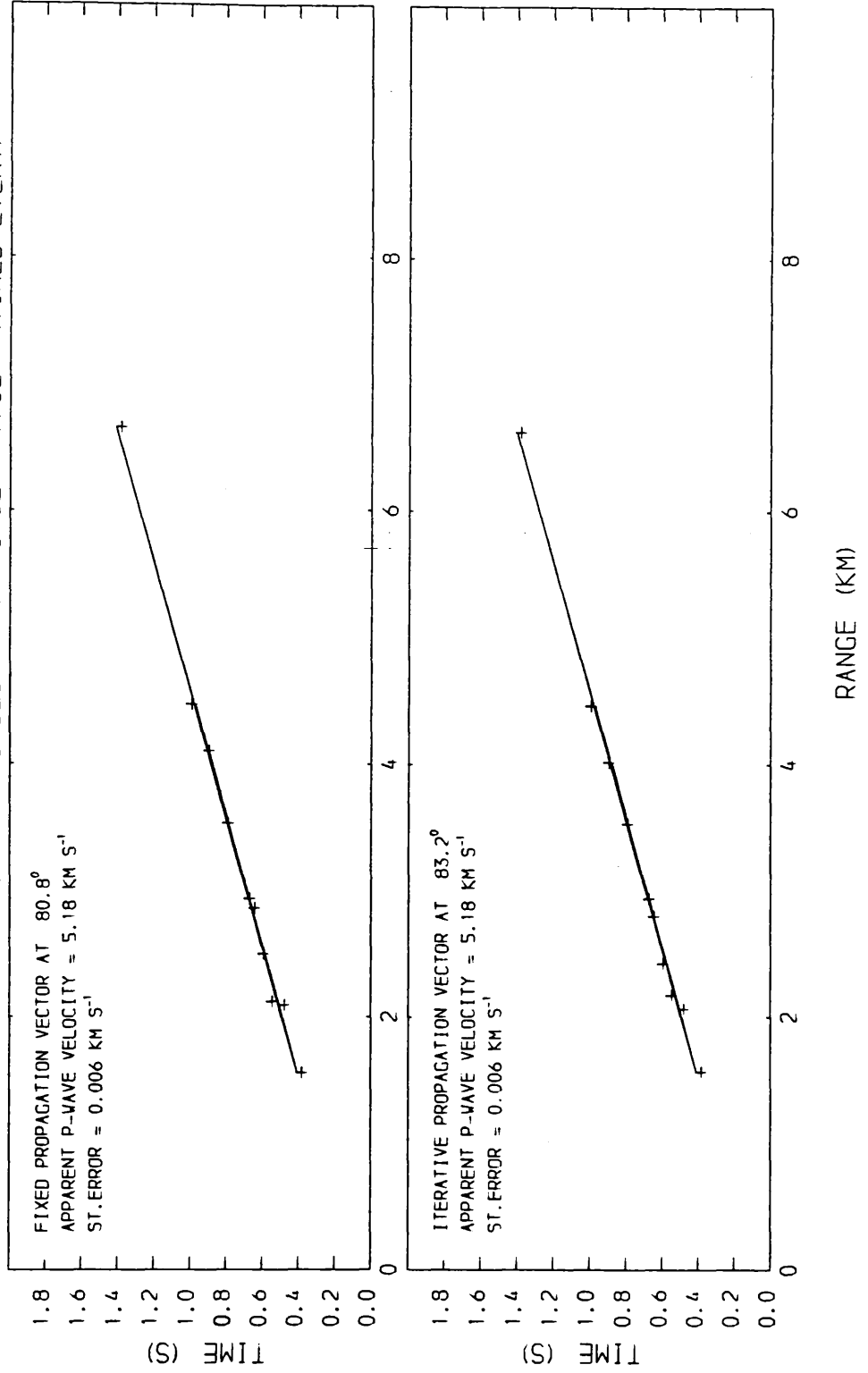
CRAIGPARK Q 30/3/77

RANGE	PT	DIST	ST ERR	TR TIME	ST ERR	RED TME	ST ERR	AZIMUTH	SITE NAME
34.940	34.940		0.122	11.398	0.014	5.575	0.025	179.934	S1 BTN
36.187	36.187		0.124	11.614	0.014	5.583	0.025	181.156	S2 BTN
36.962	36.962		0.125	11.790	0.018	5.630	0.028	182.372	S3 BTN
38.189	38.189		0.127	12.124	0.014	5.759	0.026	184.325	S4 BTN
39.178	39.178		0.129	12.516	0.014	5.986	0.026	185.757	S5 BTN
33.653	33.653		0.120	11.045	0.041	5.436	0.046	180.749	N2 BTN
35.840	35.840		0.123	11.555	0.041	5.582	0.046	177.665	N4 BTN

CRAIGPARK Q 23/2/77

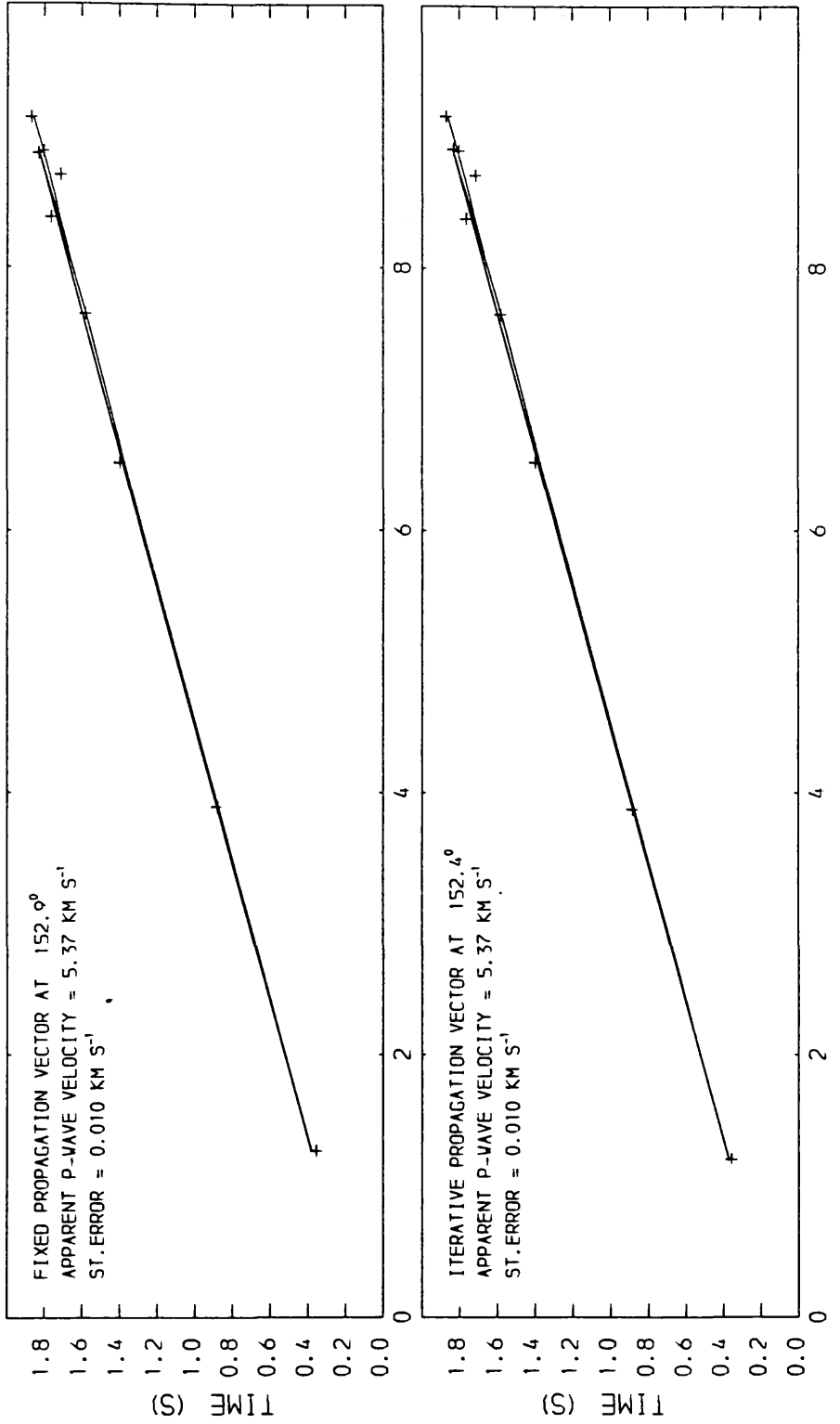
RANGE	PT	DIST	ST ERR	TR TIME	ST ERR	RED TME	ST ERR	AZIMUTH	SITE NAME
34.940	34.940		0.122	11.450	0.022	5.627	0.030	180.016	S1 BTN
36.189	36.189		0.124	11.724	0.022	5.693	0.030	181.235	S2 BTN
36.964	36.964		0.125	11.920	0.022	5.759	0.031	182.450	S3 BTN
38.193	38.193		0.127	12.293	0.022	5.928	0.031	184.400	S4 BTN
31.248	31.248		0.115	10.508	0.022	5.300	0.029	184.534	N1 BTN
33.654	33.654		0.120	10.901	0.022	5.292	0.030	180.834	N2 BTN
35.838	35.838		0.123	11.606	0.022	5.633	0.030	177.745	N4 BTN

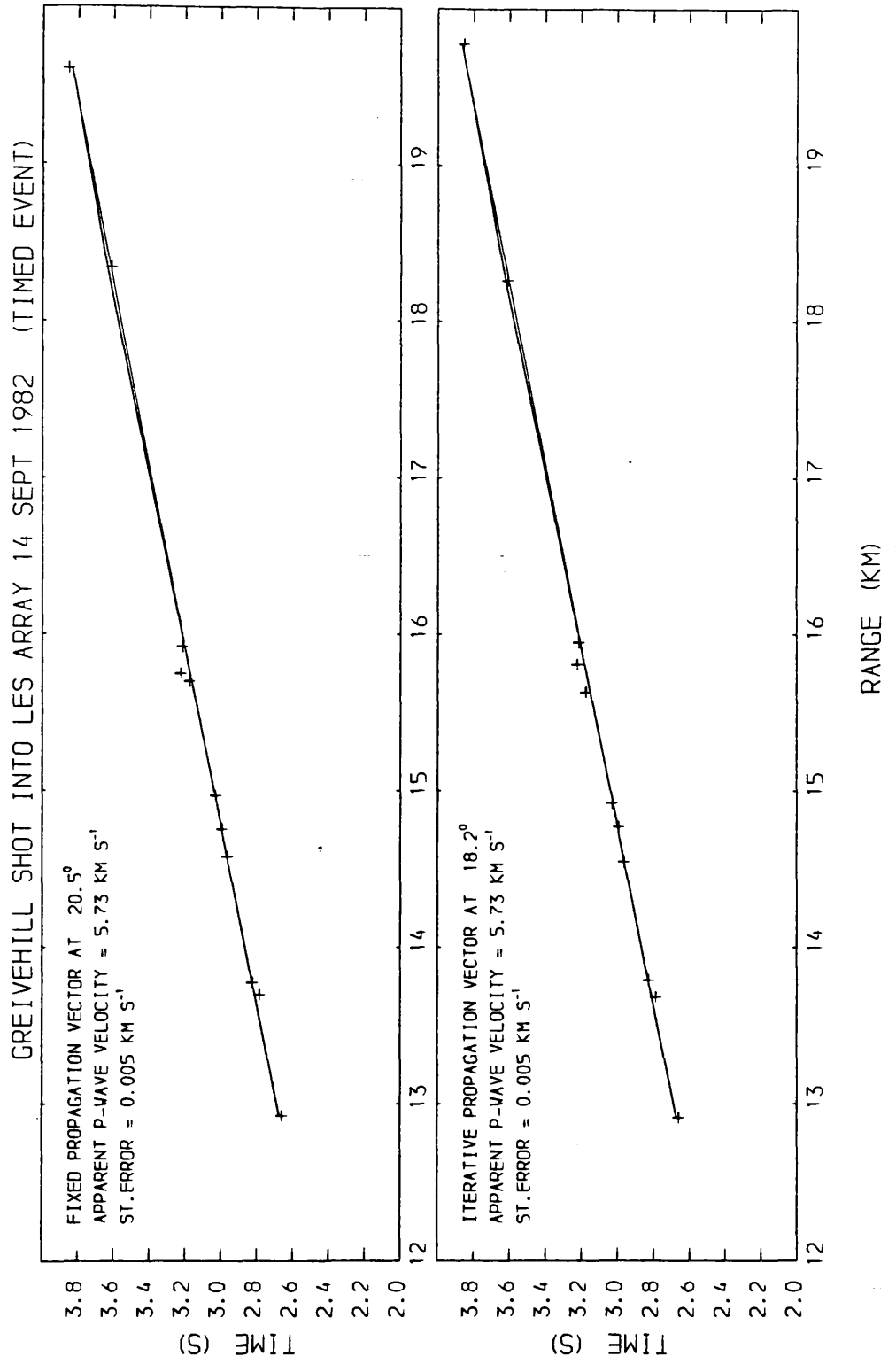
CORNSTONES SHOT INTO LES ARRAY 10 SEPT 1982 (TIMED EVENT)



Appendix 4.1

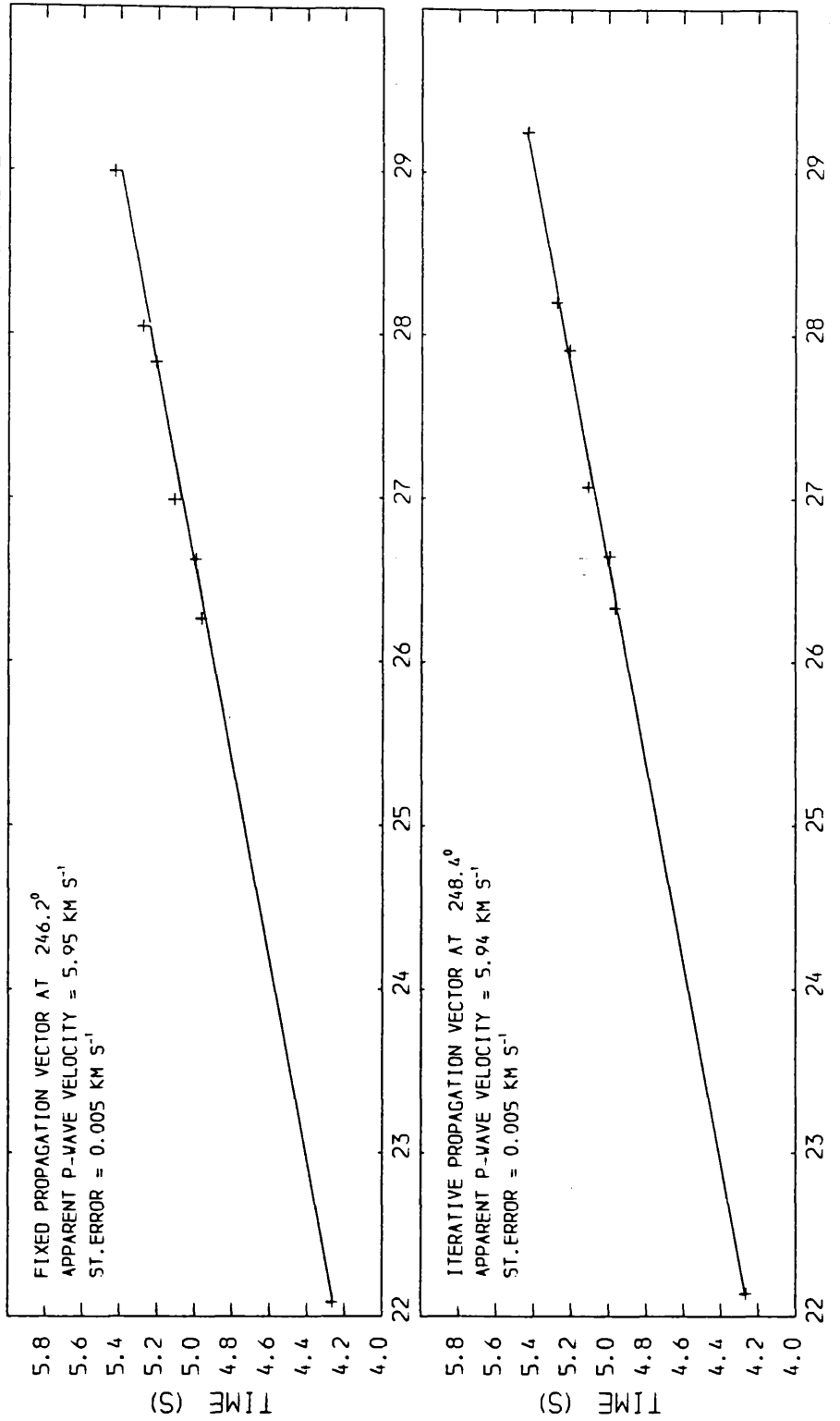
MIDDLECROFT SHOT INTO LES ARRAY 9 SEPT 1982 (TIMED EVENT)



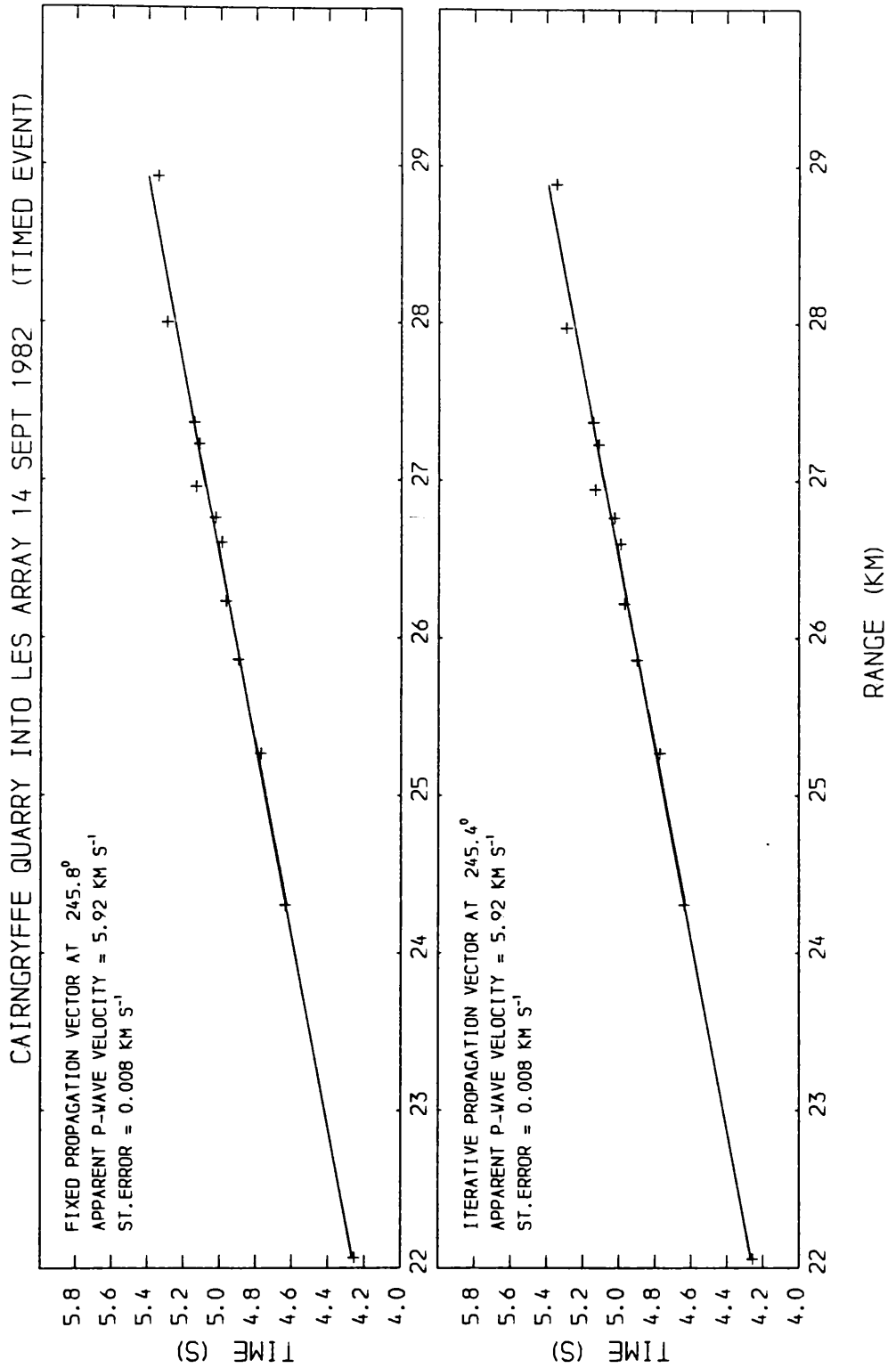


Appendix 4.3

CAIRNGRYFFE QUARRY INTO LES ARRAY 26 AUG 1982 (TIMED EVENT)

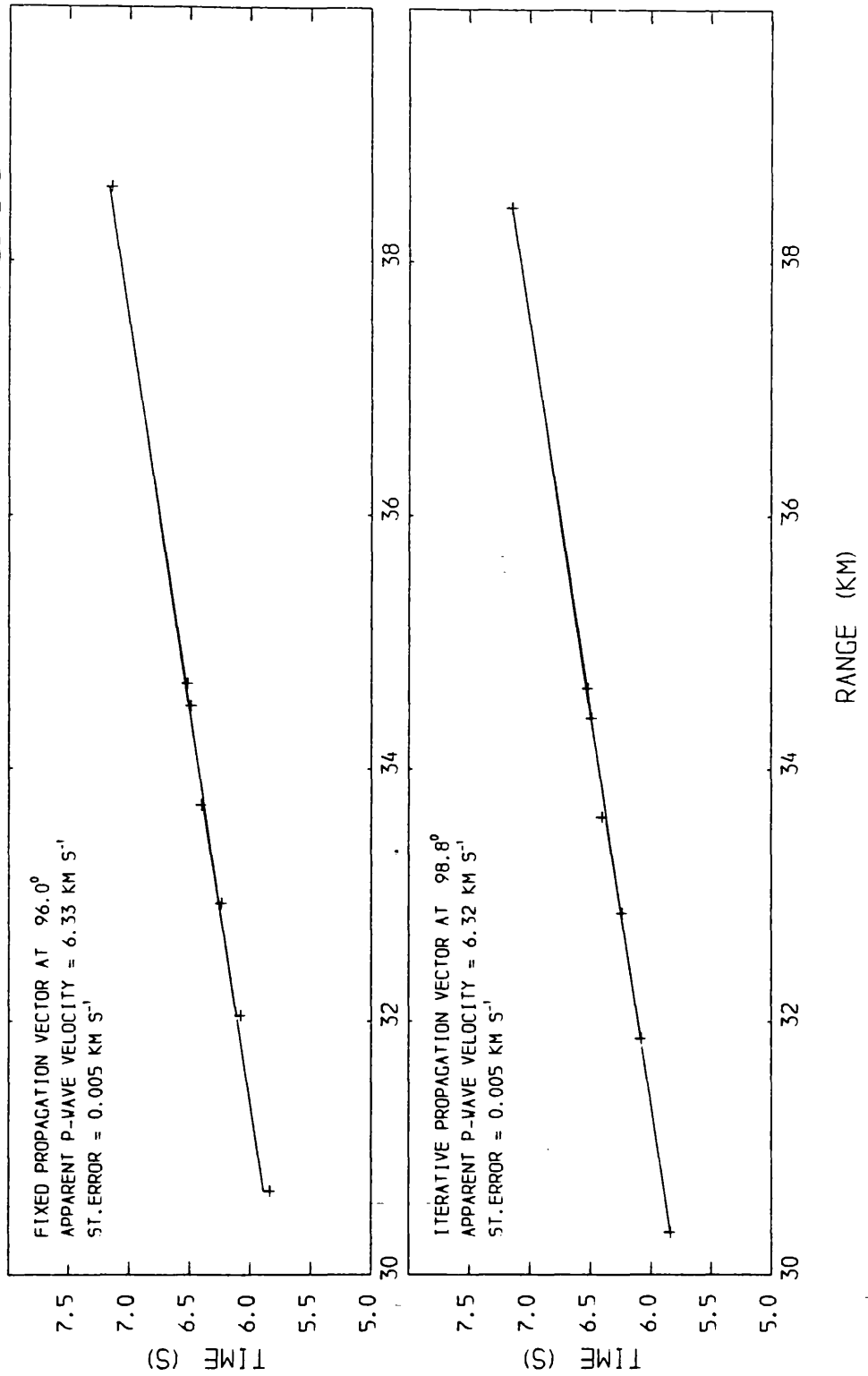


Appendix 4.4

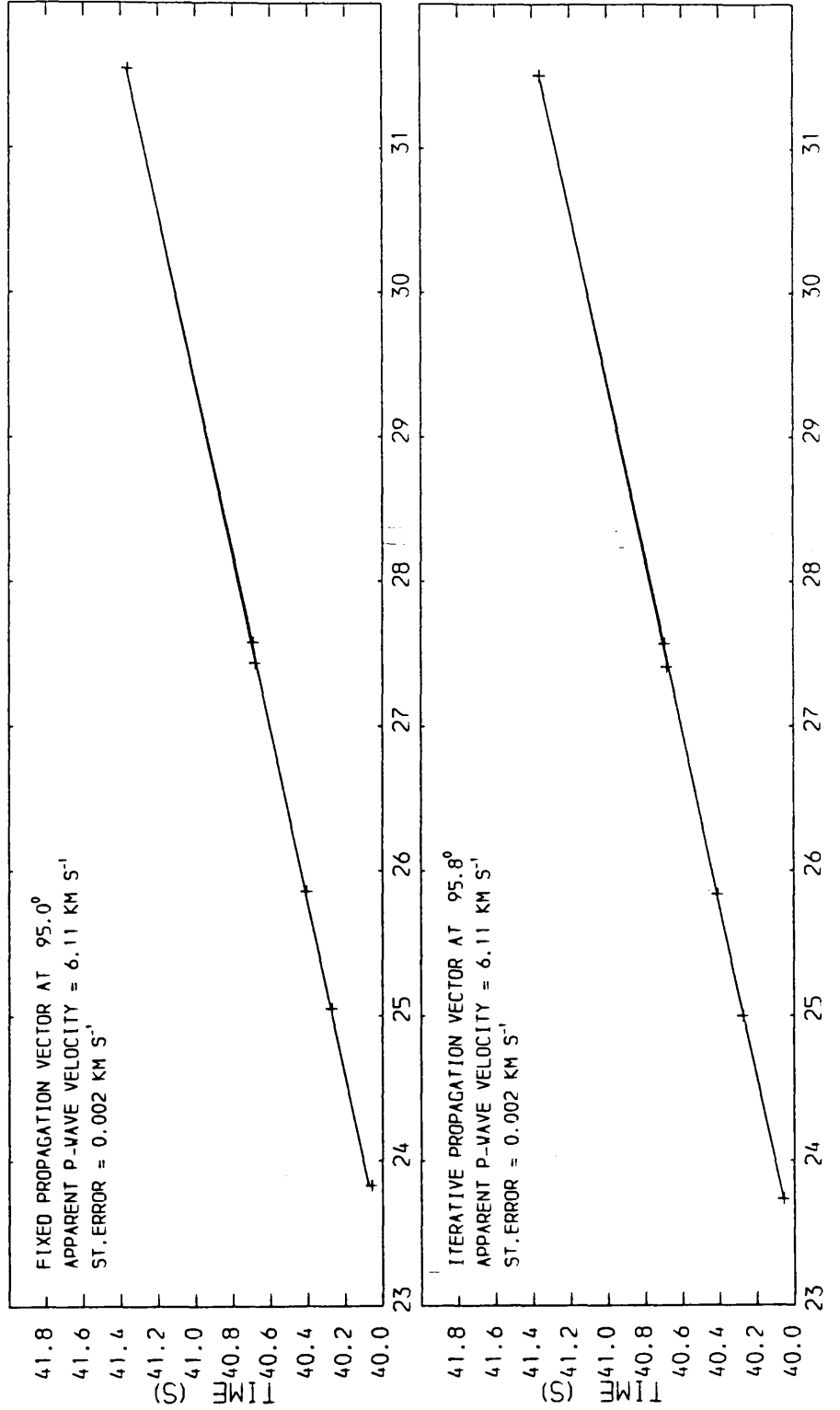


Appendix 4.5

HILLHOUSE QUARRY INTO LES ARRAY 1 SEPT 1982 (TIMED EVENT)

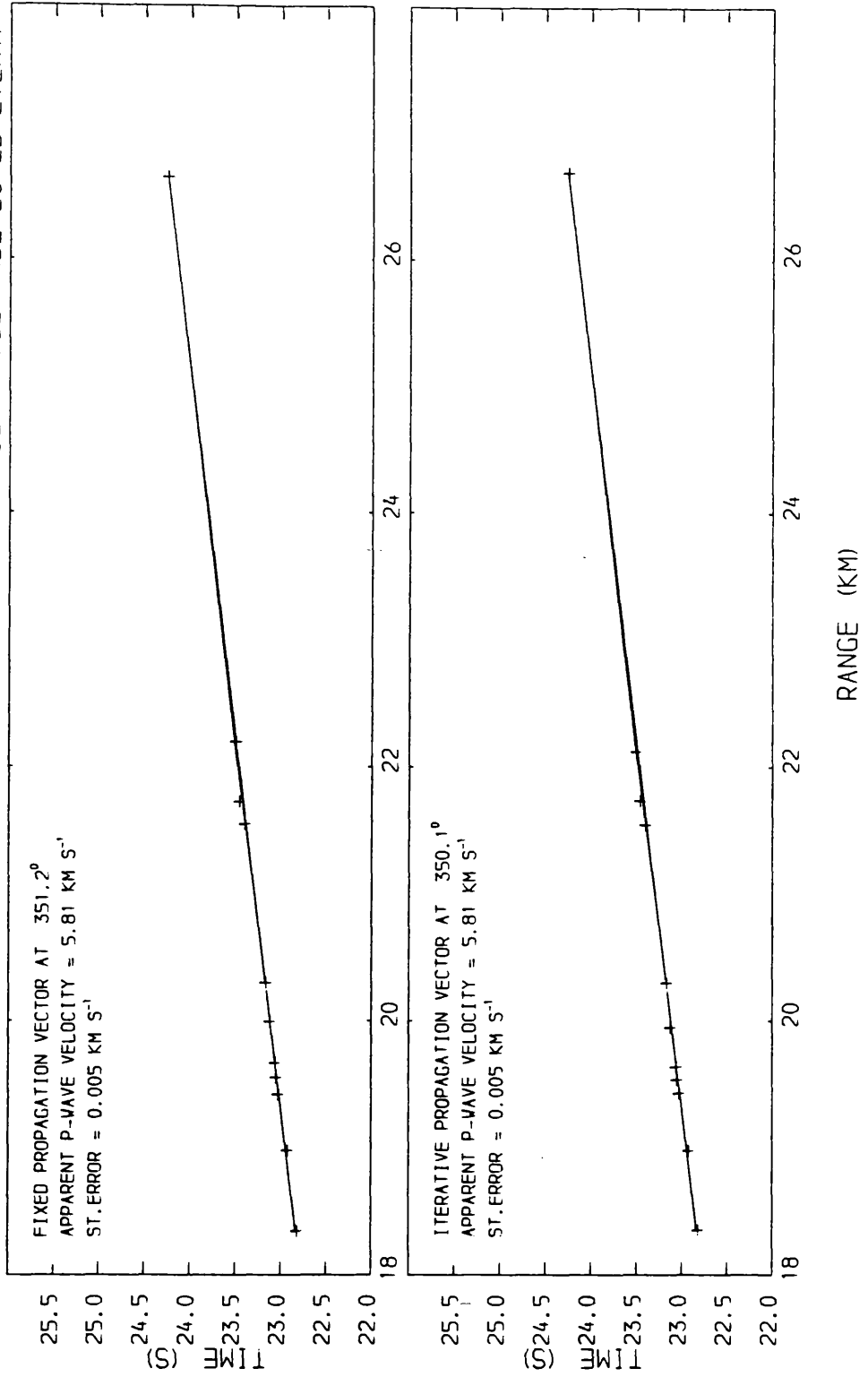


CRAIGIE QUARRY INTO LES ARRAY 26 AUG 1982 (DETECTED EVENT)



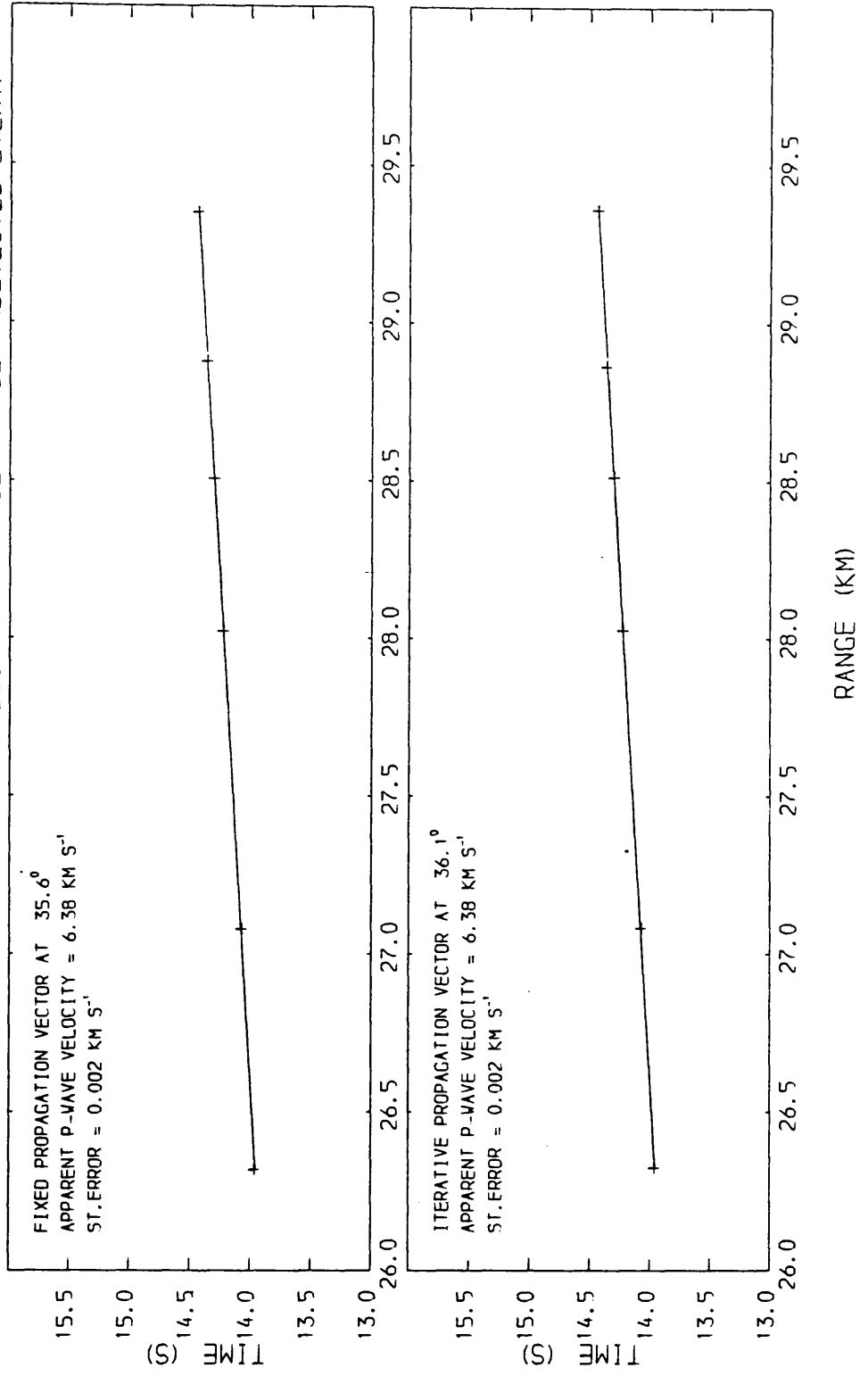
Appendix 4.7

KIRKCONNEL OPENCAST INTO LES ARRAY 14 SEPT 1982 (DETECTED EVENT)

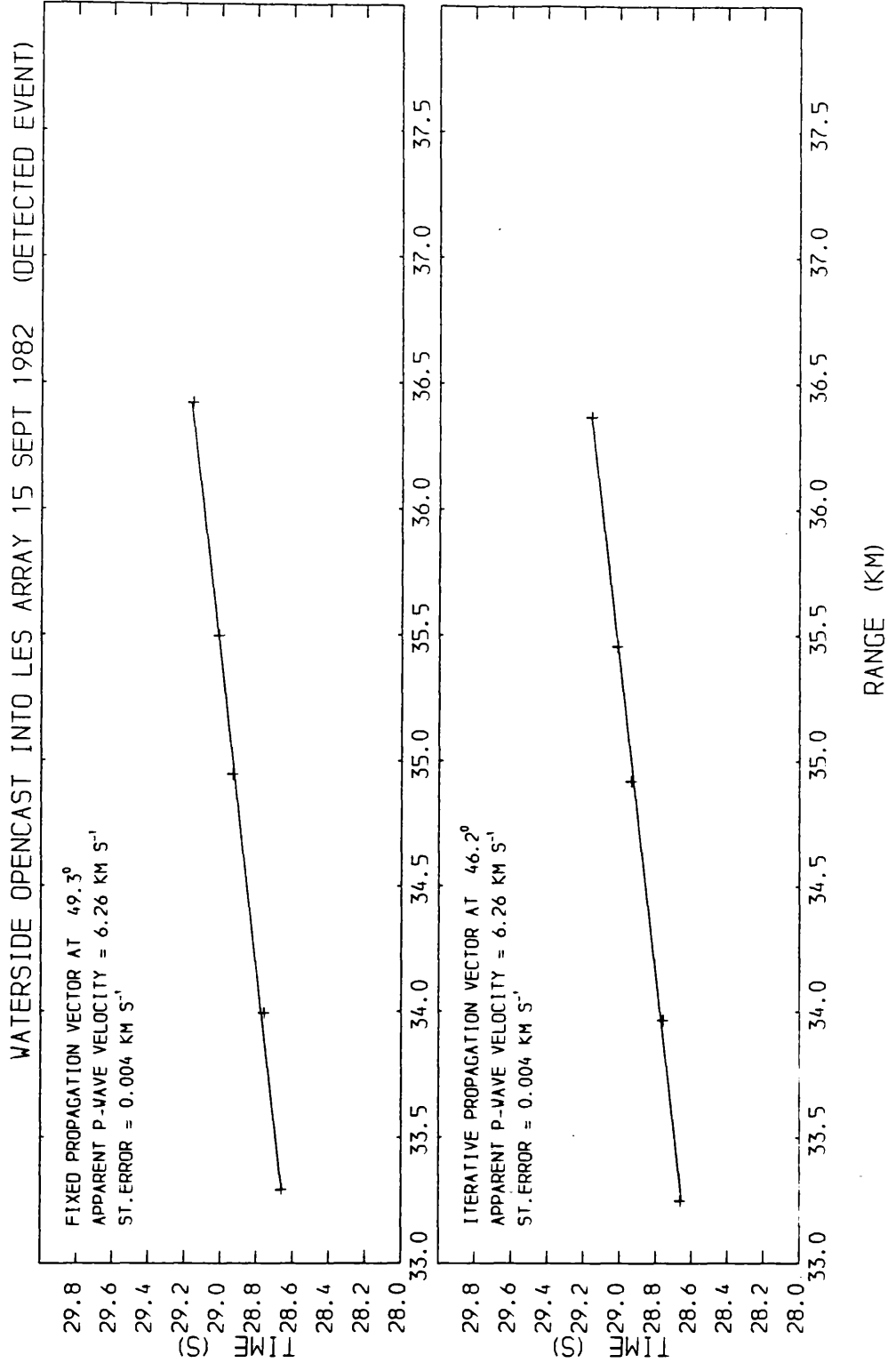


Appendix 4.8

BENBAIN OPENCASST INTO LES ARRAY 14 SEPT 1982 (DETECTED EVENT)

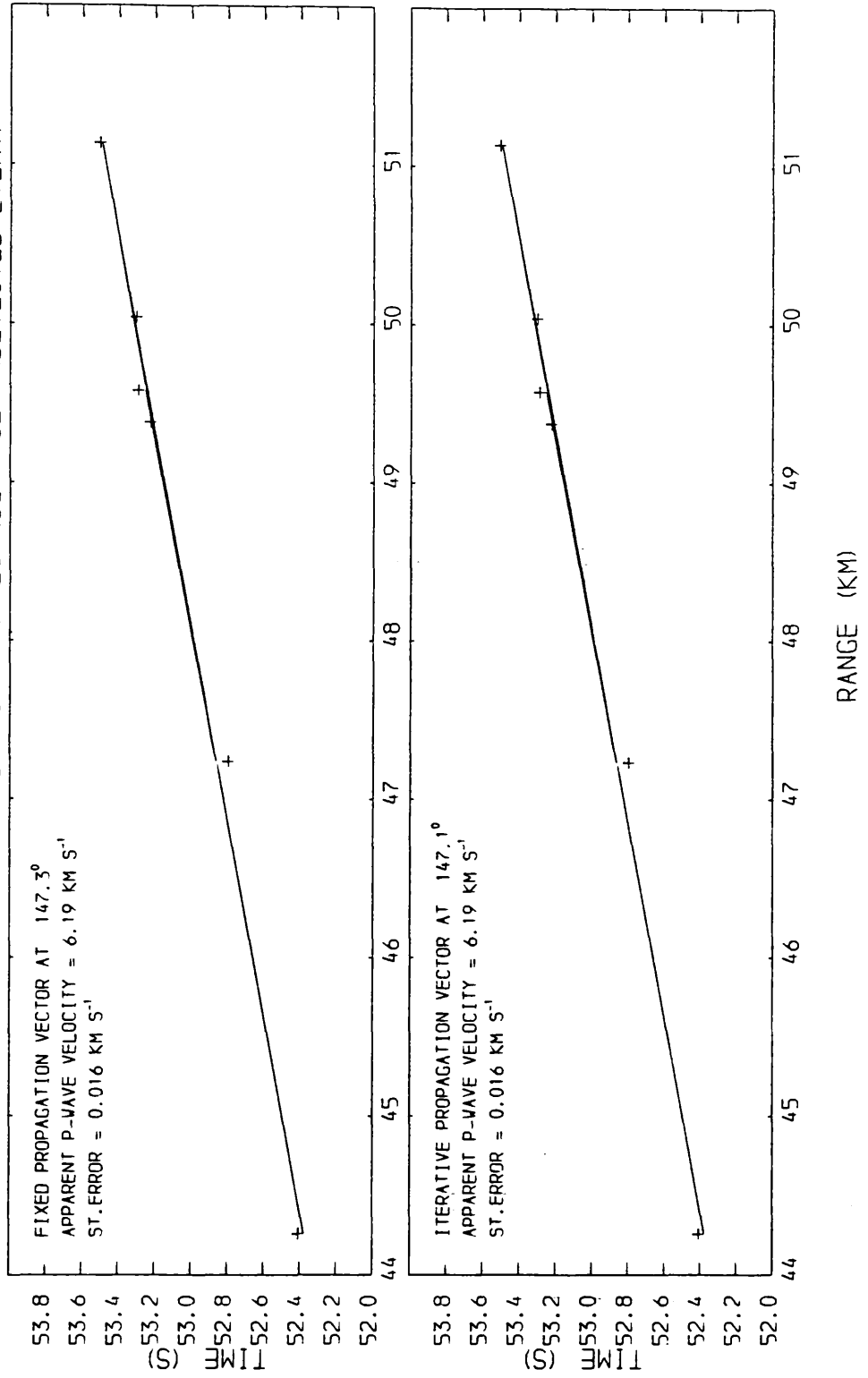


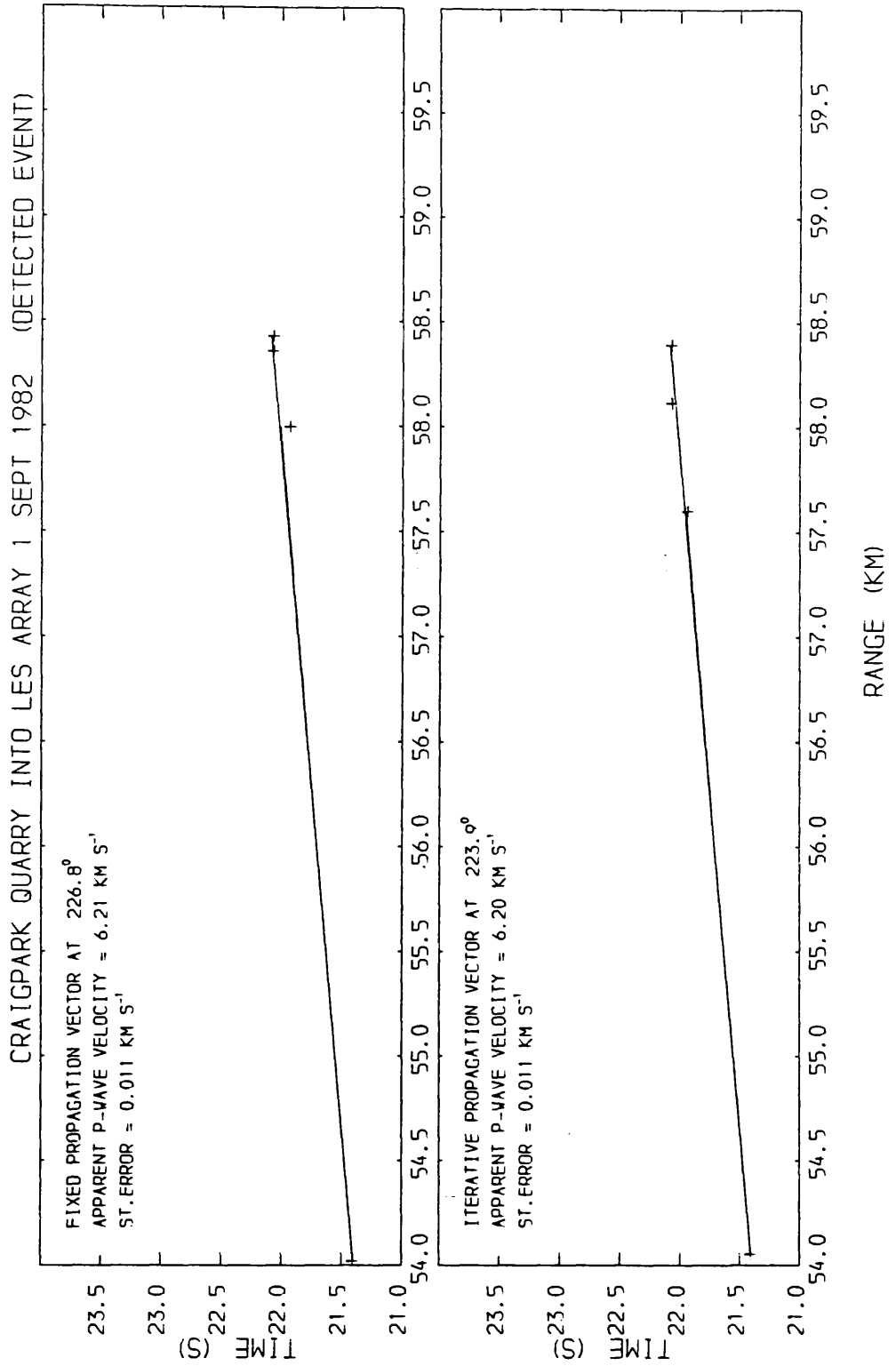
Appendix 4.9



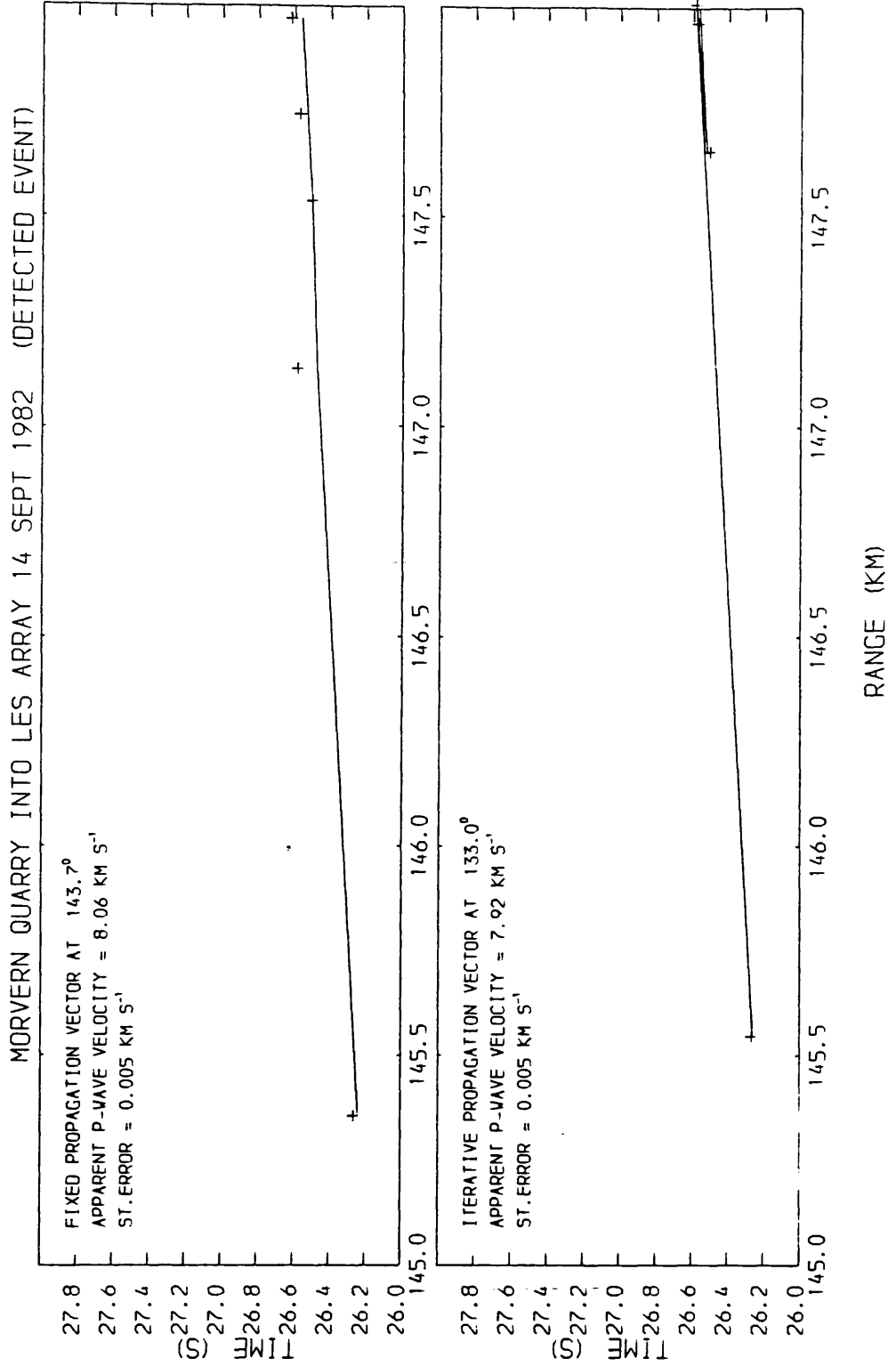
Appendix 4.10

DUMBUCK QUARRY INTO LES ARRAY 26 AUG 1982 (DETECTED EVENT)



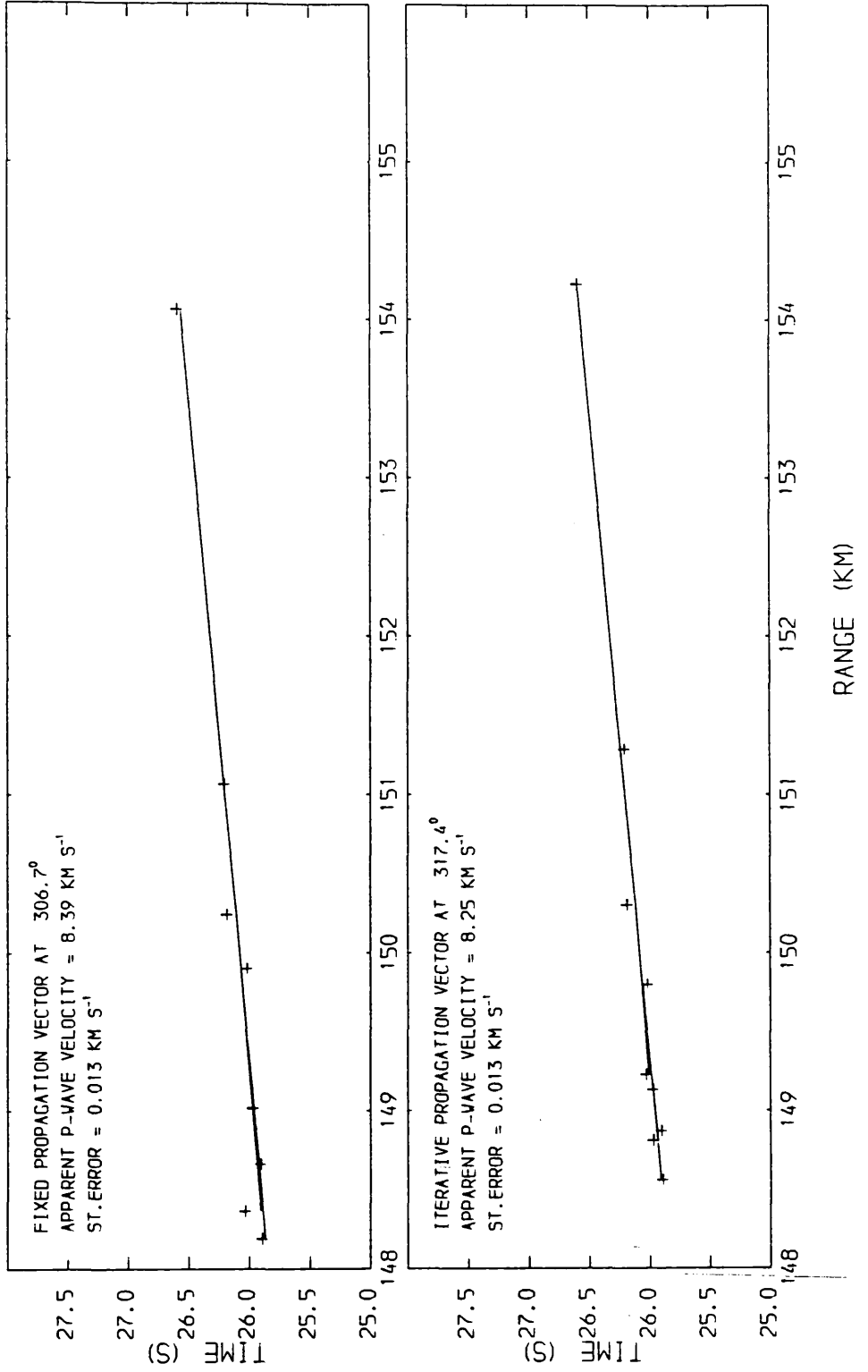


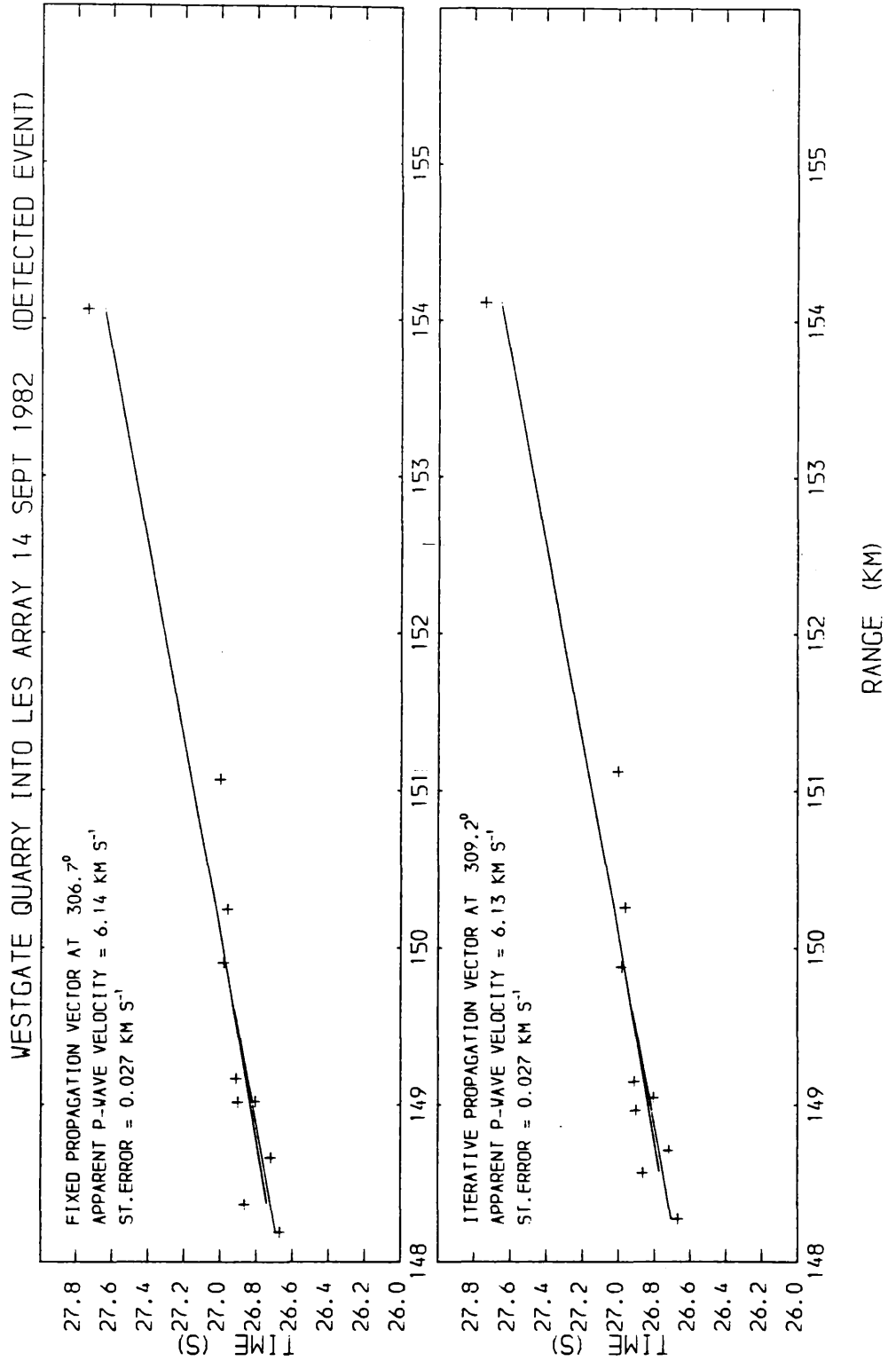
Appendix 4.12



Appendix 4.13

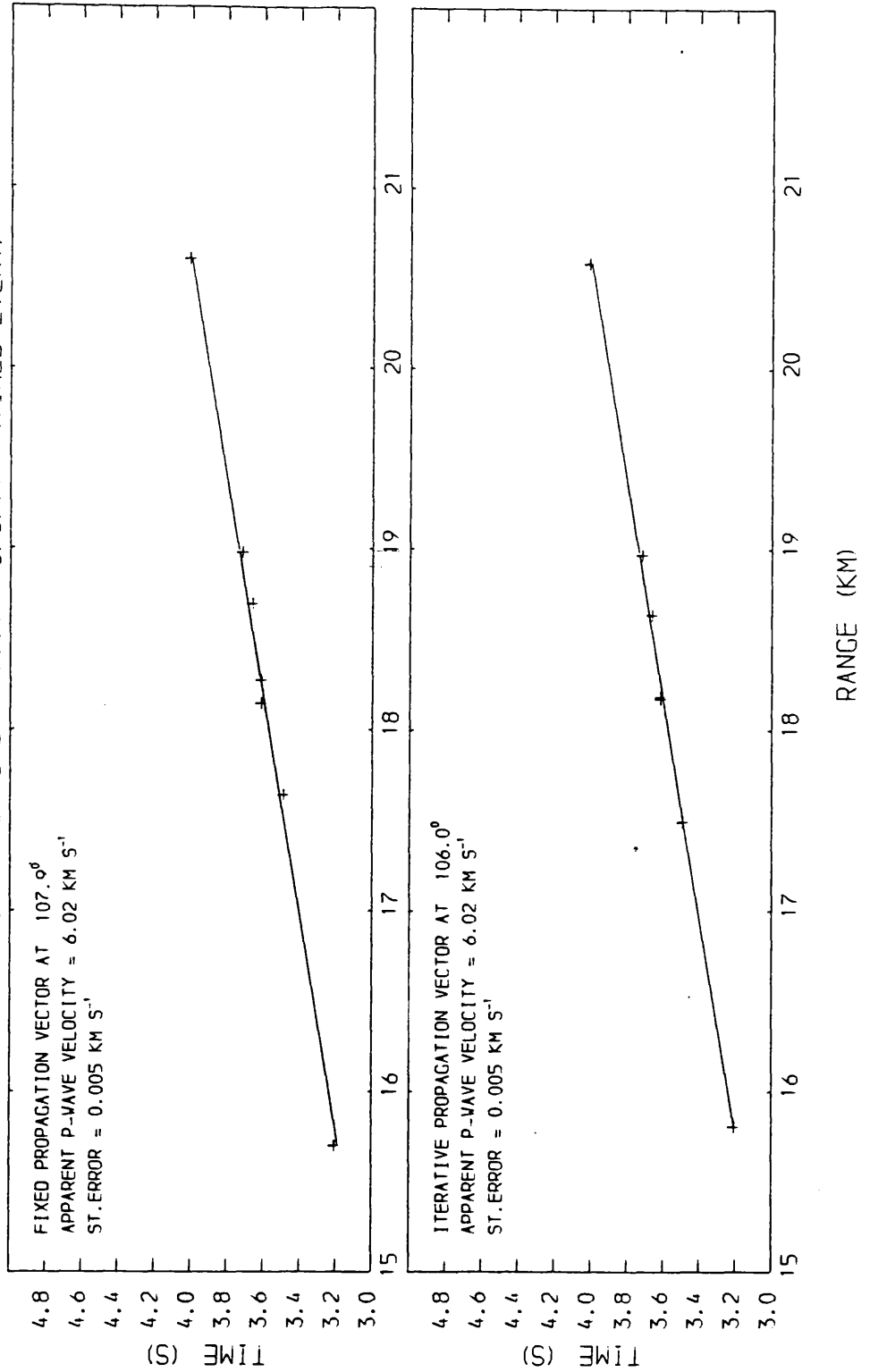
WESTGATE QUARRY INTO LES ARRAY 14 SEPT 1982 (DETECTED EVENT)



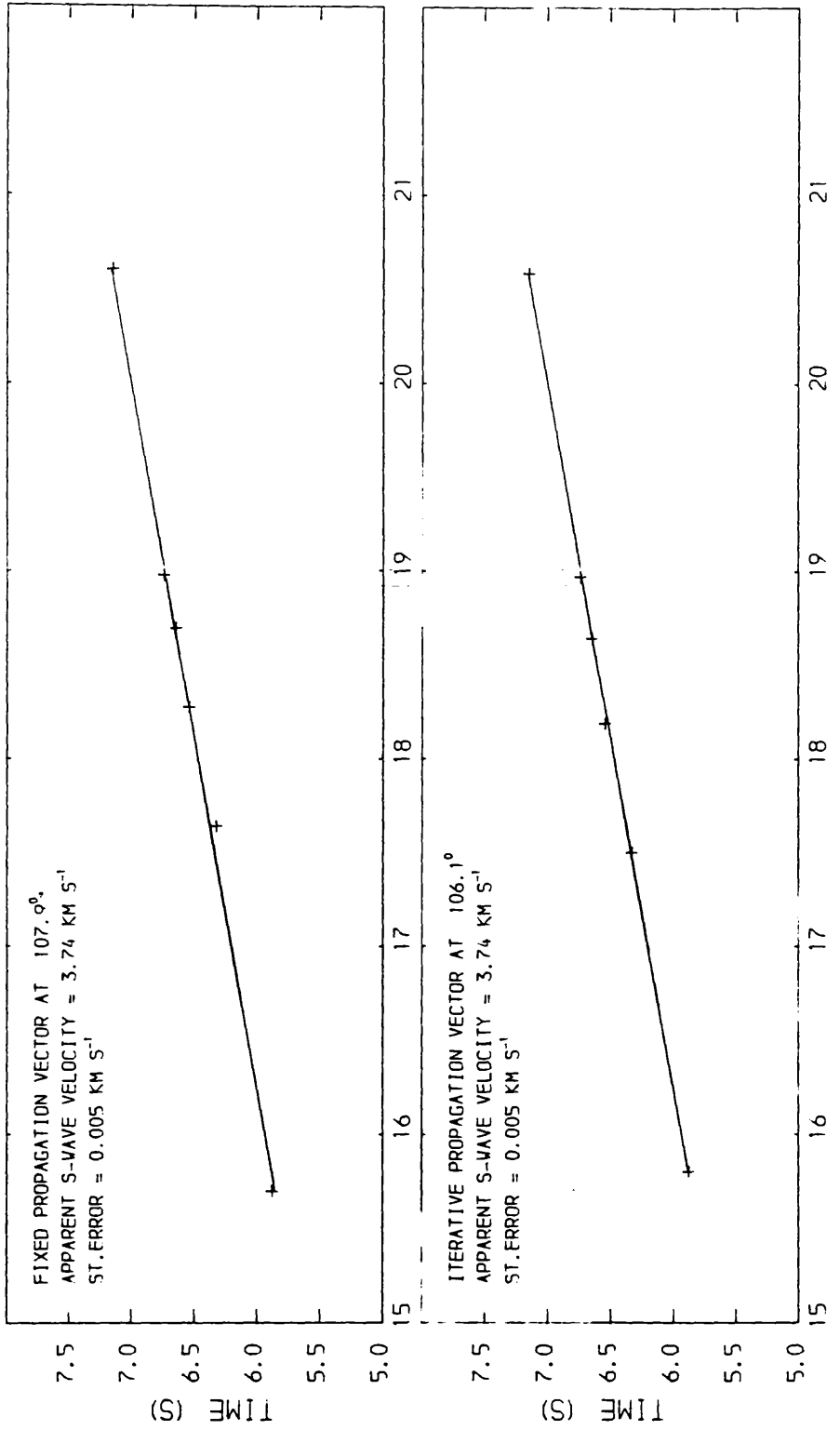


Appendix 4.15

CLOBURN QUARRY INTO BTN ARRAY 16/3/77 (TIMED EVENT)

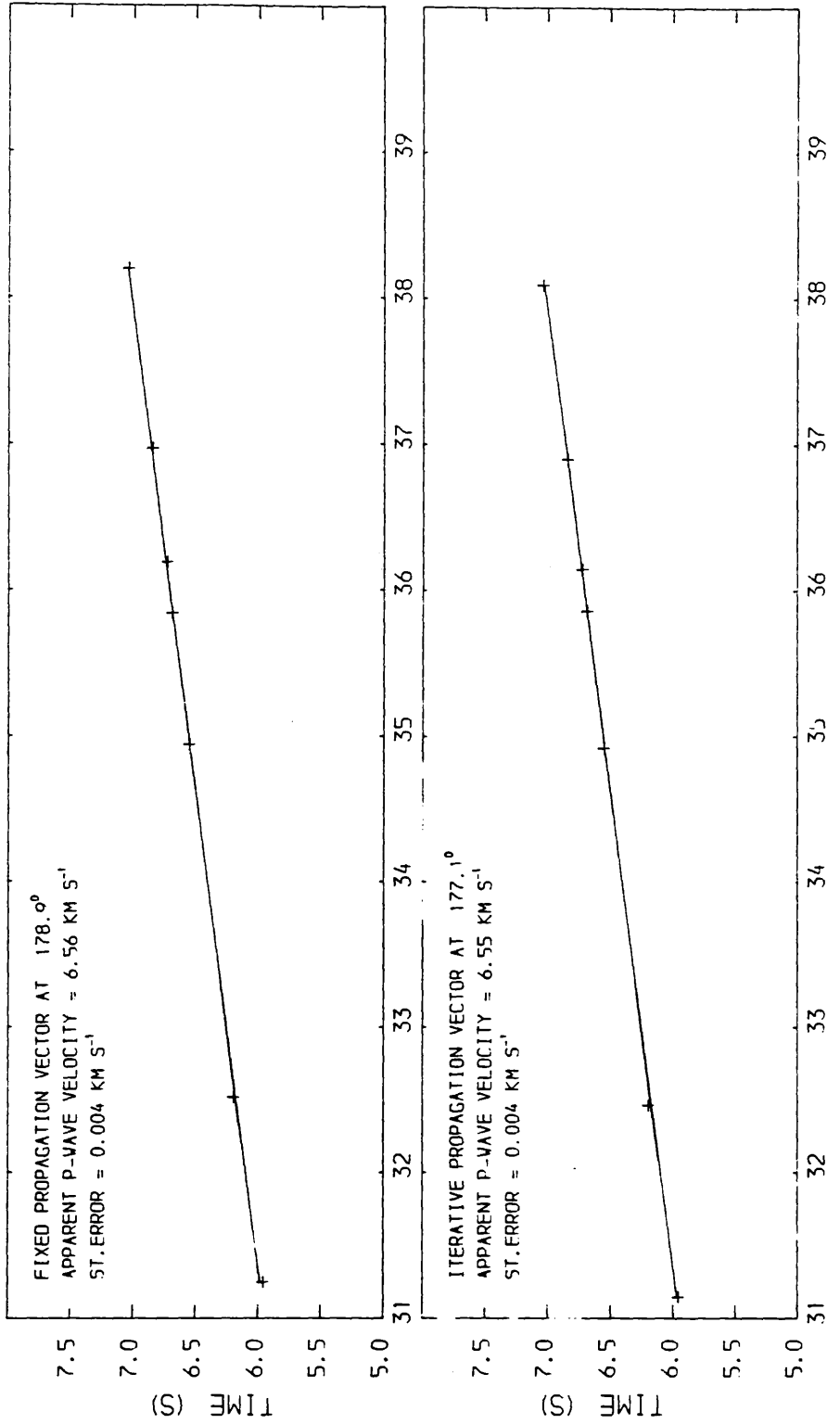


CLOBURN QUARRY INTO BTN ARRAY 16/3/77 (TIMED EVENT)



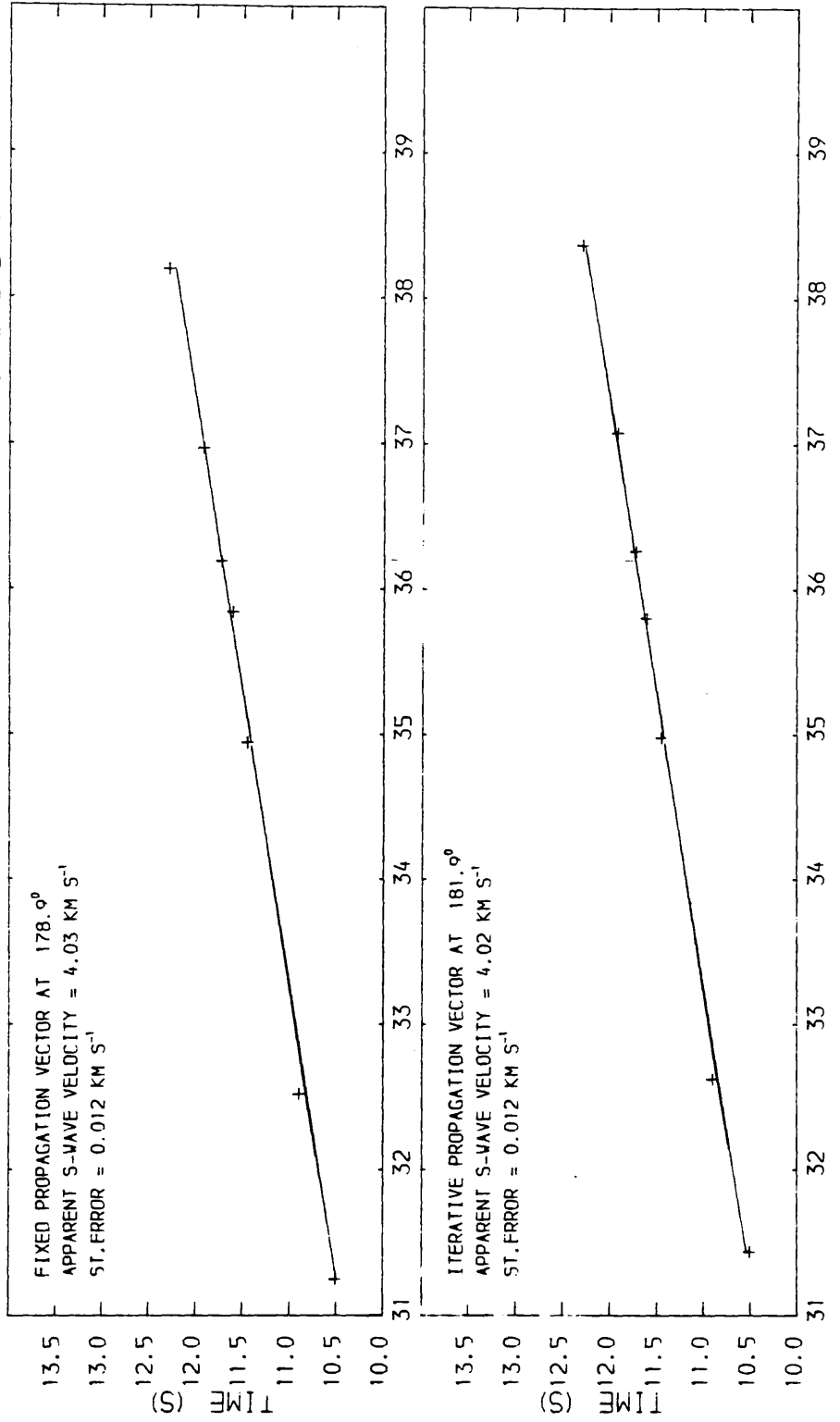
Appendix 4.17

CRAIGPARK QUARRY INTO BTN ARRAY 23/2/77 (TIMED EVENT)



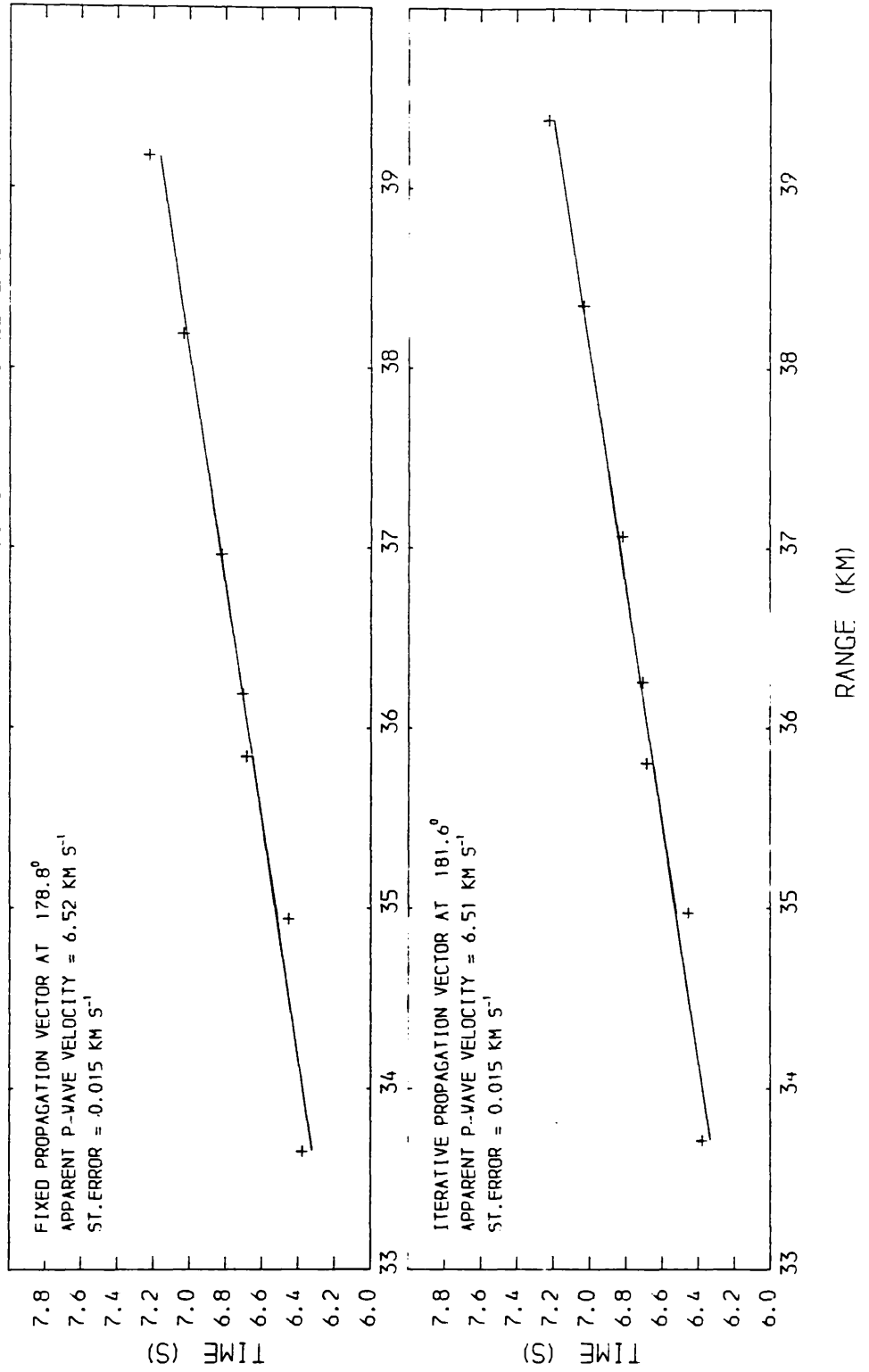
Appendix 4.18

CRAIGPARK QUARRY INTO BTN ARRAY 23/2/77 (TIMED EVENT)

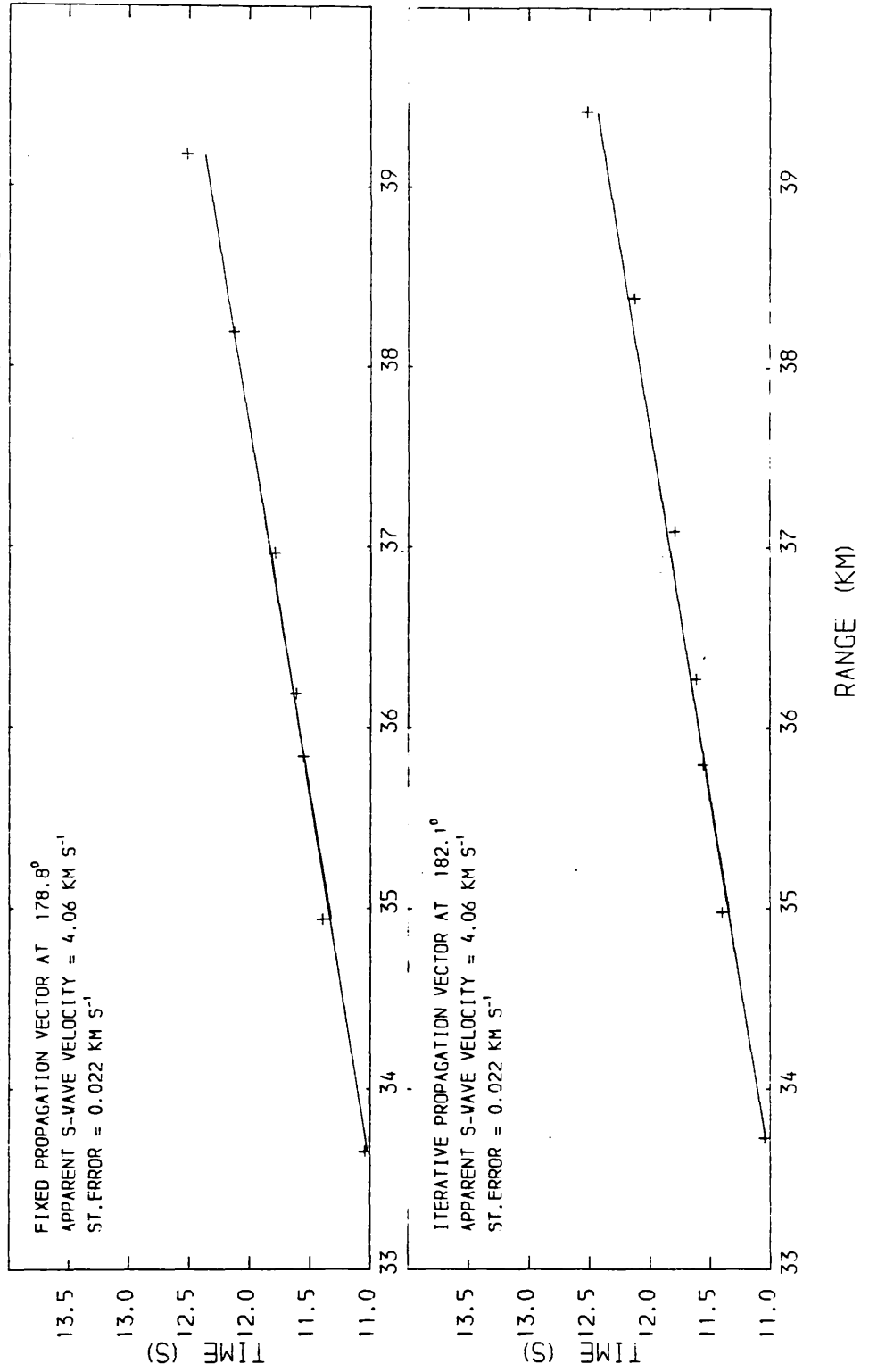


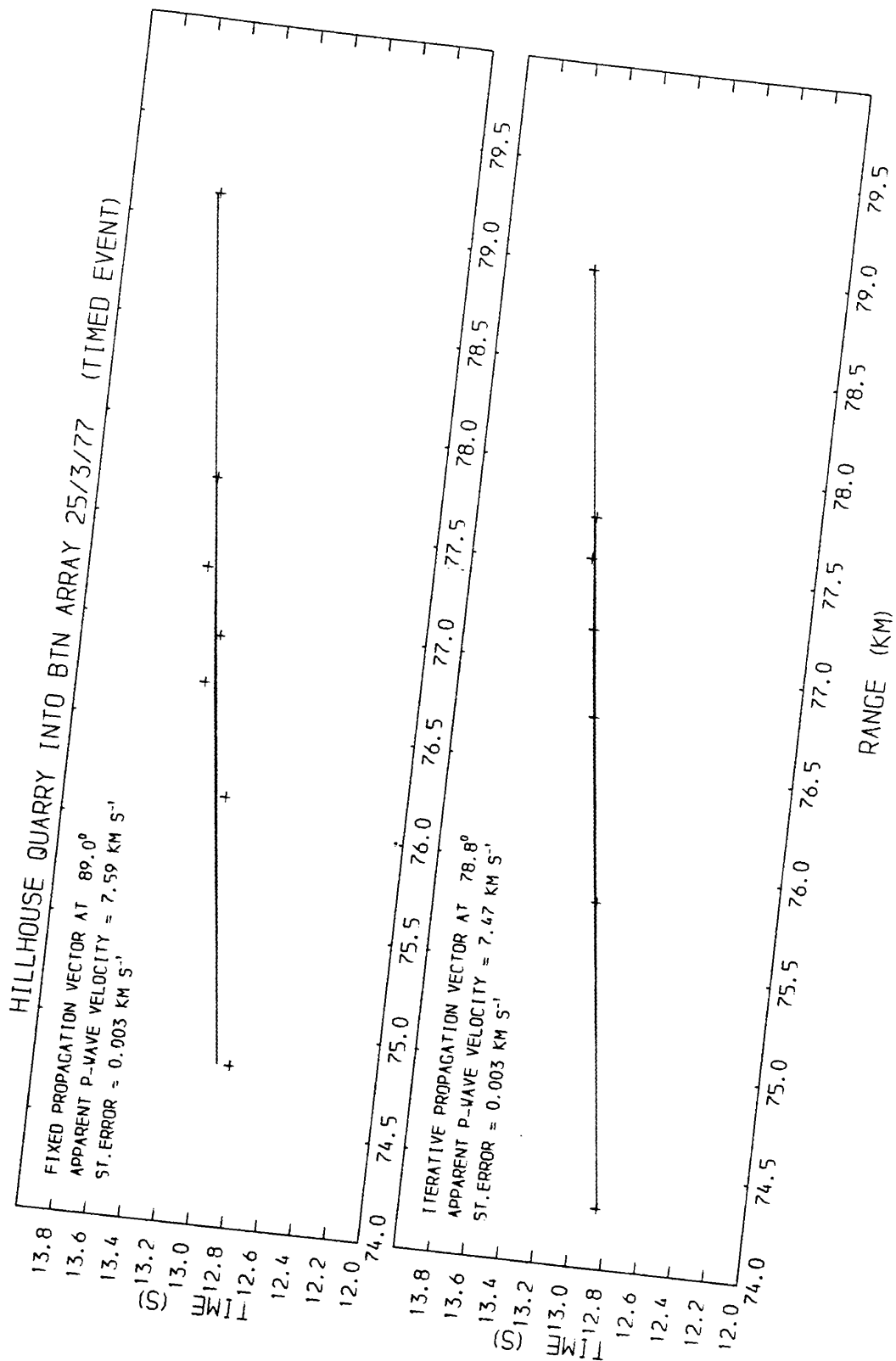
Appendix 4.19

CRAIGPARK QUARRY INTO BTN ARRAY 30/3/77 (TIMED EVENT)



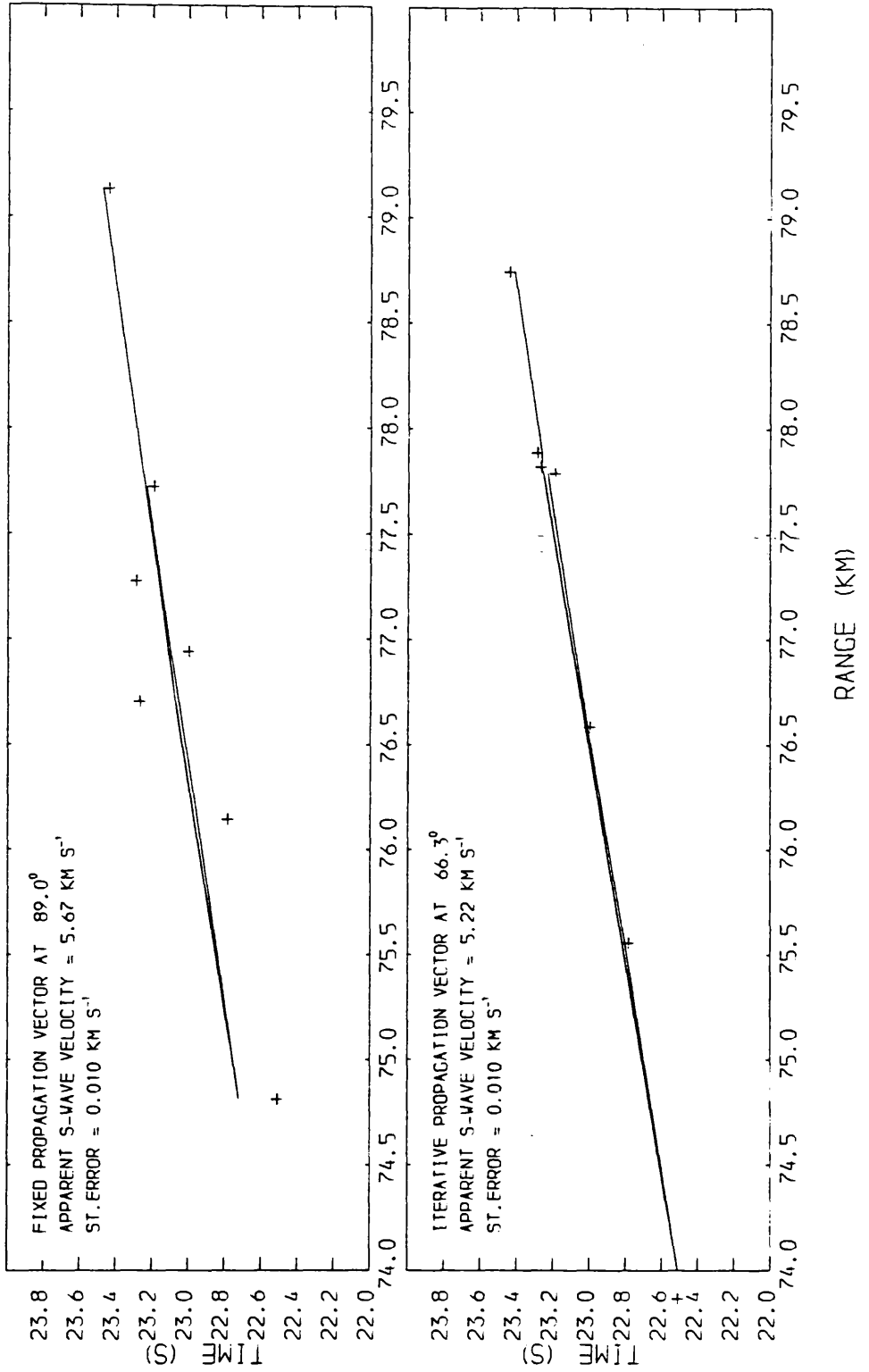
CRAIGPARK QUARRY INTO BTN ARRAY 30/3/77 (TIMED EVENT)

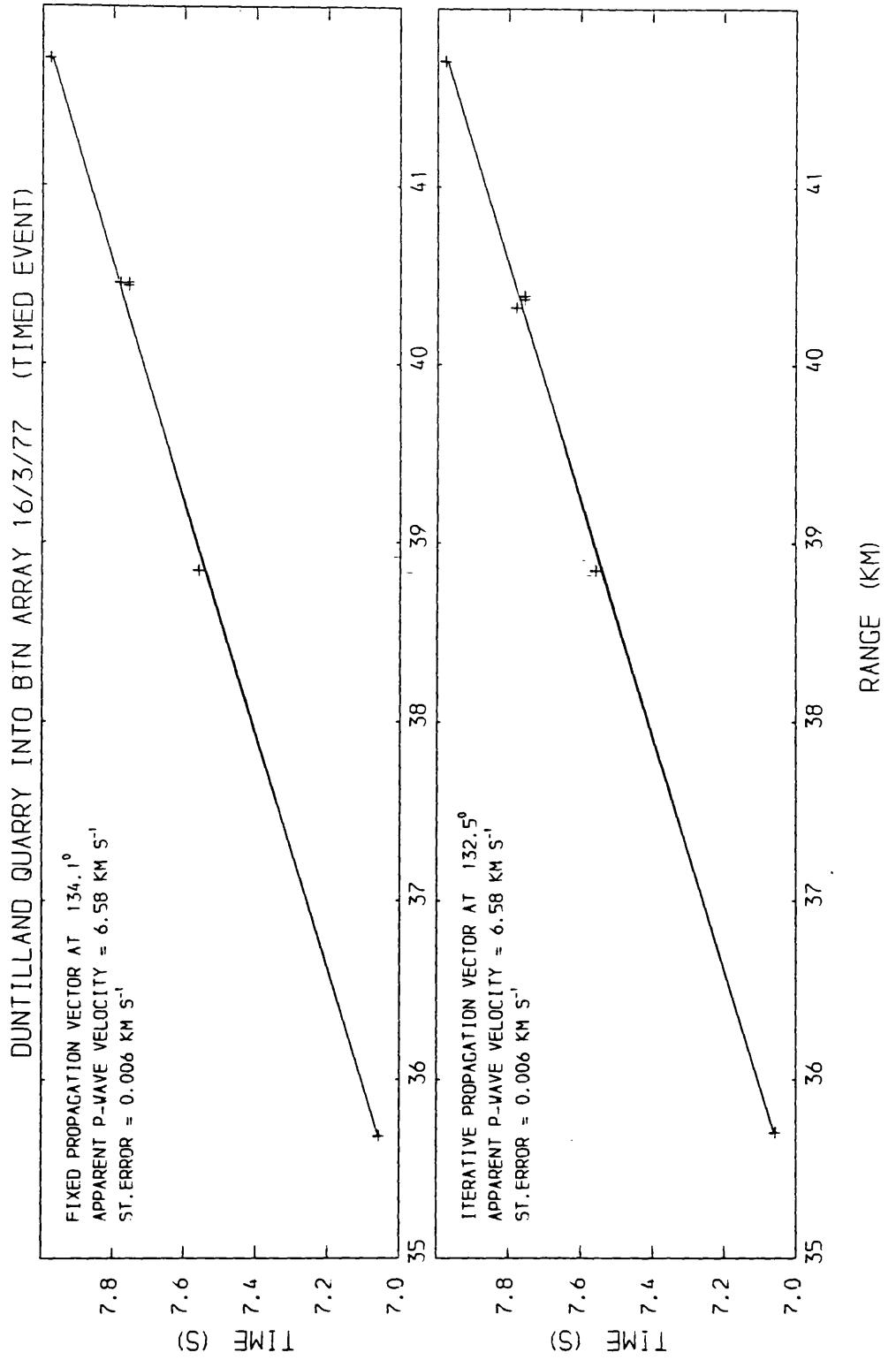




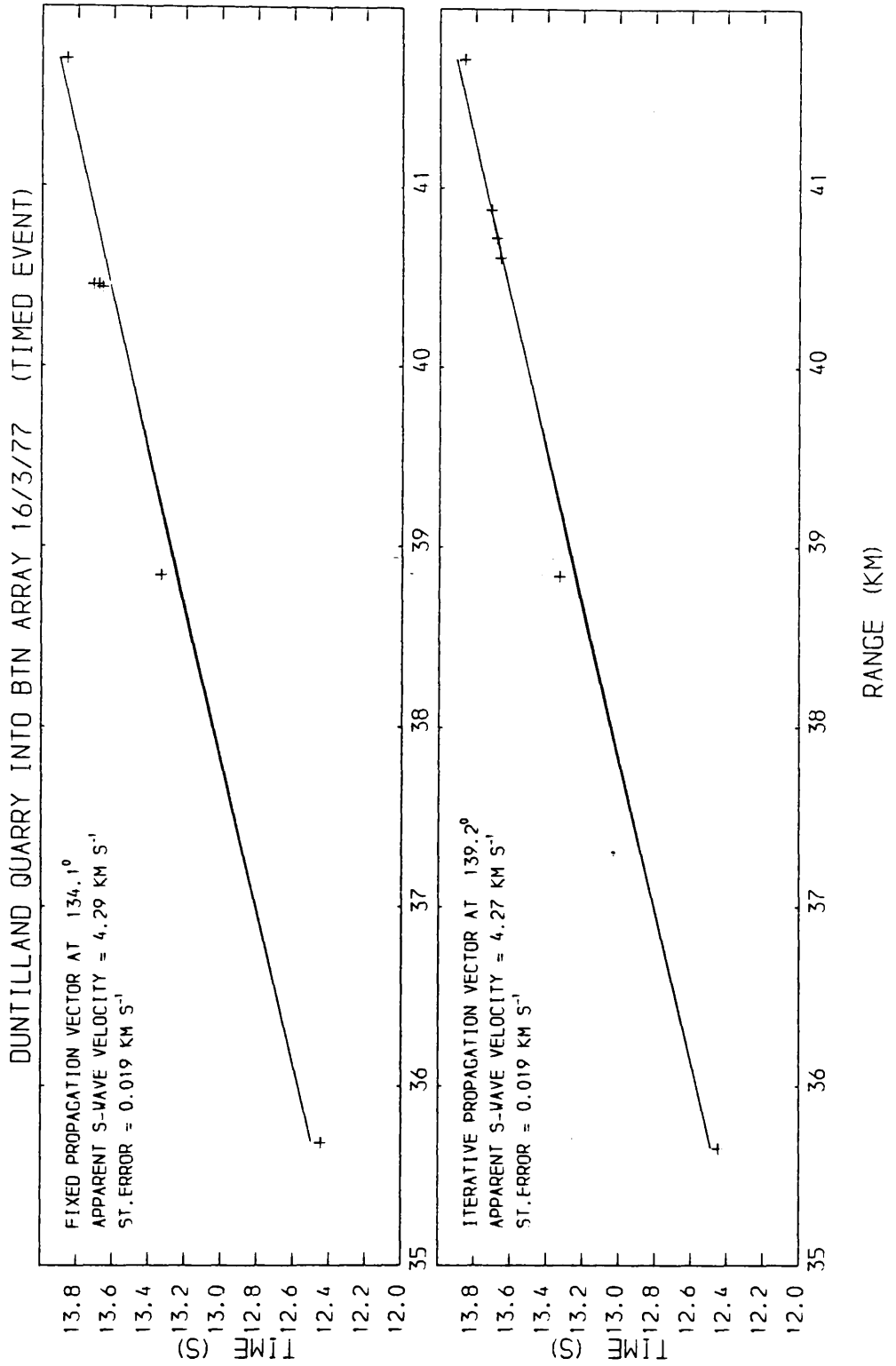
Appendix 4.22

HILLHOUSE QUARRY INTO BTN ARRAY 25/3/77 (TIMED EVENT)

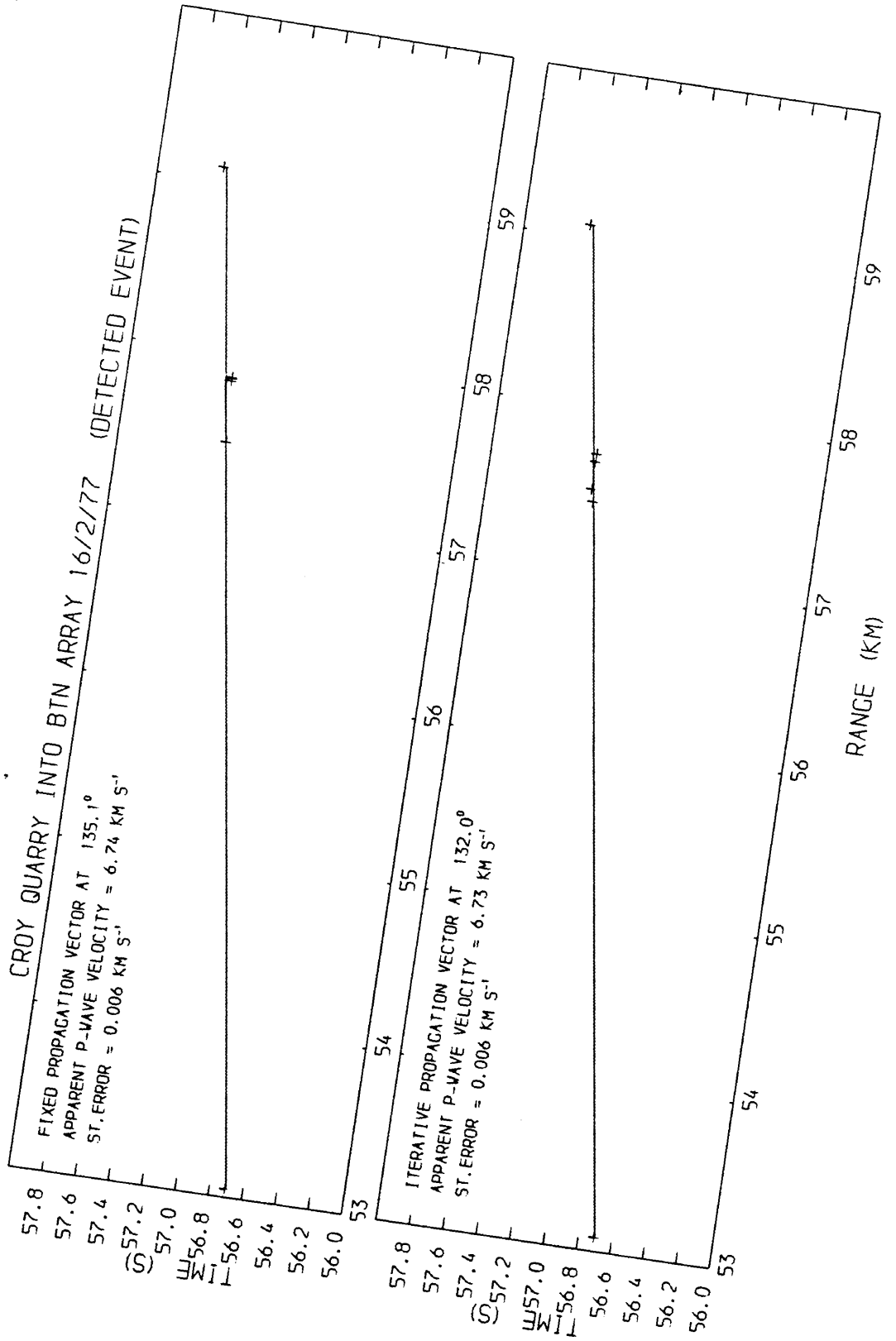




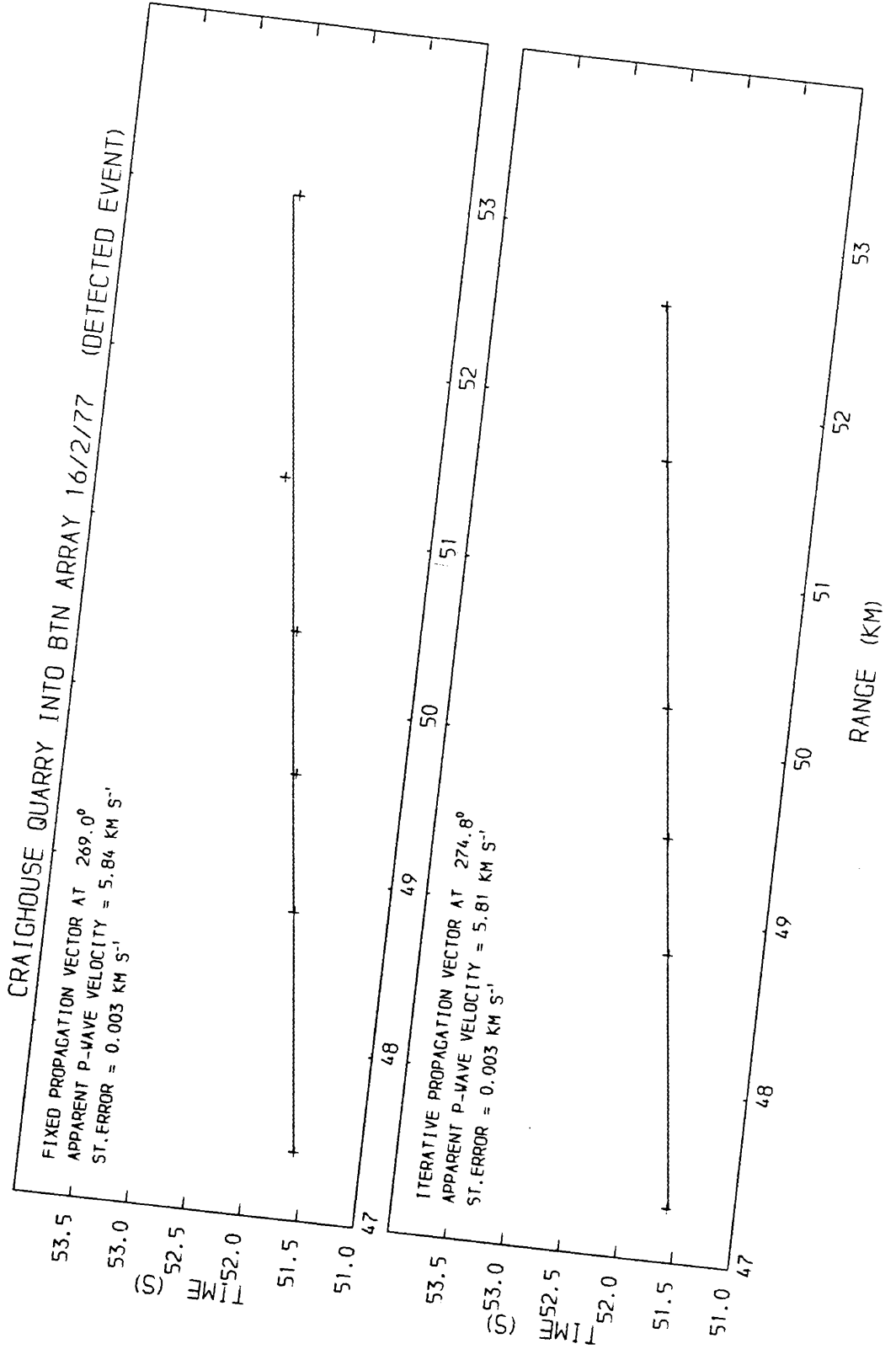
Appendix 4.24



Appendix 4.25

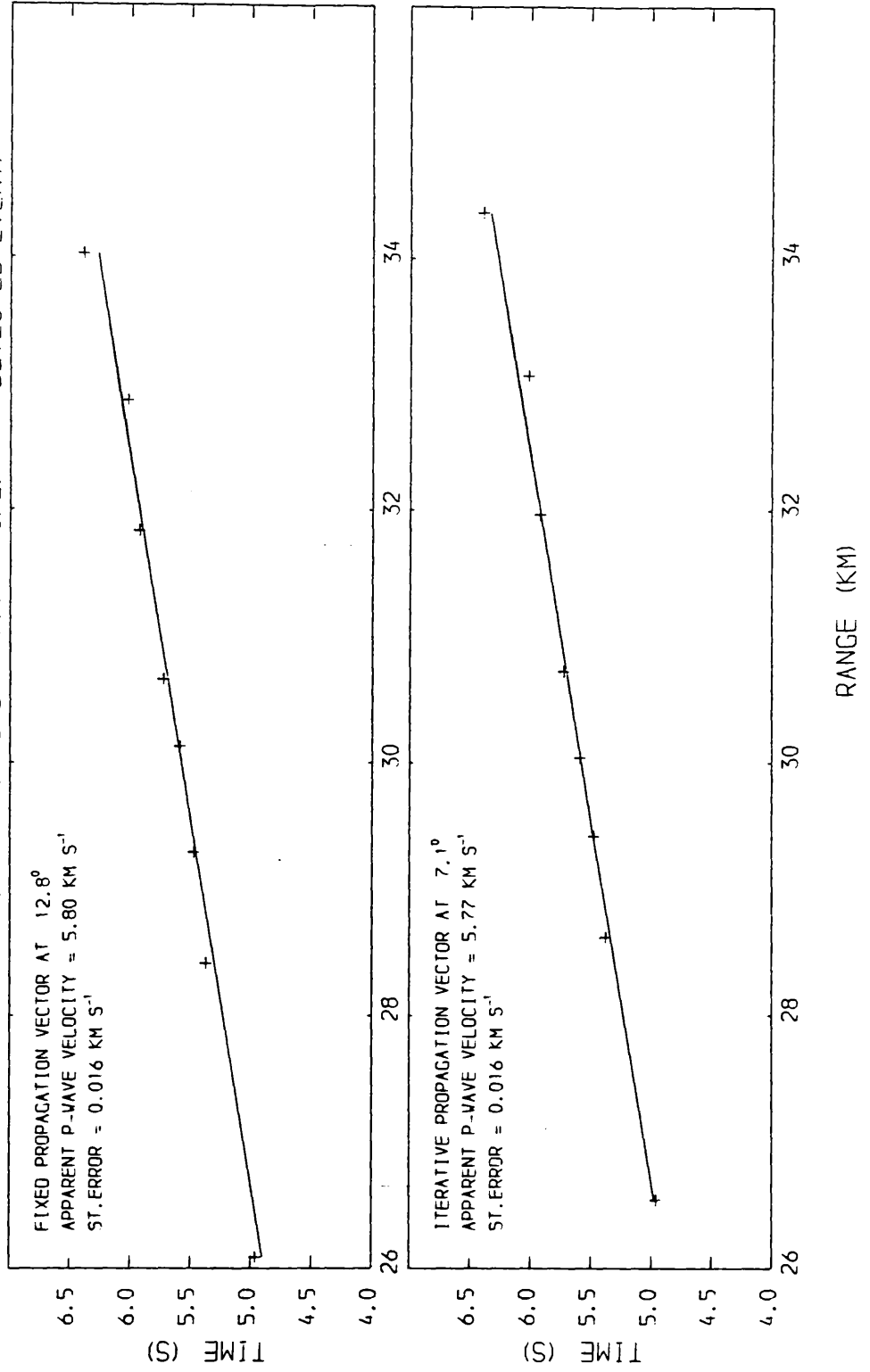


Appendix 4.26

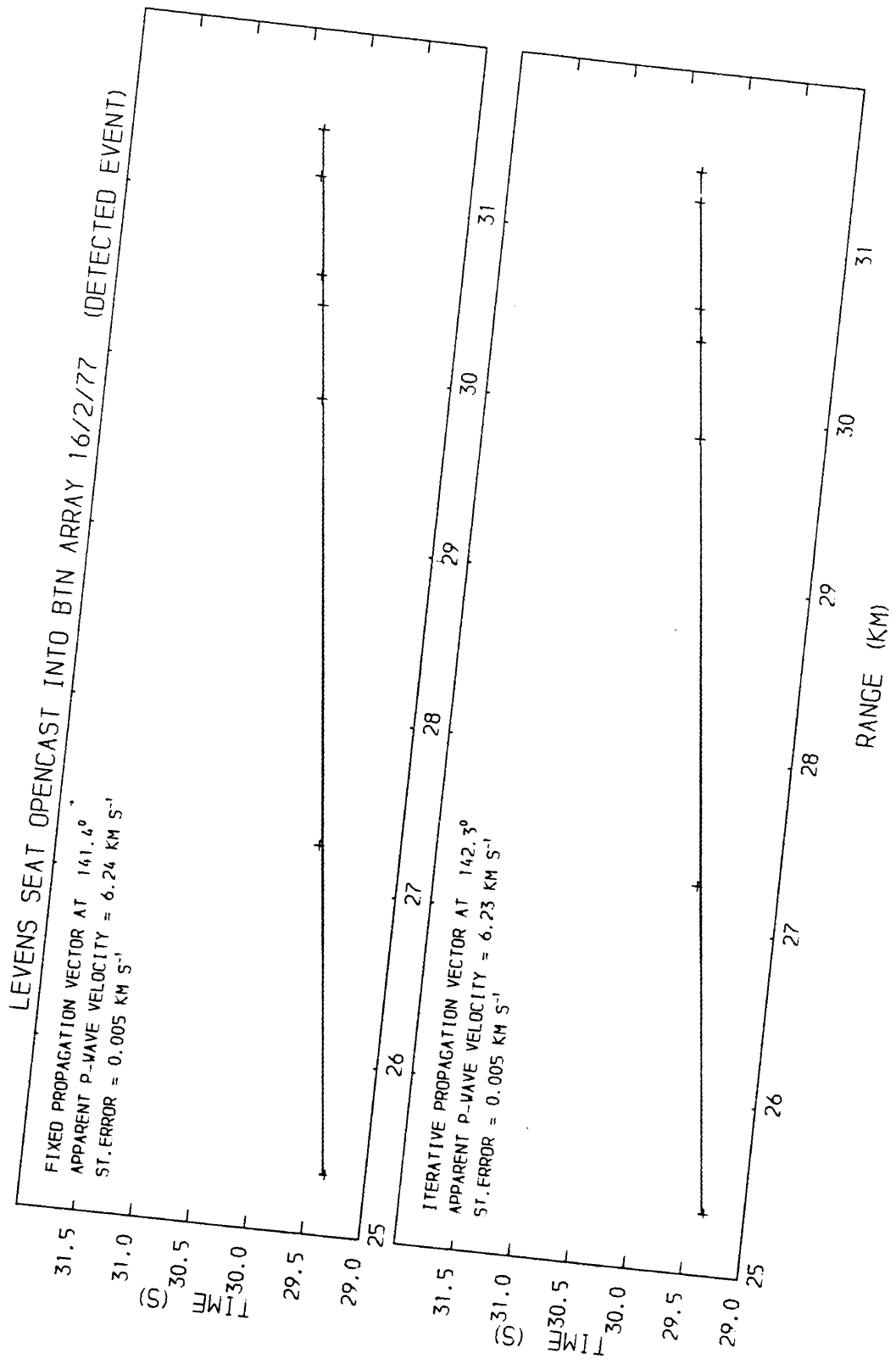


Appendix 4.27

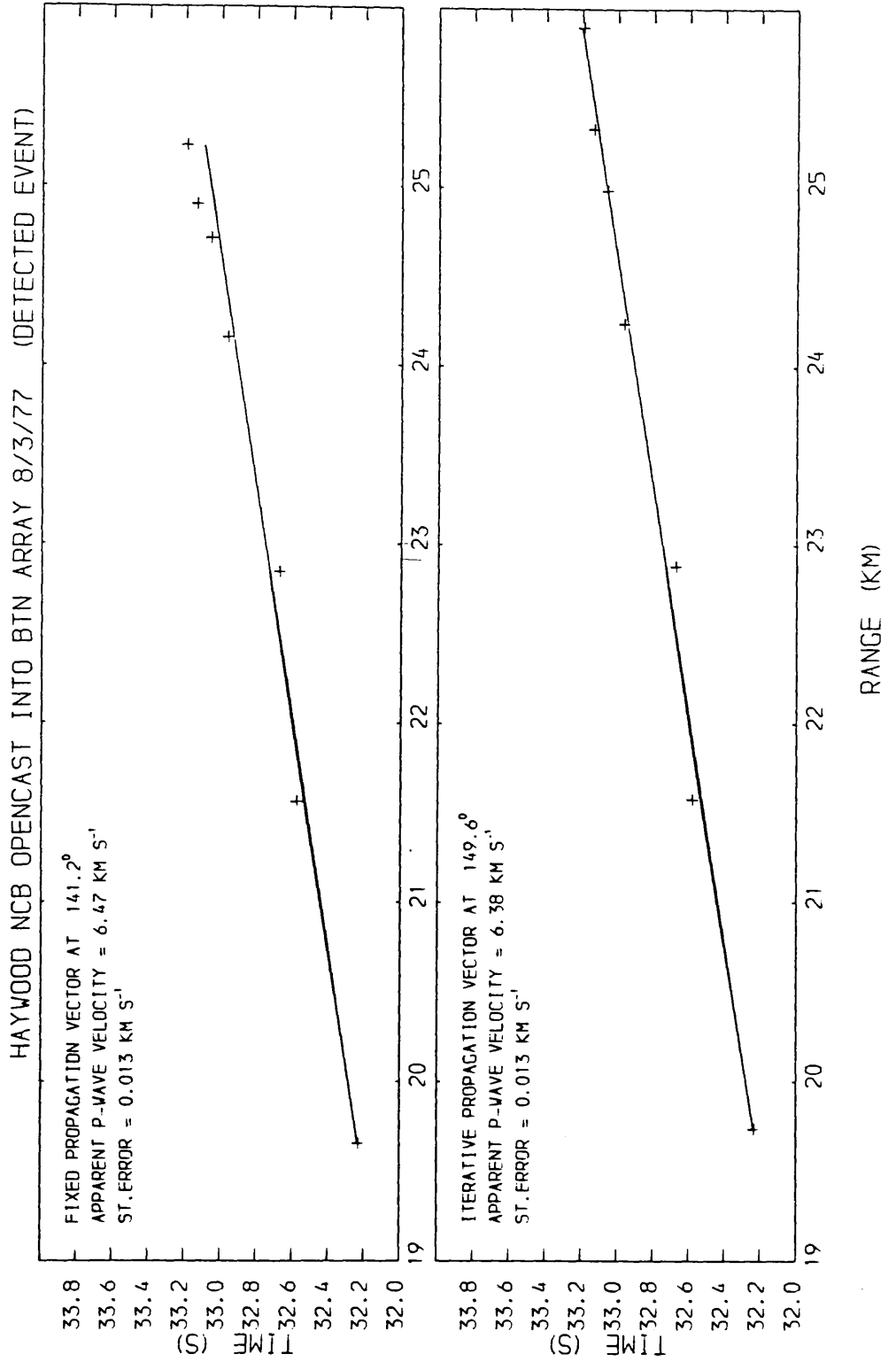
COATSGATE QUARRY INTO BTN ARRAY 16/2/77 (DETECTED EVENT)



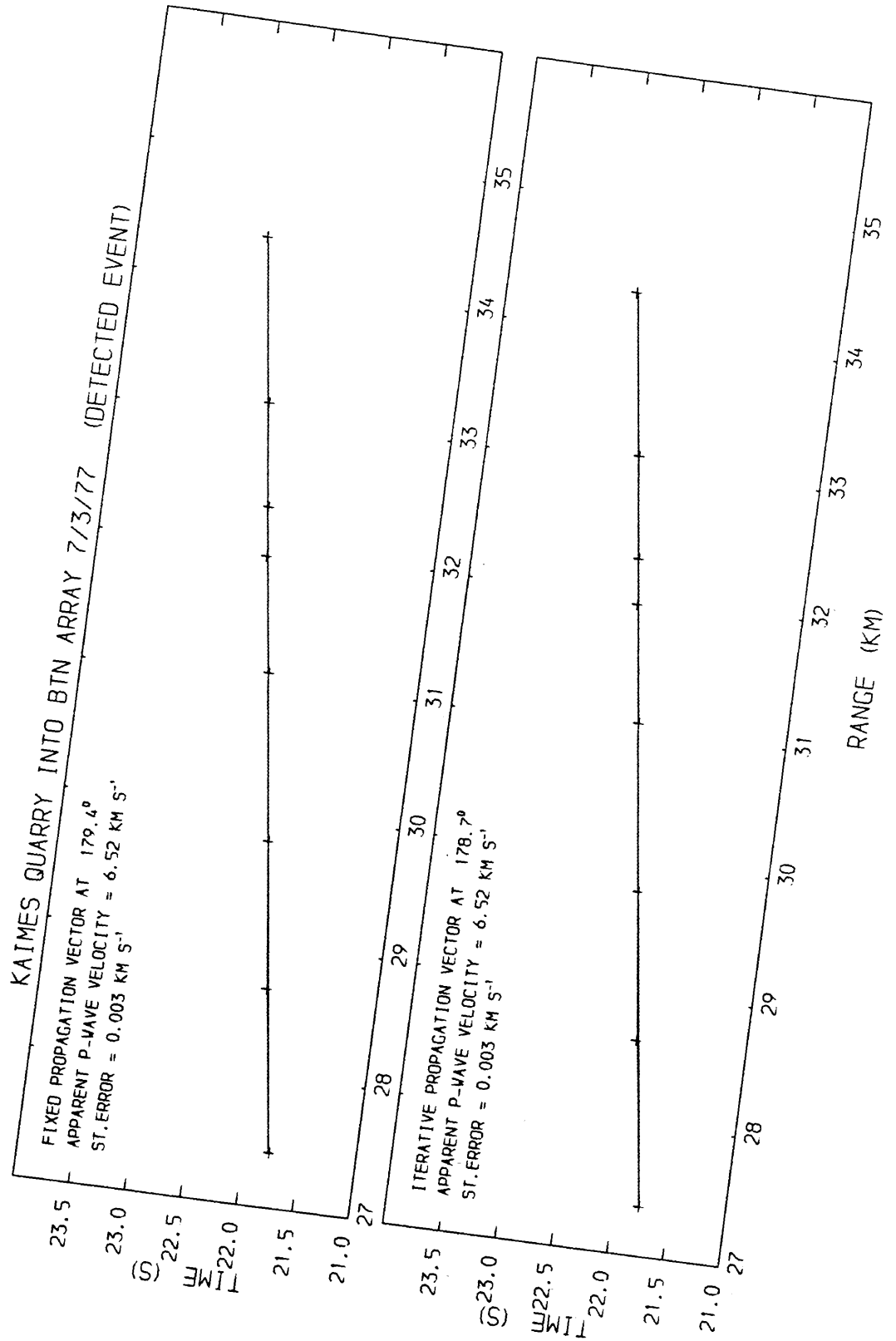
Appendix 4.28



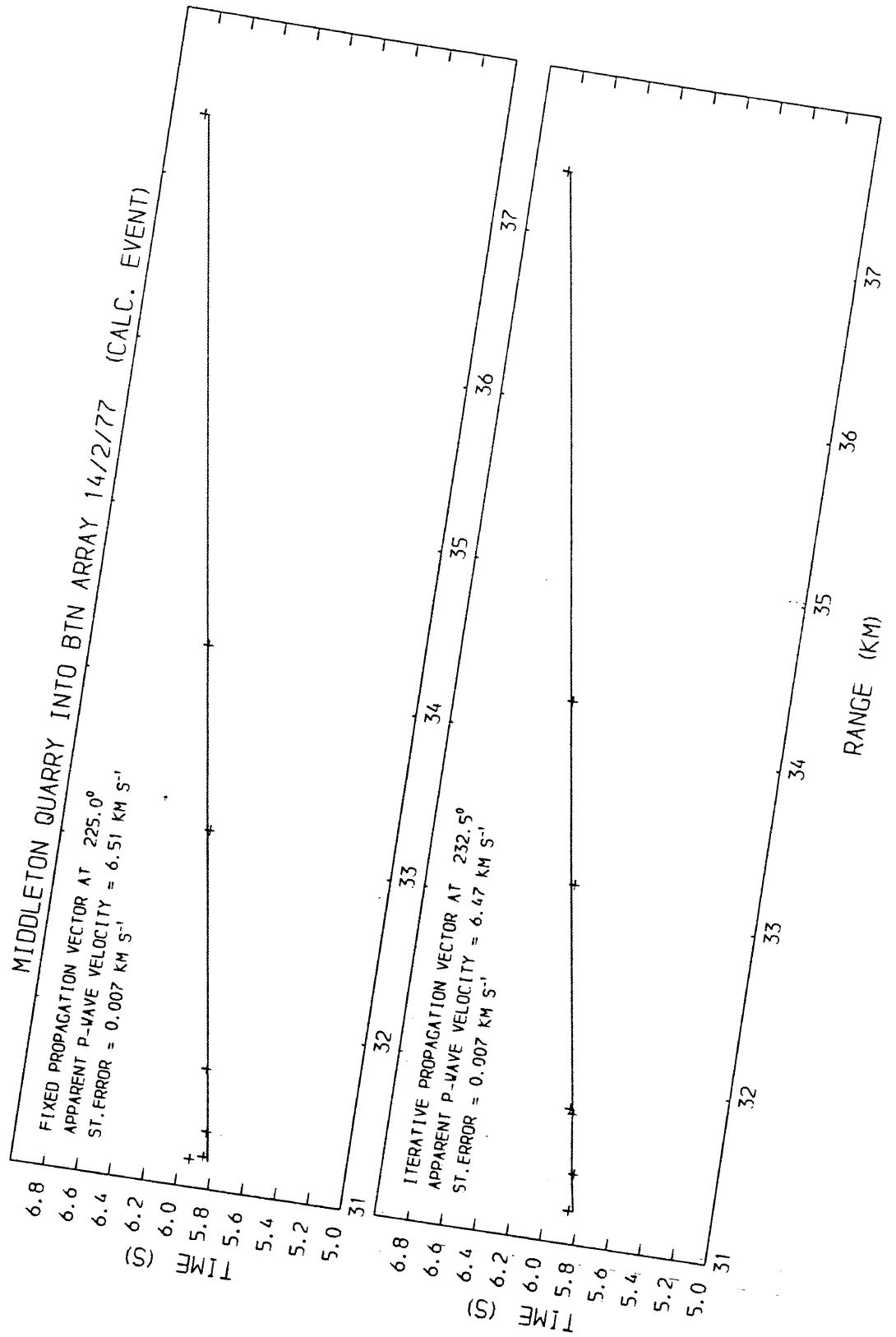
Appendix 4.29



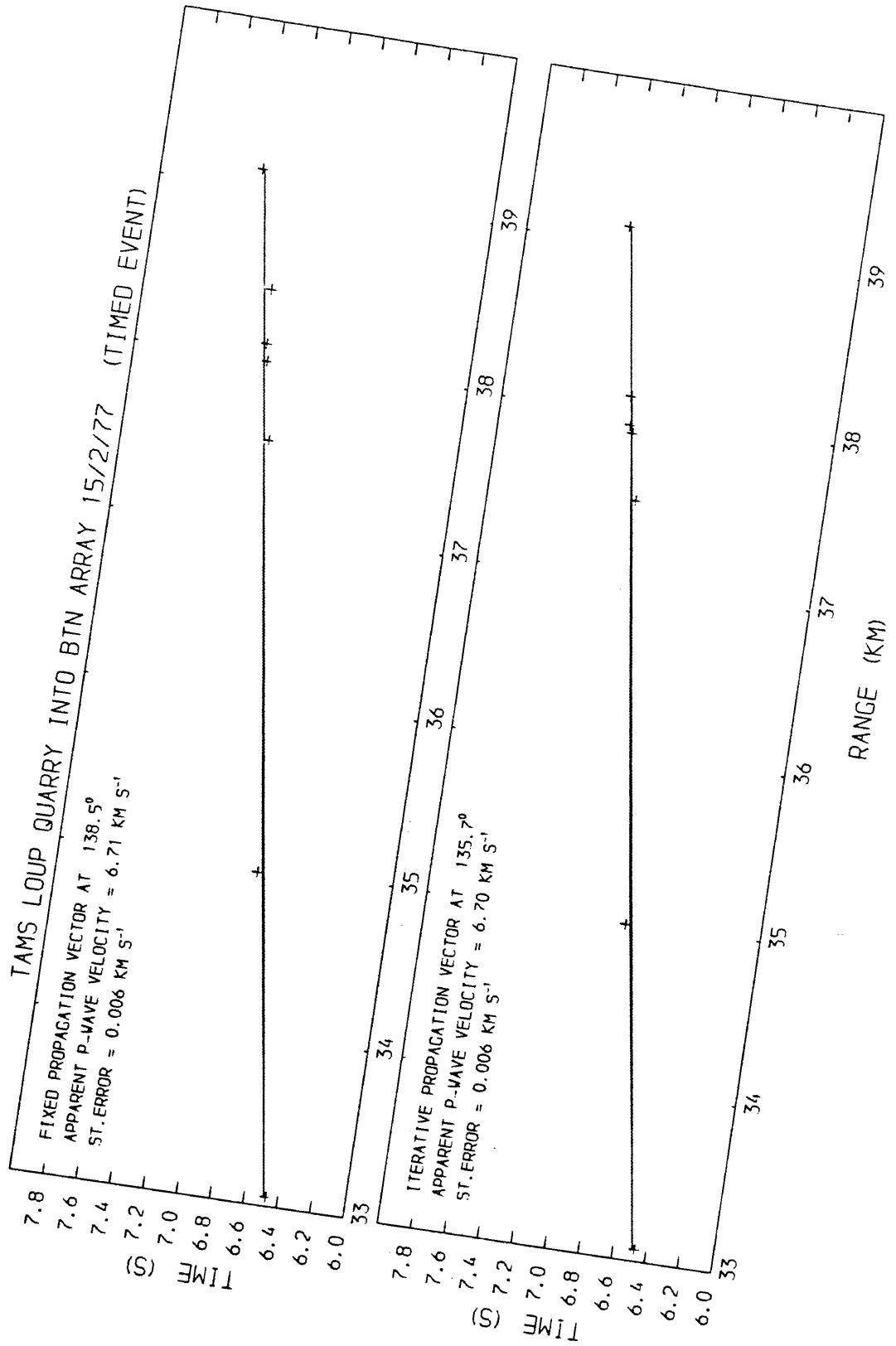
Appendix 4.30



Appendix 4.31

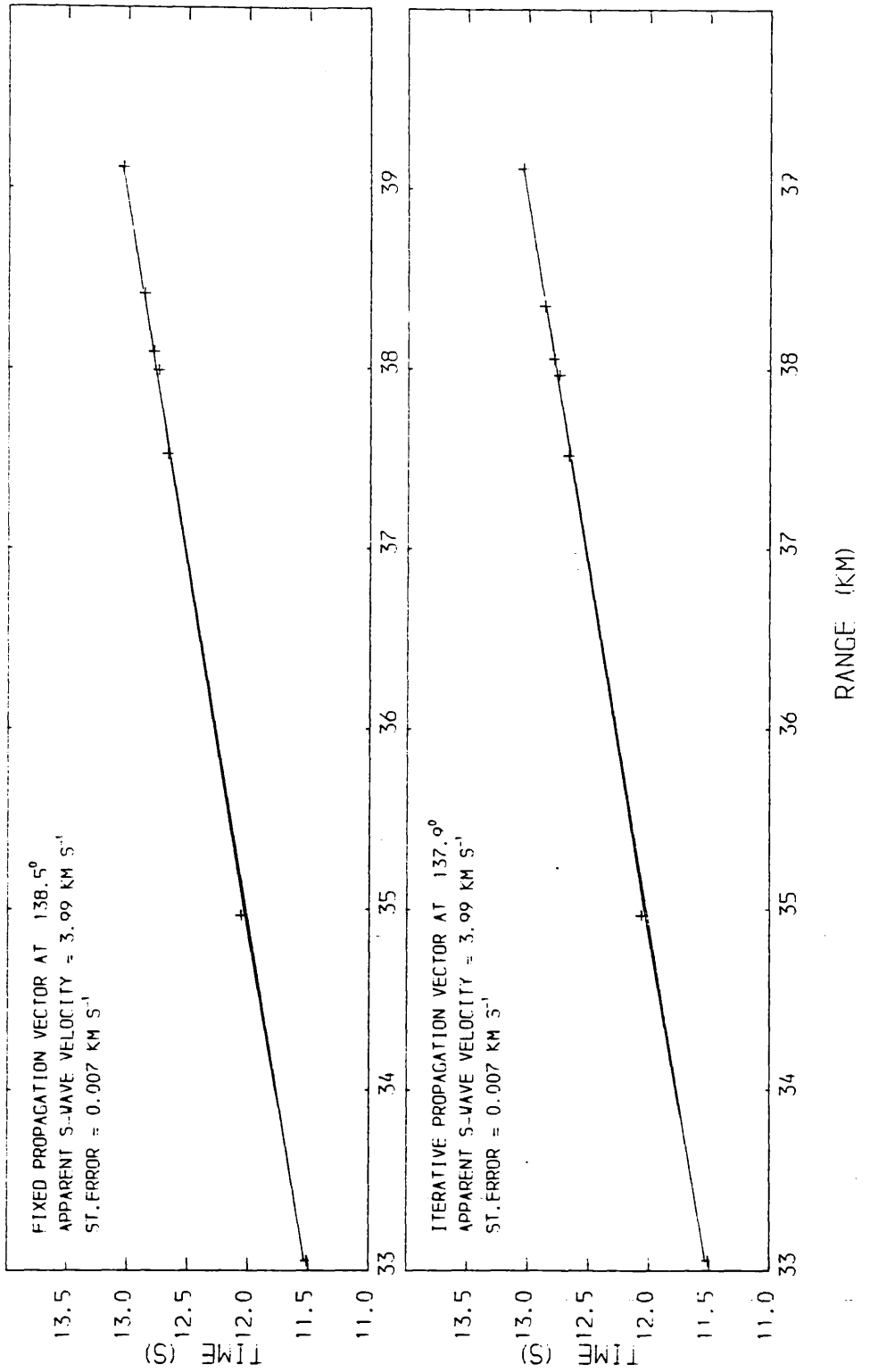


Appendix 4.32

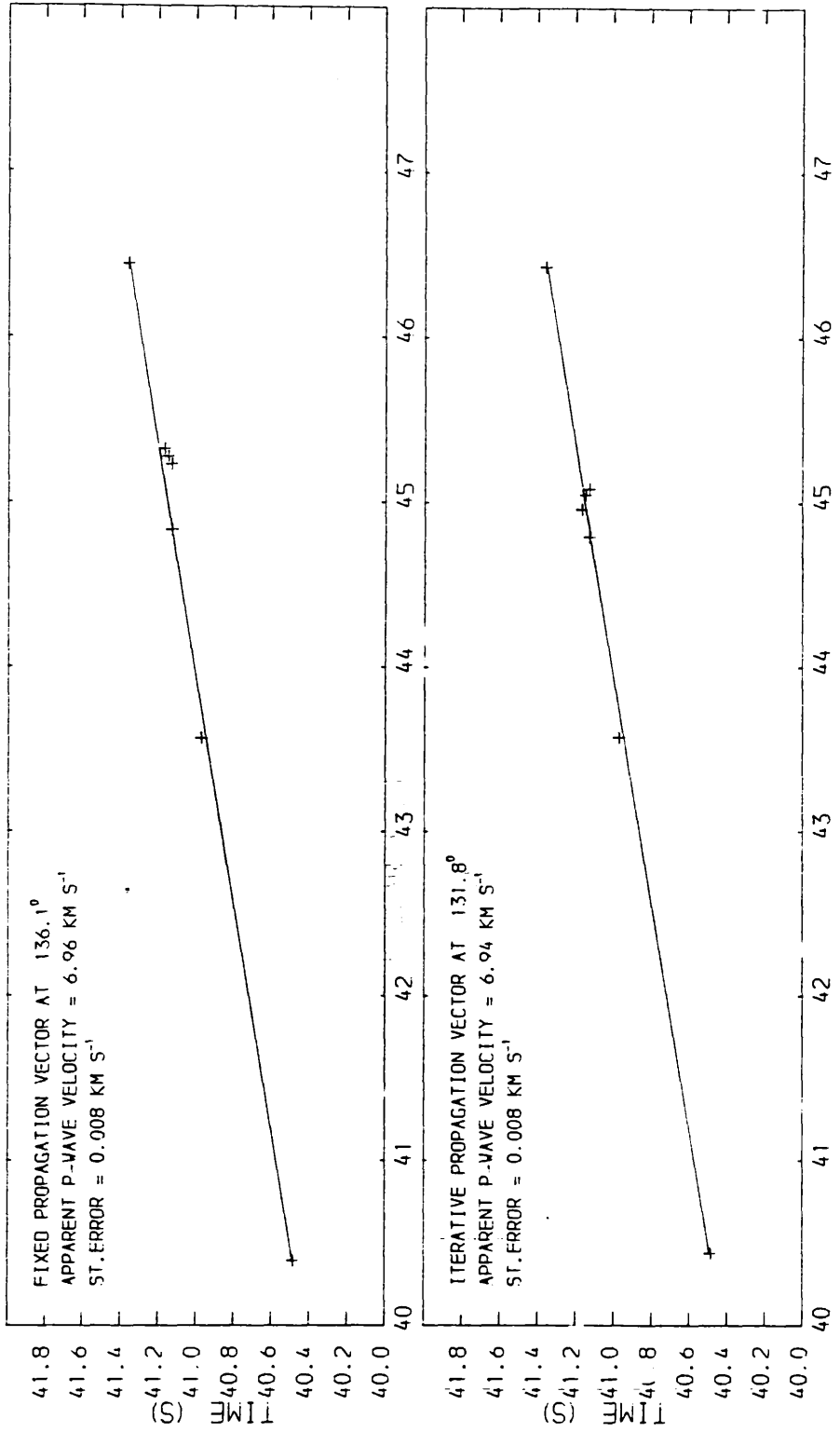


Appendix 4.33

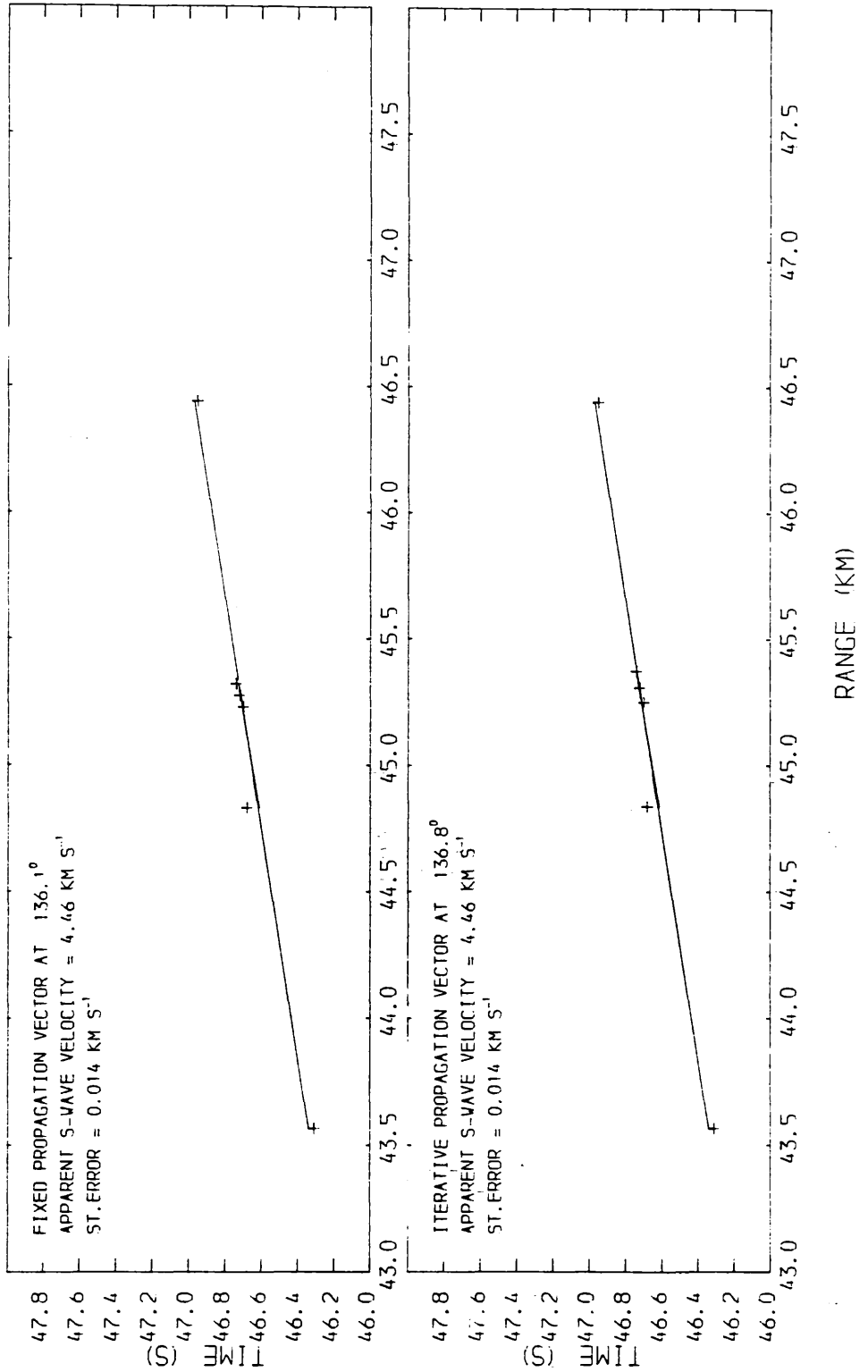
TAMS LOUP QUARRY INTO BTN ARRAY 15/2/77 (TIMED EVENT)



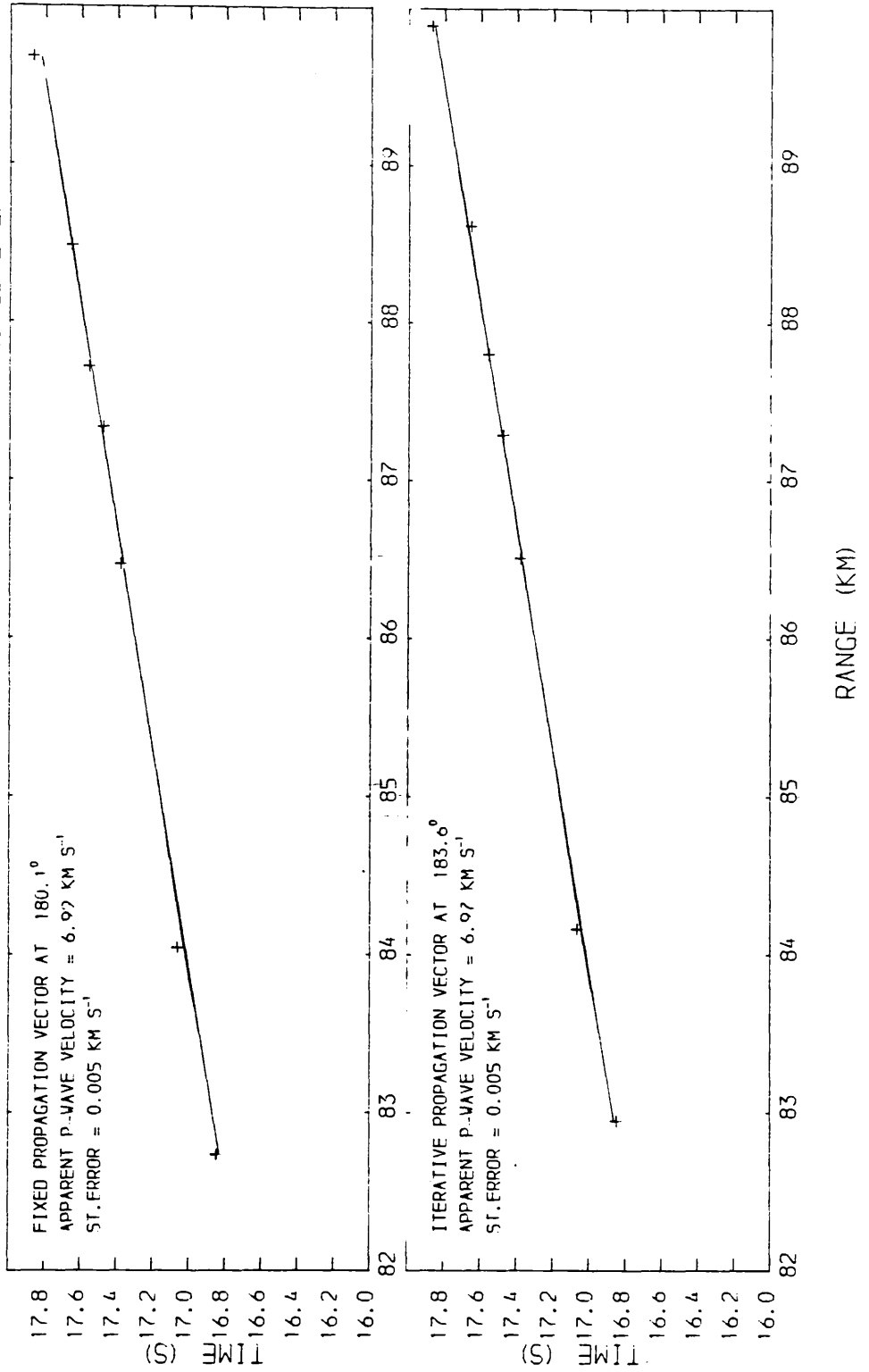
CAIRNYHILL QUARRY INTO BTN ARRAY 14/3/77 (DETECTED EVENT)



CAIRNYHILL QUARRY INTO BTN ARRAY 14/3/77 (DETECTED EVENT)



CRUICKS QUARRY INTO BTN ARRAY 21/2/77 (DETECTED EVENT)



APPENDIX 5

HILLHOUSE QUARRY EAST

SITE NAME	TR TIME	ST ERROR	MODEL TIME	RESIDUAL	PHASE
CROOKS FM	0.742	0.011	0.890	-0.148	A _S
FORTACRES FM	1.379	0.011	1.380	-0.001	"
STAFFLER RES	1.642	0.011	1.654	-0.012	"
DONKEY SITE	1.953	0.007	1.944	0.009	"
HILLHOUSE FM	2.217	0.011	2.216	0.001	A _S R
GATEHEAD FM	2.390	0.011	2.436	-0.046	"
DALLARS FM	2.517	0.011	2.531	-0.014	"
AIRD FM	2.717	0.011	2.712	0.005	"
OVERLANDS FM	2.913	0.011	2.911	0.002	"
DRUMDOCH FM	3.074	0.011	3.051	0.023	"
MILRIC FM	3.215	0.011	3.241	-0.026	"
SORNHILL FM	3.454	0.011	3.423	0.031	"
CAIRNHILL FM	3.756	0.006	3.764	-0.008	A ₀
HARDHILL SITE (1C)	4.355	0.010	4.373	-0.018	"
2C	4.656	0.007	4.652	0.004	"
ALLANTON Q (3C)	5.010	0.010	4.977	0.033	"
8A	5.838	0.006	5.820	0.018	"
2A	6.081	0.006	6.061	0.020	"
3A	6.237	0.010	6.220	0.017	"
4A	6.489	0.006	6.490	-0.001	"
5A	6.518	0.006	6.509	0.009	"
6A	7.147	0.006	7.158	-0.011	"
1D	7.488	0.005	7.598	-0.110	"
2D	8.051	0.005	8.086	-0.035	A ₁
3D	9.061	0.030	9.091	-0.030	"
1E	10.129	0.007	10.105	0.024	"
4E	11.575	0.012	11.449	0.126	"
5E	12.014	0.004	11.838	0.288	"
6E	12.094	0.040	12.043	0.051	"
KIRKLAWHILL FM	12.691	0.004	12.641	0.050	"
S4 BTN	12.859	0.014	12.854	0.005	"
S3 BTN	13.053	0.014	13.041	0.012	"
N2 BTN	13.247	0.014	13.125	0.132	"
S3 BTN	13.189	0.014	13.158	0.031	"
N2 BTN	13.305	0.014	13.207	0.102	"
S1 BTN	13.305	0.014	13.273	0.032	"
N4 BTN	13.480	0.014	13.482	-0.002	"

DUNDOFF QUARRY WEST

SITE NAME	TR TIME	ST ERROR	MODEL TIME	RESIDUAL	PHASE
1D	0.648	0.006	0.670	-0.022	AS
ARA BURN SITE	1.006	0.060	1.135	-0.074	"
6C	1.481	0.006	1.503	-0.022	ASR
ALLANTON Q SITE	3.290	0.008	3.287	0.003	"
2C	3.699	0.008	3.695	0.004	"
1C	4.105	0.008	4.078	0.027	"

DUNDOFF QUARRY EAST

SITE NAME	TR TIME	ST ERROR	MODEL TIME	RESIDUAL	PHASE
MCIRSLAND FM 2	0.329	0.007	0.344	-0.015	AS
" " 3	0.395	0.007	0.402	-0.007	"
2D	0.889	0.006	0.946	-0.057	"
BOGSIDE FM 1	0.952	0.007	0.950	-0.002	"
" " 2	0.977	0.007	0.990	-0.013	"
" " 3	1.003	0.007	1.016	-0.013	"
DARNFILLAN FM 1	1.398	0.007	1.398	0.000	"
" " 2	1.419	0.007	1.412	0.007	"
" " 3	1.431	0.007	1.426	0.005	"
3D	1.518	0.006	1.529	-0.011	"
GREENHILL FM 1	1.591	0.007	1.590	0.001	"
" " 2	1.610	0.007	1.635	-0.025	"
" " 2	1.663	0.007	1.677	-0.014	"
LANGSIDE FM 1	1.878	0.007	1.874	0.004	"
" " 2	1.923	0.007	1.915	0.008	"
" " 3	1.953	0.007	1.967	-0.016	"
1E	2.772	0.008	2.768	-0.016	ASR
3E	4.098	0.010	4.093	0.005	AO
4E	4.417	0.015	4.410	0.007	"
6E	5.104	0.008	5.131	-0.027	"

CAIRNGRYFFE-CLOBURN QUARRIES WEST

SITE NAME	TR TIME	ST ERROR	MODEL TIME	RESIDUAL	PHASE
2E	0.665	0.008	0.769	-0.104	AS
1E	0.728	0.008	0.873	-0.145	"
SANDILANDS FM	1.161	0.005	1.245	-0.084	"
LANGSIDE FM 3	1.547	0.005	1.541	0.006	"
" " 2	1.574	0.005	1.558	0.016	"
3D	2.026	0.006	2.069	-0.041	"
MCIRSLAND FM 4	3.018	0.004	3.008	0.012	"
" " 5	3.030	0.004	3.023	0.007	"

DUNDUFF Q SITE	3.380	0.005	3.347	0.033	A ₀
1D	3.586	0.006	3.711	-0.125	"
1A	5.110	0.005	3.081	0.029	"
3A	5.207	0.005	5.206	0.001	"
2A	5.275	0.005	5.240	0.035	"
8A	5.430	0.005	5.385	0.045	"
ALLANTON Q SITE	6.237	0.006	6.254	-0.017	"
2C	6.574	0.008	6.622	-0.048	"
1C	7.010	0.012	7.009	0.001	"

CAIRNGRYFFE-CLOBURN QUARRIES EAST

SITE NAME	TR TIME	ST ERROR	MODEL TIME	RESIDUAL	PHASE
3E	1.094	0.010	1.088	0.008	A _S
4E	1.500	0.008	1.512	-0.012	"
6E	2.364	0.008	2.462	-0.098	"
N1 BTN	3.207	0.011	3.179	0.028	A ₀
S4 BTN	3.490	0.011	3.492	-0.002	"
N3 BTN	3.613	0.011	3.574	0.039	"
S3 BTN	3.613	0.011	3.595	0.018	"
S2 BTN	3.660	0.011	3.665	-0.005	"
S1 BTN	3.716	0.011	3.710	0.006	"
N4 BTN	4.009	0.011	3.980	0.029	"


```

5  FORMAT(10X,I4,3F10.3)
   X(I)-X(I)-X(NS)
   Y(I)-Y(I)-Y(NS)
   Z(I)-Z(I)-Z(NS)
6  CONTINUE
   WRITE (6,212)
212 FORMAT (/10X,'FINAL OUTPUT DESCRIPTION'//
1/10X,'T OBS = OBSERVED TRAVEL TIME (IN SECS.)',
2/10X,'T CAL = CALCULATED TRAVEL TIME (IN SECS.)',
3/10X,'E(I) = CALC.TIME - OBS.TIME (IN SECS.)',
4/10X,'ZT = TRAVEL TIME IN REFRACTOR (VELA)',
5/10X,'RANGE = SOURCE SEISMOMETER DISTANCE (IN KMS.)',
6/10X,'VA = VELOCITY ACROSS ARRAY (KMS/S)',
7/10X,'AV = AVERAGE VELOCITY FROM SOURCE (IF SUBF <> 0)',
8/10X,'AV/VA = VELOCITY RATIO',
9/10X,'AZIMUTH = PROPAGATION DIRECTION OF SOURCE VECTOR TO STATION')
C
C   Read in title and travel time data for each dataset.
C
DO 13 NNN=1,NUMBR
READ(5,12) IPS,TITLE
12  FORMAT(I3,20A4)
WRITE(6,121) NNN,TITLE
121 FORMAT(//,110(' '),/10X,'DATASET NUMBER ',I3,5X,20A4,./
1110(' '),//)
IF (IPS.EQ.0) WRITE (6,122)
IF (IPS.EQ.1) WRITE (6,123)
122 FORMAT (10X,'P - WAVE DATA',/)
123 FORMAT (10X,'S - WAVE DATA',/)
DO 3 I=1,NS
T(I)=0.
K(I)=0.
3  CONTINUE
VEL1=4.0
VELA=6.0
READ (5,16) QX,QY,SVEL.
16  FORMAT(3F8.3)
WRITE(6,175)QX,QY
175 FORMAT(2X,'SOURCE COORDINATES',5X,'X',7X,'Y',/21X,2F8.3)
QQX=QX
QQY=QY
IF (SVEL.GT.0.0) VEL1=SVEL.
IF (IPS.EQ.0) GO TO 124
VEL1=VEL1/VPVS
VELA=VELA/VPVS
124 QX=CPX-QX
   QY=CPY-QY
   DELTA=SQRT(QX*QX+QY*QY)
   THETA=ASIN(QX/DELTA)
   THEID=THETA*RTOD
   IF(QY)704,705,705
704 THEID=180.-THEID
705 IF(THEID)706,707,707
706 THEID=THEID+160.
707 THEID=THEID/RTOD
   WRITE(6,14)DELTA,THEID,VEL1,VELA
14  FORMAT(/12X,'RANGE VECTOR SURFACE VA',/11X,
1' KM, DRG REES',
2' KM/S KM/S',/10X,4F8.2,RX,' ESTIMATE')
   READ(5,7)NN,SUBF,SCAF
7  FORMAT(I3,2F8.3)
DO 8 N=1,NN
READ(5,91) T,T(I)
91  FORMAT(I3,F8.3)
S(I)=X(I)*X(I)+Y(I)*Y(I)+DELTA*DELTA
K(I)=1
T(I)=T(I)/SCAF-SUBF
8  CONTINUE
C
C   First loop with propagation vector fixed, then made variable.
C
700 LP=0
   IF (KAZ.EQ.0) KK=?
   IF (KAZ.GT.0) KK=1
   IF(KAZ)999,701,702
701  WRITE(6,173)
   VELA=6.0
   IF (IPS.EQ.0) GO TO 27
   VELA=VELA/VPVS
GO TO 27
702  WRITE(6,174)
173  FORMAT(/5X,'ADJUSTABLE PROPAGATION VECTOR',/)
174  FORMAT(/5X,'FIXED PROPAGATION VECTOR',/)
   WRITE (6,18)
18  FORMAT(/,14X,'THETA',5X,'DTHETA',.6X,'VELA',.6X,'DVEL',.6X,'TCP',/)
27  LP=LP+1
708  IF(KAZ)999,709,710
709  A=0.
   B=0.
   C=0.
   D=0.

```

```

E=0.
F=0.
G=0.
H=0.
RR=VEL1*VEL1/VELA/VELA
Q=RR*RR/8.
V=(1.-RR/2.)*(1.+RR/4.+Q)/VEL1
RR=RR*(1.+RR/2.+3.*Q)/VEL1/VELA

DO 25 I=1,NS
IF(K(I))25,25,26
26 A4=SQRT(S(1))+2.*DELTA*(Y(I)*SIN(THETA)+Y(I)*COS(THETA))
A5=2.*DELTA*(X(I)*COS(THETA)-Y(I)*SIN(THETA))
A6=Z(I)*V
A7=Z(I)*HR
A8=-T(I)-(DELTA-A4)/VELA+A6
A5=A5/VELA/A4/2.
A4=(DELTA-A4)/VELA/VELA+A7
A=A+A5*A6
B=B+A5*A5
C=C+A5*A4
D=D+A4*A6
E=E+A6
F=F+A4*A4
G=G+A5
H=H+A4

25 CONTINUE

C
A6=C*G-N*H
A7=C*C-H*B
A8=E*B-A*G
A4=(D*B-A*C)*A6-A7*A8
A5=(C*C-F*B)*A6-A7*A7
DVEL=A4/A5
TCP=(A8-A7*DVEL)/A6
DTHET=(A+C*DVEL+G*TCP)/B
IF(DVEL*DVEL-0.25)34,34,331
331 IF(DVEL)332,332,333
332 DVEL=0.5
GO TO 34
333 DVEL=0.5
34 IF(DTHET*DTHET-0.04)344,344,341
341 IF(DTHET)342,342,343
342 DTHET=-0.2
GO TO 344
343 DTHET=0.2
344 IF(KAZ)999,346,345

345 DTHET=0.
346 THETA=THETA+DTHET
VELA=VELA+DVEL
WRITE (6,15) THETA, DTHET, VELA, DVEL, TCP
35 FORMAT(10X,5F10.3)
IF(DVEL*DVEL-0.000025)41,41,27
41 IF(DTHET*DTHET-0.000004)42,42,27
42 THETA=THETA*RTOD
IF(THETD)421,501,422
421 THETD=THETD+360.
GO TO 501
422 IF(THETD-360.)501,423,423
423 THETD=THETD-360.

C
501 IF (KAZ.EQ.0) GO TO 500
THET1=THETD
VELA1=VELA
TCP1=TCP
GO TO 424
500 THET2=THETD
VELA2=VELA
TCP2=TCP
424 WRITE(6,44)THETD,VELA,TCP
44 FORMAT(/,2X,'FINALLY -',F7.2,' DEGREES,',4X,F6.3,' KM/S.',4X,
1F8.3,' SECONDS AT CROSS OVER',/)
SGAR=0
WRITE(6,61)
61 FORMAT(/10X,'PIT',5X,'T OBS',5X,'T CAL',6X,'E(T)',7X,'ZT',7X,
1'RANGE',8X,'VA',8X,'AV',6X,'AV/VA AZIMUTH',/)
DS=DELTA*SIN(THETA)
DC=DELTA*COS(THETA)
TI=DELTA/VELA-TCP
V=SQRT(A4*(1./VEL1/VEL1-1./VELA/VELA))
IF (VEL1.GE.VELA) WRITE (6,126)
126 FORMAT (10X,'VELA < VFL1',/)

C
KD=0
DO 55 I=1,NS
IF(K(I))55,55,54
54 KD=KD+1
A=X(I)+DS
B=Y(I)+DC
R=SQRT(A*A+B*B)
C=DELTA-R
D=Z(I)*V
E=TCP+D
F=E-C/VELA

```



```

C      CSPACE (0.03,1.20,0.01,0.85)
C      CALL CTRMAG (15)
C      CALL PLACE (25,4)
C      CALL TYPECS (TITLE,80)
C      CALL PLACE (8,14)
C      CALL CTRORI (1.0)
C      CALL TYPECS ('TIME (S)',8)
C      CALL CTRORI (0.0)
C      CALL PLACE (8,28)
C      CALL CTRORI (1.0)
C      CALL TYPECS ('TIME (S)',8)
C      CALL CTRORI (0.0)
C      CALL PLACE (49,36)
C      CALL TYPECS ('RANGE (KM)',10)
C      CALL CTRMAG (10)

C      CALL PSPACE (0.19,1.20,0.47,0.76)
C      CALL MAP (RMIN,RMAX,TMN,TMAX)
C      CALL BORDER
C      CALL SCALES
C      CALL POSITN (RMIN+X/30,TMAX-Y/10)
C      CALL TYPECS ('FIXED PROPAGATION VECTOR AT ',28)
C      CALL TYPEPF (THEI1,1)
C      CALL SUPFIX
C      CALL TYPECS ('0',1)
C      CALL NORMAL
C      CALL POSITN (RMIN+X/30,TMAX-Y/10)
C      CALL HLINFD (3)
C      CALL TYPECS ('APPARENT ',9)
C      IF (IPS.EQ.0) CALL TYPECS ('P-WAVE ',7)
C      IF (IPS.EQ.1) CALL TYPECS ('S-WAVE ',7)
C      CALL TYPECS ('VELOCITY ',10)
C      CALL TYPEPF (VELA1,2)
C      CALL SUPFIX (' KM S',5)
C      CALL TYPECS ('-1',2)
C      CALL NORMAL
C      CALL POSITN (RMIN+X/30,TMAX-Y/10)
C      CALL HLINFD (6)
C      CALL TYPECS ('ST.ERROR = ',10)
C      CALL TYPEPF (STERR,3)
C      CALL SUPFIX (' KM S',5)
C      CALL TYPECS ('-1',2)
C      CALL NORMAL
C      CALL POSITN (RMIN+X/30,TMAX-Y/10)
C      CALL HLINFD (6)
C      CALL TYPECS ('ST.ERROR = ',10)
C      CALL TYPEPF (STERR,3)
C      CALL SUPFIX (' KM S',5)
C      CALL TYPECS ('-1',2)
C      CALL NORMAL
C      CALL CTRMAG (15)

C      CALL PSPLOT (R2,T,1,I,43)
C      CALL PTMAG (R2,F2,1,I,-2)
C      CALL CTRMAG (10)

C      CALL PSPLOT (R1,T,1,I,43)
C      CALL PTMAG (R1,F1,1,I,-2)
C      CALL CTRMAG (10)

C      Define lower graph space and plot annotation.
C      CALL PSPACE (0.19,1.20,0.15,0.44)
C      CALL MAP (RMIN,RMAX,TMN,TMAX)
C      CALL BORDER
C      CALL SCALES
C      CALL POSITN (RMIN+X/30,TMAX-Y/10)
C      CALL TYPECS ('ITERATIVE PROPAGATION VECTOR AT ',32)
C      CALL TYPEPF (THEI2,1)
C      CALL SUPFIX
C      CALL TYPECS ('0',1)
C      CALL NORMAL
C      CALL POSITN (RMIN+X/30,TMAX-Y/10)
C      CALL HLINFD (3)
C      CALL TYPECS ('APPARENT ',9)
C      IF (IPS.EQ.0) CALL TYPECS ('P-WAVE ',7)
C      IF (IPS.EQ.1) CALL TYPECS ('S-WAVE ',7)
C      CALL TYPECS ('VELOCITY ',10)
C      CALL TYPEPF (VELA2,2)
C      CALL SUPFIX (' KM S',5)
C      CALL TYPECS ('-1',2)
C      CALL NORMAL
C      CALL POSITN (RMIN+X/30,TMAX-Y/10)
C      CALL HLINFD (6)
C      CALL TYPECS ('ST.ERROR = ',10)
C      CALL TYPEPF (STERR,3)
C      CALL SUPFIX (' KM S',5)
C      CALL TYPECS ('-1',2)
C      CALL NORMAL
C      CALL CTRMAG (15)

C      Plot out travel time data as + again, and plot the final calculated
C      times for the iterated vector as a straight line.
C      CALL PSPLOT (R2,T,1,I,43)
C      CALL PTMAG (R2,F2,1,I,-2)
C      CALL CTRMAG (10)

```

C

CALL FRAME
RETURN
END


```

C Convert data into self-centring plotting coordinates and
C plot out each trace in turn
C
C 101 IT=IT-1
C
C 102 DO 200 I=1,J
A=FLOAT(IA)
DO 300 N=1,IT
IF (IGAIN.EQ.1) GO TO 103
X(N)=FLOAT(IX(N,I)+IA)
GO TO 104
103 X(N)=FLOAT(IX(N,I)/100+IA)
104 T(N)=FLOAT(N)
300 CONTINUE
CALL PTPLOT (T,X,1,IT,-2)
IA=IA+800
200 CONTINUE
C
C Write out plot details ( or error message )
C
C WRITE (6,24) TITLE,J,IT,IGAIN
GO TO 990
995 WRITE (6,25)
GO TO 990
996 WRITE (6,21)
GO TO 990
997 WRITE (6,22)
GO TO 990
998 WRITE (6,23)
C
C 990 CALL FRAME
GO TO 1
C
C Formats
C
20 FORMAT (3I3.16.10A4)
4 FORMAT (4I6)
5 FORMAT (5I6)
6 FORMAT (6I6)
7 FORMAT (7I6)
8 FORMAT (8I6)
9 FORMAT (9I6)
10 FORMAT (10I6)
11 FORMAT (11I6)
12 FORMAT (12I6)
21 FORMAT (/ ' *** DATA FILE INPUT CHANNEL NO. HAS NOT BEEN SPECIFIED
1 ***')
22 FORMAT (/ ' *** J VALUE IS OUTWITH THE CURRENT ALLOWABLE RANGE ***')
23 FORMAT (/ ' *** ERROR IN DIGITAL DATA READ STATEMENT ***')
24 FORMAT (/ ' NAME OF DATA FILE =',10A4, /
1' NUMBER OF CHANNELS =',18, / ' NUMBER OF SAMPLES READ =',18, /
2' IGAIN [ 1:1, OR 100:1 ] =',18, /)
25 FORMAT (/ ' *** SAMPLE NUMBER EXCEEDS DATA-ARRAY SIZE ***')
C
999 CALL GREN
STOP
END

```


MPLOTT=0 PLOTTING PARAMETERS ARE USER-SUPPLIED
 =1 SET INTERNALLY FOR HP TERMINAL
 =2 " " " TEKTRONICS TERMINAL
 =3 " " " ADM3A GRAPHICS TERMINAL
 =4 " " " A4 PLOTTING

THE PLOTTING AXES FOR ONE DATASET CAN BE VARIED BY
 SUPPLYING CARD-2 (NPLOT) TIMES AFTER CARD-8.

CARD-2 PLOT AXES AND PAPER SPACE PARAMETERS
 XA, XB, YA, YD FORMAT 4F10.3
 IE, MPLOT > 0
 XA, XB, YA, YB, PA, PB, PC, PD FORMAT 4F10.3, 2X, #F7.4
 XA, XR IS THE RANGE AXIS: YA, YR IS THE TIME AXIS.

CARD-3 CONTROL PARAMETERS
 NFIL, IROT, ISUB, NO, IVAR, NPARA, ISPECT, NNM, NCROSS, LNM,
 INS, MISS, CR, VEL, TIMM FORMAT(12I5, 3F5.2)

NFIL NO. OF FILES IN A DATA SET
 IROT=1 ROTATES MAP AXES BY 90 DEGREE
 ISUB=0 PRODUCES UNFILTERED SECTION
 ISUB=1 CALLS SUBROUTINES=BOX
 NO > 0 NO DIGITAL DATA IS READ IN,
 OMITT CARDS 7 - 9.
 NO = 1 GIVES FREQUENCY CHARACTERISTICS OF FILTER
 BY CALLING: FFT.
 NO = 2 GIVES IMPULSE RESPONSE OF FILTER

IVAR=0 STANDARD WIGGLER'S PLOT
 IVAR=1 VARIABLE AREA PLOTTING
 IVAR=2 CONDENSED WAVEFORM PLOTTING
 ISPECT=1 AMPLITUDE SPECTRUM OF SPECIFIED DATA WINDOW
 ISPECT=2 PHASE SPECTRUM OF SPECIFIED DATA WINDOW
 ISPECT=3 POWER SPECTRUM OF SPECIFIED DATA WINDOW
 (FOR NO > 0 SPECTRA OF A SINGLE SPIKE IS CALCULATED)
 NNM = TIME INTERVAL(IN SAMPLES) BETWEEN TWO PEAKS
 OF AUTOCORRELATION
 NCROSS=0 OMIT CROSS-CORRELATION SECTION
 NCROSS=1 CROSSCORRELATION WITH CHIRP FILTER OF
 DEFINED BANDWIDTH
 NCROSS=3 CROSSCORRELATION WITH A TRACE.(CONTINUOUSLY UPDATED)

NCROSS=2 CROSSCORRELATION WITH AVERAGE WAVELET
 GENERATED FROM FIVE PRECEDING TRACES
 (CONTINUOUSLY UPDATED)
 NCROSS=4 DECONVOLUTION WITH SPIKING FILTER
 NCROSS=5 DECONVOLUTION WITH WVPRED
 NCROSS=6 DECONVOLUTION WITH WVPRED FILTER
 (4 TO 6 GENERATES FILTER FROM EACH TRACE)
 NCROSS=7 DECONVOLUTION WITH SPIKING FILTER
 NCROSS=8 DECONVOLUTION WITH WVPRED
 NCROSS=9 DECONVOLUTION WITH WVPRED
 (7 TO 9 GENERATE FILTER(ONCE)FROM AVERAGE
 WAVELET AND TRACES ARE CONVOLVED WITH IT)
 LNM = LENGTH OF DECON FILTERS
 INS = ONSET REDUCED TIME(IN SAMPLES)
 (SUPPLIED IN CASE OF NCROSS=2 OR 7 TO 9. IT IS
 INFORMATION OF THE INITIAL TRACE WITH REFERENCE TO
 WHICH THE ONSETS OF LATER TRACES ARE FOUND AUTO-
 MATICALLY).
 MISS= NO. OF INITIAL TRACES FROM WHICH AVERAGE WAVELET
 IS TO BE GENERATED.
 CR = RATIO OF FIRST AND SECOND PEAKS OF
 AUTOCORRELATION
 VFL = REDUCTION VELOCITY(KM/S)
 TIMM= TIME GATE FOR DATA PLOTTING
 (OR Y-AXIS BOUNDS FOR OTHER CALCULATIONS)
 NPARA = 1 MEANS CHANGE OF MAP PARAMETERS IN THE NEXT FRAME

CARD-4 SHOT NAME OR TITLE OF PLOTS.
 TITLE FORMAT 12A4

CARD-5 THIS IS SUPPLIED ONLY IF ISUB=1
 INPUT REFERENCE NOS. OF FILTER SUBROUTINES TO BE CALLED
 FORMAT 10I5

FILTERS
 MS(I) = 1 :BP1 CAUSAL TAPERED ROBINSON BP FILTER
 MS(I) = 2 :BP2 MODIFIED ROBINSON BP FILTER
 MS(I) = 3 :BP3 HANNING BP FILTER
 MS(I) = 4 :HIPASS LOWCUT FILTER
 MS(I) = 5 :LOPASS HIGUT FILTER
 MS(I) = 6 :AUTOCORR AUTOCORRELATION FN
 MS(I) = 7 :CROSS CROSSCORRELATION FN

MS(I)= 8 :PROPER SWAPS DATA BETWEEN ARRAYS
 MS(I)- 9 :FASTFT ROBINSON FAST FOURIER TRANSFORM
 MS(I)=10 :WVPRD WAVELET PREDICTION FILTER
 MS(I)-11 :RV3 REVERSES CONTENTS OF AN ARRAY
 MS(I)=12 :BPH CAUSAL HANNING BP FILTER
 MS(I)-13 :BP2 STD ROBINSON BP FILTER
 MS(I)=14 :BP1 STD CAUSAL ROBINSON BP FILTER
 MS(I)=15 :FASTFT SMOOTHED ROBINSON FFT

NOTE - MORE THAN ONE FILTER CAN BE CALLED DURING A RUN, BUT THESE
 MUST BE SEPARATED BY A CALL OF FILTER 8 (SUBROUTINE PROPER),
 BEFORE EACH SUBSEQUENT FILTER.
 MAXIMUM TOTAL NUMBER OF FILTER CALLS IS SET AT 5.

CARD-6 BANDPASS FILTER PARAMETERS
 LP, DT, FL, FH, NG FORMAT (I5,3F10.3,I5)

LP= LENGTH OF FILTER(IN SAMPLES)
 DT= SAMPLE INTERVAL(IN SECONDS)
 FL= LOWER FREQUENCY(HZ)
 FH= HIGHER FREQUENCY(HZ)
 NG=1 CONVOLUTION WITH TRACE ONCE,
 (NG>1 MEANS CONV THAT MANY TIMES)

CARD-7 NTXPTS, LU
 NTXPTS > 0 FIELD TIME-DISTANCE DATA MAY BE READ IN
 AND PLOTTED WITH ERROR BARS OVER DIGITAL PLOTS
 LU = INTERNAL CHANNEL NUMBER FOR T-X READ INPUT.
 IF LU = 3, RAYPLT DATA IS READ IN
 NTXPTS CAN THEN TAKE ANY NON-ZERO VALUE

FOR LU.NE.3, NTXPTS GIVES THE NUMBER OF
 T-X POINTS TO BE READ IN (ON CHANNEL 'LU').

FOLLOWING NTXPTS-CARDS WILL BE READ IN:
 (LU.NE.3)

RANGE, DR, TIME, DT FORMAT (4F8.3)

CARD-8 MARS, IFILE, ISPEED, IPOL(J), J=1,12
 FORMAT I2, I3, I3I2

MARS =0 MEANS GEOSTORE DATA. - 9 CH (INT.CL, 7-SEISM, MSF)
 =1 MEANS MARS DATA FILE OF 4 TRACES.
 =2 MEANS MARS DATA FILE OF 5 TRACES.
 =4 GLASGOW FM SYSTEM. (4 CH SEISM)
 =5 GEOSTORE SYSTEM (5 CH)
 =7 " " (7 CH)
 =9 " " (9 CH)
 =10 " " (10 CH)
 =11 " " (11 CH)
 =12 " " (12 CH)

INPUT DATA FORMAT:
 MARS =1,2 FORMAT (5X,4/5F15.6) - LEICESTER SYSTEM
 OTHERWISE FORMAT (N.I6) - G.S.U. SYSTEM

IFILE =? INTERNAL CHANNEL NUMBER ASSIGNED TO THIS DATA
 FILE INPUT. REQUIRES AN EXTERNAL 'ASSIGN_FILE'
 STATEMENT. MAXIMUM NUMBER OF 'AFI'S = 20, FOR
 INTERACTIVE RUNNING, AND = 40, FOR BATCH JOBS.
 ISPEED=0 MEANS NORMAL RECORDING SPEED IN THE FIELD.
 =1 MEANS HALF RECORDING SPEED.
 IPOL(J) = 0 NORMAL. POLARITY ON JTH CHANNEL
 IPOL(J) = 1 REVERSED POLARITY EXISTED ON JTH SEISMOMETER
 CHANNEL (TRACE WILL BE INVERTED)

CARD-9 POSITN(J), J=1,12 FORMAT 12F7.3
 POSITN(J) GIVES THE PLOTTING POSITION (KM) OF THE JTH
 TRACE IN A FILE.

CARD-10 ISAMP, RGAIN, DIM, AMPT, LO, IR, IMP
 FORMAT I5,3F8.5,3I2

ISAMP = NUMBER OF SAMPLES (+/-) WHICH LINK THE START OF THE
 TRACE TO A SHOT ORIGIN TIME.
 RGAIN = FACTOR WHICH GIVES AMPLIFICATION TO A TRACE. IF=0.00,
 GAIN IS CALCULATED INTERNALLY, OTHERWISE RGAIN MUST
 BE USER - SUPPLIED.
 DIM > 0. OVERRIDES THE VALUE OF YA (CARD-2).
 CAN BE USED WITH TIMM (CARD-3) TO SPECIFY
 DIFFERENT Y-AXES BOUNDS FROM YA, YB (CARD-2)
 ALSO, WITH SPECTRAL ANALYSIS OF REAL DATA (IE
 ISPECT.GT.0.AND.NO.EQ.0), IS USED TO DEDINE THE


```

C   FRAME SET UP FOR ADM3A GRAPHICS TERMINALS
C   9577 PD=1.1
      PD=0.8
      GO TO 9570
C   FRAME SET UP FOR B4 PLOTTING
C   9578 PD=1.25
      PD=0.80
C   9570 PA=0.16
      PC=0.16
      READ (5,95569) XA, XD, YA, YH
      9569 FORMAT (4F10.3)
      GO TO 9568
      9574 READ(5,1)XA, XD, YA, YH, PA, PH, PC, PD
      1 FORMAT(4F10.3,2X,4F7.4)
      9568 KON=KIT*1
      WIND=YB-YA
C   INPUT CONTROL PARAMETERS.
C   IF INDEX (KIT) AND REQUIRED NO. OF PLOTS (NPLOT) > 0, SKIP INPUT
C   PARAMETERS AND MOVE TO PLOTTING FRAME SETUP.
C   IF(KIT.GT.0.AND.(LHM1.GT.0)GO TO 899
      53 READ(5,2)NFIL, IHOT, ISUB, NO, IVAR, NPARA, ISPECT, NNM, NCROSS
      2 FORMAT(12I5,3F5.2)
      READ (5,3) TITLE
      WRITE (6,3) TITLE
      3 FORMAT (12A1)
      IF(NO.EQ.0)GO TO 514
      DO 513 J1=2,7
      513 POSIT(J1)=0.
      POSIT(1)=1.0
      KF=0
      514 ISN=-1
      HN=11
      NNM2=ABS(YA*100.)+NNM-1
      WRITE(6,9571)NFIL
      9571 FORMAT(30X,'NO.OF FILES IN A DATA SET=',I5)
      IF(LPLAT.LE.4)GO TO 898
      LPLAT=1
      898 LRU=ABS(INT(YA*100.))*1
      LR=LRU+INS-1
      IF(LR.GT.20)GO TO 699
      LNR=1
      LARK1=1
      LARK2=25
      GO TO 900
      699 LRR=1.R
      LARK1=LH-20
      LARK2=LH+19
      LTQ=LH*25
      900 DO 5011 I=1,200
      B1(I)=0.
      B2(I)=0.
      B3(I)=0.
      B4(I)=0.
      B5(I)=0.
      5011 NN=0
      JP=0
      899 WRITE(6,95)KON,WIND,VEL
      95 FORMAT(2X,'PLOT NO.=',I3.5X,'WITH TIME WINDOW=',F6.2,'SEC',
      &,' AND REDUCTION VELOCITY=',F6.2)
      WRITE(6,200)
      200 FORMAT(/30X,'TITLE OF THE PLOT')
C   THIS SECTION SETS UP FRAME WITH ANNOTATION.
C   XXA=XA
      XXB=XB
      IF (MPLOT.EQ.4) CALL CTRMAG (10)
      CALL CSPACE(PA-0.15,PB+0.1,PC-0.15,PD+0.1)
      CALL PSPACE(PA,PB,PC,PD)
      IF(KPLOT.NE.0)GO TO 403
      IF(IVAR.GT.0)GO TO 403
      IF(IHOT.GT.0)GO TO 404
      CALL MAP(XXA,XXB,YA,YB)
      GO TO 31
      404 CALL MAP(YA,YB,XXA,XXB)
      GO TO 31
      403 YYA=YA
      YYB=YB
      IF(IHOT.GT.0)GO TO 1404
      CALL MAP(XXA,XXB,YYA,YYB)
      GO TO 31
      1404 CALL MAP(YYA,YYB,XXA,XXB)
      31 IF (KPLOT.GT.0) GO TO 9579
      CALL BORDER
C   9579 IF(KPLOT.EQ.0)GO TO 845

```

```

CALL SECTOR(XXA, XXH, YYA, YYH, PA, PB, PC, PD, LPLAT, IROT)
GO TO 45
845 IF(YA.GE.0.)GO TO 45
CALL POSITN(XXA,0.)
CALL JOIN(XXB,0.)
45 IF(KPLOT.NE.0)GO TO 431
CALL SCALES
GO TO 531
431 IF(LPLAT.GT.1)GO TO 214
C
C PLOT TITLE AND ANY TOP-GRAPH HEADING.
C
531 IF (MPLOT.EQ.0) GO TO 9567
IF (MPLOT.EQ.1) GO TO 9566
IF (MPLOT.EQ.2) GO TO 9565
IF (MPLOT.EQ.3) GO TO 9564
IF (MPLOT.EQ.4) GO TO 9563
9567 CALL PLACE (20,1)
CALL TYPECS (TITLE,48)
CALL PLACE (25,2)
GO TO 9562
9566 CALL PLACE (25,3)
CALL TYPECS (TITLE,48)
CALL PLACE (70,3)
GO TO 9562
9565 CALL PLACE (10,3)
CALL TYPECS (TITLE,48)
CALL PLACE (50,3)
GO TO 9562
9564 CALL PLACE (15,1)
CALL TYPECS (TITLE,48)
CALL PLACE (25,2)
GO TO 9562
9563 CALL CTMAG (15)
CALL PLACE (10,4)
CALL TYPECS (TITLE,48)
CALL PLACE (76,4)
C
9562 IF (ISPECT.EQ.0) GO TO 405
GO TO(406,407,408),ISPECT
406 CALL TYPECS('AMPLITUDE SPECTRUM',18)
WRITE(6,70)
GO TO 36
70 FORMAT(30X,'A M P L I T U D E S P E C T R U M')
407 CALL TYPECS('PHASE SPECTRUM',14)
WRITE(6,71)
71 FORMAT(30X,'P H A S E S P E C T R U M')

```

```

GO TO 36
408 CALL TYPECS('POWER SPECTRUM',14)
WRITE(6,72)
72 FORMAT(30X,'P O W E R S P E C T R U M')
GO TO 36
405 IF(IVAR.EQ.1)GO TO 5252
IF(IVAR.EQ.2)GO TO 5253
IF(NO.EQ.2)GO TO 4035
IF(VEL.GT.0.)GO TO 336
CALL TYPECS('ABSOLUTE TIME SECTION',21)
WRITE(6,774)
774 FORMAT(30X,'ABSOLUTE TIME SECTION')
GO TO 36
336 WRITE(6,75)
75 FORMAT(30X,'REDUCED TIME SECTION')
CALL TYPECS ('REDUCED TIME SECTION',20)
GO TO 36
5252 CALL TYPECS('VARIABLE AREA SECTION',21)
WRITE(6,76)
76 FORMAT(30X,'VARIABLE AREA SECTION')
GO TO 36
5253 CALL TYPECS('CONDENSED WAVEFORM TIME SECTION',31)
WRITE(6,77)
77 FORMAT(30X,'CONDENSED WAVEFORM TIME SECTION')
GO TO 36
4035 IF(NCROSS.GT.0)GO TO 36
CALL TYPECS('IMPULSE RESPONSE',16)
WRITE(6,78)
78 FORMAT(30X,'IMPULSE RESPONSE OF THE FILTER')
C
C POSITION OF X-AXIS DESCRIPTOR IS ADJUSTED FOR VARIABLE SCALE
C PLOTTING.
C
36 IF (MPLOT.EQ.0) CALL PLACE (25,35)
IF (MPLOT.EQ.1) CALL PLACE (55,37)
IF (MPLOT.EQ.2) CALL PLACE (34,33)
IF (MPLOT.EQ.3) CALL PLACE (25,29)
IF (MPLOT.EQ.4) CALL PLACE (49,38)
IF (IROT.GT.0)GO TO 410
IF (ISPECT.EQ.0) GO TO 409
IF (ISPECT.NE.0.AND.NO.EQ.0)GO TO 409
IF (ISPECT.EQ.2.AND.NO.EQ.1)GO TO 343
GO TO 38
343 CALL TYPECS('PHASE(DEGREES)',14)
GO TO 38
409 IF(NO.EQ.2)GO TO 411
CALL TYPECS('RANGE IN KM',11)

```

```

GO TO 38
411 WRITE(5,4152)
4152 FORMAT(30X,'FILTER RESPONSE')
GO TO 38
410 IF(INSPECT.EQ.0)GO TO 621
CALL TYPECS('FREQUENCY (HZ)',14)
GO TO 38
621 IF(NO.FQ.2)GO TO 655
IF(VEL.GT.0.)GO TO 656
CALL TYPECS('ABSOLUTE TIME(S)',16)
GO TO 38
656 CALL TYPECS('REDUCED TIME(S) T-X/ ',21)
CALL TYPEPF(VEL,1)
GO TO 38
655 IF (MPLT.EQ.2) CALL PLACE (38,33)
CALL TYPECS('TIME(S)',7)
C
C PLOT ANNOTATION FOR Y-AXIS
C
38 CALL PLACE (3,20)
IF (MPLT.EQ.1) CALL PLACE (2,25)
IF (MPLT.EQ.4) CALL PLACE (6,24)
CALL CTRORI (1.0)
IF (IROT.GT.0)GO TO 719
IF (INSPECT.EQ.0)GO TO 414
CALL TYPECS('FREQUENCY(HZ)',13)
GO TO 42
414 IF(NO.EQ.2)GO TO 416
IF(VEL.GT.0.)GO TO 417
CALL TYPECS('ABSOLUTE TIME(S)',16)
GO TO 42
417 CALL CTRORI (0.0)
IF (MPLT.EQ.2) CALL PLACE (3,24)
IF (MPLT.EQ.4) CALL PLACE (7,27)
CALL CTRORI (1.0)
CALL TYPECS('REDUCED TIME(S) T-X/ ',21)
GO TO 42
416 CALL TYPECS('TIME(S)',7)
GO TO 42
719 IF(INSPECT.EQ.0)GO TO 798
IF(INSPECT.EQ.2.AND.NO.EQ.1)GO TO 799
IF(NO.EQ.1.AND.INSPECT.NE.2)GO TO 42
CALL TYPECS('RANGE',5)
GO TO 42
799 CALL TYPECS('PHASE(DEGREES)',14)
GO TO 42

798 IF(NO.EQ.2)GO TO 39
CALL TYPECS('RANGE IN KM',11)
GO TO 42
39 CALL TYPECS('NORM.COEFF',10)
42 CALL CTRORI(0.0)
WRITE(6,6741)
6741 FORMAT(30X,20('-'//))
C
C SECTION-?
C
C THIS SECTION READS DATA INFORMATIONS AND PROCESSING REQUIREMENTS.
C
234 IF(KIT.GT.0.AND.IBW1.GT.0)GO TO 1149
IF(ISUB.EQ.0)GO TO 950
INPUT SUBROUTINES NUMBERS TO BE USED.
WRITE(6,61)
61 FORMAT(/30X,'(FILTERED TIME SECTION)')//)
9572 FORMAT(30X,'FILTERS BROUGHT IN ACTION')
READ(5,20)(MS(I),I=1,5)
20 FORMAT(10I5)
C
C INPUT FILTER PARAMETERS
C
950 READ(5,100)LP,DT,FL, FH, MG
100 FORNAT(I5,3F10.3,I5)
C
C DESCRIBE FILTERS USED
C
1149 IF (MPLT.EQ.0) MPLOTY=48
IF (MPLT.EQ.1) MPLOTY=47
IF (MPLT.EQ.2) MPLOTY=42
IF (MPLT.EQ.3) MPLOTY=33
IF (MPLT.EQ.4) MPLOTY=55
IF (LPLAT.EQ.2) MPLOTY=31
IF (LPLAT.GT.2) GO TO 9582
CALL CTRMAG (15)
IF (MPLT.EQ.4) CALL CTRMAG (10)
IF (ISUB.EQ.0) GO TO 9581
C
DO 9580 I=1,5
IF (MS(I).EQ.0) GO TO 9580
CALL PLACE (13,MPLOTY)
IF (MPLT.EQ.4) CALL PLACE (18,MPLOTY)
IF (MS(I).EQ.1) CALL TYPECS ('CAUSAL MOD. ROBINSON BP FILTER',30)
IF (MS(I).EQ.2) CALL TYPECS ('MOD. ROBINSON BP FILTER',23)
IF (MS(I).EQ.3) CALL TYPECS ('HANNING BP FILTER',17)

```

```

IF (MS(I).EQ.4.OR.MS(I).EQ.5.OR.MS(I).EQ.6.OR.MS(I).EQ.7.OR.MS(I).
1EQ.8) GO TO 9584
IF (MS(I).EQ.9) CALL TYPECS ('ROBINSON FAST FOURIER TRANSFORM',31)
IF (MS(I).EQ.10.OR.MS(I).EQ.11) GO TO 9584
IF (MS(I).EQ.12) CALL TYPECS ('CAUSAL HANNING BP FILTER',24)
IF (MS(I).EQ.13) CALL TYPECS ('ROBINSON BP FILTER',18)
IF (MS(I).EQ.14) CALL TYPECS ('CAUSAL ROBINSON BP FILTER',25)
IF (MS(I).EQ.15) CALL TYPECS ('SMOOTHED ROBINSON FAST FOURIER TRAN
1SFORM',40)
IF (MS(I).EQ.9.OR.MS(I).EQ.15) GO TO 9580
CALL TYPEFN (FL,1)
CALL TYPECS ('-',1)
CALL TYPEFN (FH,1)
CALL TYPECS ('H7',2)
9584 IF (MS(I).NE.4) GO TO 9586
CALL TYPECS ('LOWCUT FILTER',13)
CALL TYPEFN (FL,1)
CALL TYPECS ('HZ',2)
9586 IF (MS(I).NE.5) GO TO 9585
CALL TYPECS ('HICUT FILTER',12)
CALL TYPEFN (FH,1)
CALL TYPECS ('HZ',2)
9585 IF (MS(I).EQ.10) CALL TYPECS ('WAVELET PREDICTION FILTER',25)
IF (MS(I).EQ.6.OR.MS(I).EQ.7.OR.MS(I).EQ.8.OR.MS(I).EQ.9.OR.MS(I).
1EQ.11.OR.MS(I).EQ.15) GO TO 9580
CALL TYPECS ('LEM:TH =',10)
CALL TYPEFN (LP,4)
MPLQTY=MPLQTY+1
9580 CONTINUE
GO TO 9582
9581 CALL PLACE (13,MPLQTY)
IF (MPLQTY.EQ.4) CALL PLACE (18,MPLQTY)
CALL TYPECS ('UNFILTERED SECTION',18)
C
9582 CALL CTRMAG (20)
IF (KIT.GT.0.AND.(DM1.GT.0) GO TO 1150
IF (NCROSS.NE.0.OR.ISUB.NE.0)GO TO 951
WRITE(A,62)
62 FORMAT(/20X,'UNFILTERED TIME SECTION'//)
951 KOUNT=0
CALL ICI9HEMASK(64,IRES)
IF (NO.SQ.0) GO TO 5002
IF (NCROSS.EQ.0.AND.NO.NE.0)GO TO 1381
C
READ IN FIELD TIME-DISTANCE DATA IF REQUIRED.
C
C
5002 READ (5,2524) NTXPTS,LU

```

```

2524 FORMAT (2I3)
IF (NTXPTS.EQ.0) GO TO 50
CALL TXPLTS (NTXPTS,VEL,LU,XA)
C
C
INPUT FILE PARAMETERS FOR EACH DATA FILE.
50 READ(5,4) MARS,IFILE,ISPEED,(IPOL(J),J=1,12)
READ (5,40) (POSIT(J),J=1,12)
4 FORMAT (I2,I3,13I2)
40 FORMAT (12F7.3)
KUS=KOUNT+1
C
C
THIS SECTION READS DATA FILES.
C
C
JI = NUMBER OF SECONDS OF RECORD TO BE READ IN * 100 SAMPLES/SEC
VALUE OF JI IS RELATED TO THE REQUIRED TIME PLOTTING WINDOW (TIMH)
AS WELL AS THE REDUCED TIME COMPONENT XB/VEL.
C
IF JI > NUMBER OF LINES ON ANY SUPPLIED DATA FILE - PROGRAM READS
IN ALL DATA PRESENT IN THAT FILE.
C
IF IFILE IS NOT SUPPLIED, PROGRAM ENDS
C
C
IF(IFILE.EQ.0)GO TO 55
IF (VEL.EQ.0.) GO TO 1410
DXD=XB
IF (ARS(XA).GT.XB) DXD=ARS(XA)
JI=IFIX((TIMH+DXD/VEL)*100)
GO TO 1411
1410 JI=IFIX(TIMH*100)
1411 IF (JI.GT.2500) JI=2500
III=0.
C
DO 6 I=1,JI
IF (MARS.EQ.0) READ(IFILE,765,FRR=50,END=1421)IDUMMY,
1(ITRACE(I,J),J=1,7),IDUMMY
IF (MARS.EQ.1) READ(IFILE,766,ERR=50,END=1421)(TRACE(J,I),J=1,4),
1DUMMY
IF (MARS.EQ.2) READ(IFILE,767,ERR=50,END=1421)(TRACE(J,I),J=1,4),
1DUMMY
IF (MARS.EQ.12)READ(IFILE,781,FRR=50,END=1421)(ITRACE(J,I),J=1,12)
IF (MARS.EQ.11)READ(IFILE,780,ERR=50,END=1421)(ITRACE(J,I),J=1,11)
IF (MARS.EQ.10)READ(IFILE,768,ERR=50,END=1421)(ITRACE(J,I),J=1,10)
IF (MARS.EQ.9) READ(IFILE,765,ERR=50,END=1421)(ITRACE(J,I),J=1,9)
IF (MARS.EQ.7) READ(IFILE,769,ERR=50,END=1421)(ITRACE(J,I),J=1,7)
IF (MARS.EQ.5) READ(IFILE,770,ERR=50,END=1421)(ITRACE(J,I),J=1,5)
IF (MARS.EQ.4) READ(IFILE,771,ERR=50,END=1421)(ITRACE(J,I),J=1,4)
III=III+1
6 CONTINUE
C

```

```

766 FORMAT (5X,4F15.6)
767 FORMAT (5X,5F15.6)
771 FORMAT (4I6)
770 FORMAT (5I6)
769 FORMAT (7I6)
765 FORMAT (9I6)
768 FORMAT (10I6)
780 FORMAT (11I6)
781 FORMAT (12I6)
C
1421 III=III+1
C
C IN = NO. OF SAMPLES ACTUALLY READ IN.
C TPO= NO. OF SECONDS OF DATA (AT 100 S/SEC) OF DATA ACTUALLY READ IN
C
IN=III-1
TPO=FLOAT(IN)/100.
JP=JP+1
KF=0
C
C THIS PART IS CONCERNED WITH RECORDING MACHINE SPEED.
C
C IF(ISPEED.EQ.1)GO TO 9545
SD=1.0
SSD=1.0
GO TO 1370
9545 SD=0.5
SSD=2.0
C
C MAIN PROCESSING LOOP.
C
C THIS SECTION PREPARES ABSOLUTE TIME SECTION.
C
WR1 = RANGE
WR2 = RANGE/RED.VEL
WR3 = ZERO-AVERAGE
WR4 = CALC.AVERAGE GAIN
WR5 = SEISMOMETER POLARITY INDEX
C
1370 JK1=12
GO TO 1383
1381 JKJ=1
1383 DO 11 J=1,JK1
IF (NCROSS,"Q.O.AND.NO.NE.0) GO TO 1382
IF (POSIT(J).EQ.0)GO TO 11
C
FOR EACH TRACE TO BE PROCESSED - READ IN TRACE PARAMETERS.
C
C READ (5,7) ISAMP, GAIN, DIM, AMPT, LQ, IP, IWP
7 FORMAT (I5,3F8.5,3I2)
IF (DIM.EQ.0.) GO TO 1382
YA=DIM
KF=KF+1
1382 IF (NCROSS.EQ.0.AND.NO.GT.0)GO TO 516
NN=NN+1
PAK=POSIT(J)
WR1(KF)=POSIT(J)
WR5(KF)=IPOL(J)
IF(VEL.GI.0.)GO TO 8
IF(ISAMP.LI.0)GO TO 9
KK= ISAMP+INT(YA*100.*SD)
GO TO 10
9 KK=ISAMP+1+INT(YA*100.*SD)
GO TO 10
C
C THIS SECTION PREPARES REDUCED TIME SECTION.
C
8 RITA=ABS(POSIT(J))/VEL.
REDT=RITA*100.*SD
KK=INT(REDT+0.005+YA*100.*SD)+ISAMP
10 K=MAX(KK,1)
KR2(KF)=KK
WR2(KF)=RITA
C
C IN THIS SECTION POSITION OF 1ST SAMPLES ARE FOUND WITH RESPECT
C TO REDUCTION VELOCITIES 6.0KM/S & 3.5KM/S.
C
REDT2=(ABS(POSIT(J))/6.0)*SD*100.+0.005
KK2=INT(REDT2)+ISAMP
K2=MAX(KK2,1)
REDT3=(ABS(POSIT(J))/3.5)*SD*100.+0.005
KK3=INT(REDT3)+ISAMP
K3=MAX(KK3,1)
C
C THIS PART DEALS WITH POLARITY CASE.
C
IF(IPOL(J).EQ.0)GO TO 3333
PL=-1.0
GO TO 510
3333 PL=1.0
510 IF(MARS.EQ.1.OR.MARS.EQ.2)GO TO 2411
DO 515 I=1,IN

```

```

515 XX(I)=FLOAT(ITRACE(J,I))*PL
GO TO 2415
2411 DO 535 I=1,IN
535 XX(I)=TRACE(J,I)*400.*PL
2415 IF(CH.LT.1.0)GO TO 3411
CALL PROPER(IN,XX,X)
GO TO 3412

C THIS SECTION REMOVES DIRECT COMPONENT AND RUBLE EFFECT
C FROM THE DATA.
3413 WR3(KF)=0.
WR4(KF)=0.

C DO 1516 I=K2,IN
1516 Y(I-K2+1)=XX(I)

C REMA PRODUCES ZERO-AVERAGED DATA BY ADDING ALL SAMPLES,
C AVERAGING, AND FINDING THE RESIDUAL ON EACH SAMPLE.
C JUST= "WORVING" DATA L.H.H.T.H - (P.LOTTING)
C Y = INPUT ARRAY (DATA)
C R = OUTPUT ARRAY (RESIDUALS)
C JUST=IN-K2+1
CALL REMA(JUST,Y,R,AVF)

C WR3(KF)=AVF
IF(NN.GT.1)GO TO 3420
WRITE(6,3421)
3421 FORMAT(50X,"ZERO-AVERAGE FILTER")
3420 IF(ID.EQ.1)GO TO 3422
CALL PROPER(JUST,Y,C)
GO TO 3423
3422 CALL BUBBLE(JUST,R,CR,NNM,C)
WRITE(6,4434)
4434 FORMAT(50X,"BUBBLE FILTER")

C IF I < K2 (FIRST SAMPLE), X(I) = XX(I)
C I >= K2 X(I) = C(1 TO JUST)
3423 DO 3414 I=1,IN
IF(I.LT.K2)GO TO 3415
X(I)=C(I-K2+1)
GO TO 3414
3415 X(I)-XX(I)

3414 CONTINUE
C SUPPLIED TIME GATE FOR DATA TO PROCESS
3412 KITT=IN-K+1
IF(TIMM.EQ.0.)GO TO 868
NP=INT(TIMM*100.*SD)+1
IF(NP.GE.KITT)GO TO 868
GO TO 869
868 NP=KITT
869 DO 1591 I=1,NP
1591 XX(I)=X(I+K-1)

C SECTION=4
C CROSSCORRELATION SECTION
C NCROSS=1 CROSSCORRELATION WITH CHIRP FILTER OF SUPPLIED
C FREQUENCY BAND.
C NCROSS=2 CROSSCORRELATION WITH A GENERATED UPDATED
C AVERAGE WAVELET FROM PRECEDING 5 TRACES.
C NCROSS=3 CROSSCORRELATION WITH A DEFINED GOOD TRACE

C IF(NCROSS.EQ.0)GO TO 516
C IF(NCROSS.GT.3.AND.NCROSS.LT.7)GO TO 1154
C IF(NCROSS.GE.7)GO TO 1152
C GO TO(1151,1152,1153),NCROSS
C CROSSCORRELATION WITH CHIRP FILTER
1153 IF(NN.GT.1)GO TO 6111
C CHIRP FILTER IS A GENERATED SINE WAVE OF GIVEN BANDWIDTH
C (FROM THE FILTER PARAMETERS CARD) OF DURATION EQUAL TO THE
C DEFINED TIME WINDOW.
C CHIRP FILTER TT=SIN(2*PI*3.1416(F1+(F2-F1)*T/2L)T)
C L LENGTH OF FILTER; T IS PERIOD OF SINE WAVE
C F1 LOWER FREQUENCY; F2 IS HIGHER FREQUENCY
C AL=FLOAT(NP-1)/2.
C DO 3135 I=1,NP
C AT=FLOAT(I-1)
C W=FL+(FH-FL)*AT/(2.*AL)
C LP=NP
3135 TT(I)-SIN(2.*PI*3.1416*W*AT)
WRITE(6,1131)
1131 FORMAT(50X,"CROSSCORRELATION WITH CHIRP FILTER")

```

```

IF(NO.EQ.0)GO TO 6111
IF(NO.EQ.1)GO TO 2121
CALL PROPER(NP, TT, X)
GO TO 16
2121 CALL PROPER(NP, TT, XX)
GO TO 6341
6111 CALL BP3(LP, DT, FI, FI, NG, NP, XX, LXX, X)
CALL CROSS(NP, X, NP, TT, NP, XX)
GO TO 516
C
C CROSSCORRELATION WITH A TRACE CONTINUOUSLY UPDATED BY
C CROSSCORRELATION WITH THE PREVIOUS ADJACENT TRACE. THE INITIAL
C TRACE IS TO BE SUPPLIED.
C
C CROSSCORRELATION WITH SELECTED TRACE
C
1151 CALL BP3(LP, DT, FI, FI, NG, NP, XX, NP, X)
IF(NN.GT.1)GO TO 6112
WRITE(6,1132)
1132 FORMAT(50X, 'CROSSCORRELATION WITH TRACE')
CALL PROPER(NP, X, TT)
GO TO 11
6112 CALL CROSS(NP, X, NP, TT, NP, XX)
CALL PROPER(NP, XX, TT)
GO TO 516
C
C GENERATION OF WAVELET AND CROSSCORRELATION WITH IT
C
1152 IF(NO.EQ.0)GO TO 1182
CR2=0.9
GO TO 5020
1182 IF(NN.GT.MISS.AND.NCROSS.GE.7)GO TO 1254
CALL BP3(LP, DT, FI, FI, NG, NP, XX, NP, X)
IF(NN.LE.MISS)GO TO 619
CALL FFOLD(NP, X, IXP XCP.I.XX, XX)
CALL PROPER(NP, XX, X)
619 IF(NN.GT.1)GO TO 5019
NET=LR+49
DO 5012 I=LR, NET
IT=I-LR+1
IF(IT.GT.25)GO TO 1159
WW(IT)=X(I)
GO TO 5012
1159 WW(IT)=0.
5012 CONTINUE
LWW=IT

GO TO 5020
5019 IF(LO.EQ.0)GO TO 5020
DO 5021 J=1,49
WW(I)=DR(I)
B1(I)=DB(I)
B2(I)=DB(I)
B3(I)=DB(I)
B4(I)=DB(I)
5021 B5(I)=DB(I)
ISA=LRR
LQ=0
GO TO 5023
5020 ISA=LR
5023 ISA1=ISA-R
ISA2=ISA+8
IF(NO.GT.0)GO TO 2713
NET2=LW/2
CALL CROSS(NP, X, NET2, WW, NP, XX)
CALL MAXSN2(ISA1, ISA2, XX, RMAX, LR)
CALL CROSS3(NP, XX, NET2, WW, LR, I, Y, CR2)
2713 CALL MAXSN2(ISA1, ISA2, XX, RMAX, LRD)
LR=LRD-1
IF(LR.GE.LARK1.AND.IR.LE.LARK2)GO TO 1999
LR=LRR
1999 INAM(KF)=LR
IF(NO.GT.0)GO TO 517
IF(NN.GT.MISS.AND.APS(CR2).I.T.O.7)GO TO 516
517 NET=LR+49
DO 3888 I=LR, NET
IT=I-LR+1
IF(IT.GT.25)GO TO 3817
Y(IT)=XX(I)
GO TO 3888
3817 Y(IT)=0.
3888 CONTINUE
DO 5013 IR=1,49
B1(IR)=B2(IR)
B2(IR)=B3(IR)
B3(IR)=B4(IR)
B4(IR)=B5(IR)
5013 B5(IR)=Y(IR)
DO 5014 I=1,49
WW(I)=B1(I)+B2(I)+B3(I)+B4(I)+B5(I)
5014 CALL MAXSN(49, WW, XMAX, LZ)
WW(KF)=XMAX
IF(YMAX.NE.0.)GO TO 5001
XMAX=1.0

```

```

5001 DO 5018 I=1,49
5018 WW(I)-WW(I)/XMA
IF(NN.EQ.MISS)GO TO 5015
IF(NN.GT.MISS)GO TO 516
GO TO 11
5015 CALL PROPER(49,WW,DR)
CALL PEF(49,DR,1.3,LXCP,XCP,IZA)
WRITE(6,1729)(XCP(IV).IV=1,1,XCP)
1729 FORMAT(10F8.4)
1133 WRITE(6,1133)
FORMAT(30X,'AVERAGE WAVELET')
IF(NCROSS.GE.7)GO TO 2516
IF(NO.EQ.0)GO TO 11
DO 1222 I=1,49
IF(1.LT.25)GO TO 1223
X(I)-WW(I-24)
GO TO 1222
1223 X(I)-WW(26-I)
1222 CONTINUE
IF(NO.EQ.1)GO TO 1221
LP=49
GO TO 16
1221 NP=49
CALL PROPER(NP,X,XX)
GO TO 6341
C
C SECTION-5
C
C DECONVOLUTION(PART-A)
C FILTER GENERATED FROM INDIVIDUAL TRACE
C
1154 IF(NCROSS.GE.7)GO TO 2516
CALL BP3(LP,DT,FL,FI,NG,NP,XX,NP,X)
NCT=1R+1,UM
DO 6146 I=L,R,NCT
ND=I-LR+1
6146 Y(ND)=X(I)
CALL MAXSH(ND,Y,FUK,LRT)
DO 4687 I=1,ND
4687 DB(I)=Y(I)/FUK
NCR2=NCROSS-3
WN=1.3
GO TO(1155,1156,1157),NCR2
1155 CALL SPIKE(ND,DB,WN,ND,XCP,ERROR,IZA)
LXCP=ND
IF(NN.GT.1)GO TO 1911
WRITE(6,1134)
1134 FORMAT(50X,'SPIKING GEN. FROM EACH TRACE')
1911 IF(NO.EQ.0)GO TO 121
GO TO 131
1156 CALL PEF(ND,DB,WN,LXCP,XCP,IZA)
IF(NN.GT.1)GO TO 1912
WRITE(6,1135)
1135 FORMAT(50X,'PEF GEN. FROM EACH TRACE')
1912 IF(NO.EQ.0)GO TO 121
GO TO 131
1157 CALL WVPRED(ND,DB,10,1,XCP,XCP)
IF(NN.GT.1)GO TO 1913
WRITE(6,1136)
1136 FORMAT(50X,'WVPRED GEN. FROM EACH TRACE')
1913 IF(NO.EQ.0)GO TO 121
131 NP=LXCP
LP=NP
IF(NO.EQ.1)GO TO 132
CALL PROPER(LP,XCP,X)
GO TO 16
132 CALL PROPER(NP,XCP,XX)
GO TO 6341
121 CALL FFOLD(NP,X,1,XCP,XCP,LXX,XX)
IF(NCR2.GT.1)GO TO 516
LXC1=LXCP/?
DO 2333 I=LXC1,LXX
II=I-LXC1+1
2333 X(II)=XX(I)
DO 3334 I=1,NP
IF(ILE,IL)GO TO 3335
XX(I)=0.
GO TO 3334
3335 XX(I)-X(I)
3334 CONTINUE
GO TO 516
C
C DFCONVOLUTION(PART-B)
C
C DECONVOLUTION WITH THE FILTER GENERATED FROM AVE.WAVELET.
2516 NCR3=NCROSS-6
WN=1.3
ND=49
IF(NN.GT.MISS)GO TO 1254
GO TO(1251,1252,1253),NCR3
1251 CALL SPIKE(ND,DB,WN,ND,XCP,ERROR,IZA)
WRITE(6,1137)
1137 FORMAT(30X,'SPIKING GEN. FROM AVE.WAVELET')

```

```

LXCP=ND
GO TO 1254
1252 CALL PEF(ND,DB,WN,LXCP,XCP,IZA)
WRITE(6,1138)
1138 FORMAT(30X,'PEF GEN. FROM AVE.WAVELET')
GO TO 1254
1253 CALL WVPRED(ND,DB,LNM,LXCP,XCP)
WRITE(6,1139)
1139 FORMAT(30X,'WVPRED GEN. FROM AVE.WAVELET')
1254 IF(NO.EQ.0)GO TO 1255
GO TO 131
1255 IF(NN.EQ.MISS)GO TO 11
CALL BP3(LP,DT,FL,NG,NP,XX,LXX,X)
CALL FFOLD(NP,X,LXCP,XCP,LXX,XX)
IF(NCR3.GT.1)GO TO 516
LXC1=LXCP/2
IL=LXX-LXC1+1
DO 4444 I=1,TL
4444 X(I)=XX(I+LXC1-1)
DO 4445 I=1,NP
IF(I.LE.IL)GO TO 4446
XX(I)=0.
GO TO 4445
4446 XX(I)=X(I)
4445 CONTINUE
SECTION-6
C 516 IF(TSUB.LE.0)GO TO 16
C THIS SECTION DOES FILTERING OF EITHER DIGITAL DATA OR A
C SINGLE SPIKE (NO > 0).
C
C IF(NO.EQ.0)GO TO 6341
NP=1
KNP=1
CALL IMPULS (NP,XX,KNP)
C
C 6341 DO 21 I=1,5
IF(NS(I).EQ.0) GO TO 212
IF(MS(I).EQ.1.OR.MS(I).EQ.14) GO TO 1101
IF(NS(I).EQ.2.OR.MS(I).EQ.13) GO TO 1102
IF(NS(I).EQ.3) GO TO 1103
IF(NS(I).EQ.4) GO TO 1104
IF(MS(I).EQ.5) GO TO 1105
IF(NS(I).EQ.6) GO TO 1106
IF(MS(I).EQ.7) GO TO 1107
IF(NS(I).EQ.8) GO TO 1108
IF(MS(I).EQ.9.OR.MS(I).EQ.15.OR.MS(I).EQ.16) GO TO 1109
IF(NS(I).EQ.10)GO TO 1110
IF(MS(I).EQ.11)GO TO 1111
IF(NS(I).EQ.12)GO TO 1112
C CAUSAL BANDPASS FILTER BY ROBINSON
IMS=0
IF (MS(I).EQ.14) IMS=1
CALL BP1(LP,DT,FL,NG,NP,XX,LXX,X,IMS)
IF(JP.GT.1)GO TO 21
WRITE(6,3023)
3023 FORMAT(50X,'BANDPASS FILTER(ROBINSON)')
GO TO 21
C MODIFIED ROBINSON'S BANDPASS FILTER
IMS=0
IF (MS(I).EQ.13) IMS=1
CALL BP2(LP,DT,FL,NG,NP,XX,LXX,X,IMS)
IF(JP.GT.1)GO TO 21
WRITE(6,6758)
6758 FORMAT(50X,'BANDPASS FILTER(MODIFIED ROBINSON)')
GO TO 21
C HANNING BANDPASS
1103 CALL BP3(LP,DT,FL,NG,NP,XX,LXX,X)
IF(JP.GT.1)GO TO 21
WRITE(6,5121)
5121 FORMAT(50X,'HANNING BANDPASS')
GO TO 21
C LOWCUT FILTER
1104 CALL HIPASS(LP,DT,FL,NG,NP,XX,LXX,X)
IF(JP.GT.1)GO TO 21
WRITE(6,3024)
3024 FORMAT(50X,'HIPASS FILTER')
GO TO 21
C HICUT FILTER
1105 CALL LOPASS(LP,DT,FL,NG,NP,XX,LXX,X)
IF(JP.GT.1)GO TO 21
WRITE(6,3025)
3025 FORMAT(50X,'LOPASS FILTER')
GO TO 21
C DOES AUTOCORRELATION
1106 CALL AUTOCCR(NP,XX,NP,X)

```

```

IF(JP.GT.1)GO TO 21
WRITE(6,9995)
9995 FORMAT(50X,'AUTOCORRELATION')
GO TO 21
C
C DOES CROSSCORRELATION
1107 CALL CROSS(NP,XX,NP,XX,NP,X)
IF(JP.GT.1)GO TO 21
WRITE(6,9994)
9994 FORMAT(50X,'CROSSCORRELATION')
GO TO 21
C
C PUTS DATA FROM ONE ARRAY TO THE OTHER
1108 IF(N0.EQ.0)GO TO 5108
NP=LP
5108 CALL PROPER(NP,X,XX)
IF(JP.GT.1)GO TO 21
WRITE(6,9993)
9993 FORMAT(50X,'PROPER')
GO TO 21
C
C FAST FOURIER TRANSFORM
1109 SIGN=-1.0
IF (ISN.EQ.1) SIGN=1.0
IF (NCROSS.EQ.0.AND.HO.NE.0) GO TO 4045
C
C ZERO-AVERAGE THE TIME SERIES
CALL REMA(NP,XX,X.FTAVE)
CALL PROPER(NP,X,XX)
C
4045 IF (MS(I).EQ.9.OR.M3(I).EQ.15) CALL FASTFT(XX,NP,I.T.IF.SPECT.SIGN)
IF (MS(I).EQ.15) CALL SMOOTH(XX,LT)
C
IF(JP.GT.1)GO TO 21
IF (MS(I).EQ.9) WRITE (6,8887)
IF (MS(I).EQ.15) WRITE (6,8889)
8887 FORMAT(50X,'FAST FOURIER TRANSFORM')
8889 FORMAT(50X,'SMOOTHED FAST FOURIER TRANSFORM')
GO TO 21
C
WAVELET PREDICTION FILTER
1110 CALL WVPRED(NP,XX,20,LXCP,XCP)
IF(JP.GT.1)GO TO 21
WRITE(6,5115)
5115 FORMAT(50X,'WAVELET PREDICTION FILTERING')

```

```

GO TO 21
C
C REVERSE ARRAYS
1111 CALL RVS(NP,XX,X)
GO TO 21
C
C CAUSAL HANNING BANDPASS FILTER
1112 CALL BP4(LP,DT,FL,FM,NG,NP,XX,NP,X)
IF(JP.GT.1)GO TO 21
WRITE(6,6321)
6321 FORMAT(50X,'CAUSAL HANNING BANDPASS')
21 CONTINUE
C
C SECTION-7
C
C THIS SECTION DOES PLOTTING.
212 IF(N0.EQ.2)GO TO 866
IF (ISPECT.GT.0)GO TO 865
PAK=POSIT(J)
PAKI=PAK-0.2
GREEN=PAK+0.1
CALL PROPER(NP,X,XX)
C
C THIS PART IS RELATED WITH AMPLITUDE NORMALISATION OF THE DATA.
RGAIN > 0.0000, GAIN FACTOR SET EXTERNALLY.
AMPT = SCALE FACTOR FOR AUTOMATIC TRACE NORMALISATION
16 IF(N0.EQ.2)GO TO 866
IF (RGAIN.GT.0.0000) GO TO 716
MP=IFIX(TIMH*100.)
C
CALL PROPER (MP,XX,AX)
CALL MAXSN(MP,AX,XMAX,INDEX)
IF (ISUB.EQ.0.AND.XMAX.LT.0.00000001) XMAX=0.00000001
WR4(KF)=XMAX
IF (AMPT.I.T.0.001) AMPT=1.000
GAIN=(0.8/XMAX)*AMPT
GO TO 3636
716 GAIN=RGAIN
C
3636 DO 1586 I=1,NP
IT=I+K-1
1586 X(IT)=X(I)*GAIN
C
C DOES PLOTTING OF TIME SECTION

```

```

C      DOES PLOTTING OF FILTER SPECTRUM
C
      865 IF(NN.GT.1)GO TO 875
      WRITE(6,7171)
      7171 FORMAT(50X,'AMPLITUDE/POWER OR PHASE SPECTRUM')
      875 CALL PROPER(LT,XX,AX)
      IF(I*P*CT.EQ.2)GO TO 4415
      CALL MAXSH(LT,AX,XMAX,INDEX)
      IF (NO.EQ.0) XMAX=XMAX*0.25
      WR4(KF)=XMAX
      IF(XMAX.NE.0.)GO TO 1391
      4415 XMAX=1.0
      1391 GAIN=1./XMAX
      FAC=50./FLOAT(LT-1)
      DO 738 I=1,I1
      TIME(I)=FLOAT(I-1)*FAC
      IF(NO.EQ.0)GO TO 749
      PX(I)=AX(I)*GAIN
      GO TO 738
      749 PX(I)=AX(I)*GAIN+PAK
      738 CONTINUE
      IF(I*P,I.T.3)GO TO 4046
      WRITE(6,4047)((TIME(I),PX(I)),I=1,LT)
      4047 FORMAT(2X,F7.3,5X,F10.3)
      4046 IF(I*ROT.GT.0)GO TO 34
      CALL PTPLOT(PX,TIME,1,I.T,-2)
      IF(NO.GT.0)GO TO 2523
      GO TO 7141
      34 CALL PTPLOT(TIME,PX,1,I.T,-2)
      IF(NO.GT.0)GO TO 2523
      GO TO 7141
C
C      DOES PLOTTING OF THE FILTER IN TIME DOMAIN.
C
      866 TIME(1)=0
      LPXX=200
      DO 466 I=2,I*PXX
      TIME(I)=TIME(I-1)+0.01
      466 CALL PROPER(I*P,X,PP)
      CALL MAXSH(LP,PP,XMAX,INDEX)
      IF (XMAX,I.T.0.00000001) XMAX=0.00000001
      DO 467 I=1,LP
      467 PX(I)=PP(I)/XMAX
C
C      IF THE FILTER LENGTH IS LESS THAN THE X-AXIS LENGTH
C      (IE LP=200 SAMPLES) THEN FILL GAP WITH ZEROS.
C
      11=NP+K-1
      DO 101 I=K,11
      IF(IVAR.EQ.0.OR.IVAR.GT.1)GO TO 1960
      IF(X(I).LE.-0.2)GO TO 101
      IF(X(I).GT.0.7)GO TO 1705
      IF(X(I).GT.-0.2.AND.X(I).LE.0.7)GO TO 1706
      1705 X(I)=0.7
C
C      CONVERT WAVEFORM TO PLOTTING COORDINATES
C
      1706 PX(I)=POSIT(J)*X(I)
      GO TO 703
      1960 PY(I)=POSIT(J)*X(I)
      703 IF(VEL.GT.0)GO TO 704
      IF(I*AMP.I.T.0)GO TO 748
      TIME(I)=(FLOAT(I-1-15AMP))*SSD)/100.
      GO TO 1901
      788 TIME(I)=(FLOAT(I-1-15AMP)*SSD)/100.
      GO TO 1901
      704 TIME(I)=(FLOAT(I-15AMP)-REDT)*SSD)/100.
C
C      DOES VARIABLE AREA PLOTTING
C
      1901 IF(IVAR.EQ.0)GO TO 101
      PINK=PX(I)
      BLUE=TIME(I)
      GO TO(1703,1704),IVAR
      1703 CALL POSIT(PAKI,BLUE)
      CALL JOIN(PINK,BLUE)
      GO TO 101
      1704 IF(GREEN.GT.PINK)GO TO 101
      CALL POSITN(GREEN,BLUE)
      CALL JOIN(PINK,BLUE)
      101 CONTINUE
      IF(I*P.NE.2)GO TO 4051
      WRITE(6,4055)((TIME(I),X(I)),I=K,11)
      4055 FORMAT(5X,8F15.8)
      4051 IF(IVAR.EQ.1.OR.LBW1.GT.0)GO TO 2523
      IF(I*ROT.GT.0)GO TO 888
C
C      PLOT OUT TRACE
C
      CALL PTPLOT(PX,TIME,K,11,-2)
      GO TO 7141
      888 CALL PTPLOT(TIME,PY,K,11,-2)
      GO TO 7141
C

```

```

IF (LPLGT.LPXX-?) GO TO 469
L.PXY=L.P+1
DO 470 I=1,PXY,'PXX
470 PX(I)=0.0
C
469 IF (IROT.GT.0) GO TO 468
CALL TPLOT(PX,TIME,1,LPXX,-2)
GO TO 2523
468 CALL TPLOT(TIME,PX,1,LPXX,-2)
2523 IF (LBM1.EQ.0) GO TO 7141
NN2=NR-MISS
BIG(NN2)=PAK
KUSS(NN2)=K
KUSS1(NN2)=II
DO 2522 JET=1,1
JET=NR2
DO 2522 I=K,II
TV1(I,JET)=PX(I)
2522 TV2(I,JET)-TIME(I)
C
C PRINT OUT RESULT PARAMETERS
C
7141 IF (NCROSS.EQ.0.AND.NO.GT.0) GO TO 11
WRITE(6,707)
707 FORMAT (/)
WRITE(6,8883)KUS,IS:AMP
8883 FORMAT(5X,'FILE NO.:',13.3X,'SAMPLES TO LINK FILE WITH SHOT=',I5)
11 CONTINUE
C
WRITE(6,8884)(WR1(NT),NT=1,KF)
8884 FORMAT(5X,'TRACE POSITIONS',12F9.3)
WRITE(6,8882)(IPOS(NT),NT=1,KF)
8882 FORMAT(5X,'TRACE POLARITY',12I9)
IF (VFL.EQ.0.) GO TO 8890
WRITE(6,8885)(WR2(NT),NT=1,KF)
8885 FORMAT(5X,'REDUCED TIMES',12F9.3)
8890 WRITE(6,8886)(KR2(NT),NT=1,KF)
8886 FORMAT(5X,'FIRST SAMPLE NO',12I9)
WRITE(6,6667)(WR3(NT),NT=1,KF)
6667 FORMAT(5X,'A V A H A G E 3',12E10.7)
IF (NO.GT.0.AND.NCROSS.EQ.0) GO TO 111
WRITE(6,8888)(WR4(NT),NT=1,KF)
8888 FORMAT(5X,'GAIN VALUES',12E10.2,/)
IF (UCROSS.LT.' OR.'NCROSS.GT.2.AND.NCROSS.LT.7)) GO TO 111
WRITE(6,7143)(INAM(NT),NT=1,KF)
7143 FORMAT(5X,'INITIAL 3AH MV',12I9)
C
END OF DATA PROCESSING LOOP.
C
111 KOUNT=KOUNT+1
C
IF INDEX (KOUNT) < NO. OF FILES, THEN RETURN AND READ IN NEXT FILE
IF (KOUNT.NE.HFIL) GO TO 50
C
THIS SECTION IS ONLY FOR 4-QUAD PLOTTING (KPLOT=1)
IF (KPLOT.EQ.0) GO TO 1150
LPLAT=LPLAT+1
IF (LPLAT.GT.4) GO TO 1150
C
RETURN FOR NEXT DATASET OR NEW MAPPING PARAMETERS
IF (NPARA.EQ.1) GO TO 54
GO TO 53
C
1150 KIT=KIT+1
IF (NO.GT.0) GO TO 1147
WRITE(6,1989)KUS
1989 FORMAT(/,10X,'TOTAL NO. OF FILES PROCESSED =',I5)
WRITE(6,1991)NN
1991 FORMAT(10X,'TOTAL NO. OF TRACES PROCESSED=',I5,/)
1147 IF (LBM1.GT.0) GO TO 1148
IF (KIT.LT.NPLOT) GO TO 367
GO TO 55
C
IF KIT = NPLOT, FINISH ALL CALCULATIONS
C
1148 MISS2=MISS+1
DO 858 LF=MISS2,NN2
K=KUSS(LF)
II=KUSS1(LF)
PAK=BIG(LF)
PAKI=PAK-0.2
GEEH=PAK+0.1
DO 859 LS=K,II
TIME(LS)=TV2(LS,LF)
PX(LS)=TV1(LS,LF)
IF (TVAR.EQ.0) GO TO 859
C
VARIABLE AREA PLOTTING
GO TO (7859,2860).IVAR
2859 PINK=PX(LS)

```

```

BLUE=TIME(LS)
CALL POSITN(PAKI, BLUE)
CALL JOIN(PINK, BLUE)
GO TO 859
2860 IF(GREEN.GT.PINK)GO TO 859
CALL POSITN(GREEN, BLUE)
CALL JOIN(PINK, BLUE)
CONTINUE
859 IF(IVAR.EQ.1)GO TO 858
C
C TIME SECTION PLOTTING
C
IF(IROT.GT.0)GO TO 2882
CALL PIPLOT(PX, TIME, K, II, -2)
GO TO 858
2882 CALL PIPLOT(TIME, PX, K, II, -2)
858 CONTINUE
367 WRITE(6, 967)KIT
967 FORMAT(20X, 'FRAME NUMBER=', I3//)
CALL FRAME
C
C RETURN FOR NEXT DATASET OR FOR NEW MAPPING PARAMETERS
C
IF(KIT.LT.NPLOT.AND.NPARA.EQ.0)GO TO 53
IF(KIT.LT.NPLOT.AND.NPARA.EQ.1)GO TO 54
55 CALL GRENDD
STOP
END
C
C END OF MAIN PROGRAM
C
SUBROUTINE HP1(LP, DT, FL, FH, NG, NP, XX, LXX, X, IMS)
ROBINSON 1078; 1066
CALCULATES CAUSAL HANDPA'S (ROX) FILTER WHICH PASSES
FREQUENCIES IN THE RANGE OF FL AND FH.
C
LP =LENGTH OF ONE LOBE PLUS ONE CENTRE POINT.
C
FLT =THE OUTPUT FILTER OF LENGTH LP(CAUSAL PART).
C
FL =LOWER FREQUENCY PASSED.
C
FH =HIGHER FREQUENCY(HZ)
C
DT =DATA INTERVAL IN SECONDS.
C
DIMENSION PP(500) XX(2500), X(2500)
KAP=0
IF((FH-FL)-1.0/(DT*FN))11,31,31
8 FN=LP
IF((FH-FL)-1.0/(DT*FN))11,31,31
11 FC=(FH+FL)/2.0
WL=6.2832*(FC*DT-0.5/FN)
WH=6.2832*(FC*DT+0.5/FN)
GO TO 41
31 WL=FL*DT*6.2832
WH=FH*DT*6.2832
41 PP(1)=WH-WL
DO 51 IT=2, LP
FIT=FLOAT(IT-1)
PP(IT)=(SIN(WH*FIT)-SIN(WL*FIT))/FIT
51 CONTINUE
DO 50 I=1, LP
FI=I-1
FM1=LP-1
W=0.54+0.46*COS(3.1416*FI/FM1)
IF (IMS.EQ.1) W=1.000
50 PP(I)=PP(I)*W/3.1416
610 CALL FFOLD(NP, XX, LP, PP, LXX, X)
IF(NP.NE.1)GO TO 100
LXX=LP
GO TO 611
100 KAP=KAP+1
IF(KAP.EQ.NG)GO TO 634
CALL RVSNP(X, XX)
GO TO 610
634 IF(NG.EQ.1)GO TO 612
CALL PROPER(NP, X, XX)
CALL RVSNP(NP, XX, X)
612 LXX=NP
611 RETURN
C
C SUBROUTINE BP2(LP, DT, FL, FH, NG, NP, XX, LXX, X, IMS)
C
C GENERATES A TWO-SIDED BOX FILTER BASED ON SUBROUTINE BP1.
C
DIMENSION XX(2500), X(2500), PP(500)
KAP=0
PP(LP)-0.
M=(LP+1)/2
FM=N
IF((FH-FL)-1.0/(DT*FN))1,2,2

```



```

DIMENSION PP(500),XX(2500),X(2500)
KAP=0
N=(LP+1)/2
PP(1)=(FH-FL)*DT
WH=6.2832*FH*DT
WL=6.2832*FL*DT
DO 20 I=2,N
FI=FLOAT(I-1)
XF=FI*(FH-FL)*DT
IF(XF.EQ.1.000)XF=1.001
HI=1.0-XF**2
HI=6.2832*FI*HI
LP=M
20 PP(I)=(-SIN(FI*WH)-SIN(FI*WL))/HI
72 CALL FFOLD(NP,XX,LP,PP,LXX,X)
IF(NP.NE.1)GO TO 575
LXX=LP
GO TO 576
575 KAP=KAP+1
IF(KAP.EQ.HI)GO TO 71
CALL RV(S(NP,X,XX))
GO TO 72
71 IF(HI.EQ.1)GO TO 73
CALL PROPER(NP,X,XX)
CALL RV(S(NP,XX,X))
73 LXX=NP
576 RETURN
END
C
C
SUBROUTINE HIPASS(LP,DT,FH,NG,NP,XX,LXX,X)
WARREN 1981
GENERATES LOCUT FILTER BASED ON THE CAUSAL ROBINSON
BANDPASS FILTER.
DIMENSION PP(500),XX(2500),X(2500)
KAP=0
IF(FH*DT-0.5)H,8.70
WH=FI*DT*2.0
WHI=3.1416*WH
WHI2=-2.0*WHI
PP(1)=1.0-WH
DO 20 I=2,LP
FI=FLOAT(I-1)
PP(I)=(-SIN(WHI*FI))/(WHI*FI)*WHI2
DO 50 I=1,LP
KAP=KAP+1
IF(KAP.EQ.HI)GO TO 111
CALL RV(S(NP,X,XX))

```

```

FI=FLOAT(I-1)
FM1=FLOAT(LP-1)
W=0.54+0.46*COS(3.1416*FI/FM1)
50 PP(I)=PP(I)*W/3.1416
87 CALL FFOLD(NP,XX,LP,PP,LXX,X)
IF(NP.NE.1)GO TO 55
LXX=LP
GO TO 70
55 KAP=KAP+1
IF(KAP.EQ.HI)GO TO 88
CALL RV(S(NP,X,XX))
GO TO 87
88 IF(HI.EQ.1)GO TO 89
CALL PROPER(NP,X,XX)
CALL RV(S(NP,XX,X))
89 LXX=NP
70 RETURN
END
C
C
SUBROUTINE LOPASS(LP,DT,FL,NG,NP,XX,LXX,X)
WARREN 1981
GENERATES HICUT FILTER BASED ON THE CAUSAL ROBINSON
BANDPASS FILTER.
DIMENSION PP(500),XX(2500),X(2500)
KAP=0
IF(FL*DT-0.5)R,8.70
WL=2.0*DT*FL
PP(1)=WL
WL2=3.1416*WL
DO 20 I=2,LP
FI=FLOAT(I-1)
20 PP(I)=2.0*WL*(SIN(WL2*FI))/(WL2*FI)
DO 50 I=1,LP
FI=FLOAT(I-1)
FM1=FLOAT(LP-1)
W=0.54+0.46*COS(3.1416*FI/FM1)
50 PP(I)=PP(I)*W/3.1416
112 CALL FFOLD(NP,XX,LP,PP,LXX,X)
IF(NP.NE.1)GO TO 33
LXX=LP
GO TO 70
33 KAP=KAP+1
IF(KAP.EQ.HI)GO TO 111
CALL RV(S(NP,X,XX))

```



```

IT=I-LR2+1
4 C(IT)=CC(I)
CALL PROPER(IT,C,X)
NR=IT-LM+1
DO 3 J=1, NR
COF(J)=0.
SUM1=0.
SUM2=0.
SUM3=0.
SUM4=0.
SUM5=0.
DO 2 I=1, M
SUM1=SUM1+Y(I)
SUM2=SUM2+Y(I)**2
SUM3=SUM3+X(I+J-1)
SUM4=SUM4+X(I+J-1)**2
SUM5=SUM5+Y(I)*X(I+J-1)
SY=FLOAT(LM)*SUM4-SUM3**2
SY=FLOAT(LM)*SUM2-SUM1**2
ST=FLOAT(LM)*SUM5-SUM3*SUM1
COF(J)=ST/(SQRT(SX)*SQRT(SY))
3 CONTINUE
LY=NR
WRITE(6,55)(COF(J),J=1,NR)
55 FORMAT(5X,'COF=',8F9.3)
RETURN
END

SUBROUTINE CRS123(CC,LC,ICR1,ICR2,ICR3)
FINDS THE 1ST, 2ND AND 3RD ZERO-CROSSINGS OF THE WAVELET
INPUT IS THE WAVELET.
DIMENSION CC(2500)
I=0
1 I=I+1
IF(CC(I))3,3,2
2 ICR1=I
IF(CC(I-1)**2.LT.CC(I)**2) ICR1=I-1
I=I+1
IF(CC(I))4,5,5
5 ICR2=I
IF(CC(I-1)**2.LT.CC(I)**2) ICR2=I-1
I=I+1
IF(CC(I))7,7,6
6 I=I+1
IF(CC(I-1)**2.LT.CC(I)**2) ICR3=I
7 ICR3=I

IF(CC(I-1)**2.LT.CC(I)**2) ICR3=I-1
LF=LC
RETURN
END

SUBROUTINE AUTOGR(LX,XX,LP,X)
ALI 1983
COMPUTES TUKEY AUTOCORRELATION OF XX.
LP=LARGEST LAG
X IS THE UNNORMALISED OUTPUT
DIMENSION XX(2500),X(2500)
DO 1627 IT=1,LP
X(IT)=0.0
MM=LX-IT+1
IF(IT.GT.LX)GO TO 4
DO 1628 IE=1,MM
JF=IE+IT-1
1628 X(IT)=XX(JE)*XX(IE)+X(IT)
4 CONTINUE
1627 RETURN
END

SUBROUTINE WVPRED(LX,XX,LALPHA,LA,XCP)
WAVELET PREDICTION FILTERING.
XCP IS THE PREDICTION FILTER
DIMENSION XX(2500),XCP(2500),X(2500)
KAP=0
JM=LX+LALPHA
LALPH2=LALPHA+1
J1=JM+1
LA=LX
CALL AUTOGR(LX,XX,JM,SPACE)
CALL PROPER(JM,SPACE,X)
CALL EUREKA(LA,SPACE,SPACE(LALPH2),XCP,SPACE(J1))
98 CALL FFOURD(LX,XX,LA,XCP,LXX,X)
CALL DOT(LA,XCP,SPACE(LALPH2),AG)
SPACE(2)=1-AG/SPACE(1)
CALL DOT(LALPHA,XX,XX,SPACE(3))
SPACE(3)=SPACE(3)/SPACE(1)
SPACE(4)=SPACE(2)-SPACE(3)

```



```

DE3=PC+PPH#FLOAT(LPLAT-3)
GO TO 86
87 DE3=PC+PPH#FLOAT(LPLAT-3)+0.03
88 IF(LPLAT.EQ.4)GO TO 89
DE4=PC+PPH#FLOAT(LPLAT-2)-0.03
GO TO 20
89 DE4=PC+PPH#FLOAT(LPLAT-2)
20 CALL PSPACE(DE1,DE2,DE3,DE4)
IF(IROT.FO.0)GO TO 32
CALL MAP(YA,YB,XA,XB)
GO TO 34
32 CALL MAP(XA,XB,YA,YB)
34 CALL BORDER
IF(YA.GE.0.)GO TO 33
CALL POSITN(XA,0.)
CALL JOIN(YB,0.)
33 CALL CTRMAG(10)
CALL SCALES
CALL CTRMAG(20)
RETURN
END
C
C
SUBROUTINE TXPLTS (NTXPTS,VEL,LU,XA)
C
C DAVINSON 1985,
C Subroutine TXPLTS reads in and plots optional T-X , with errors,
C on the same plot(s) as the digital traces.
C
C If LU=1, output from HAYPL1?? is extracted and will be plotted
C as straight lines.
C Otherwise, field data with errors will be plotted.
C
DIMENSTOR RAYX(100),RAYT(100)
REWIND LU
CALL REOPEN
C
IF (LU.EQ.3) GO TO 1
DO 100 N=1,NTXPTS
READ (LU,10) RANGE,DR,TIME,DT
IF (VEL.EQ.0.) GO TO 3
DTR=SQRT(DT**2+(DR/VFL)**2)
T=TIME-ABS(RANGE)/VFL
GO TO 2
3 DTR=DT
T=TIME
2 CALL POSITN ( RANGE-DR,T)
DE3=PC+PPH#FLOAT(LPLAT-3)
GO TO 86
CALL JOIN (RANGE+DR,T)
CALL POSITN (RANGE,T+DTR)
CALL JOIN (RANGE,T-DTR)
100 CONTINUE
GO TO 4
C
1 READ (LU,11) KK
IF (KK.EQ.999) GO TO 4
IF (KK.GT.100) WRITE (6,13)
DO 101 N=1,KK
READ (LU,12) RAYX(N),T
IF (XA.T.T.0.0) RAYX(N)=RAYX(N)+XA
IF (VEL.GT.0.) GO TO 5
RAYT(N)=T+ABS(RAYX(N))/VFL.
GO TO 101
5 RAYT(N)=T
101 CONTINUE
C
CALL PTPLOT (RAYX, RAYT, 1, KK, -2)
GO TO 1
C
10 FORMAT (4F8.3)
11 FORMAT (I3)
12 FORMAT (2F8.3)
13 FORMAT ('// *** ERROR IN SUBROUTINE TXPLTS *** ',/,/,
1' INPUT DATA GREATER THAN ARRAY DIMENSIONS ',/,/)
C
4 CALL BLKPEN
C
RETURN
END
C
C

```



```

IF(IPL0T.EQ.'ADM3AG') CALL ADM3AG
IF(IPL0T.EQ.'HP747') CALL HP747
IF(IPL0T.EQ.'HP2647') CALL HP2647
IF(IPL0T.EQ.'GP39') CALL GP39
IF(IPL0T.EQ.'GP39W') CALL GP39W
IF(IPL0T.EQ.'S75680') CALL S75680

IF(IPL0T.EQ.'T4010'.OR.'T4014') CALL PICCIE

C
C Some terminals require a reduction of plot size. This is carried
C out by CALL UNITS. Not required for the central plotter or the
C Sigma S75680 terminal.
C
IF(IPL0T.EQ.'S75680') GOTO 35
IF(IPL0T.EQ.'GP39'.OR.'IPL0T.EQ.'GP39W') GOTO 35
CALL UNITS(1.0)

C
35 CALL WINDOW(2)

C
IF(IPL0T.NE.'HP2647') GOTO 39
XORIGL=XORIGL*0.25
ZORIGL=ZORIGL*0.25

C
C Read in plotting parameters from control file.
C
39 READ (2,10) YLEN,XLEN,XSCMIN,XSCMAX,XINT,ZLEN,ZSCMIN,ZSCMAX,ZINT

C
C If last card of control file is blank, set default plotting
C parameters.
C
IF (YLEN.EQ.0.) YLEN=200.0
IF (XLEN.EQ.0.) XLEN=120.0
IF (XSCMIN.EQ.0.) XSCMIN=0.0
IF (XSCMAX.EQ.0.) XSCMAX=8.0
IF (XINT.EQ.0.) XINT=8
IF (ZLEN.EQ.0.) ZLEN=100.0
IF (ZSCMIN.EQ.0.) ZSCMIN=0.0
IF (ZSCMAX.EQ.0.) ZSCMAX=10.0
IF (ZINT.EQ.0.) ZINT=11

C
IF (IPL0T.EQ.'GP39') CALL DEVVAP (XORIGL+XLEN+100.,264.,0)
IF (IPL0T.EQ.'GP39W') CALL DEVVAP (XORIGL+XLEN+100.,829.,0)

C
C Read in required number of profiles (IXINC) and number of
C depth increments (IZINC, in multiples of 50m), from SEIS81
C output file.
C

```

```

READ (1,9) IXINC, IZINC
IF (IZINC.GT.300) WRITE (6,12)

C
C Read in velocity matrix, ending at END-OF-FILE or when I=IZINC.
C
DO 101 N=1, IZINC
  J=J+1
  READ (1,11) Z(N), (VZ(I,N,1), I=1, IXINC)
  IF (Z(N).EQ.999.) GO TO 20
  READ (1,11) Z(N), (VZ(I,N,2), I=1, IXINC)
  READ (1,11) Z(N), (VZ(I,N,3), I=1, IXINC)

C
C Calculate VP/Vs and Poisson's ratio matrices
C
DO 106 I=1, IXINC
  IF (VZ(I,N,2).LT.0.05) GO TO 23
  PSR(I,N)=VZ(I,N,1)/VZ(I,N,2)
  PSNR(I,N)=(PSR(I,N)**2/2-1)/(PSR(I,N)**2-1)
  GO TO 106
23 PSR(I,N)=0.
  PSNR(I,N)=0.
106 CONTINUE
101 CONTINUE
GO TO 21

C
20 IZINC=J-1

C
C This section produces plots of V-7 curves from L to R across the
C Velocity-Depth-Range matrix
C
21 IF (IC.EQ.0) THEN
  DYLEN=YLEN/(IXINC-1)
  DI(1)=0.0
  X(1)=0.0
  Y(1)=0.0

C
C Define increments and angle (from horizontal) for the plotted
C Range axis
C
DO 103 I=2, IXINC
  DY(I)=DY(I-1)+DYLEN
  X(I)=DY(I)*SIN(THETA)
  Y(I)=DY(I)*COS(THETA)
103 CONTINUE

C
C Position and write out axis annotations.
C

```

```

XXX=X(IXINC/2)-20.0
YYY=Y(IYINC/2)+3.0
CALL CHAANG (THETA)
CALL MOVTO2 (XORIGL+XXX,ZORIGL+ZLEN+YYY)
CALL CHAHOL (7HRANGE*)
CALL CHAHOL (7H (KM)*)
CALL CHAANG (0.0)
CALL MOVTO2 (XORIGL+XLEN*1.0/5.0,ZORIGL-12.0)
IF (I.P.LT.3) THEN
CALL CHAHOL (8HVELOCI*)
CALL CHAHOL (5HTY *)
CALL CHAHOL (8H(KM/S)*)
ELSE IF (I.P.EQ.3) THEN
CALL CHAHOL (8HVP/V*)
CALL CHAHOL (7HRATIO*)
ELSE IF (I.P.EQ.4) THEN
CALL CHAHOL (8HPOISSO*)
CALL CHAHOL (8HNS RAT*)
CALL CHAHOL (4HIO*)
ELSE IF (I.P.EQ.5) THEN
CALL CHAHOL (8HIDENSIT*)
CALL CHAHOL (8HY (MG/*)
CALL CHAHOL (5HM3)*)
END IF
CALL MOVTO2 (XORIGL-10.0,ZORIGL+ZLEN*3.3/10.0)
CALL CHAANG (90.0)
CALL CHAHOL (7HDEPTH*)
CALL CHAHOL (7H (KM)*)
CALL CHAANG (0.0)
C
C Position and write out range values
C TSCALE is used to provide the illusion of perspective
C
IF (IXINC.GT.51) II=5
IF (IXINC.GT.21.AND.IXINC.LT.51) II=4
IF (IXINC.LE.21) II=3
TSCALE=1.0
X(1)=0.0
Y(1)=0.0
C
DO 104 I=1,IYINC,II
IF (IXINC-I.LT.II) GO TO 104
IK=I-1
XC=X(I)
YC=Y(I)
CALL SCALE2 (TSCALE,TSCALE)
IF (I.EQ.1) CALL MOVTO2 (XORIGL+XC-8.0,ZORIGL+ZLEN+YC)
XXX=X(IXINC/2)-20.0
YYY=Y(IYINC/2)+3.0
CALL CHAANG (THETA)
CALL MOVTO2 (XORIGL+XXX,ZORIGL+ZLEN+YYY)
CALL CHAHOL (7HRANGE*)
CALL CHAHOL (7H (KM)*)
CALL CHAANG (0.0)
CALL MOVTO2 (XORIGL+XLEN*1.0/5.0,ZORIGL-12.0)
IF (I.P.LT.3) THEN
CALL CHAHOL (8HVELOCI*)
CALL CHAHOL (5HTY *)
CALL CHAHOL (8H(KM/S)*)
ELSE IF (I.P.EQ.3) THEN
CALL CHAHOL (8HVP/V*)
CALL CHAHOL (7HRATIO*)
ELSE IF (I.P.EQ.4) THEN
CALL CHAHOL (8HPOISSO*)
CALL CHAHOL (8HNS RAT*)
CALL CHAHOL (4HIO*)
ELSE IF (I.P.EQ.5) THEN
CALL CHAHOL (8HIDENSIT*)
CALL CHAHOL (8HY (MG/*)
CALL CHAHOL (5HM3)*)
END IF
CALL MOVTO2 (XORIGL-10.0,ZORIGL+ZLEN*3.3/10.0)
CALL CHAANG (90.0)
CALL CHAHOL (7HDEPTH*)
CALL CHAHOL (7H (KM)*)
CALL CHAANG (0.0)
C
C Draw out V-7 curve.
C
3 CALL GRAMOV (XSCHMIN,ZSCHMIN)
DO 100 N=1,IZINC
IF (I.P.EQ.1) VZZ=VZ(I,N,1)
IF (I.P.EQ.2) VZZ=VZ(I,N,2)
IF (I.P.EQ.3) VZZ=PSR(I,N)
IF (I.P.EQ.4) VZZ=PSWR(I,N)
IF (I.P.EQ.5) VZZ=VZ(I,N,3)
VZ=Z(N)
IF (VZZ.GT.XSCHMIN.AND.VZZ.LE.XSCHMAX.AND.ZZ.GT.ZSCHMIN.AND.ZZ.LE.ZSCH
1MAX) GO TO 22
CALL GRAMOV (XSCHMIN,ZZ)
GO TO 100
22 CALL GRALIN (VZZ,ZZ)
100 CONTINUE
C
IF (I.GT.1) CALL MOVTO2 (XORIGL+XC-12.0,ZORIGL+ZLEN+YC)
CALL CHAINT (IK,3)
TSCALE=TSCALE-0.03/IXINC
104 CONTINUE
C
TSCALE=1.0
C Define V-Z axes and plot out V-7 curve for each range.
C
DO 102 I=1,IXINC
CALL SCALE2 (TSCALE,TSCALE)
XORIG=XORIGL+X(I)
ZORIG=ZORIGL+Y(I)
IF (I.GT.1) GO TO 6
CALL AXIPOS(1,XORIG,ZORIG,XLEN,1)
CALL AXISCA(3,XINT,XSCHMIN,XSCHMAX,1)
CALL AXIDRA(2,1,1)
6 CALL AXIPOS(1,XORIG,ZORIG+ZLEN,XLEN,1)
IF (I.LT.IXINC) GO TO 2
CALL AXIPOS(1,XORIG,ZORIG,XLEN,1)
CALL AXISCA(3,XINT,XSCHMIN,XSCHMAX,1)
CALL AXIDRA(-2,-1,1)
2 IF (I.LT.IXINC) GO TO 7
CALL AXIPOS(1,XORIG+XLEN,ZORIG,ZLEN,2)
CALL AXISCA(3,ZINT,ZSCHMAX,ZSCHMIN,2)
CALL AXIDRA(2,1,2)
7 CALL AXIPOS(1,XORIG,ZORIG,ZLEN,2)
IF (I.GT.1) GO TO 3
CALL AXIPOS(1,XORIG,ZORIG,ZLEN,2)
CALL AXISCA(3,ZINT,ZSCHMAX,ZSCHMIN,2)
CALL AXIDRA(-2,-1,2)
C
C Draw out V-7 curve.
C
3 CALL GRAMOV (XSCHMIN,ZSCHMIN)
DO 100 N=1,IZINC
IF (I.P.EQ.1) VZZ=VZ(I,N,1)
IF (I.P.EQ.2) VZZ=VZ(I,N,2)
IF (I.P.EQ.3) VZZ=PSR(I,N)
IF (I.P.EQ.4) VZZ=PSWR(I,N)
IF (I.P.EQ.5) VZZ=VZ(I,N,3)
VZ=Z(N)
IF (VZZ.GT.XSCHMIN.AND.VZZ.LE.XSCHMAX.AND.ZZ.GT.ZSCHMIN.AND.ZZ.LE.ZSCH
1MAX) GO TO 22
CALL GRAMOV (XSCHMIN,ZZ)
GO TO 100
22 CALL GRALIN (VZZ,ZZ)
100 CONTINUE
C

```

```

C  Draw Range axis by incrementing plotting origin after each plot.
C
IF (I.EQ.1) GO TO 4
XORG=XORIGL+X(I-1)
ZORG=ZORIGL+Y(I-1)
CALL MOVTO2 (XORG,ZORIG)
CALL LINTO2 (XORG,ZORG)
CALL MOVTO2 (XORIG,ZORIG+ZLEN)
CALL LINTO2 (XORG,ZORG+ZLEN)
CALL MOVTO2 (XORIG+XLEN,ZORIG)
CALL LINTO2 (XORG+XLEN,ZORG)
IF (I.EQ.IXINC) GO TO 4
GO TO 5
4 CALL MOVTO2 (XORIG,ZORIG)
CALL LINTO2 (XORIG+XLEN,ZORIG)
5 CALL MOVTO2 (XORIG,ZORIG+ZLEN)
TSCALE=TSCALE-0.001/IXINC
102 CONTINUE
C
C This section contours the VGD matrix with respect to range and
C depth
C
ELSE IF (IC.EQ.1) THEN
IZ=IZINC
DO 107 N=1,I7INC
DO 108 I=1,IXINC
IF (IP.FO.1) VGD(I,I7)=V7(I,N,1)
IF (IP.EQ.2) VGD(I,I2)=V2(I,N,2)
IF (IP.EQ.3) VGD(I,I7)=PSR(I,N)
IF (IP.EQ.4) VGD(I,I2)=PSR(I,N)
IF (IP.FO.5) VGD(I,I2)=V7(I,N,3)
108 CONTINUE
I7=I7-1
WRITE (6,14) (VGD(I,N),I=1,IXINC)
14 FORMAT (25F5.1)
107 CONTINUE
CALL DEVFAP (XLFN,ZLEN,0)
CALL LEVELS (XSCMIN,XSCMAX)
IYX=XINT/IFIX(XSCHAX-XSCHIN)
CALL LABCON (IX,1,0.,0)
CALL SETSCA (10.,1.,1.25)
CALL DRACON (IXINC,0.,40.0,I7INC,-15.,1.,VGD,XINT,0.,R5000,W
1)
END IF
C
C Formats
C

```

```

8 FORMAT (2I3,F6.2,A6)
9 FORMAT (2I5)
10 FORMAT (F6.1,2(3F6.1,I6))
11 FORMAT (F6.2,1X,101F5.2)
12 FORMAT (' *** IZINC > 300
REDUCE IZINC OR ENLARGE ARRAYS *** ')
CALL DEVEND
STOP
END

```



```

IF (VO, EQ.9998.) GO TO 99
IK=IK+1
L=L+1
4 READ (5,12) X(L),T(L)
IF (X(L),EQ.9999.) GO TO 5
IF (JJ,LT.0) THEN
TR(L)=T(L)
T(L)=TR(L)+X(L)/RVEL
ENDIF
IF (JJ,GT.0) TR(L)=T(L)-X(L)/RVEL
IF (L,GT.1) GO TO 1
XINT(L)=X(L)
TINT(L)=T(L)
GO TO 4
1 XINT(L)=X(L)-X(L-1)
TINT(L)=T(L)-T(L-1)
2 V(L)=XINT(L)/TINT(L)
GO TO 4
5 J=L-1
M=J-1
IF (VO, EQ.0) VO=V(1)
Q=VO/VO**2
Calculate p and tau
DO 102 L=1,M
VPT(L)=0.5*(V(L)+V(L+1))
TAU(L)=T(L)-X(L)/VPT(L)
P(L)=VPT(L)/VPT(L)**2
U(L)=SQRT(P(L)**2+Q**2)
102 CONTINUE
C Calculate depths using tau-p method
ZZ(1)=(TAU(?)#0.5)/(SQRT(Q**2-P(?)**2))
NN=M-1
DO 103 L=2,NN
ZF=SQRT(Q**2-P(L+1)**2)
ZG=SQRT(U(L)**2-P(L+1)**2)
ZH=(TAU(L+1)#0.5)+(ZZ(L-1)#ZF)
ZZ(L)=ZH/ZG
103 CONTINUE
C Write out the results table
DO 104 L=1,NN
WRITE (6,14) X(L),T(L),TR(L),VPT(L),TAU(L),P(L),ZZ(L)
CONTINUE
104 WRITE (6,15) X(M),T(M),TR(M),VPT(M),TAU(M),P(M)
WRITE (6,16) X(J),T(J),TR(J)
C Plotting commands
IF (N, EQ.1) THEN
IF (IK, EQ.1) THEN
CALL POSITN (0.,0.)
CALL JOIN (X(1),TR(1))
END IF
CALL PTPLOT (X, TR, 1, J, -2)
C
ELSE IF (N, EQ.2) THEN
CALL PSPACE (0.15,0.62,0.10,0.40)
CALL MAP (0.12,0.26,0.0,TAUMAX)
CALL PTPLOT (P,TAU,1,M,43)
IF (J, LE.30) CALL PTPLOT (P,TAU,1,M,-2)
C
CALL PSPACE (0.73,1.20,0.10,0.40)
CALL MAP (VMIN,VMAX,ZMAX,0.)
IF (IK, EQ.1) THEN
CALL PLOTNC (VO,0.,43)
CALL JOIN (VPT(1),ZZ(1))
END IF
CALL PTPLOT (VPT, ZZ, 1, NN, 43)
IF (J, LE.30) CALL PTPLOT (VPT, ZZ, 1, NN, -2)
C
CALL PSPACE (0.15,0.62,0.48,0.78)
CALL MAP (XMIN,XMAX,0.26,0.12)
CALL PTPLOT (X,P,1,M,43)
IF (J, LE.30) CALL PTPLOT (X,P,1,M,-2)
C
CALL PSPACE (0.73,1.20,0.48,0.78)
CALL MAP (0.12,0.26, YMIN, YMAX)
CALL PTPLOT (P, TR, 1, M, 43)
IF (J, LE.30) CALL PTPLOT (P, TR, 1, M, -2)
C
END IF
C Return to read in next set of data
GO TO 6
C
99 CALL GRENDA
C

```



```

CALL TYPECS ('VELOCITY (KM.S-1)',17)
CALL PLACE (24,20)
CALL TYPECS ('RANGE (KM)',10)
CALL PLACE (68,20)
CALL TYPECS ('P (S.KM-1)',10)
CALL PLACE (4,13)
CALL CTROI (1,0)
CALL TYPECS ('P (S.KM-1)',10)
CALL CTROI (0,0)
CALL PLACE (51,13)
CALL CTROI (1,0)
CALL TYPECS ('TR (S)',6)
CALL CTROI (0,0)
CALL PLACE (4,11)
CALL CTROI (1,0)
CALL TYPECS ('TAU (S)',7)
CALL CTROI (0,0)
CALL PLACE (51,32)
CALL CTROI (1,0)
CALL TYPECS ('DEPTH (KM)',10)
CALL CTROI (0,0)
CALL PSPACE (0.15,0.62,0.09,0.30)
CALL MAP (0.12,0.26,0.0,TAUMAX)
CALL BORDER
CALL SCALES
CALL PSPACE (0.73,1.20,0.09,0.30)
CALL MAP (VMIN,VMAX,ZMAX,0.0)
CALL BORDER
CALL SCALES
CALL PSPACE (0.15,0.62,0.47,0.77)
CALL MAP (XMIN,XMAX,0.26,0.12)
CALL BORDER
CALL SCALES
CALL PSPACE (0.73,1.20,0.47,0.77)
CALL MAP (0.12,0.26,YMIN,YMAX)
CALL BORDER
CALL SCALES
RETURN
END

```

```

C C PLOTTING COORDINATES
C C HXMIN, HXMAX, HYMIN, HYMAX ARE MAXIMUM AND MINIMUM PLOTTING
C C COORDINATES (RANGE AND REDUCED-TIME)
C C HYMN, HYMX ARE MINIMUM AND MAXIMUM COORDS. FOR T-X GRAPHS
C C
C C 3: IPT, J, VRED, X0          FORMAT (2I3,2F8.3)
C C
C C IPT = GHOST GRAPHICAL SYMBOL (SEE GHOST MANUAL).
C C J = NORMALLY VALUES OF BETWEEN 50 - 56 ARE USED
C C VRED = NUMBER OF GEOPHONES IN EACH DATASET
C C X0 = REDUCTION VELOCITY IN KM/S
C C REPRESENTS THE DISTANCE ALONG THE PROFILE (IN KM)
C C TO THE SOURCE (FOR SPLIT SPREAD PROFILES)
C C
C C 4: XSORC, DXSORC, YSORC, ZSORC, DZSORC, TSORC, DTSORC, QSITE
C C          FORMAT (4(F8.3,F6.3),5A8)
C C
C C XSORC, YSORC, ZSORC, TSORC ARE ORIGIN COORDS AND SHOT
C C INSTANT TIME
C C DXSORC ETC. ARE ASSOCIATED OBSERVED ERRORS.
C C QSITE IS THE QUARRY/SHOT NAME
C C
C C 5: XSEIS, DXSEIS, YSEIS, DYSEIS, ZSEIS, DZSEIS, TSEIS, DTSEIS, SITE
C C          FORMAT (4(F8.3,F6.3),5A8)
C C
C C XSEIS, YSEIS, ZSEIS, TSEIS ARE GEOPHONE STATION COORDS. AND
C C ARRIVAL TIMES
C C DXSEIS ETC. ARE ASSOCIATED OBSERVED ERRORS.
C C SITE IS THE GEOPHONE SITE NAME
C C
C C OR IF IX = 1
C C 5: XSEIS, DXSEIS, YSEIS, DYSEIS, ZSEIS, DZSEIS, TSEIS, DTSEIS, AINC
C C          VINC, SITE          FORMAT (4(F8.3,F6.3),
C C                               2F6.3,5A8)
C C
C C AS ABOVE BUT WITH:
C C AINC IS HEIGHT ABOVE DATUM
C C VINC IS VELOCITY OF SURFACE LAYER
C C
C C IF IP = 2 OR 3 THEN MODEL REDUCED-TIME DISTANCE DATA IS READ IN
C C ON CHANNEL 3. (INPUT IS IDENTICAL TO THE
C C COMPLIMENTARY OUTPUT FROM PROGRAM RAYPLT)
C C (SEE GLASGOW VERSION OF THE SEIS81 PACKAGE)
C C
C C KK
C C HXRAY, HTRAY (FROM 1 TO KK)          FORMAT I3
C C                                         FORMAT 2F8.3

```

```

C C -----
C C PROGRAM TX3E
C C -----
C C PROGRAM 'TX3D' IS DESIGNED TO READ IN RAW TIME-DISTANCE FIELD
C C DATA, CONVERT TO TRAVEL-TIMES, REDUCE TO A COMMON DATUM (IF
C C REQUIRED), AND PLOT DATA AS TRAVEL-TIME OR REDUCED-TIME DISTANCE
C C GRAPHS.
C C
C C PROGRAM COMPLETES IN FORTRAN77 ON THE ICI:2988 UNDER VME AT THE
C C GUCS, AND USES GHOST GRAPHICAL ROUTINES.
C C WRITTEN BY          K. DAVIDSON,          1981
C C                   DEPARTMENT OF GEOLOGY,
C C                   UNIVERSITY OF GLASGOW,
C C                   GLASGOW G12 8QQ.
C C
C C INPUT DATA:
C C 1: IP, IX, IE, NUMB, TITLE          FORMAT (3I2, I3, 5A8)
C C
C C IP = 0: A4 PLOTS OF REDUCED TIME ARE PRODUCED
C C = 1: LARGE PLOTS OF REDUCED TIME ARE PRODUCED
C C = 2: SAME AS 0 BUT WITH RAY-TRACE DATA ON CHANNEL 3
C C = 3: SAME AS 1, " " " " " " " "
C C = 4: A4 PLOTS OF TRAVEL TIME - DISTANCE ARE PRODUCED
C C = 5: SAME AS 4, BUT WITH RAY-TRACE DATA ON CHANNEL 3
C C
C C IX = 0: ONLY NAT.GRID & ELEVATION COORDS SUPPLIED.
C C = 1: ABOVE + SURFACE CORRECTION ESTIMATES.
C C IE = 0: PREDEFINED GHOST GRAPHICAL SYMBOLS ARE PLOTTED
C C AT ALL POINTS.
C C = 1: ERROR BARS ARE PLOTTED AT ALL POINTS
C C NUMB= NUMBER OF DATASETS
C C TITLE TITLE OF PROFILE
C C
C C 2: AZLN, HXMIN, HXMAX, HYMIN, HYMX, HYMN, HYMX          FORMAT (F5.1,6F8.3)
C C
C C AZLN DEFINES THE BEARING OF THE PROFILE FROM THE LHS
C C OF THE PLOT. USED TO DISTINGUISH RANGE AND

```



```

DZDIST=ZDIST**2+DSQRT(DZSEIS(N)**2+DZSORC**2)
DZINV2=DSQRT(DXDIST**2+DYDIST**2+DZDIST**2)
DZINV=0.5*(1.0/DSQRT(ZINV))*DZINV2
DTIME=DSQRT(DTSEIS(N)**2+DTSORC**2)
DTRED=DSQRT(DTTIME**2+(DZINV/VRED)**2)

C
C
C
PLACE AZ IN CORRECT QUADRANT
IF (XDIST.LT.0..AND.YDIST.LT.0.) GO TO 35
IF (XDIST.LT.0..AND.YDIST.GT.0.) GO TO 36
IF (XDIST.GT.0..AND.YDIST.GT.0.) GO TO 37
IF (XDIST.GT.0..AND.YDIST.LT.0.) GO TO 38
35 AZ=270-(DATAN2(DABS(YDIST),DABS(XDIST))*RAD)
GO TO 39
36 AZ=270+(DATAN2(YDIST,DABS(YDIST))*RAD)
GO TO 39
37 AZ=90-(DATAN2(YDIST,XDIST)*RAD)
GO TO 39
38 AZ=90+(DATAN2(DABS(YDIST),XDIST)*RAD)
39 AZLN1=AZLN-90.00
AZLN2=AZLN+90.00

C
C
C
TEST FOR POSITIVE OR NEGATIVE DIRECTION OF SOURCE FROM RECEIVERS.
IF -90 < AZ < +90, RELATIVE TO AZLN - POSITIVE ZINV
IF +90 < AZ < -90, RELATIVE TO AZLN - NEGATIVE ZINV
IF (A7.LT.A7LN2.AND.A7.GT.A7LN1) GO TO 3
ZINV=0.000-ZINV

C
3 IF (IX.FQ.0) GO TO 4
XCOR=ZDIST/DTAN(AINC(N))
TCOR=ZDIST/DSIN(AINC(N))/VINC(N)
ZINV=ZINV-XCOR
TTIME=TTIME-TCOR
4 HXO(N)=XO+ZINV
TRED=TTIME-DABS(ZINV/VRED)
HTRED(N)=TRED
HDZINV=DZINV
HDTRD=DTRED
IF (IP.GE.4) THEN
HTRED(N)=TTIME
HDTRD=DTIME
END IF
IF (IX.FQ.0) GO TO 7
WRITE (6,50) ZINV,HXO(N),XDIST,YDIST,ZDIST,XCOR,
1TTIME,TCOR,TRED,AZ,(SITE(N),M=1,5)
GO TO 100

7 WRITE (6,40) ZINV,HXO(N),DZINV,TTIME,DTRED,DTRED,
1AZ,(SITE(N),M=1,5)
IF (IE.EQ.0) GO TO 100
CALL POSITN (HXO(N)-HDZINV,HTRED(N))
CALL JOIN (HXO(N)+HDZINV,HTRED(N))
CALL POSITN (HXO(N),HTRED(N)+0.030)
CALL JOIN (HXO(N),HTRED(N)-0.030)
100 CONTINUE
WRITE (6,63)
C
IF (IE.GT.0) GO TO 200
CALL PTPLOT (HXO,HTRED,1,N,IPT)
C
200 CONTINUE
C
C
C
FORMATS
10 FORMAT (2I3,8X,F8.3)
13 FORMAT (I3)
15 FORMAT (2F8.3)
20 FORMAT (4(F8.3,F6.3),5A8)
30 FORMAT (4(F8.3,F6.3),2F6.3,5A8)
40 FORMAT (8F8.3,4X,5A8)
41 FORMAT (' RANGE', PT DIST, ST ERR, TR TIME, SITE NAME, ST ERR,
1 RED TIME, ST ERR, AZIMUTH, XCOR, YDIST, YDIST, ELEV,
1 XCOR, TOT TIME, TCOR, RED TIME, AZIMUTH,
2 SITE NAME, /100(' '), //)
52 FORMAT (/100(' '),/20X,'PROGRAM DESIGNED TO PROCESS ANALOGUE',
1 TIME-DISTANCE DATA',/100(' '),//)
60 FORMAT (/20X,'INPUT DATA',//)
62 FORMAT (/20X,'OUTPUT RESULTS',10X,5A8,//)
63 FORMAT (/100(' '))
70 FORMAT (3I2,13F8.3,5A8)
75 FORMAT (F5.1,6F8.3)
76 FORMAT (/5X,*** ERROR - NUMBER OF SAMPLES IS GREATER THAN THE',
1 ARRAY BOUNDS ***,//,10X,'INCREASE ALL SOURCE PROGRAM ARRAYS',
1 TO',I4, //)
C
C
999 CALL GRENDD
STOP
END
C
C
SUBROUTINE TO ANNOTATE REDUCED TIME GRAPH.

```

```

CALL CTRORI (1.0)
CALL TYPECS ('TRANSIT TIME (SECS)',19)
CALL CTRORI (0.0)
CALL PLACE (20,1)
CALL TYPECS (TITLE,40)
CALL BORDER
CALL CTRMAG (10)
CALL AXES
CALL CTRMAG (20)
RETURN
END

```

```

C SUBROUTINE PLTT1 (VRED,IP,HXMIN,HXMAX,HYMIN,HYMAX)
  IMPLICIT DOUBLE PRECISION (A-G,O-Z)
  COMMON TITLE (5)

```

```

C IF (IP.EQ.1.OR.IP.EQ.3) GO TO 1
  CALL CSPACE (0.03,1.20,0.01,0.85)
  CALL PSPACE (0.20,1.20,0.15,0.76)
  GO TO 2
  1 CALL CSPACE (0.05,1.35,0.05,1.00)
  CALL PSPACE (0.15,1.35,0.2,0.94)
  2 CALL MAP (HXMIN,HXMAX,HYMIN,HYMAX)
  IF (IP.EQ.1.OR.IP.EQ.3) GO TO 3
  CALL PLACE (35,27)
  GO TO 4

```

```

  3 CALL PLACE (35,31)
  4 CALL TYPECS ('RANGE (KM)',10)
  IF (IP.EQ.1.OR.IP.EQ.3) GO TO 5
  CALL PLACE (5,20)
  GO TO 6

```

```

  5 CALL PLACE (2,21)
  6 CALL CTRORI (1.0)
  CALL TYPECS ('REDUCED TIME (T-X)',18)
  CALL TYPEFN (VRED,1)
  CALL TYPECS ('',1)
  CALL CTRORI (0.0)
  CALL PLACE (20,2)
  CALL TYPECS (TITLE,40)
  CALL BORDER
  CALL CTRMAG (10)
  CALL AXES
  CALL CTRMAG (20)
  RETURN
  END

```

```

C SUBROUTINE TO ANNOTATE T-X GRAPH.

```

```

C SUBROUTINE PLTT2 (HXMIN,HXMAX,HYMIN,HYMX)
  IMPLICIT DOUBLE PRECISION (A-G,O-Z)
  COMMON TITLE (5)

```

```

C CALL CSPACE (0.03,1.20,0.01,0.85)
  CALL PSPACE (0.20,1.20,0.15,0.76)
  CALL MAP (HXMIN,HXMAX,HYMIN,HYMX)
  CALL PLACE (35,27)
  CALL TYPECS ('RANGE (KM)',10)
  CALL PLACE (5,20)

```



```

VU(J)=U(J)/U(J)**2
IF (NCODE3.EQ.2) WRITE (10,201) ZZ(J),VPT(J)
WRITE (6,101) DIST(J),T(J),VPT(J),VU(J),P(J),Q,TAU(J),Z(J),
17Z(J)
46 CONTINUE
C
C PLOTTING SEQUENCE.
C
C READ (5,109) NTXPTS,LU
C
C READ IN PICKED TIME-DISTANCE DATA AND PLOT OUT WITH MODEL DATA
C
C IF (NCODE1.EQ.0) GO TO 1
CALL WHBPL0 (RVEL,XMIN,VMX,TMN,TMX)
IF (NTXPTS.EQ.0) GO TO 11
CALL TXPLTS (NTXPTS,RVEL,LU)
11 CALL POSITH (0.,0.)
DO 45 J=1,M
45 CALL JOIN (DIST(J),TRED(J))
CALL FRAME
1 IF (NCODE2.EQ.0) GO TO 2
CALL WHBPL1 (XMIN,XMAX,ZRO,ZMX)
CALL PTPL0T (DIST,Z,1,M,43)
CALL FRAME
2 IF (NCODE3.EQ.0) GO TO 3
CALL WHBPL2 (VMN,VMX,ZRO,ZMX)
CALL PTPL0T (VPT,Z,1,M,43)
CALL PTPL0T (VPT,Z,1,M,-2)
IF (NCODE3.EQ.1) GO TO 4
CALL PLOTNC (VO,0,44)
CALL JOIN (VPT(1),ZZ(1))
CALL PTPL0T (VPT,ZZ,1,NN,44)
CALL PTPL0T (VPT,ZZ,1,NN,-2)
4 CALL FRAME
3 IF (NCODE4.EQ.0) GO TO 50
CALL WHBPL3
CALL PTPL0T (P,TAU,1,M,43)
CALL PTPL0T (P,TAU,1,M,-2)
CALL FRAME
50 CONTINUE
C
C FORMATS.
C
100 FORMAT (I5,9F8.3)
101 FORMAT (10F8.3)
102 FORMAT (4X,F7.3,7X,F6.3,4X,F7.3,8X,F7.3,F10.3,6X,F7.3,AX,F
17.3)
103 FORMAT (//6X,' DETERMINATION OF VELOCITY-DEPTH FUNCTION',/6X,' BY WIE
1CHERT-HERGLOTZ-BATEMAN INTEGRAL',/1X,' DEPTH (KM)',2X,' VELOCITY (KM
2/S)',2X,' TAU (S)',2X,' SLOWNESS (S/KM)', ' TIME (S)',2X,' RED. TIME',2
3X,' DISTANCE (KM)',2X,' GRADIENT (S-1)'//)
104 FORMAT (5I5)
105 FORMAT (////2X,' PROBLEM NUMBER',I3.10A4)
106 FORMAT (10A4)
109 FORMAT (2I3)
110 FORMAT (2F8.3)
111 FORMAT (9F8.3)
CALL GREND
STOP
END
C
C SUBROUTINE TO ANNOTATE PLOT OF RANGE AGAINST DEPTH.
C
SUBROUTINE WHBPL1 (XMIN,XMAX,ZRO,ZMX)
COMMON TITLE (10)
CALL CSPACE (0.05,1.1,0.05,0.82)
CALL PSPACE (0.2,1.1,0.2,0.76)
CALL MAP (XMIN,XMAX,ZMX,ZRO)
CALL PLACE (20,1)
CALL TYPECS (TITLE,40)
CALL PLACE (30,24)
CALL TYPECS ('RANGE (KM)',10)
CALL PLACE (4,15)
CALL CTRORI (1.0)
CALL TYPECS ('DEPTH (KM)',10)
CALL CTRORI (0.0)
CALL BORDER
CALL CTRMAG (10)
CALL SCALES
CALL CTRMAG (20)
RETURN
END
C
C SUBROUTINE TO ANNOTATE PLOT OF VELOCITY AGAINST DEPTH.
C
SUBROUTINE WHBPL2 (VMN,VMX,ZRO,ZMX)
COMMON TITLE (10)
CALL CSPACE (0.05,1.1,0.05,0.82)
CALL PSPACE (0.2,1.1,0.2,0.76)
CALL MAP (VMN,VMX,ZMX,ZRO)
CALL PLACE (20,1)
CALL TYPECS (TITLE,40)
CALL PLACE (30,24)
CALL TYPECS ('VELOCITY (KM/S)',15)

```

```

CALL PLACE (4,14)
CALL CTRORI (1.0)
CALL TYPECS ('DEPTH (KM)',10)
CALL CTRORI (0.0)
CALL BORDER
CALL CTRMAG (10)
CALL SCALES
CALL CTRMAG (20)
RETURN
END

C
C
C
SUBROUTINE TO ANNOTATE PLOT OF COMPUTED REDUCED TIME AGAINST RANGE.
C
C
SUBROUTINE WHBPLO (RVEL, XMIN, XMN, THN, THX)
COMMON TITLE (10)
CALL CSPACE (0.05,1.1-0.05,0.82)
CALL PSPACE (0.2,1.1,0.2,0.76)
CALL MAP (XMIN, XMN, THN, THX)
CALL PLACE (20,1)
CALL TYPECS (TITLE,40)
CALL PLACE (30,24)
CALL TYPECS ('RANGE (°M)',10)
CALL PLACE (4,19)
CALL CTRORI (1.0)
CALL TYPECS ('REDUCED TIME (T-X)',18)
CALL TYPEFN (RVEL,1)
CALL TYPECS ('',1)
CALL CTRORI (0.0)
CALL BORDER
CALL CTRMAG (10)
CALL AXES
CALL CTRMAG (20)
RETURN
END

C
C
C
SUBROUTINE TO ANNOTATE PLOT OF TAU AGAINST SLOWNESS (P).
C
C
SUBROUTINE WHBP13
COMMON TITLE (10)
CALL CSPACE (0.05,1.1-0.05,0.82)
CALL PSPACE (0.2,1.1,0.2,0.76)
CALL MAP (0.3,0.1,0.3,0.0)
CALL PLACE (20,1)
CALL TYPECS (TITLE,40)
CALL PLACE (24,24)
CALL TYPECS ('RAY PARAMETER - P (S/KM)',24)
CALL PLACE (4,16)

```

```

CALL CTRORI (1.0)
CALL TYPECS ('TAU (T-PX) (S-1)',16)
CALL CTRORI (0.0)
CALL BORDER
CALL CTRMAG (10)
CALL SCALES
CALL CTRMAG (20)
RETURN
END

```

```

SUBROUTINE TXPLTS (NTXPTS, RVEL, LU)

```

Subroutine TXPLTS reads in and plots optional T-X, with errors, on the same plot(s) as the digital traces.

```

REWIND LU
CALL REDPEN

```

```

DO 100 N=1,NTXPTS
READ (LU,1) RANGE,DR,TIME,DT
IF (RVEL.EQ.0.) GO TO 3
DTR=SQRT(DT**2+(DR/RVEL)**2)
T=TIME-RANGE/RVEL
GO TO 2
3 DTR=DT
T=TIME
2 CALL POSITN (RANGE-DR, T)
CALL JOIN (RANGE+DR, T)
CALL POSITN (RANGE, T+DTR)
CALL JOIN (RANGE, T-DTR)
100 CONTINUE
1 FORMAT (4F8.3)

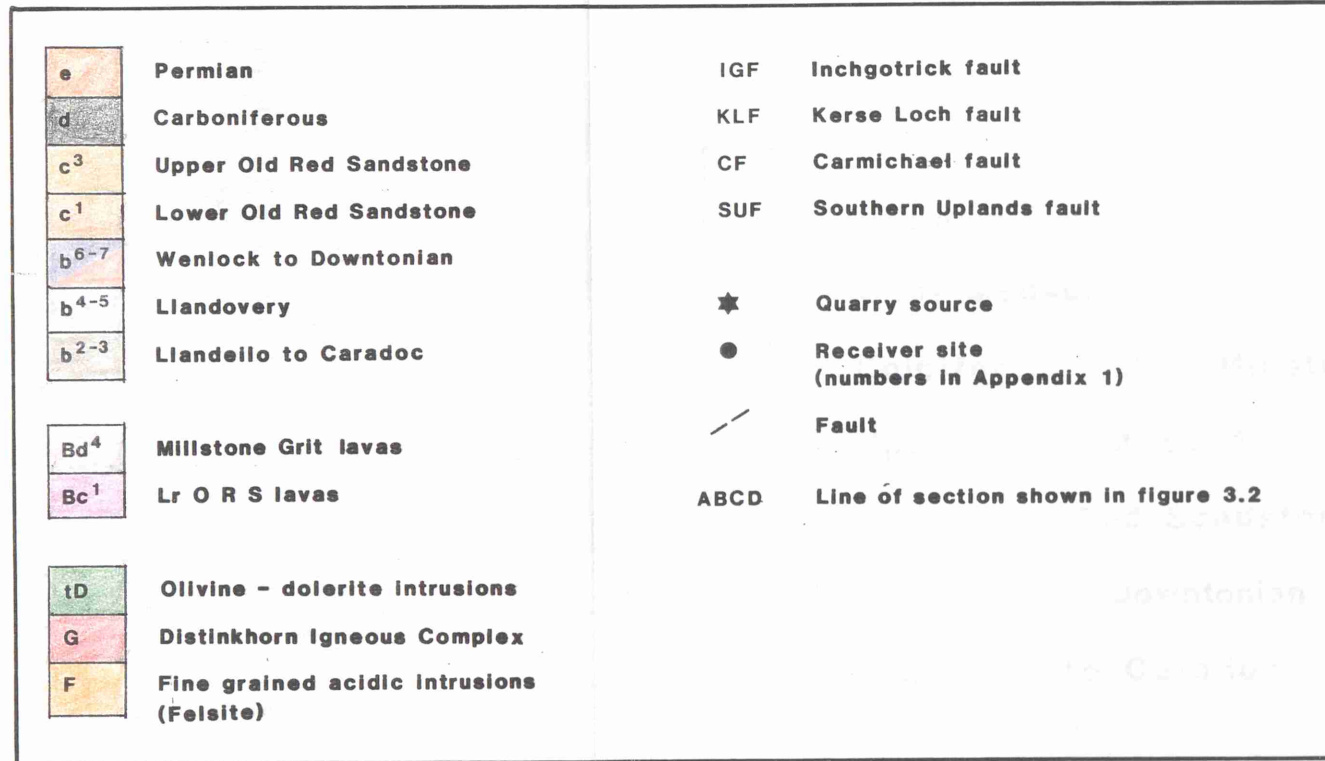
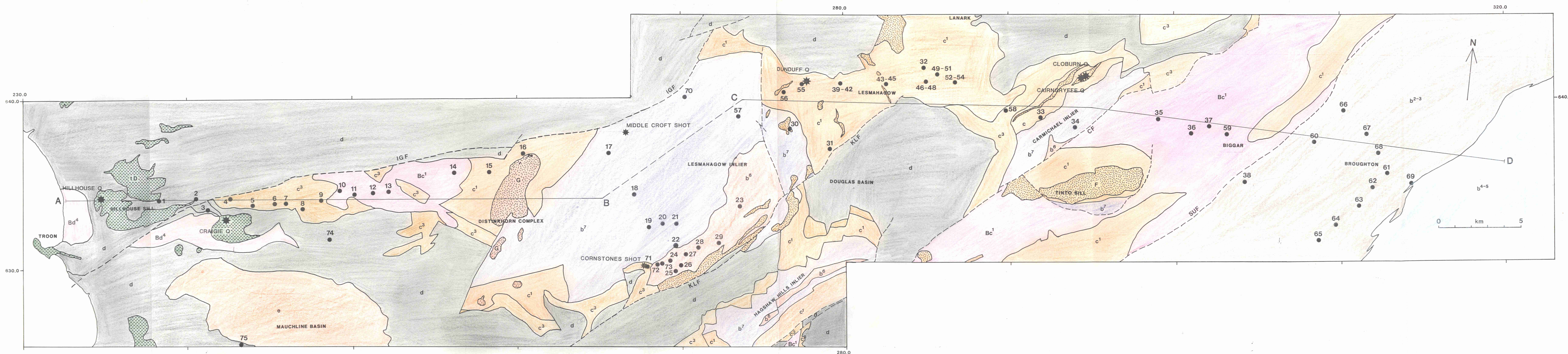
```

```

CALL BLKPEN
RETURN
END

```





Location map for the Hillhouse - Broughton profile and adjacent regions.